CONTINENTAL SHELF PROCESSES AFFECTING THE OCEANOGRAPHY OF THE SOUTH ATLANTIC BIGHT

Progress Report

Contract No. EY-76-S-09-0902

NOTICE

This report was prepared as an account of work sponsored by the United States Government. Neither the United States nor the United States Department of Energy, nor any of their employees, nor any of their contractors, subcontractors, or their employees, makes any warranty, express or implied, or assumes any legal liability or responsibility for the accuracy, completeness or usefulness of any information, apparatus, product or process disclosed, or represents that its use would not infringe privately owned rights.

DISTRIBUTION OF THIS DOCUMENT IS UNLIMITED

DISCLAIMER

This report was prepared as an account of work sponsored by an agency of the United States Government. Neither the United States Government nor any agency Thereof, nor any of their employees, makes any warranty, express or implied, or assumes any legal liability or responsibility for the accuracy, completeness, or usefulness of any information, apparatus, product, or process disclosed, or represents that its use would not infringe privately owned rights. Reference herein to any specific commercial product, process, or service by trade name, trademark, manufacturer, or otherwise does not necessarily constitute or imply its endorsement, recommendation, or favoring by the United States Government or any agency thereof. The views and opinions of authors expressed herein do not necessarily state or reflect those of the United States Government or any agency thereof.

DISCLAIMER

Portions of this document may be illegible in electronic image products. Images are produced from the best available original document.

2

SRO-902-5

MASTER

DISTRIBUTION OF THIS DOCUMENT IS UNLIMITED

SRO-902-5

CONTINENTAL SHELF PROCESSES AFFECTING THE OCEANOGRAPHY OF THE SOUTH ATLANTIC BIGHT

Progress Report

By

North Carolina State University
School of Physical and Mathematical Sciences
Raleigh, North Carolina 27650

Leonard J. Pietrafesa
Principal Investigator

1 March, 1978

"This report was prepared as an account of work sponsored by the United States Government. Neither the United States nor the United States Department of Energy, nor any of their employees, nor any of their contractors, subcontractors, or their employees, makes any warranty, express or implied, or assumes any legal liability or responsibility for the accuracy, completeness or usefulness of any information, apparatus, product or process disclosed, or represents that its use would not infringe privately-owned rights."

ABSTRACT

The objectives of the project were to determine the physical/dynamical processes controlling/affecting the distribution of phytoplankton nutrients on the continental shelf in the South Atlantic Bight. The initial objectives were to determine the short term, i.e., 2 to 10 day and longer term flux of nutrients onto the continental shelf. This is clearly related to the more general problem of combined physical and biogenic control of phytoplankton nutrients.

Pietrafesa (North Carolina State University) and Atkinson (Skidaway Institute of Oceanography) conducted a pilot experiment on the "Summer" (August-September) and "Fall" (October-December) circulation and hydrography on the North Carolina continental shelf in 1975. The experiment did produce the first results from which processes, their causes and effects, and their frequency of occurrence and persistence, could be appreciated and studied. The current meter data suggested that there is both tidal and sub-tidal energy on the North Carolina shelf and that the sub-tidal variability is strongly atmospherically and Gulf Stream influenced.

Atkinson, Pietrafesa, Dunstan (Skidaway Institute of Oceanography) and Paffenhofer (Skidaway Institute of Oceanography) conducted a more extensive and comprehensive field experiment in Onslow Bay during the period June thru September, 1976. The objectives of this second year (of funding) experiment included both the direct measurement of the along-shelf, cross-shelf and vertical structure of the "late Spring-Summer-early Fall" current, temperature, conductivity and pressure fields from fixed point, vertical moorings and a continuation of the hydrographic and biological sampling by SKIO personnel.

Additionally, Pietrafesa's Onslow Bay moorings have been maintained during the periods Dec., 1976 - April, 1977; July, 1977 - Dec., 1977 and Dec., 1977 - the present. During these periods, efforts have been co-ordinated in the Georgia Bight and Onslow Bay regions.

Results of the filed efforts, integrations of the physical, chemical and biological data and mathematical models of all data set types have also been accomplished.

'Twas brillig, and the slithy toves
Did gyre and gimble in the wabe:
All mimsy were the borogoves
And the mome raths outgrabe.

- Lewis Carroll -

TABLE OF CONTENTS

		Page
	Frontispiece	i
	List of Figures	v
	List of Tables	xii
I.	SUMMARY OF ACCOMPLISHMENTS	1
	APPLICATIONS TO THE DEPARTMENT OF ENERGY	5
II.	INTRODUCTION	6
	SCOPE OF REPORT	8
	OCEANIC AND ATMOSPHERIC SETTING	11
	The Gulf Stream Influence	11
	Background	11
	Continental Shelf Flushing by Gulf Stream and Wind	25
	Possible Downstream Effects of the Charleston Bump	45
	Hydrography of a Gulf Stream Spinoff Filament; 19-21 April, 1977	63
	Continental Margin Atmospheric Climatology and Coastal Sea Level	91
	Horizontal Wind Coherence	108
	Atmospheric Pressure Coherence	120
	Sea Level	129
III.	MEASUREMENT PROGRAM AND CO-ORDINATION	158
	EQUIPMENT AND MOORING DESCRIPTION	160
	Mooring Deployment and Recovery	170
	Deployment	170
	Recovery	171
	Calibration Techniques	172
	Speed	172

		Page
	Direction	173
	Pressure	174
	Temperature and Conductivity	174
	Data Processing	175
	Aanderaa Current Meters	175
IV.	DATA PRODUCTS	183
V.	PRELIMINARY PHYSICAL DYNAMICAL ANALYSIS	185
VI.	MODELS	246
	BIOLOGICAL MODELING	246
	Biological Processes	257
	Nitrate Uptake	257
	Extracellular Release by Phytoplankton	258
	Zooplankton Excretion	258
	Fish Excretion	259
	Decomposition of Particulate Matter	259
	Nitrogen Fixation by Blue-Greens	260
	Regeneration from Bottom Sediments	261
	Scale Analysis	261
	Examples of Results	262
	Conclusions	271
	BUOYANCY FLUX MODEL	275
	SHOHAT RENORMALIZATION TECHNIQUE	277
	DIAGNOSTIC AND PROGNOSTIC MODELS	283
	SHELF RESPONSE TO A MOVING STORM MODEL	284
VII.	MOMENTUM AND HEAT FLUX CALCULATIONS	286
VIII.	BIOLOGICAL FOULING	293
IX.	HURRICANE BELLE	294

	Page
X. PLANS AND OBJECTIVES	295
OBJECTIVES TO BE ADDRESSED: 1 MARCH, 1978 - 31 MAY, 1979	297
REFERENCES	300

LIST OF FIGURES

		Page
1.	Carolina Capes region, Onslow Bay	9
2.	Satellite imagery at 1315Z, April 8, 1977	19
3.	Satellite imagery at 0125Z, April 10, 1977	20
4.	Satellite imagery at 1421Z, April 11, 1977	21
5.	Satellite imagery at 1336Z, April 11, 1977	22
6.	Satellite imagery at 1405Z, April 13, 1977	23
7.	Satellite imagery at 1501Z, April 17, 1977	24
8.	Case Study of Bottom intrusion during period Aug. 9-24, 1975	28
8a.	Averaged vectors of wind stress and currents	29
9.	SK10/NCSU Onslow Bay/ocean/hydrographic grid	35
10.	Onslow Bay surface temperatures, September 3-13, 1975	37
11.	Onslow Bay bottom temperatures, September 3-13, 1975	38
12.	Onslow Bay vertical distribution of temperature, September 3-13, 1975	39
13.	Onslow Bay surface temperatures in July and August, 1975	41
14.	Onslow Bay bottom temperatures in July and August, 1975	42
15.	Onslow Bay vertical distribution of temperature, July 14-15, 1975	43
16.	Onslow Bay vertical distribution of temperature, August 4-6, 1975	44
17.	Topography of South Atlantic Bight showing feature known as "Charleston Bump"	47
18.	Several test cases of model	50
19.	Model of "Charleston Bump"	51
20.	Western edge of Gulf Stream on March 7, 1974	53
21.	Western edge of Gulf Stream on December 22, 1974	54
22.	Space-time history representative of the Gulf Stream front	57
23.	South Atlantic Bight average surface temperature, Jan.-Mar. (NODC)	59

24. South Atlantic Bight average temperature at 50 m, Jan.-Mar. (NODC) 60
25. South Atlantic Bight average temperature at 50 m, Jan.-Mar. (NODC) 61
26. Mooring locations 65
27. Surface temperature, April, 18-22, 1977 66
28. Surface salinity, April 18-22, 1977 67
29. Surface temperature, April 18-22, 1977 68
30. Surface salinity, April 18-22, 1977 69
31. Temperature profile, April 18-22, 1977 70
32. Temperature profile, April 18-22, 1977 71
33. Temperature profile, April 18-22, 1977 72
34. Temperature and salinity profile, site G, 7 July, 1977 73
35. T-S diagram, site G, 7 July, 1977 74
36. Temperature and salinity profile, site K, 7 July, 1977 75
37. T-S diagram, site K, 7 July, 1977 76
38. Temperature and salinity profile, site H, 7 July, 1977 77
39. T-S diagram, site H, 7 July, 1977 78
40. Temperature and salinity profile, site E, 7 July, 1977 79
41. T-S diagram, site E, 7 July, 1977 80
42. Temperature and salinity profile, site C, 7 July, 1977 81
43. T-S diagram, site C, 7 July, 1977 82
44. Temperature and salinity profile, site B, 7 July, 1977 83
45. T-S diagram, site B, 7 July, 1977 84
46. Temperature and salinity profile, site J, 7 July, 1977 85
47. T-S diagram, site J, 7 July, 1977 86
48. Temperature and salinity profile, site M, 8 July, 1977 87
49. T-S diagram, site M, 8 July, 1977 88
50. Surface temperature, 20 April, 1977 89

51. Surface temperature, 27 April, 1977 90

52. South Atlantic Bight 99

53. Energy response envelope of 40 hr. low pass filter 102

54. Meteorological data, Cape Hatteras, N.C., March-April 1974 104

55. Meteorological data, Wilmington, N.C., March-April 1974 105

56. Meteorological data, Charleston, S.C., March-April 1974 106

57. Meteorological data, Savannah, Ga., March-April 1974 107

58. Wind stress, March-April 1974 110

59. Wind stress, July-August 1974 111

60. Wind stress, September-October 1974 112

61. Wind stress, March-April 1975 113

62. Wind stress, July-August 1975 114

63. Wind stress, September-October 1975 115

64. HAT-WIL onshore wind coherence, April-July 1974 116

65. HAT-WIL alongshore wind coherence, April-July 1974 117

66. HAT-WIL onshore wind coherence, September-December 1974 118

67. HAT-WIL alongshore wind coherence, September-December 1974 119

68. HAT-WIL pressure coherence, September-December 1974 121

69. HAT-SAV pressure coherence, September-December 1974 122

70. CHS-SAV pressure coherence, September-December 1974 123

71. HAT-WIL pressure coherence, April-July 1974 124

72. WIL-CHS pressure coherence, April-July 1974 125

73. CHS-SAV pressure coherence, April-July 1974 126

74. HAT-CHS pressure coherence, April-July 1974 127

75. HAT-SAV pressure coherence, April-July 1974 128

76. CHS alongshore wind stress vs. CHS adjusted sea level, 1974 131

77. CHS alongshore wind stress vs. CHS adjusted sea level, Apr-Jul 1974 132

78. CHS offshore wind stress vs. CHS adjusted sea level, Apr-Jul 1974 133

79. CHS alongshore wind stress vs. CHS adjusted sea level, Sept-Dec 1974 134
80. CHS offshore wind stress vs. CHS adjusted sea level, Sept-Dec 1974 135
81. Meteorological data, Cape Hatteras, Jan-Feb 1974 138
82. Sea level data, Jan-Feb 1974 139
83. Wind stress, Jan-Feb 1974 141
84. Adjusted sea level, Mar-Apr 1974 142
85. Adjusted sea level, Sept-Oct 1974 143
86. Adjusted sea level, Nov-Dec 1974 144
87. BFT vs. CHS adjusted sea level coherence, Apr-Jul 1974 146
88. BFT vs. CHS adjusted sea level coherence, Sept-Dec 1974 147
89. FRY vs. BFT adjusted sea level coherence, Sept-Dec 1974 148
90. FRY vs. CHS adjusted sea level coherence, Sept-Dec 1974 149
91. HAT u vs. v wind stress coherence, Sept-Dec 1974 150
92. WIL u vs. v wind stress coherence, Sept-Dec 1974 151
93. CHS u vs. v wind stress coherence, Sept-Dec 1974 152
94. SAV u vs. v wind stress coherence, Sept-Dec 1974 153
95. Onslow Bay, North Carolina - study area 161
96. SKIO/NCSU hydrography/biological grid 162
97. Mooring site locations, Spring-Summer 1976 163
98. Vertical section of instrument depths 164
99. Mooring site locations for Fall-Winter 1976 165
100. Mooring site locations for Summer 1977 166
101. Fixed position current meter moorings 168
102. Sample Aanderaa calibration curves 176
103. Three hour low pass velocity components from A_{top} 187
104. Three hour low pass velocity components from B_{top} 188
105. Three hour low pass velocity components from C_{top} 189
106. Three hour low pass velocity components from C_{bot} 190

107. Three hour low pass velocity components from D_{top} 191
108. Three hour low pass velocity components from D_{bot} 192
109. Three hour low pass velocity components from E_{top} 193
110. Three hour low pass velocity components from E_{bot} 194
111. Three hour low pass velocity components from F_{bot} 195
112. Mean velocity for Summer 1976 197
113. Mean velocity for July 23-August 22, 1976 (top meters) 198
114. Progressive vector diagram A_{top} 199
115. Progressive vector diagram B_{top} 200
116. Progressive vector diagram C_{top} 201
117. Progressive vector diagram D_{top} 202
118. Progressive vector diagram E_{top} 203
119. Progressive vector diagram F_{bot} 204
120. Low pass current from C_{top} 205
121. Low pass current from C_{bot} 206
122. Histogram from C_{top} 207
123. Histogram from C_{bot} 208
124. Histogram from D_{top} 209
125. Histogram from D_{bot} 210
126. Histogram from E_{top} 211
127. Histogram from E_{bot} 212
128. Histogram from F_{top} 213
129. Kinetic energy density spectra u component C_{top} 215
130. Kinetic energy density spectra v component C_{top} 216
131. Kinetic energy density spectra u component C_{bot} 217
132. Kinetic energy density spectra v component C_{bot} 218
133. Principle axes and RMS velocity at moorings A-F 219

134. Rotary spectrum: clockwise C_{top} 221
135. Rotary spectrum: anticlockwise, C_{top} 222
136. Hodograph parameters from C_{top} 224
137. Tidal ellipses for Summer 1976 227
138. Tidal ellipses for July 23-August 22, 1976 (top meters) 228
139. Energy fraction vs. frequency C_{top} - total current 235
140. Energy fraction vs. frequency C_{top} - offshore current 236
141. Energy fraction vs. frequency C_{top} - alongshore current 237
142. Energy fraction vs. frequency C_{bot} - total current 238
143. Energy fraction vs. frequency C_{bot} - offshore current 239
144. Energy fraction vs. frequency C_{bot} - alongshore current 240
145. Offshore current coherence, D_{bot} vs. D_{top} 243
146. Alongshore current coherence, D_{bot} vs. D_{top} 244
147. Bottom profiles 252
148. Streamline contours - day one 255
149. Streamline contours - day five 255
150. Streamline contours - day one 256
151. Streamline contours - day five 256
152. Nitrate profiles - day one 263
153. Nitrate profiles - day four 263
154. Nitrate profiles - day one 264
155. Nitrate profiles - day four 264
156. Nitrate profile in Onslow Bay, July 14-15, 1976 266
157. Nitrate profile in Onslow Bay, August 14-15, 1976 266
158. Nitrate profiles - day one 267
159. Nitrate profiles - day four 267
160. Nitrate profiles - day one 269
161. Nitrate profiles - day four 269

162. Nitrate profiles - day one 270

163. Nitrate profiles - day four 270

164. Nitrate profiles - day one 272

165. Nitrate profiles - day four 272

166. Nitrate profiles - day one 273

167. Nitrate profiles - day four 273

168. Case 18 u velocity profile 278

169. Case 18 v velocity profile 279

170. Case 18 temperature profile 280

171. Horizontal momentum correlation variance E_{top}, Summer 1976 288

172. Heat correlation variance in the x-direction for E_{top}, Summer 1976 289

173. Heat correlation variance in the y-direction for E_{top}, Summer 1976 290

174. Spectra for temperature and u velocity from E_{top} 291

175. Cospectra of temperature vs. u velocity for E_{top} 292

LIST OF TABLES

		Page
1.	Data summary from moored instrumentations in Onslow Bay	27
2.	Cruise Information	36
3.	Hypsometric data for Onslow Bay, N. C.	36
4.	Meteorological stations	92
5.	Sea level stations	92
6.	Instrument moorings and element locations	169
7.	Data particulars	178
8.	First order statistics - "alongshore" rotation (56°)	179
9.	First order statistics - principle axis rotation	180
10.	Tidal constituents in Onslow Bay observed during the summer of 1976	230
11.	Buoyancy flux model parameters	281

I. SUMMARY OF ACCOMPLISHMENTS

During the period from 1 June, 1975 to date, our study of the continental shelf processes affecting the oceanography of the South Atlantic Bight has been principally involved with a substantial, co-ordinated field effort. The success of the data acquisition phase of the program has now required an intensive data analysis phase which has been slowing increasing in effort.

The present year is the third of Department of Energy funding for studies of continental shelf processes affecting the oceanography of the South Atlantic Bight. The main phase of the field program, located in Onslow Bay, has been completed and the data are being analyzed and written up for publication. The Onslow Bay and Carolina Capes have yielded several manuscripts for publication to date but our main efforts during the past 2½ years have been devoted to data acquisition, filtering, reduction and initial presentation. We have now reached the analyses and publication phase of our extensive field efforts to date. Additionally, during the next proposed year of funding we will be planning our large scale experiments which are scheduled to occur in 1979 and 1981.

During our first three years of AEC, ERDA, DOE support, we have made 20 cruises into the Carolina Capes part of the South Atlantic Bight and have contributed, with personnel assistance from NCSU provided, to several Skidaway Institute of Oceanography (SKIO) and University of Miami (UM) cruises. Six papers are presently either in press or in submission to journals, five data reports which include preliminary discussion of

data are available and nine papers have been delivered at national conferences; presenting the partial results of our work to date.

The preliminary accomplishments of our research efforts to date are as follows:

Tidal Effects - The tides in the SAB tend to be predominantly semi-diurnal, increase in amplitude from Cape Hatteras to function of location, Savannah, propagate as a Poincare Wave, contain 40% - 55% of the total, as a 18% of the alongshore and 65% of the on-shore variances of the currents, (at site C) respectively, are topographically steered and are very stable.

Gulf Stream Meandering/Intrusion, Incursion Events - The Gulf Stream derived events which peretrate onto the continental shelf in the vicinity of an in Onslow Bay represent a major source of the fraction of energy inputed into this system. These intrusion events also are the major source of nutrients supplied to Onslow Bay and displace 11 to 36% of the volume of Onslow Bay during their occurrence. They occur at a periodicity of four to twelve days and impart in varying degrees vertical and horizontal dynamical stability to the water column in their life history.

Onslow Bay Flushing - Gulf Stream spawned and wind driven events which flush the Bay waters have been identified, qualitatively described and quantitatively defined. The flushing rate is estimated to be of the order of 2-3 months for Onslow Bay.

Eddy Incursion Event in the Carolina Capes - During the period 18-22 April, 1977 in the shelf waters of upper Long and Onslow Bays, the hydrography of a Gulf Stream spin-off filament was sighted and mapped by NCSU and observed in satellite imagery; comparisons of the satellite and ocean station data have been made.

Effects of the Charleston "Bump" - The downstream effects of the topographic feature known as the Charleston "Bump" have been observed as meanders of the Gulf Stream Front in the region of the Carolina Capes; the results of a mathematical model (Pietrafesa and Janowitz) for topographic Rossby Waves generated by the "bump" have been compared, quite favorably to NOAA/NESS satellite imagery. This feature may be part of the reason for the meandering, eddy-shedding processes undergone by the Gulf Stream.

Nutrient Modeling - A time-dependent, vertical plane numerical model of the distribution of nutrients on the South Atlantic Bight during an intrusion event has been developed and favorably compared to data (Hofmann and Pietrafesa).

Coastal, Atmospheric Climatology - Coastal winds and pressure have been statistically analyzed and described in space and time.

Coastal Sea Level - Tide gage data has been statistically analyzed and described in space and time.

Meteorology/Sea Level - Intercomparisons have been made between sea level and meteorological input for years 1974 and 1975 and during the Onslow Bay studies. Cross-spectral analyses of the two indicate that sea level responds to atmospheric pressure and wind over discrete frequency bands and that Ekman convergences and divergences, direct response to traveling met systems as well as the possible generation of long waves which are observed to propagate north, north of Frying Pan shoals.

Topographic Effects - The effects of the cuspate topography in Onslow Bay has been shown to steer the principal axes of low frequency motion as well as the tidal ellipses. The shoals are shown to act as both source and sink to Onslow Bay, at either end.

Flux of Heat - Calculations derived from a turbulence approach to the data and consideration of co-spectra between cross-analyses of current and temperature indicate fluxes of heat on at the top, heat off at the bottom in the mid-to central shelf break portion of Onslow Bay over event periods the order of 4-10 days. These fluxes of heat, and preliminary fluxes of mass calculations describe the frequency and nature of wind induced and Gulf Stream spawned events in both qualitative and quantitative ways.

Flux of Momentum - Calculations of Reynolds' stresses have been accomplished and indicate large fluxes of momentum along and across the shelf break during wind induced and Gulf Stream spawned events.

Hurricane Belle - Our moored arrays of current, temperature, pressure and salinity sensors detected the passage of this event in August, 1976 and characterized the dramatic shelf response: currents the order of 50-90 cm/sec in the interior and 20-70 cm/sec 3 m. above the bottom; temperature changes the order of 2-9°C over a several day period.

Wind effects - The relationship of currents to winds indicates that the shallow, inner shelf of Onslow Bay is strongly wind influenced while the mid-shelf region tends to be a region of Gulf Stream and wind influence and the outer shelf shows good correlations to the wind at selective frequencies and though this region tends to be principally Gulf Stream influenced, there seem to be relationships between wind intensity and direction and Gulf Stream Front location. Offshore winds seem to tweak the GSF offshore, in the central, shelf break region of Onslow Bay resulting in reduced alongshore currents to the north and decreases in local temperature; the opposite wind field results in opposite effects in u, v and T.

A mathematical model of the effects of the atmospheric seasonal heating/cooling/etc. cycle on the circulation of a baroclinic continental shelf, indicates that surface buoyancy fluxes may be responsible for much of the low frequency variability of currents as well as the structure of the temperature and salinity fields. The effects of mechanical wind forcing are also included in the model and can either enhance, modify or dominate the buoyancy driven modes of circulation and hydrography. (Pietrafesa and Janowitz)

Northward propagating wave like events appear in the current meter data at 3-3½ day periods and are supported by a northward propagation of sea level over the same period band.

During the summer period, Onslow Bay is physically and dynamically banded both across the shelf and along the shelf. The inner region is very strongly wind influenced, though wind events are obvious in the current fields. The mid shelf region contains a complex mixture of atmospheric and Gulf Stream induced currents. The inner, northerly shelf corner of the Bay tends to have a predominantly barotropic character while the inner southwesterly corner displays both barotropic and baroclinic modes of response.

Intrusions of Gulf Stream water, which occur during the summer months, are typically advected shoreward in the southerly portion of the bay, due to the forcing of the predominantly southwesterly winds, subsequently either surface and are driven northeasterly across the Bay, seaward or rotate clockwise, more northerly towards the inner northern extent of the Bay and become either stranded and decay through mixing processes, or leak out south and east of the Cape Lookout Shoals, all as a function of the magnitude and direction of the wind.

Diagnostic and Prognostic Models - Hydrographic and current data are being used to develope both diagnostic and prognostic models to both aid in our understanding of the processes and to direct our efforts towards a predictive capability.

APPLICATIONS TO THE DEPARTMENT OF ENERGY

The coastal zone area of the South Atlantic Bight is presently undergoing a dramatic increase in energy related activities. Oil exploration is presently active, with preliminary indications suggesting that the SAB may contain major oil reserves. Additionally, offshore nuclear power plants which could use the up-welled cold waters, derived from the Gulf Stream, as an energy source and the ambient coastal waters as thermal coolants may be a future reality. Additionally, rivers and estuaries are discharging, industrial, agricultural and human wastes into the coastal zone from the lateral side and the atmosphere is dumping wind borne pollutants into the oceanic environment from above. The environmental implications of these activities is not yet known since we are presently trying to understand the environment itself.

Energy related activities such as offshore oil production, OTEC power plants, offshore nuclear power plants and coastal based energy production, each present a possible source of contaminant introduction to the shelf waters. We are beginning to identify the mechanisms for contaminant transport and the natural processes for maintaining safe and biologically conducive water quality standards. This information will eventually lead to a better predictive capability of shelf water motions so that possible effects of environmental degradation can be minimized.

II. INTRODUCTION

The southeast U.S. continental margin region extending from Cape Hatteras to Cape Canaveral (termed the South Atlantic Bight, S.A.B., by Bumpus, 1973) after years of relative academic and industrial neglect has recently become a focal point of energy-related activities. Oil exploration is presently underway and present expectations are for a major oil reserve te be discovered in the near future. Offshore thermal power plants which will utilize the up-lifted cold water energy source of the Gulf Stream to transmit electricity to east coast metropolitan areas are being considered as a viable form of solar energy. Offshore nuclear power plants may someday be a reality. In addition a number of rivers are discharging industrial by-products into the coastal zone. The environmental impacts of these activities are presently unknown. The guiding scientific objective of the study described in this report is to imporve the capability for prediction of the physical environment on the SAB continental shelf; the principal scientific task is to determine the relative importance of driving mechanisms and to measure the shelf response on seasonal time and space scales. This work is part of a larger coordinated multi-University, interdisciplinary investigation aimed at understanding the physical, chemical and biological processes of the SAB.

The collective experience obtained from direct observations on continental shelves has exposed a number of important generalizations about the forces that may be responsible for driving or damping shelf circulation and the nature of the shelf response to these forces. These observations have been carried out in many specific locations; but due to a lack of coordination and focus, they have precluded a general, coherent development

of the dynamics of entire geographical shelf areas. Indeed, we have discovered that wind, tidal, and offshore forces, such as those imposed by the Gulf Stream, may be responsible for driving shelf circulation; however, as a corollary, we also have learned that to understand the specific nature of each force and to weigh the relative importance of each is not possible without viewing large sections of the shelf as a hydrodynamic continuum.

Shelf regimes have been categorized historically by the character of their seasonal hydrographic persistence because there has been a lack of direct measurements of circulation. We are conducting a study to provide the direct observations of the nature of the driving and the magnitude of the circulation in the South Atlantic Bight shelf regime; i.e., we are attempting to measure the relative influence of the offshore current and meteorological forces in maintaining the large-scale shelf circulation.

Given the above it is deemed essential to develop an understanding of biological/chemical/physical functioning of the nearshore and continental shelf regimes and as nearly as possible to quantify general circulation patterns that control biological production and the dispersal of pollutants, whatever their source.

The marine environment of the SAB is subject to changes which take place in time scales ranging from minutes to decades. Life processes in the S.A.B. continental shelf are largely controlled by water circulation which produce dramatic changes on scales of days to years. Without an understanding of the coupling of circulation and biological production, the magnitude of these influences and where they occur, little in the way of predictive capability or establishing cause and effect relationships can be achieved.

The DOE sponsored Southeast Continental Shelf Program was developed in an orderly, sequential manner and is aimed at gaining an understanding of natural processes which control biological activity and the dispersal of selected potential pollutants. Over the long run, with such knowledge, it should be possible to separate and explain natural changes from those which may be induced by man's activities in the coastal-continental shelf environment. The basic philosophy of DOE and the principals involved in this study is that effective management decisions are ultimately based on obtaining predictive capability and to achieve this an understanding of ecosystem function is required.

SCOPE OF REPORT

This Progress Report covers all research conducted under U.S. Department of Energy (Formerly U.S. Energy Research and Development Administration, U.S. Atomic Energy Commission) Contract No. E(38-1)-902, by personnel at North Carolina State University under the direction of Dr. Leonard J. Pietrafesa (Principal Investigator), Associate Professor of Oceanography (at N.C.S.U.), during the period 1 June, 1975 through the present, 1 March, 1978.

The report covers the research investigations of continental shelf processes which affect the oceanography in the Carolina Capes region, specifically Onslow Bay, (cf. Figure 1) of the South Atlantic Blight, which were accomplished by Dr. L.J. Pietrafesa (N.C.S.U.) as a part of a multi-disciplinary, multi-institutional effort (the South East Continental Shelf Program).

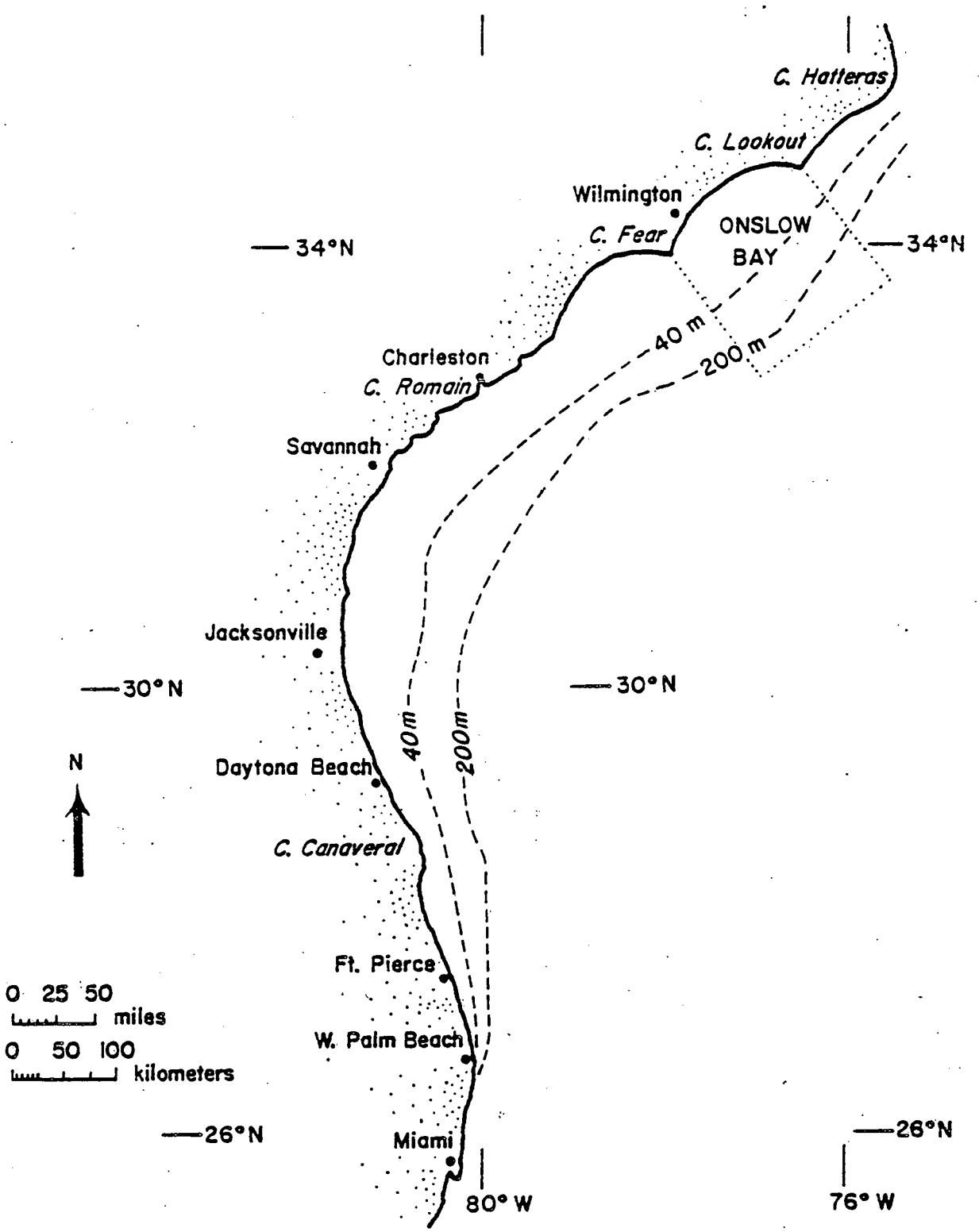

Figure 1. South Atlantic Bight

The initial phase of this study began in August, 1975 wherein Dr. L.P. Atkinson (Skidaway Institute of Oceanography) and Dr. L.J. Pietrafesa (N.C.S.U.) conducted the first hydrographic and biological survey and deployed moored current meters in Onslow Bay, North Carolina. Subsequent cruises involved integrated, co-ordinated biological, chemical and hydrographic sampling and mooring recoveries and redeployments involving additional N.C.S.U. and SKIO personnel (Drs. H. Windom, W. Dunstan and G. Paffenhofer). During the winter, 1977 the University of Miami began moored meter work in the Georgia Bight and the SKIO emphasis shifted to that region while the N.C.S.U. emphasis continued in the Carolina Capes region. This co-ordinated, integrated experiment and those which have followed, to date, are now yielding the extensive temporal and spatial ranges and domains of data which were deemed necessary to fully study the continental shelf processes affecting the oceanography of the whole of the South Atlantic Bight.

Gulf Stream Influence

Background

The influence of the western boundary current, the Gulf Stream, which persists generally along the seaward edge of the continental margin between Capes Hatteras and Canaveral, upon the continental shelf between these end points, may be considerable in terms of physical, chemical and biological aspects of the oceanography of the South Atlantic Bight. Our (NCSU, SKIO and UM) studies have yielded much valuable information to date and may, in fact, be of essential importance in the more complete understanding of the dynamics and influence of the Gulf Stream, which to date, has been lacking in terms of being spatial and temporal synoptic. The DOE sponsored studies have been the most synoptic, complete studies of the Gulf Stream influence, to date. It is of reiterative note (Niiler, 1975; Pietrafesa, 1976; Lee, 1977) here to review some of our understanding of the Gulf Stream influence, and then to procede in an overview analysis of how our (NCSU) present studies have served to either reinforce, modify, re-explain or describe anew the phenomonology of the Gulf Stream influence on the shelf waters of the South Atlantic Bight.

A "Multiple Ship Survey" of 1950, reported on by Fuglister and Worthington (1951), was the first large scale, multi-vessel study of Gulf Stream fluctuations. The name "meanders" was introduced for the slow undulations observed in the location and structure of the Gulf Stream downstream of Cape Hatteras.

It is of historical note herein to point out that Abbe (1895) presented the following description of the eddy phenomonology in relationship to the formation and maintainance of the cuspate shape of the three Carolina Capes:

> The Gulf Stream produces an eddy current which washes the coast southwardly, and the sand bars, so common on the coast, are formed in the diagonal or resultant of these two currents. Those formed at the mouth of rivers must also, it seems to me, be influenced by the force and direction of their waters. These bars, however, are generally formed directly by the ocean, and not by the waters of the rivers.
>
> A satisfactory hypothesis must then account for the southwestward intention of the cuspate capes, the evidence of inflow at the hook, and the tendency of the capes to travel southwestward.
>
> It is therefore suggested that a set of back-set eddies is here produced by the northeastward-flowing Gulf Stream, and that these eddies, aided by waves from the prevailingly northeast and southeast storms of this area, have produced the cuspate capes which we have studied. The currents of the back-set eddies setting from northeast to southwest would serve to determine the general trend of movement and of cutting, and would also explain the cross currents that formed the hooked-spit of Cape Lookout.
>
> As to the actual existence of such a set of eddies on this portion of the coast, though not rigidly proved, we may with some show of reason infer that they exist. For on other parts of our own coast and on foreign coasts, such as along the south coast of Alaska, and on the northern coast of the Isthmus of Panama, we find such eddies set up by the great ocean currents.
>
> Our assumption, then, of a set of back-eddies is not a violent one, and it seems to suit our needs better than previous explanations.

The existence of these Gulf Stream events had thus not gone undetected even before the oceanographic multiship survey and or satellite imagery.

Several studies provide evidence for eddying, entrainment, and intrusion of Gulf Stream and shelf waters. Von Arx, Bumpus, and Richardson (1955) found northeasterly oriented filaments of Gulf Stream water along the shelf break with dimensions of ten kilometers to one hundred kilometers. These "shingles" or "sausages" could be mapped by the filaments in the thermal, velocity, and water type properties of the surface; the subsurface isothermal slopes, or patterns, remained unknown at that time.

During a 28-day study in May and June, 1958, Webster (1961a) made 120 consecutive crossings of the Gulf Stream axis off Onslow Bay, North Carolina. Measurements of surface velocity and salinity were made, and bathythermograph temperatures were taken half-hourly to a depth of 200 m. Webster found that the axis of the current meandered laterally, with a peak displacement of about 10 km. He found a strong correlation between the axis offshore distance and the alongshore surface atmospheric pressure gradient, when the latter was lagged about four days. The alongshore pressure gradient was presumed to be representative of the offshore geostrophic wind component over Onslow Bay. Correlation with the pressure gradient perpendicular to the current axis was not found. The dominant period of the axis meanders was about seven days; Webster estimated the alongstream meander scale to be about 100 km. Webster thus noted a strong apparent correlation with the onshore-offshore wind component, but he estimated the wind effect to be one or two orders of magnitude too weak to be the source of energy for the meanders. Three regions of local mechanical energy transfer between eddies and the mean motion can be noted. Webster (1961b) thus demonstrated

that fluctuations on the 1-day to 1-week time scale were locally deriving mechanical energy from shear of the mean current on the surface at the shelf break. In the cyclonic shear zone, both the eddies and the mean flow were losing mechanical energy. On the anticyclonic side, the eddies were driving the mean flow. On the cross-stream average from Miami to Onslow Bay, he found a net flux to the mean Gulf Stream which could rapidly double the average surface speed of the Florida Current. Such an acceleration is not observed; work of opposite sign is done by the pressure gradients near the surface. Recently, Sturges (1974) has made estimates of the mean downstream pressure gradient from coastal sea levels along the South Atlantic Bight and the Florida Straits; and he has found it to be large enough to provide the energy flux, at least at the shelf break, to balance the work done on the eddies. Following Webster's analysis, Oort (1964), using the thermal flux data corresponding to Webster's momentum flux data, found a counter-gradient heat flux in the surface layer which would sharpen the surface front. He also raised the question of a lower layer source for heat flux and intense potential energy release. Blanton (1971) combined a few short current meter records at the shelf break with hydrographic sections and interpreted the results two-dimensionally. He found near-bottom intrusions of Gulf Stream water, which had been suggested by Bumpus (1954), followed by vertical mixing with shelf waters and subsequent offshore flow of near-surface shelf water, which would give a counter-gradient heat flux near the surface. Schmitz and Niiler (1969) analyzed a new data set, i.e.,

dropsonde data, in an analogous fashion. They concluded that there existed negligible net transfer of kinetic energy between the eddies and the mean motion in the surface layer on the cross-stream average; instead, and internal redistribution of kinetic energy was occurring, as described above. Schmitz (1969) concluded that the interior of the Florida Current off Miami was essentially in inertial balance; Niiler (1975) found that the inertial balance is slowly eroded along the shelf break, and there is a vorticity flux into the Gulf Stream from the shelf.

Hansen (1970) traced the position of the Gulf Stream thermal front off North Carolina for twelve consecutive months in 1965 and 1966. He summarized the observed meanders as wave patterns of 200 to 400 km wave-length moving eastward with speeds of about 10 cm/sec.

Several theoretical accounts have been attempted for the meandering, eddying motion of the Florida Current/continental shelf system. Niiler and Mysak (1971) considered subinertial waves in a barotropic Gulf Stream with horizontal shear and variable cross-stream bottom topography; i.e., a model with potential vorticity gradients commensurate with the magnitude and form of the depth-integrated Florida Current was examined. They concluded that long waves could propagate north and south on the sheared current and that short waves could propagate northward and were unstable. The most unstable waves had a period of about 10 days and wave lengths of 150 kilometers in the vicinity of the Blake Plateau (South Atlantic Bight). Orlanski (1969) considered a model with two "active" layers and bottom topography and found baroclinic

instabilities to be possible for the parametric range observed in the South Atlantic Bight. The most unstable waves had a period of about 10 days and wave lengths of about 220 kilometers. Orlanski also noted the need for observations through the water column to determine the various energy exchanges. Orlanski and Cox (1973) carried out analogous calculations for a continuously stratified system, with similar results. Additionally, finite-amplitude effects reduced the growth rate; maximum amplitudes were reached in about one week.

Recent studies of the Florida Current provide some further consideration. Richardson, Schmitz, and Niiler (1969) show mean velocity sections for the Florida Current, two of which are located off the South Atlantic Bight. The mean Florida Current extends over the relatively shallow shelf break (50 to 100 meters deep); the bulk of the Florida Current lies over a deep shelf (~800 meters deep). Surface velocities up to 100 cm sec^{-1} occur over the shelf break. From 1/3 to 1/2 of the total volume transport occurs in the upper 200 meters of the water column; thus, the outer shelf spans much of the Florida Current. Schmitz and Richardson (1968) found that the transport fluctuations were $\pm 1/3$ of the mean transport, 75% of the transport fluctuations were tidal, and no more than 10% occurred at periods greater than one day. Niiler and Richardson (1973) made a more precise estimate of the seasonal variation, finding a prominent maximum in summer (June). They concluded that the seasonal variations accounted for 45% of the transport variance.

Recently, De Szoeke (1975) found a bottom slope-induced hybrid instability which arises from an interaction between a topographically trapped baroclinic wave and a "thermal" baroclinic Rossby wave. De Szoeke states that the hybrid instability is not "fundamental in nature," but rather serves to redistribute the energy from the classical baroclinic energy source (cf. Pedlosky, 1964). De Szoeke's application of the hybrid mechanism to the Florida Current neglected the importance of horizontal velocity shear to the overall vorticity dynamics.

Saltzman and Tang (1975) used an analytical model to demonstrate how second-order, nongeostrophic effects can modify a two-layer baroclinic wave system that grows exponentially from a small perturbation in a uniform zonal ocean current. It is shown that many of the asymmetric features characteristic of meandering ocean currents develop, including fronts and cutoff cyclonic cold pools to the south and anticyclonic warm pools to the north of the axis of the mean current. The implication is that all of these features can be viewed as being the simultaneous consequence of baroclinic instability of a broader, more unifrom current that might tend to be forced externally by the wind stress thermohaline processes.

The Very-High-Resolution Radiometer on the NOAA-2 (National Oceanic and Atmospheric Administration) satellite has recently obtained imagery in the visible channel over a major portion of the coastal waters off the eastern seaboard of the United States. Strong and DeRycke (1973) indicated an abrupt change in surface roughness

at the shoreward edge of the Gulf Stream Current from Florida to Cape Hatteras that could result from the opposition of waves propagating against the flow of the Gulf Stream. Herein, DeRycke, Rao (1973) pointed out an apparent relationship between the occurrence of eddies along the western side of the Gulf Stream and strong westerly winds.

Mysak and Hamon (1969) found evidence for a nonbarometric response of sea level from the North Carolina coast, especially at periods of 3 to 10 days. The phase relations were consistent with southward propagation of barotropic continental shelf waves, with seasonal modulation of the phase speed due to seasonal variations of the Florida Current. They also noted a broad peak in the sea level spectra centered on a period of about 15 days.

Satellite images (Legeckis, 1975; Stumpf and Rao, 1975) suggest that the eddies evolve from growing instabilities (Florida Current meander), which may initially be wind induced. They manifest themselves as warm, southward-oriented, tongue-like extrusions of Florida Current water onto the shelf, similar to the shingle structure observed by Von Arx, Bumpus and Richardson (1955). In the Florida Straits they are confined by the narrow shelf coastal boundary and observed diameters range from 10 to 30 km. Eddy vertical extent is approximately 200m. Lee (1975) concludes that spin-off eddies are a dominant mechanism for shelf water mass exchange off southeast Florida and estimates the shelf residence time as 1 week due to eddy water renewal. Singer, et. al. (1977) and Blanton and Pietrafesa (1978) have essentially concluded that the similar flushing mechanism is at work throughout the whole of the South Atlantic Bight. Satellite imagery (Figures 2 thru 7)

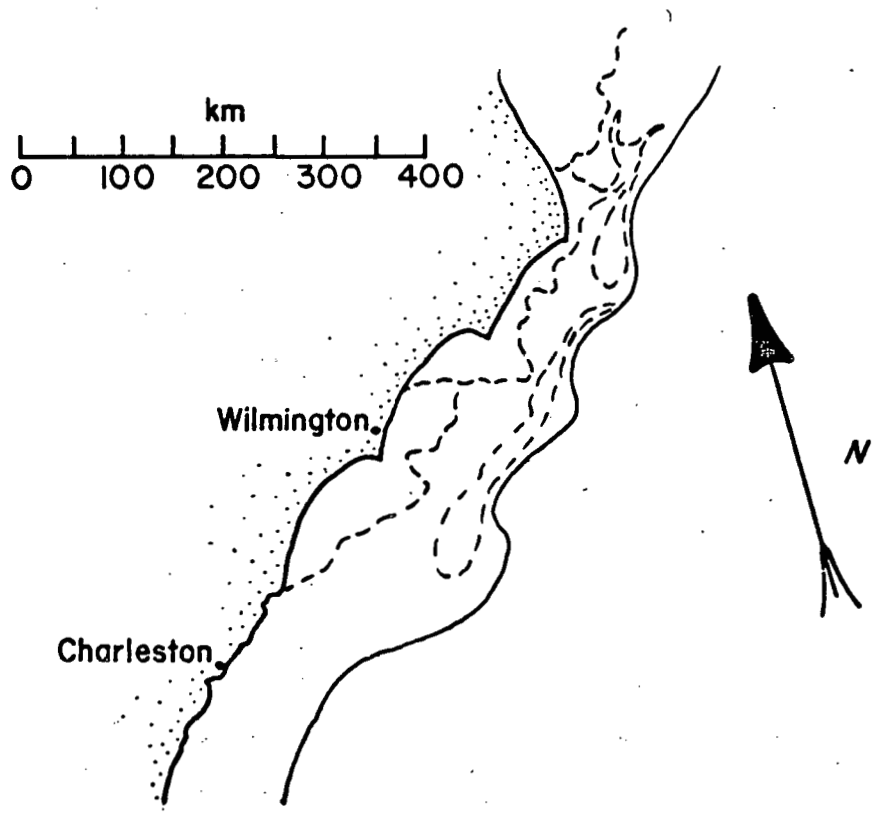

Figure 2. Satellite imagery at 1351Z, April 8, 1977 (solid line is GSF)

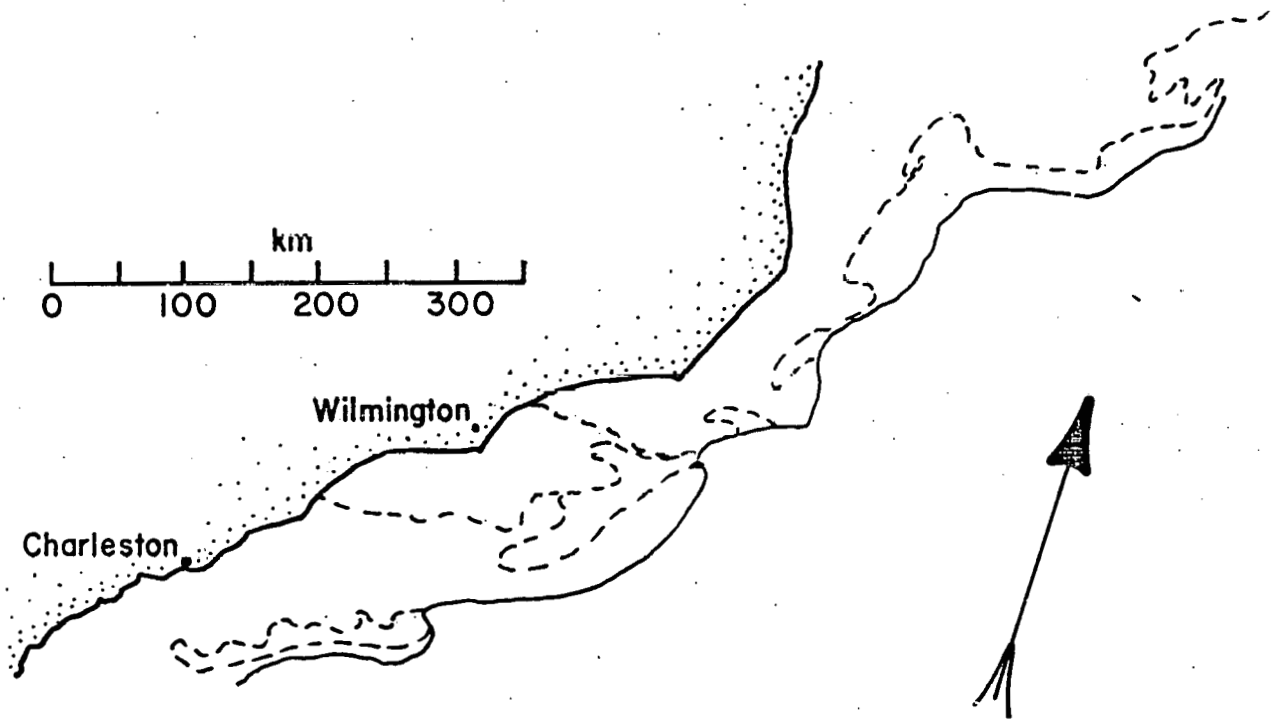

Figure 3. Satellite imagery at 0125Z, April 10, 1977 (solid line is GSF)

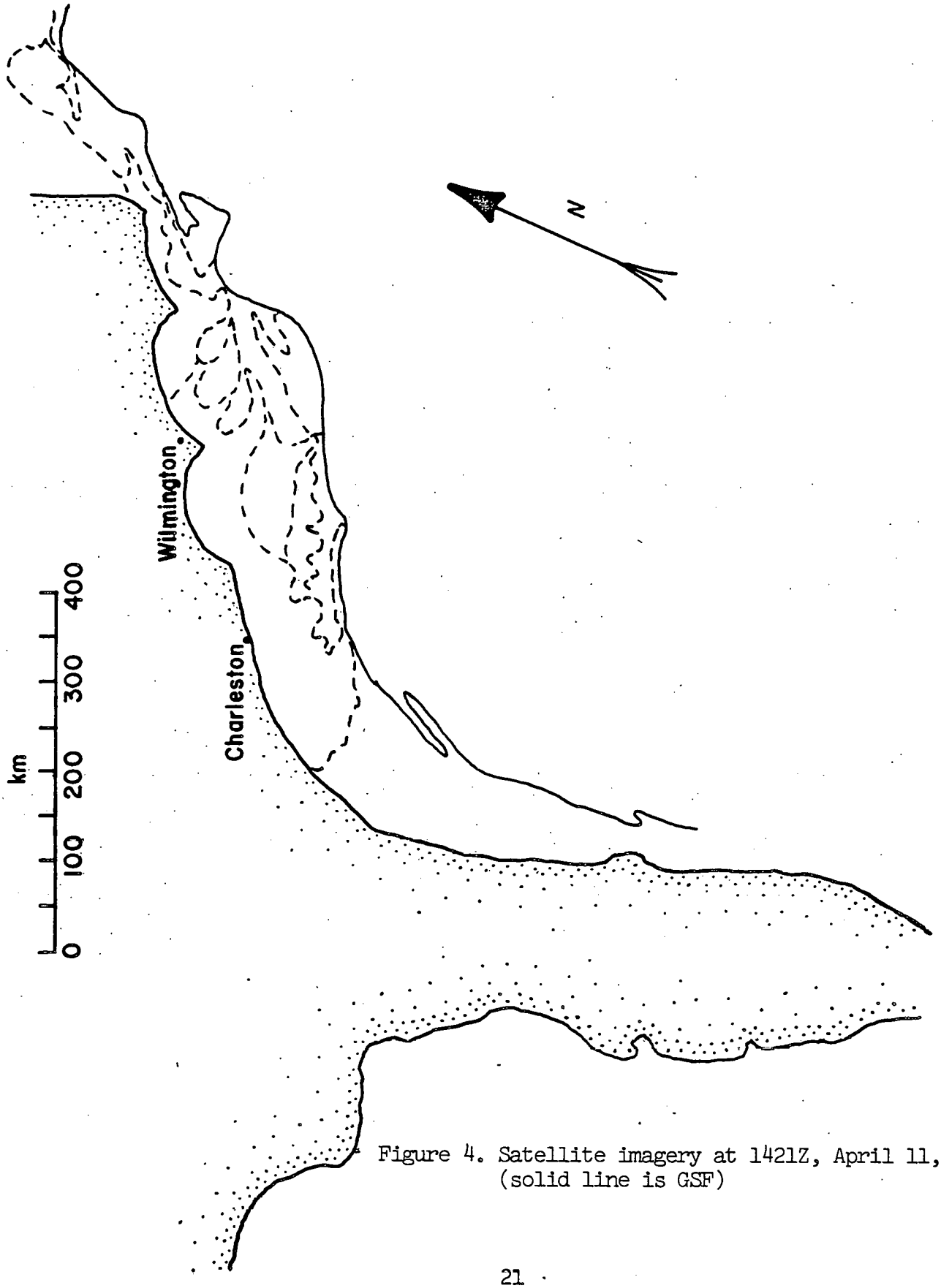

Figure 4. Satellite imagery at 1421Z, April 11, 1977
(solid line is GSF)

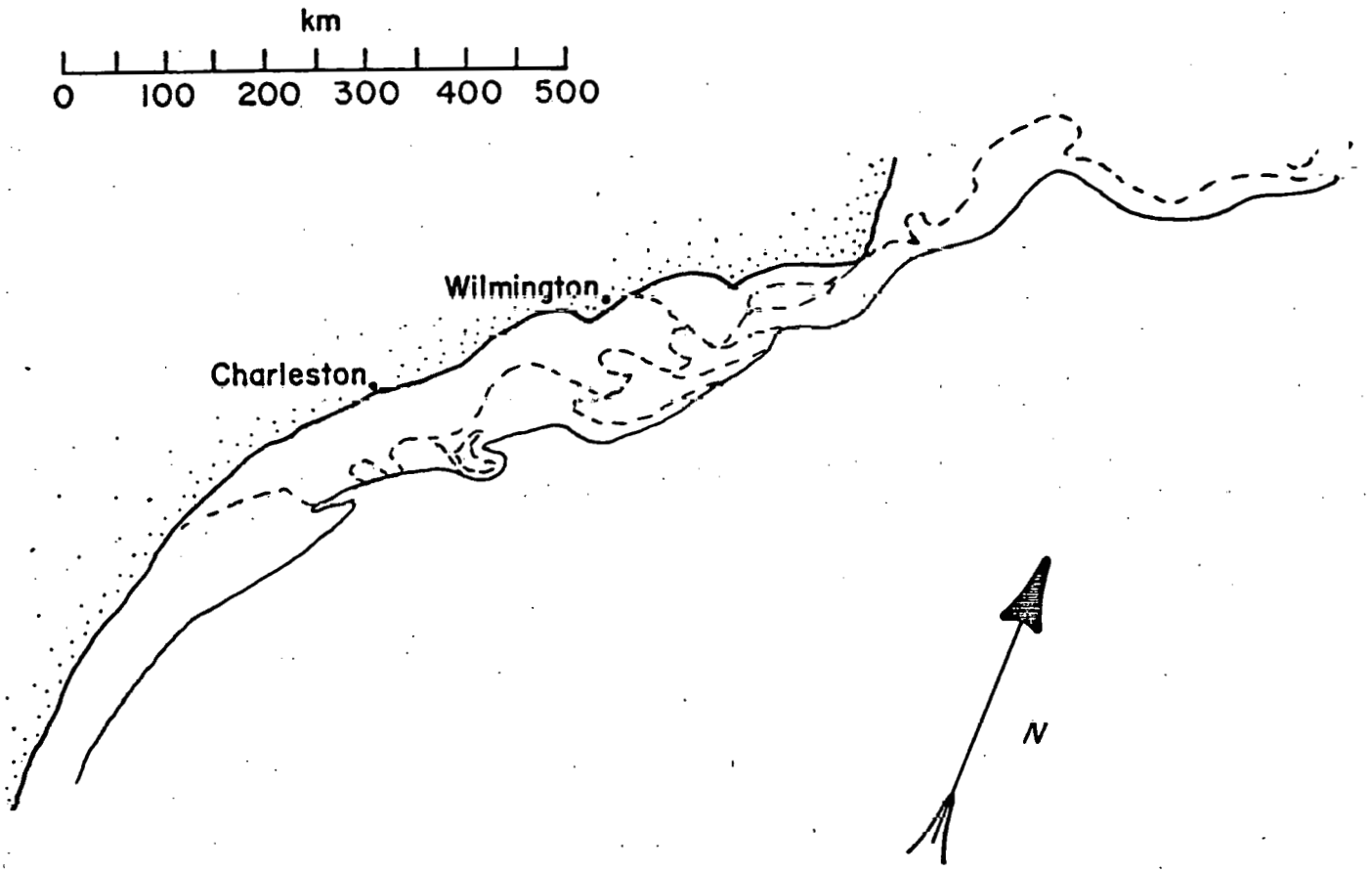

Figure 5. Satellite imagery at 1336Z, April 11, 1977 (solid line is GSF)

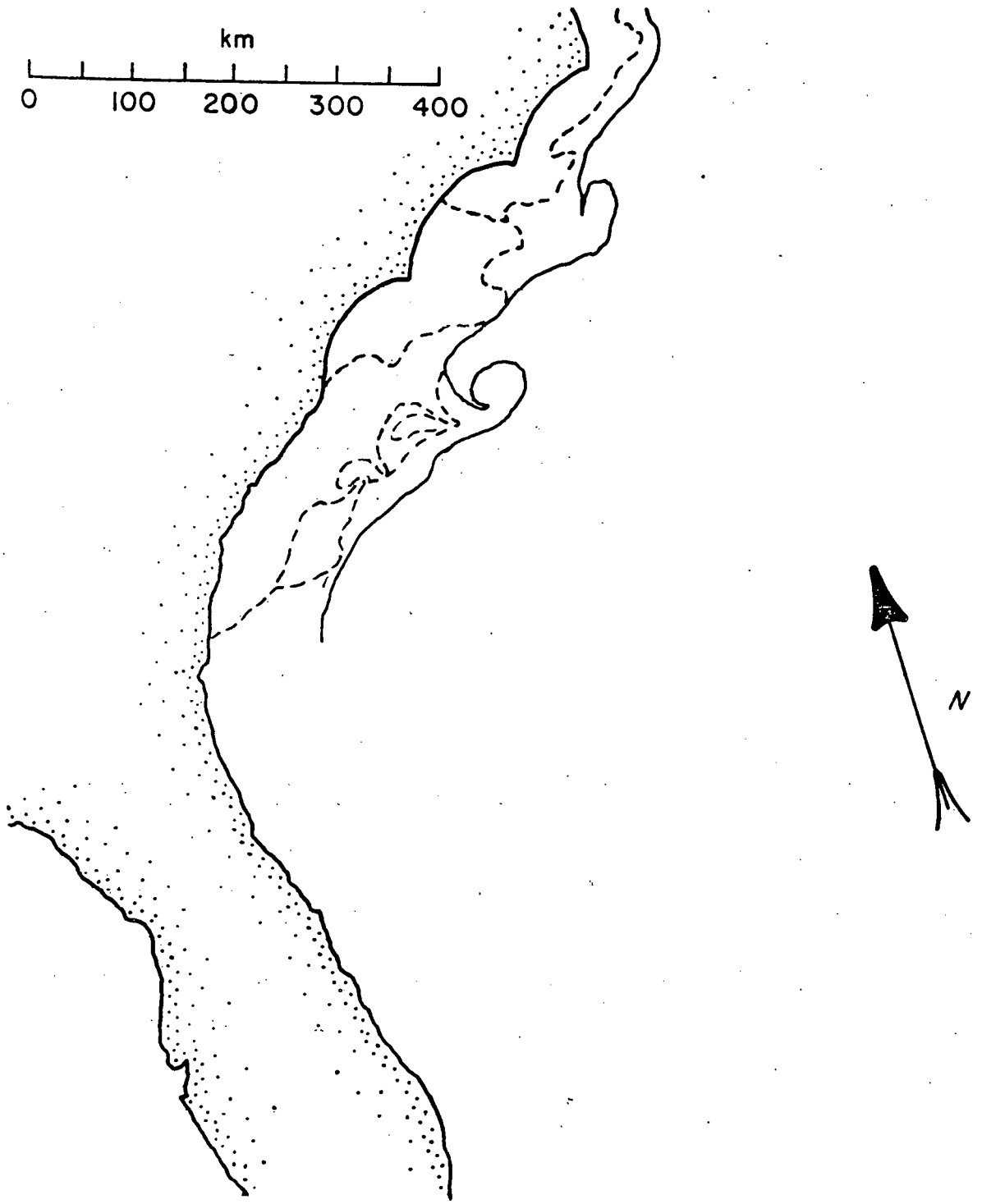

Figure 6. Satellite imagery at 1405Z, April 13, 1977 (solid line is GSF)

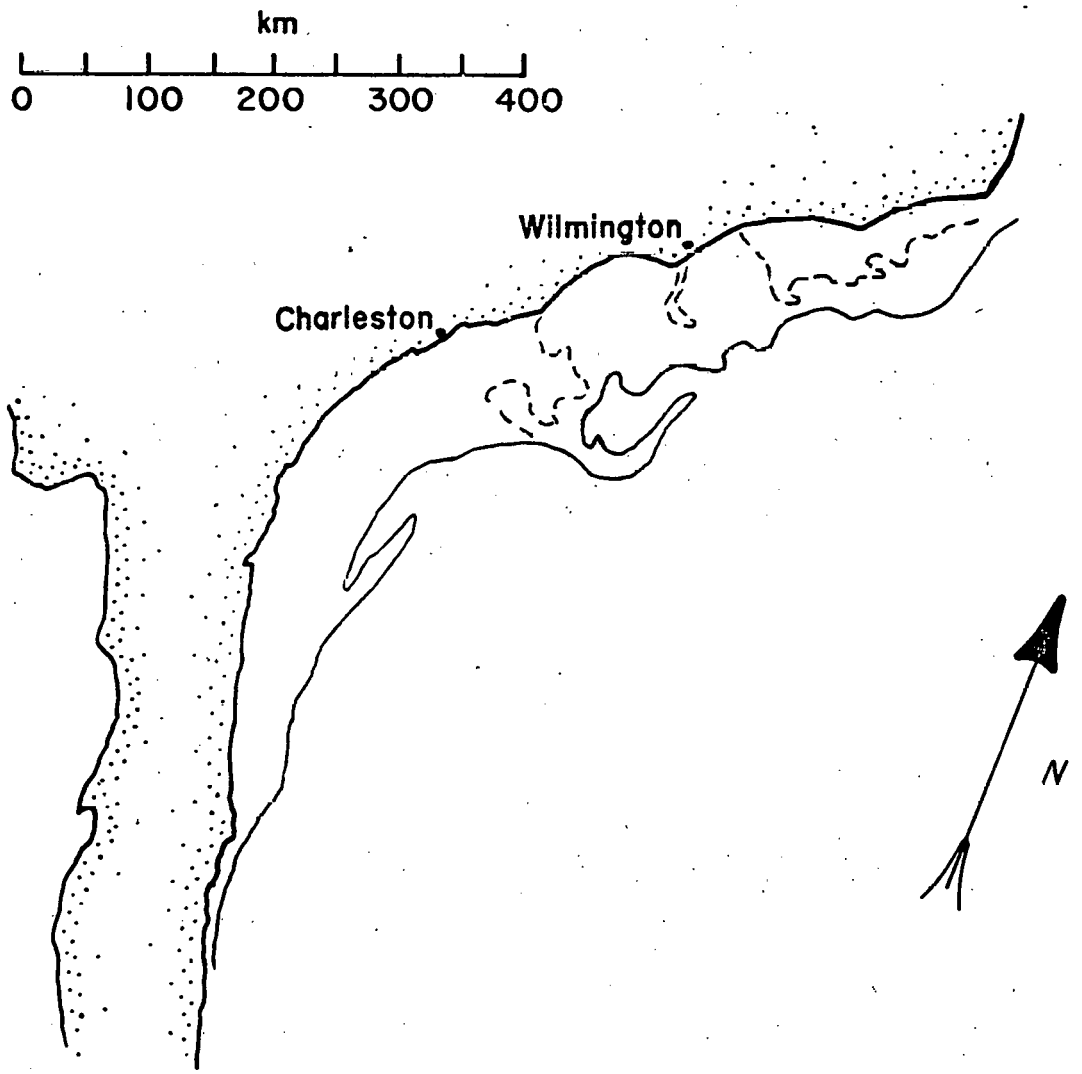

Figure 7. Satellite imagery at 1501Z, April 17, 1977 (solid line is GSF)

show that eddy-like excursions are a consistent feature along the shelf break of the SAB and appear to grow to much larger proportions.

Continental Shelf Flushing by Gulf Stream and Wind

Near the shelf break (50 to 75 m isobaths) Gulf stream frontal instability processes, such as wave-like meanders and spin-off eddies become a significant contributor to current variability and water mass exchange (Lee, 1975; Lee and Mayer, 1977; Pietrafesa, 1977). The Gulf Stream surface front may meander about 10 to 25 km in the east-west direction with a wave length of 100 to 200 km. These meanders are known to grow at times into the tongue-like disturbances (shingles, sausages or eddies). The cyclonic circulation in the eddies transports shelf water offshore in the southern region of the vorticity, which provides a mechanism for rapid water exchange. It is thus appreciated that eddy like events displace large volumes of shelf water with onshore flows of Gulf Stream waters at the surface and bottom and offshore shelf water displacement and subsequent entrainment into the slope waters.

Flushing frequency is thought to tie directly to the frequency with which meanders and eddy events occur. Conventional wisdom is that meanders and eddy events occur at frequencies between 0.1 and 0.2 cycles per day; figures which embrace the pioneering study by Webster (1961), as well as studies of sea level by Mysak and Hamon (1969), and present current studies. We should point out that studies have yet to unambigously link onshore/offshore flow cycles on the North Carolina Shelf with meanders or accelerations of the Gulf Stream. From the Lee and Pietrafesa DOE data sets, it is

obvious that large amplitude current fluctuations with periods ranging from several days to several weeks are common features on the continental shelfs off both Georgia and North Carolina. These current meter data (Pietrafesa, et. al., 1977, 1978) indicate that cycles in onshore/offshore flow often precede local wind events occurring more or less simultaneously at Cape Hatteras and Wilmington, North Carolina (separation-distance about 120 km). Perturbations in the Gulf Stream represent a mechanism which could be causing those flow cycles in mid-shelf that seem poorly correlated with local winds.

Blanton and Pietrafesa (1978), to be referred to as BP, considered data covering 42 days collected during 1975 by Pietrafesa (1976) and outlined in Table 1. Over this period, eight cycles of onshore/offshore flow occurred, about one cycle each 5 days. The most dramatic onshore/offshore event occurred at the SW mooring from 10-22 August 1975 (Fig. 8). The other seven cycles in the SW had durations from 4 to 5 days long. The onshore flow in all but one cycle lasted 2 to 4 times longer than the following offshore flow, indicating that that flow was predominantly onshore in the SW corner near bottom. Onshore/offshore flow cycles near bottom in the NE were weak and poorly coherent with near bottom flow in the SW. The average flow from the smoothed record is shown in Figure 8a where averages were computed for the entire 42-day record. The near bottom flow in the SW is clearly stronger than that observed in the NE. The strong average northeastward flow near surface in the northeast is closely aligned with the

Table 1. Data summary from moored instrumentations in Onslow Bay.

Mooring	Water Depth	Instrument Type	Depth	Record Duration
NE	28 m	Endeco-105	10 m	6 August-26 September 1975
		Endeco-105	25 m	
SW	28 m	GO- 3070	11 m	6 August-26 September 1975
		Endeco-105	25 m	

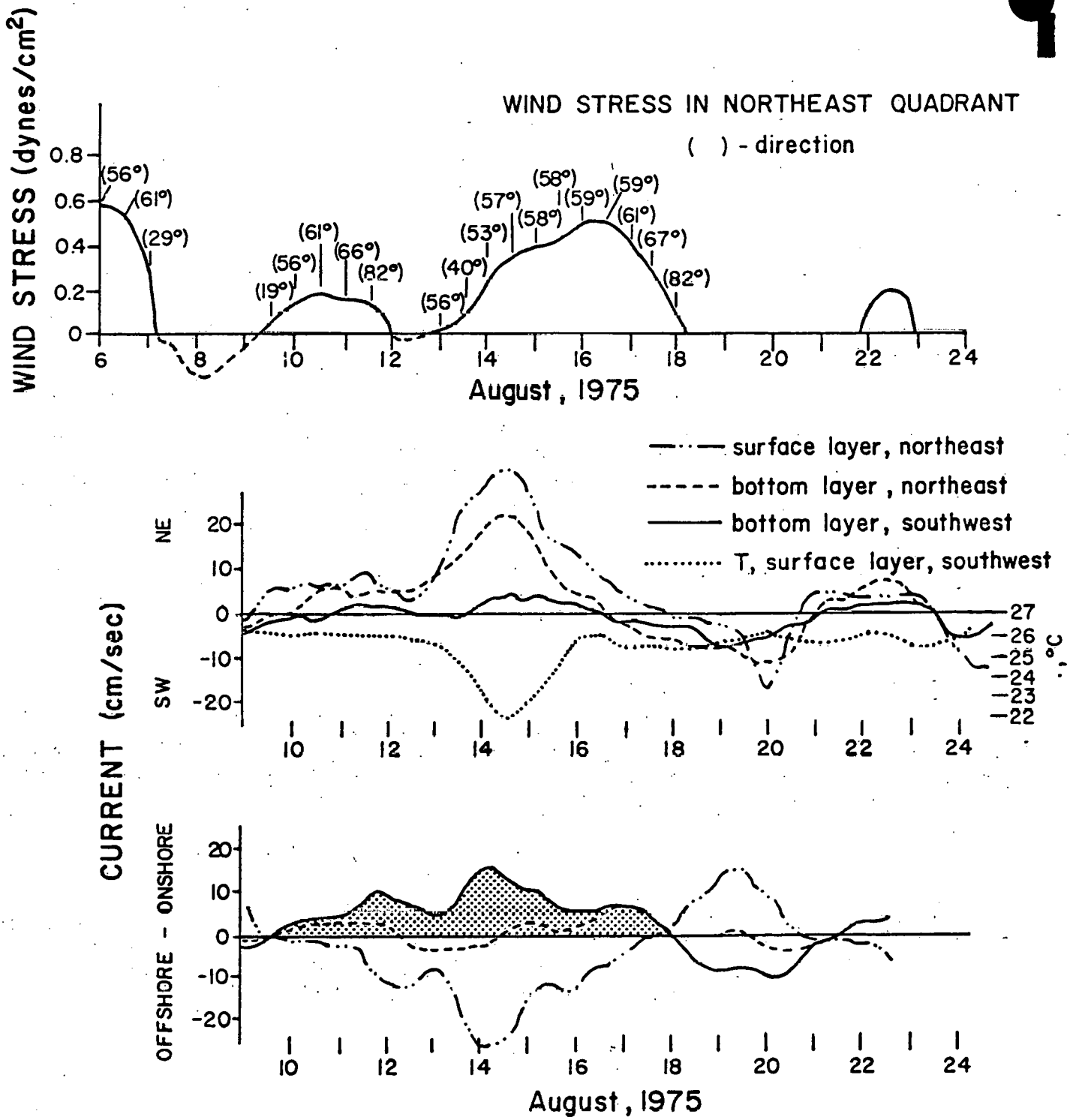

Figure 8. Cast study of bottom intrusion during period Aug. 9-24, 1975

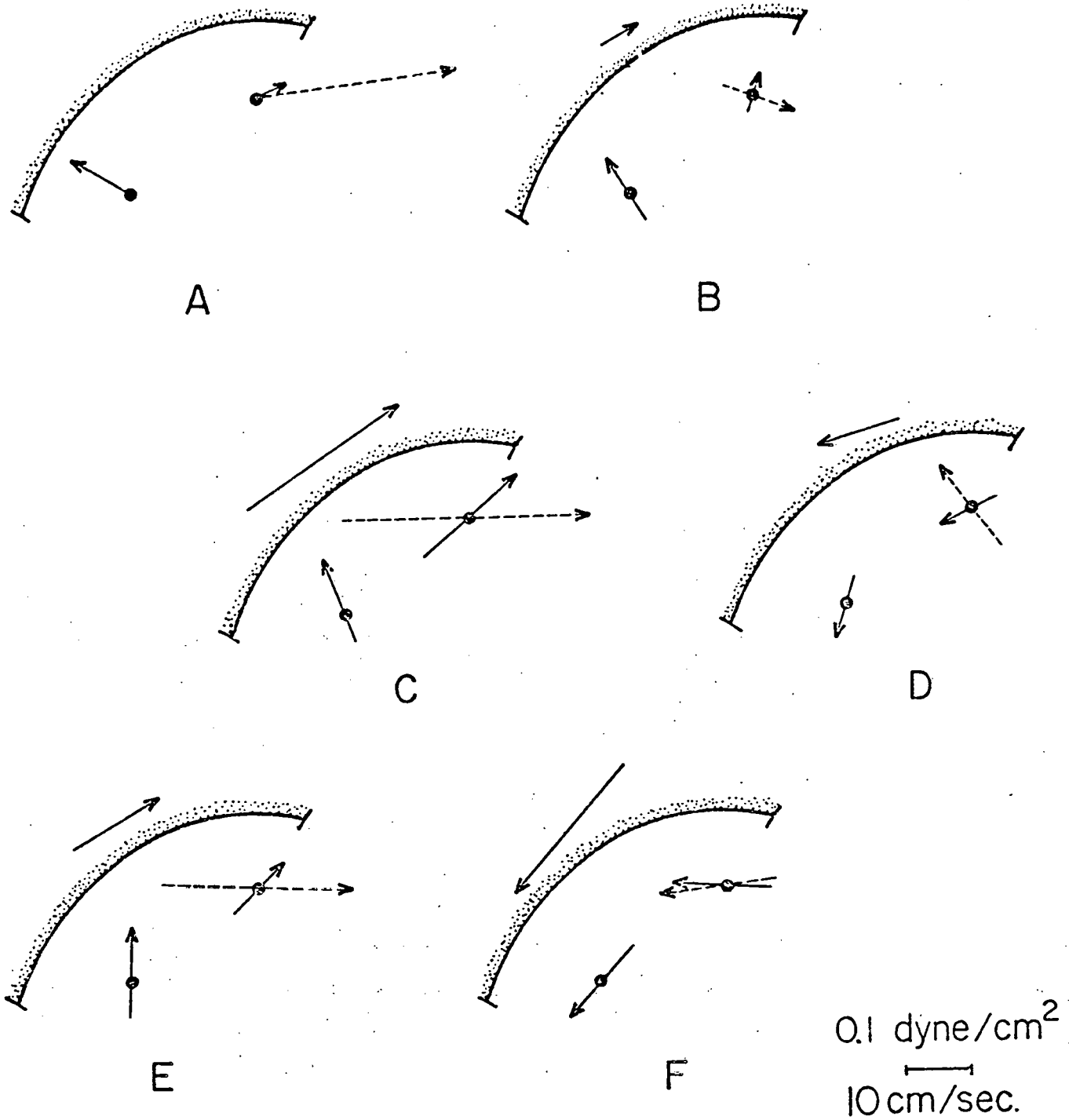

Figure 8a. Daily averaged vectors of wind stress squared (Cape Hatteras) and currents during specific events of wind. (a) 42-day average currents (only); (b) NE wind stress, 12 Aug.; (c) NE wind stress, 14 Aug.; (d) SW wind stress, 19 Aug.; (e) NE wind stress, 12 Sept.; (f) SW wind stress, 14 Sept. Wind stress vectors are depicted northwest of the shoreline in each illustration except the first. In (a), multiply vector lengths by 0.05 for true speeds. Dotted arrows represent currents at 10 meters depth; solid arrows represent currents at 25 meters depth.

prevailing northeastward wind stress during the summer season in a conventional Ekman barotropic geostrophic sense. Onslow Bay responds to discrete wind events from the SW (prevailing) and the NE (after frontal passages). Blanton and Pietrafesa selected five days of the 42-day record to demonstrate this response (Fig. 8a). Three illustrations cover northeastward wind stress whose daily average varied from less than 1 dyne/cm^2 to almost 3 dynes/cm^2. Under these conditions, only the surface flow in the northeast increases with increasing wind stress. The onshore flow in the SW averaged 10-15 cm/sec during the day under the three different stress magnitudes. Two other illustrations cover episodes of southwestward wind stress. The first daily average stress was about 1 dyne/cm^2; the second was almost 3 dynes/cm^2. Bottom flow tended to follow the trend of the isobaths. It was not clearly proportional to the wind's strength. Neither was the surface flow.

Hydrographic data obtained at the time the two moorings were set showed Onslow Bay to be highly stratified in the vertical with a well mixed surface layer of about 27.5°C and salinites less than 35.5°/oo over a well mixed bottom layer whose temperature ranged from 25.5°C less than 20 km offshore to less than 22.5°C near the shelf break. Salinities were everywhere greater than 36°/oo in the lower layer. The bottom meters were within this bottom layer. Temperature and salinity (Atkinson, et.al., 1976) confirm that the onshore/offshore flow cycles in this bottom layer transported water of Gulf Stream origin.

Onslow Bay seems to respond in a discrete manner to different directions of the alongshelf wind stress. Northeastward stress induces offshore flow near the surface almost 45° to the right of the wind. This is really no support of Ekman drift since the Cape Lookout Shoals in the NE corner undoubtedly deflect, i.e. steer the flow to some degree. The occasional insensitivity of the bottom flow to wind stress magnitude implies another driving source which we will discuss below. Southwestward wind stress reverses the sense of the near surface flow and bottom flow is more clearly aligned with the isobaths. There was strong onshore bottom flow observed in the SW between 10-18 August (Fig. 8). The along shelf component was very small. Bottom topography in this region is quite complex, and it is entirely possible that this strong onshore component is following the local topography. Nevertheless, water is clearly being carried toward the inner portion of the embayment. Three points can be stressed here. First, strong bottom flow began at least two days before strong northeastward winds. Secondly, the maximum current speeds occurred 2 to 3 days before the strongest winds. Thirdly, the currents diminished and reversed while the winds still blew hard toward the northeast. In fact, the strongest observed winds occurred on 18 August. The effect of this strong onshore flow in the SW can be seen in the temperature data at 11 meters depth in the NE. The temperature at this point was approximately 26°C for the entire 42 day record except between 14 and 16 August (Fig. 8). At this time, the temperature dropped on 14 August to 22°C. The low

temperature occurred simultaneously with the strongest bottom flow in the SW which had been acting for the previous 3 days at only slightly lesser speed. These facts suggest that the dramatic onshore/offshore event was triggered by a large-scale disturbance, probably originating in the Gulf Stream and enhanced by the upwelling favorable, subsequent winds. The onshore flow carried relatively cold temperature water of Gulf Stream origin (Atkinson, et.al., 1976) to the inner portions of the embayment where vertical mixing in the shallow water cooled the entire water column to around 22°C. This water was returned offshore in the upper portions of the water column where it passed by the NE mooring on 14 August.

The other seven cycles in the 42-day record had much less effect on the inner portions of Onslow Bay because they were not as strong nor did they persist as long. Nevertheless, these cycles represent processes that remove or flush water from the embayment. Our data seem to indicate that such cycles occur about once every 5 days.

The Cape Fear i.e. Frying Pan, and Cape Lookout shoals bounding the southern and northern parts respectively of Onslow Bay appear to exert a degree of topographic control on the circulation. The response of Onslow Bay to onshore flow events indicate that water tends to cross the embayment predominantly in the southern portion. We assumed therefore, that the onshore flow occurs over one-half the along shelf length or L - 50 km. The average thickness of this flow was estimated from extensive hydrographic data taken over

several years. The sharp thermocline that separates the surface shelf water from the more saline and colder bottom water (Blanton, 1971) averages roughly 10 meters off of the bottom (Atkinson, et.al., 1976; Pietrafesa, 1978). Thus the onshore flow is typically about 10 meters thick. Average onshore speeds are about 7 to 10 cm/sec at the SW mooring which last on the average of about 3 days. Using the above values, we calculate the volume flux of onshore flow across a half length of the embayment to be about 1.3×10^{16} cm^3 over a 3-day duration. The embayment's total volume (100 km x 50 km x 30 m) is about 1.5×10^{17} cm^3. Thus 12 onshore events are required to remove the total volume of Onslow Bay. If these events occur each 5 days, a replacement rate = 12 events x 5 day/ events = 60 days. Thus about 2 months are required to flush Onslow Bay by these onshore flow cycles.

This flushing rate of 2 months can be compared with other calculations for the shelf south of Cape Hatteras. Atkinson, Blanton and Haines (1977) calculated an overall flushing rate of 2.7 months based on the freshwater distribution and input to the Georgia Bight area. In that paper, it was shown that this rate was remarkedly constant from season to season, and a Gulf Stream entrainment model was proposed to account for the rate at which freshwater could be removed from the Continental Shelf. Using typical freshwater filament dimensions and salinities observed by satellite and hydrographic cruises and assuming that the stream entrains one of these filaments each five days, it is speculated that about 2 to 3 months are required to remove the freshwater observed on the Continental shelf in the South Atlantic Bight.

The volume of the subsurface intrusions typically observed in the summer in Onslow Bay was calculated by Atkinson and Pietrafesa (1978) in the following way. Each ocean/hydrographic station was assumed to represent a 10 x 20 km ($200km^2$) area (cf. Figure 9). The product of the layer thickness at a station, which is determined by examination of the vertical profiles, times $200km^2$ yields the volume of intruded water in that region. Summing the regional volumes then gives the total intrusion volume. The difficulty with this approach is in the differention on between intruded water and resident Onslow Bay water which may be old Gulf Stream water. Tables 2, 3 indicate the pertinent cruises, dates, stations, depths, volumes, cumulative sums and Bay volume percentages.

Observations in Onslow Bay in September 3-13, 1975 identified one subsurface water mass (Figures 10,11,12) with minimum temperatures of 25.0C. The stranded intrusion was located in the inner part of the Bay and current meter and hydrographic evidence indicates it was draining from the Bay east of Cape Lookout. The results of the last hydrographic grid (11-12-13 September 1975) indicated that at that time the water mass was either thoroughly mixed into the water column or advected from the Bay. The volume was determined from the 8-9-10 September data. The bounding isotherm was 27.5C and the area is cross-hatched in Figures 10 and 11. This observation is an attempt at estimation of an intrusion volume. The calculated volume of $47km^3$ represents 11% of the Bay volume. Considering that the intrusion was situated in the inner Bay, represents more than 20% on the inner Bay volume.

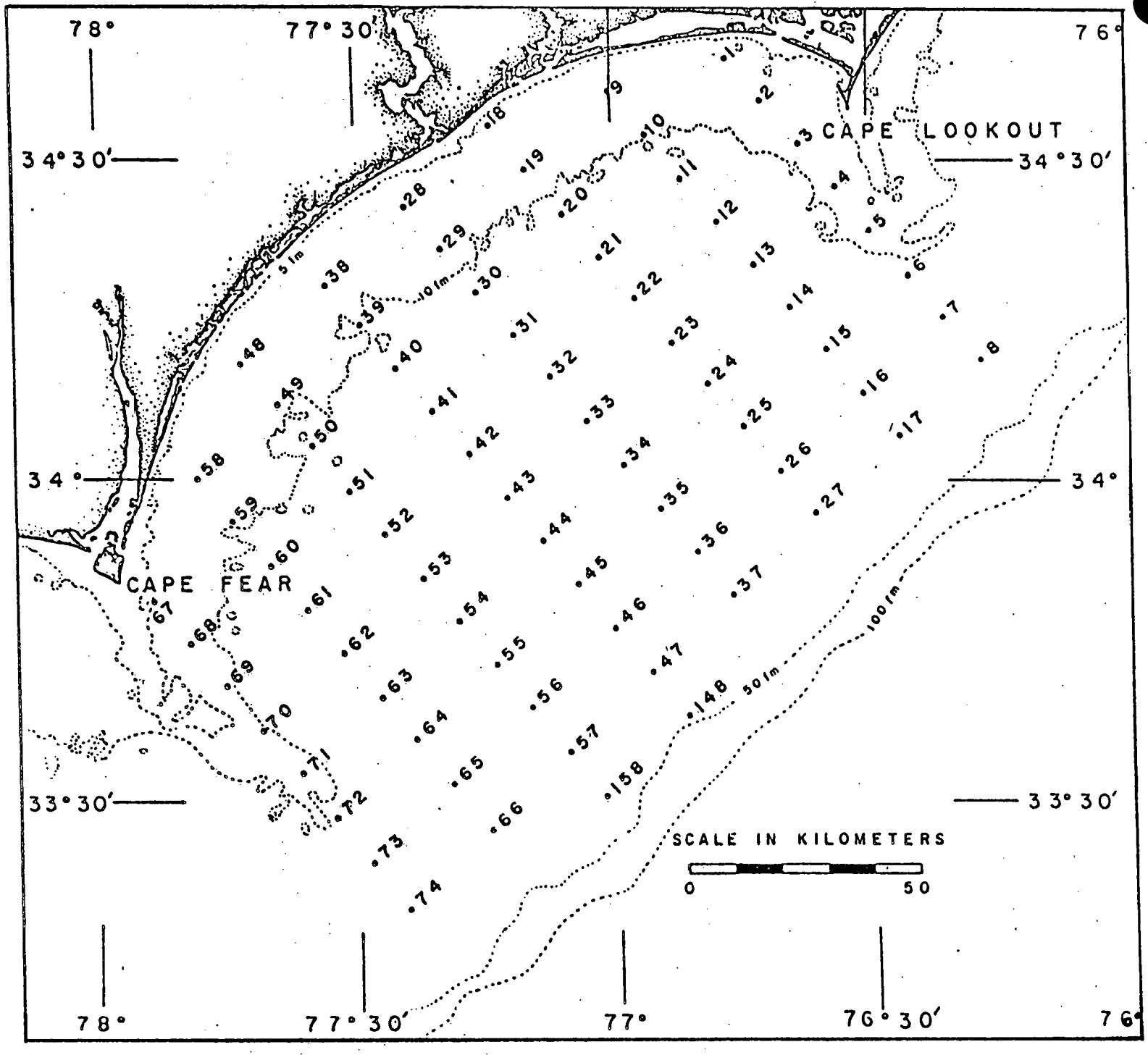

Figure 9 3KIO/NCSU Onslow Bay Ocean/hydrographic grid

Table 2

Cruise	Dates	#Stations	Onshore/Offshore #Sections	Data Report
OBIS I	6-7 August 1975	14	2	1
OBIS II	September 1975			2
OBIS III	13-14 October 1975	18	2	1
OBIS IV	8-11 December 1975	12	7	1
OBIS V	14 July-18 Aug. 1976	100	24	3
OB5 Cruise Leg	14-18 July 1976	53	5	4
OB6	21-23 July 1976	46	5	4
OB7	28 July-6Augst 1976	44	9	4
OB8	14-16 August 1976	42	6	4
OB9	18 August	4	0(one Along-shore)	4
	Totals	333	60	28

Table 3 Hypsometric data for Onslow Bay, North Carolina

Depth Range (m)	Volume (km^3)	Cumulative Sum (km^3)	%of Bay volume
0-9.1(0-5f)	2.4	2	0.6
9.1-18.3(5-10f)	48.2	51	11
18.3-27.4(10-15f)	102	153	24
27.4-36.6(15-20f)	165	318	39
36.6-45.7(20-25f)	105	423	25

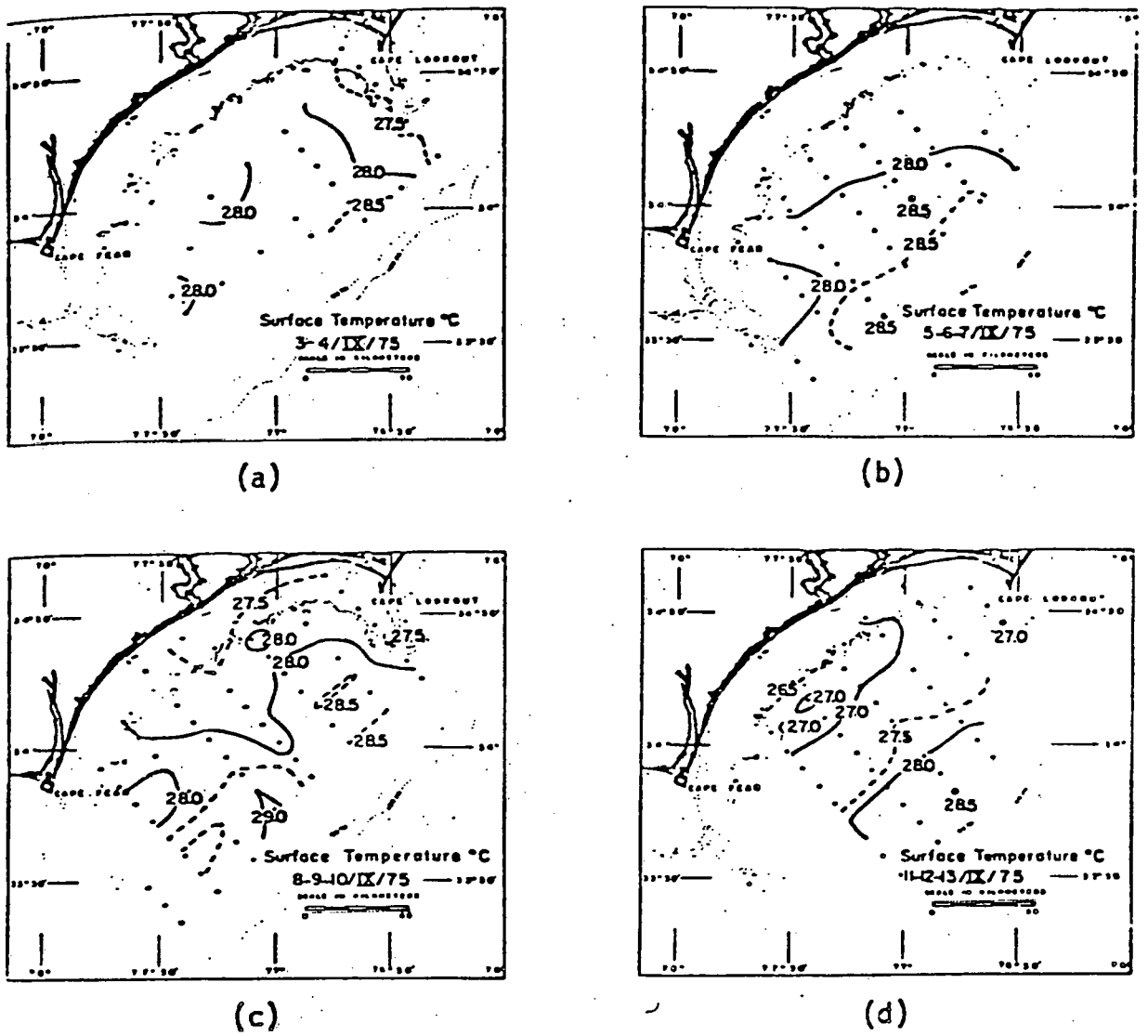

Figure 10 Onslow Bay surface temperatures September 3-13, 1975

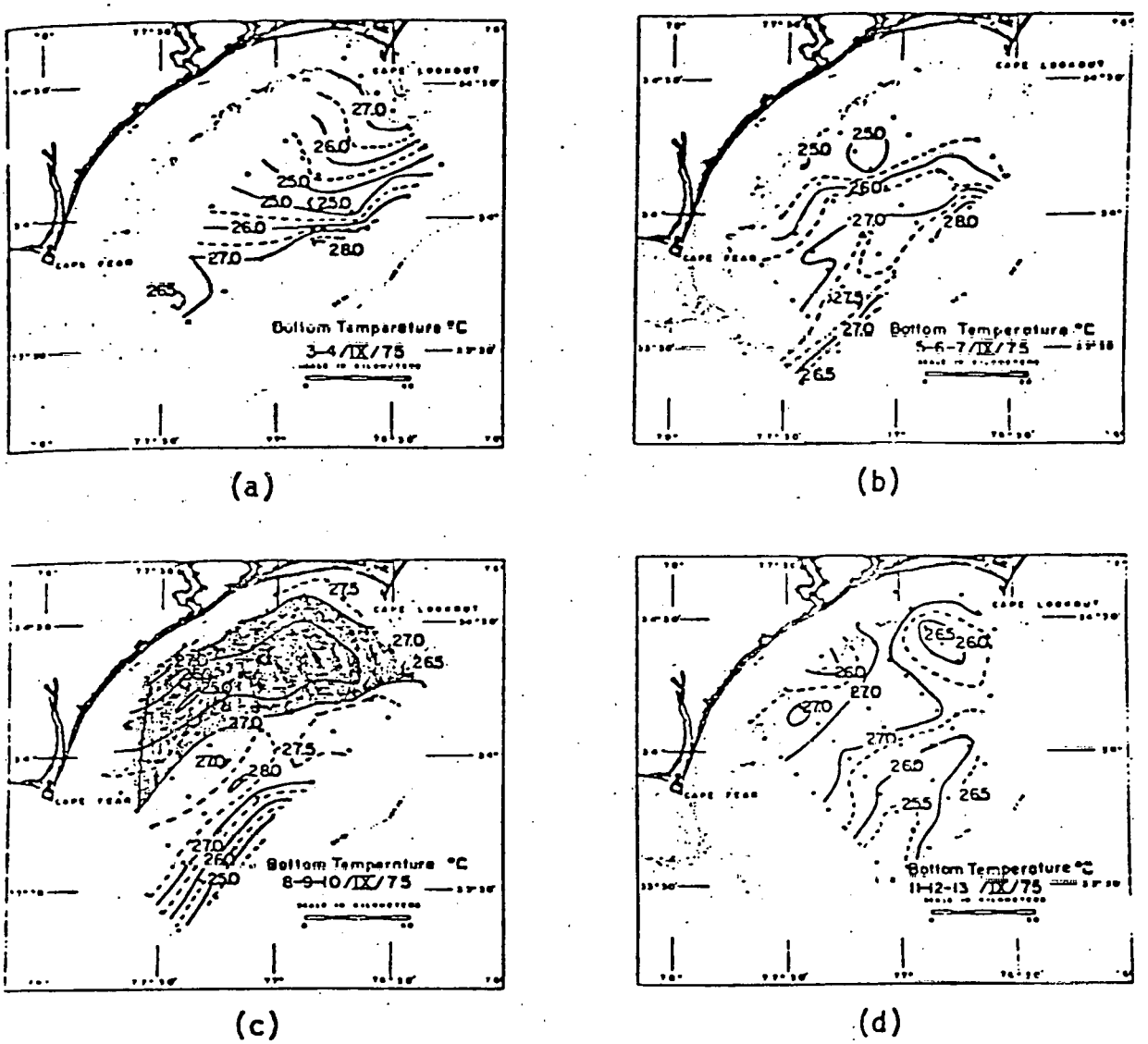

Figure 11 Onslow Bay bottom temperatures September 3-13, 1975

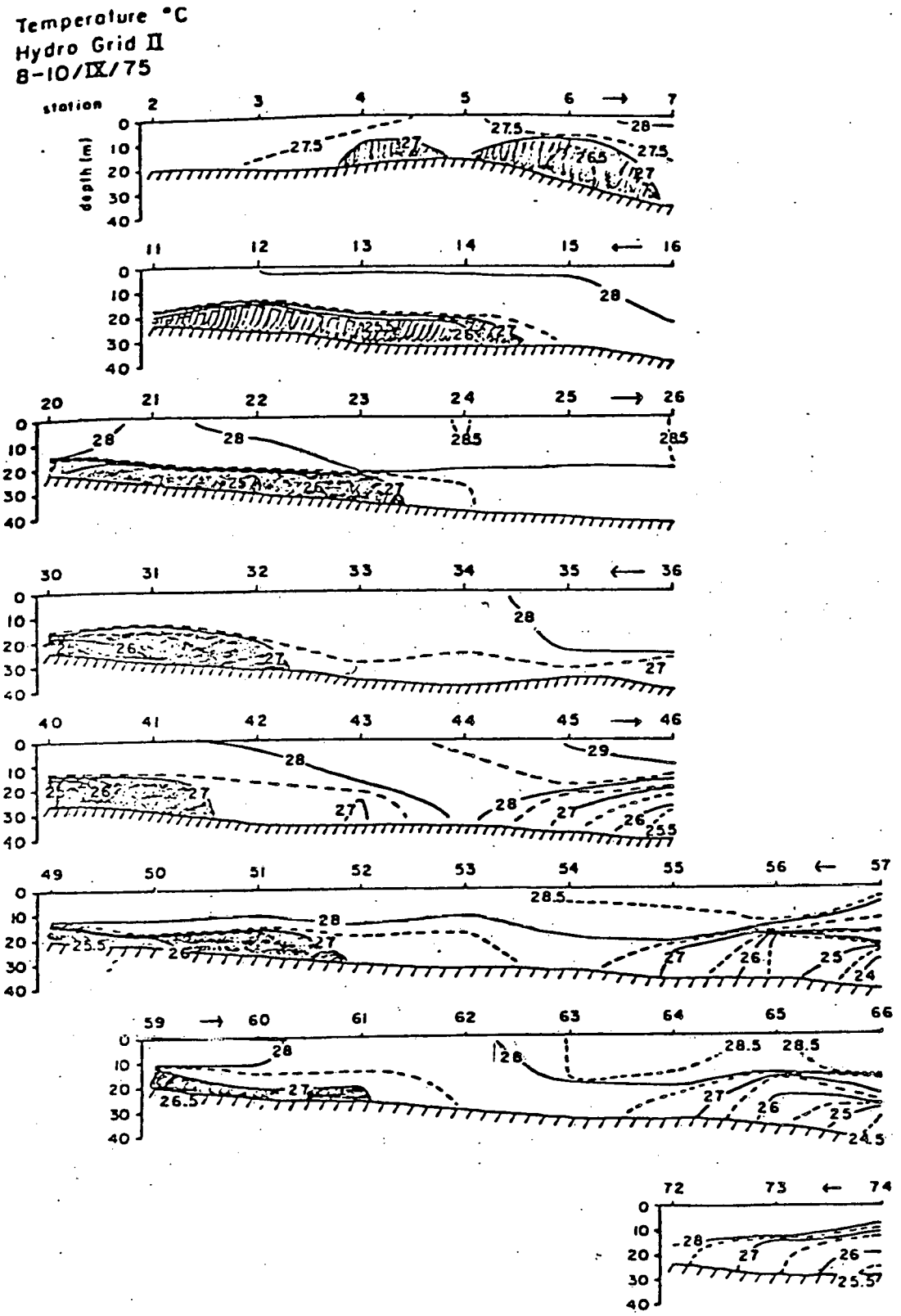

Figure 12 Onslow Bay vertical distribution of temperature September 3-13, 1975

The remaining four measurements of subsurface intrusion volumes result from intensive observations in Onslow Bay in July and August 1976. During the period surface temperatures (Figure 13) gradually warmed from 26 to 27C with lower temperatures near Frying Pan Shoals and nearshore and higher temperatures in the Gulf Stream. Bottom temperatures (Figure 14) indicate that the Bay was repeatedly invaded by deeper, cold Gulf Stream waters with temperatures as low as 21.5C. The variation in near bottom temperatures indicates that various water masses were invading the Bay rather than the remote possibility that one intrusion maintains its integrity and migrates spatially, to and fro in time.

Observations made in Onslow Bay during 14-15, July, 1976 indicated the presence of a large subsurface mass of colder water. There is a question concerning its temporal origin, if not its spatial characteristics. The intrusion was cut off (stranded) from the stream in the northern area (Figures 14,15, stations 8 and 109). The calculated volume, of this intrusion, of 151 km^3 represents 36% of the Bay volume.

The 21-23, July, 1976 grid included an observation of a water mass of 23-24°C stranded in the Bay. This water mass could be either the same water observed the 14-15 July or a new one. The calculated volume of 86 km^3 represents 20% of the Bay volume. The 4-6, August observations identified à new subsurface water mass in the Bay with minimum temperatures of 21.5^{o}C compared to the previous lows of 23°C. The intrusion was stranded in the Bay, by a mass of 23-24°C water at the shelf break (Figures 14,16). The calculated volume of 46 km^3 represents 11% of the Bay volume.

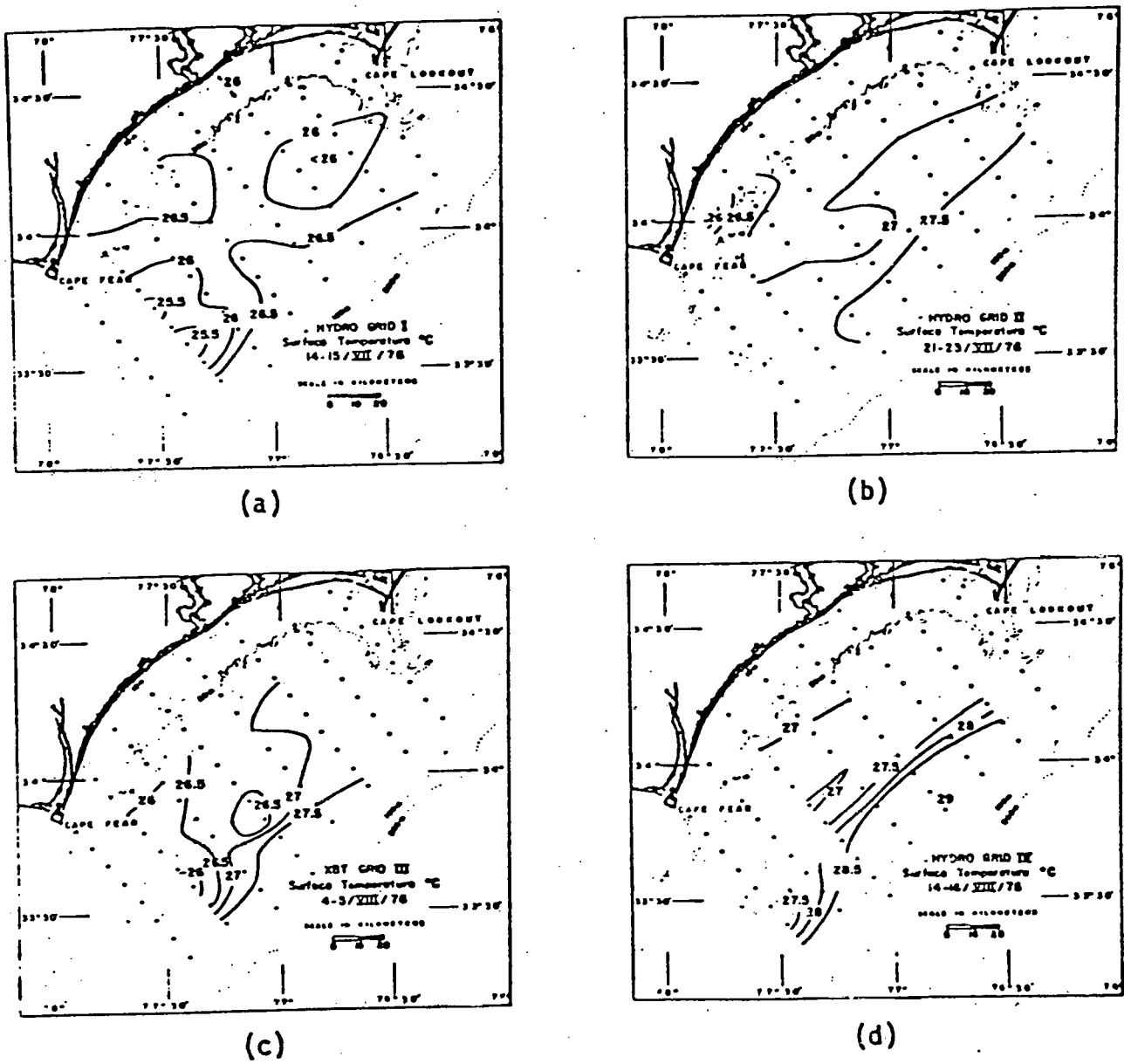

Figure 13 Onslow Bay surface temperatures in July and August, 1975

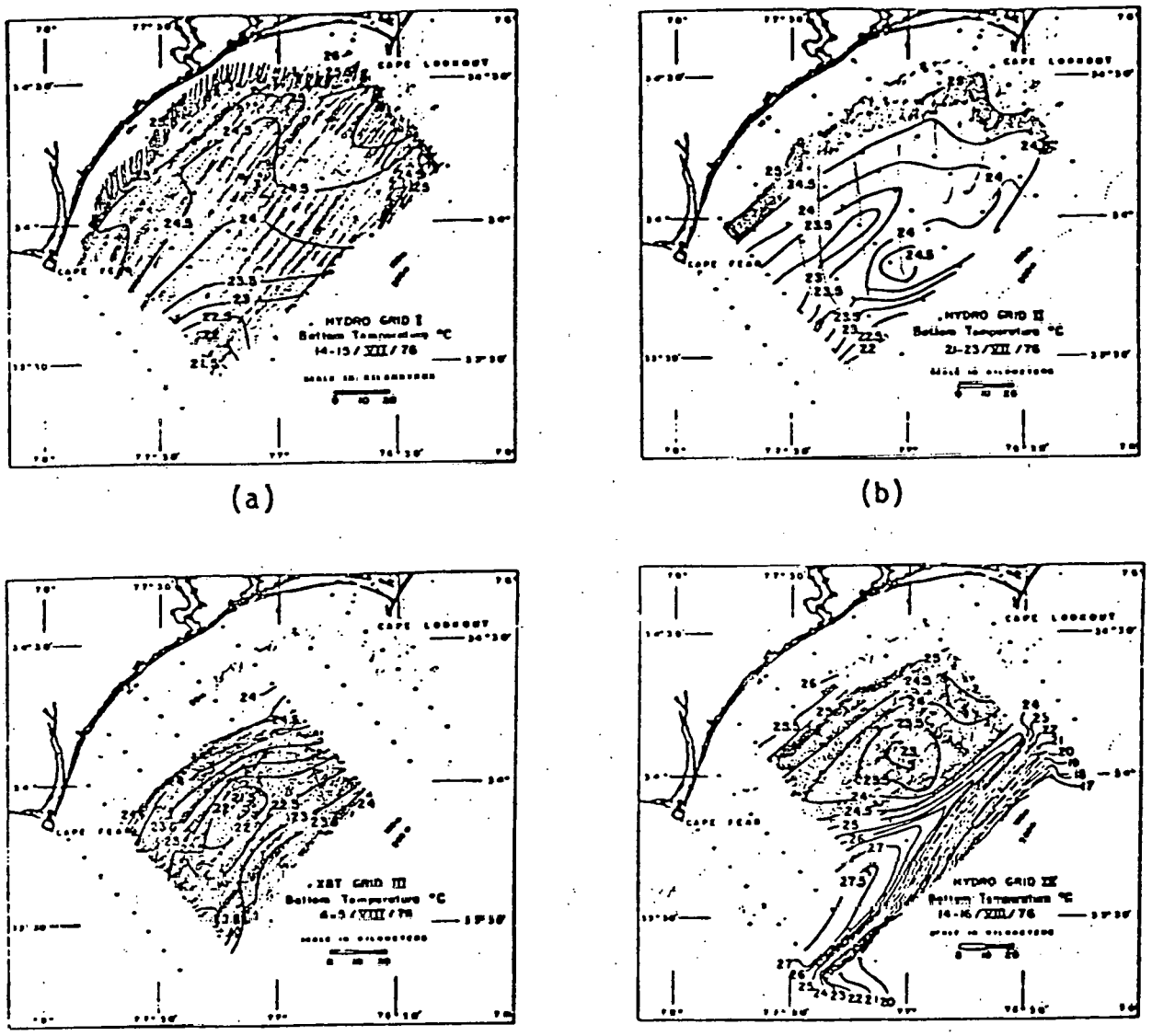

Figure 14 Onslow Bay bottom temperatures in July and August, 1975

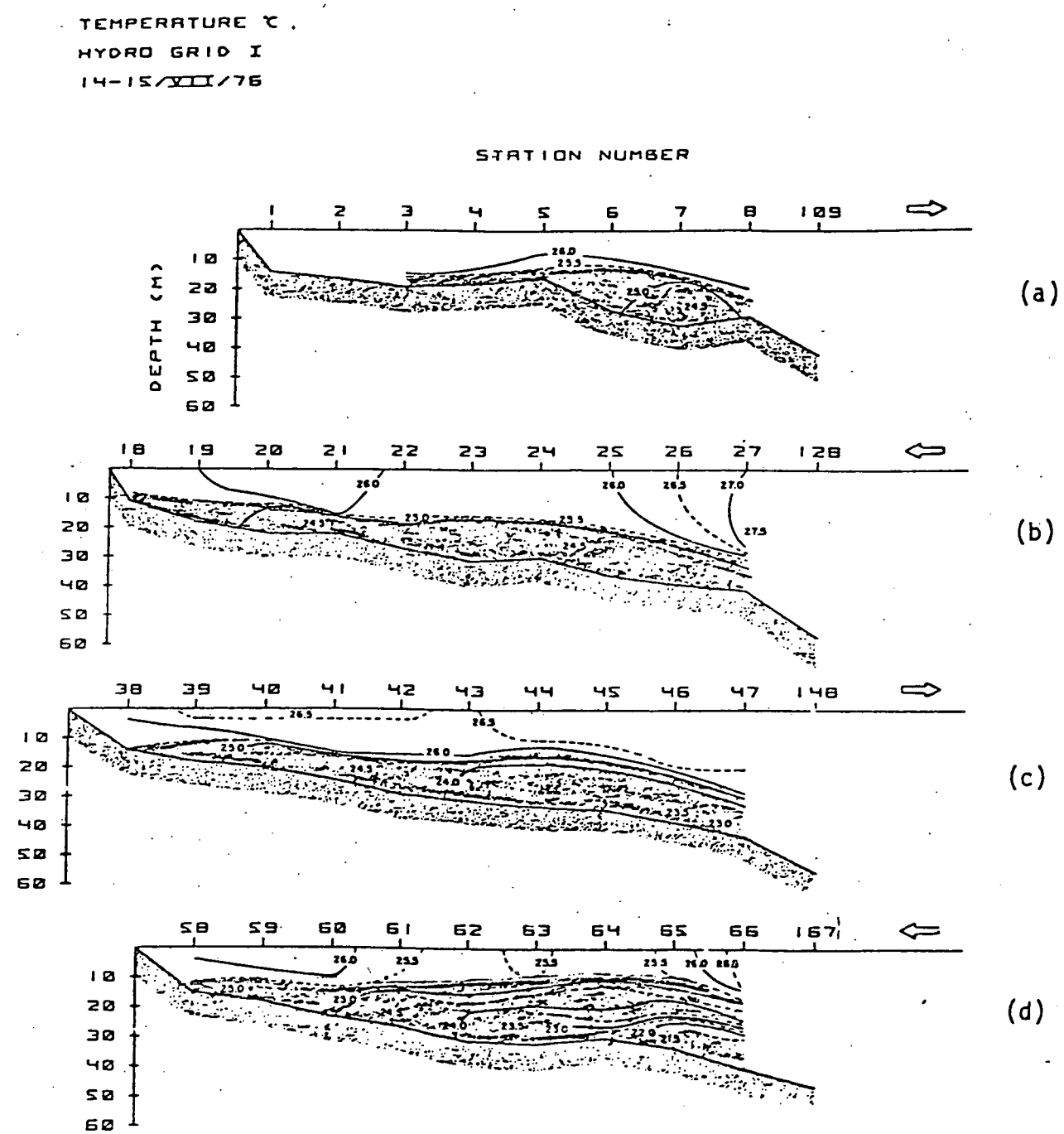

Figure 15 Onslow Bay vertical distribution of temperature July 14-15, 1975

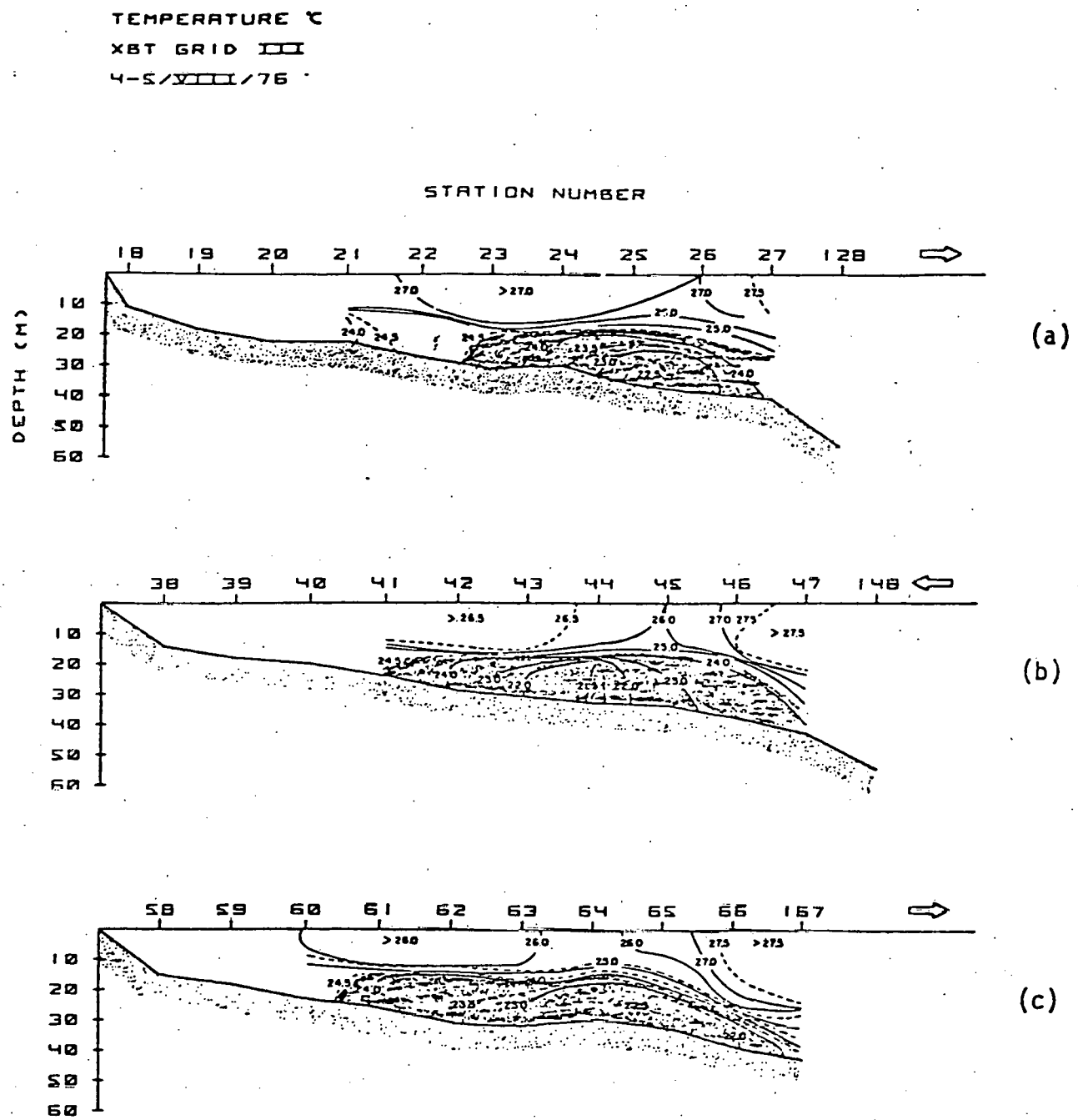

Figure 16 Onslow Bay vertical distribution of temperature August 4-6, 1975

Subsurface intrusions, which are responsible for the appearance of cold, dense, Gulf Stream derived waters typically in the bottom layer at the southern extent of Onslow Bay, in effect transport vertical physical/dynamical stability to the water column. This stability can be measured by an increase in the vertical gradient of density, whereby a portion of the energy being externally inputed to the system is used to increase the potential energy, thereby reducing the relative level of turbulent, mixing intensity. It is our belief, herein, that this increased stability is of essential importance from either a biological or chemical viewpoint.

The questions at this point seems to involve those of a basic nature, i.e.: what generates these frontal, eddy events and during their existence, what are the physical, dynamical and ultimately, biological, chemical and geological consequences of their appearance and persistence.

Possible Downstream Effects of the Charleston Bump

A significant feature within the surface thermal (Very High Resolution Radiometer, VHRR) satellite imagery being collected and processed by NOAA/NESS is the quasi-permanent northward to eastward to northward large scale meander of the relatively warm Gulf Stream water away from the coast between Savannah, Ga. to Charleston, S. C. to Cape Fear, N. C. This feature has become known as the "Charleston Bump" (probably Legeckis, 1975) and seems to be evident, in varying degrees, during all of the seasons.

It is this permanancy or persistence of the feature, which is both surface and subsurface in nature which led DOE investigators Pietrafesa (NCSU) and Atkinson (SKIÖ) to speculate that the feature was topographically, orographically induced, since topographic variations occur within the isobaths along the continental slope and are suggestive of a topographically generated wave or series of waves, called Topographic Rossby Waves which "stand" downstream of the "Bump" to Cape Hatteras.

Pietrafesa and a colleague at NCSU (Dr. G.S. Janowitz) have computed the characteristics of a downstream standing Topographic Rossby Wave (TRW) generated by a bump sitting on a continental slope below a barotropic jet on a β-plane. The theory involved in the solutions as well as the characteristic values used are presented in the following development. The basic questions being addressed are: could the topographic feature shown in Figure 17 induce a "lee-wave" or downstream standing TRW; if so, then do these waves, which would vary as the mean current varies, bear a relationship to the quasi-permanent meander in the Gulf Stream offshore of South Carolina; if so, then is the surface thermal imagery, as well as the subsurface hydrography downstream of the "Bump" a resultant feature of these TRW's; if so, then are the eddy events observed in the NOAA/NESS, VHRR imagery and Pietrafesa's hydrographic and moored current, temperature and conductivity sensors a resultant of TRW's presenting a mechanism wherein the baroclinic jet, i.e. the Gulf Stream, undergoes a baroclinic instability which grown in time and space, goes unstable and spins

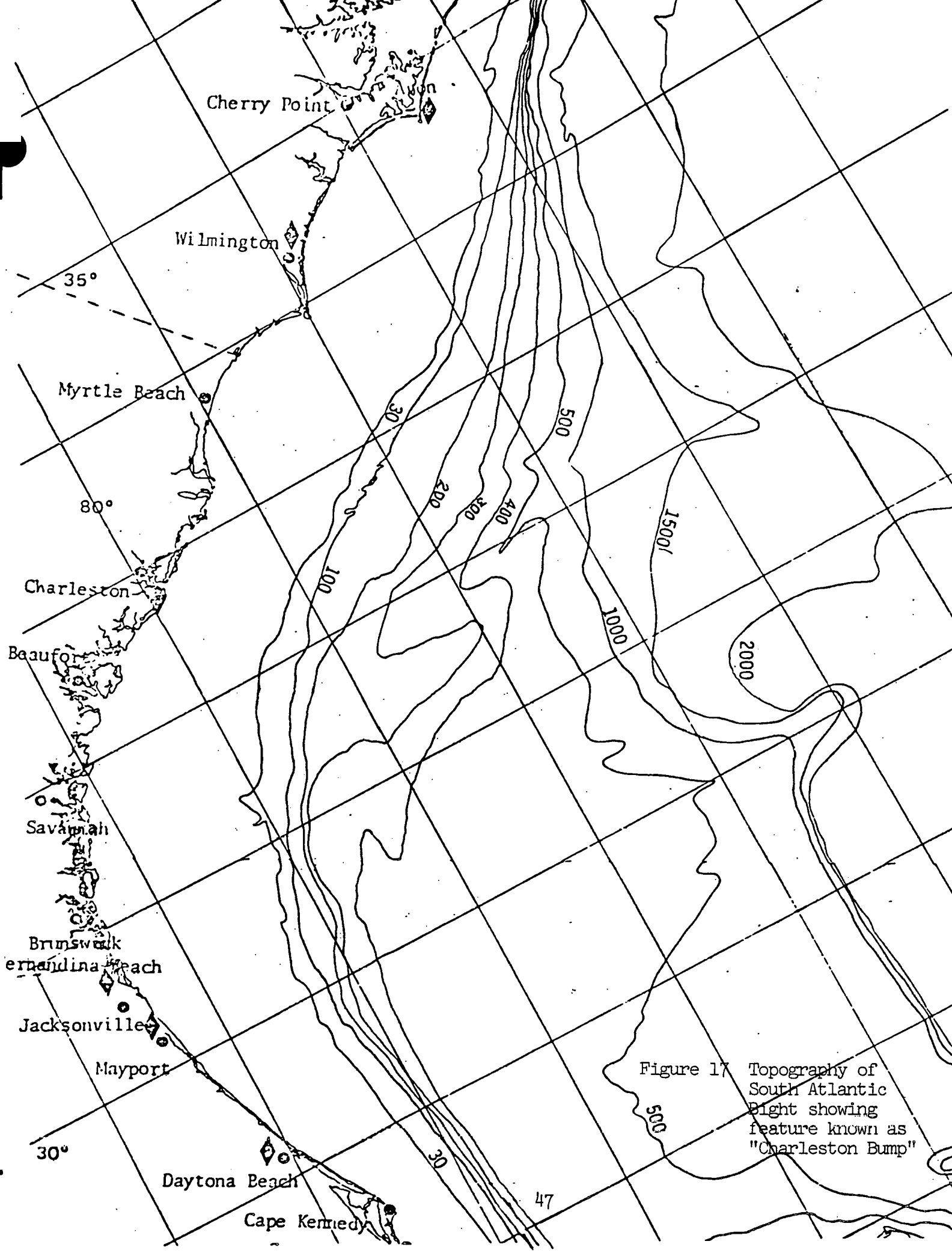

Figure 17 Topography of South Atlantic Bight showing feature known as "Charleston Bump"

off an eddy, shingle, sausage feature to relieve itself of the instability. The mean current fluctuates in time and as a result, even a simple barotropic model would result in a superposition of standing "lee" waves, which differ in wave characteristics from one the other as a function of temporal fluctuations in the mean current.

A simple model of a barotropic (density equal to a constant, for this initial case) model of the characterization of a jet flowing over a bump is now formulated. Consider the following system of equations and boundary conditions:

$\rho_o \frac{Du}{Dt} - f_o v = -P_x$, in zonal direction,

$\rho_o \frac{Dv}{Dt} + f_o u = -P_y$, in meridional direction,

$P_x = -\rho_o g$, in vertical,

where ρ_o , f_o denote constant density and constant Coriolis parameter,

and with boundary conditions,

$\hat{v} \to U\hat{i}$, as $x \to -\infty$ (the offshore constraint),

$w = o$, at $z = H$ (the rigid lid),

$w = \frac{Dh}{Dt}$, at $z = h\ (x,y)$ (the kinematic condition),

$v = o$, at $y = L$ (the lateral boundary on the western side),

and $h = \theta y + \hat{h}\ (x,y)$

where θ = a constant slope ($\sim 10^{-2}$) and where $\hat{h}$ denotes a"bump".

The vorticity equation derived from this system is

$$(P')_{xx} + (P')_{yy} + \alpha^2 (P' + \rho_o f_o U_o y) + \frac{\rho_o f_o^2 \hat{h}}{H} = 0 \quad ,$$

where $P' = P + \rho_o g z$

and $\alpha^2 = f_o \theta / UH$.

The solution of this equation can now be written as

$$\frac{P'}{\rho_o f U L} = -y + \sum_{m=1}^{8} C_m \left(-2H(x-x_m) \int_0^1 \frac{\sin T(x-x_m)}{T} \cos K(y-y_m) dk + \int_1^\infty \frac{e^{-T|x-x_m|}}{T} \cdot \cos K(y-y_m) dK\right)$$

where $T = (|K^2-1|)^{1/2}$

$$H(x) = \begin{cases} 1 , & x > 0 \\ 0 , & x < 0 \end{cases} ,$$

$C_4 = C_1 = C_2 = C_3 = 0.2$,

$C_5 = C_6 = C_7 = C_8 = -0.2$,

$x_5 = x_1$, $x_6 = x_2$, $x_7 = x_3$, $x_8 = x_4$,

$y_5 = -y_1$, $y_6 = -y_2$, $y_7 = -y_3$ and $y_8 = -y_4$.

The flow field results of several test cases are depicted in Figure 18 for the topography, including an idealized, pie-shaped bump sitting atop a linearly sloped continental slope, as depicted in Figure 19 . The flow field suggests a topographically induced meander, just downstream of the Bump, where the meander is in reality part of a damped Rossby Wave which decays in amplitude in the downstream direction like r^{-1} so that the upstream effects are of lesser importance. The wavelength of the standing Rossby Wave is

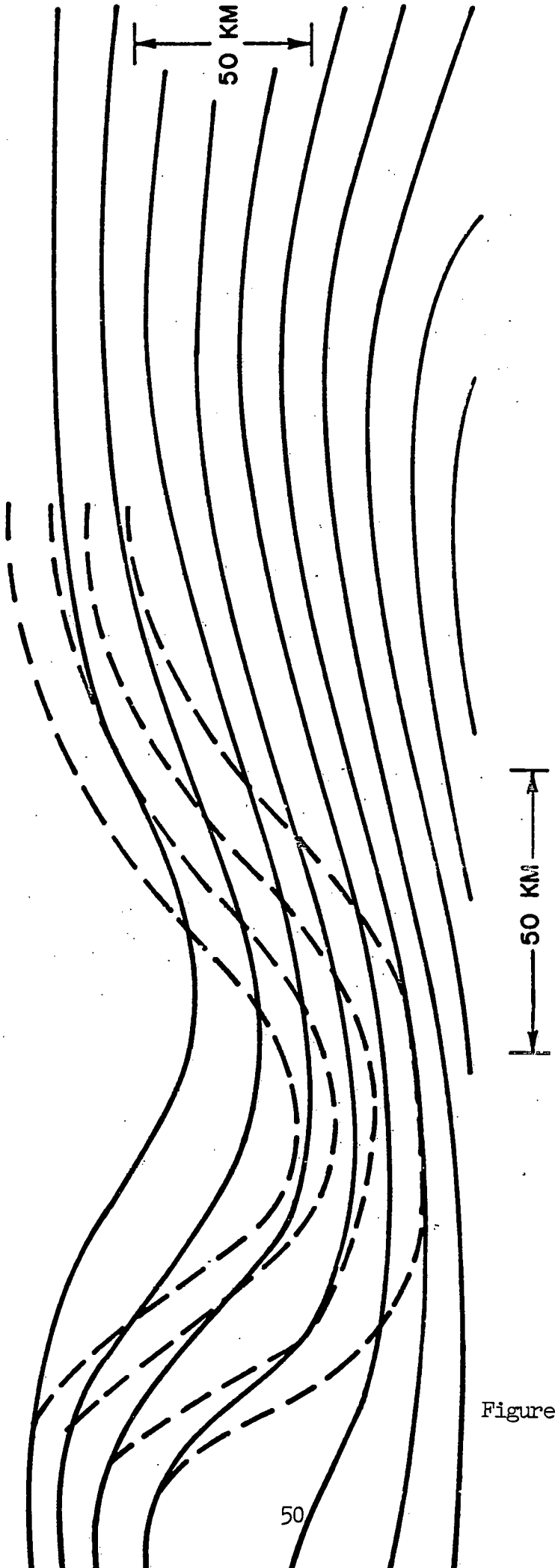

Figure 18 Several test case
of model

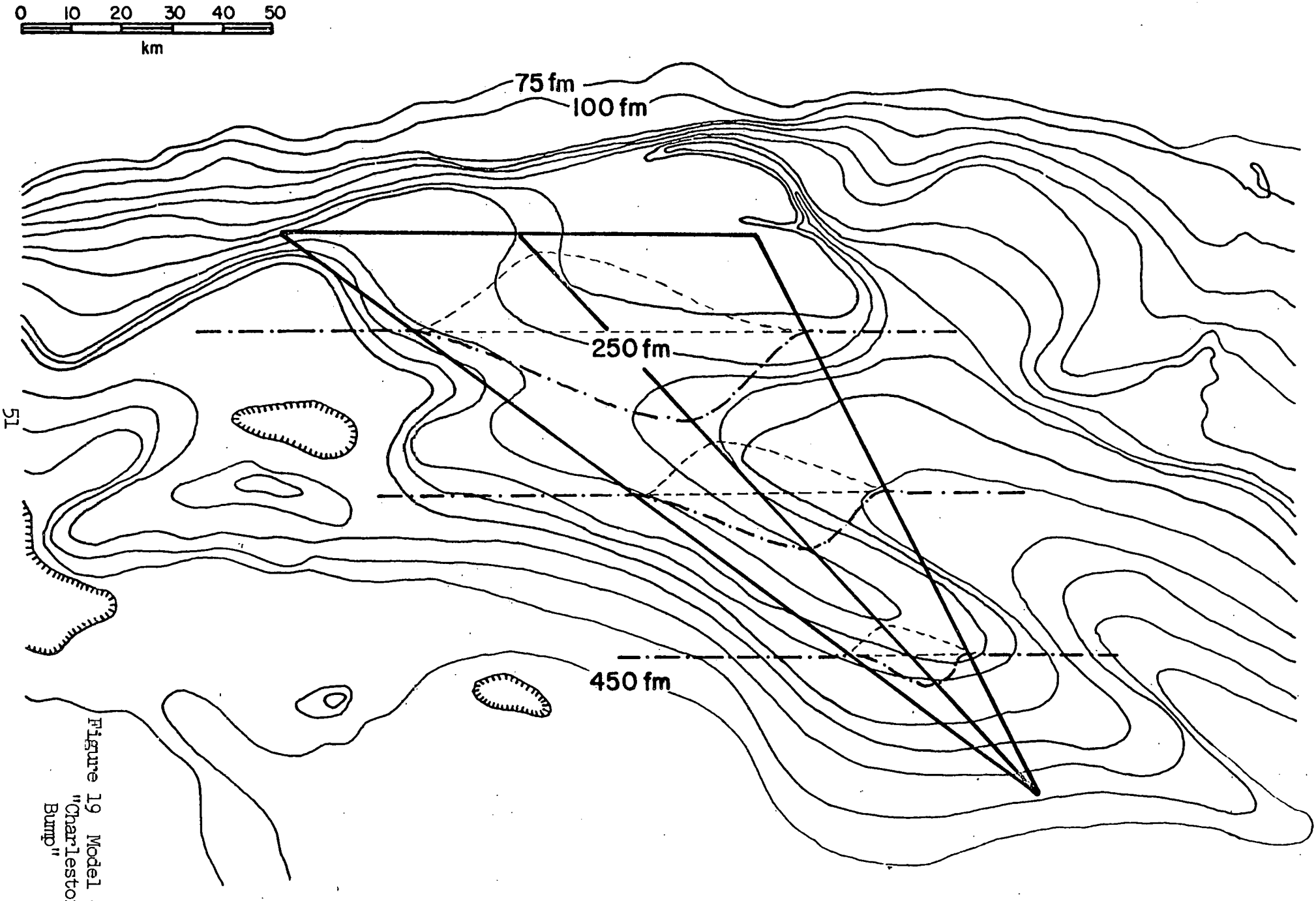

Figure 19 Model of "Charleston Bump"

approximately 200 and 160 kilometers for the two different cases depicted, and the maximum offshore deflection of the jet due to the Bump is shown to be approximately 50 and 75 kilometers for the 2 cases presented. The 2 cases separately assume a mean current of 150 cm/sec and 100 cm/sec or 75 Sverdrups and 50 Sverdrups of transport, separately. In general, the wavelength of the Topographic Rossby Wave generated downstream increases as $U^{1/2}$, the amplitude as $U^{-1/2}$ and the deflection as U^{-1}. It is of note also that the β- effect would cause the wavelength to change like β^{-1}, in the downstream direction. The model figures are compared to several NOAA/NESS VHRR products (complements of Dr. R. Legeckis, NOAA/NESS) in Figures 20 and 21.

Presumably, one could proceed by incorporating density structure, the β- effect, more general topography, vertical and horizontal velocity shear and temporal variability thereof. The model would necessarily have to be solved numerically. The point remains though that the essentials of the fact of the Gulf Stream deflection east of Charleston and of the appearance of wave forms downstream of this deflection are in the model presented herein. The implications of an oscillating baroclinic jet, especially in the region of the frontal zone remains an intriging problem. These implications may include the evolution and formation of the shingle-eddy events through a baroclinic instability process.

The Gulf Stream could then be controlled by mean potential vorticity variations which not only have their origins in total water depth columns shrinking and stretching but also in mean along current variations in the cross-stream directions and mean cross

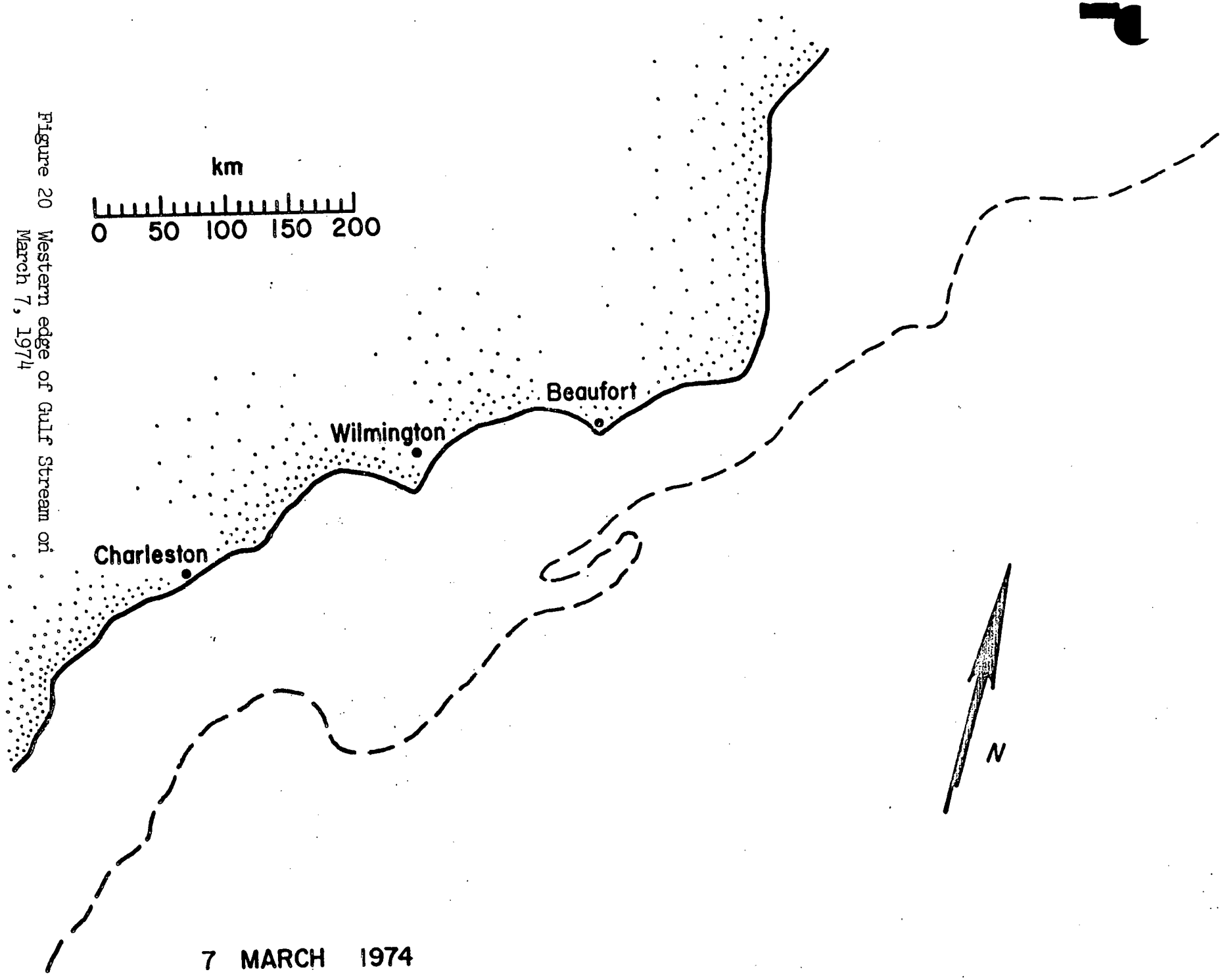

Figure 20 Western edge of Gulf Stream on March 7, 1974

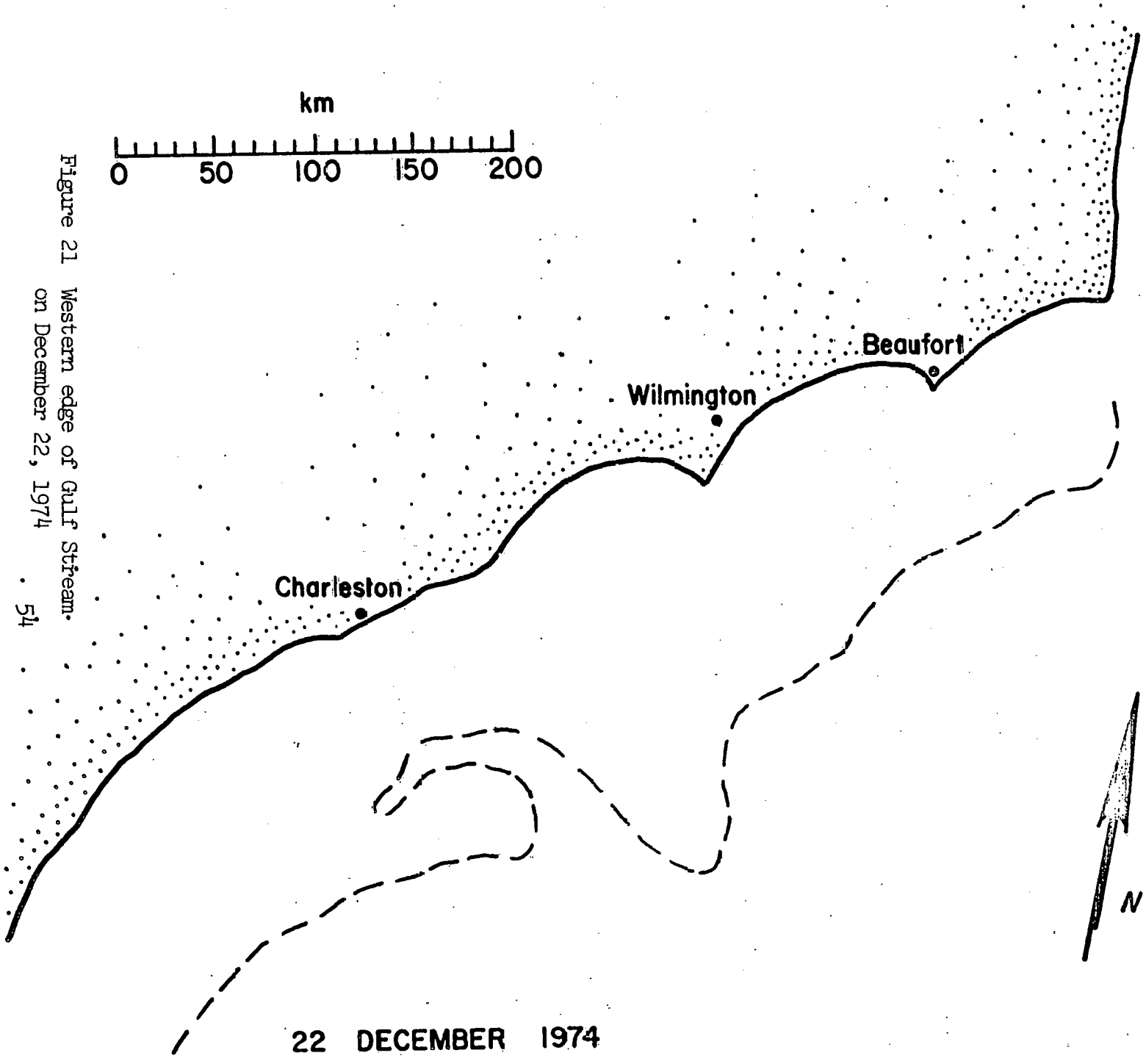

Figure 21 Western edge of Gulf Stream on December 22, 1974

current variations in the downstream direction. An example which partially characterizes the topographic wave induction process is given by the following balance of

$$|(f + \zeta)h_x| \quad \text{vs.} \quad |h\beta| \text{ , where } \zeta = V_x - U_y \text{ : now,}$$

if Left Hand Side >> Right Hand Side, then waves are possible and this inequality is certainly true in our area of interest.

The following scenario is presented as an explaination of the meandering and eddy shedding processes which the Gulf Stream undergoes: South of the Charleston Bump, between approximately the Florida Straits and Savannah, Ga., the Stream may meander due to some process and eddies may form due to some instability process, perhaps related to an off-shore wind tweaking the Gulf Stream Front (GSF) which then differentially decelerates and accelerates the Gulf Stream. The Gulf Stream then flows towards the Charleston, S.C. latitude, encounters a topographic constraint and as a function of its mean speed at the time, is deflected offshore as the origin site of a topographically generated, standing Rossby Wave appearing downstream of the Bump. The Gulf Stream assumes this wave like form, downstream of the Charleston Bump. The wave like form can change in amplitude and wavelength as a function of the vertical velocity variability of the Stream upstream of the Bump, of the position of the Stream before it encounters the Bump, of the variability of horizontal and vertical shears within the Stream, of baroclinic structure within the Stream and as a function of where the crests and troughs of this standing wave are located in relation

to the continental margin topographic variations which may resteer the flow. The GSF may occasionally go unstable through some baroclinic instability process, perhaps induced by wind tweaking or by some other mechanism, which may be investigated by considering the works of Pedlosky (1971) and Orlanski (1969). This instability, most likely baroclinic in nature because of the fact that the shingles generally orient themselves to the southwest as they erupt out of the Stream, can occur as a growing perturbation on the order of several days to nearly several weeks in frequency, grow and orient themselves west to south west, become sheared off from the Gulf Stream, finally detach and dissipate on the shelf or become reentrained in the Stream.

Topographic lee waves would be characterized by appearing to be stationary, but they presumably could propagate due to alongshore variations in the cross-slope bottom topography, of which there are a considerable number in the region of the Carolina Capes, also due to the temporal variability of the mean flow, i.e. the importance of U_t in the momentum balance and also that the steady barotropic wave may be inherently unstable and consequently undergo temporal variations related to a propagation in space.

Dr. R. Legeckis (NOAA/NESS) has kindly supplied this author with a space-time history representation of the GSF. This characterization is shown in Figure 22 and seems to indicate a downstream propagation of wave/shingle like features at rates the order of 25-75 km/day. Such analyses may be of invaluable worth in aiding our understanding of the Gulf Stream influence on the continental shelf in the South Atlantic Bight.

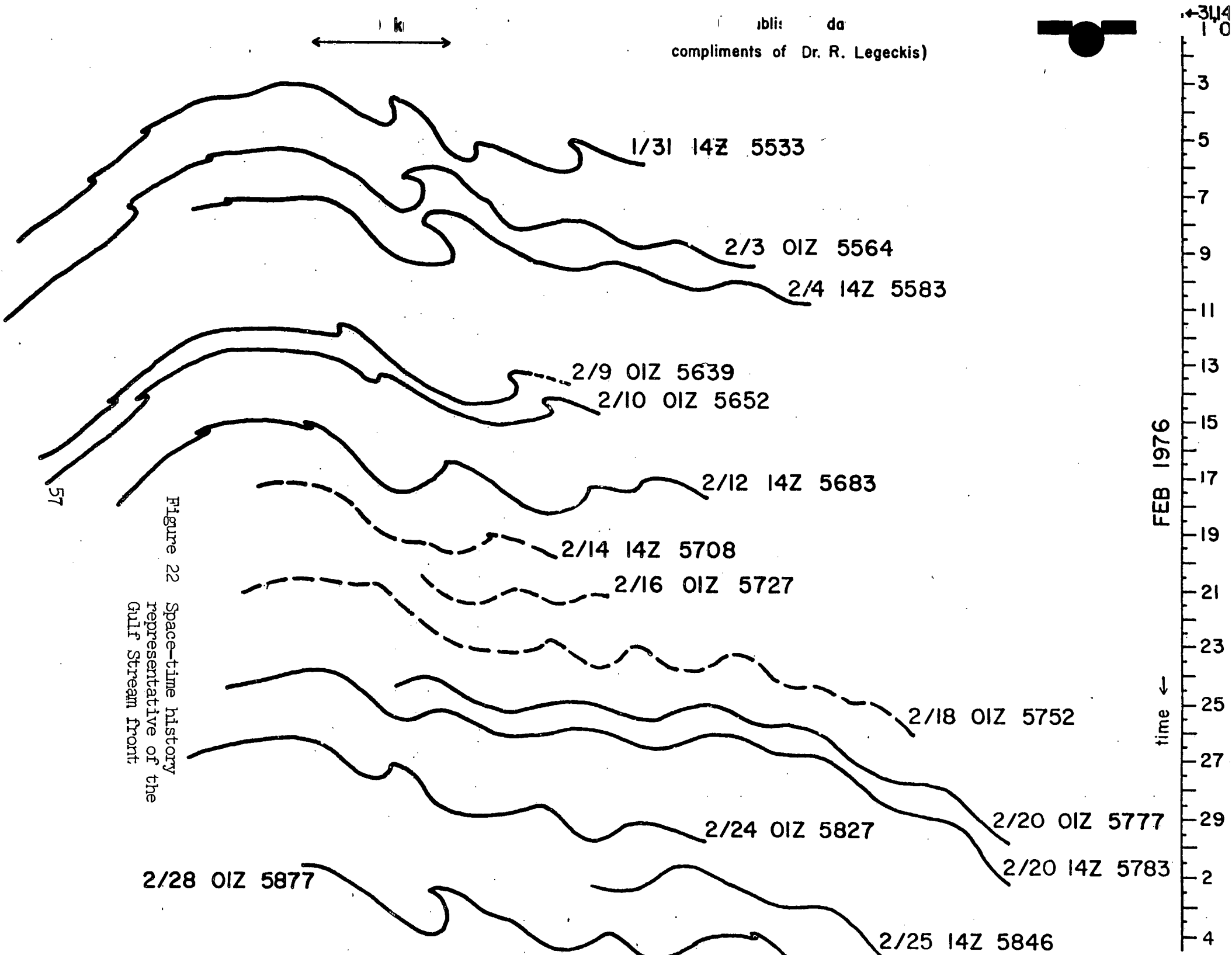

Figure 22 Space-time history representative of the Gulf Stream front

A time series of VHRR imagery of the Southeastern U. S. continental margin and ocean waters, extending from 7-18 April, 1977 (supplied by Dr. R. Legeckis, NOAA/NESS), as well as other spot imagery indicate waves of the order of 140-200 kilometers in length and with crest to trough amplitudes of 10 to 75 kilometers propagating (10-75 km/day) downstream of, and seemingly stemming from, the Charleston Bump. A seemingly permanent eastward meander of the Gulf Stream in the downstream vicinity of the Bump indicates a deflection of the order of 50-75 kilometers.

It is of note herein that the Pietrafesa-Janowitz model results predict a deflection of 50-75 kilometers and downstream waves with lengths the order of 160 to 200 km.

It is of additional note that temperature data obtained from NODC (T.B. Curtin, personnal communication) indicate that there is a deflection in the T data southeast of Charleston from the surface down to at least 50 meters (eg. Figures 23 - 24). These data further suggest that this deflection is present the entire year but has its largest amplitude during the fall (Figure 25 - Curtin, 1978), probably reflecting the decrease in transport during this season (Fuglister, 1951; Iselin, 1940). This T data is entirely consistent with the Pietrafesa-Janowitz "Charleston" bump model presented.

Hydrographic surveys in the Carolina Capes region planned for Spring, Summer and Fall, 1978 will hopefully result in the quasisynoptic mapping of several of these events, whereby we may be able to determine definitevely whether the eruptions are baroclinic instabilities or not. The surveys will be conducted when the ocean is visible to the VHRR so that we may intercompare our ground truth to the VHRR imagery. March/April/May, are months

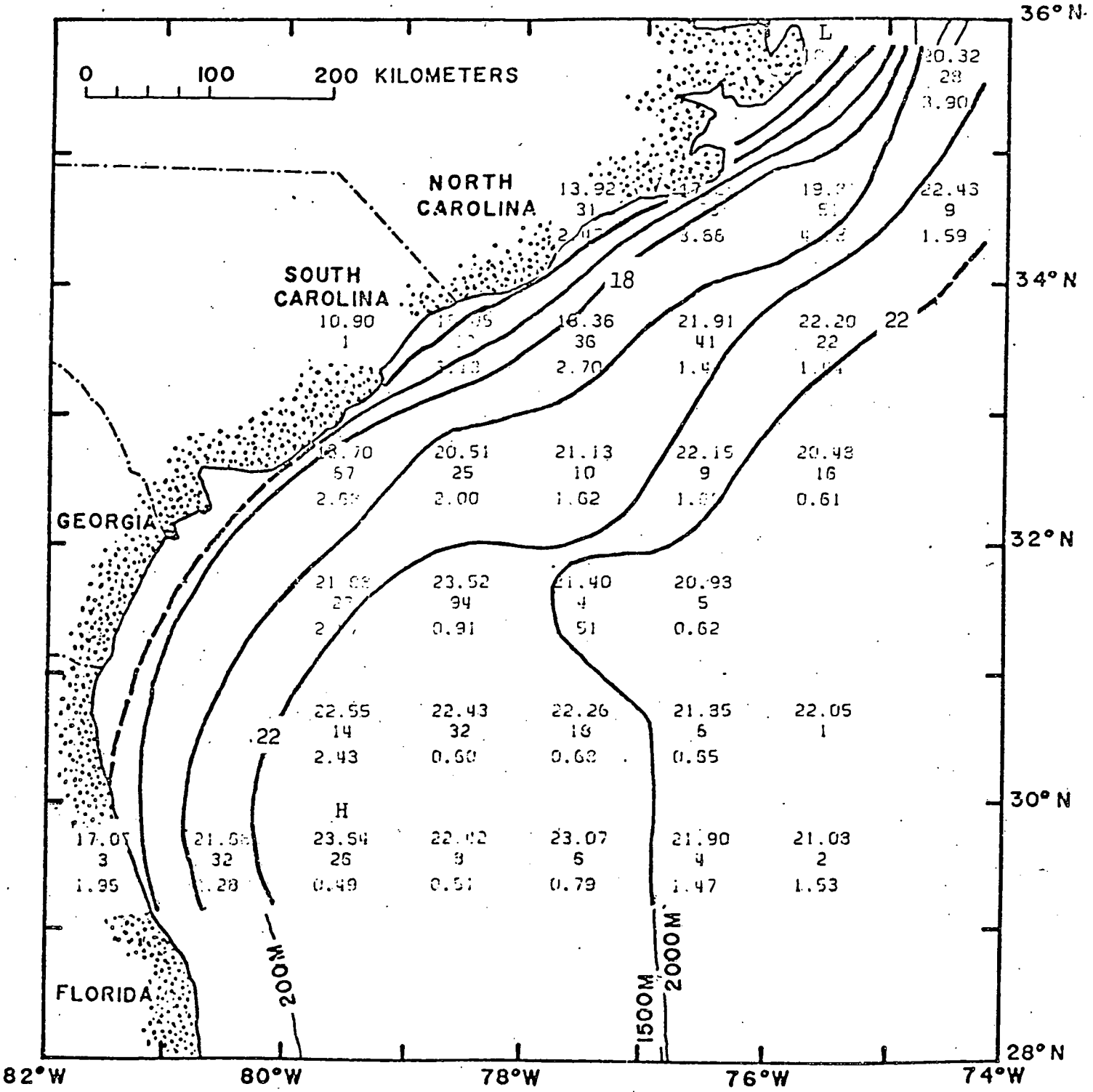

Figure 23 South Atlantic Bight average surface temperature, Jan.-March (NODC)

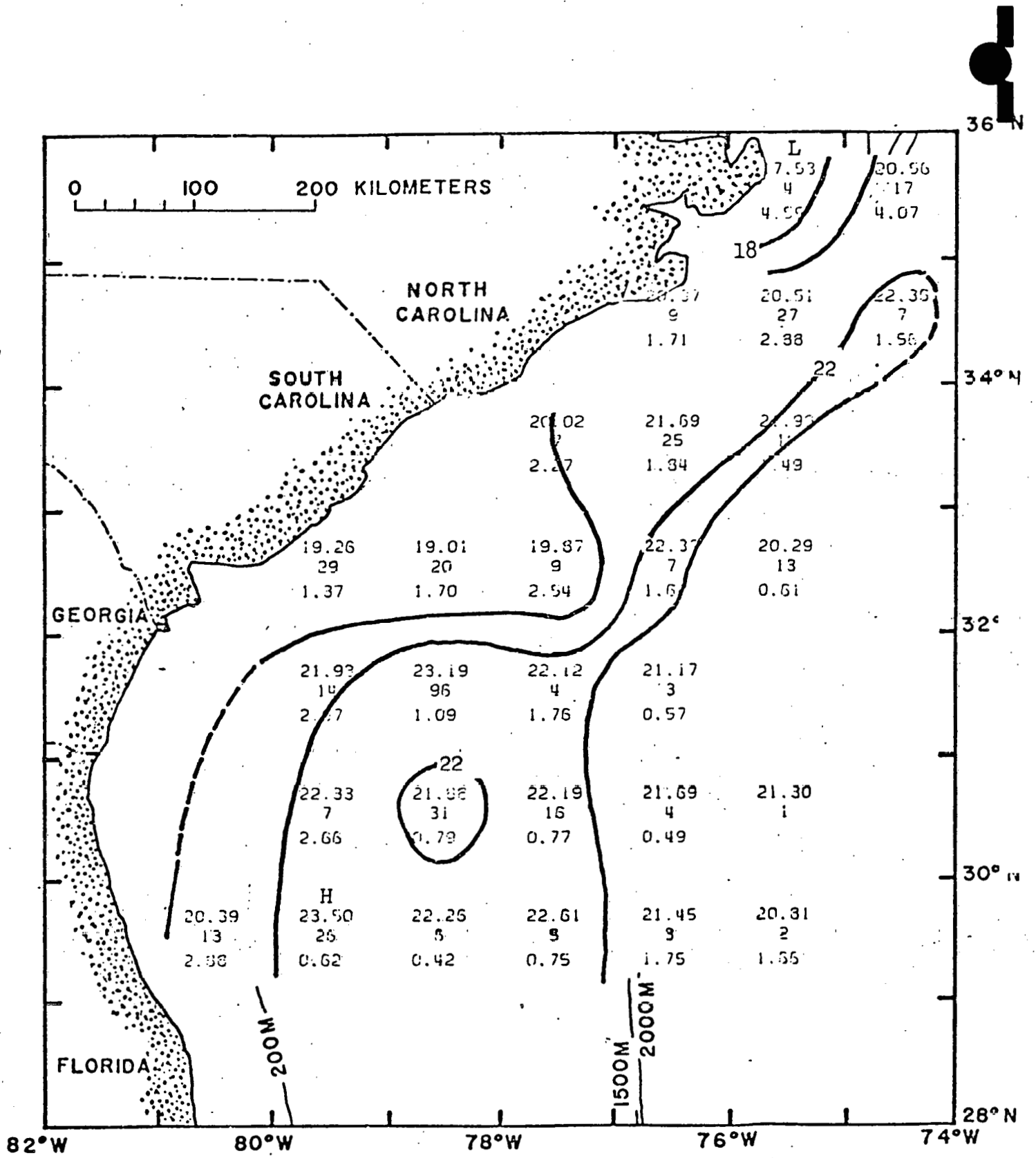

Figure 24 South Atlantic Bight average temperature at 50m, Jan.-Mar. (NODC)

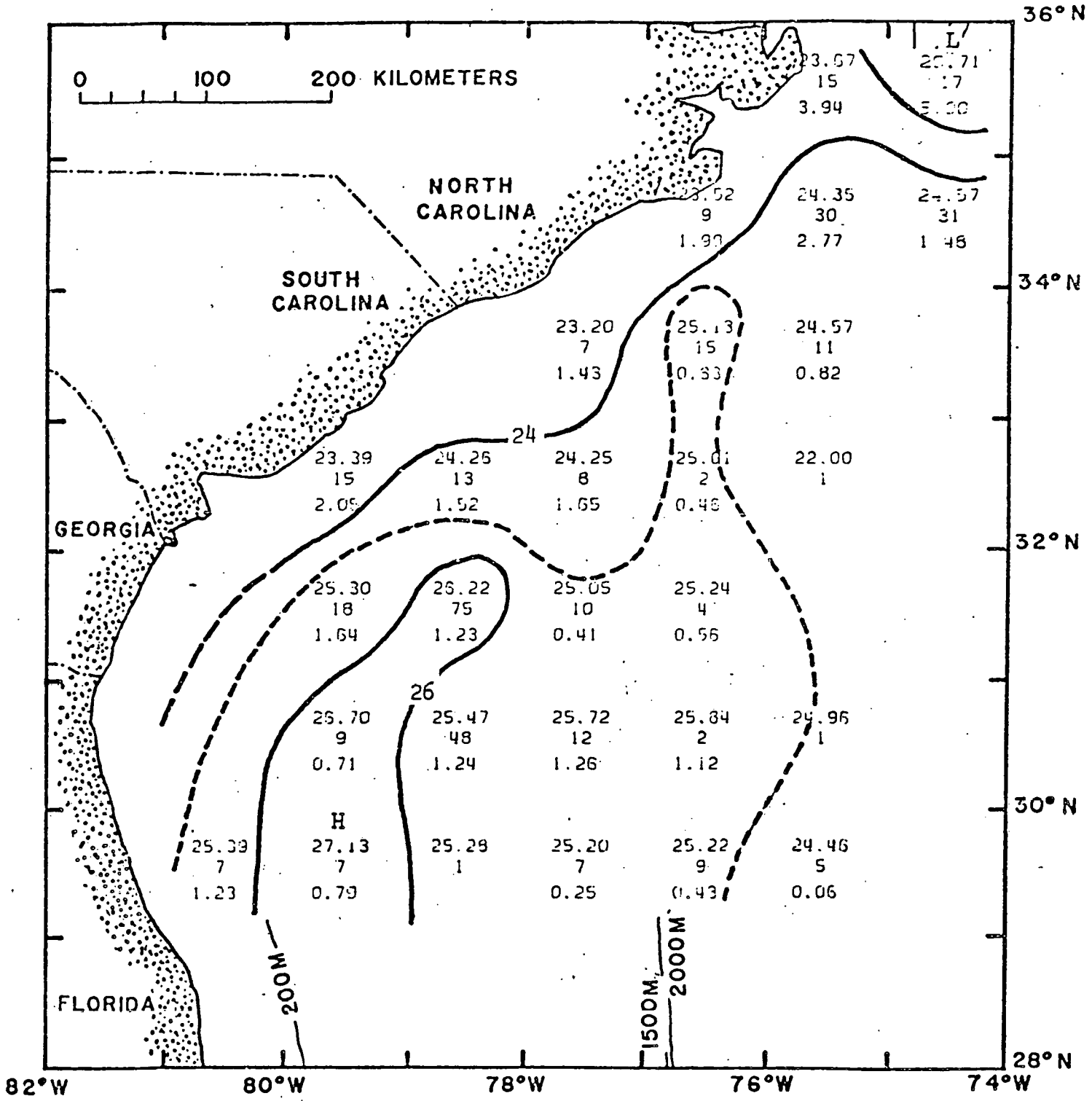

Figure 25 South Atlantic Bight average temperature at 50m, Oct.-Dec. (NODC)

when the ocean surface has been visible in the past, so that it is planned to conduct the described hydro survey during a mooring retrieval-deployment cruise during March-May, 1978.

This scenario of possibilities may well describe a series of mechanisms which lead to a flushing of the shelf waters, in the Carolina Capes region, as well as a continual pumping of the shelf with new, fresh supplies of larvae and nutrients.

So rests the case for topographically generated downstream-of-the-"Bump"-waves and subsequent-eruptions.

Hydrography of a Gulf Stream Spin-off Filament; 19-21 April, 1977

As previously indicated in this part of the report, the Gulf Stream occasionally sheds filaments, along it's western wall, onto the continental margin in the South Atlantic Bight. The actual mechanism(s) which produce these eruptions is strictly speculative at this time, but we are beginning to gain an appreciation for the frequency and size of these events through satellite imagery, moored current meter observations and through fortuitous hydrographic mapping of an event or events.

During the period 18-22 April, 1977 a current meter retrieval cruise was conducted by NCSU in the region of the Carolina Capes (under DOE funding). At that time, a hydrographic survey was conducted (in the hope that an eruption event would be present) as part of our normal routine. Fortuitously, we were able to map one of these Stream shed events using our hydro gear, including a Sippican XBT, a Guidline CTD, a Plessey STD and a Plessey Thermosalinograph. The event which we mapped, as shown in Figures 26 - 49 was also observed by the Naval Oceanographic Office in its Experimental Ocean Frontal Analysis (EOFA) products (cf. Figures 50 - 51), complements of Mr. R. Perchall and by NOAA/NESS, in the previously discussed time series (Figures 2 - 7). This latter time series also includes an event south of the Charleston Bump, which was mapped by Atkinson (SKIO) and Lee (UM) as part of the DOE work.

From the T, S data one can see that the event was of a size of the order of 150 km x 50 km in the horizontal and at least 200m in vertical extent. A general feature throughout the axis, center of the filament is a salty, warm lense of water near the surface and a doming up of isotherms from the bottom up as is conceptualized in classical models of stratified, cyclonic, warm core eddies. A point herein is to suggest that these events are not eddies in the conventional sense; they are best referred to as "spin off-events" or "filament eruptions". In any case, it is obvious that these events are biologically important on the continental shelf in so far as they not only transport larve-laden, nutrient rich Gulf Stream waters onto the continental shelf, but they also pump the nutrients and larvae up into the upper portion of the water column, the "doming-up" effect and the frequency of their occurence insures the biological community of a continual supply of nutrients. The Menhaden fish may well be an end result of a food chain process which begins with the onset of a spin-off event and thrives on reoccurences of the same.

Another consequence of these events, in concert with the mechanical forcing of the wind, is that they displace resident shelf waters, which are often entrained into the Gulf Stream on the southeasterly side or offshore edge of the spin off event. As discussed earlier, this entrainment of shelf waters serves to flush the shelf of mature, nutrient depleted resident shelf waters and replace the void with Gulf Stream garden delights.

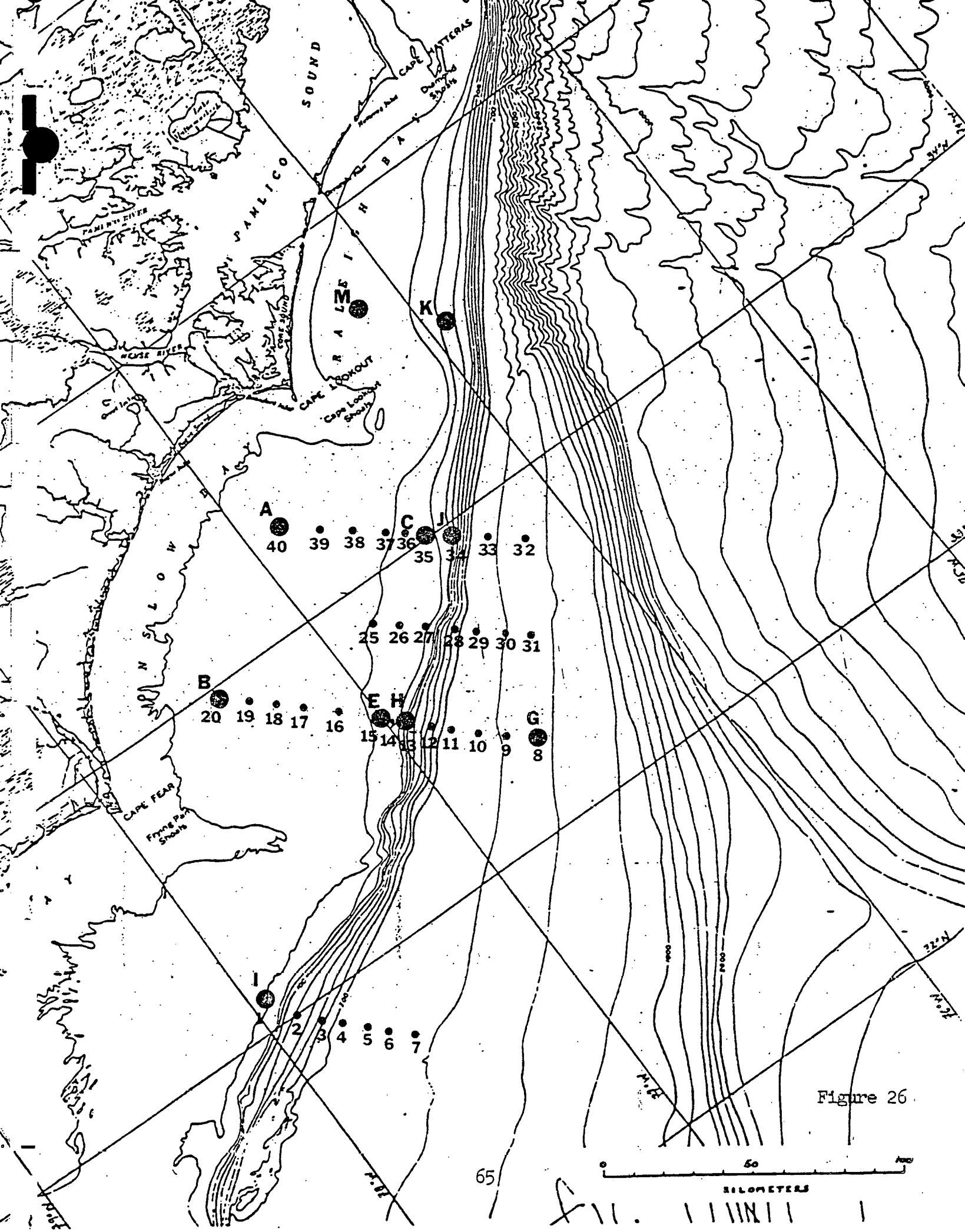
PAMLICO SOUND
CAPE HATTERAS
Diamond Shoals
RALEIGH BAY
PAMLICO RIVER
NEUSE RIVER
CAPE LOOKOUT
Cape Lookout Shoals
LOW BAY
CAPE FEAR
Frying Pan Shoals
A
B
C
E
G
H
I
J
K
M
40 39 38 37 36 35 34 33 32
25 26 27 28 29 30 31
20 19 18 17 16 15 14 13 12 11 10 9 8
1 2 3 4 5 6 7
0 50 100
KILOMETERS

Figure 26

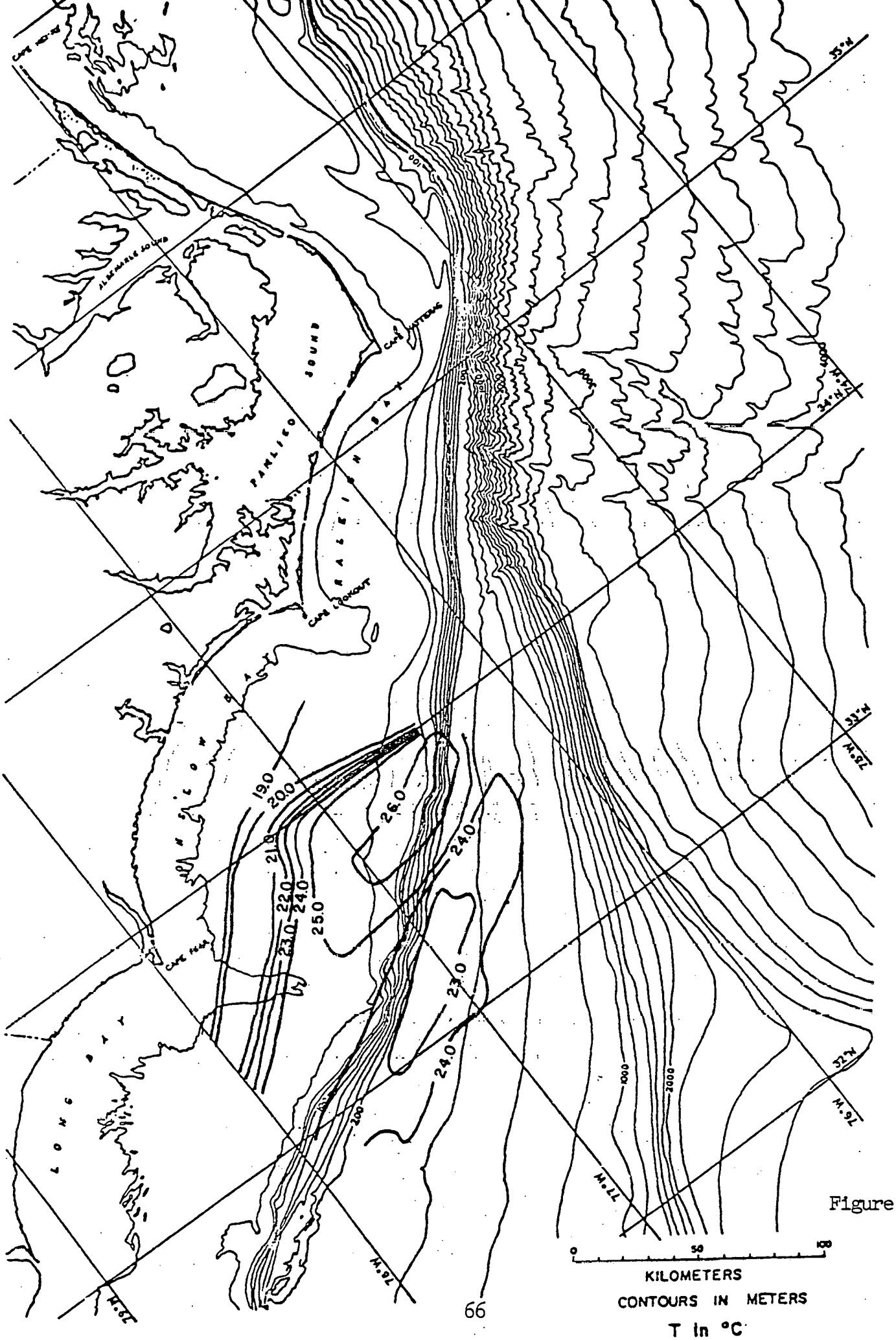
CAPE HENRY
ALBEMARLE SOUND
PAMLICO SOUND
CAPE HATTERAS
CAPE LOOKOUT
CAPE FEAR
LONG BAY
19.0
20.0
21.0
22.0
23.0
24.0
25.0
26.0
24.0
23.0
24.0
100
200
1000
2000
35°N
34°N
33°N
32°N
78°W
77°W
76°W
0
50
100
KILOMETERS
CONTOURS IN METERS
T in °C

Figure 27

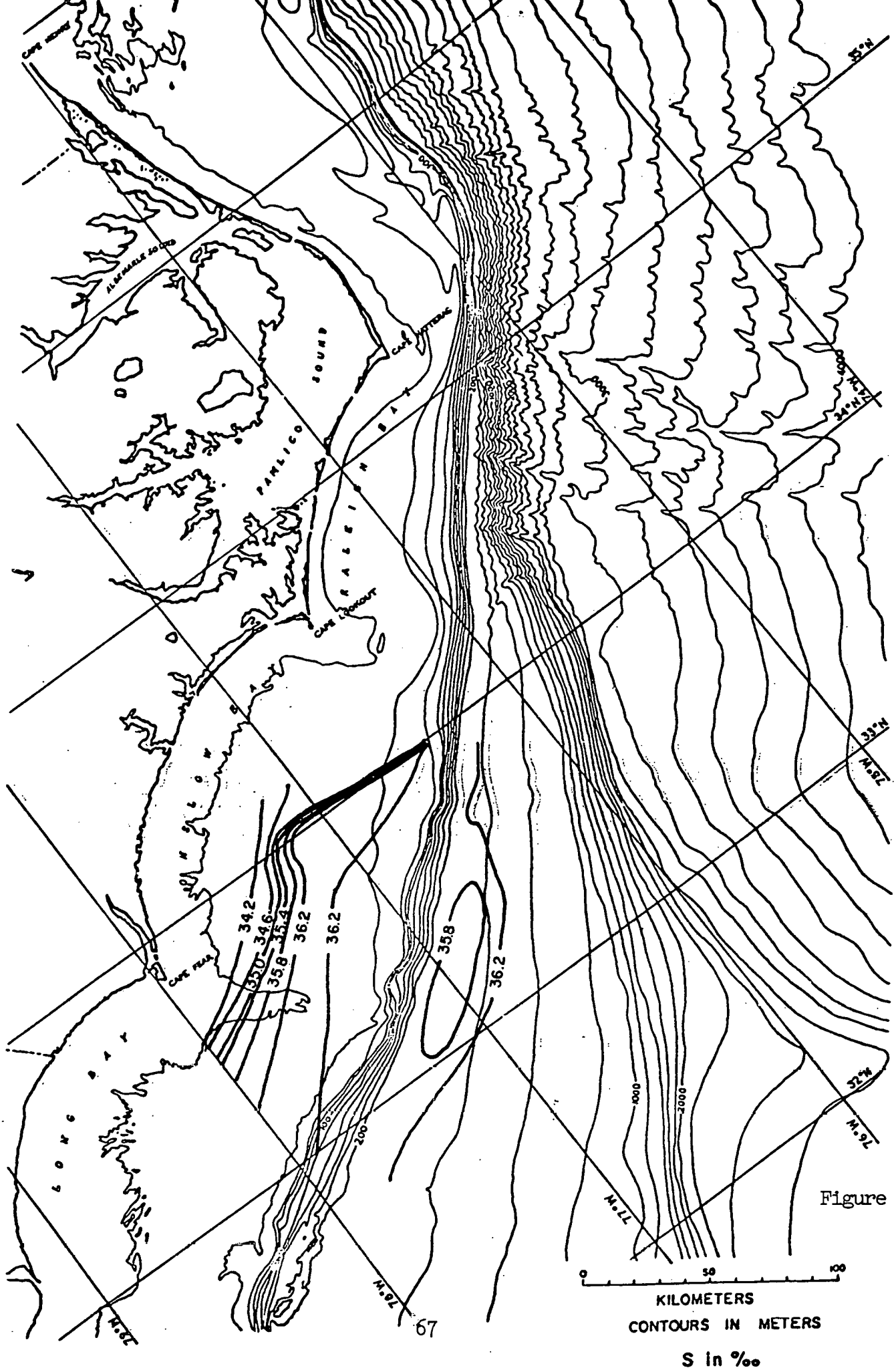
CAPE HENRY
ALBEMARLE SOUND
PAMLICO SOUND
CAPE HATTERAS
CAPE LOOKOUT
CAPE FEAR
LONG BAY
34.2
34.6
35.0
35.4
35.8
36.2
36.2
35.8
36.2
200
1000
2000
35°N
34°N
33°N
32°N
78°W
76°W
77°W
76°W
0
50
100
KILOMETERS
CONTOURS IN METERS
S in ‰

Figure 28

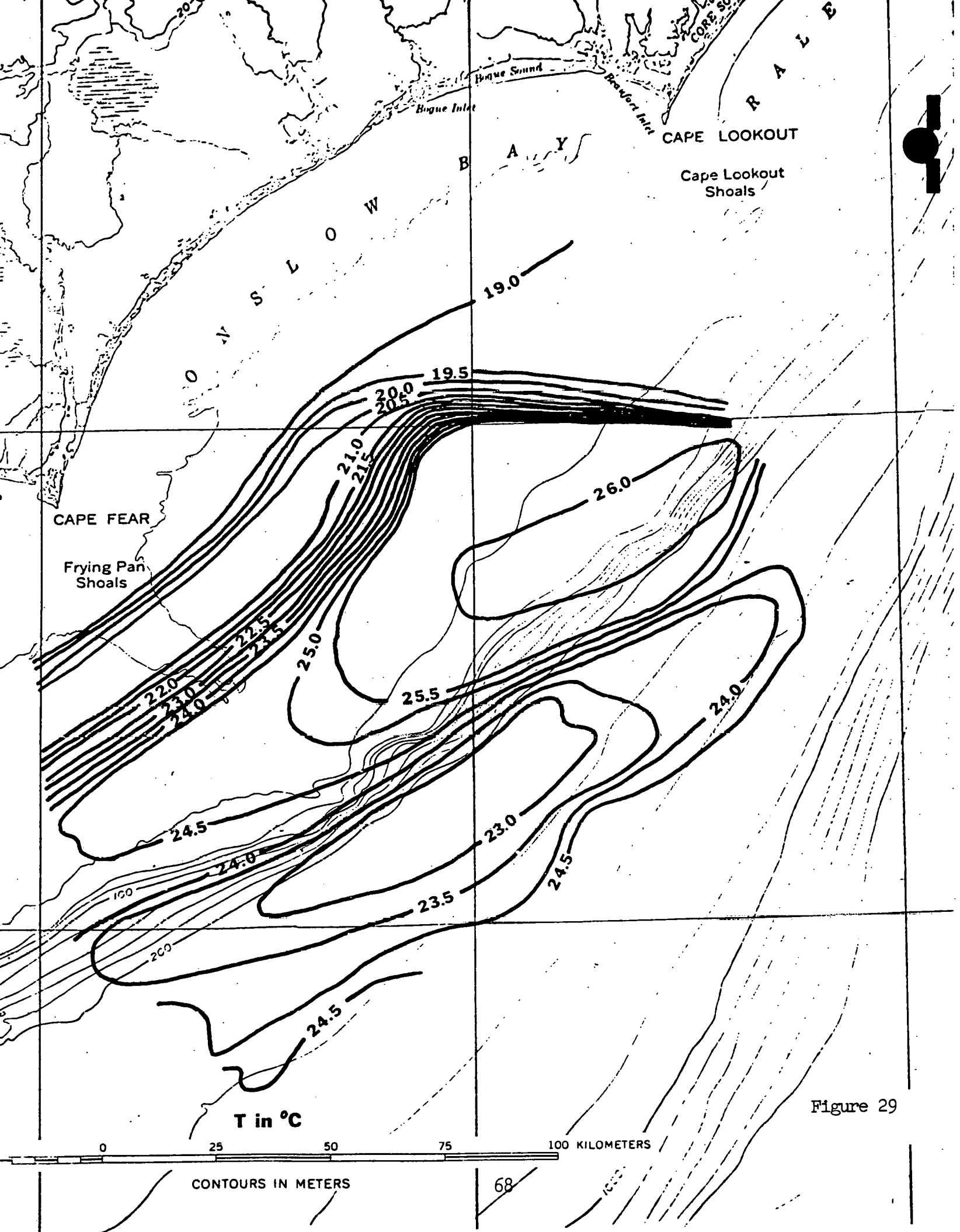
Bogue Sound
Bogue Inlet
Beaufort Inlet
CORE SOUND
CAPE LOOKOUT
Cape Lookout Shoals
ONSLOW BAY
CAPE FEAR
Frying Pan Shoals
19.0
19.5
20.0
20.5
21.0
21.5
22.0
22.5
23.0
23.5
24.0
24.5
25.0
25.5
26.0
100
200
T in °C
0
25
50
75
100 KILOMETERS
CONTOURS IN METERS

Figure 29

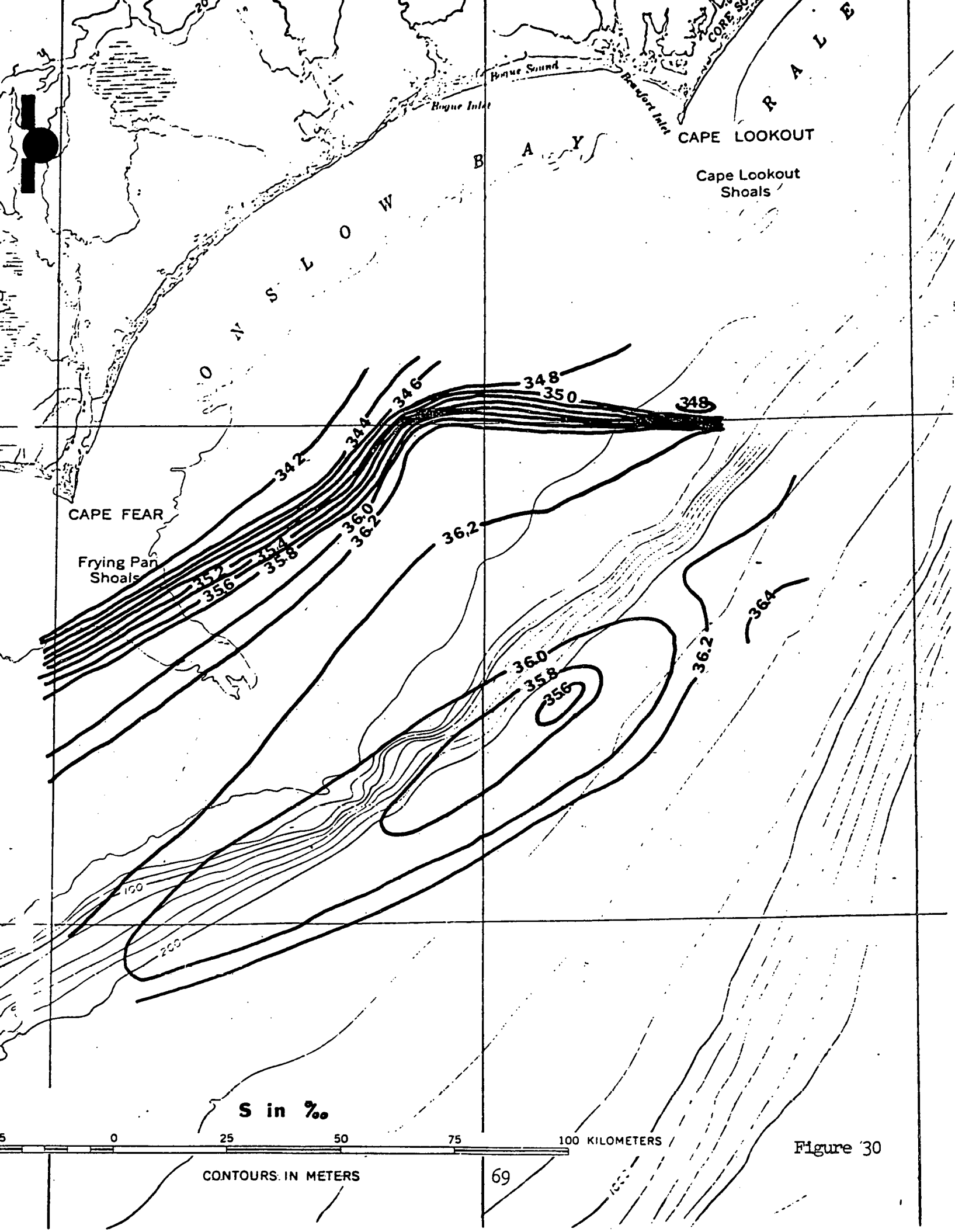
Bogue Sound
Bogue Inlet
Beaufort Inlet
CORE SO
CAPE LOOKOUT
Cape Lookout Shoals
ONSLOW BAY
CAPE FEAR
Frying Pan Shoals
34.2
34.4
34.6
34.8
35.0
34.8
35.2
35.4
35.6
35.8
36.0
36.2
36.2
36.4
36.0
35.8
35.6
36.2
100
200
S in ‰
0
25
50
75
100 KILOMETERS
CONTOURS IN METERS

Figure 30

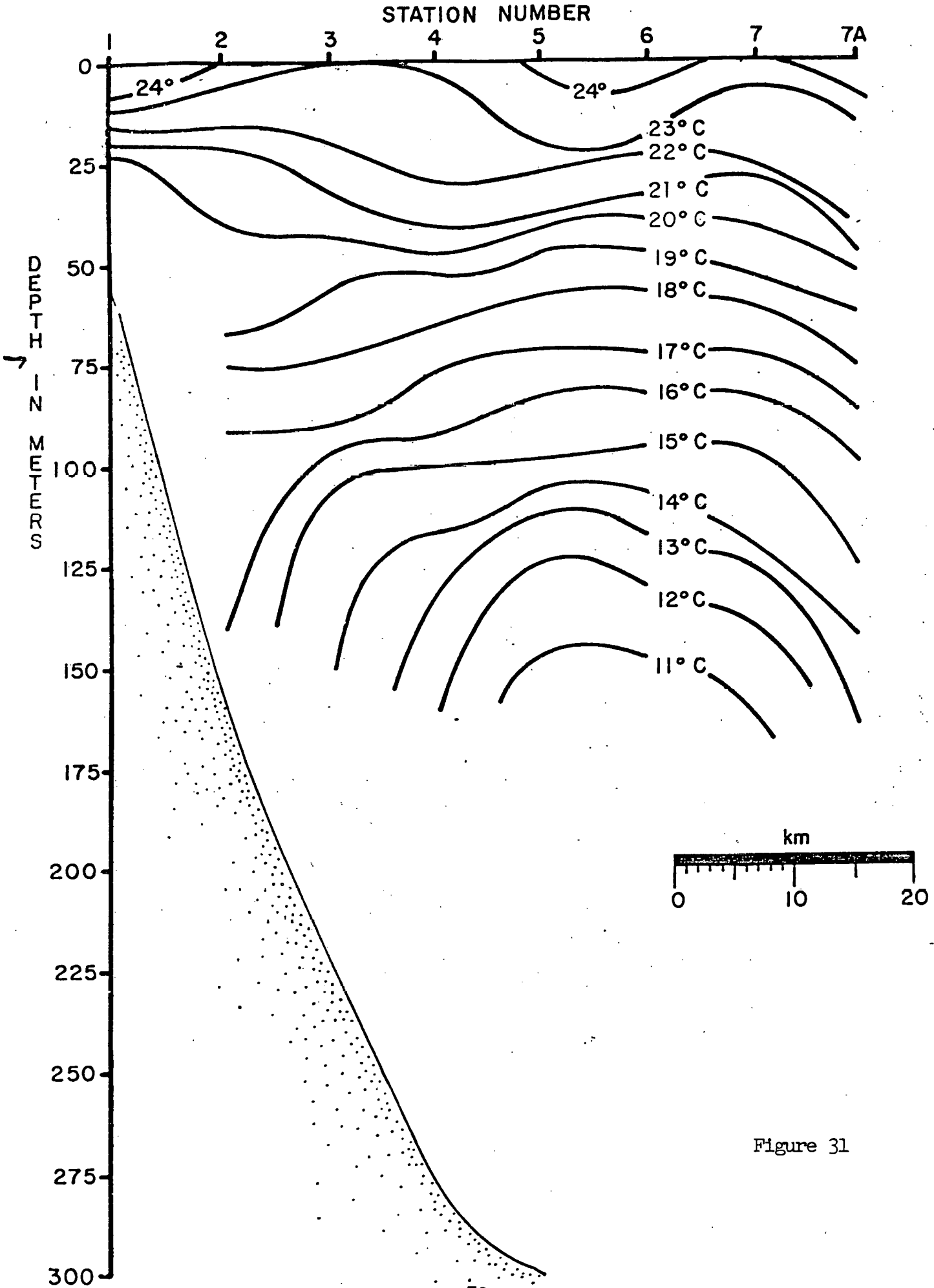
STATION NUMBER
1
2
3
4
5
6
7
7A
DEPTH IN METERS
0
25
50
75
100
125
150
175
200
225
250
275
300
24°
24°
23° C
22° C
21° C
20° C
19° C
18° C
17° C
16° C
15° C
14° C
13° C
12° C
11° C
km
0
10
20

Figure 31

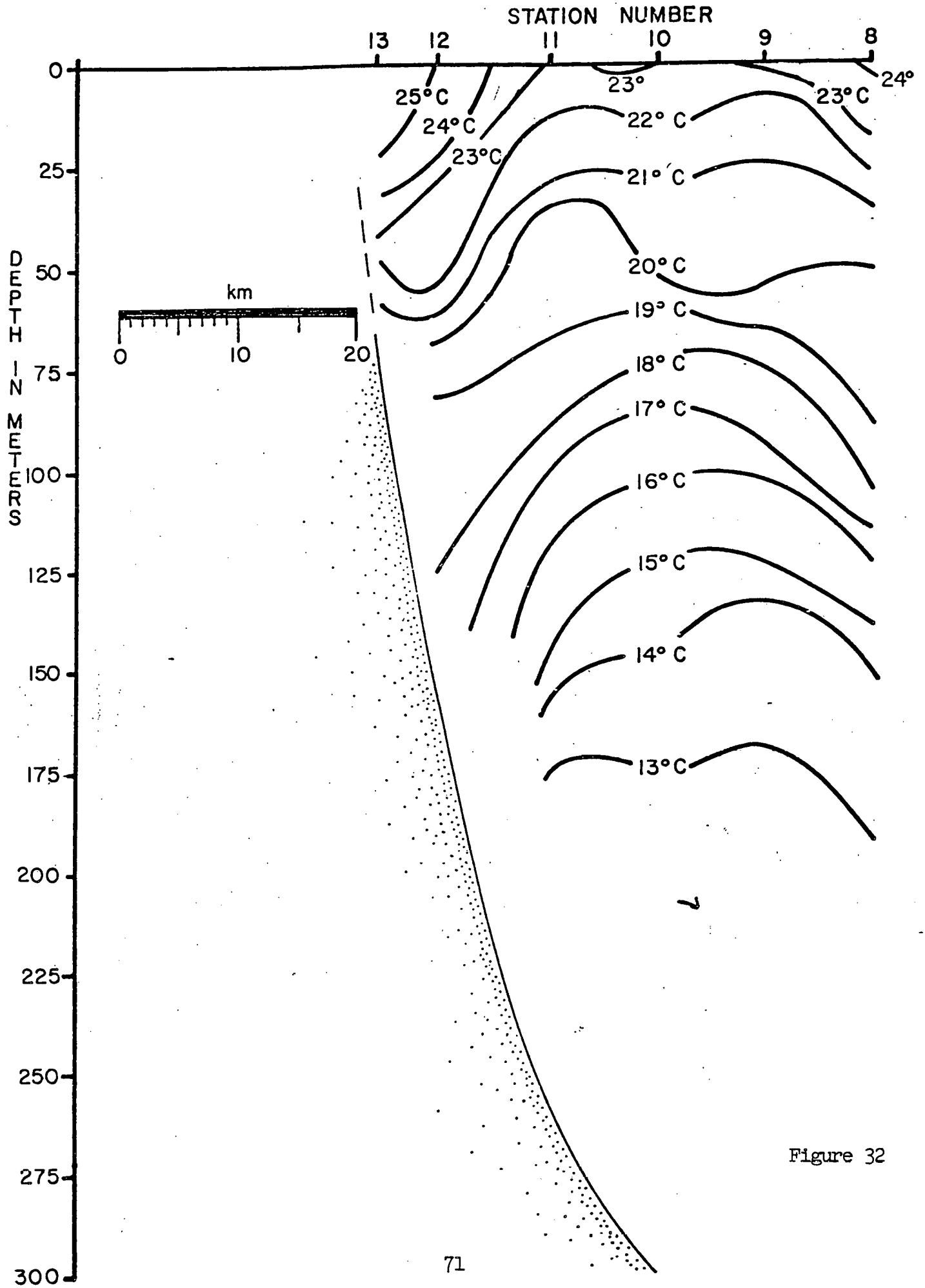
STATION NUMBER
13
12
11
10
9
8
DEPTH IN METERS
0
25
50
75
100
125
150
175
200
225
250
275
300
km
0
10
20
25°C
24°C
23°C
23°
22° C
21° C
20° C
19° C
18° C
17° C
16° C
15° C
14° C
13° C
23° C
24°

Figure 32

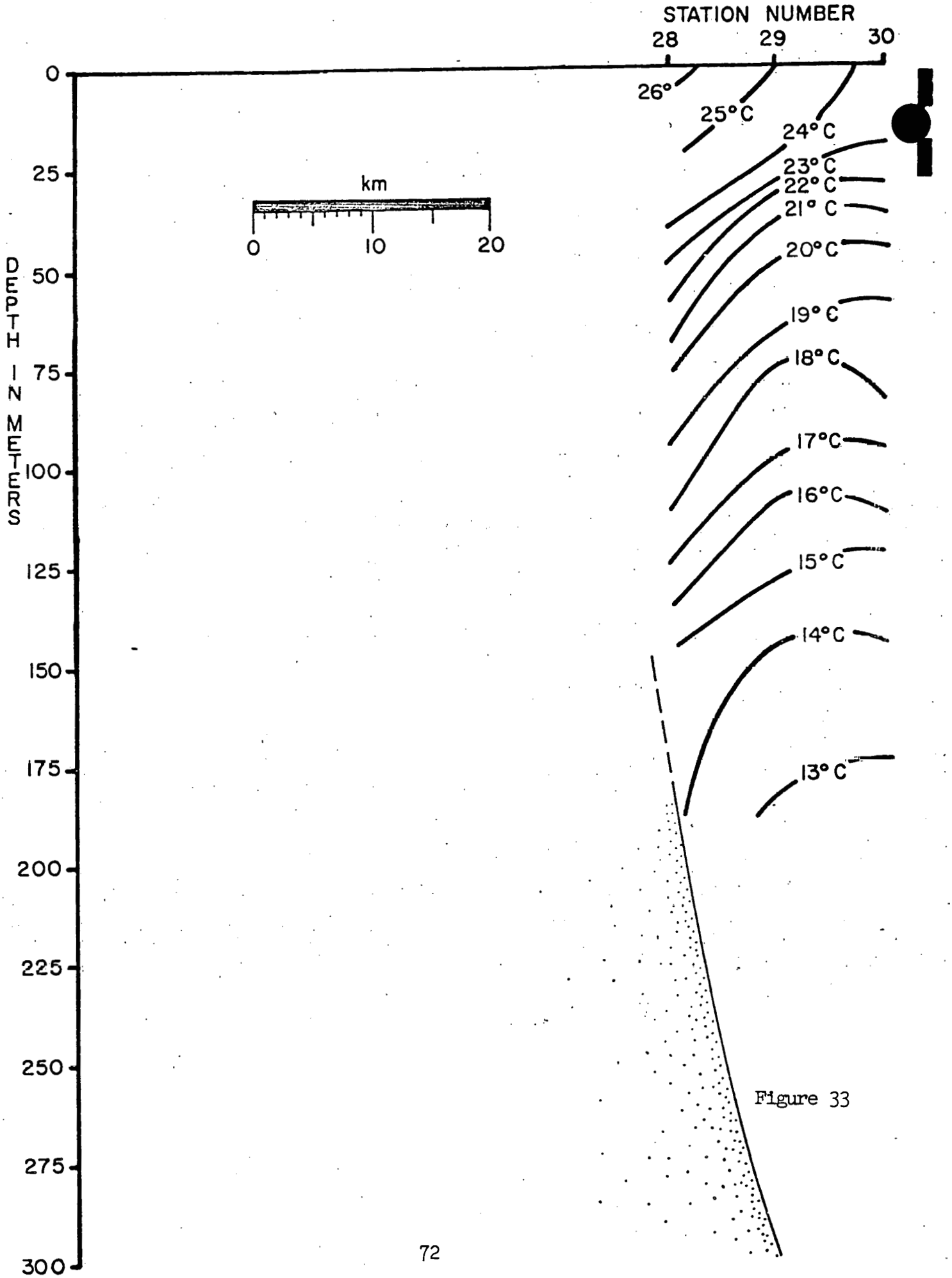
STATION NUMBER
28
29
30
26°
25°C
24°C
23°C
22°C
21° C
20°C
19° C
18° C
17°C
16°C
15° C
14°C
13° C
km
0
10
20
DEPTH IN METERS
0
25
50
75
100
125
150
175
200
225
250
275
300

Figure 33

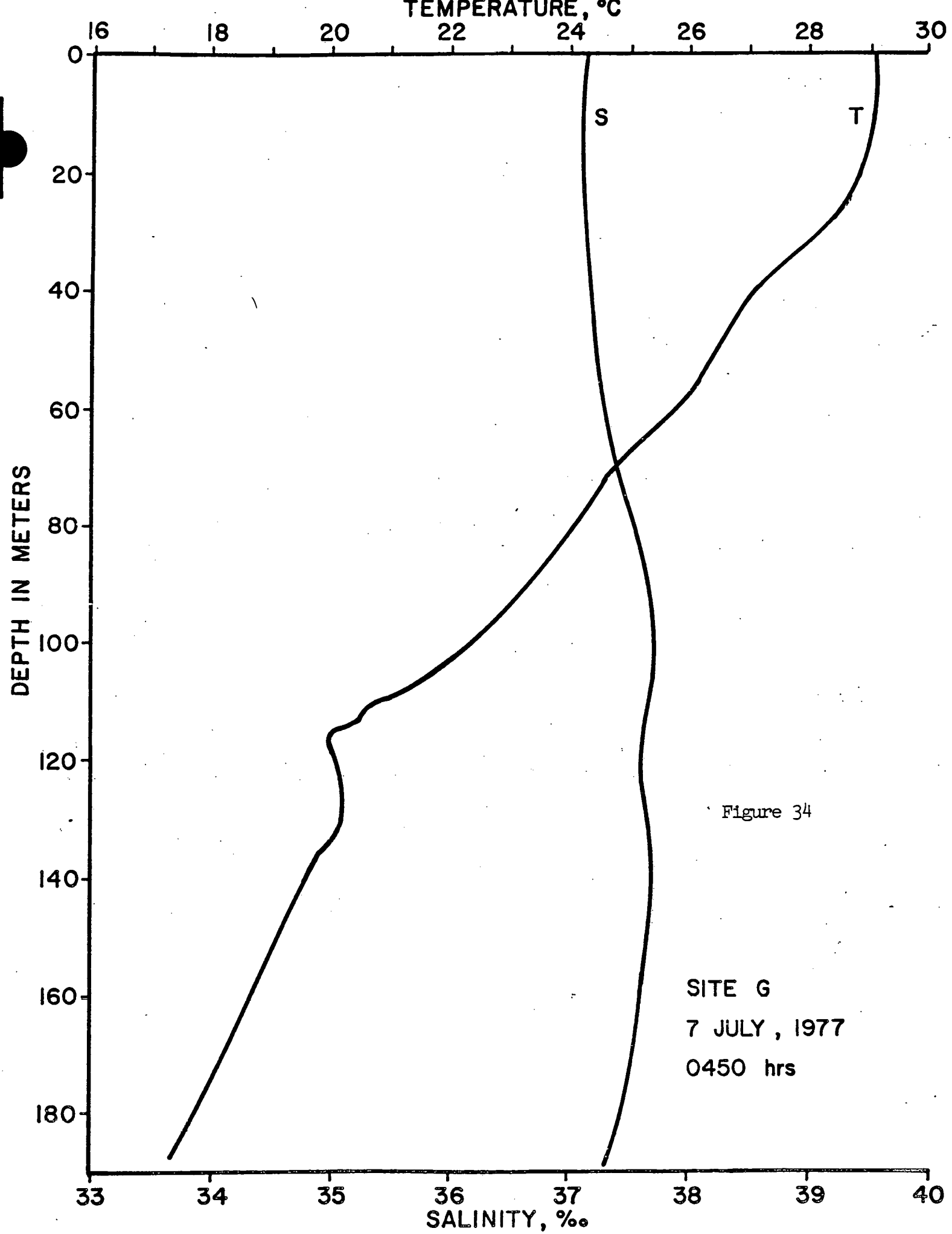
TEMPERATURE, °C
16
18
20
22
24
26
28
30
0
20
40
60
80
100
120
140
160
180
DEPTH IN METERS
S
T
SITE G
7 JULY, 1977
0450 hrs
33
34
35
36
37
38
39
40
SALINITY, ‰

Figure 34

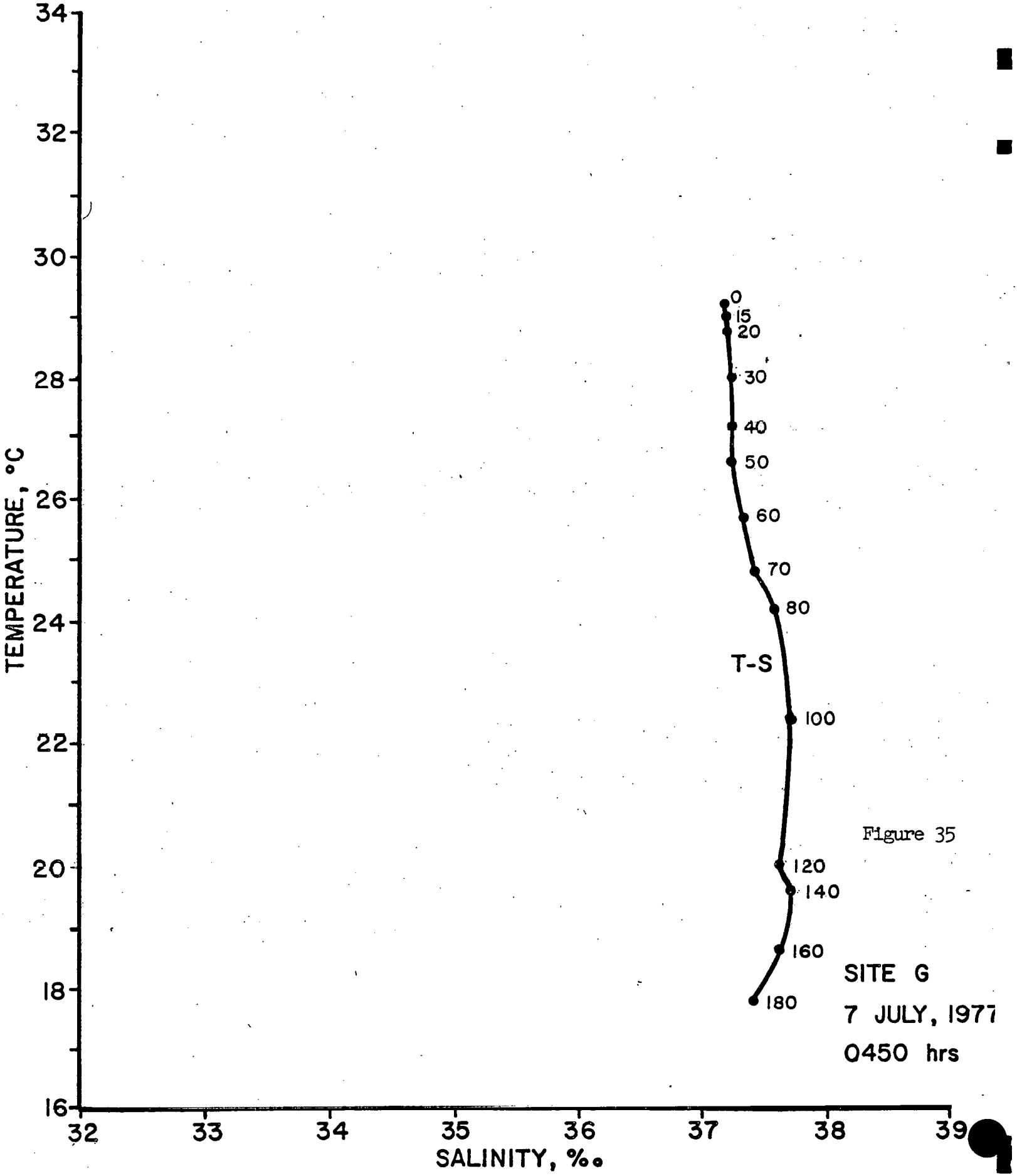
TEMPERATURE, °C
SALINITY, ‰
T-S
0
15
20
30
40
50
60
70
80
100
120
140
160
180
SITE G
7 JULY, 1977
0450 hrs

Figure 35

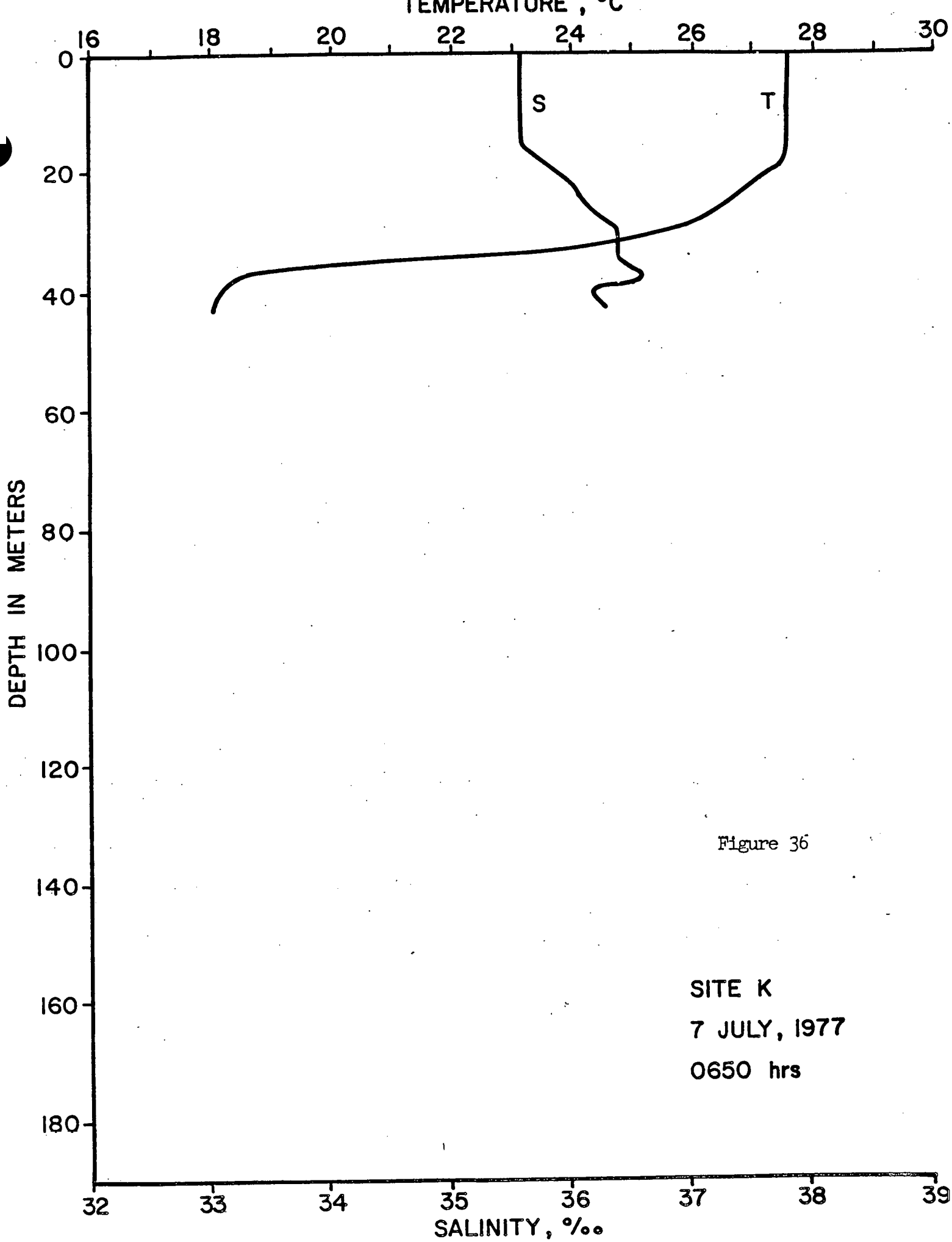
TEMPERATURE, °C
16
18
20
22
24
26
28
30
S
T
DEPTH IN METERS
0
20
40
60
80
100
120
140
160
180
SITE K
7 JULY, 1977
0650 hrs
32
33
34
35
36
37
38
39
SALINITY, ‰

Figure 36

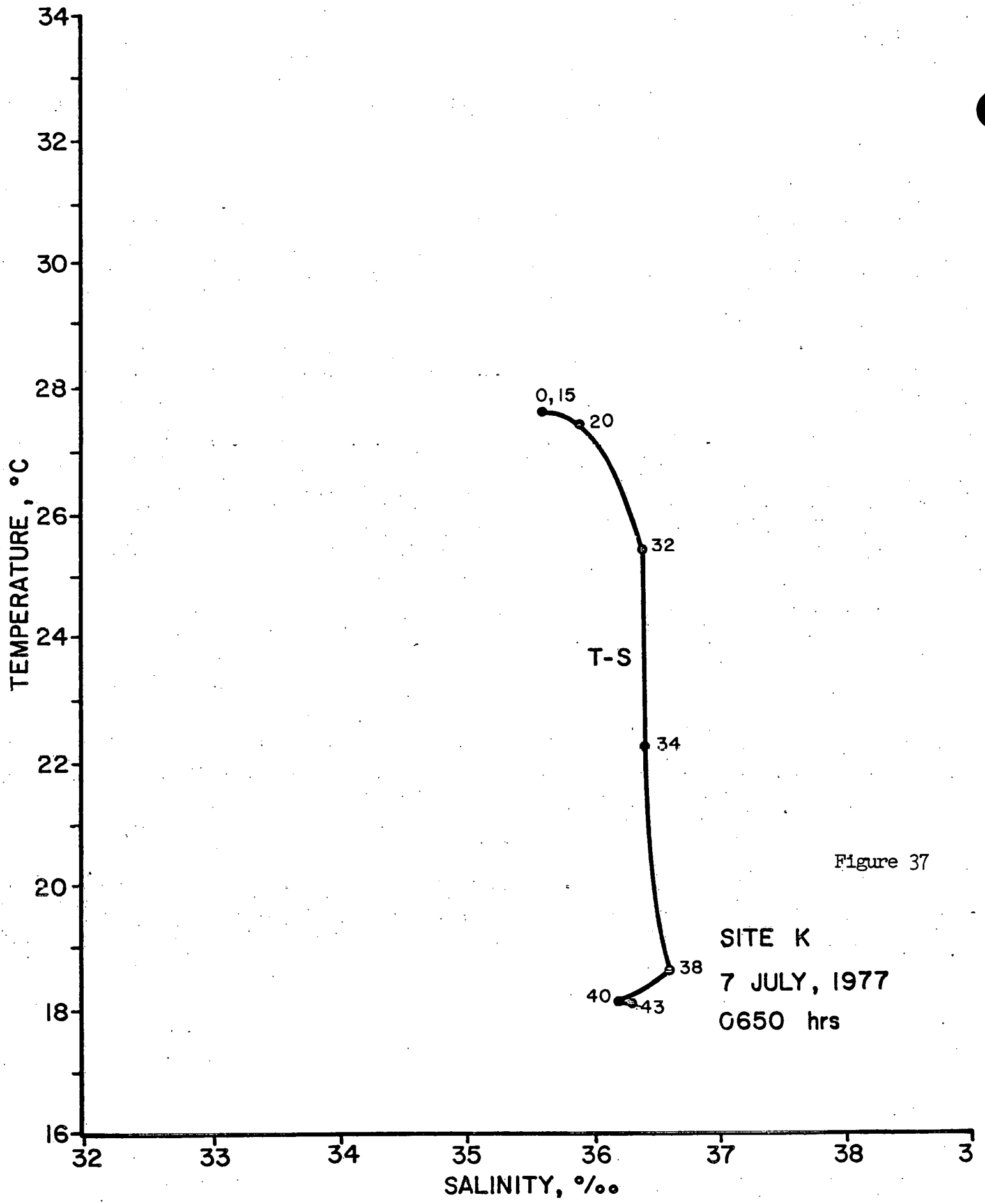
34
32
30
28
26
24
22
20
18
16
TEMPERATURE, °C
32
33
34
35
36
37
38
3
SALINITY, ‰
0,15
20
32
T-S
34
38
40
43
SITE K
7 JULY, 1977
0650 hrs

Figure 37

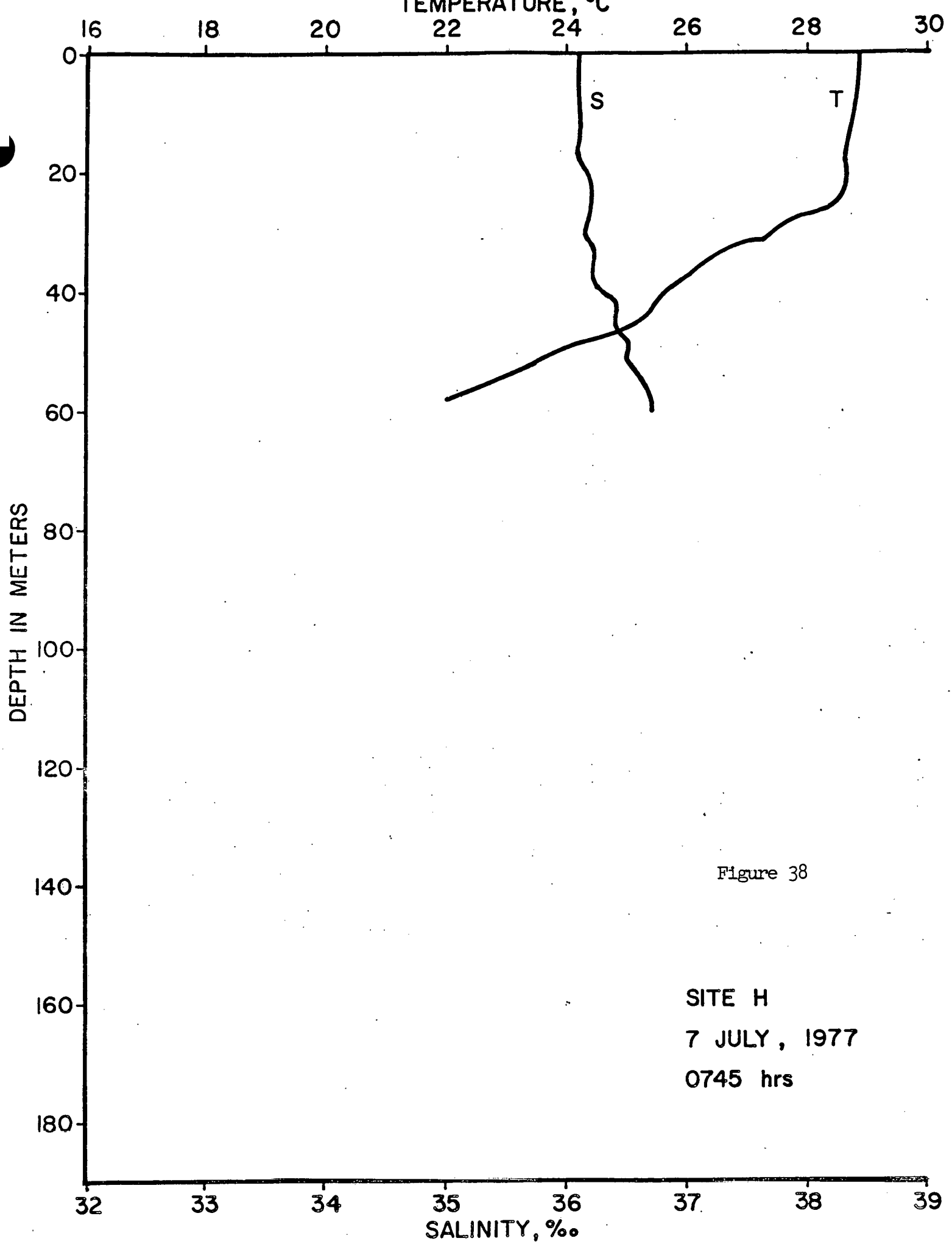
TEMPERATURE, °C
16
18
20
22
24
26
28
30
S
T
DEPTH IN METERS
0
20
40
60
80
100
120
140
160
180
SITE H
7 JULY, 1977
0745 hrs
32
33
34
35
36
37
38
39
SALINITY, ‰

Figure 38

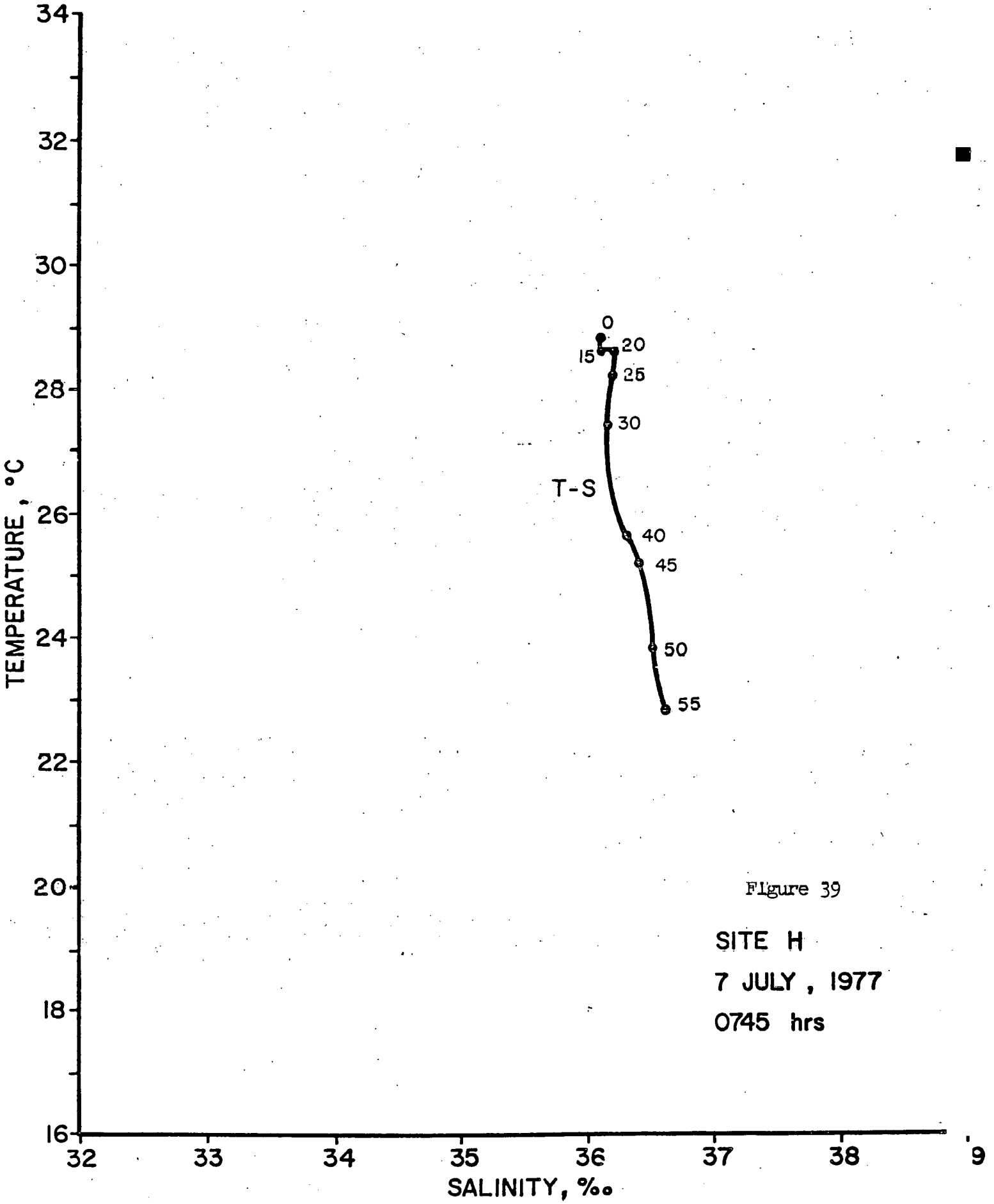
34
32
30
28
26
24
22
20
18
16
TEMPERATURE, °C
32
33
34
35
36
37
38
9
SALINITY, ‰
0
15
20
25
30
T-S
40
45
50
55
SITE H
7 JULY, 1977
0745 hrs

Figure 39

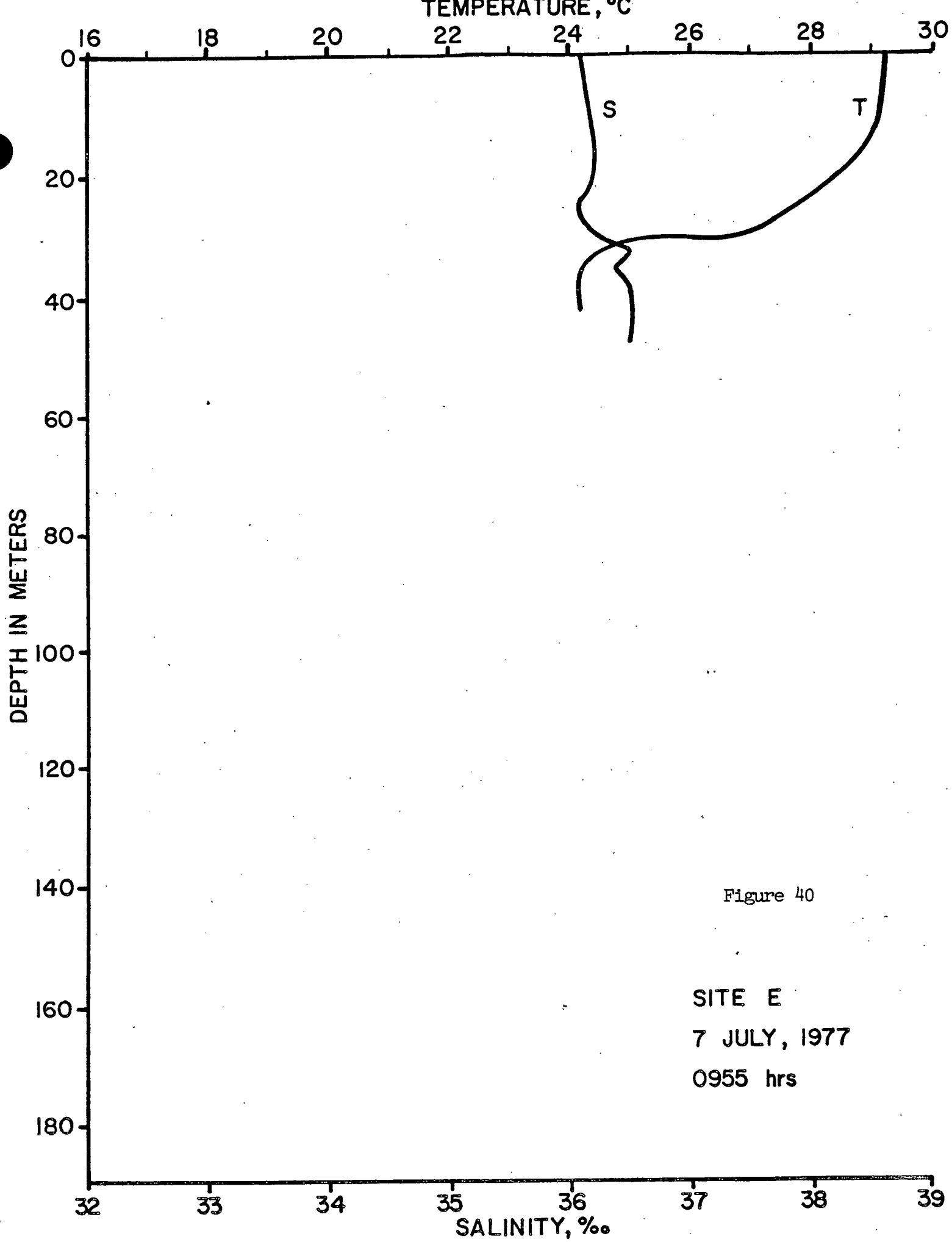
TEMPERATURE, °C
16
18
20
22
24
26
28
30
0
20
40
60
80
100
120
140
160
180
DEPTH IN METERS
S
T
32
33
34
35
36
37
38
39
SALINITY, ‰
SITE E
7 JULY, 1977
0955 hrs

Figure 40

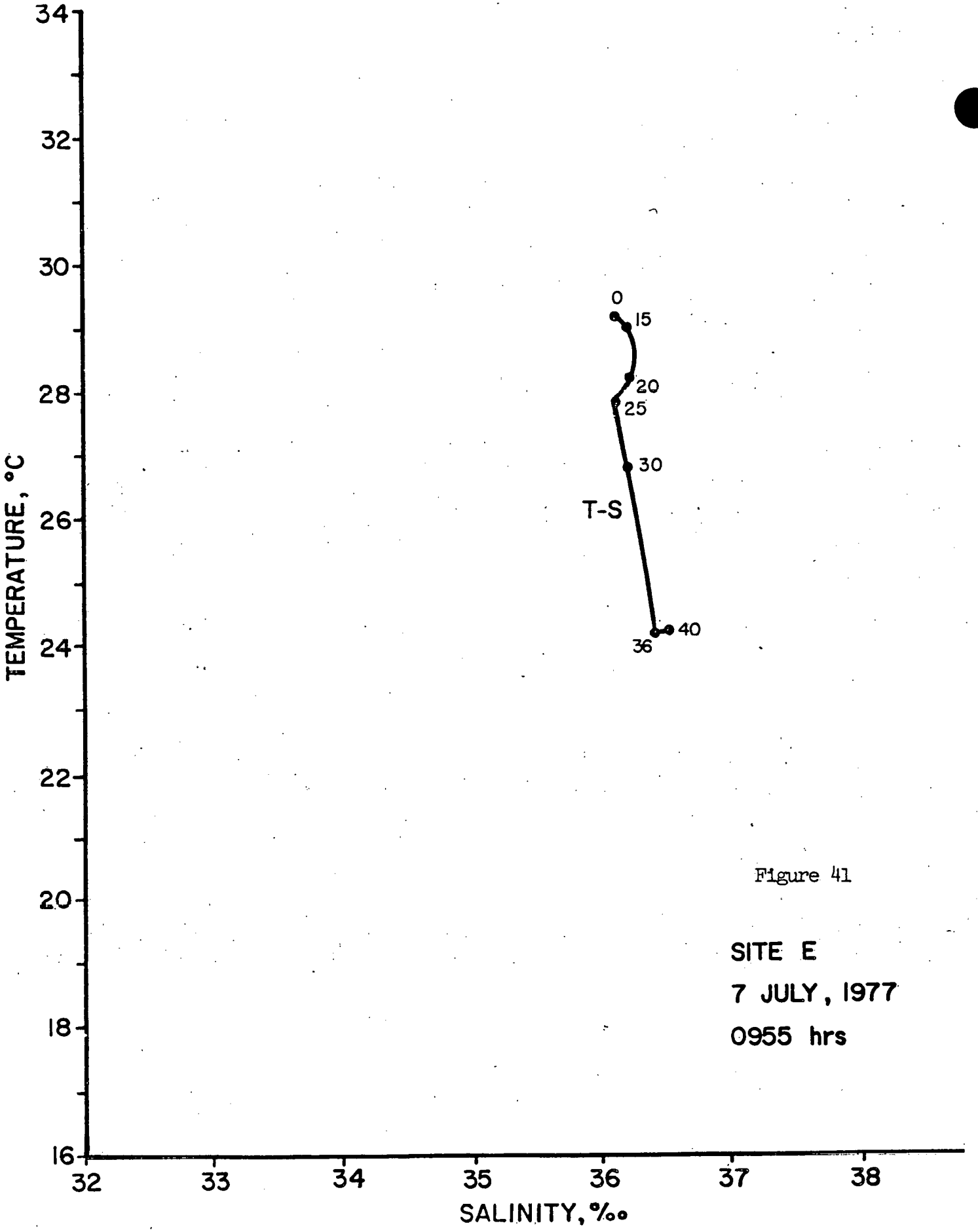
34
32
30
28
26
24
22
20
18
16
TEMPERATURE, °C
32
33
34
35
36
37
38
SALINITY, ‰
0
15
20
25
30
T-S
36
40
SITE E
7 JULY, 1977
0955 hrs

Figure 41

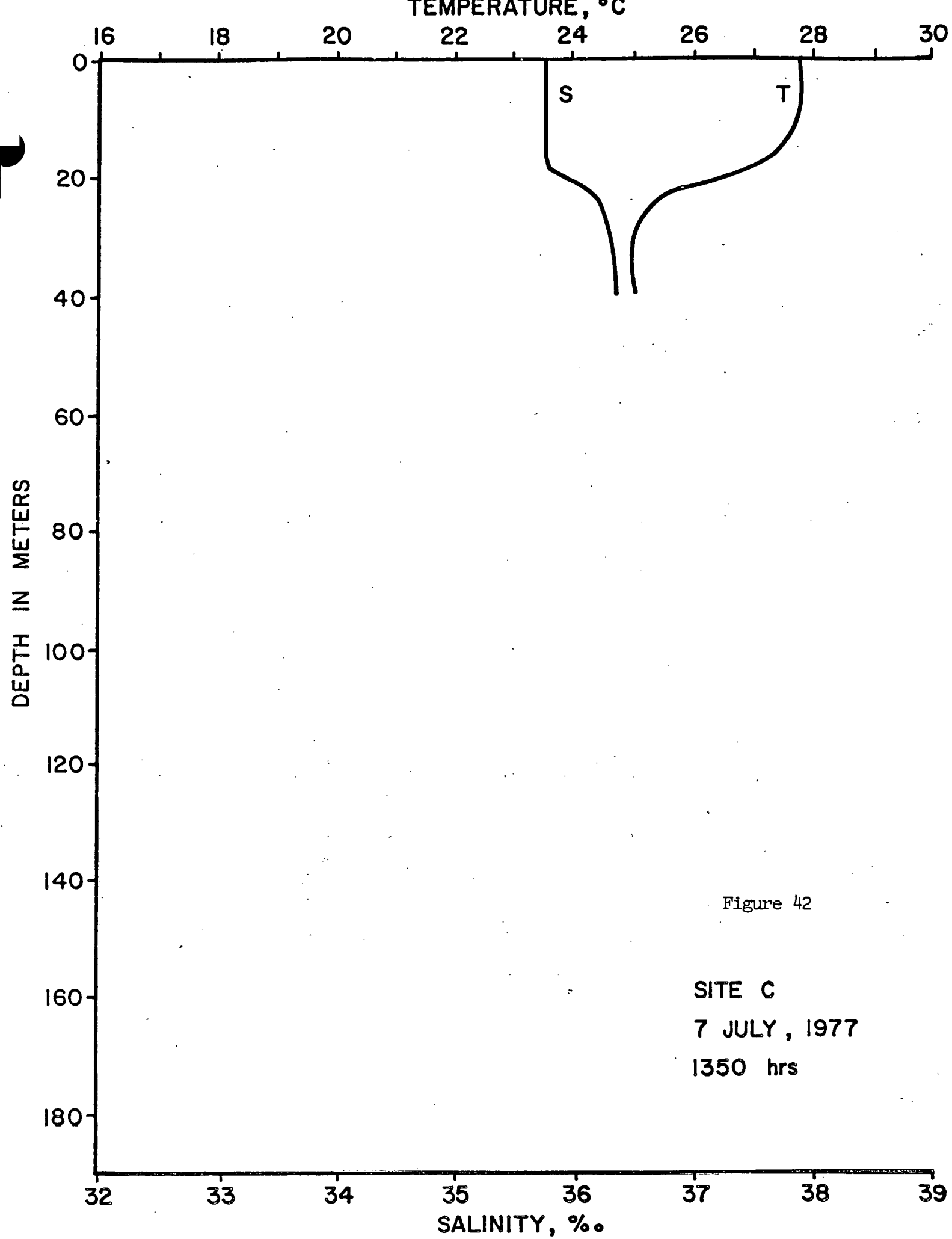
TEMPERATURE, °C
16
18
20
22
24
26
28
30
S
T
DEPTH IN METERS
0
20
40
60
80
100
120
140
160
180
SITE C
7 JULY, 1977
1350 hrs
32
33
34
35
36
37
38
39
SALINITY, ‰

Figure 42

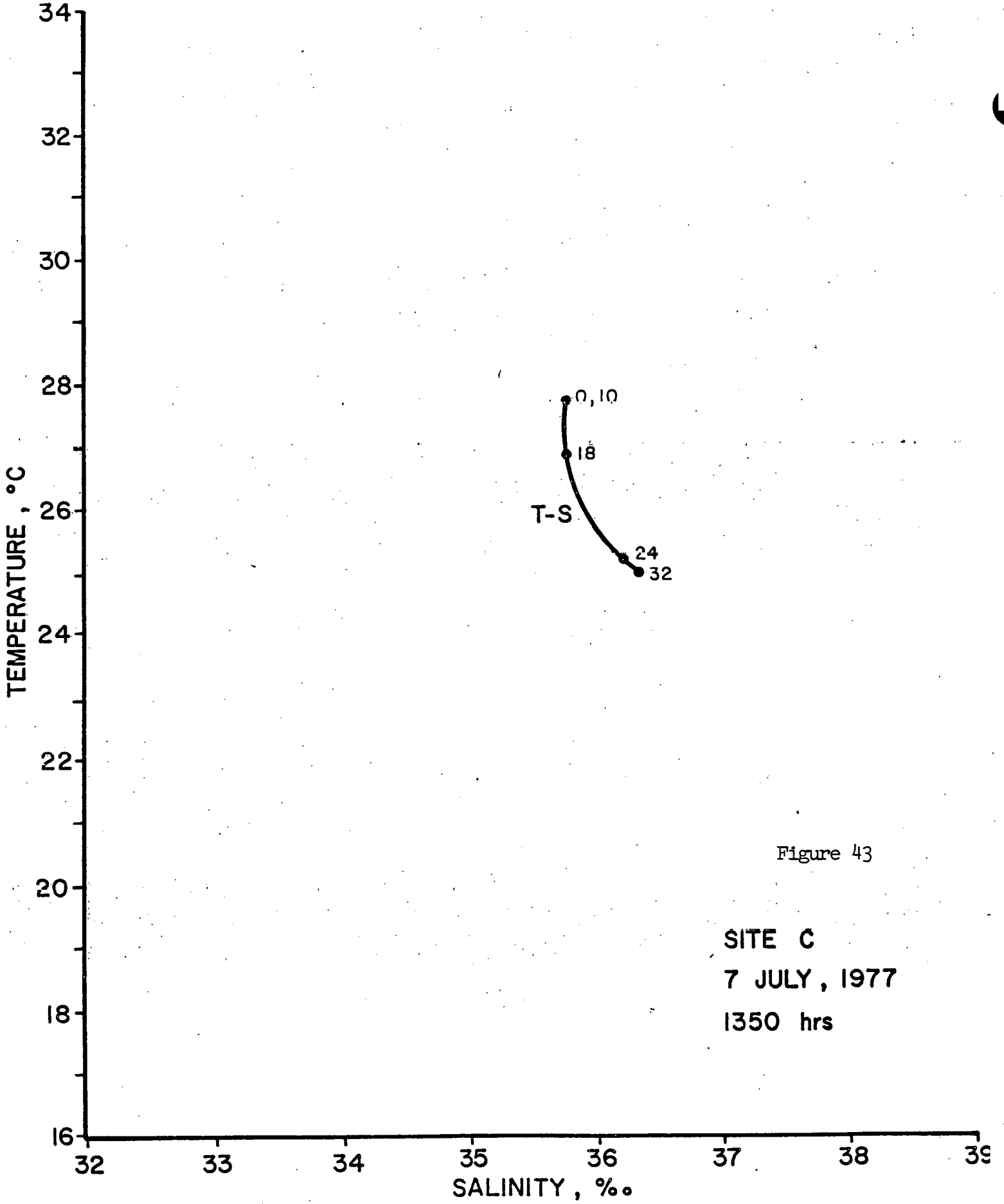
34
32
30
28
26
24
22
20
18
16
TEMPERATURE , °C
0,10
18
T-S
24
32
32
33
34
35
36
37
38
39
SALINITY , ‰
SITE C
7 JULY , 1977
1350 hrs

Figure 43

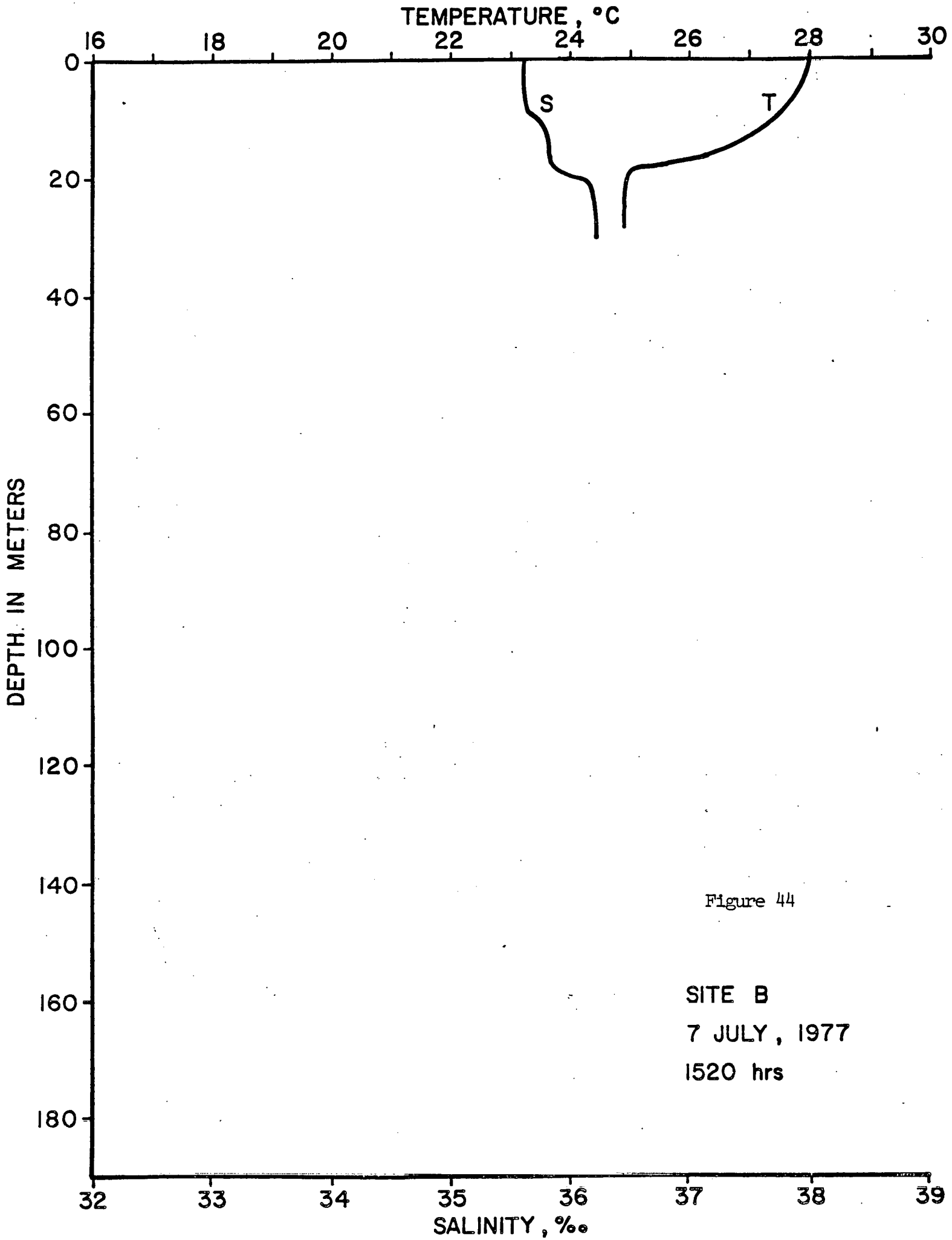
TEMPERATURE, °C
16
18
20
22
24
26
28
30
0
20
40
60
80
100
120
140
160
180
DEPTH IN METERS
S
T
32
33
34
35
36
37
38
39
SALINITY, ‰
SITE B
7 JULY, 1977
1520 hrs

Figure 44

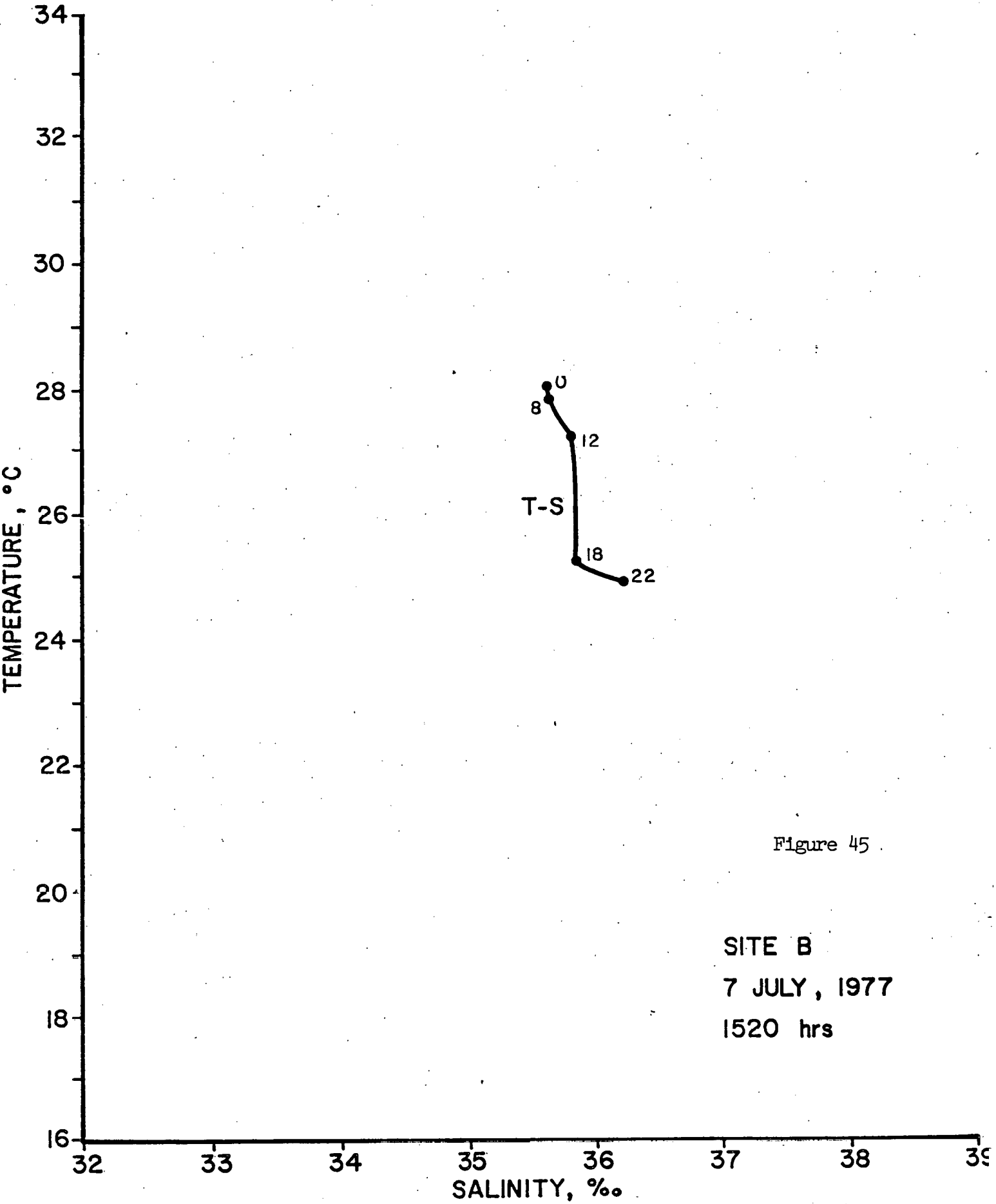
34
32
30
28
26
24
22
20
18
16
TEMPERATURE, °C
32
33
34
35
36
37
38
39
SALINITY, ‰
0
8
12
T-S
18
22
SITE B
7 JULY, 1977
1520 hrs

Figure 45

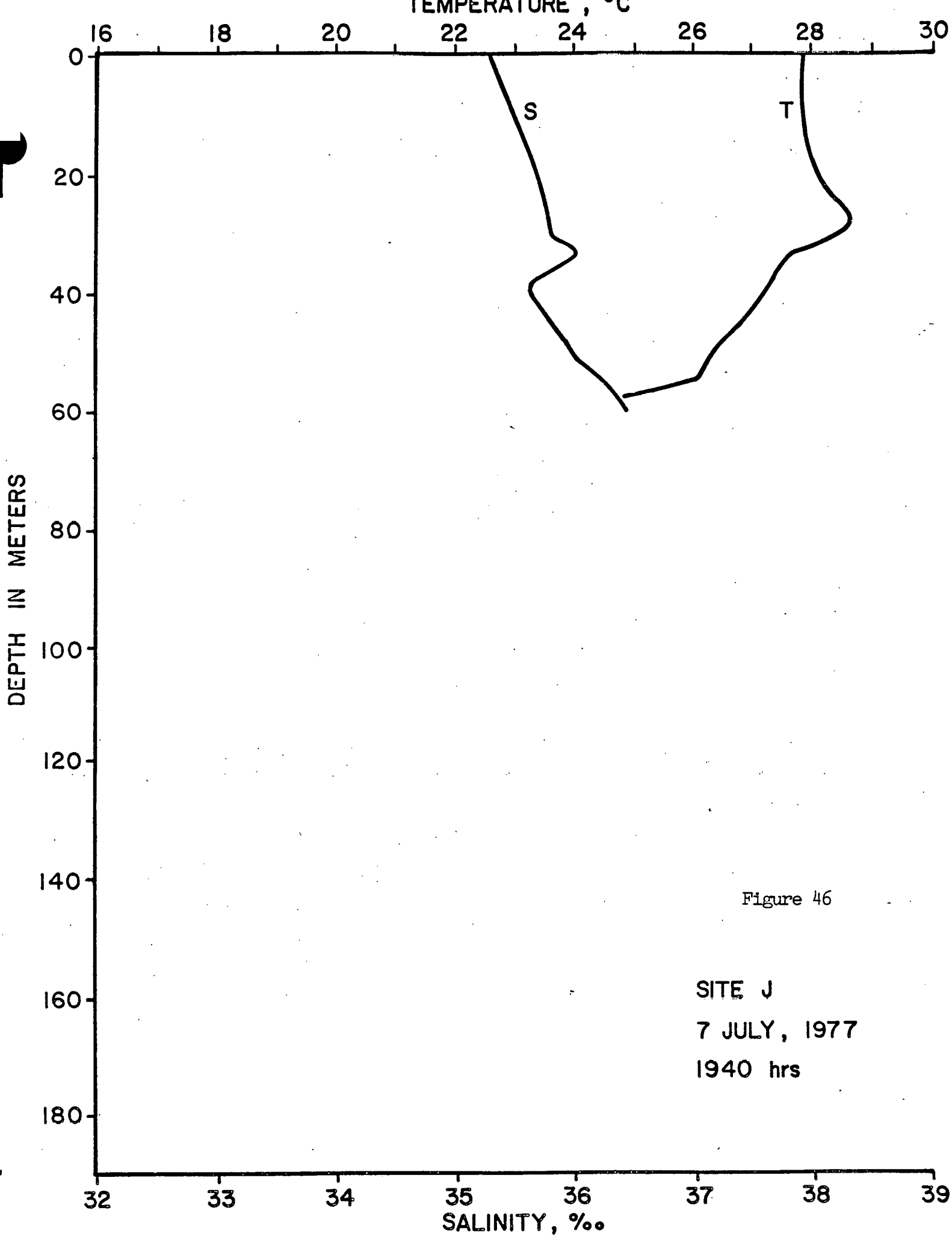
TEMPERATURE, °C
16
18
20
22
24
26
28
30
S
T
DEPTH IN METERS
0
20
40
60
80
100
120
140
160
180
SITE J
7 JULY, 1977
1940 hrs
32
33
34
35
36
37
38
39
SALINITY, ‰

Figure 46

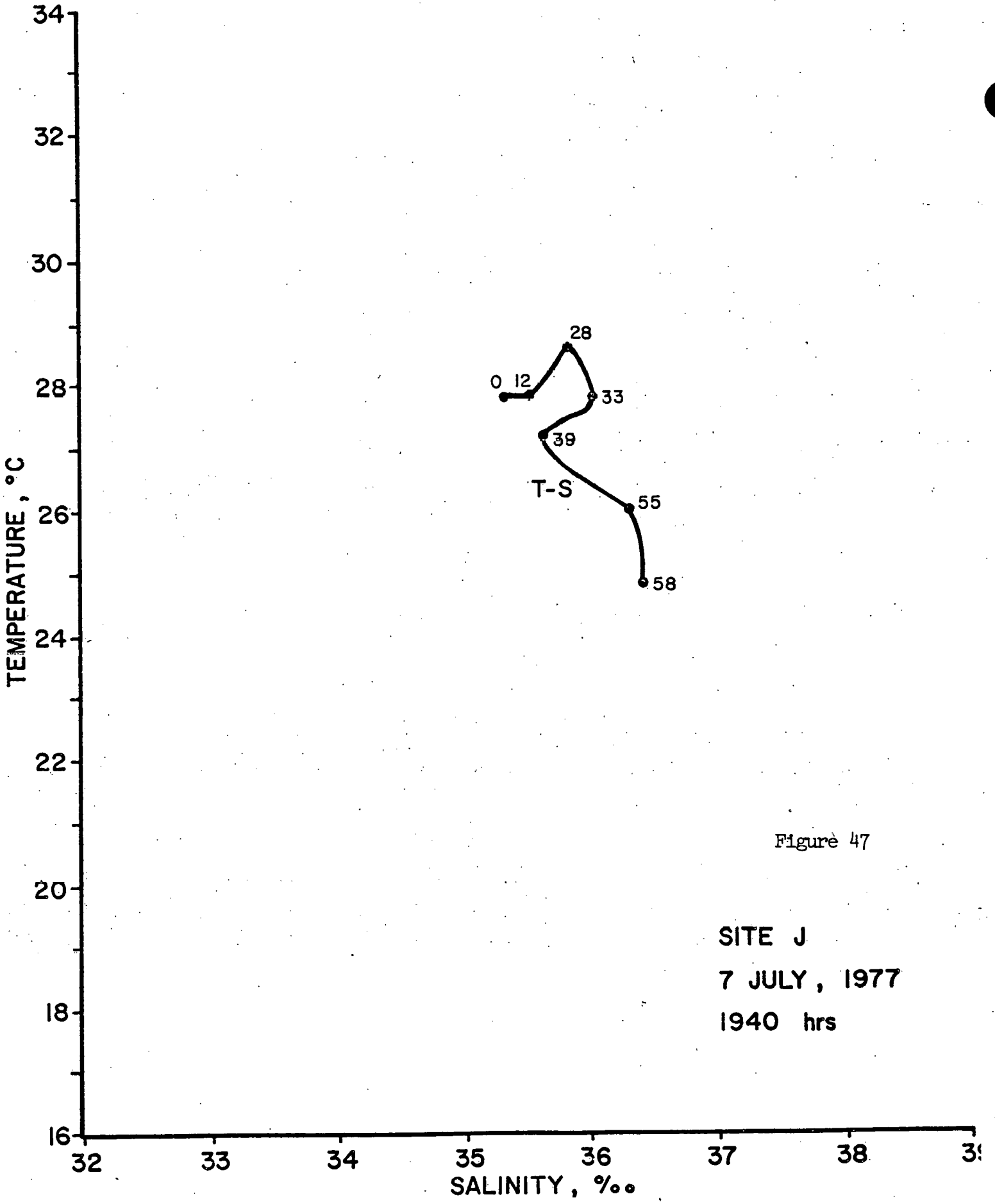
34
32
30
28
26
24
22
20
18
16
TEMPERATURE, °C
32
33
34
35
36
37
38
39
SALINITY, ‰
0
12
28
33
39
55
58
T-S
SITE J
7 JULY, 1977
1940 hrs

Figure 47

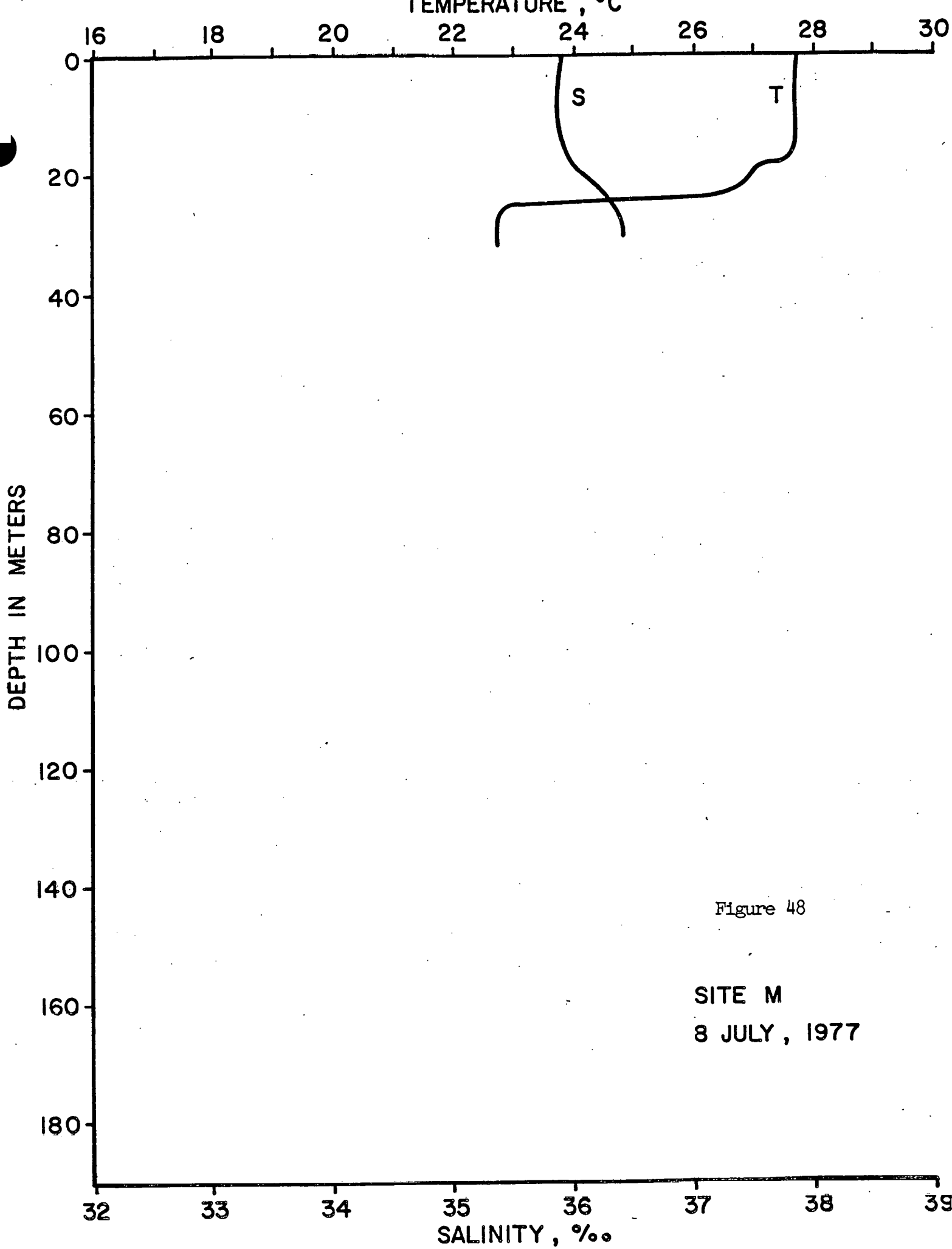
TEMPERATURE, °C
16
18
20
22
24
26
28
30
S
T
DEPTH IN METERS
0
20
40
60
80
100
120
140
160
180
SITE M
8 JULY, 1977
32
33
34
35
36
37
38
39
SALINITY, ‰

Figure 48

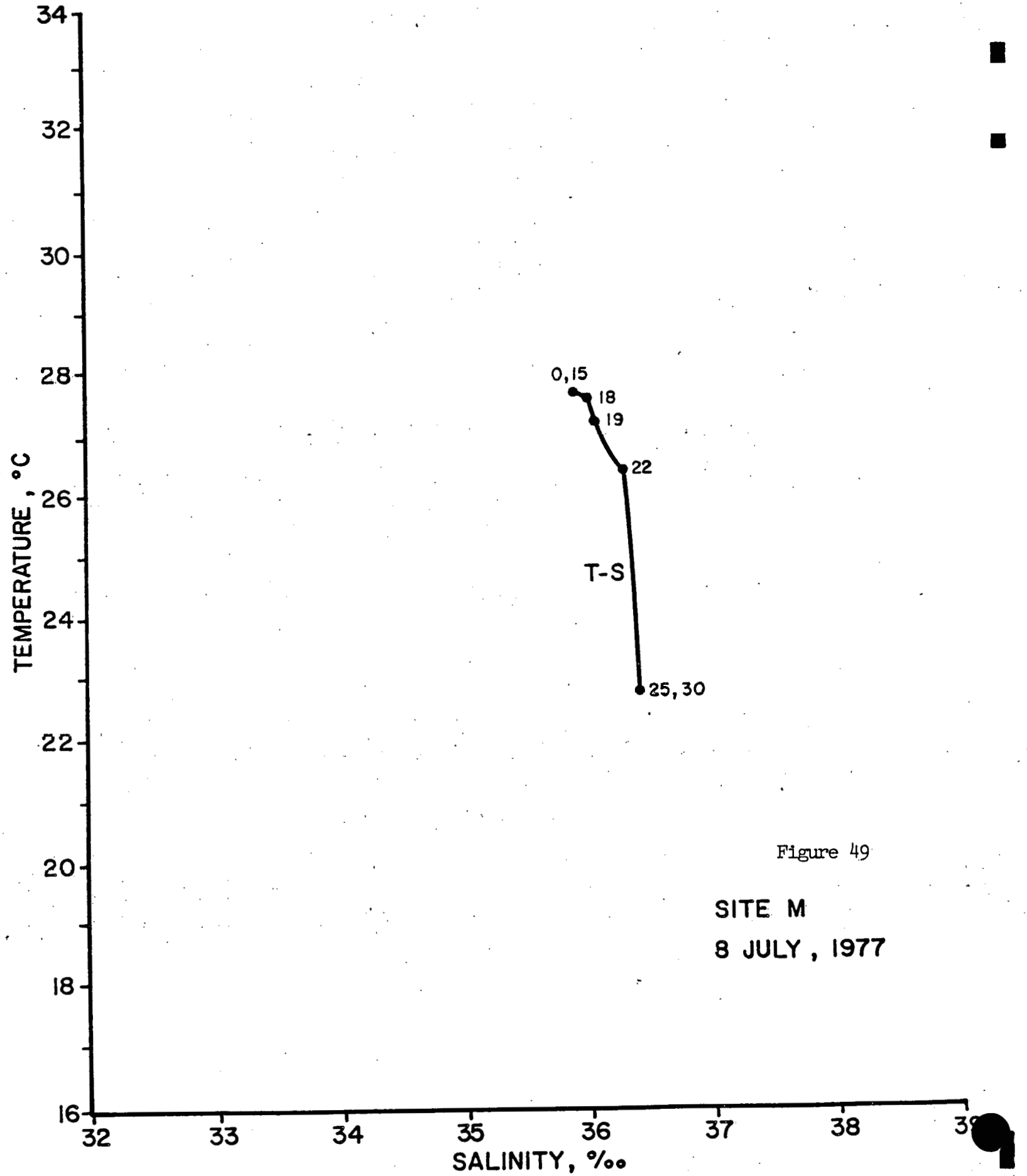
34
32
30
28
26
24
22
20
18
16
TEMPERATURE, °C
32
33
34
35
36
37
38
SALINITY, ‰
0,15
18
19
22
T-S
25,30
SITE M
8 JULY, 1977

Figure 49

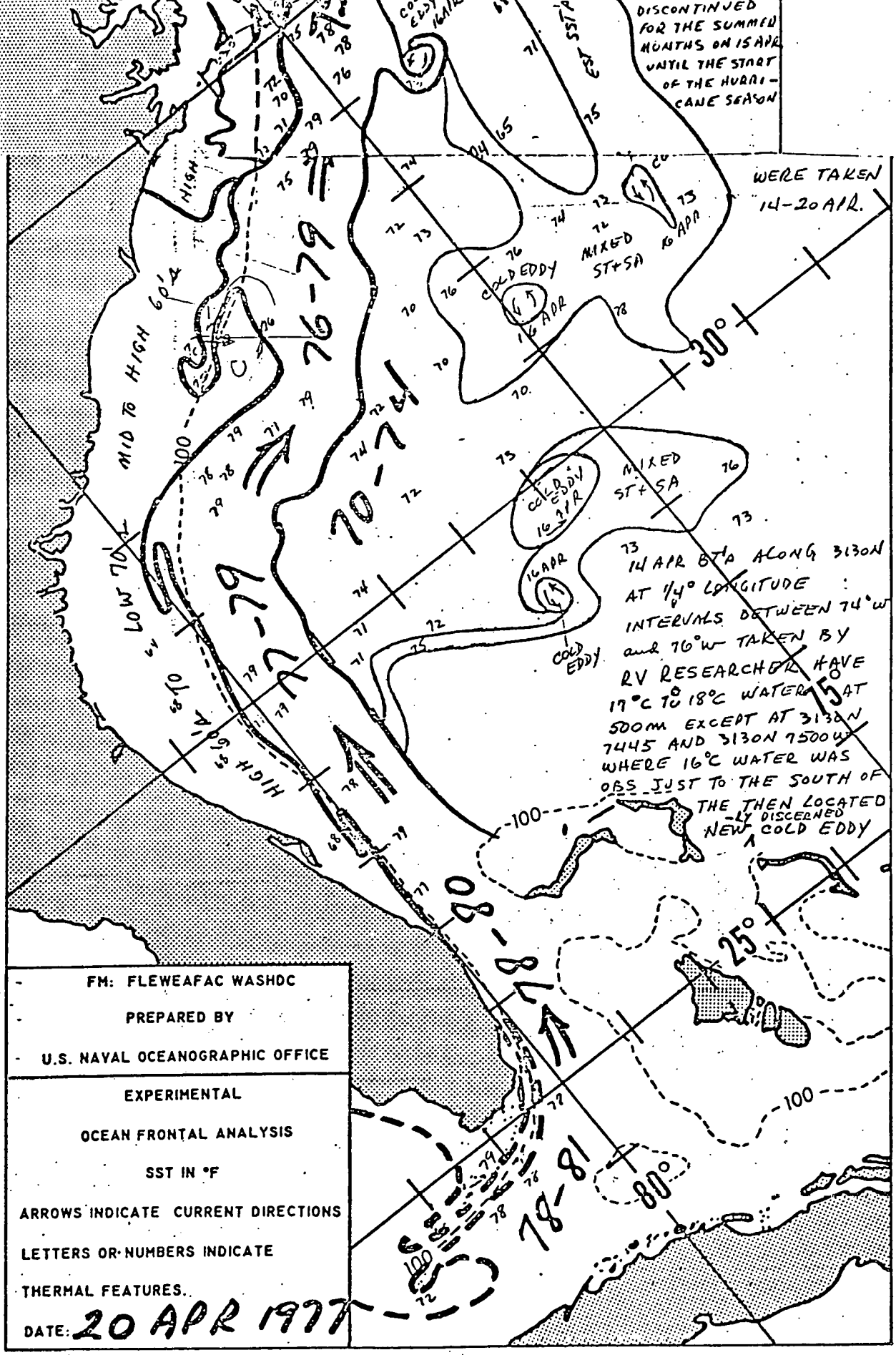
DISCONTINUED FOR THE SUMMER MONTHS ON 15 APR UNTIL THE START OF THE HURRICANE SEASON
WERE TAKEN 14-20 APR.
COLD EDDY 16 APR
MIXED ST+SA
16 APR
MID TO HIGH 60's
LOW 70's
HIGH 85 to 90
76-79
70-74
78-80
78-81
30°
25°
80°
100
14 APR BT'S ALONG 31°30N AT 1/4° LONGITUDE INTERVALS BETWEEN 74°W and 76°W TAKEN BY RV RESEARCHER HAVE 17°C TO 18°C WATER AT 500m EXCEPT AT 31°30N 74°45 AND 31°30N 75°00W WHERE 16°C WATER WAS OBS JUST TO THE SOUTH OF THE THEN LOCATED -LY DISCERNED NEW COLD EDDY
FM: FLEWEAFAC WASHDC
PREPARED BY
U.S. NAVAL OCEANOGRAPHIC OFFICE
EXPERIMENTAL
OCEAN FRONTAL ANALYSIS
SST IN °F
ARROWS INDICATE CURRENT DIRECTIONS
LETTERS OR NUMBERS INDICATE
THERMAL FEATURES.
DATE: 20 APR 1977

Figure 50

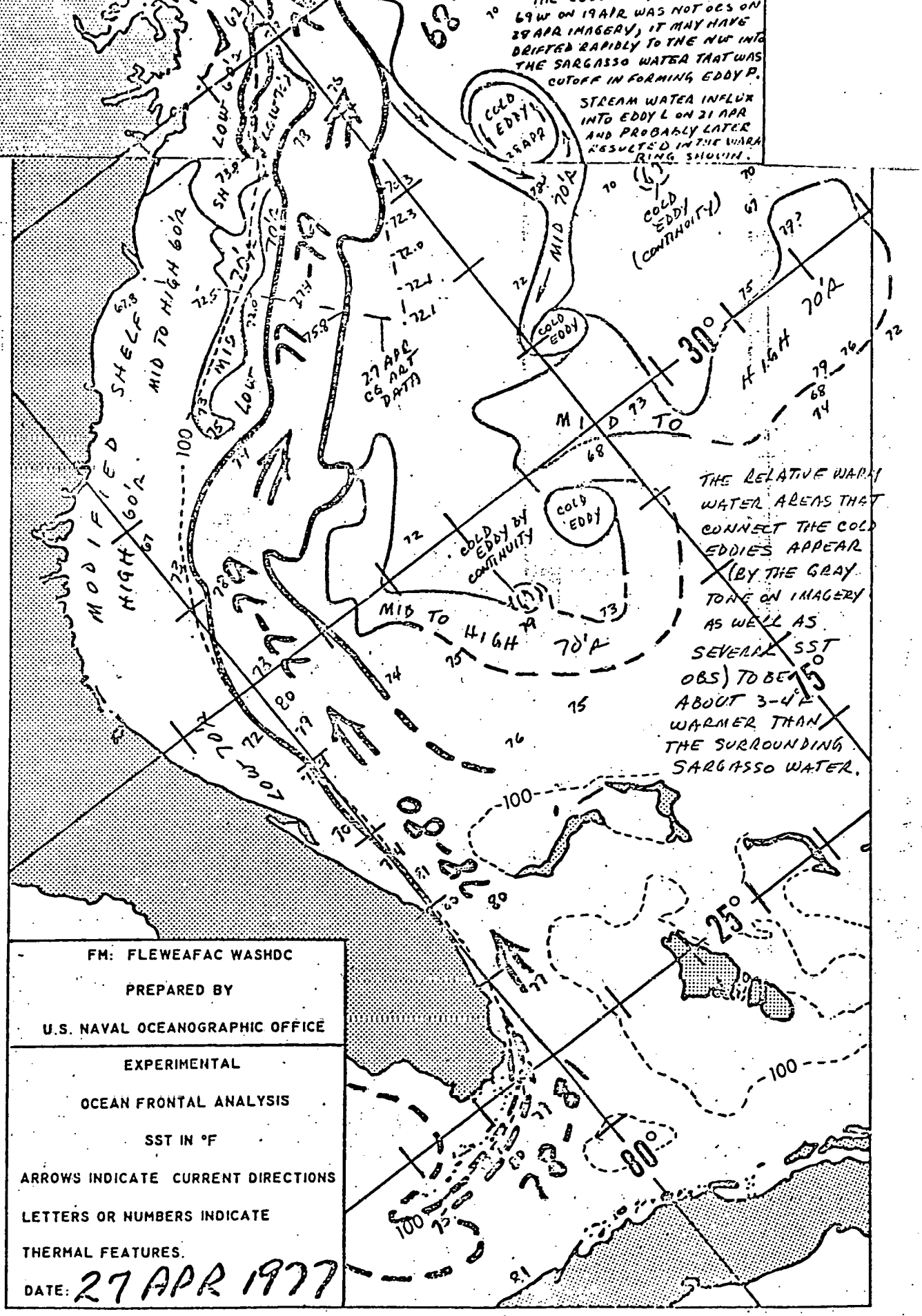
69W ON 19 APR WAS NOT OCS ON 27 APR IMAGERY, IT MAY HAVE DRIFTED RAPIDLY TO THE NW INTO THE SARGASSO WATER THAT WAS CUTOFF IN FORMING EDDY P.
STREAM WATER INFLUX INTO EDDY L ON 21 APR AND PROBABLY LATER RESULTED IN THE WARM RING SHOWN.
COLD EDDY 25 APR
COLD EDDY (CONTINUITY)
COLD EDDY
27 APR CG ART DATA
MID TO HIGH 70'A
MID TO HIGH 60'A
MODIFIED SHELF
LOW 70'A
COLD EDDY BY CONTINUITY
THE RELATIVE WARM WATER AREAS THAT CONNECT THE COLD EDDIES APPEAR (BY THE GRAY TONE ON IMAGERY AS WELL AS SEVERAL SST OBS) TO BE ABOUT 3-4°F WARMER THAN THE SURROUNDING SARGASSO WATER.
FM: FLEWEAFAC WASHDC
PREPARED BY
U.S. NAVAL OCEANOGRAPHIC OFFICE
EXPERIMENTAL
OCEAN FRONTAL ANALYSIS
SST IN °F
ARROWS INDICATE CURRENT DIRECTIONS
LETTERS OR NUMBERS INDICATE
THERMAL FEATURES.
DATE: 27 APR 1977

Figure 51

Continental Margin Atmospheric Climatology and Coastal Sea Level

From the many continental shelf dynamics studies which have been made in the past decade, it has become increasingly apparent that a detailed analysis of continental margin waters can only be accomplished with an appreciation of the coastal meteorology. Fortunately, coastal meteorological and, in addition, coastal sea level data have been archived and thus provide coastal oceanographers with inexpensive, priceless and complimentary data sets. Past coastal sea level studies have demonstrated that these data contain not only tidal data but also sub-inertial frequency information which measurably details shelf response to atmospheric forcing. Additionally, a particular region, such as the South Atlantic Bight, can be characterized by the statistics of the temporal spectra of both data sets as well by the alongshore coherences which may exist between stations. In this study, atmospheric wind and pressure have been examined and correlated with coastal sea level changes at various coastal stations along the South Atlantic Bight (Tables 4 and 5).

The atmospheric climate overlying the South Atlantic Bight is determined by both polar and tropical marine air masses, resulting in a "temperate rainy" climate with mild winters, long hot summers, and adequate moisture in all seasons, according to Koppen (see Pettersen, 1969). The north-south surface temperature gradient over the eastern U.S. reaches a seasonal maximum in late winter of approximately 1.5°C per degree latitude, which is about four times the summer gradient. The polar front, the

Table 4

Meteorological Stations

Station	Latitude	Longitude
Cape Hatteras, N.C.	35°16'N	75°33'W
Wilmington, N.C.	34°14'N	77°57'W
Charleston, S.C.	32°46'N	79°56'W
Savannah, Ga.	32°05'N	81°06'W

Table 5

Sea Level Stations

Station	Latitude	Longitude
Beaufort, N.C.	34°432'N	76°40.2'W
Beaufort Inlet, N.C.	34°41.6'N	76°42.7'W
Wilmington, N.C.	34°13.6'N	77°57.2'W
Frying Pan Shoals, N.C.	33°29.1'N	77°35.4'W
Charleston, S.C.	32°46'N	79°56'W

actual zone of maximum temperature contrast which separates the colder continental air from the warmer, more moist tropical air, both intensifies and shifts southward in the winter to near Cape Hatteras, resulting in a region of intense cyclogenesis stretching along the eastern U.S. seaboard from Florida towards northern Europe. Most of the intense extratropical lows develop over the southeast U.S. but show their greatest growth as the storms move offshore over the warmer ocean, especially in the neighborhood of the Gulf Stream. The mean speed of these synoptic-scale cyclones is 5-7 m/sec (10-15 kts), with less than 20% of the storms moving at speeds greater than 12.5 m/sec (25 kts) (NOAA, 1970).

These wintertime extratropical cyclones (and to a lesser extent the accompanying anticyclones) can affect the coastal oceanic circulation in a number of direct and indirect ways. The surface pressure and wind stress patterns for a mature low can be coherent over 600 kms., can persist for 3 to 4 days, and can directly drive a large-scale coastal current. Intense lows are frequently accompanied by trailing outbreaks of very cold polar air, causing sharp cold fronts which move southeastward over the southeastern states; and they can bring freezing weather and strong winds as far south as Florida. Smaller scale waves can develop along the polar front near the southeastern coast which exhibit highly variable stress and precipitation patterns on the subsynoptic (10-100 km) scale (Bosart, Vando, and Helsdon, 1972; Bosart, 1973). Bosart and Cussen (1973) have found surface pressure fluctuations of 4-5 mb amplitude along the coast

and have attributed these perturbations to atmospheric gravity wave generation by accompanying frontogenesis. Perhaps the most intense atmospheric pressure and surface wind stress patterns are associated with the large-scale tropical storms and hurricanes which develop primarily in August-October and occasionally migrate along the Southeast coast, visiting the Carolina coast with a frequency of about one severe storm every two years (U.S. Navy, 1970). The meteorological forcing on the Carolina Shelf is thus dominated in winter by transient extratropical storms with considerable variability in strength, structure, and persistence of the important meteorological fields. The predominant winds are northwesterly to northeasterly, with some 30% of the observed speeds reported to NOAA (1970) exceeding 8 m/sec (16 kts).

The summer meteorological regime along the Carolina coast is controlled by a strong weakening of the polar front and an intensification of the Azores-Bermuda high. The region of most intense cyclogenesis has shifted north of Cape Hatteras and while some active frontogenesis and cyclogenesis continues over the Southeast U.S. shelf, the atmospheric variability there is decreased in summer. The predominant winds are lighter and southerly to southwesterly. Some 60% of the NOAA-collected surface observations (NOAA, 1970) indicate wind speeds of less than 5 m/sec (10 kts), while 15% indicate wind speeds greater than 8 m/sec (16 kts). The standard deviation of the surface pressure shows both a strong seasonal fluctuation and a steady

decrease with decreasing latitude south of Cape Hatteras (U.S. Navy, 1970). The standard deviation of the surface pressure at Charleston, S.C., is about one-half its mean winter value of 7 mb. Ward (1925) and his more recent co-workers suggest that a transition from a northern cyclonic-controlled climate to a more Gulf-like climate with higher temperatures and less dramatic weather occurs along the Southeast shelf near the latitude of Charleston.

On localized scales; an appreciable diurnal sea/land breeze, as well as an apparent semi-diurnal harmonic thereof, are in evidence along the North Carolina coast (Pietrafesa, et. al., 1977).

The recent work of Saunders (1977) suggests that there is a great deal of offshore as well as alongshore structure to the mean wind fields which gives rise to the need for meteorological buoys which would allow for an assessment of the curl and divergence of the wind field as well as a mass and heat air/sea interaction evaluation. Saunders also points out an offshore wind stress maximum which occurs during early fall; he finds no apparent reason for this but it seems likely that the air-sea temperature gradients may be largest during this time of the year, thereby increasing the drag coefficient and subsequently the relative stress field.

Another line of investigation has pursued the influence of meteorological forcing, albeit in a less systematic manner. In the summer season, near coastal winds with northward (alongshore) components are common and often persistent. Green (1944) and Taylor and Steward (1959) reported evidence for summer coastal

upwelling of northeast North Carolina. Bumpus (1973) then inferred that wind-driven upwelling probably occurred throughout the South Atlantic Bight in the summer season. Wunsch, Hansen, and Zetler (1969) examined many years of sea level and meteorological data from the Florida Straits region; they found no evidence for a significant, systematic meteorological influence on the Florida Current.

The response of coastal surface elevation to continental atmospheric forcing has been examined, by a number of investigators. Miller (1957 and 1958) studied the New England and New Jersey coasts; Hamon (1962, 1963, 1966) studied the Australian coasts; Panshin (1967), Mooers and Smith (1968), Pietrafesa (1970), Cutchin and Smith (1973), Smith (1974), Kundu, Allen and Smith (1975) and Huyer, Hickey, Smith, Smith and Pillsbury (1975) have separately and in part investigated the effects of atmospheric forcing on sea level along the Pacific Northwest coast; Mysak and Hamon (1969) partially studied the North Carolina coast; Cragg and Sturges (1974) did an in depth study of the West Florida shelf while Brooks and Mooers (1977) considered sea level response along the East Florida shelf.

Sea surface elevations along coastlines are related to both alongshore and transhore winds. Simple Ekman theory (Ekman, 1905) and subsequent studies of both set-up and set-down (Hidaka, 1953; Welander, 1957) and shelf wave generation (Hamon, 1962, 1963, 1966; Mysak and Hamon, 1967; Cutchin and Smith, 1973; Huyer, et. al., 1975); have supported the evidence for subinertial frequency correlations between atmospheric forcing and sea level signature.

This review presents cross analyses of surface wind and atmospheric pressure which are then shown to provide the sea level response function to meteorological forcing. The implications which these results bear for shelf circulation investigations can then be inferred and supported with current meter data collected in the area of interest (Pietrafesa, et. al., 1978a and 1978b).

The literature cited suggests that variations in atmospheric pressure, wind speed and direction, currents and subinertial phenomena, such as shelf waves, can significantly affect the coastal sea level signature. Sea level response to variations in coastal meteorological pressure fields can be expressed in terms of a factor which is frequency dependent. It can be best appreciated as the relationship between the input to a filter and the subsequent convolved output. Generally, a one centimeter per millibar depression (rise) in sea level per increase (decrease) in barometric pressure is observed.

While the evidence for the existence of continental shelf waves has been at times inferred from the cross-statistical analyses of tidal and meteorological data, these have been few actual current meter observations made at sufficiently extensive longshore stations to corroborate the passage of these phenomena. Huyer, et. al. (1976) confirmed the existence of such phenomena along the Oregon-Washington coast and the ongoing Department of Energy current meter study between Cape Lookout and Savannah by Dr. T. N. Lee (of the University of Miami) and Dr. L. J. Pietrafesa (of North Carolina State University) could confirm

the Mysak and Hamon (1969) contention of their existence. Pietrafesa, et. al. (1978) have produced current meter spectra from Onslow Bay, N. C. which show energy peaks at the 2.5-4, 5-7 and 8-11 day period bands, which could be associated with south/ northward propagating wave phenomena. Nontheless, without further corroboration, such as the Pietrafesa study may yield, the separation of free or forced Rossby wave sea level response from wind induced stationary sea level fluctuations is no more than speculation.

Wunsch, et. al. resolved that astronomical tides were responsible for most of the sea level variations. Herein, it is of note that low frequency fluctuations, within the 0.5-08 cpd frequency range, are an observed feature of the Gulf Stream. Pillsbury (1890), Parr (1937), Duing, Mooers and Lee (1977), Duing (1975), Schmitz and Richardson (1968) and Lee and Mayer (1977) all independently observe such lateral, onshore-offshore periodicities of the current regime in the Gulf Stream off of the Florida Coast. Webster (1961) found a 0.14 cpd cross-shelf meander of the Gulf Stream front off of Onslow Bay, which seemed to be correlated with the cross-shelf wind component. Orlanski (1969), Niiler and Mysak (1971) and Orlanski and Cox (1973) independently suggest that inherent baroclinic instabilities of the Gulf Stream can be responsible for the energy which appears in the aforementioned frequency domain range. These instabilities would then force a shelf water response which could appear in the sea level signature. A contemporaneous description

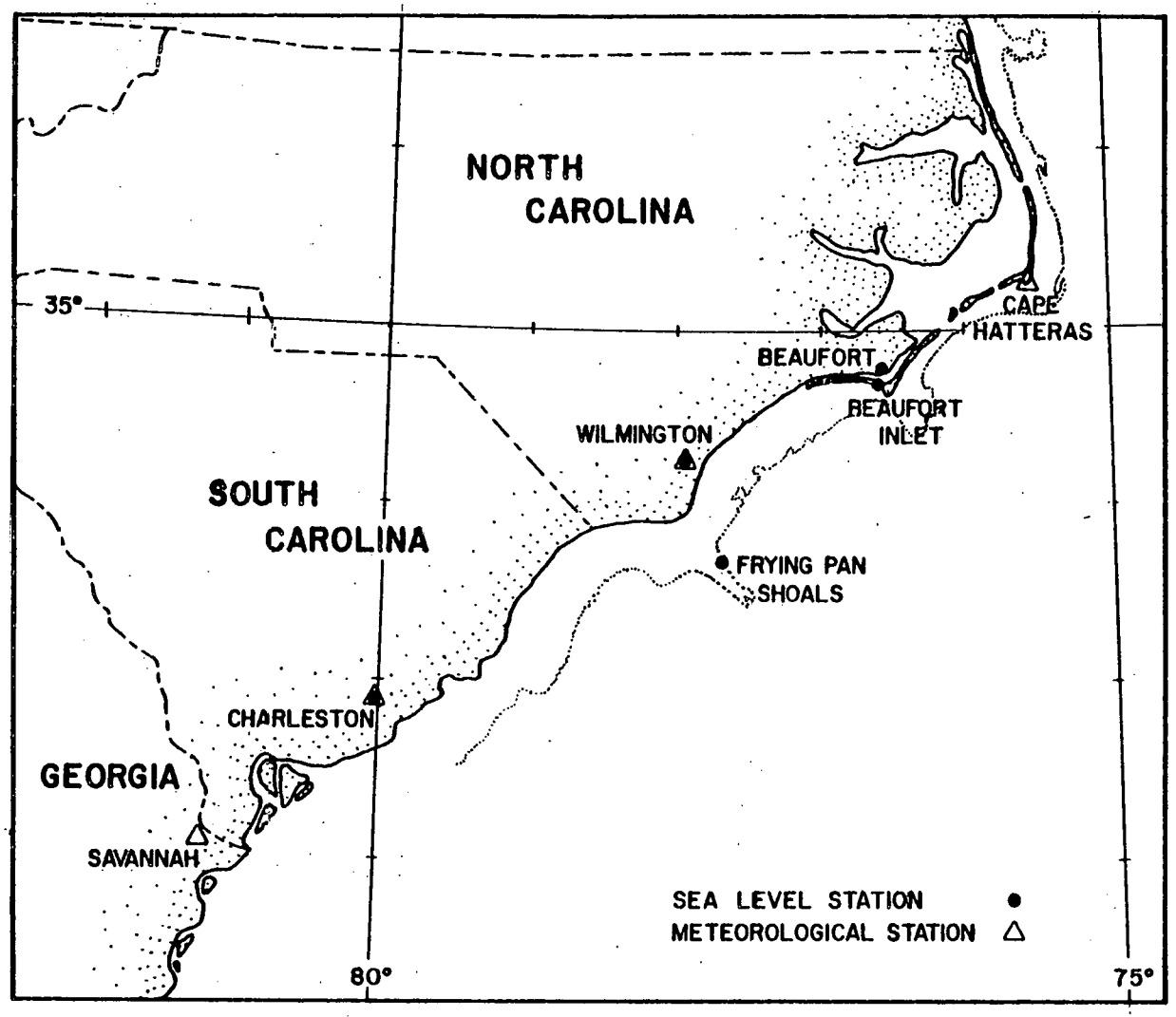

Figure 52. Location of meteorological and sea level stations

of coastal current, sea level, Gulf Stream dynamic character and atmospheric forcing needs to be accomplished; such a study is included in the aforementioned Lee and Pietrafesa field studies extending from Florida to Cape Hatteras, but in this report we shall simply report on some coastal meteorological and sea level relationships.

Meteorological stations and tide gauge stations chosen for this study are respectively: Cape Hatteras, Wilmington, Charleston and Savannah; Beaufort, Beaufort Inlet, Frying Pan Shoals, Wilmington, and Charleston. These are geographically depicted in Figure 52. Throughout this area the continental shelf tends to be shallow and generally broad with the major exception of a narrowing at Cape Hatteras and occasional incursions of shoals seaward of Capes Hatteras, Lookout and Fear (cf. Figure 52). The shelf break is typically at the 75 meter isobath. Though the topography in the vicinity of each gage varies considerably, the similarity between the low frequency, low passed sea level records at the various stations supports the assumption that there is minimal location influence apparent in the spectral ranges considered, save for the Frying Pan Shoal and Wilmington data, which may be geographically and or topographically influenced.

For this project progress report, two years of hourly heights, recorded to the nearest 2-3 centimeters were analyzed at each sea level station. Three hourly observations at atmospheric pressure and wind speed direction were obtained from the Savannah and Wilmington airports and Charleston and Cape

Hatteras coastal stations. The airport data are undoubtedly contaminated by topographic boundary layer effects and may thus show considerably diminished magnitudes, as well possible rotations in direction relative to the coastal stations. It is further appreciated that the coastal meteorological data may show both phase differences as well as magnitude and direction variations with the actual, at sea, marine atmospheric climatology. This contention is strongly suggested in the comparison of the Saunders (1977) offshore, at-sea meteorological statistics to the Ruzecki (1974) coastal, land based results.

The data analyzed are from coastal sea level, i.e. tide gauge, and meteorological stations located in Figure 52 . Hourly values of sea level height for 1974 were obtained from the National Ocean Survey, NOAA, Rockville, Maryland, for stations at Beaufort (BFT), Frying Pan Shoals (FPS) and Wilmington (WIL), North Carolina, and at Charleston (CHS), South Carolina. Three-hourly values of surface wind speed, wind direction, and atmospheric pressure for 1974 were obtained from the National Climatic Center, NOAA, Asheville, North Carolina for stations at Cape Hatteras, N.C., (HAT), Wilmington, N.C. (WIL), Charleston, S.C. (CHS) and Savannah, Ga. (SAV).

The sea level data were low pass filtered using a Lanczos filter taper to attenuate the daily and semidaily tides and inertial fluctuations (the inertial periods at/are: SAV/22.64 hr; CHS/22.04 hr; WIL-FPS/21.46 hr; BFT/21.1 hr; and HAT/20.9 hr. The envelope of the forty (40) hour low pass filter energy response functions are shown in Figure 53. Attenuation

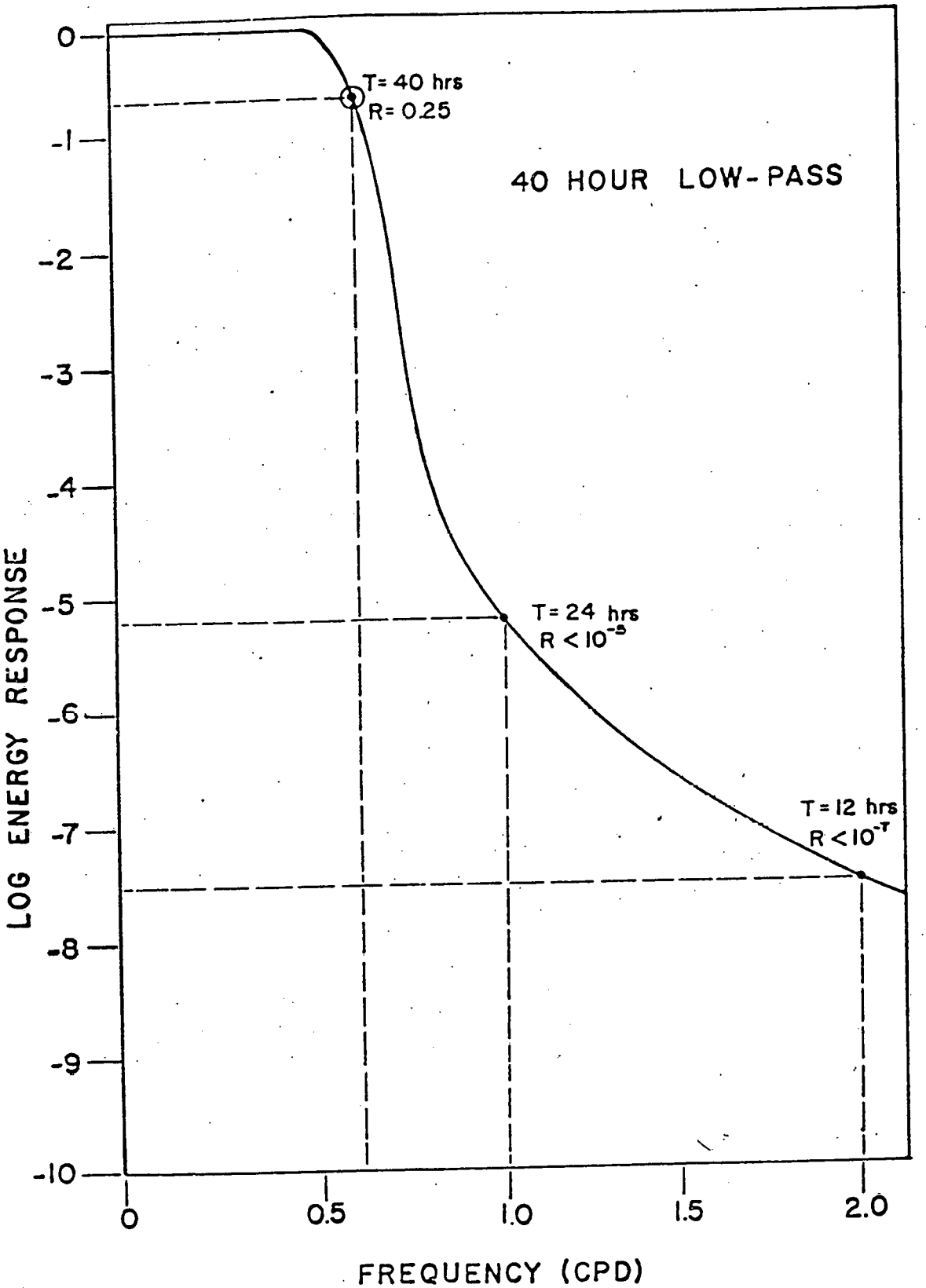

Figure 53. Filter energy response envelope, 40HRLP

at diurnal and higher frequencies is greater than 10^6 and 10^5 respectively. After filtering, the sea level data were resampled at 8 and 6 hourly intervals, for the two separate filtering intervals, respectively.

The radial distances between these stations are approximately: SAV-CHS/130 km; SAV-WIL/380 km; SAV-BFT/480 km; SAV-HAT/620 km; CHS-WIL/240 km; CHS-BFT/340 km; CHS-HAT/480 km; WIL-BFT/100 km; WIL-HAT/240 km; and BFT-HAT/140 km.

Three-hourly wind stress vector components in a right-handed rotated coordinate system, such that the alongshore component is 55.6° East of North, were computed from the raw wind speed and direction data, with the positive vector sense in the direction toward which the wind blows. The stress components were computed using a quadratic drag law with the drag coefficient $C_D = 1.5 \times 10^{-3}$ (Pond, 1976). The wind stress components and atmospheric pressure time series were low pass filtered, using a filter with the response characteristics shown in Figure 53. The atmospheric data were then subsampled at 9-hour intervals and linearly interpolated to 8 and 6 hourly intervals to be commensurate with the respective sea level data.

The filtered atmospheric pressure time series indicates that the SAV, CHS, WIL, and HAT stations (Figs. 54-57) are well correlated over most of the large and even small amplitude variations which is indicative of the high degree of horizontal coherence over length scales of the pressure field much greater than the SAV-HAT radial separation distance which is 620 km. The large horizontal coherence distance presumably reflects the

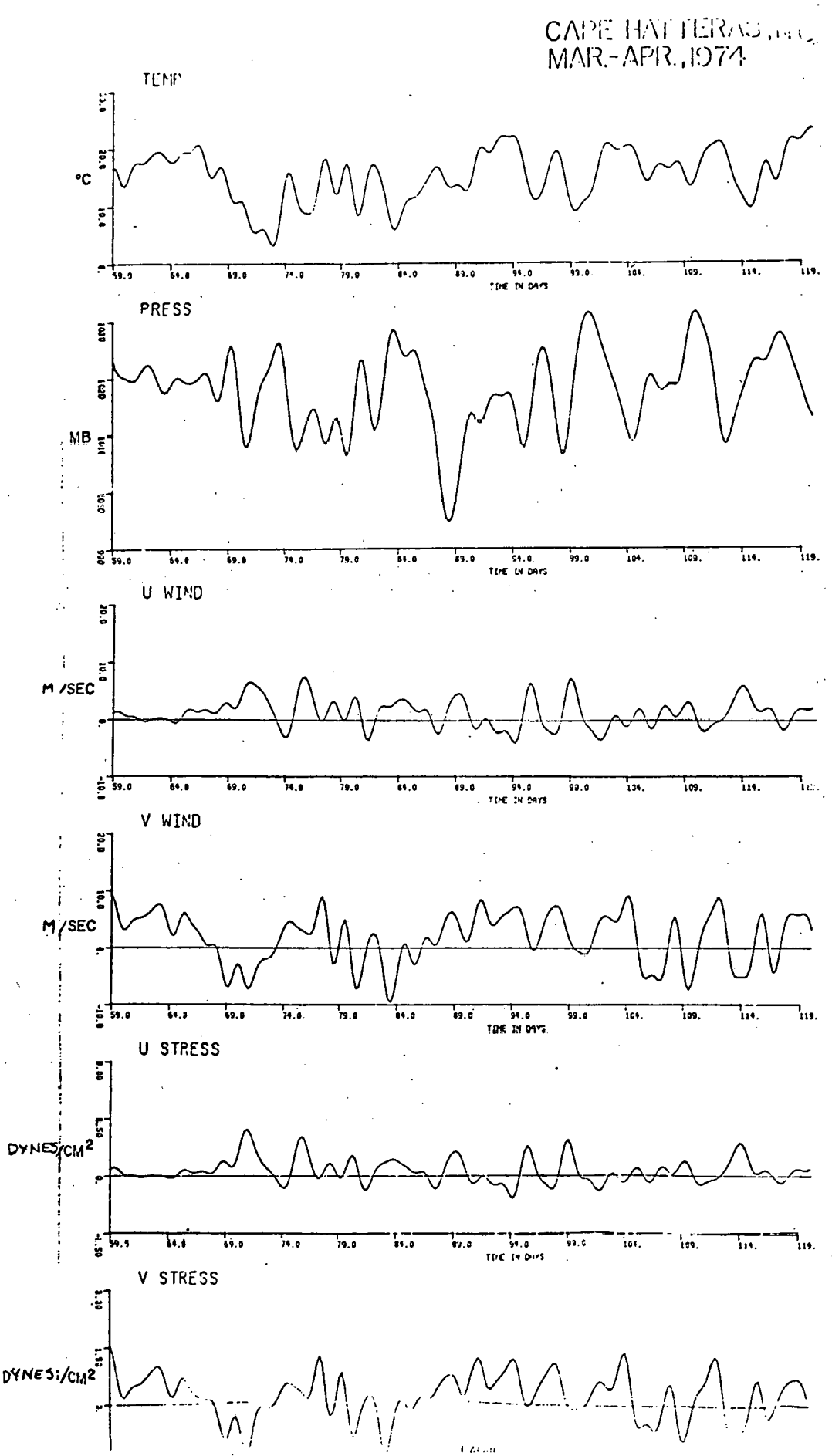

Figure 54. Temperature, pressure, wind velocity components and wind stress components at Cape Hatteras, N. C., Mar. through Apr., 1974

WILMINGTON, N.C.
MAR.-APR., 1974

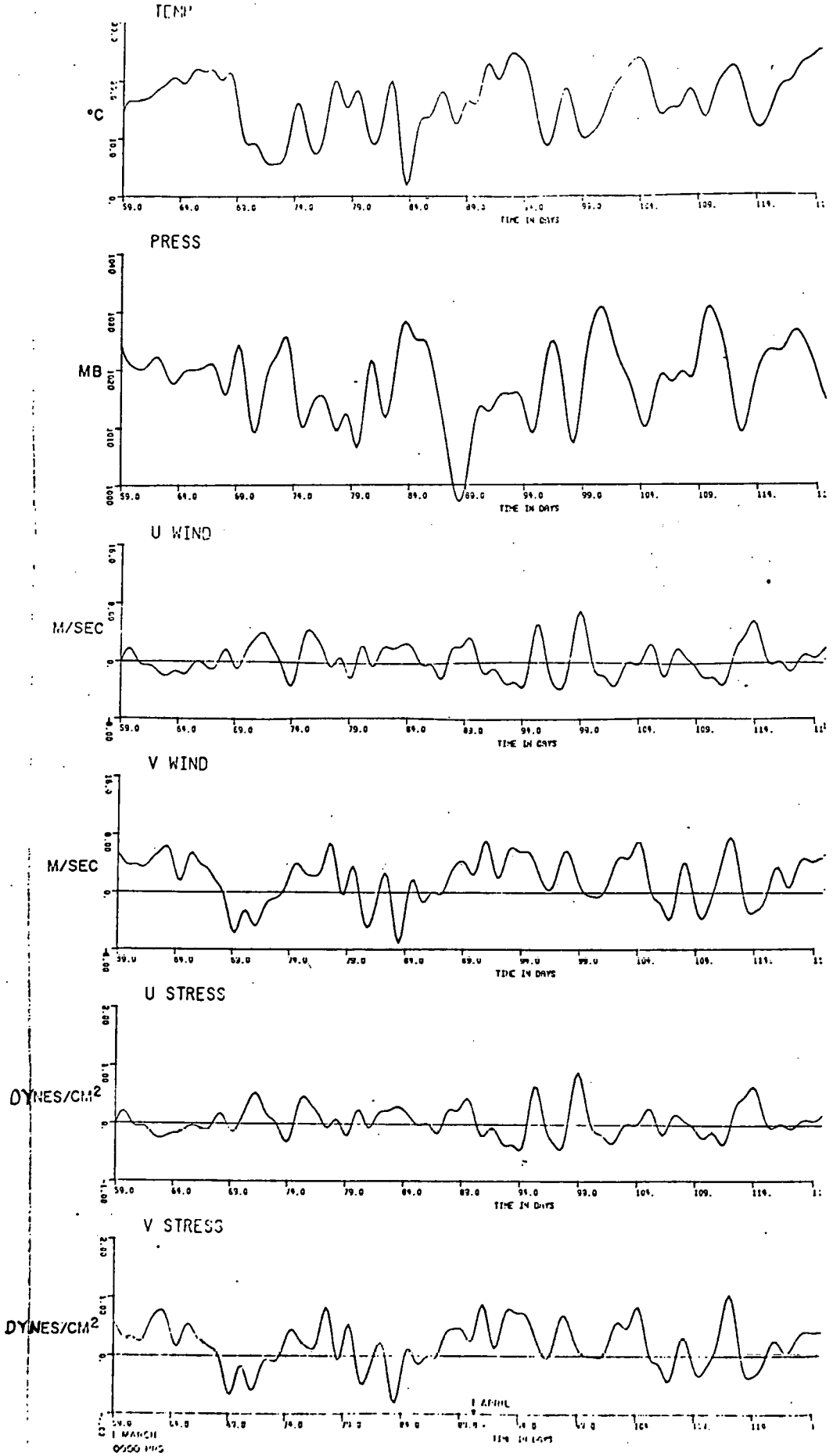

Figure 55. Temperature, pressure, wind velocity components and wind stress components at Wilmington, N. C., Mar. through Apr., 1974

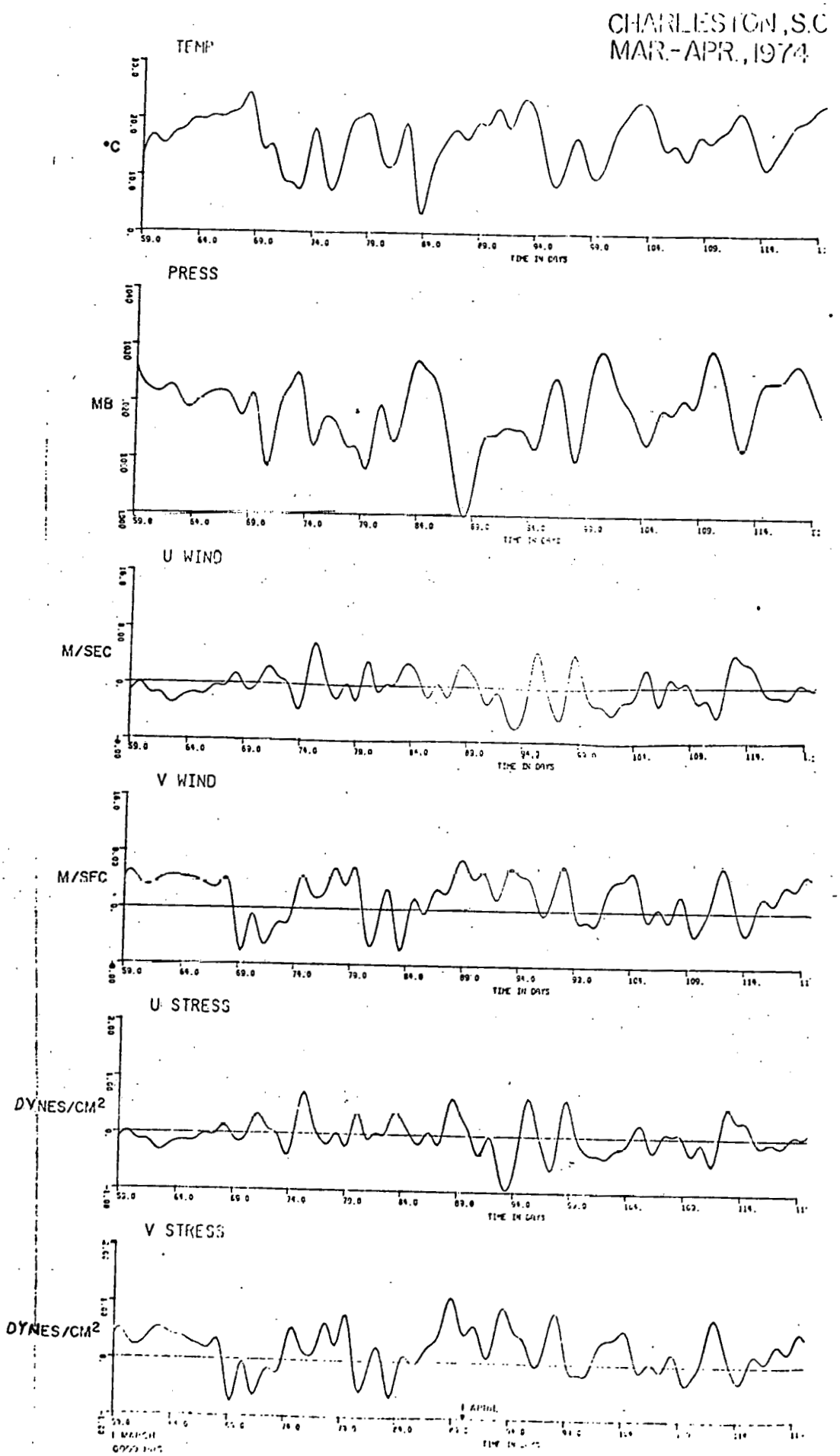

Figure 56. Temperature, pressure, wind velocity components and wind stress components at Charleston, S. C., Mar. through Apr., 1974

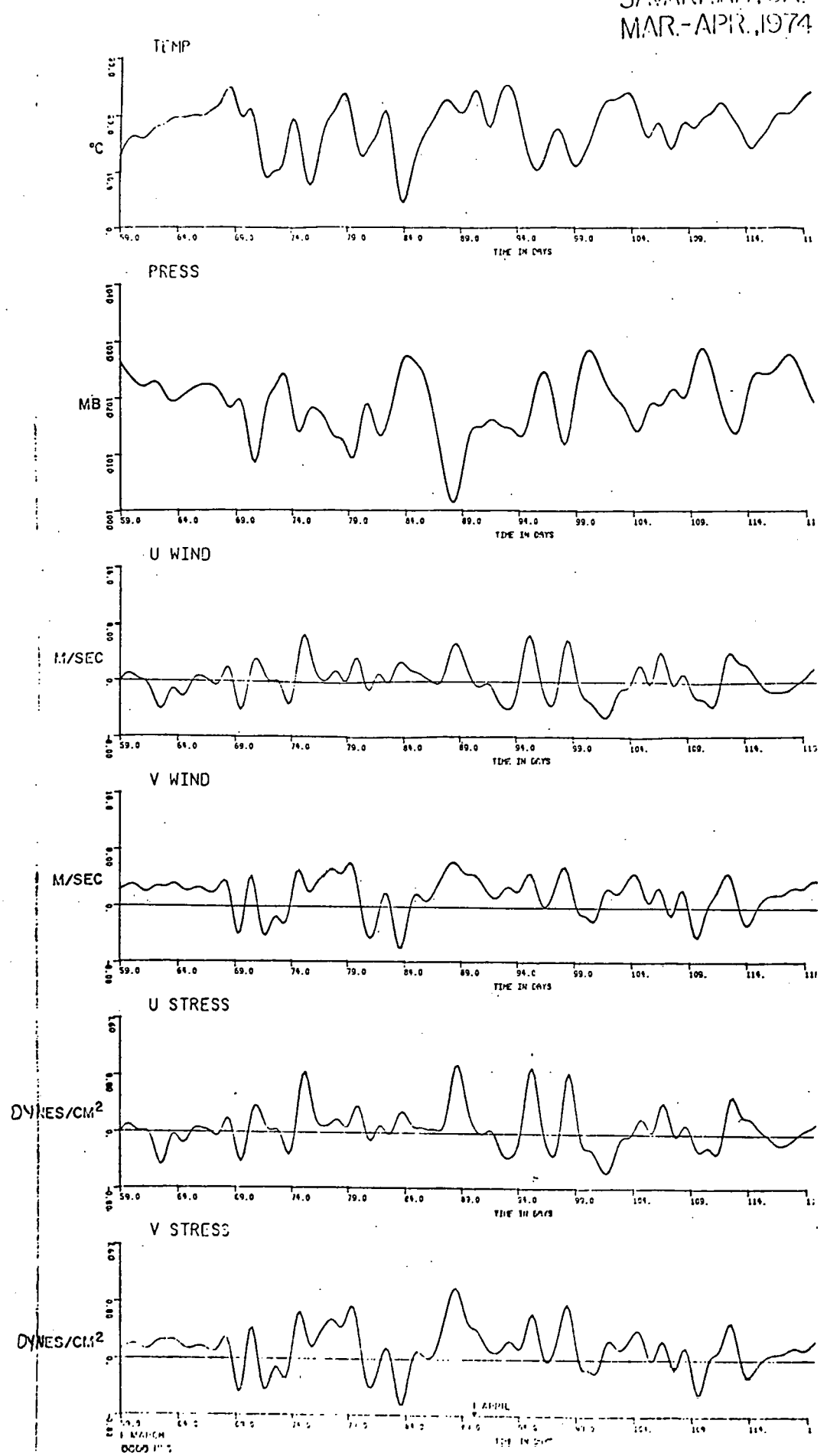

Figure 57. Temperature, pressure, wind velocity components and wind stress components at Savannah, Ga., Mar. through Apr., 1974

synoptic meteorological scales associated with mid-latitude atmospheric disturbances, especially during the fall, winter, spring periods. The alongshore wind stress components (Figs. 58 thru 63) also show essential correlation over the SAV-HAT separation distance, but variations in intensity and structure between stations are more apparent than in the pressure time series. Vector representations or stacks of stick diagrams, of the wind stress during passage of cold front events indicate the clockwise rotation usually associated with the passage of such an event over the station(s). Here it is noted that HAT typically shows the largest stress magnitudes. Alongshore winds tend to dominate both in magnitude and duration relative to the cross-shelf components. Wind stress reversals, noted at all of the met stations,occurred on time scales of several days to several weeks, which is the typical periods of forcing within the atmospheric stress continuum.

Horizontal Wind Coherence:

Figures 64 through 69 indicate the Kinetic Energy Density (KED) spectra of alongshelf and transshelf wind components at stations SAV, CHS, WIL, and HAT. The spectra indicate that within the temporal period 2-14 days, there is a rise in the energy density as approximately the frequency to the minus three halves power, which is consistent with the findings of Oort and Taylor (1969) and Cragg and Sturges (1974) for other coastal regions and is attributed to the passages of cyclones and anticyclones. The KED curve flattens out at periods in excess of 14 days. Within the temporal ranges of interest of the continental shelf studies of

Pietrafesa, the range from the order several days to a month, alongshore winds show a remarkably high degree of visual correlation, save for occasional several day departures, in the station time series shown in Figures 54 through 57. One can observe similarly good visual correlation between transshelf wind components between station pairs over the whole of the radial separation distance with occasional departures, in the same figure series as above.

Over the entire frequency range of 0.5-0.05 cpd, alongshore winds are more energetic than cross-shelf winds. Figures 64 through 67 show this in the KED's for WIL and HAT. Note the strong diurnal signal in the on/off direction.

During the April-July, 1974 subset, alongshore wind components between station pairs are in general more coherent than off/on shore winds at frequencies below 0.23 cpd and vice versa at frequencies above 0.23 cpd. The exceptions are WIL-HAT where C^2 is always higher for alongshore vs. transshore winds and WIL-HAT where alongshore winds are more coherent below 0.3 cpd and transshore winds are more coherent above 0.3 cpd. The Sept.-Dec., 1974 subset offers greater complexity in that, with minor variations, alongshore winds are generally more coherent than cross-shore winds at frequencies below 0.12 cpd, higher between 0.14 and 0.28 cpd at the northerly stations variable pair to pair above the latter frequency. Figures 64 through 75 depict the various cross-correlations. Alongshore wind pairs display less phase shifts, which are typically less than a few hours, than cross-shelf wind pairs. This is evident from both the time series and the cross-correlations. Additionally, it is noted that alongshore winds have C^2's above 0.5 and typically higher than 0.65 over radial separation distances of 630km below frequencies of 0.3 cpd but tend to

Figure 58. Wind stress vectors at Cape Hatteras, N. C., Wilmington, N. C. Charleston, S. C. and Savannah, Ga., Mar. through Apr., 1974

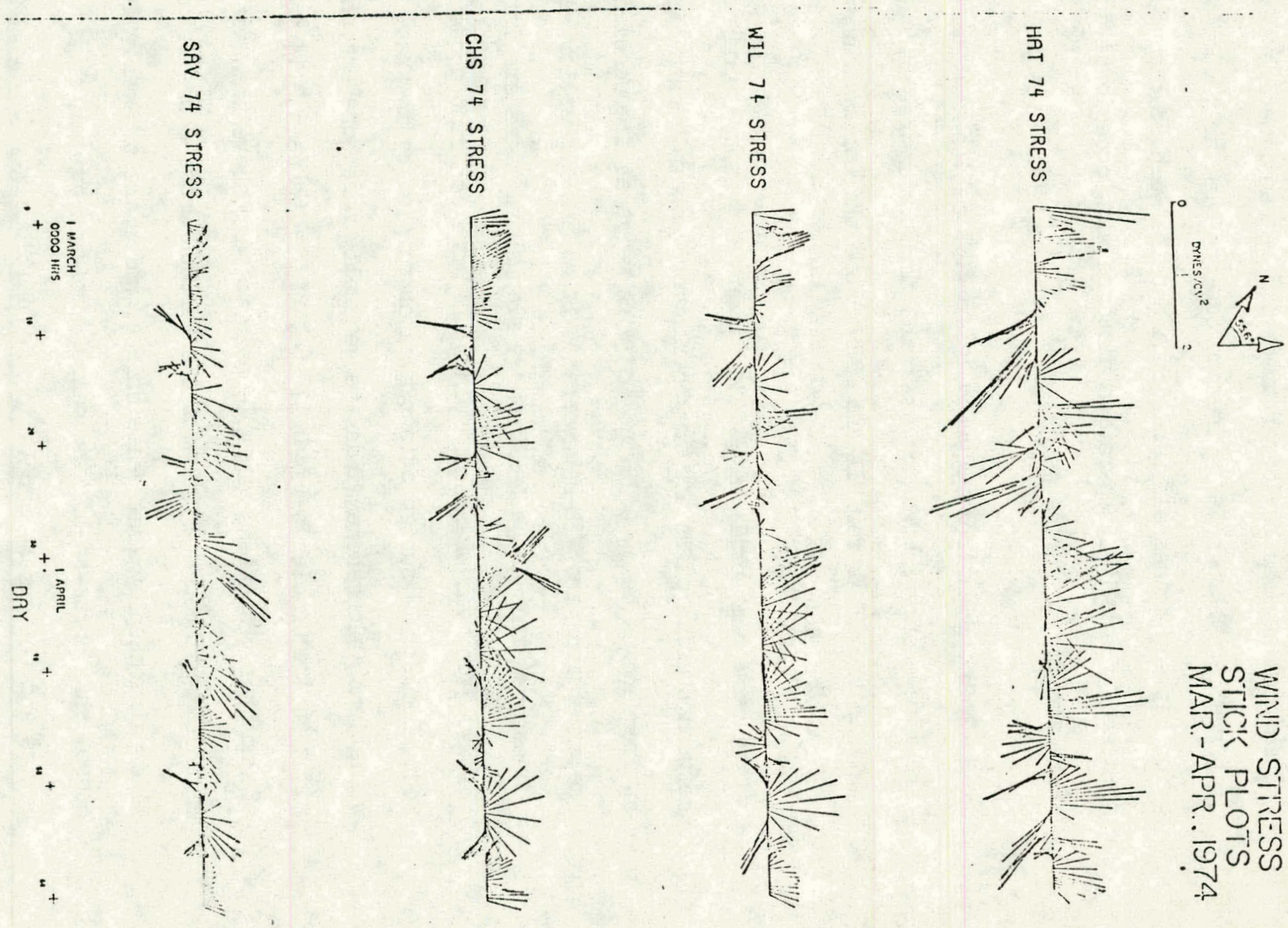

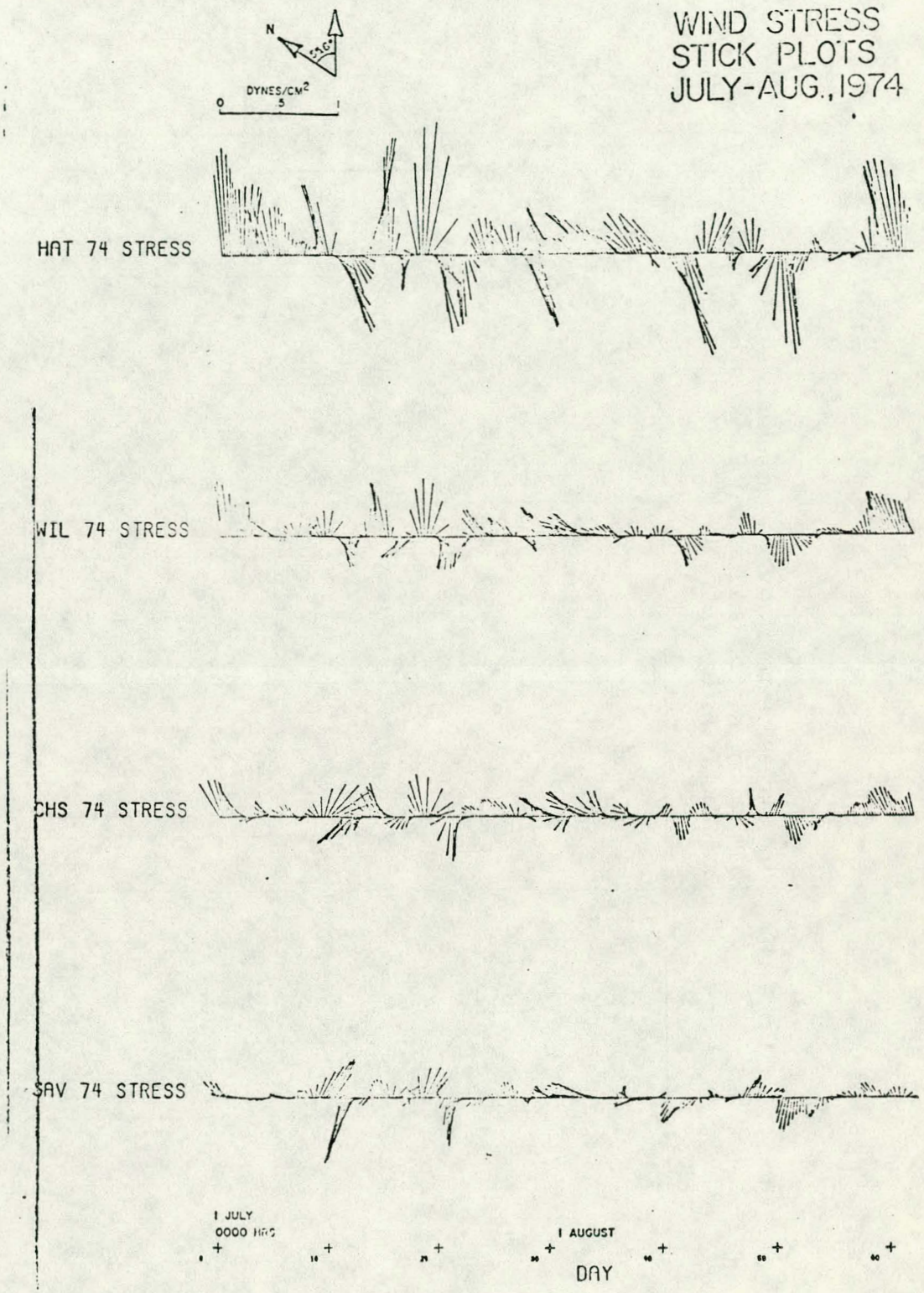

Figure 59. Wind stress vectors at Cape Hatteras, N. C., Wilmington, N. C., Charleston, S. C. and Savannah, Ga., July through Aug., 1974

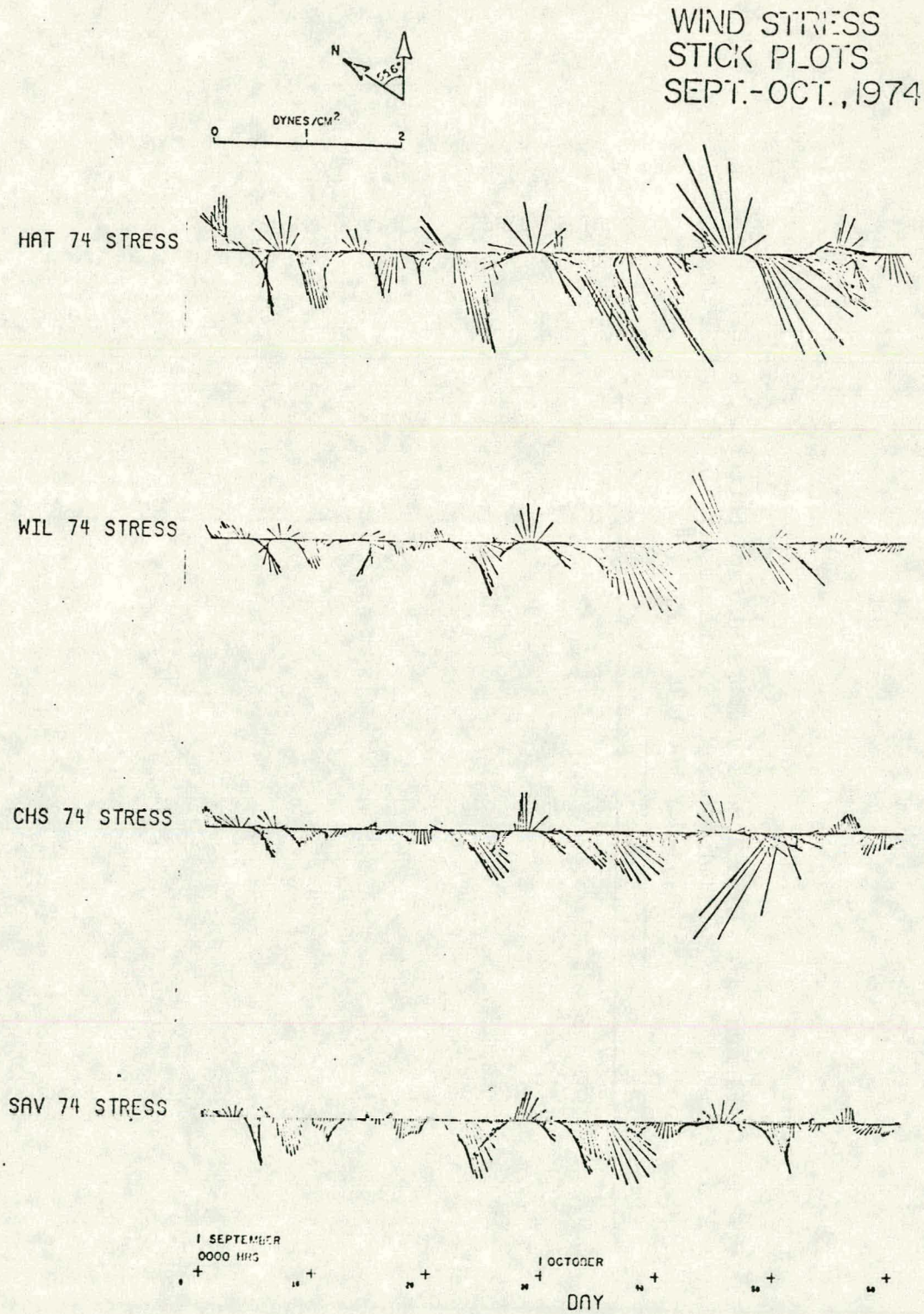

Figure 60. Wind stress vectors at Cape Hatteras, N. C., Wilmington, N. C., Charleston, S. C. and Savannah, Ga., Sept. through Oct., 1974

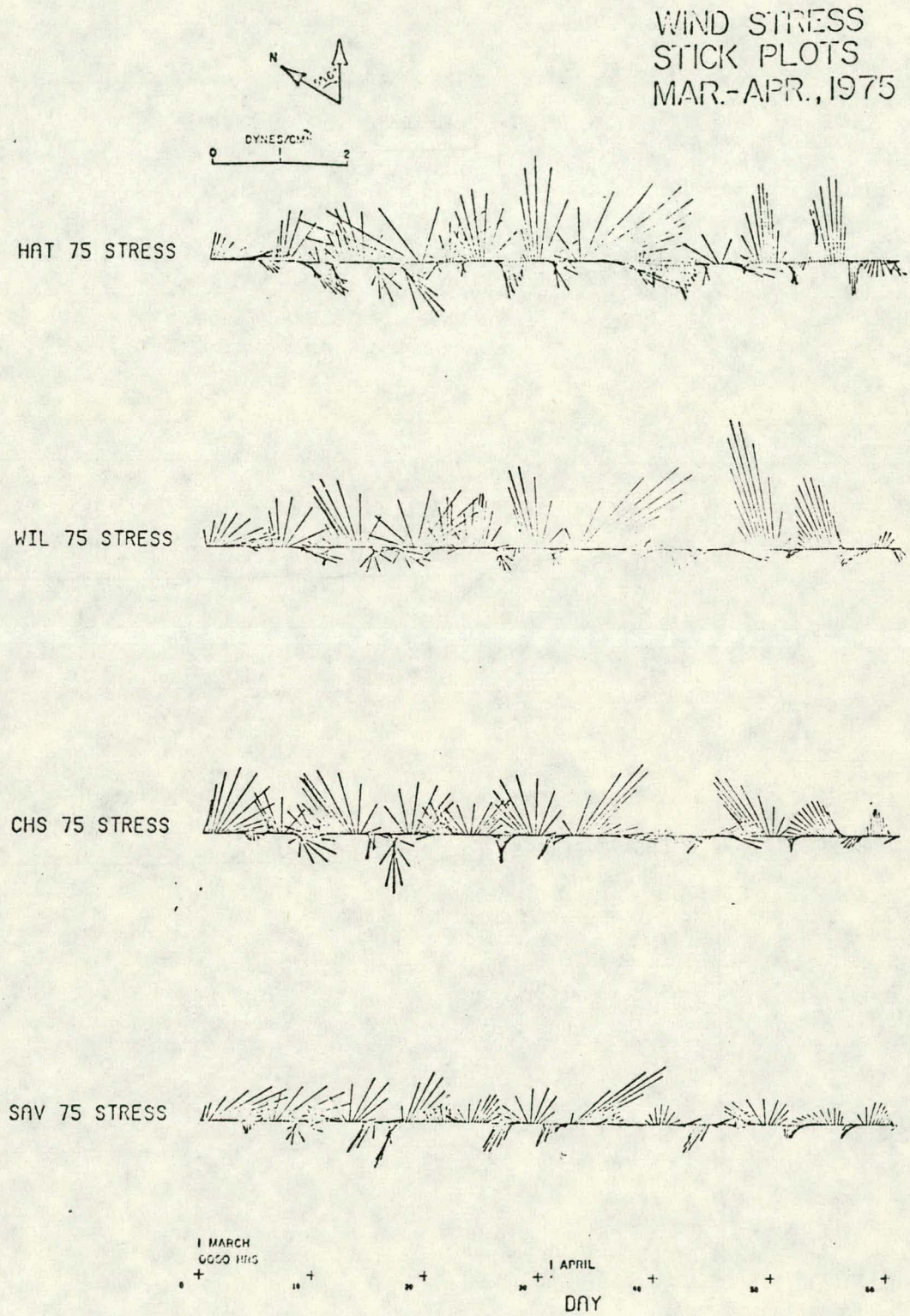

Figure 61. Wind stress vectors at Cape Hatteras, N. C., Wilmington, N. C., Charleston, S. C. and Savannah, Ga., Mar. through Apr., 1975

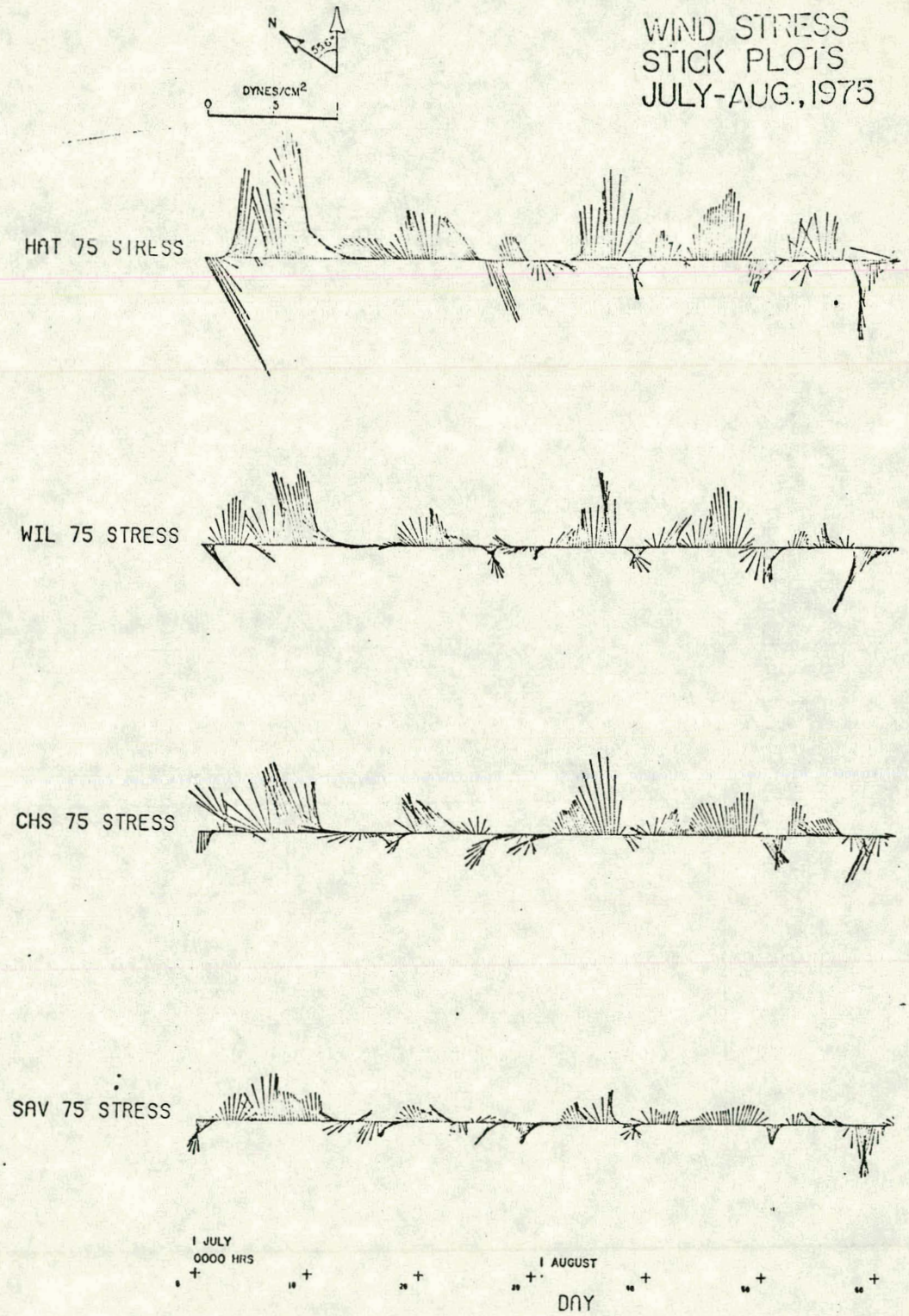
WIND STRESS
STICK PLOTS
JULY-AUG., 1975
N
DYNES/CM2
0
5
HAT 75 STRESS
WIL 75 STRESS
CHS 75 STRESS
SAV 75 STRESS
1 JULY
0000 HRS
1 AUGUST
DAY

Figure 62

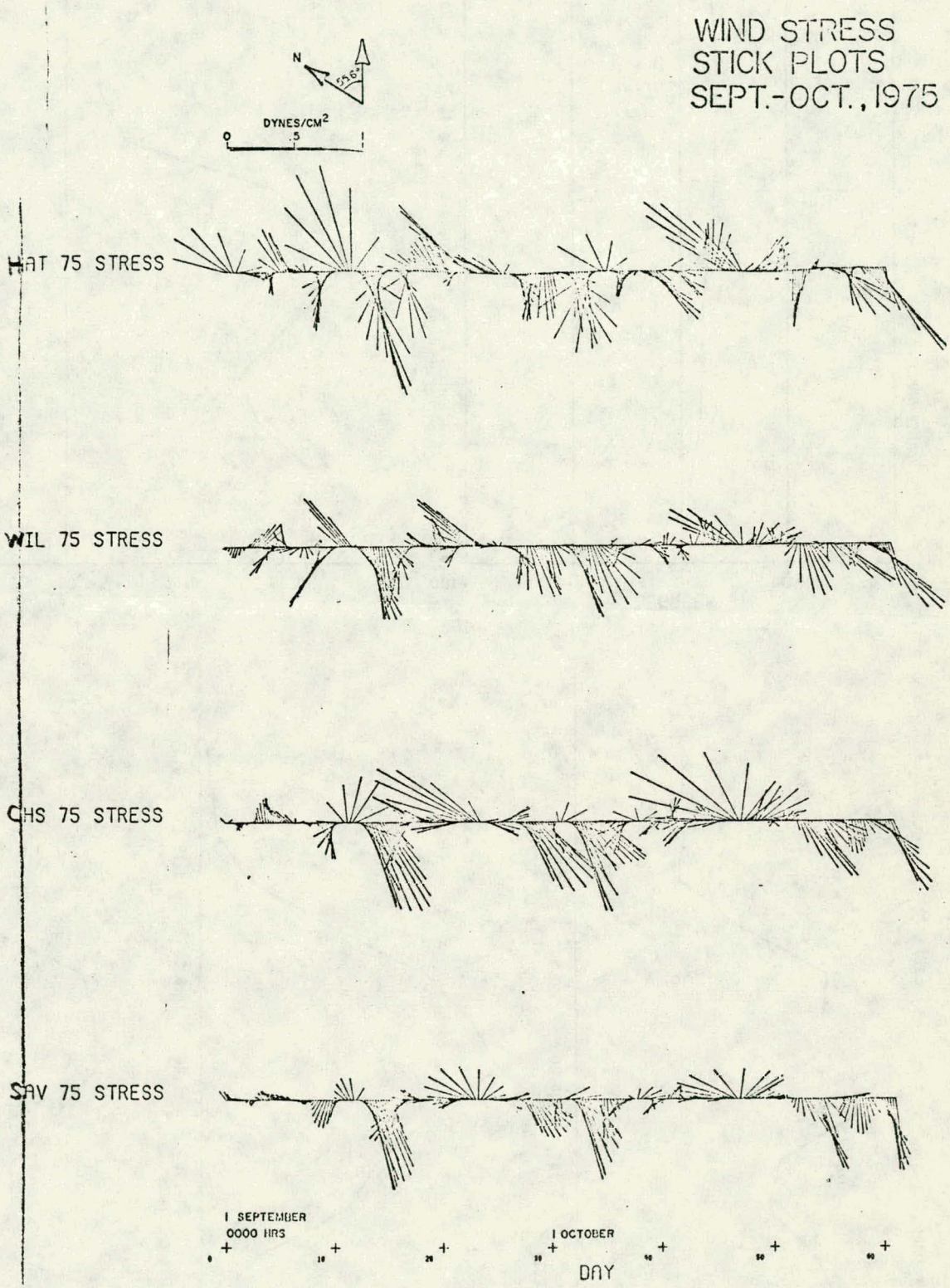
WIND STRESS
STICK PLOTS
SEPT.-OCT., 1975
N
DYNES/CM2
0
.5
1
HAT 75 STRESS
WIL 75 STRESS
CHS 75 STRESS
SAV 75 STRESS
1 SEPTEMBER
0000 HRS
1 OCTOBER
DAY

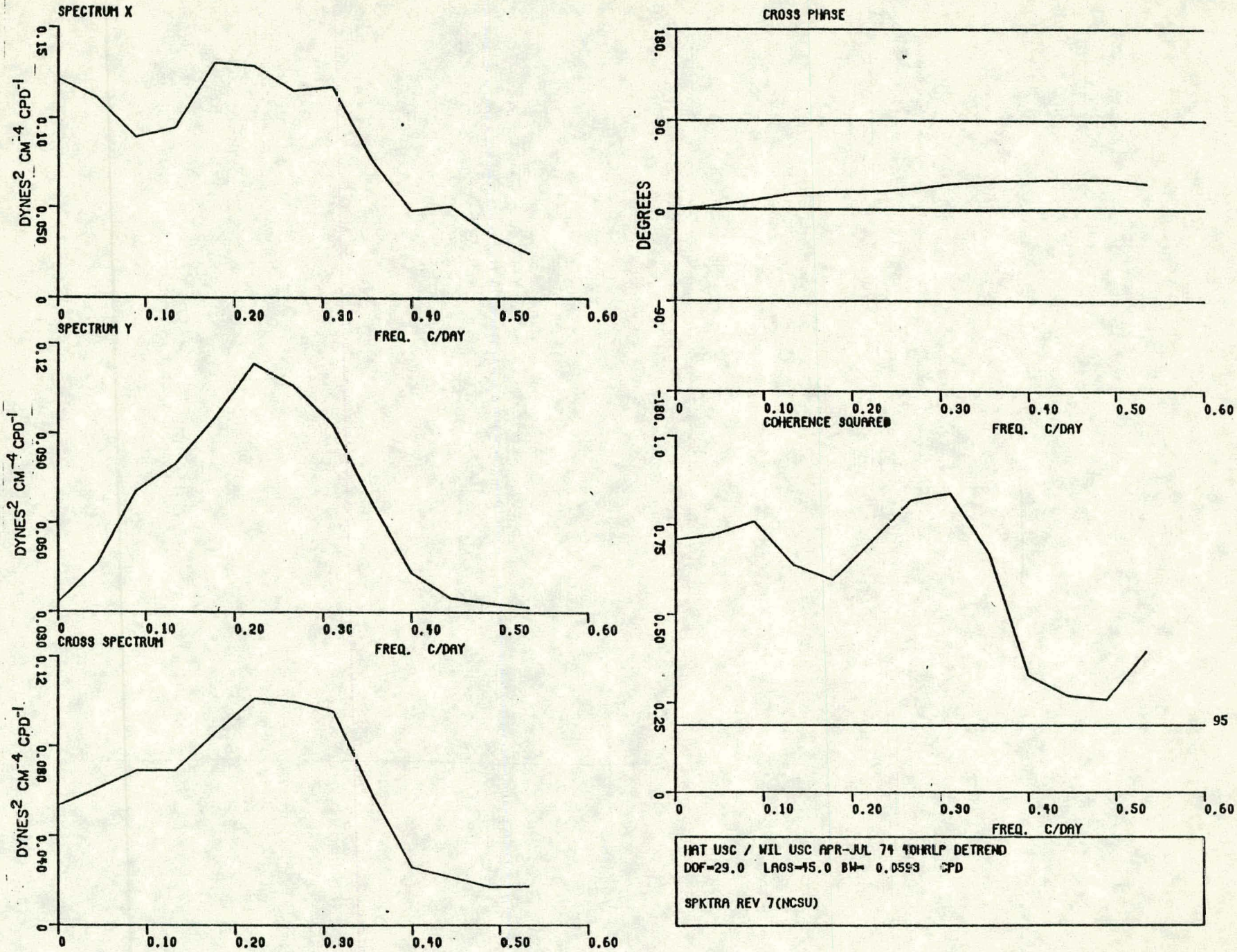
SPECTRUM X
DYNES^2 CM^{-4} CPD^{-1}
0.15
0.10
0.050
0
0.10
0.20
0.30
0.40
0.50
0.60
FREQ. C/DAY
SPECTRUM Y
DYNES^2 CM^{-4} CPD^{-1}
0.12
0.090
0.060
0.030
CROSS SPECTRUM
DYNES^2 CM^{-4} CPD^{-1}
0.120
0.080
0.040
CROSS PHASE
DEGREES
180.
90.
0
-90.
-180.
COHERENCE SQUARED
1.0
0.75
0.50
0.25
95
HAT USC / WIL USC APR-JUL 74 40HRLP DETREND
DOF=29.0 LAGS=45.0 BW= 0.0593 CPD
SPKTRA REV 7(NCSU)

Figure 64

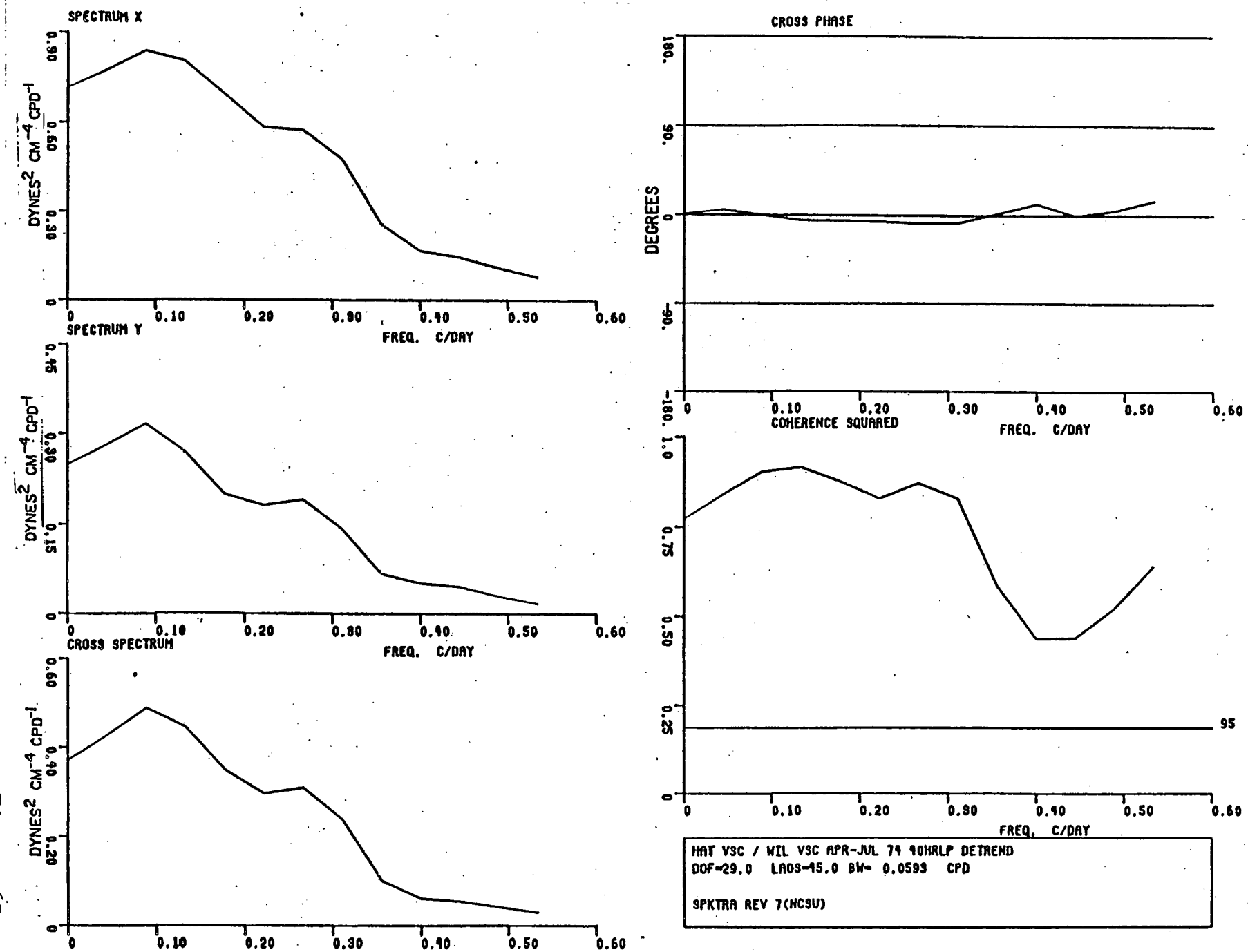
SPECTRUM X
DYNES^2 CM^{-4} CPD^{-1}
0.90
0.60
0.30
0
0.10
0.20
0.30
0.40
0.50
0.60
FREQ. C/DAY
SPECTRUM Y
DYNES^2 CM^{-4} CPD^{-1}
0.45
0.30
0.15
0
FREQ. C/DAY
CROSS SPECTRUM
DYNES^2 CM^{-4} CPD^{-1}
0.60
0.40
0.20
0
FREQ. C/DAY
CROSS PHASE
DEGREES
180.
90.
0
-90.
-180.
FREQ. C/DAY
COHERENCE SQUARED
1.0
0.75
0.50
0.25
0
95
FREQ. C/DAY
HAT VSC / WIL VSC APR-JUL 74 40HRLP DETREND
DOF=29.0 LAGS=45.0 BW= 0.0593 CPD
SPKTRA REV 7(NCSU)

Figure 65

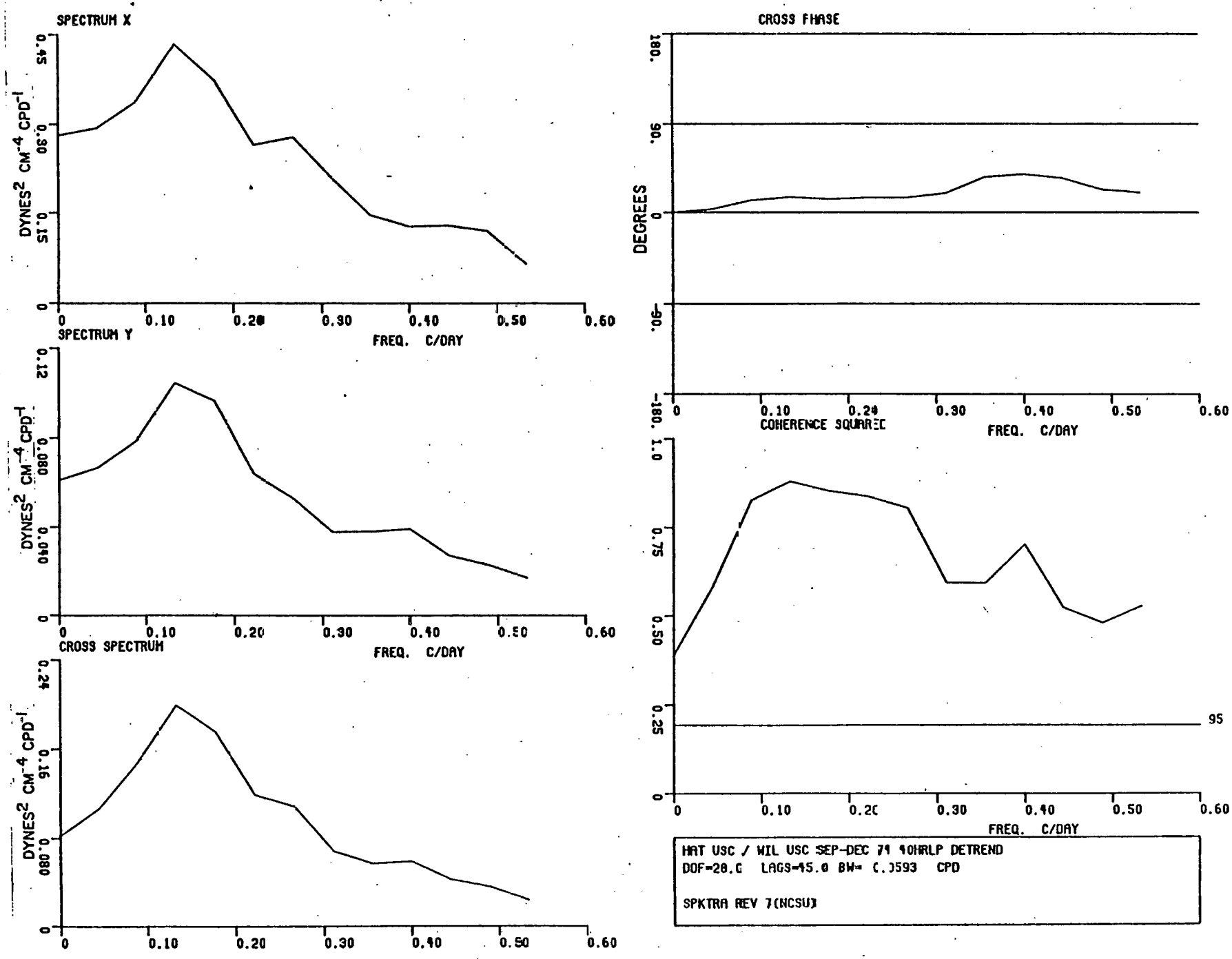
SPECTRUM X
DYNES^2 CM^{-4} CPD^{-1}
0.45
0.30
0.15
0
0.10
0.20
0.30
0.40
0.50
0.60
FREQ. C/DAY
SPECTRUM Y
DYNES^2 CM^{-4} CPD^{-1}
0.12
0.080
0.040
0
0.10
0.20
0.30
0.40
0.50
0.60
FREQ. C/DAY
CROSS SPECTRUM
DYNES^2 CM^{-4} CPD^{-1}
0.24
0.16
0.080
0
0.10
0.20
0.30
0.40
0.50
0.60
CROSS PHASE
DEGREES
180.
90.
0
-90.
-180.
0.10
0.20
0.30
0.40
0.50
0.60
FREQ. C/DAY
COHERENCE SQUARED
1.0
0.75
0.50
0.25
0
95
0.10
0.20
0.30
0.40
0.50
0.60
FREQ. C/DAY
HAT USC / WIL USC SEP-DEC 71 40HRLP DETREND
DOF=20.0 LAGS=45.0 BW= 0.0593 CPD
SPKTRA REV 7(NCSU)

Figure 66

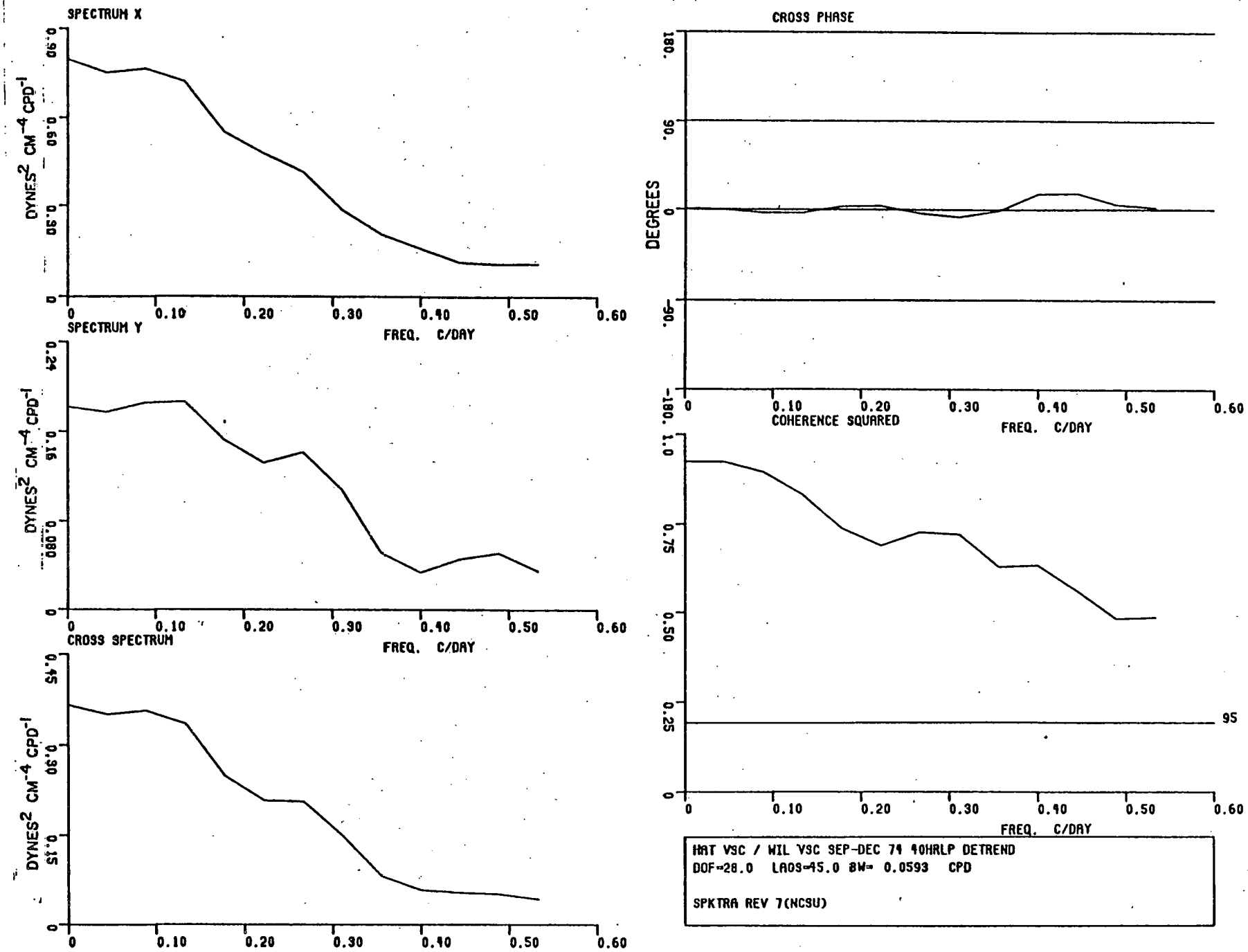
SPECTRUM X
DYNES^2 CM^{-4} CPD^{-1}
0.90
0.60
0.30
0
0.10
0.20
0.30
0.40
0.50
0.60
FREQ. C/DAY
SPECTRUM Y
DYNES^2 CM^{-4} CPD^{-1}
0.24
0.16
0.080
0
0.10
0.20
0.30
0.40
0.50
0.60
FREQ. C/DAY
CROSS SPECTRUM
DYNES^2 CM^{-4} CPD^{-1}
0.45
0.30
0.15
0
0.10
0.20
0.30
0.40
0.50
0.60
FREQ. C/DAY
CROSS PHASE
DEGREES
180.
90.
0
-90.
-180.
0.10
0.20
0.30
0.40
0.50
0.60
FREQ. C/DAY
COHERENCE SQUARED
1.0
0.75
0.50
0.25
0
95
0.10
0.20
0.30
0.40
0.50
0.60
FREQ. C/DAY
HAT VSC / WIL VSC SEP-DEC 74 40HRLP DETREND
DOF=28.0 LAGS=45.0 BW= 0.0593 CPD
SPKTRA REV 7(NCSU)

Figure 67

decrease at a rate of 0.1 per 150km increase in radial station pair distance.

It can therefore be concluded that winds recorded at any one of the coastal stations could, at least qualitatively, be representative of the wind fields at any of the other stations, with appropriate reservation. The adequacy of representation is an event, season, location sensitive variable, but for events within the frequency band 0.3 to 0.05 cpd the contention is not without evidential basis. What is suggested herein is that the divergence of the alongshore wind stress may not be large, and furthermore that possibly the curl of the cross-shore wind stress may not be large but the data indicates little of a definitive nature about the curl of $\tau^{(y)}$ or the divergence of $\tau^{(x)}$ and moreover nothing about the offshore wind field structure, which is the actual mechanical forcing function.

Atmospheric Pressure Coherence

Forty hour low-passed atmospheric pressure from the met stations indicate a high degree of coherence with daily pressures rarely differing by more than several millibars between stations. The phase shifts are nearly zero at all frequencies save for shifts of the order of 0-20 degrees over radial distances the order of 100-650kms (egs. HAT/WIL, Fig. 68; HAT/SAV, Fig. 69; CHS/SAV, Fig. 70). The southerly met stations typically lead the more northerly stations (eg. CHS leads HAT) for the entire separate series lengths of years 1974 and 1975. Considering the 4 month block, April-July 1974, though: HAT lags WIL only at frequencies greater than 0.2 cpd, below that the pair are in 0 degree phase; WIL leads CHS from 0.1-0.2 cpd, lags above and is in 0 degree phase below; CHS leads

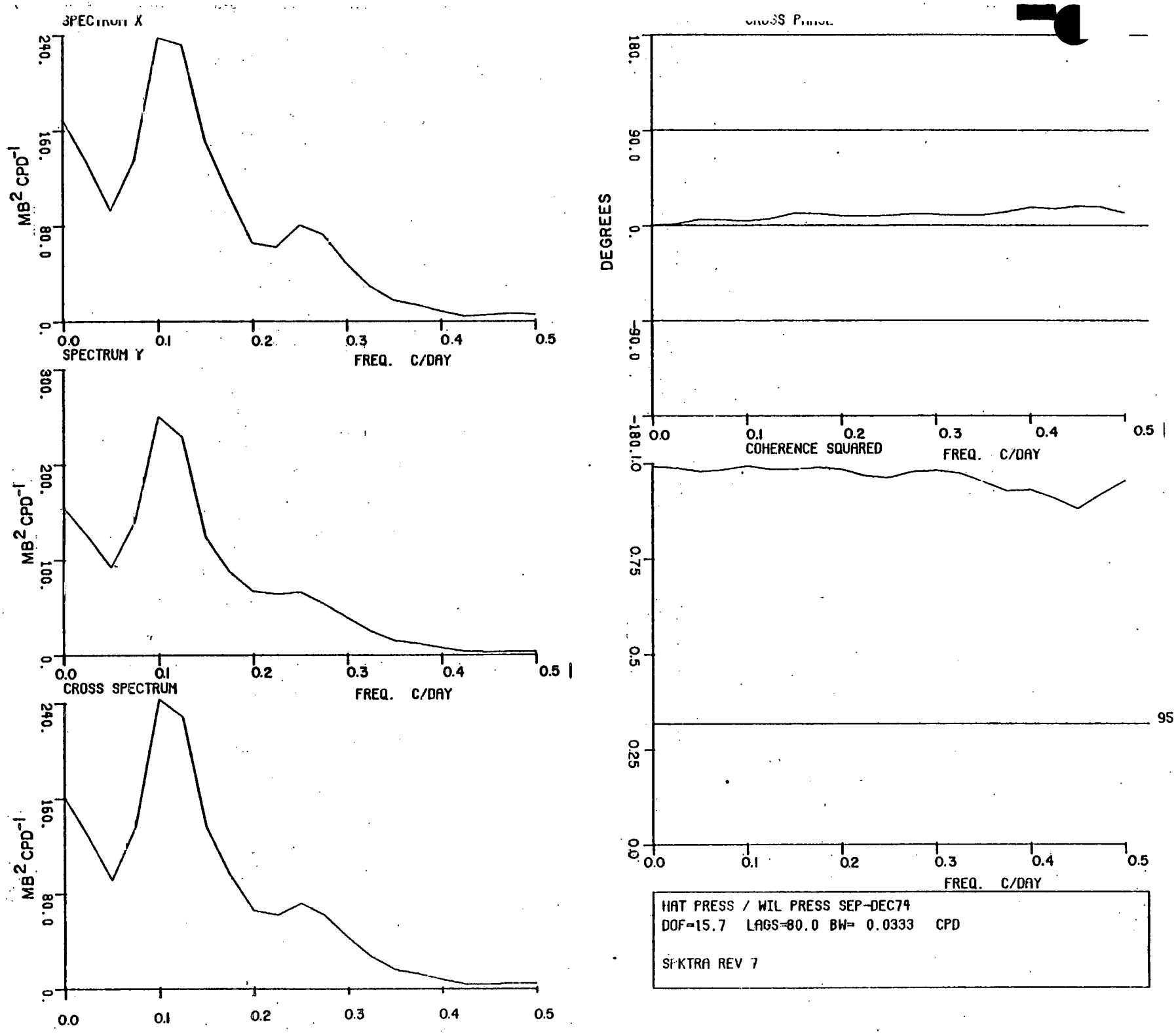
SPECTRUM X
MB2 CPD-1
FREQ. C/DAY
SPECTRUM Y
MB2 CPD-1
FREQ. C/DAY
CROSS SPECTRUM
MB2 CPD-1
FREQ. C/DAY
CROSS PHASE
DEGREES
FREQ. C/DAY
COHERENCE SQUARED
95
FREQ. C/DAY
HAT PRESS / WIL PRESS SEP-DEC74
DOF=15.7 LAGS=80.0 BW= 0.0333 CPD
SPKTRA REV 7

Figure 60

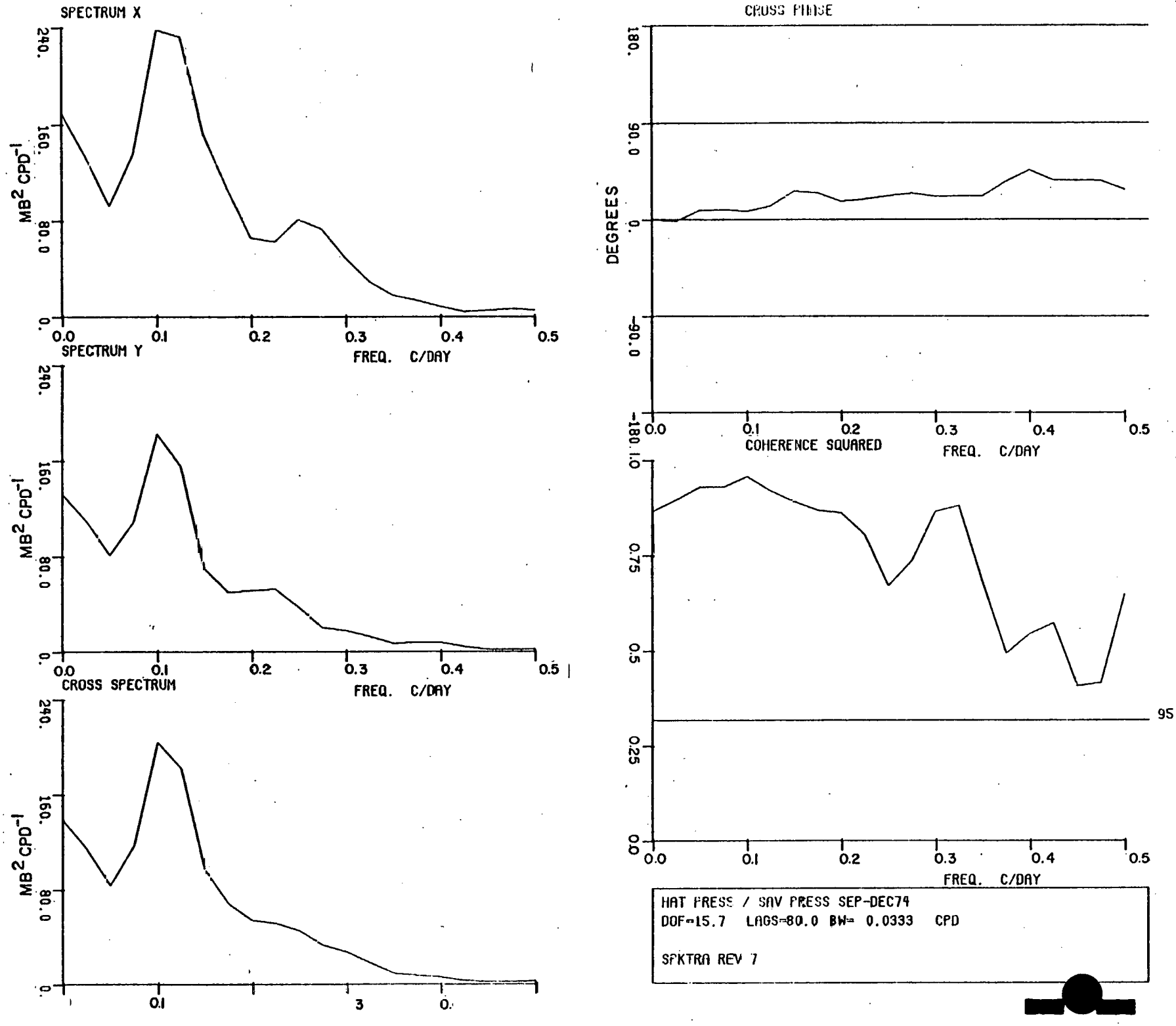
SPECTRUM X
MB2 CPD-1
FREQ. C/DAY
SPECTRUM Y
MB2 CPD-1
FREQ. C/DAY
CROSS SPECTRUM
MB2 CPD-1
CROSS PHASE
DEGREES
FREQ. C/DAY
COHERENCE SQUARED
FREQ. C/DAY
95
HAT PRESS / SAV PRESS SEP-DEC74
DOF=15.7 LAGS=80.0 BW= 0.0333 CPD
SPKTRA REV 7

Figure 69

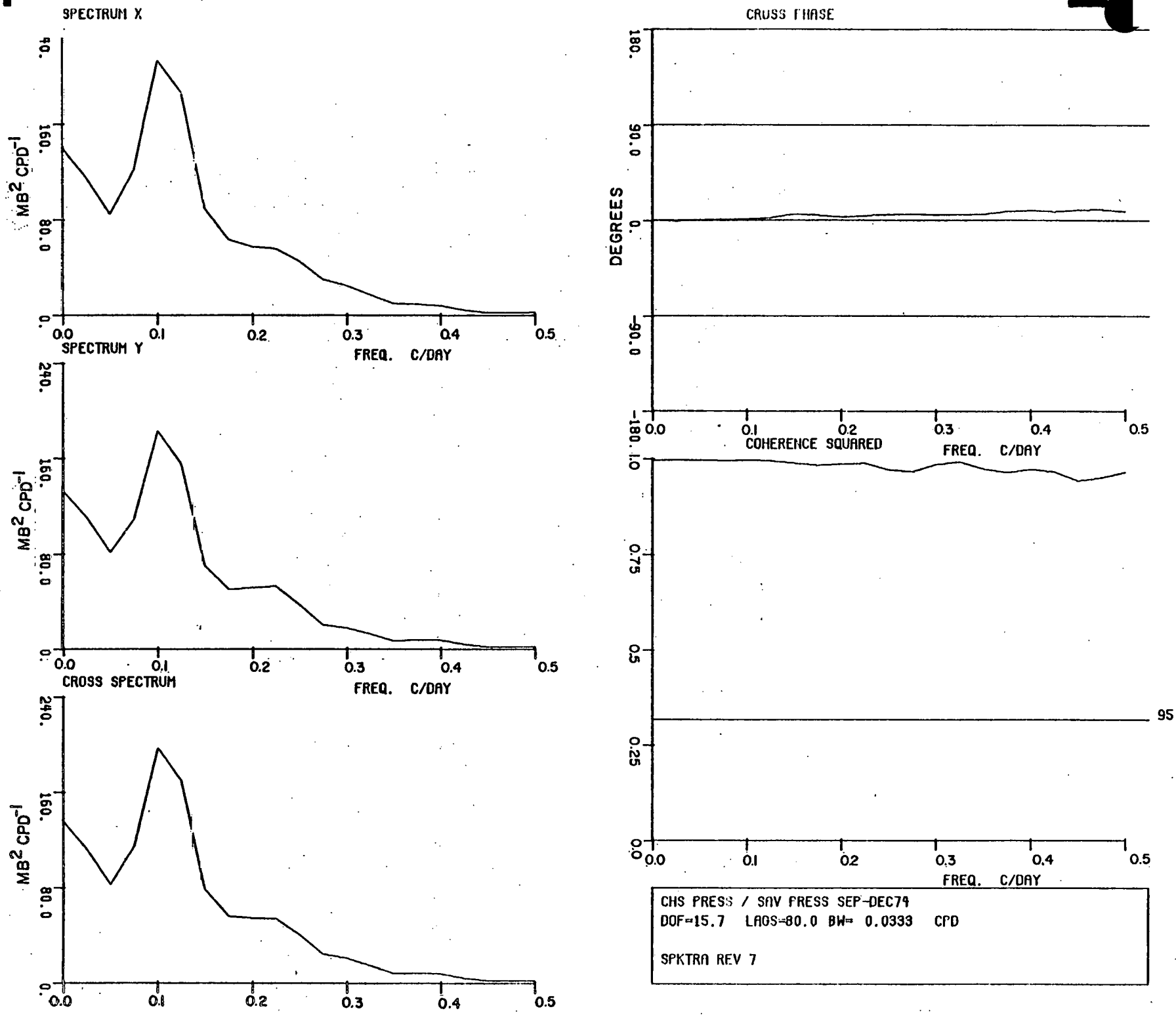
SPECTRUM X
MB2 CPD-1
FREQ. C/DAY
SPECTRUM Y
MB2 CPD-1
FREQ. C/DAY
CROSS SPECTRUM
MB2 CPD-1
FREQ. C/DAY
CROSS PHASE
DEGREES
FREQ. C/DAY
COHERENCE SQUARED
95
FREQ. C/DAY
CHS PRESS / SAV PRESS SEP-DEC74
DOF=15.7 LAGS=80.0 BW= 0.0333 CPD
SPKTRA REV 7

Figure 70

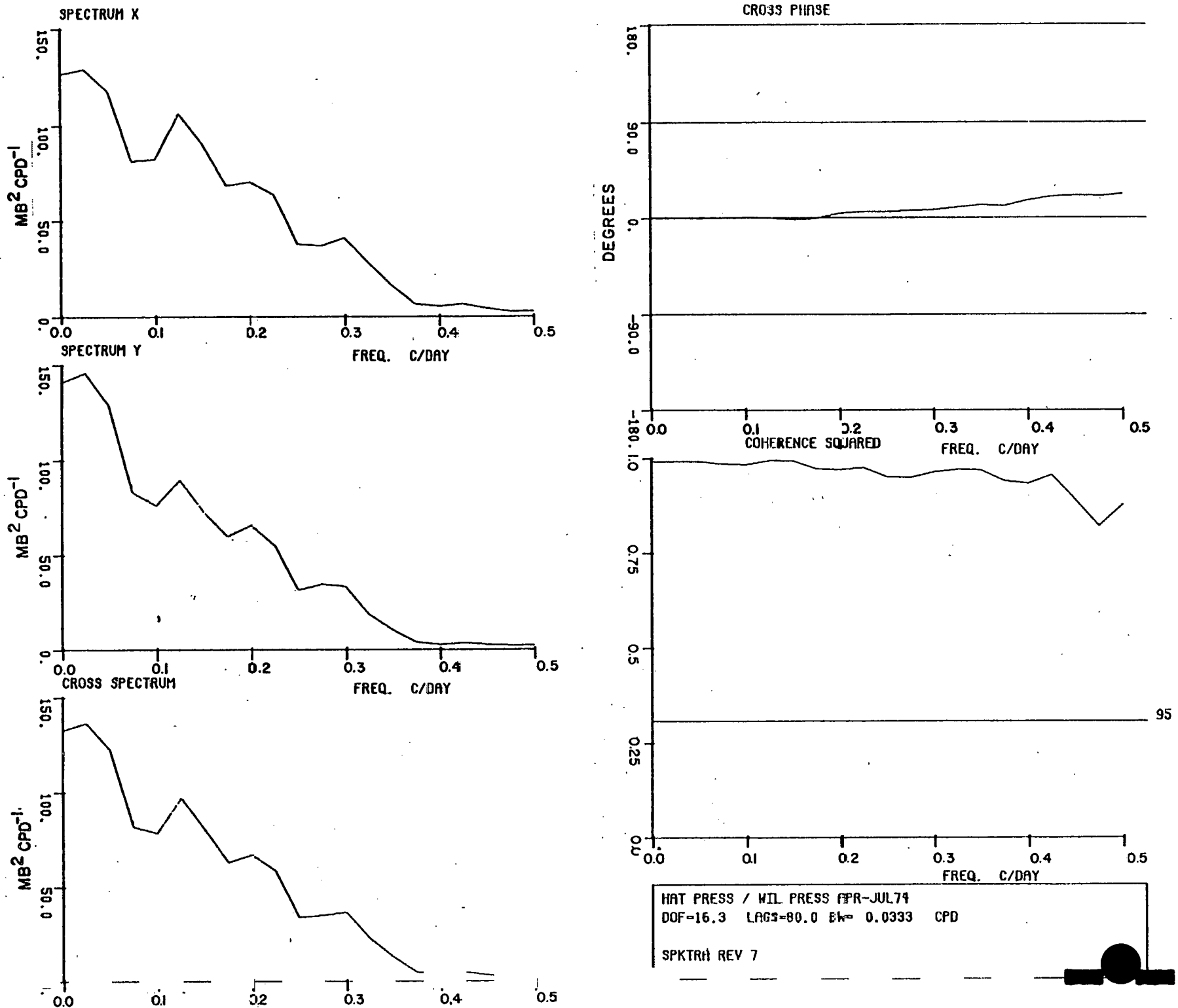
SPECTRUM X
MB2 CPD-1
FREQ. C/DAY
SPECTRUM Y
MB2 CPD-1
FREQ. C/DAY
CROSS SPECTRUM
MB2 CPD-1
CROSS PHASE
DEGREES
FREQ. C/DAY
COHERENCE SQUARED
FREQ. C/DAY
95
HAT PRESS / WIL PRESS APR-JUL74
DOF=16.3 LAGS=80.0 BW= 0.0333 CPD
SPKTRA REV 7

Figure 71

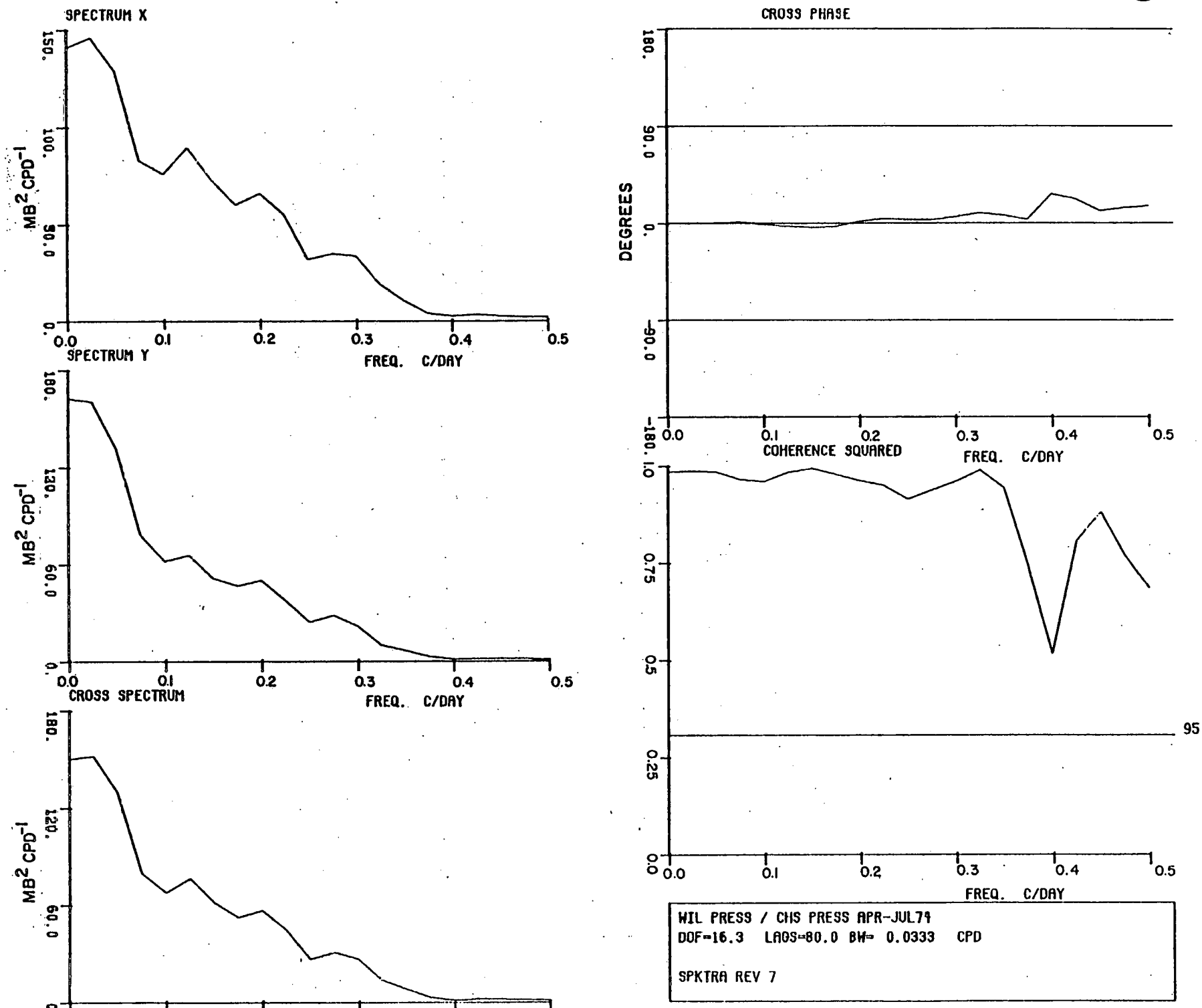
SPECTRUM X
MB2 CPD-1
FREQ. C/DAY
SPECTRUM Y
MB2 CPD-1
FREQ. C/DAY
CROSS SPECTRUM
MB2 CPD-1
FREQ. C/DAY
CROSS PHASE
DEGREES
FREQ. C/DAY
COHERENCE SQUARED
FREQ. C/DAY
95
WIL PRESS / CHS PRESS APR-JUL74
DOF=16.3 LAGS=80.0 BW= 0.0333 CPD
SPKTRA REV 7

Figure 72

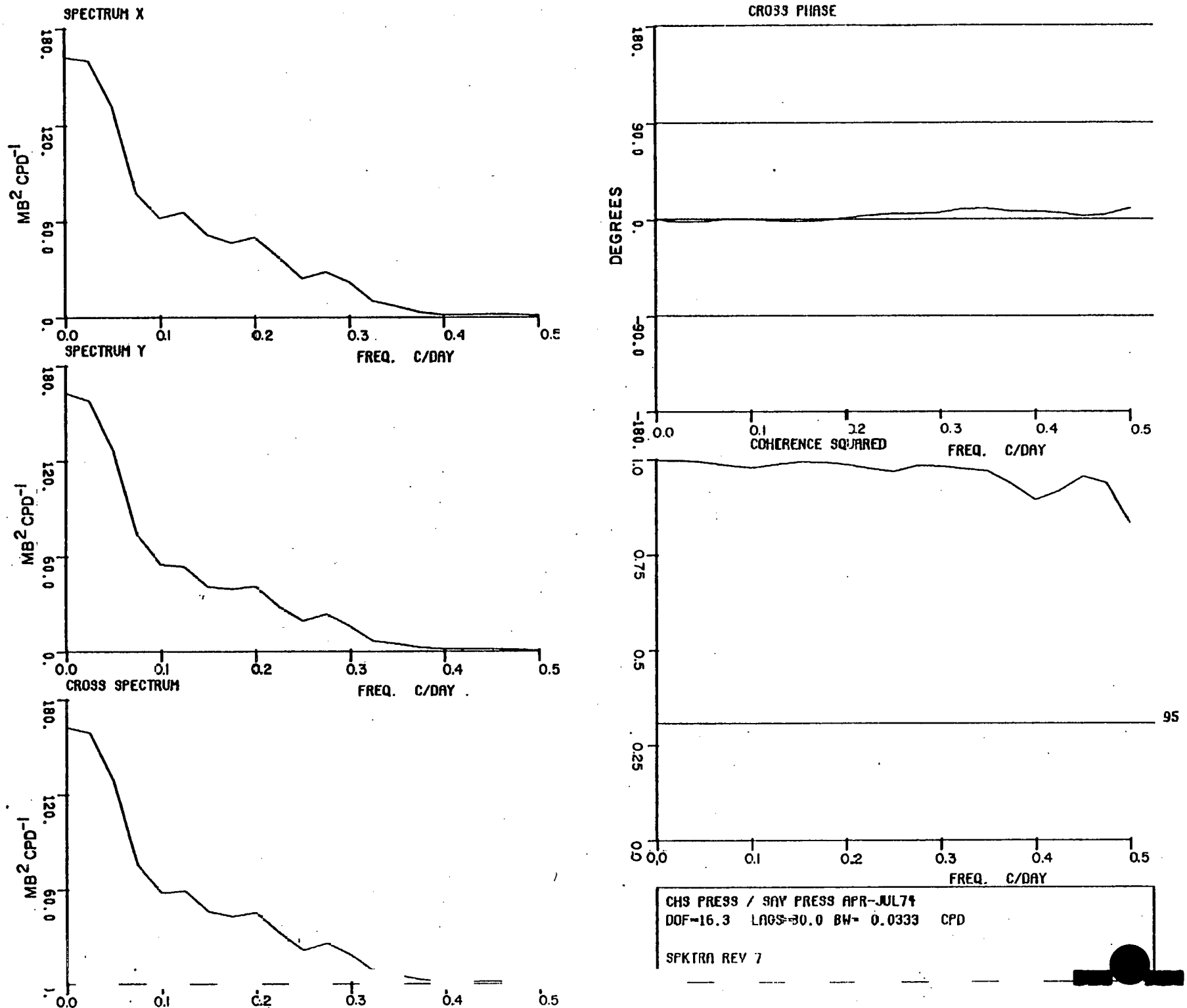
SPECTRUM X
MB2 CPD-1
FREQ. C/DAY
SPECTRUM Y
MB2 CPD-1
FREQ. C/DAY
CROSS SPECTRUM
MB2 CPD-1
FREQ. C/DAY
CROSS PHASE
DEGREES
FREQ. C/DAY
COHERENCE SQUARED
95
FREQ. C/DAY
CHS PRESS / SAY PRESS APR-JUL74
DOF=16.3 LAGS=30.0 BW= 0.0333 CPD
SPKTRA REV 7

Figure 73

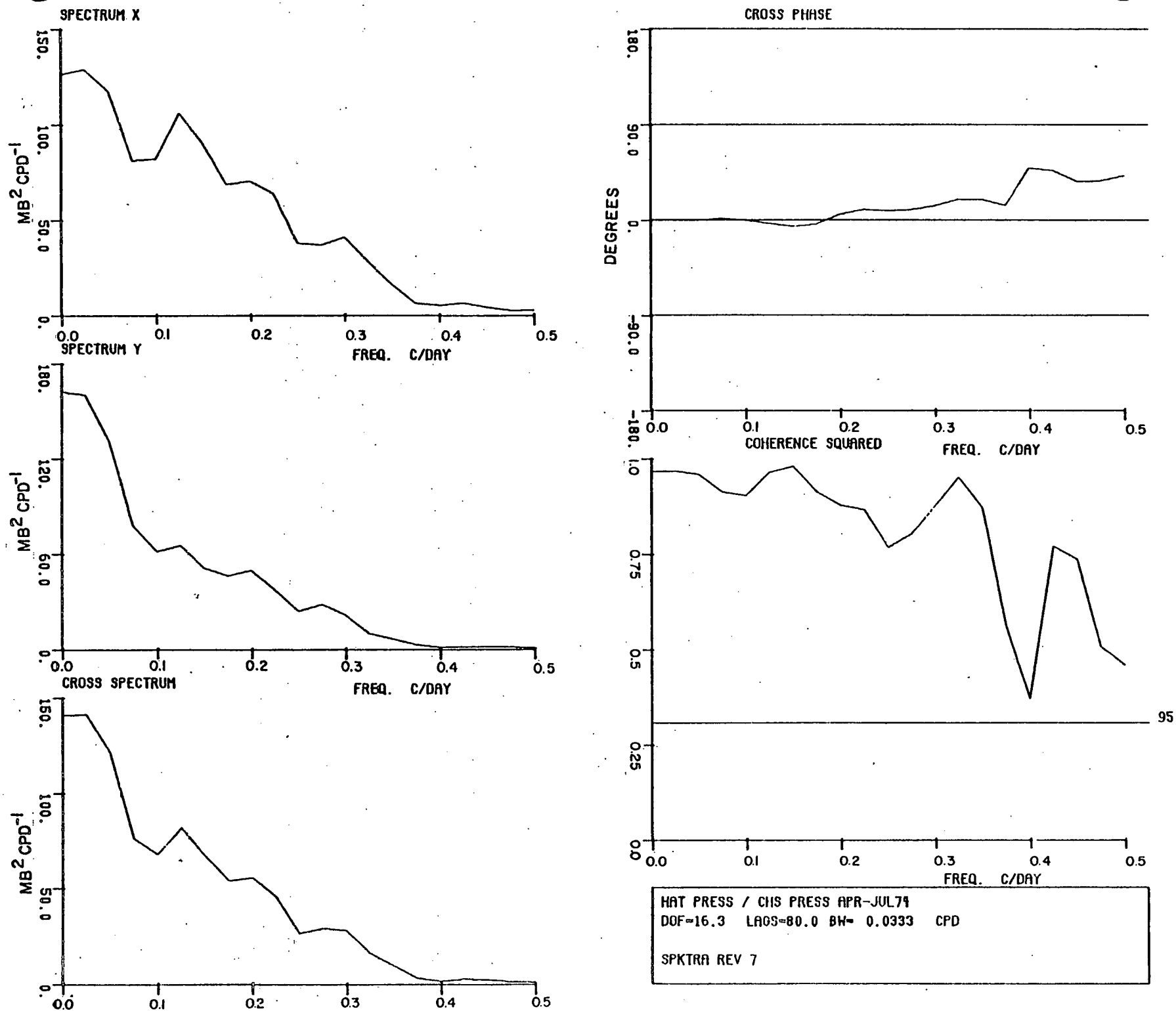
SPECTRUM X
MB2 CPD-1
150.
100.
50.0
0.
0.0
0.1
0.2
0.3
0.4
0.5
FREQ. C/DAY
SPECTRUM Y
MB2 CPD-1
180.
120.
60.0
0.
CROSS SPECTRUM
MB2 CPD-1
CROSS PHASE
DEGREES
180.
90.0
0.
-90.0
-180.
COHERENCE SQUARED
1.0
0.75
0.5
0.25
0.0
95
HAT PRESS / CHS PRESS APR-JUL79
DOF=16.3 LAGS=80.0 BW= 0.0333 CPD
SPKTRA REV 7

Figure 74

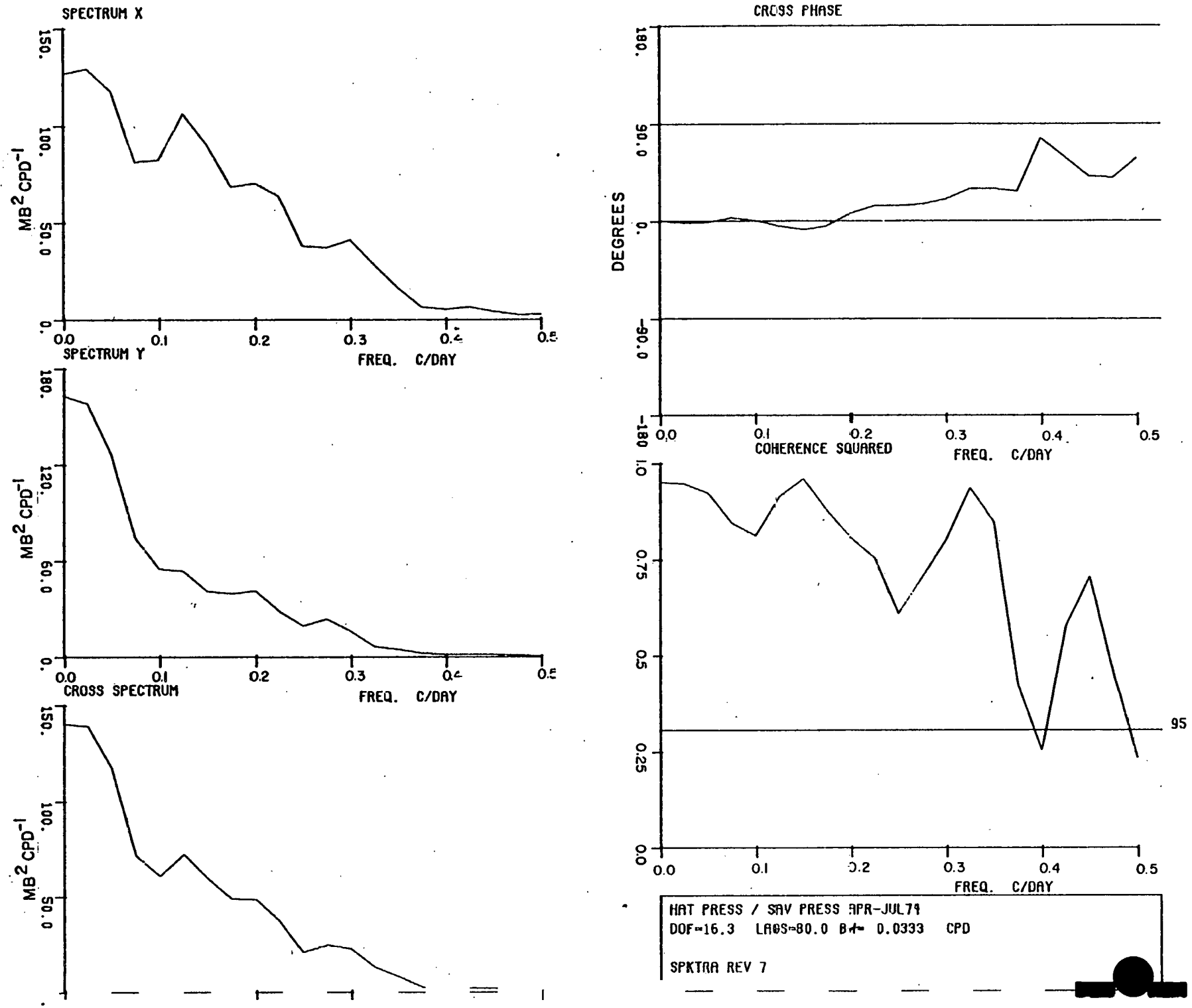
SPECTRUM X
MB² CPD⁻¹
FREQ. C/DAY
SPECTRUM Y
MB² CPD⁻¹
FREQ. C/DAY
CROSS SPECTRUM
MB² CPD⁻¹
CROSS PHASE
DEGREES
FREQ. C/DAY
COHERENCE SQUARED
95
FREQ. C/DAY
HAT PRESS / SAV PRESS APR-JUL79
DOF=16.3 LAGS=80.0 BW= 0.0333 CPD
SPKTRA REV 7

Figure 75

SAV from below 0.2 cpd and lags above 0.2 cpd; HAT leads CHS between 0.2-0.1 cpd, lags above and is in phase below; HAT leads SAV between 0.2-0.1 cpd and lags below. During the period Sept.-Dec., 1974, the southerly stations consistently lead the more northerly station pair, over all frequencies, with no exceptions. It certainly appears, herein, from the cross-correlations between station pairs that the pressure spectrum at any individual station is reasonably representative of that at any other with minor adjustments in phase as a function of the pairing and the frequency. Coherence squared (C^2) is typically in excess of 0.9 over station radial separation distances the order of 200km and drops off from 0.95 to 0.5 at distances in excess of 400km in the 0.1-0.5 cpd band. Exceptions to the rule are noted for: WIL-CHS, C^2 of 0.5 at 0.4 cpd during April-July, 1974; HAT-CHS, C^2 of 0.3 at 0.4 cpd during April-July, 1974; HAT-SAV, C^2 of 0.25 at 0.4 cpd during Sept.-Dec., 1974; and WIL-CHS, C^2 of 0.75 at 0.4 cpd during Sept.-Dec., 1974.

Sea Level

As described earlier, the sea level data were low pass filtered using a Lanczos filter taper to attenuate the diurnal and semi-diurnal tides and inertial fluctuations (cf. Figure 53).

Among factors which significantly affect sea level, particular note is made to the variations in atmospheric pressure, atmospheric winds, oceanic currents and long, shelf wave phenomena. The response of the level of the sea surface to varying atmospheric pressure is more correctly expressed in terms of a frequency dependent barometric factor, i.e., a transfer function for the pressure and sea level system. Herein, the sea level data was "adjusted" (as well as left "unadjusted") for the so-called "barometric effect." For frequencies below 1 cpd, the sea surface responds

to changes in atmospheric pressure in a reasonably regular, nearly instantaneous fashion. The adjustment suggested over nearly the entire frequency range of interest in this study (eg. Roden, 1960; Mysak and Hamon, 1969) for sea level fluctuations due to varying barometric pressure is about 1.0 cm/mbar, i.e., a one millibar increase (decrease) in pressure depresses (elevates) the sea surface approximately 1 centimeter.

Spectral analyses of alongshore and cross-shore winds, separately, and sea level are shown in the series of Figures 76 through 80. Remarkably high C^2 results between sea level and alongshore winds, especially at frequencies below 0.35 cpd, over the 1974 and 1975 yearly series, as well as the 4 month series blocks, April-July and Sept.-Dec., 1974. The cross-coast wind vs. sea level comparisons, at co-incident or nearby sites, indicate more selective coherence bands. Some of the potential hazards which should be noted in this preliminary comparison are that the Wilmington tide gage is located 27 miles from the mouth of the Cape Fear River Estuary, a tidally influenced coastal plain estuary which undoubtedly has a sea level response signature very different from that of an open, coastal station. Consequently, any intercomparisons of sea level at WIL and any other station, save for one at the mouth or between, in the Cape Fear River Estuary, as was done by Brooks (1977) to confirm the existence and southerly propagation of continental shelf waves, must be done so with appropriate reservation. Likewise, the incomparisons of HAT atmospheric data and BFT sea level must be considered in view of the 140 km radial separation of the two stations.

C^2's the order of 0.7 to 0.95 between wind and sea level appear over period bands 3-4 days and 5-10 days in the alongshore wind intercomparisons (eg. CHS v stress vs. CHS ADJ SEALVL APR-JUL 74, Fig. 77 and SEP-DEC 74,

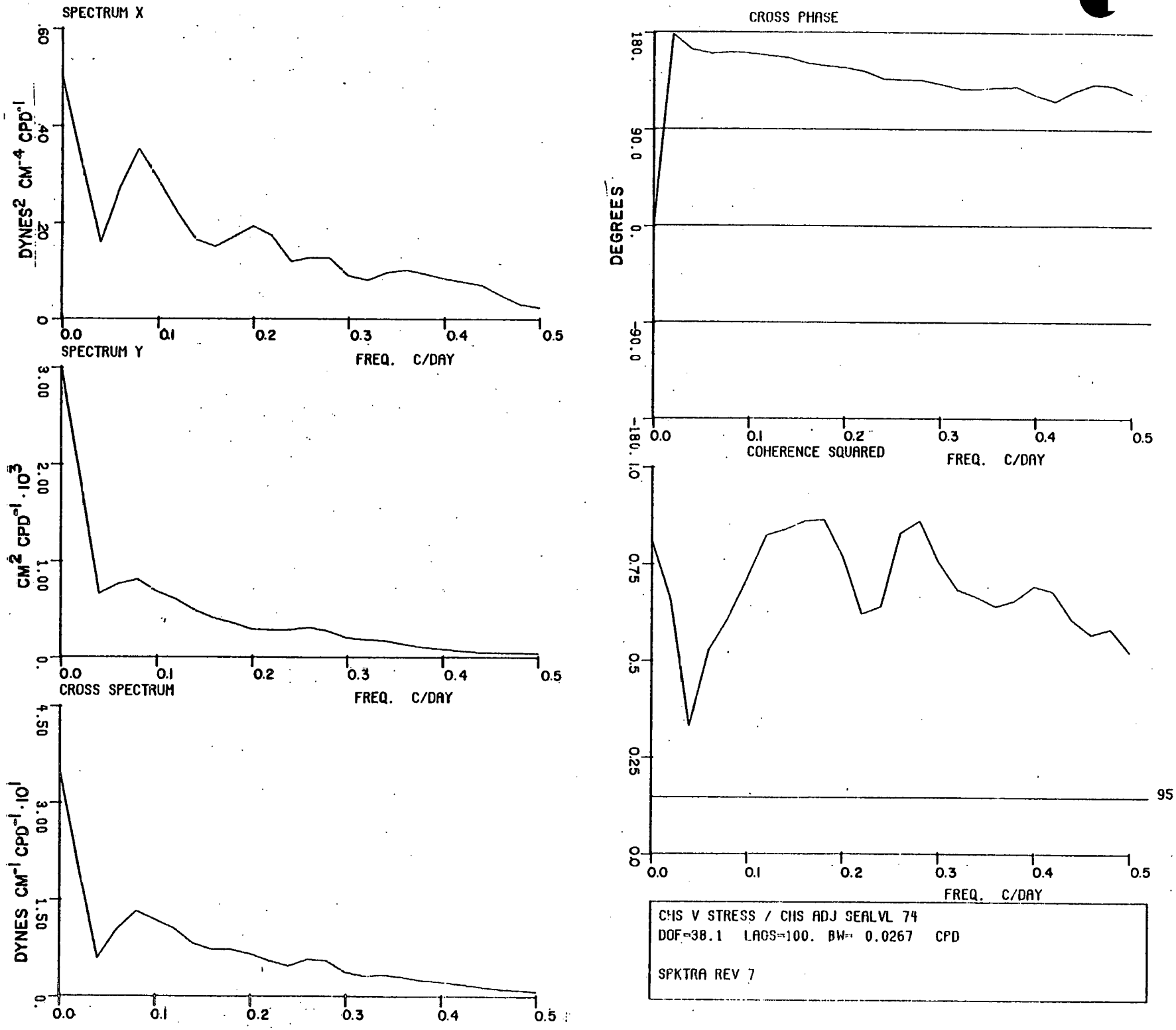
SPECTRUM X
DYNES² CM⁻⁴ CPD⁻¹
FREQ. C/DAY
SPECTRUM Y
CM² CPD⁻¹ · 10³
FREQ. C/DAY
CROSS SPECTRUM
DYNES CM⁻¹ CPD⁻¹ · 10¹
FREQ. C/DAY
CROSS PHASE
DEGREES
FREQ. C/DAY
COHERENCE SQUARED
95
FREQ. C/DAY
CHS V STRESS / CHS ADJ SEALVL 74
DOF=38.1 LAGS=100. BW= 0.0267 CPD
SPKTRA REV 7

Figure 76

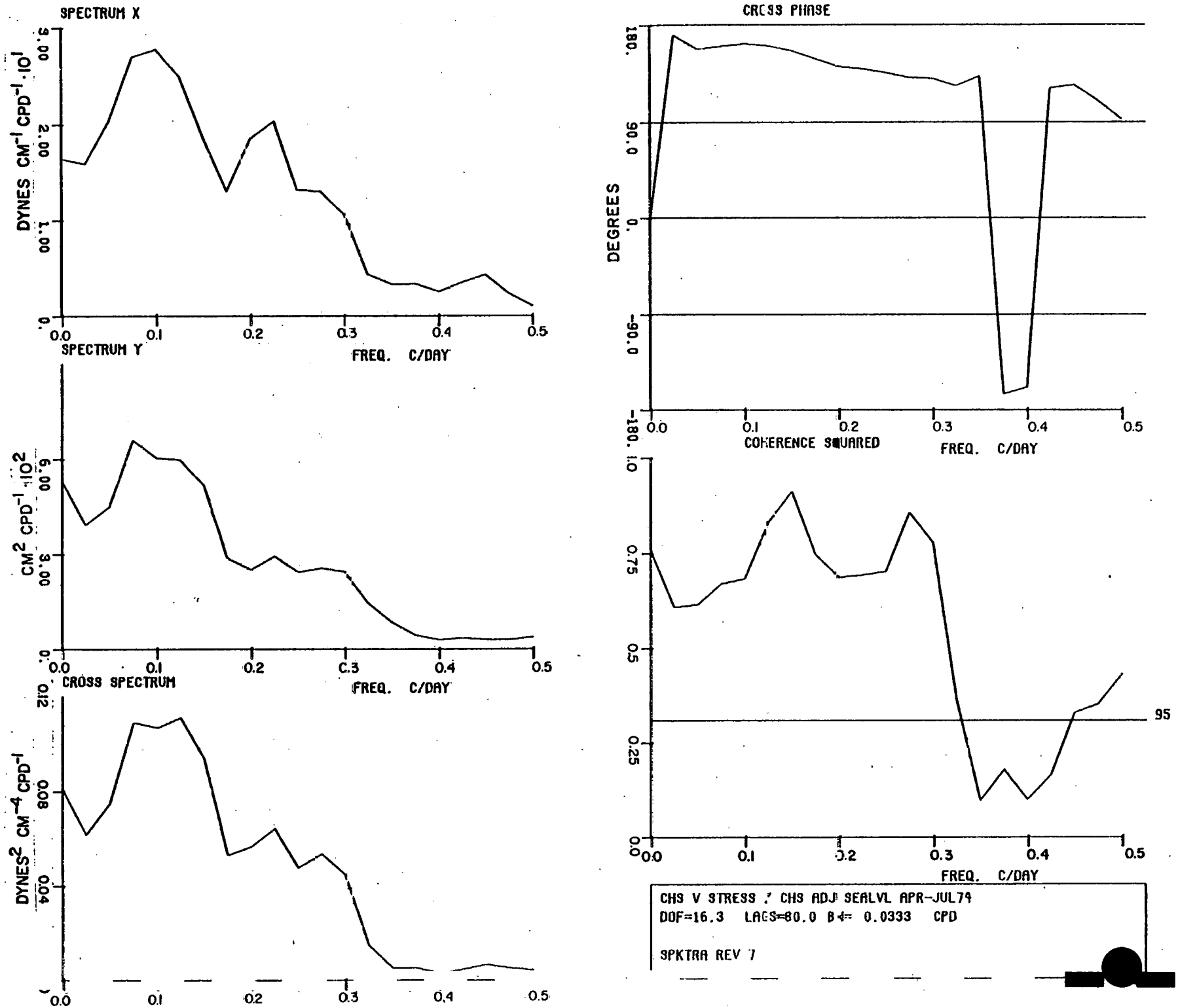
SPECTRUM X
DYNES CM^{-1} CPD^{-1} $\cdot 10^1$
FREQ. C/DAY
SPECTRUM Y
CM^2 CPD^{-1} $\cdot 10^2$
FREQ. C/DAY
CROSS SPECTRUM
DYNES^2 CM^{-4} CPD^{-1}
FREQ. C/DAY
CROSS PHASE
DEGREES
FREQ. C/DAY
COHERENCE SQUARED
FREQ. C/DAY
95
CHS V STRESS / CHS ADJ SEALVL APR-JUL79
DOF=16.3 LAGS=80.0 BW= 0.0333 CPD
SPKTRA REV 7

Figure 77

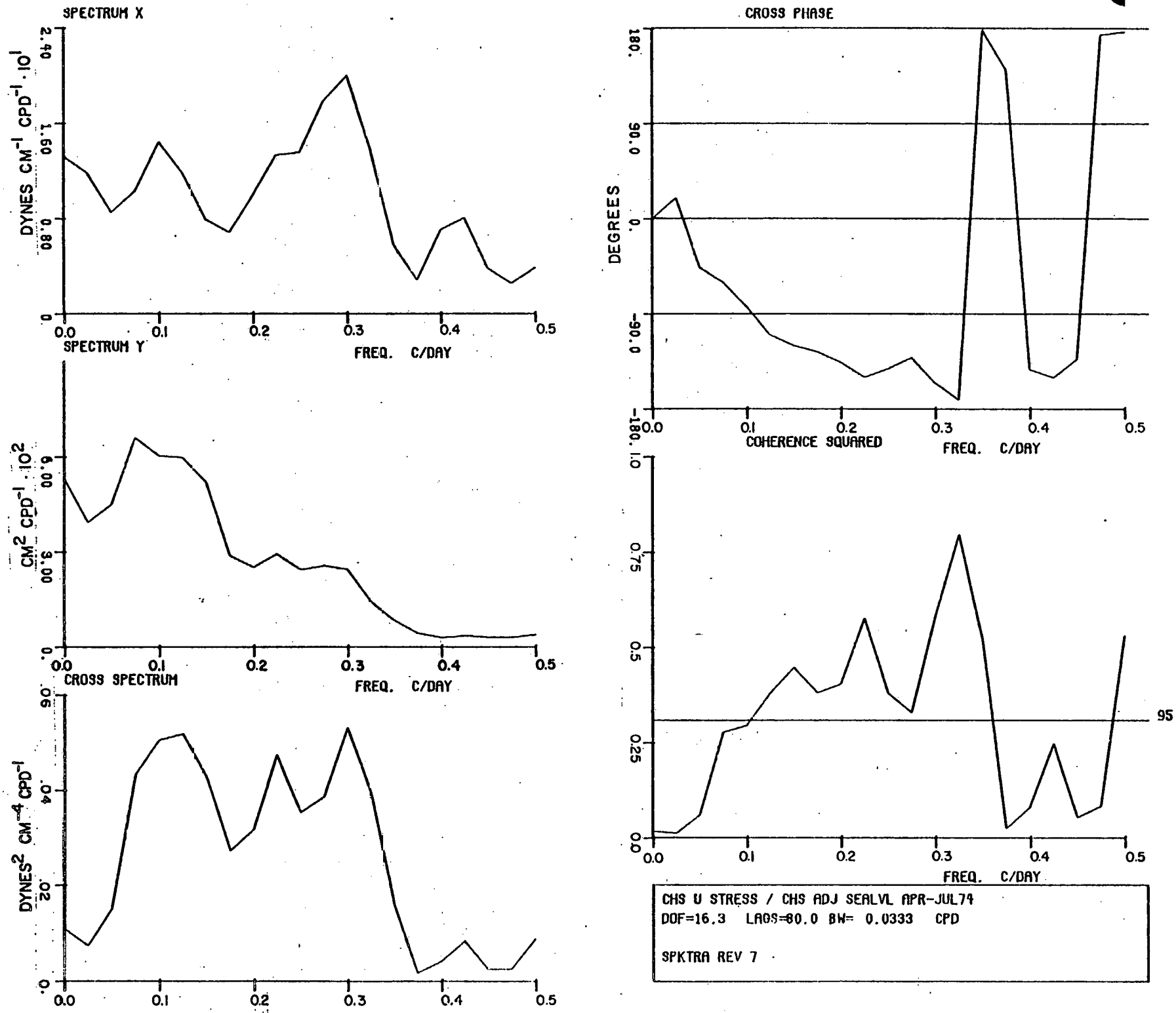
SPECTRUM X
DYNES CM^{-1} CPD^{-1} · 10^{1}
2.40
1.60
0.80
0
0.0
0.1
0.2
0.3
0.4
0.5
FREQ. C/DAY
SPECTRUM Y
CM^{2} CPD^{-1} · 10^{2}
6.00
3.00
0.
CROSS SPECTRUM
DYNES^{2} CM^{-4} CPD^{-1}
.06
.04
.02
CROSS PHASE
DEGREES
180.
90.0
0.
-90.0
-180.
COHERENCE SQUARED
1.0
0.75
0.5
0.25
95
CHS U STRESS / CHS ADJ SEALVL APR-JUL74
DOF=16.3 LAGS=80.0 BW= 0.0333 CPD
SPKTRA REV 7

Figure 78

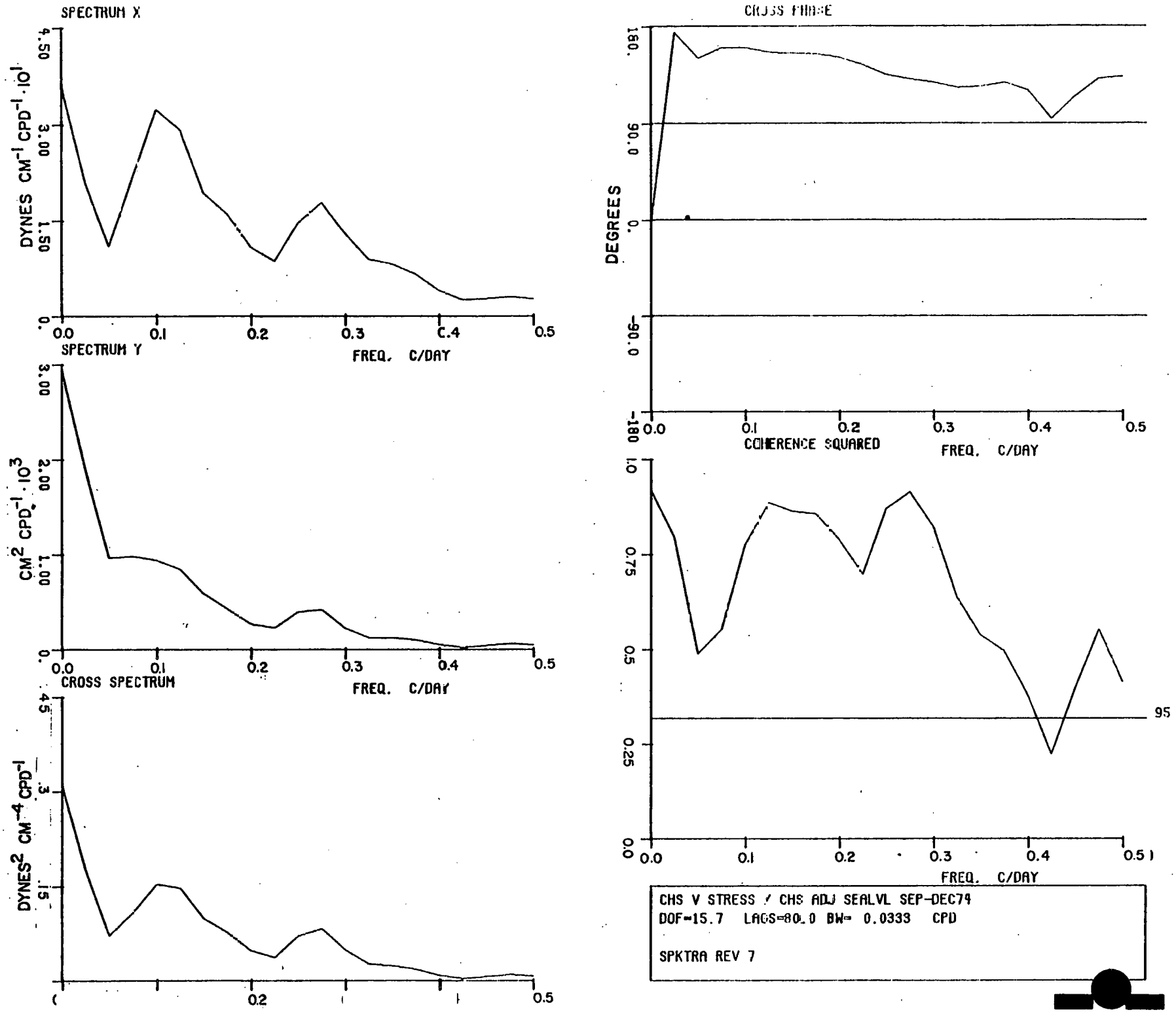
SPECTRUM X
DYNES CM^{-1} CPD^{-1} $\cdot 10^{1}$
4.50
3.00
1.50
0.
0.0
0.1
0.2
0.3
0.4
0.5
FREQ. C/DAY
SPECTRUM Y
CM^{2} CPD^{-1} $\cdot 10^{3}$
3.00
2.00
1.00
0.
FREQ. C/DAY
CROSS SPECTRUM
DYNES^{2} CM^{-4} CPD^{-1}
FREQ.
CROSS PHASE
DEGREES
180.
90.0
0.
-90.0
-180
COHERENCE SQUARED
1.0
0.75
0.5
0.25
0.0
95
CHS V STRESS / CHS ADJ SEALVL SEP-DEC74
DOF=15.7 LAGS=80.0 BW= 0.0333 CPD
SPKTRA REV 7

Figure 79

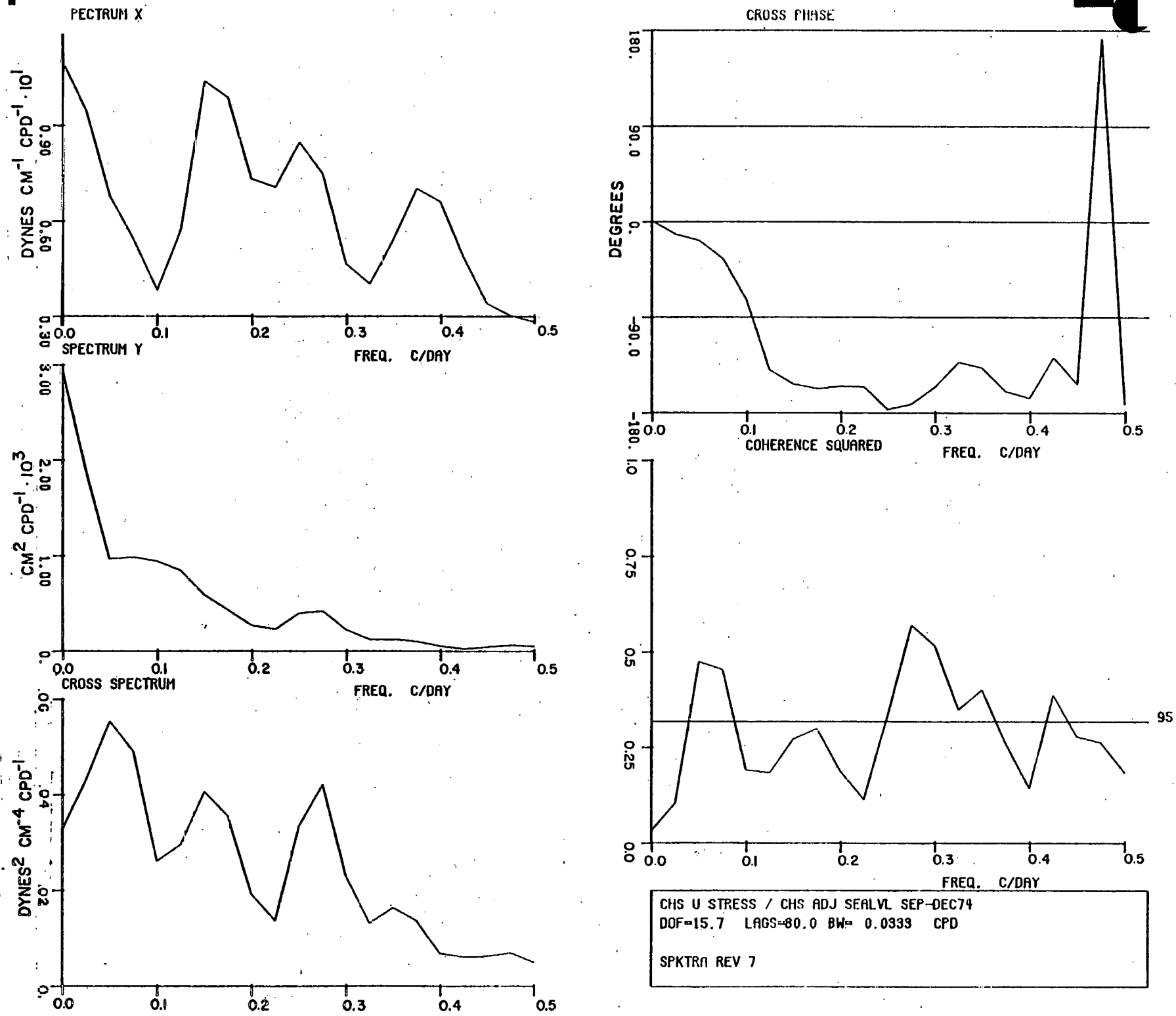
PECTRUM X
DYNES CM^{-1} CPD^{-1} $\cdot 10^{1}$
0.90
0.60
0.30
0.0
0.1
0.2
0.3
0.4
0.5
FREQ. C/DAY
SPECTRUM Y
CM^{2} CPD^{-1} $\cdot 10^{3}$
3.00
2.00
1.00
0.
CROSS SPECTRUM
DYNES^{2} CM^{-4} CPD^{-1}
.06
.04
.02
CROSS PHASE
DEGREES
180.
90.0
0.
-90.0
-180.
COHERENCE SQUARED
1.0
0.75
0.5
0.25
0.0
95
CHS U STRESS / CHS ADJ SEALVL SEP-DEC74
DOF=15.7 LAGS=80.0 BW= 0.0333 CPD
SPKTRA REV 7

Figure 80

Fig. 121). The overall C^2 level is much lower in the transshelf wind cases, with C^2's in excess of 0.5 at periods of 3-4 days.

These spectra imply that there is a substantial and coherent coupling between the sea level response variable and the wind input variable, particularly at selective frequencies, i.e., in simplistic terms the membrane responds to the forcing within the band of the forcing frequencies. In fact the KED's of sea level demonstrate the same rise of energy to the minus three-halfs power of frequency over periods of several days to several weeks which is shown in the wind spectra (Figures 76 and 80).

It is of note herein that the KED's indicate a rise in energy levels from north to south, i.e., from BFT to FPS to CHS (Figs. 87-90) over the entire frequency range. This is consistent, at the semi-diurnal period of 12-41 hours, with the notion of the semi-diurnal tide propagating as a Poincare wave which increases in amplitude as the shelf widens, as it does from Cape Hatteras to Savannah. A doublet spike at the diurnal period appears in all of the sea level KED's; there is no immediate explanation for this phenomenon.

It was deemed necessary, at this point, to proceed in the data analysis of the met/sea level time series by computing multiple coherences between pressure, wind components and sea level and to compute in phase transfer functions between the atmospheric variables and sea level. Since pressure and wind are coherent over varying frequency bands, between each other, as well as separately with sea level, it is enlightening to input one atmospheric variable, then another and finally another and watch the C^2's with sea level be either augmented, enhanced or reduced. It is useful to compute the ratio of the co-spectrum of sea level and alongshore

or cross-shore winds or pressure to the autospectrum of the respective atmospheric variable; a uniform (nonuniform) ratio over some spectral range would then be indicative of no preferential (of a preferential) frequency band within which air-sea momentum transfers are more efficient which is further indicative of no resonance (of resonance) between the atmosphere and sea level.

These latter kinds of data products are buried in the data presented but need to be formally accomplished.

Considering the alongshore and cross-shelf wind stress components (heretofore $\tau^{(y)}$ and $\tau^{(x)}$) and adjusted sea level, it is noted that sea level consistently, without exception, lags $\tau^{(x)}$ but leads $\tau^{(y)}$. Additionally, it should be noted that $\tau^{(y)}$ leads $\tau^{(x)}$ over the most coherent bands, between the two, and in fact the two components tend to be in quadrature. This is entirely consistent with the scenario of sea level falling at the coast due to increasing offshore or southwesterly, alongshore winds and rising with increased onshore or northeasterly winds.

It appears that sea level (SL) from CHS to BFT responds, to some measure, in a conventional Ekman sense, i.e., SL fluctuates up or down in direct response to wind stress both in the alongshore and transshore directions. Southwesterly (northeasterly) winds produce a setdown (setup) of SL at the coast and offshore (onshore) winds produce a setdown (setup) of SL at the coast. A clear example of this is shown in the time series of sea level at CHS and the wind stress field at CHS from 5-20 January, 1974 (days 5-20 in Figures 81 and 82). The coastal Ekman scenario follows so well that even a relaxation in the magnitude of the stress field, which was directed to the northeast on days 9 and 10 was

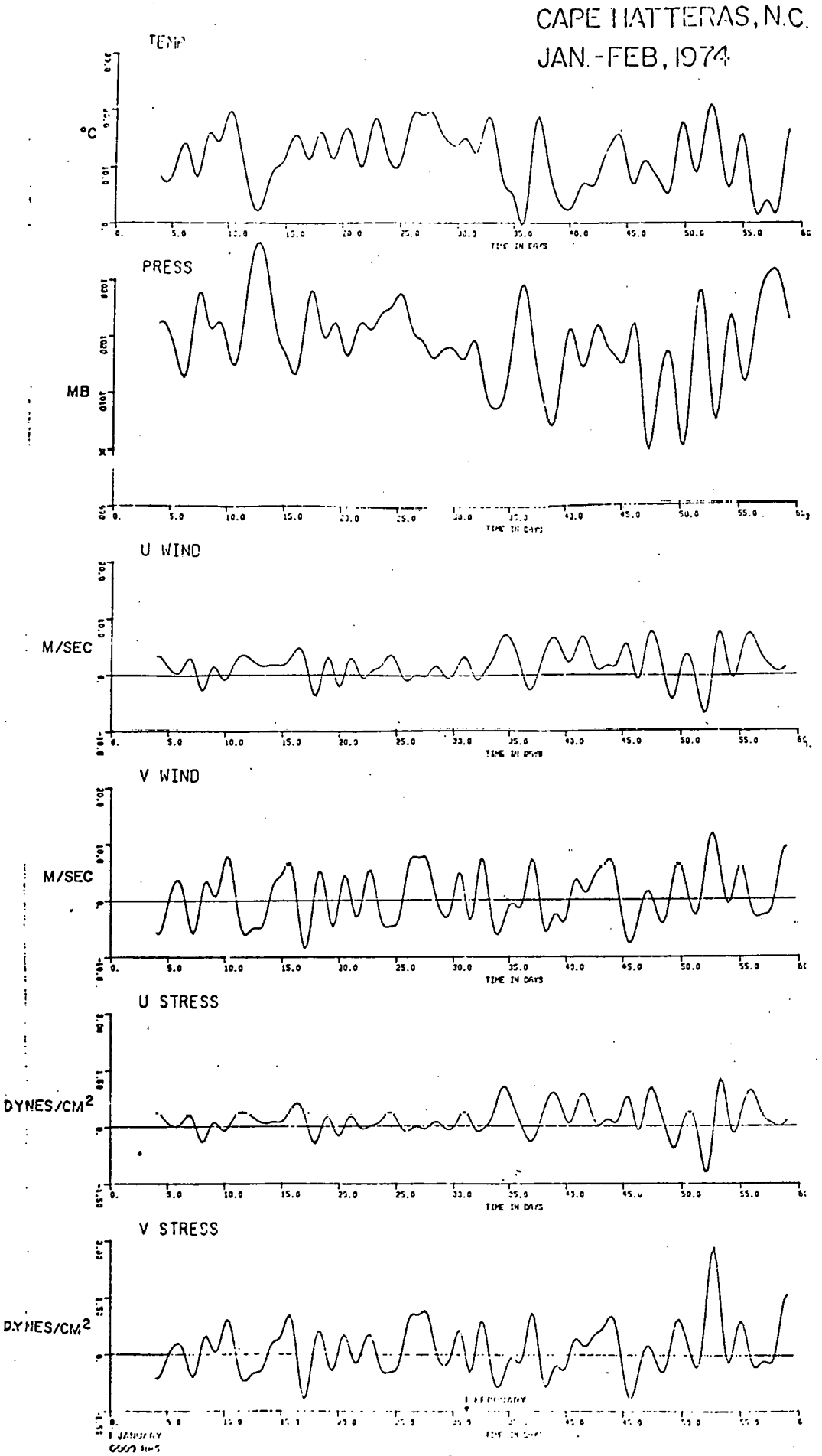

Figure 81 Temperature, pressure, wind velocity components and wind stress components at Cape Hatteras, N. C., Jan. through Feb., 1974

Figure 82 Sea level measurements at Beaufort, N. C., Beaufort Inlet, N. C., Wilmington, N. C. and Charleston, S. C., Jan. through Feb., 1974

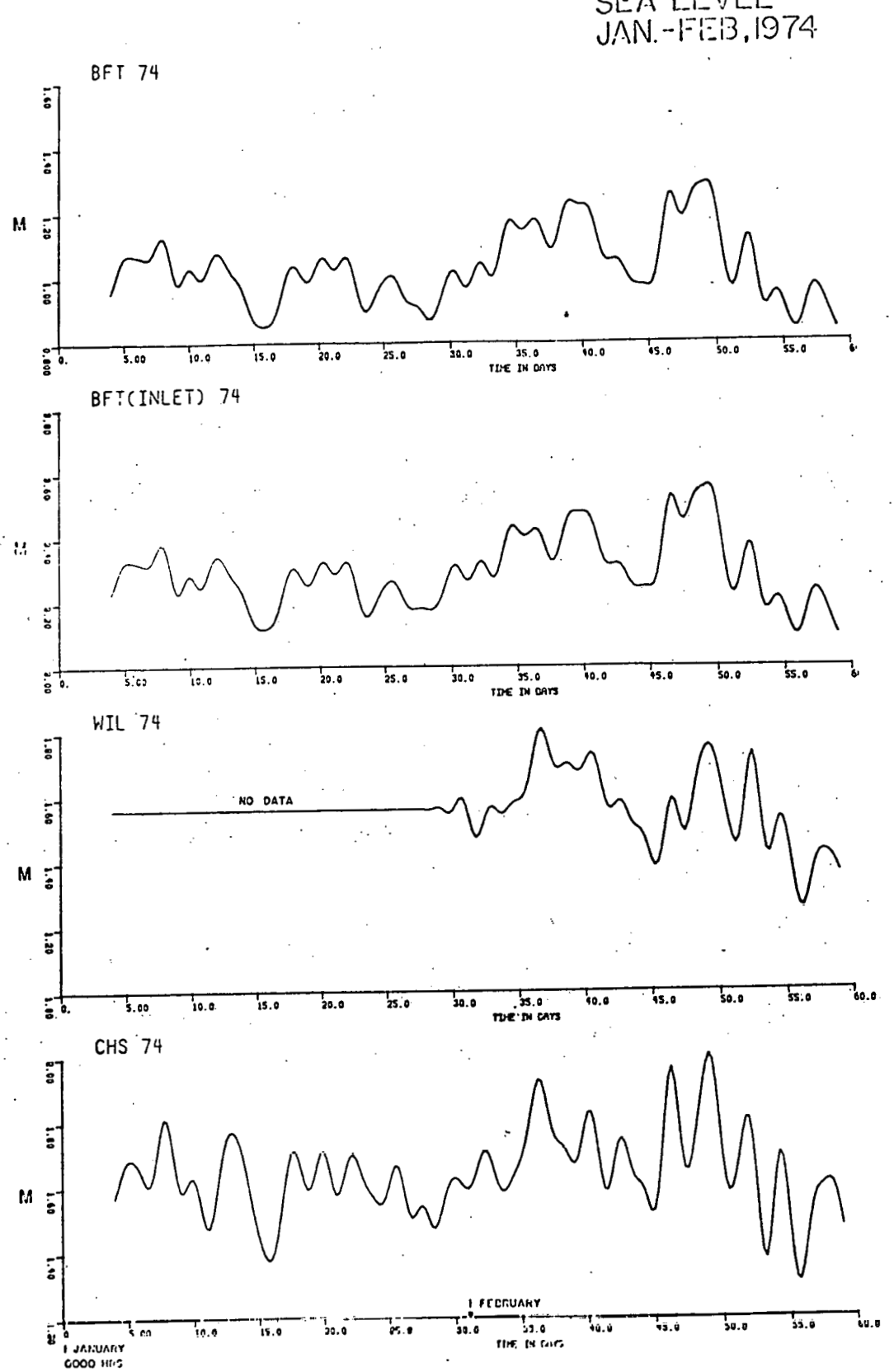

mirrored in a slight increase in sea level. BFT-SL is entirely consistent with the CHS Ekman scenario during this period given the agreement of the HAT, WIL and CHS winds. The southwesterly to northeasterly wind reversal which occured during day 11 (11 Jan., 1974), consistent with the clockwise wind stress vector rotation of a cold front, Figure 81, from $\tau^{(y)} \sim 0.6$ dynes/cm^2 to $\tau^{(y)} \sim -0.5$ dynes/cm^2 resulted a drop in sea level of approximately 55 cm.

It is of note here that the sea level data, particularly intercomparisons of the BFT/FPS time series because they imply that not only transshelf but also alongshelf slopes of sea surface, consistent with a piling up of the surface waters in the direction of the wind, exist. On 1 December 1974 a large southwesterly wind event occurred and not only dropped sea level at FPS and BFT, which were both at 130cm height at the event onset, but created a 50cm rise in sea level from FPS to BFT, a radial distance of 150km. This is evident in Figure 82 which shows evidence for the existence of longshore pressure gradients, which were hypothesized to exist by Garvine (1971) and used in a mathematical model of coastal dynamics by Pietrafesa (1973) to drive a cross-shelf interior flow thereby eliminating the necessity of a bottom, frictional layer to balance the offshore Ekman transport. In a barotropic geostrophic sense the cross-shelf flow induced by this longshore pressure gradient, using the relation $u = -(gf^{-1})\zeta_y$, is of the order of 23 cm/sec. The longshore variations in sea level observed between Capes Lookout and Fear, which define Onslow Bay in the alongshore direction, are certainly no proof of the existence of Garvine's contention nor a justification of Pietrafesa's use of the longshore pressure gradient in his model, since both of these investigators were dealing with straight coastlines having no longitudinal constraints and the cape shoals do

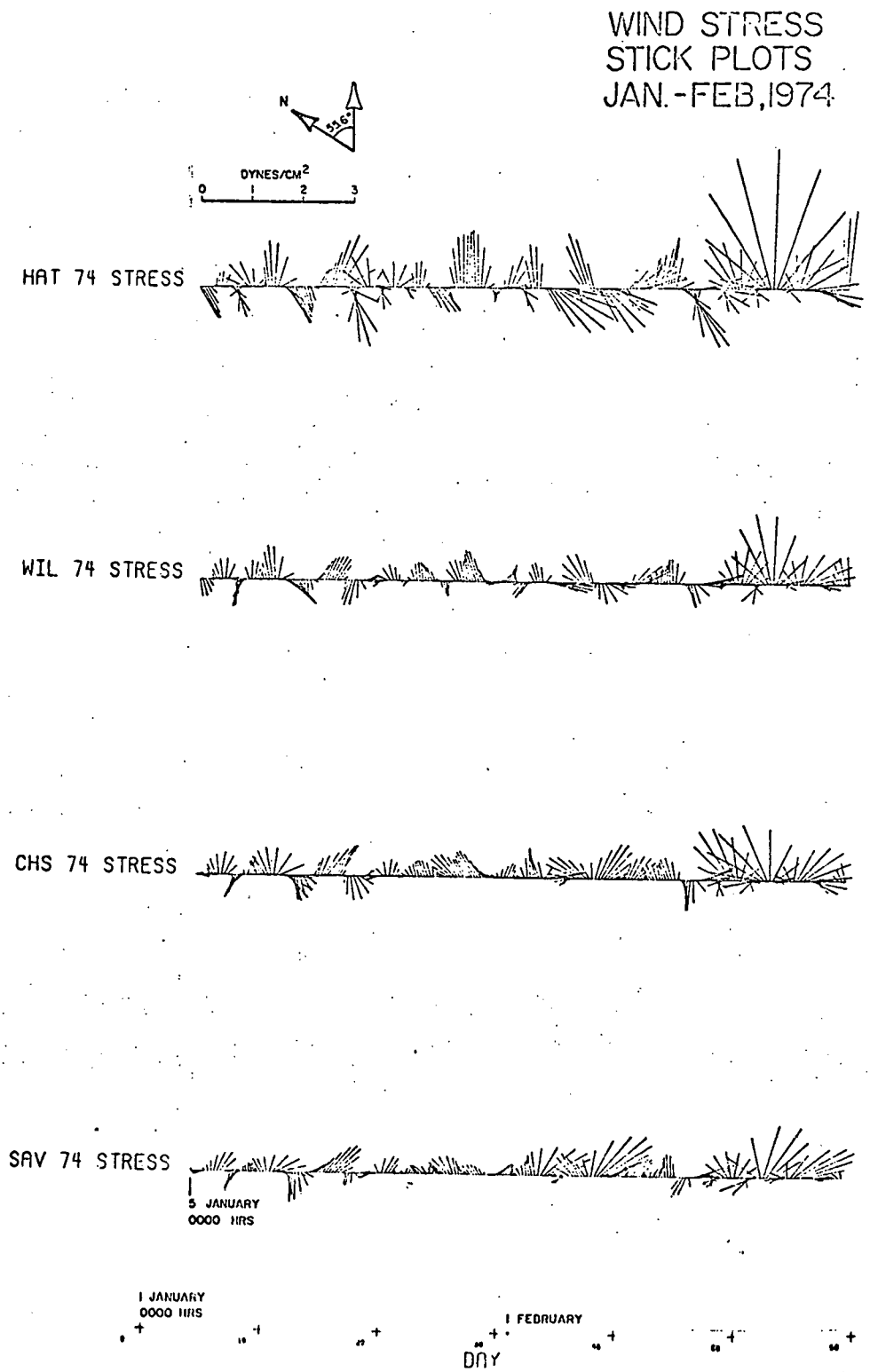
WIND STRESS
STICK PLOTS
JAN.-FEB,1974
N
53.6°
DYNES/CM²
0
1
2
3
HAT 74 STRESS
WIL 74 STRESS
CHS 74 STRESS
SAV 74 STRESS
5 JANUARY
0000 HRS
1 JANUARY
0000 HRS
1 FEBRUARY
DAY

Figure 83

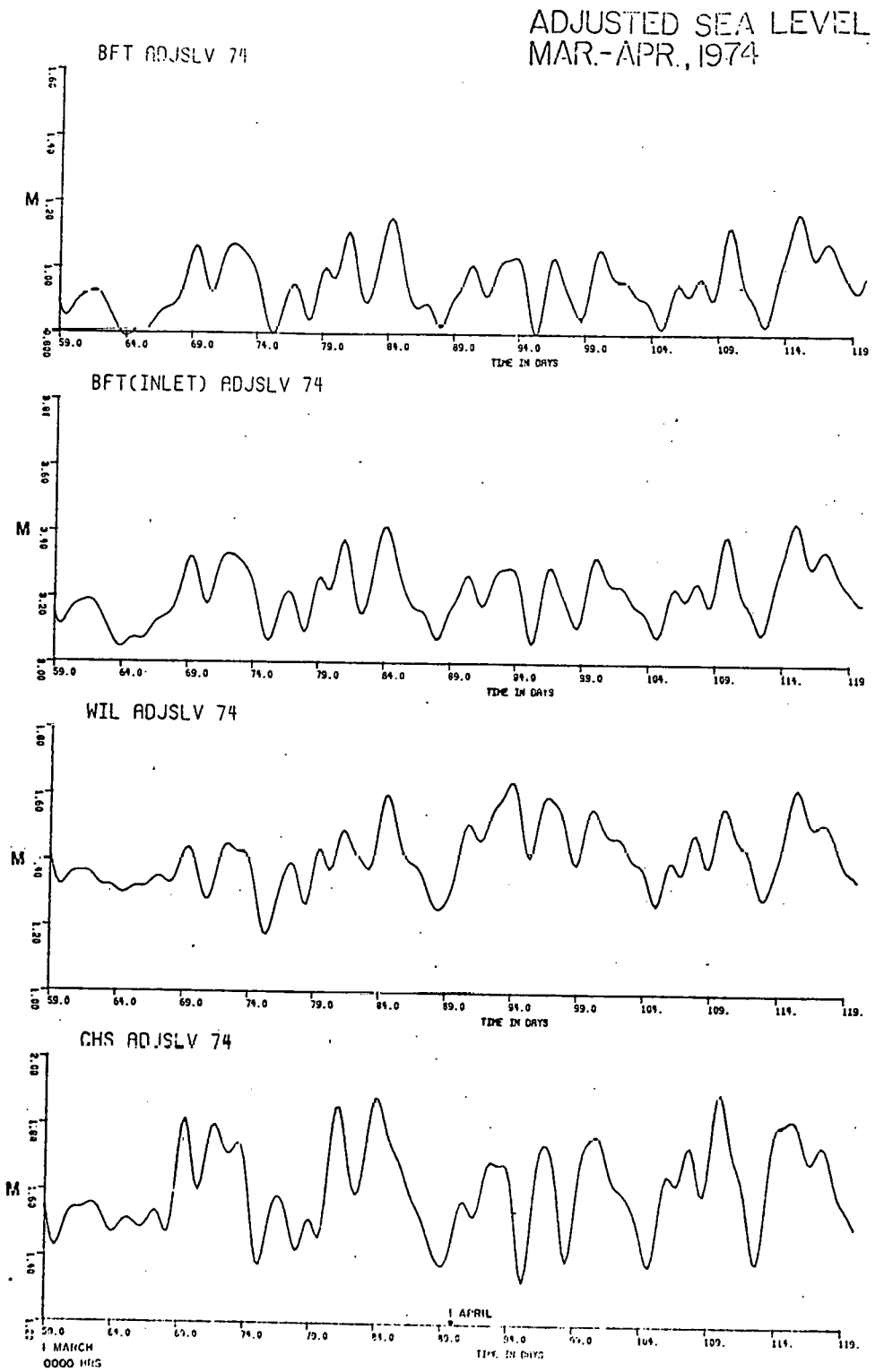
ADJUSTED SEA LEVEL
MAR.-APR., 1974
BFT ADJSLV 74
M
TIME IN DAYS
BFT(INLET) ADJSLV 74
M
TIME IN DAYS
WIL ADJSLV 74
M
TIME IN DAYS
CHS ADJSLV 74
M
1 MARCH
0000 HRS
1 APRIL

Figure 84

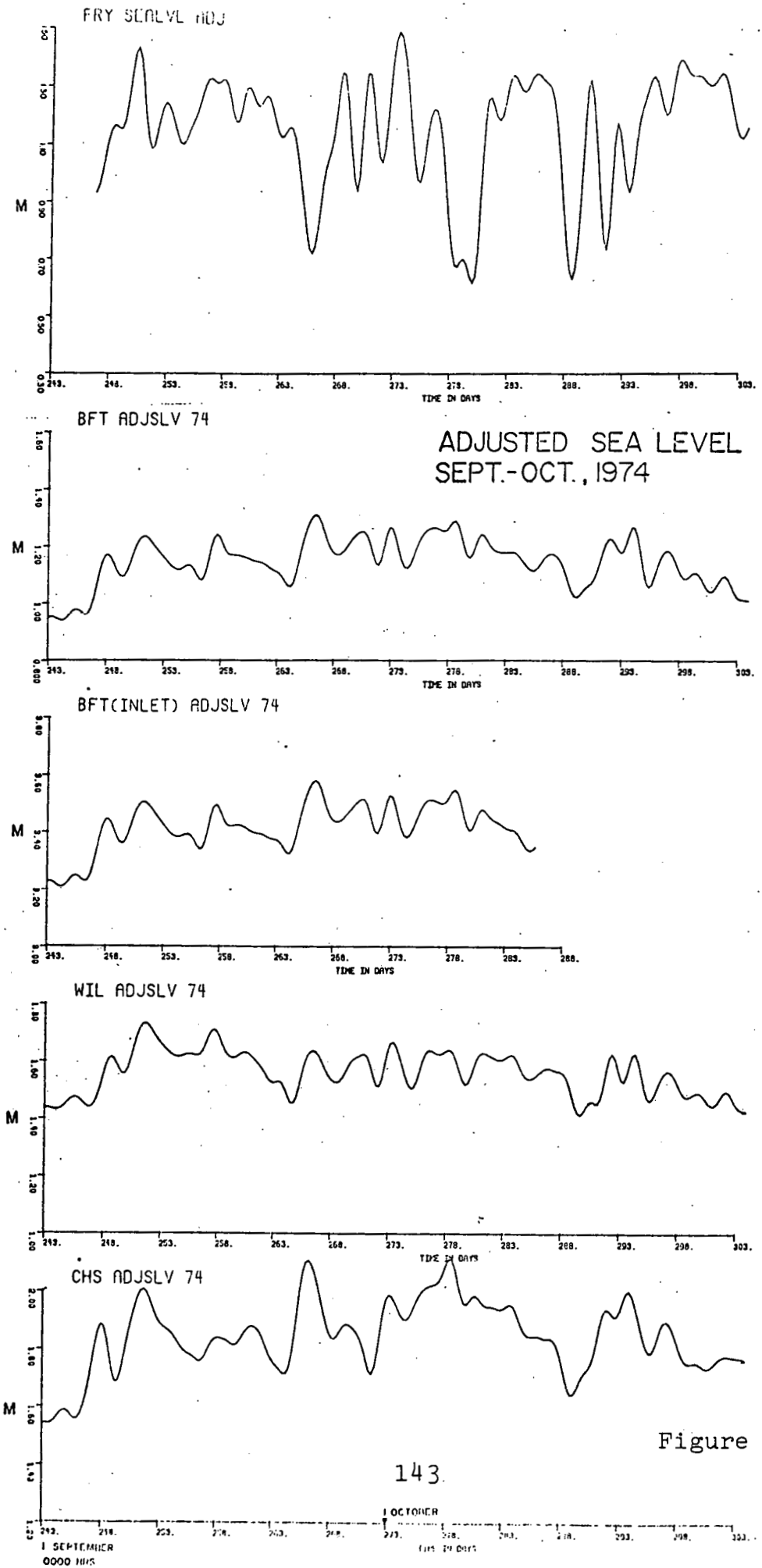
FRY SEALVL ADJ
BFT ADJSLV 74
ADJUSTED SEA LEVEL
SEPT.-OCT., 1974
BFT(INLET) ADJSLV 74
WIL ADJSLV 74
CHS ADJSLV 74
M
TIME IN DAYS
1 OCTOBER
1 SEPTEMBER
0000 HRS

Figure 85

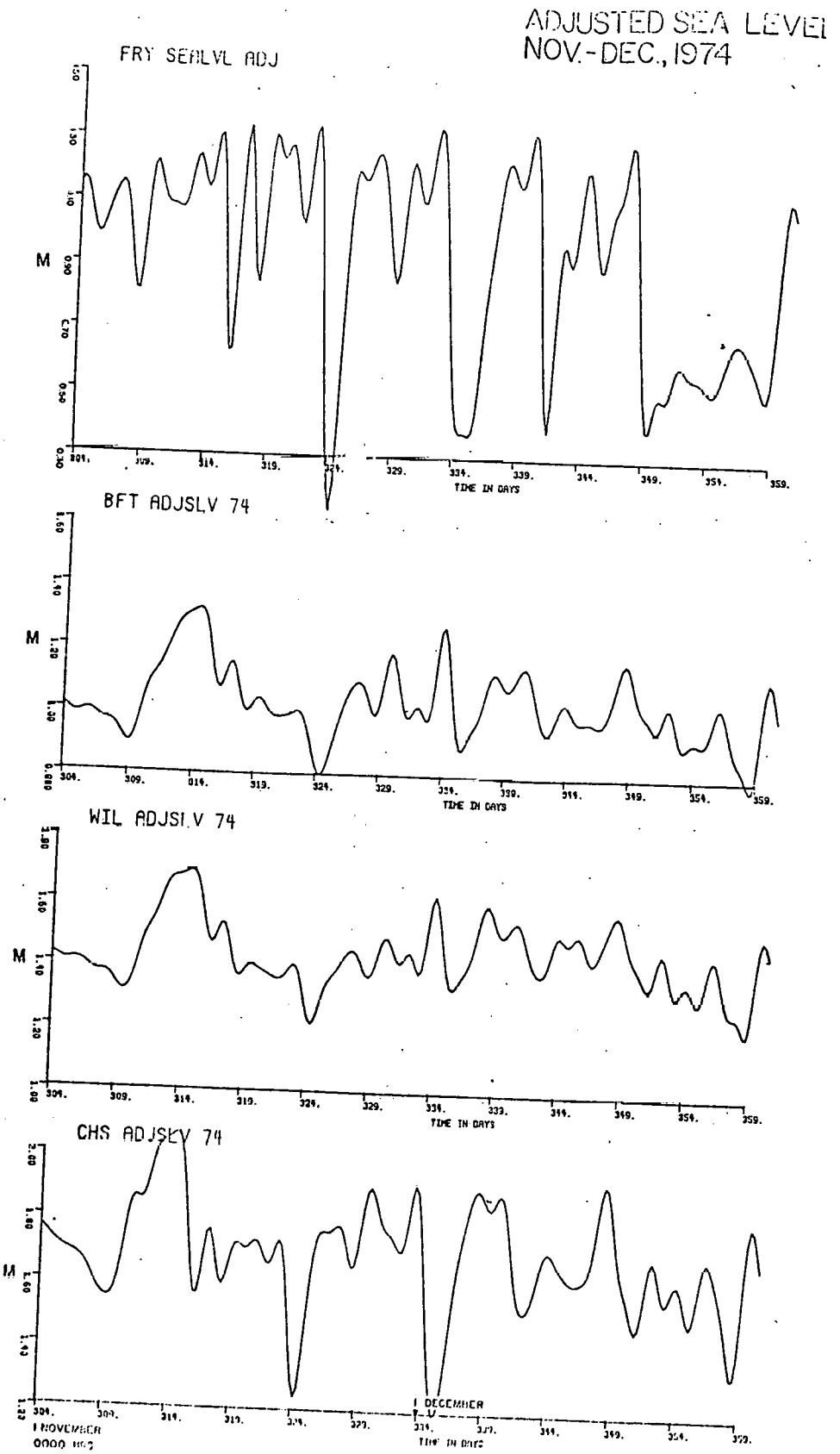
ADJUSTED SEA LEVEL
NOV.-DEC., 1974
FRY SEALVL ADJ
M
TIME IN DAYS
BFT ADJSLV 74
M
TIME IN DAYS
WIL ADJSLV 74
M
TIME IN DAYS
CHS ADJSLV 74
M
1 NOVEMBER
1 DECEMBER

Figure 86

constrain the hydrodynamics within. CHS vs. SAV sea level intercomparisons would offer a more generic look at the question of existence of a ζ_y in concert with an imposed $\tau^{(y)}$ at the surface.

A simplified balance in the alongshore direction could be written as $\zeta_y \sim \tau^{(y)}$ g D where D is the depth of the direct wind induced layer (the layer within which the wind is piled up). The example presented above of a $\Delta\zeta$ of 50 cm from BFT to FPS, 150 km, with a $|\tau^{(y)}|$ of 0.9 dynes/cm^2 indicates a D of 2.8 meters.

A great deal of visual correlation is obvious in the time series of filtered sea level (Figures 84 through 86. The Kinetic Energy Density representations (Figures 87 - 90) also indicate that BFT, FPS and CHS contain the similar energetics, save for the fact that the energy level rises from north to south, especially in the shape of the curve, as was described earlier in the text.

The cross analyses of sea level, including some of the pairing combinations, between CHS, BFT, WIL and FPS are shown in Figures 87 thru 90. Consider several subsets, not including WIL in the discussion because of the aforementioned fact that WIL is 27 miles (45 km) from the mouth of the tidal, wind, and river runoff influenced Cape Fear River Estuary.

During the Sept.-Dec., 1974 subset, (Fig. 88) BFT and CHS are coherent (above the 95% confidence level, which loses some credible meaning at C^2's too low) over the entire frequency range. There are several highly significant period bands which should be noted: at 2.25 days, $C^2 \sim 0.8$ and CHS leads BFT by 4½ hours; at 3.6 days, $C^2 \sim 0.85$, CHS leads BFT by 4 1/3 hours; at periods above 10 days the two stations are essentially in phase. During this same period: CHS $\tau^{(y)}$ and $\tau^{(x)}$ are most coherent at periods encompassing 3 and 6-7 days and are close to quadrature (60-90°) with $\tau^{(y)}$ leading $\tau^{(x)}$; SAV $\tau^{(y)}$ and $\tau^{(x)}$ are more broadly

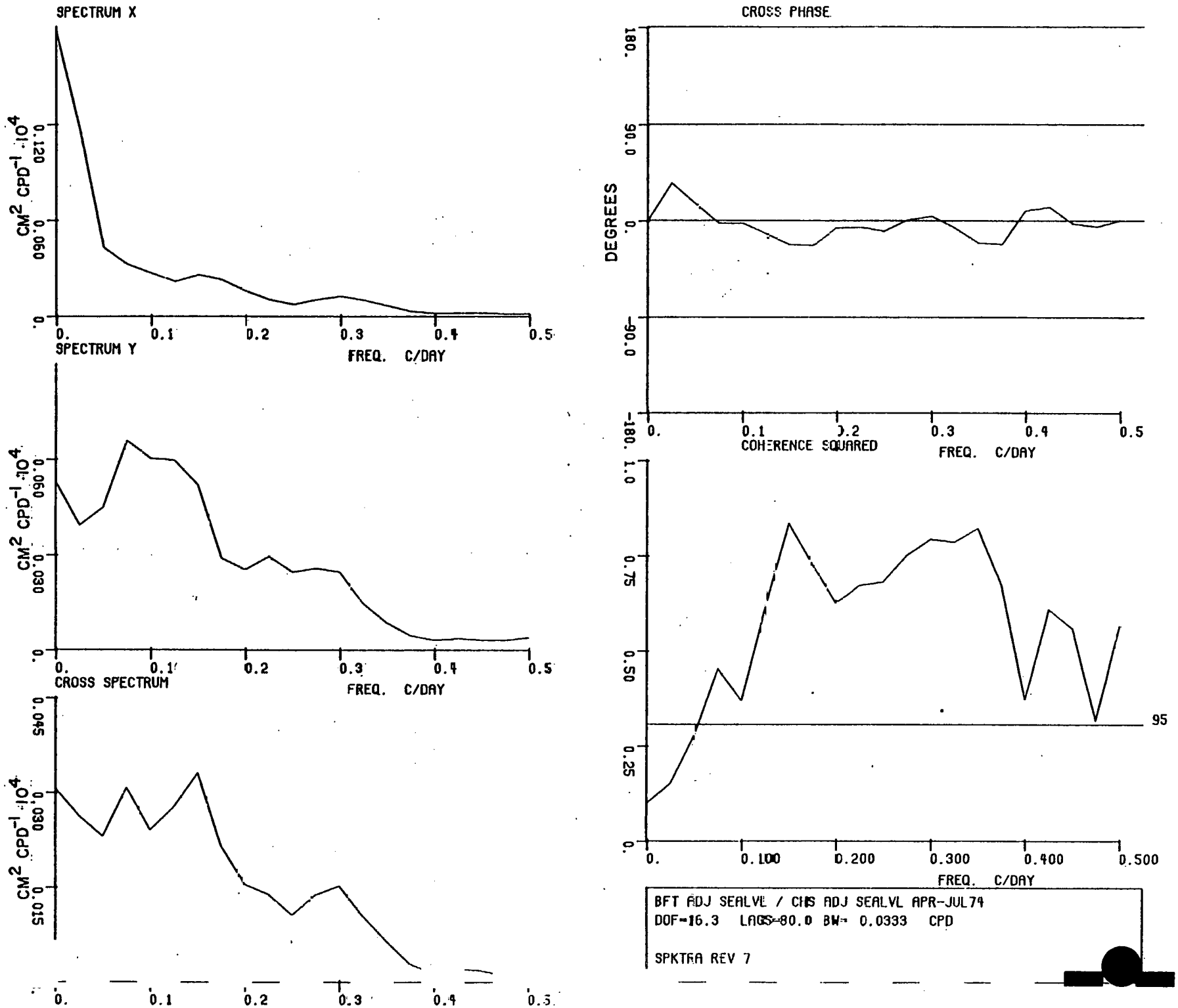
SPECTRUM X
CM2 CPD-1 ·10^4
0.120
0.060
0.
0.
0.1
0.2
0.3
0.4
0.5
FREQ. C/DAY
SPECTRUM Y
CM2 CPD-1 ·10^4
0.060
0.030
0.
0.
0.1
0.2
0.3
0.4
0.5
FREQ. C/DAY
CROSS SPECTRUM
CM2 CPD-1 ·10^4
0.045
0.030
0.015
0.
0.1
0.2
0.3
0.4
0.5
CROSS PHASE
DEGREES
180.
90.0
0.
-90.0
-180.
0.
0.1
0.2
0.3
0.4
0.5
FREQ. C/DAY
COHERENCE SQUARED
1.0
0.75
0.50
0.25
0.
95
0.
0.100
0.200
0.300
0.400
0.500
FREQ. C/DAY
BFT ADJ SEALVL / CHS ADJ SEALVL APR-JUL74
DOF=16.3 LAGS=80.0 BW= 0.0333 CPD
SPKTRA REV 7

Figure 87

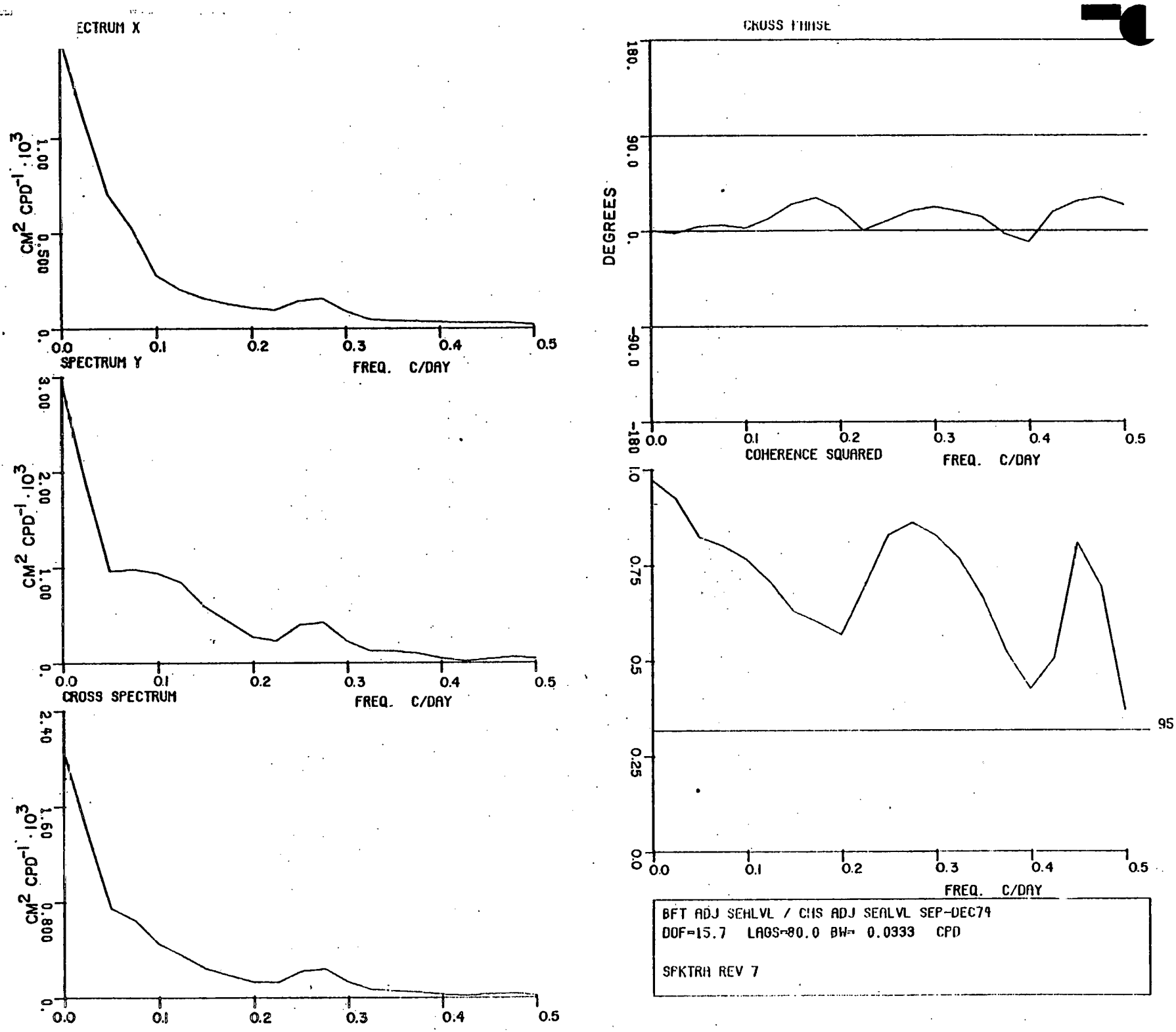
ECTRUM X
CM2 CPD-1 · 10^3
SPECTRUM Y
FREQ. C/DAY
CROSS SPECTRUM
CROSS PHASE
DEGREES
COHERENCE SQUARED
95
BFT ADJ SEALVL / CHS ADJ SEALVL SEP-DEC79
DOF=15.7 LAGS=80.0 BW= 0.0333 CPD
SPKTRA REV 7

Figure 88

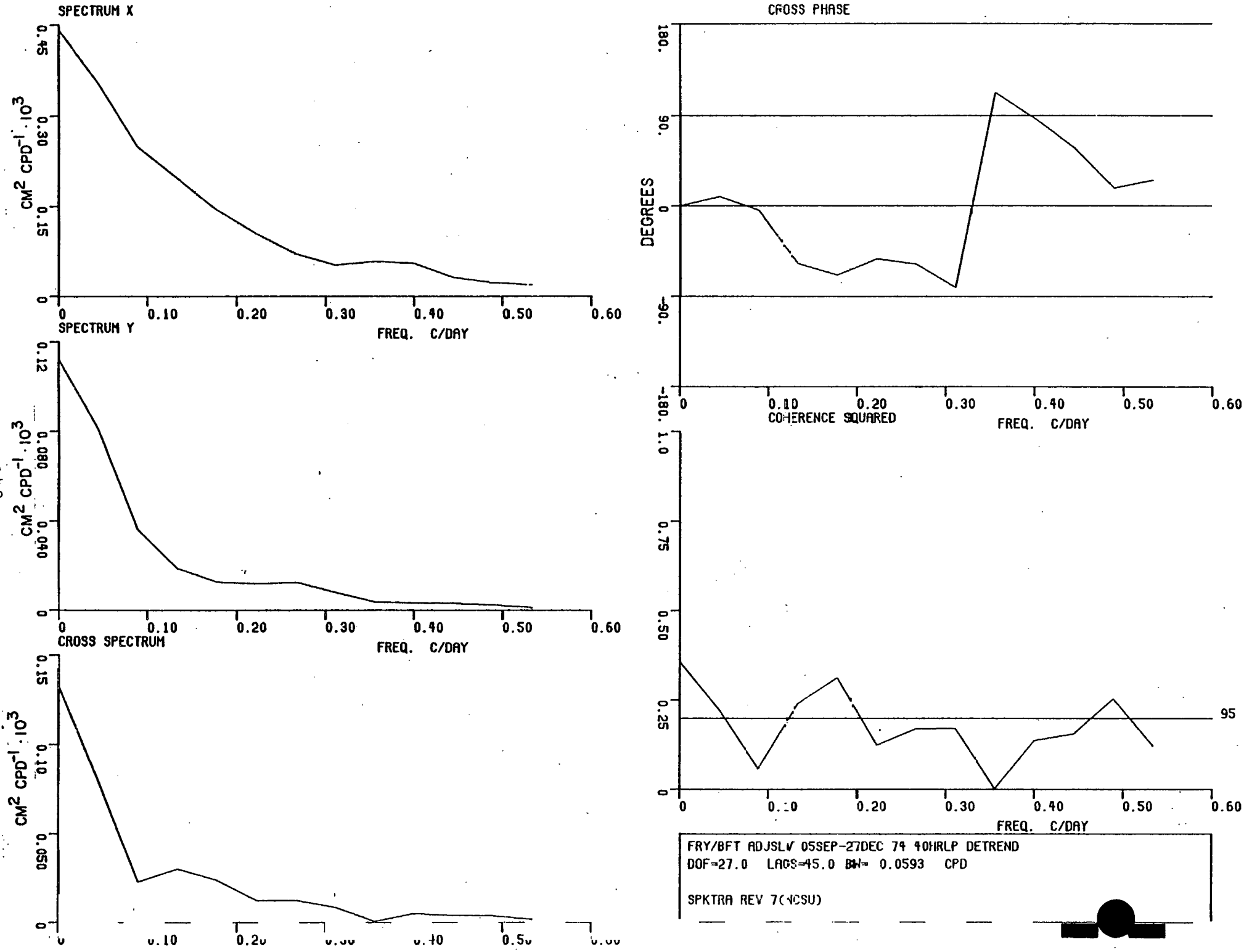
SPECTRUM X
CM2 CPD-1 . 10^3
0.45
0.30
0.15
0
0.10
0.20
0.30
0.40
0.50
0.60
FREQ. C/DAY
SPECTRUM Y
CM2 CPD-1 . 10^3
0.12
0.080
0.040
CROSS SPECTRUM
CM2 CPD-1 . 10^3
0.15
0.10
0.050
CROSS PHASE
DEGREES
180.
90.
0
-90.
-180.
COHERENCE SQUARED
1.0
0.75
0.50
0.25
95
FRY/BFT ADJSLW 05SEP-27DEC 74 40HRLP DETREND
DOF=27.0 LAGS=45.0 BW= 0.0593 CPD
SPKTRA REV 7(NCSU)

Figure 89

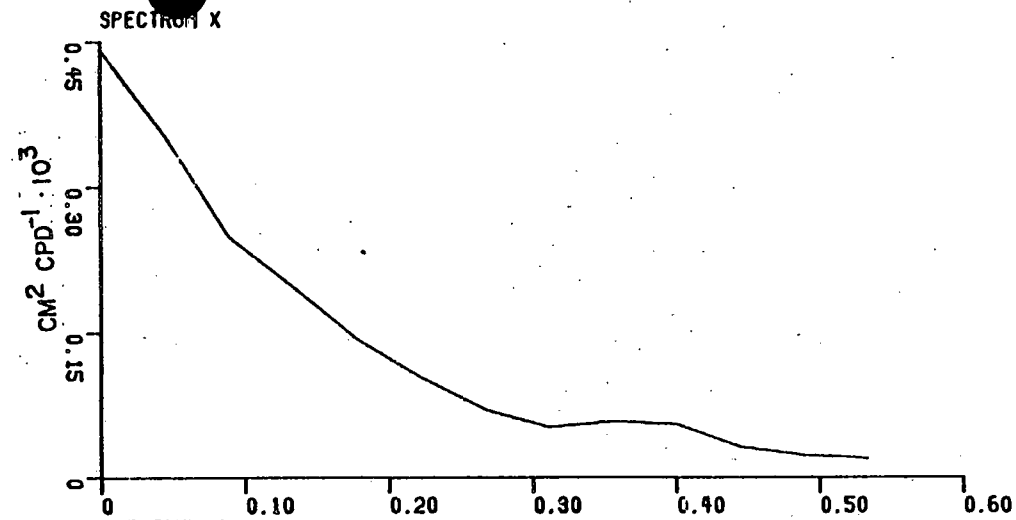

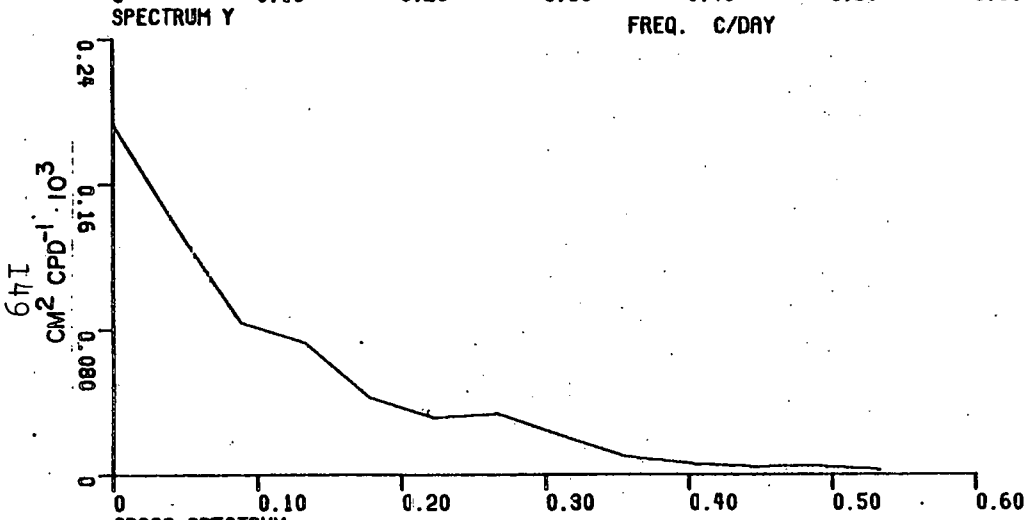

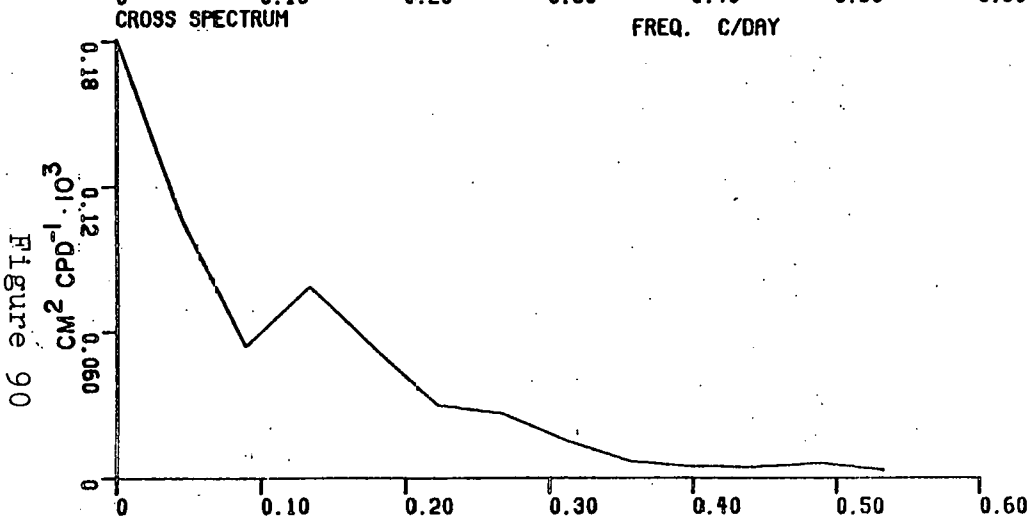

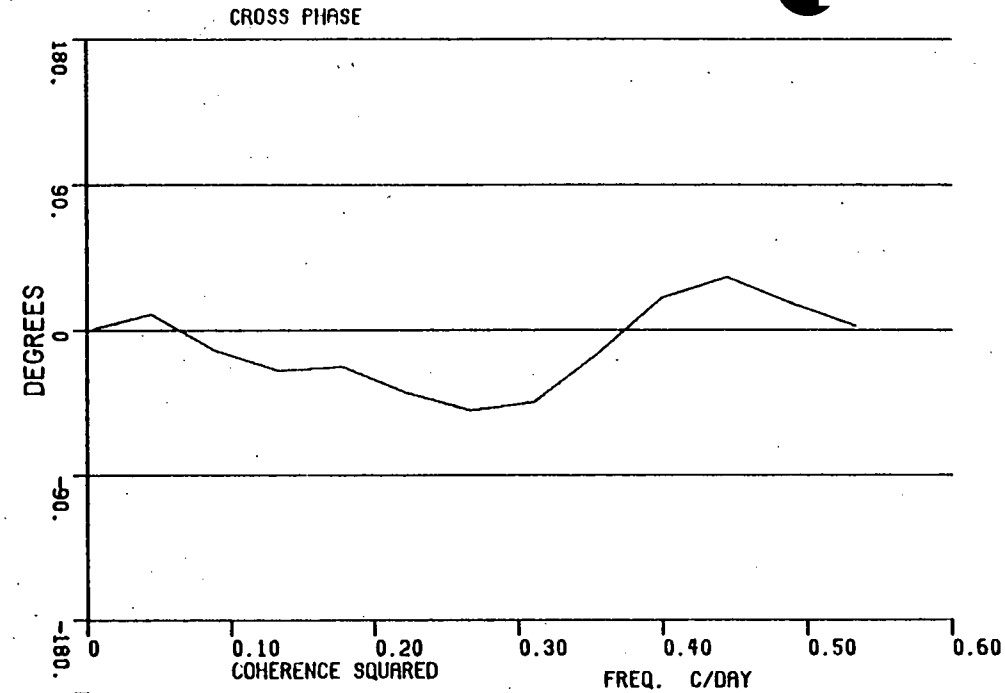

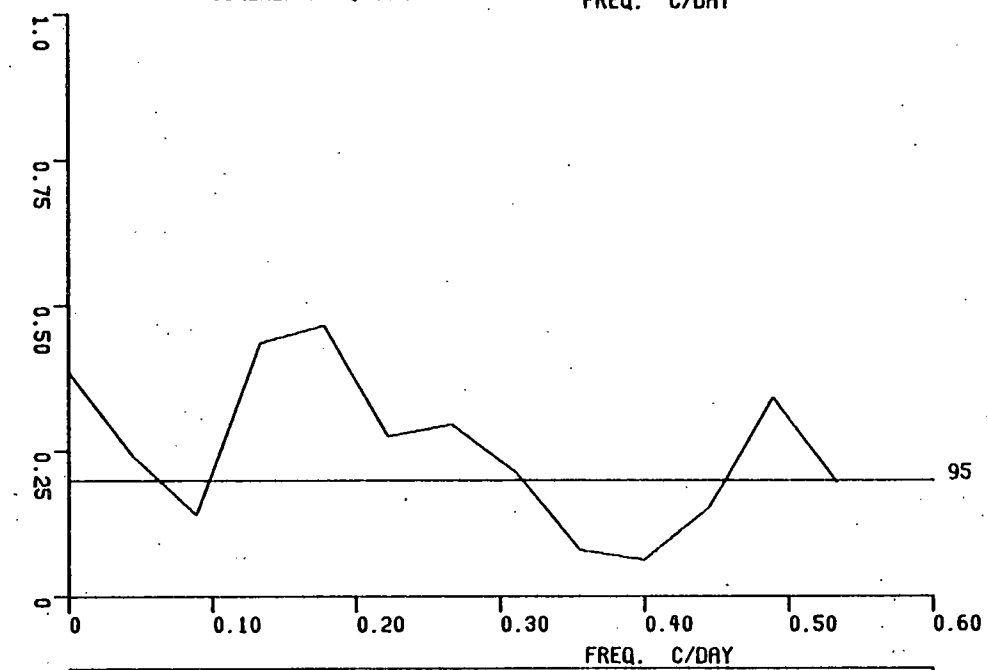

FRY/CHS ADJSLV 05SEP-27DEC 79 40HRLP DETREND
DOF=27.0 LAGS=45.0 BW= 0.0593 CPD

SPKTRA REV 7(NCSU)

Figure 90

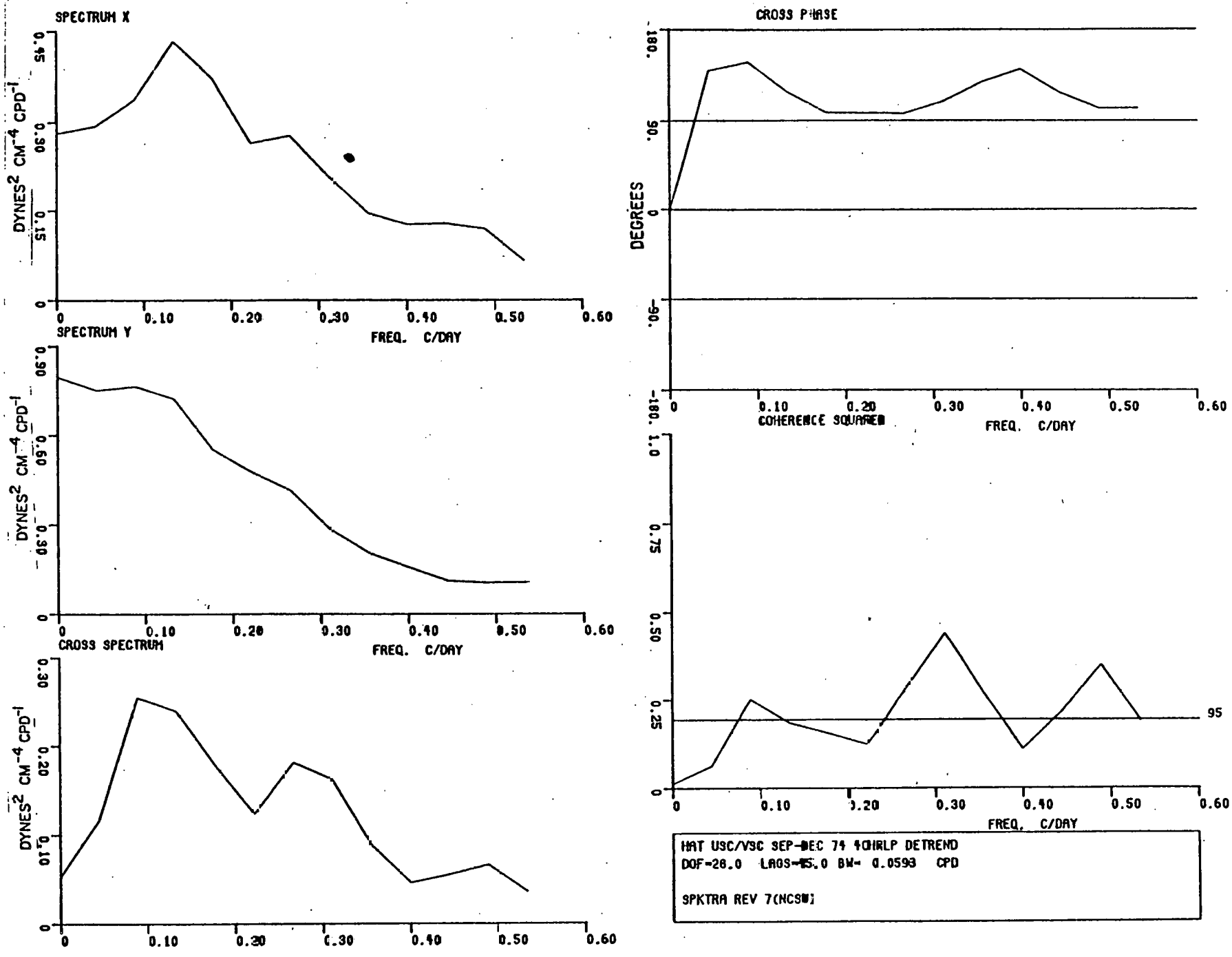
SPECTRUM X
DYNES^2 CM^{-4} CPD^{-1}
0.45
0.30
0.15
0
0.10
0.20
0.30
0.40
0.50
0.60
FREQ. C/DAY
SPECTRUM Y
DYNES^2 CM^{-4} CPD^{-1}
0.90
0.60
0.30
0
FREQ. C/DAY
CROSS SPECTRUM
DYNES^2 CM^{-4} CPD^{-1}
0.30
0.20
0.10
0
FREQ. C/DAY
CROSS PHASE
DEGREES
180.
90.
0
-90.
-180.
COHERENCE SQUARED
1.0
0.75
0.50
0.25
0
95
FREQ. C/DAY
HAT USC/VSC SEP-DEC 74 4CHRLP DETREND
DOF=28.0 LAGS=15.0 BW= 0.0593 CPD
SPKTRA REV 7(NCSW)

Figure 91

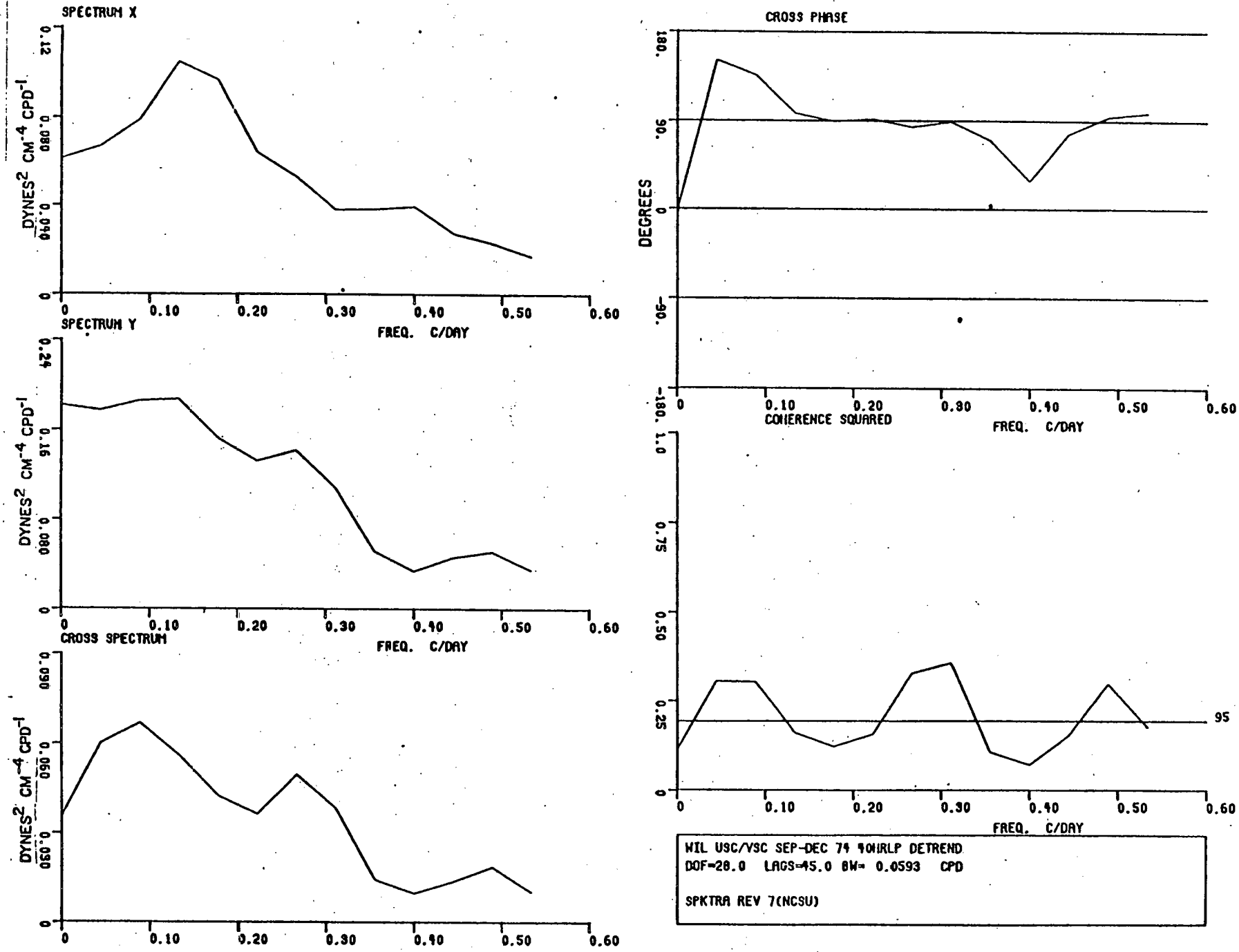
SPECTRUM X
DYNES^2 CM^{-4} CPD^{-1}
0.120
0.080
0.040
0
0.10
0.20
0.30
0.40
0.50
0.60
FREQ. C/DAY
SPECTRUM Y
DYNES^2 CM^{-4} CPD^{-1}
0.24
0.16
0.080
CROSS SPECTRUM
DYNES^2 CM^{-4} CPD^{-1}
0.090
0.060
0.030
CROSS PHASE
DEGREES
180.
90.
0
-90.
-180.
COHERENCE SQUARED
1.0
0.75
0.50
0.25
95
WIL USC/VSC SEP-DEC 74 %WIRLP DETREND
DOF=28.0 LAGS=45.0 BW= 0.0593 CPD
SPKTRA REV 7(NCSU)

Figure 92

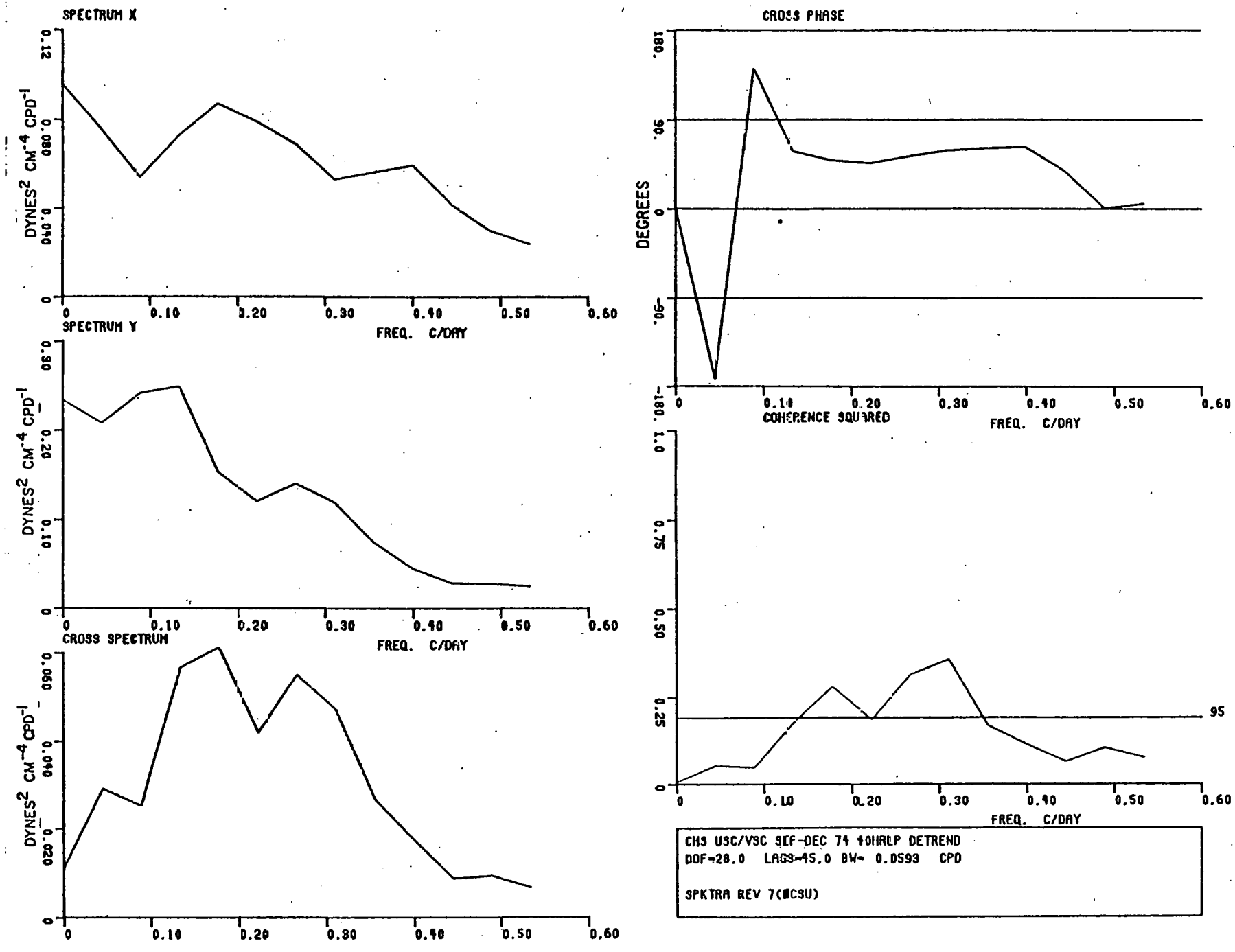
SPECTRUM X
DYNES^2 CM^{-4} CPD^{-1}
FREQ. C/DAY
SPECTRUM Y
DYNES^2 CM^{-4} CPD^{-1}
FREQ. C/DAY
CROSS SPECTRUM
DYNES^2 CM^{-4} CPD^{-1}
FREQ. C/DAY
CROSS PHASE
DEGREES
FREQ. C/DAY
COHERENCE SQUARED
95
FREQ. C/DAY
CH3 USC/VSC SEP-DEC 74 HOURLY DETREND
DOF=28.0 LAGS=45.0 BW= 0.0593 CPD
SPKTRA REV 7(USC)

Figure 93

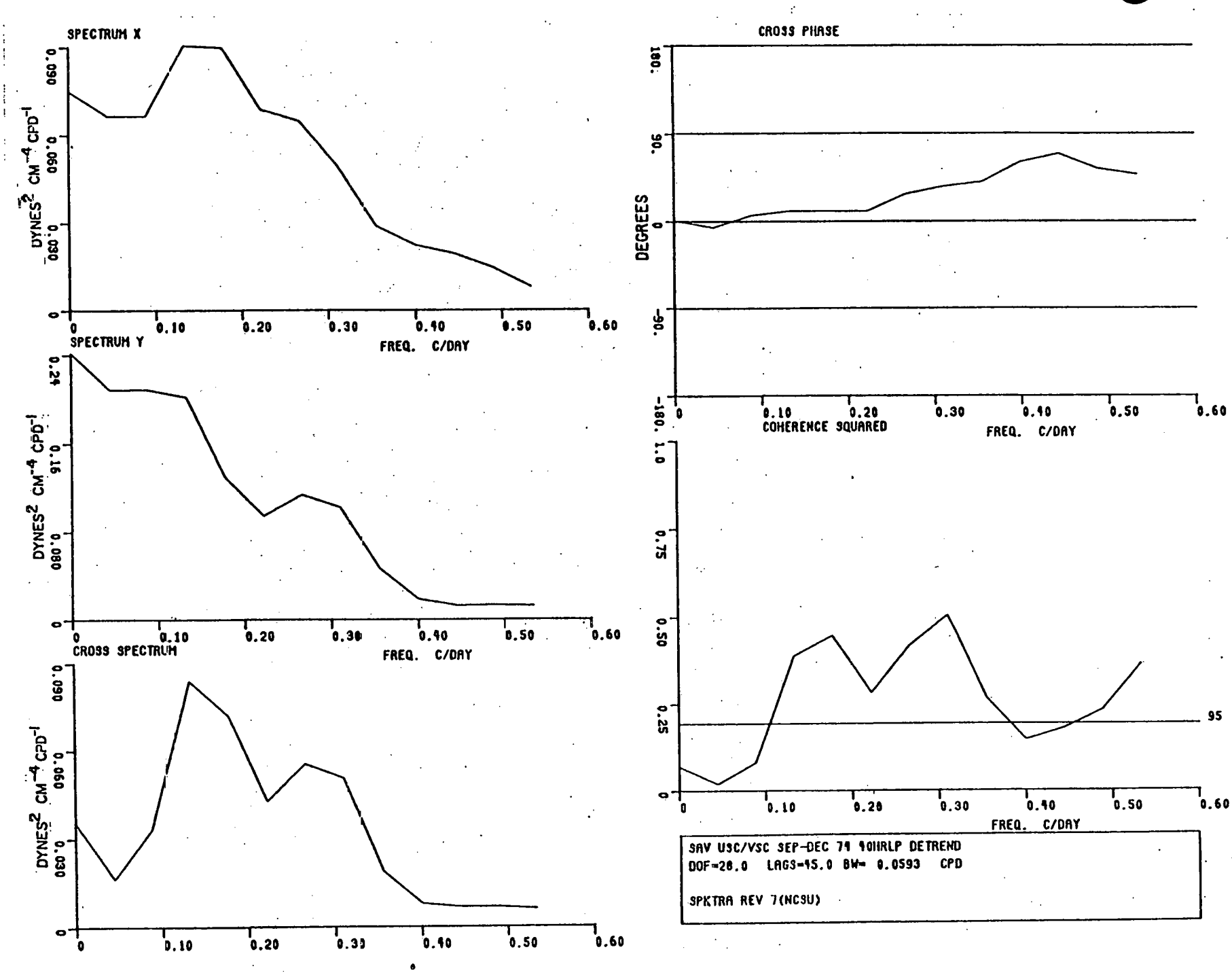
SPECTRUM X
DYNES^2 CM^{-4} CPD^{-1}
FREQ. C/DAY
SPECTRUM Y
DYNES^2 CM^{-4} CPD^{-1}
FREQ. C/DAY
CROSS SPECTRUM
DYNES^2 CM^{-4} CPD^{-1}
FREQ. C/DAY
CROSS PHASE
DEGREES
FREQ. C/DAY
COHERENCE SQUARED
95
FREQ. C/DAY
SAV USC/VSC SEP-DEC 79 40HRLP DETREND
DOF=28.0 LAGS=15.0 BW= 0.0593 CPD
SPKTRA REV 7(NCSU)

Figure 94

coherent, over the period range 2.8 - 10 days and also indicate $\tau^{(y)}$ leading $\tau^{(x)}$ by approximately 60°-80°; HAT $\tau^{(y)}$ leads $\tau^{(x)}$ (Fig. 93) at 2+, 3 and 10 day periods by 90°-110°. WIL $\tau^{(x)}$ and $\tau^{(y)}$ relationships (Fig. 94) closely follow those of SAV with the two components being very close to quadrature. The phase relationships between these wind components and to sea level indicate a lowering of sea level with increasing positive $\tau^{(y)}$ and $\tau^{(x)}$ wind stress with the offshore propagation of an anti-cyclone cold front whereby, from the coast seaward a southeasterly wind would begin to rotate clockwise, while sea level dropped to some maximum low as the wind became southwesterly, then began to rise as the wind rotated to be northwesterly to northerly and so-on.

During this same Sept.-Dec., 1974 period: FPS was coherent with BFT (Fig. 89) at 2 and 5-8 day periods, with minimal coherence (90% confidence level) at 3 day periods, with FPS leading BFT at the 3 and 5-8 day periods by about 15 hours and 25-40 hours; FPS and CHS (F. 90) are coherent at 2 and 3-9 day periods (esp. at 6-8 days) with FPS leading CHS by 0.45 days, at 0.275 cpd and 0.4 days between 0.16 and 0.12 cpd frequencies suggesting an event propagation speed of 5 m/sec. from Frying Pan Shoals to Charleston.

One could investigate the phase differences between wind stress components and adjusted sea level by adjusting the two time series so that the phase lag between the two is eliminated and then reconsider the correlation between the two time series. One could also consider the average ratio of sea level amplitude to wind speed magnitude, a value to be compared to the magnitude of the average of the ratio of the co-spectrum of sea level and wind component to the auto-spectrum of the wind component. These calculations will be done in a report to follow.

Monthly to seasonal to annual variations in sea level, due to the thermal variability of the water column and the changes in the atmospheric, marine climatology will be investigated in the report to follow. Seasonal

to annual harmonics could be eliminated from the time series, thereby suppressing the long period contamination of the short period correlations.

By extracting data which represents a change in only one of the atmospheric variables, while the other variables remain below some greatest lower bound, one could plot the sea level response to changes in that variable alone. There, a functional relationship between sea level and atmospheric pressure and wind could be obtained in an empirical fashion.

This type of procedure could be done for winds blowing in any direction and should result in a curve which indicates the changes in sea level as a function of wind direction, station by station.

Because of the problems which were encountered in obtaining tide gage data from NOAA/NOS, we do not have all of the data which is probably available for both the years and area of interest. We did not receive the Frying Pan Shoal sea level data until recently and so were not able to fully incorporate this invaluable data set into our analysis to date. Fortunately though, this is a preliminary assessment of the atmospheric climatology and sea level in the Carolina Capes region of the South Atlantic Bight and the report to follow this initial effort will be more inclusive and extensive and will incorporate the moored current, temperature, pressure, conductivity data as has been done by other investigators (eg: Smith, 1974; Cragg and Sturges, 1974).

Herein it should be noted that Brooks (1977) has used sea level data from BFT and WIL to predicate the existence of zero group speed continental shelf waves of the barotropic, clockwise rotating variety. It is the

conclusion of this author (Pietrafesa) that the Brooks' conclusions were premature, at best, and that no new evidence yet exists for the southerly propagation of a barotropic continental shelf wave. In fact, and to the contrary of Brooks' contention, FPS vs. BFT and CHS vs. BFT (all sea level) both would argue that there is a northerly propagation of events, definitely atmospherically induced.

The passage of large scale meteorological disturbances, such as are seen to occur in the data shown within the met/sea level report (Pietrafesa, 1978c), along a coastline can generate waves of the continental shelf wave variety (Gill and Schumann, 1974). However, as suggested by Niiler and Mysak (1971), the vorticity associated with the mean current over a continental margin may be of the order of the Coriolis parameter and the shelf waves could be advected by the mean current or even be amplified and grow unstable. The former possibility has recently been investigated by McKee (1978) who showed that a sheared geostrophic current could change the direction of phase propagation of the waves. Grimshaw (1978) has extended McKee's work and found that the presence of a boundary sheared current in a continental shelf wave field could result in the continental shelf waves having negative phase speeds. Additionally, Grimshaw suggests that the background vorticity provided by the sheared boundary current may result in the amplitude of the shelf waves being modulated/increased and that the amplified waves may become unstable.

Pietrafesa (1978 a and b) shows evidence for the northerly propagation of events which show up as wavelike features in the current meter data, i.e. u and v are in quadrature, with u leading v. This evidence is in contradiction with the Brooks' contention that southerly propagating barotropic CSW's

exist since the Pietrafesa data was collected well within the offshore extent of the first node, within which the Brooks' wave must rotate clockwise contrary to the Pietrafesa evidence that the event rotates cyclonically at periods of 3-3½ days. What may be happening herein is that the shelf waves may be getting advected with the mean current, towards the north. If the waves have a phase speed within the range of that of the speed of the mean current, and moreover due to the fact that both v_x and h_x are large, in the region of the shelf break, slope, it may appear to the observed (the current meter) that the waves are propagating northward and rotating cyclonically. The fact that h_y is varying, in the Capes region, may also influence the characteristics of any possible shelf waves modes.

It should also be noted that there is little consistent co-herence within the period band of interest (eg. site D, Figures 127 - 128) from top to bottom at mooring sites, ruling out the possibility of a strictly barotropic phenomenon.

Superimposed on all of this is the fact that $\tau^{(y)}$, and $\tau^{(x)}$ are very coherent over these periods, with $\tau^{(y)}$ leading $\tau^{(x)}$, that currents are coherent with the wind at these periods and that, for example, in the inner shelf region, the southerly currents lead the northerly currents over the period bond 3-3½ days, consistent with the wind forcing.

Dr. T.N. Lee (UM) has reported (personal communication) findings in the Georgia Bight similar to those shown by this author (Pietrafesa) for Carolina Capes region so that the two regions are not at dynamical variance in qualitative comparison herein.

III. MEASUREMENT PROGRAM AND CO-ORDINATION

In August, 1975 a set of Summer and Fall studies were begun in Onslow Bay, N. C. These studies constituted part of the North Carolina State University (NCSU) - Skidaway Institute of Oceanography (SKIO) combined efforts to contemporaneously measure: the temperature and salinity, i.e., hydrography; the current speeds and direction at several locations; and sea level and meteorology local and regional to Onslow Bay, North Carolina. Personnel from SKIO also measured various biological parameters along the hydrographic grid (cf. Figure 96). This work constituted the initial effort of a multi-discipline, multi-institutional program sponsored by the Energy Research and Development Administration to study the continental shelf processes affecting the oceanography of the South Atlantic Bight and is detailed in Pietrafesa, et.al., (1978). The immediate problems being addressed were those of understanding the processes by which nutrients are transported onto the North Carolina Shelf from offshore and to establish possible transport pathways for effluents discharged into North Carolina coastal waters.

Cruises were conducted to deploy (retrieve) fixed position current meter moorings (Figure 95) and to make detailed hydrographic and biological parametric measurements in Onslow Bay. The results of the latter surveys are presented in a series of SKIO data reports: Atkinson, et.al., (1976a,b), Dunstan, et.al. (1976), Atkinson, et.al. (1977) and Singer, et.al. (1977).

Endeco 105 current meters were used to measure speed and direction at specified temporal intervals and spatial locations.

The essential part of the 1975 Summer-Fall experiment was a fixed-level array of 4 Endeco 105-film recording current meters and 4 General Oceanics film - recording thermographs. Two moorings were set at the "focal points", locations A and B (Figure 95) of the cuspate shaped Onslow Bay. The current meters were set two to a mooring at depths of 10 and 25 meters from the surface in 28 meters of water, at each of the mooring sites, A and B. The array was designed to observe the propagation of phenomena across and along the inner to mid-shelf and to establish insights into the physics of the vertical and horizontal modal structure of the horizontal currents.

Onslow Bay was chosen as an initial study site in the context of a study of the whole of the continental margin of the South Atlantic Bight because it is the more densely populated region of the North Carolina coast and, consequently, the waste disposal problem is more critical there than elsewhere. The reason for siting the study of the intrusion of nutrients onto the continental shelf of the South Atlantic Bight in Onslow Bay was primarily based on the fact that there is/has been more historical data, i.e., background information needed to plan such a study, collected in Onslow Bay than anywhere else in the South Atlantic Bight.

Encouraged by the relative success of the 1975 pilot study, Atkinson and Pietrafesa conducted a more extensive and comprehensive field experiment in Onslow Bay during the period June thru September, 1976. The objectives of this second year experiment included both the direct measurement of the along-shelf, cross-shelf and vertical structure of the "late Spring-Summer-early Fall" current, temperature, conductivity and pressure fields from fixed point, vertical moorings and a continuation of the hydrographic and biological sampling, along the 1975 grid (Figure 96) by SKIO personnel. The mooring locations and vertical configurations are shown in

Figures 97 and 98. A total of 8 Endeco and General Oceanic current meters and thermographs were used at the 30 meter locations (sites A and B) and 8 Aanderaa RCM-4, with temperature, pressure and conductivity sensors, were used at the three 45 meter and one 70 meter sites (C, D, E and F). Several major and minor quasisynoptic hydrographic and biological surveys were made during the moored array experiment to study the variability of the shelf water and biological properties and to better determine the spatial and temporal distributions therein. Meteorological and coastal sea level data were collected from the stations listed in Tables 4 and 5.

Additionally: the moorings were re-established in December, 1976 and were retrieved in late April, 1977; and the deployment - retrieval scenario was conducted again during the period July-December, 1977 (as shown in Figures 99 and 100). From December, 1977, through the present a reduced array has been deployed. Drs. T.N. Lee (University of Miami) and Pietrafesa have co-ordinated a series of Georgia Bight - Carolina Capes experiments. These experiments will yield the first major alongshore South Atlantic Bight physical data.

EQUIPMENT AND MOORING DESCRIPTION

The moorings, established at sites A-F during the summer of 1976, had a taut line (wire) configuration. One or more subsurface floats were used to keep a bottom anchored cable taut. Fixed level recording equipment was attached to and suspended (away) from the cable. For mooring A and B a bottom anchored, auxiliary surface marker was located some distance from the main mooring line. The bottom "auxiliary" anchor was connected to the "main" anchor by a polypropylene ground line, which floats approximately a meter from the ocean floor. Moorings C-F did not have a surface marker.

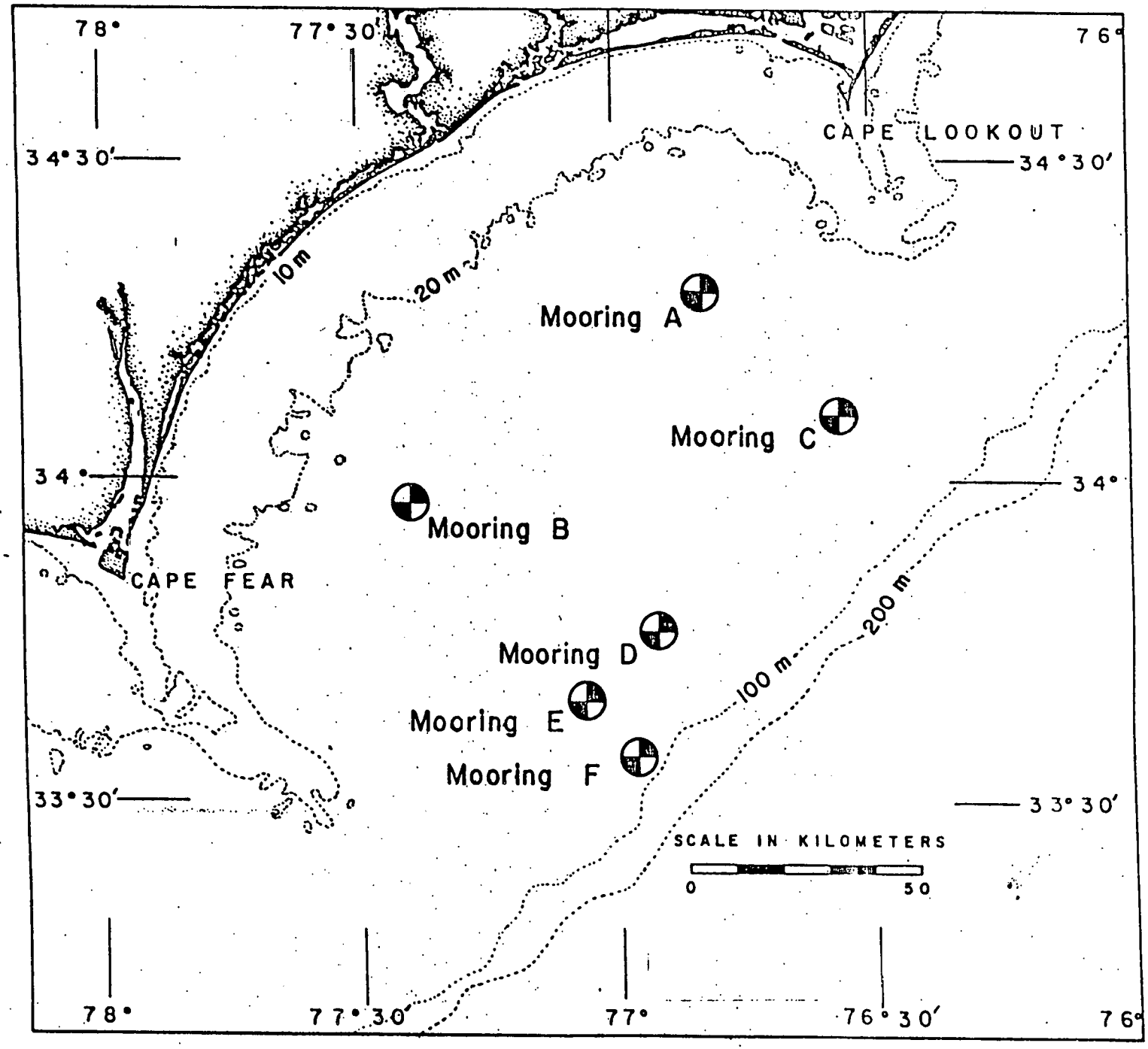

Figure 95. Onslow Bay, North Carolina-Study Area

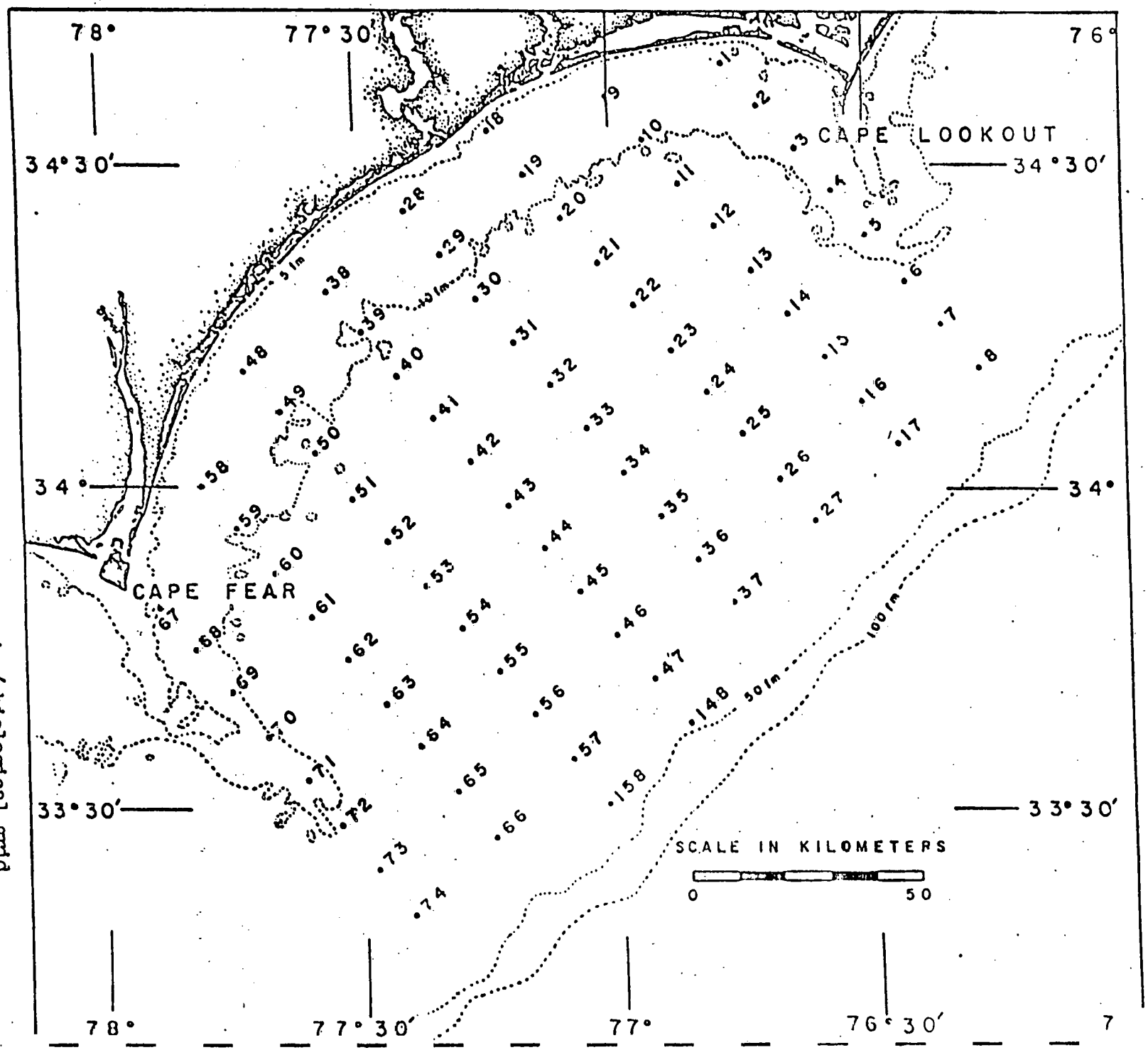

Figure 96 SK10/NCSU hydrography/ biological grid

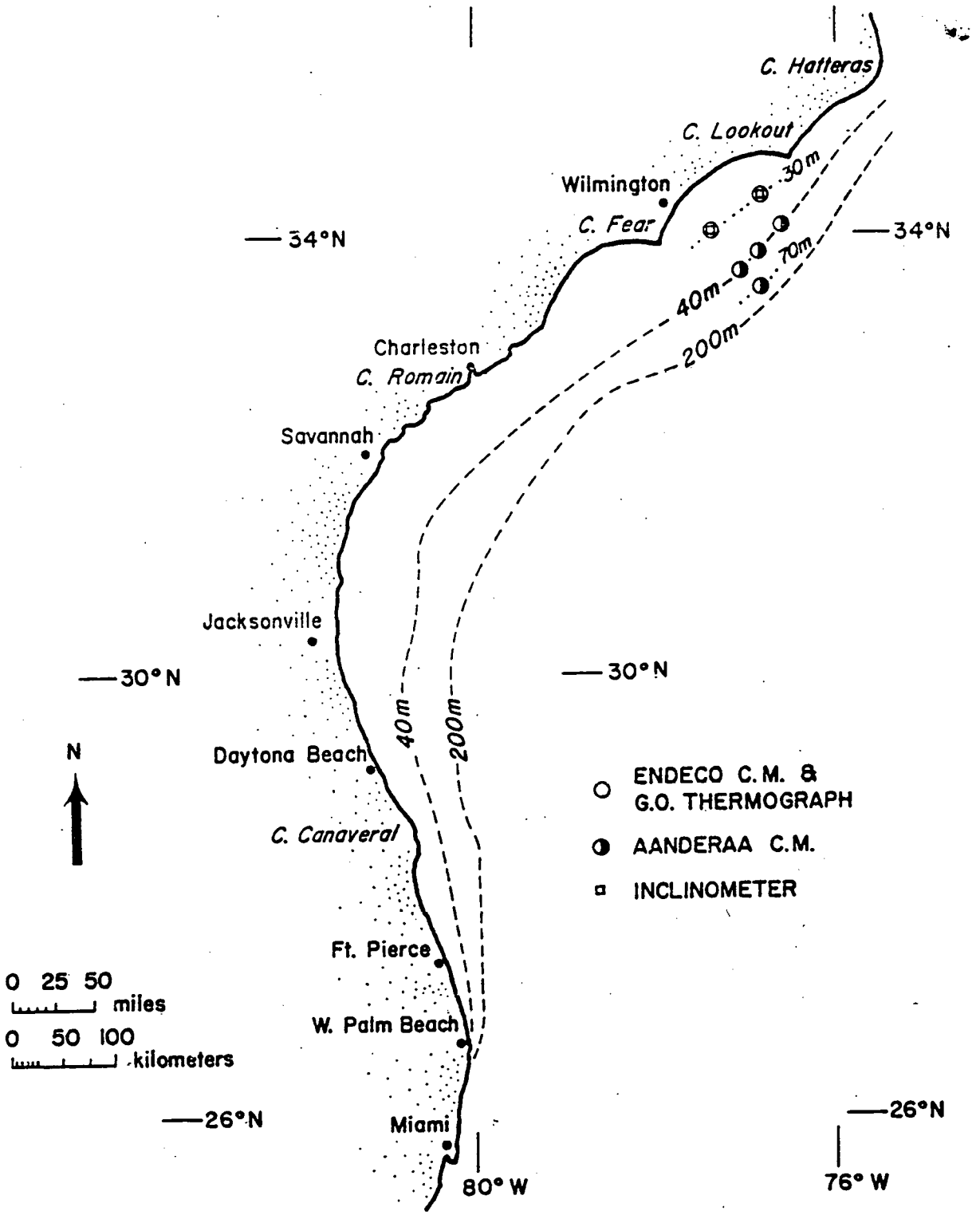

Figure 97. Mooring site locations; Spring-Summer 1976

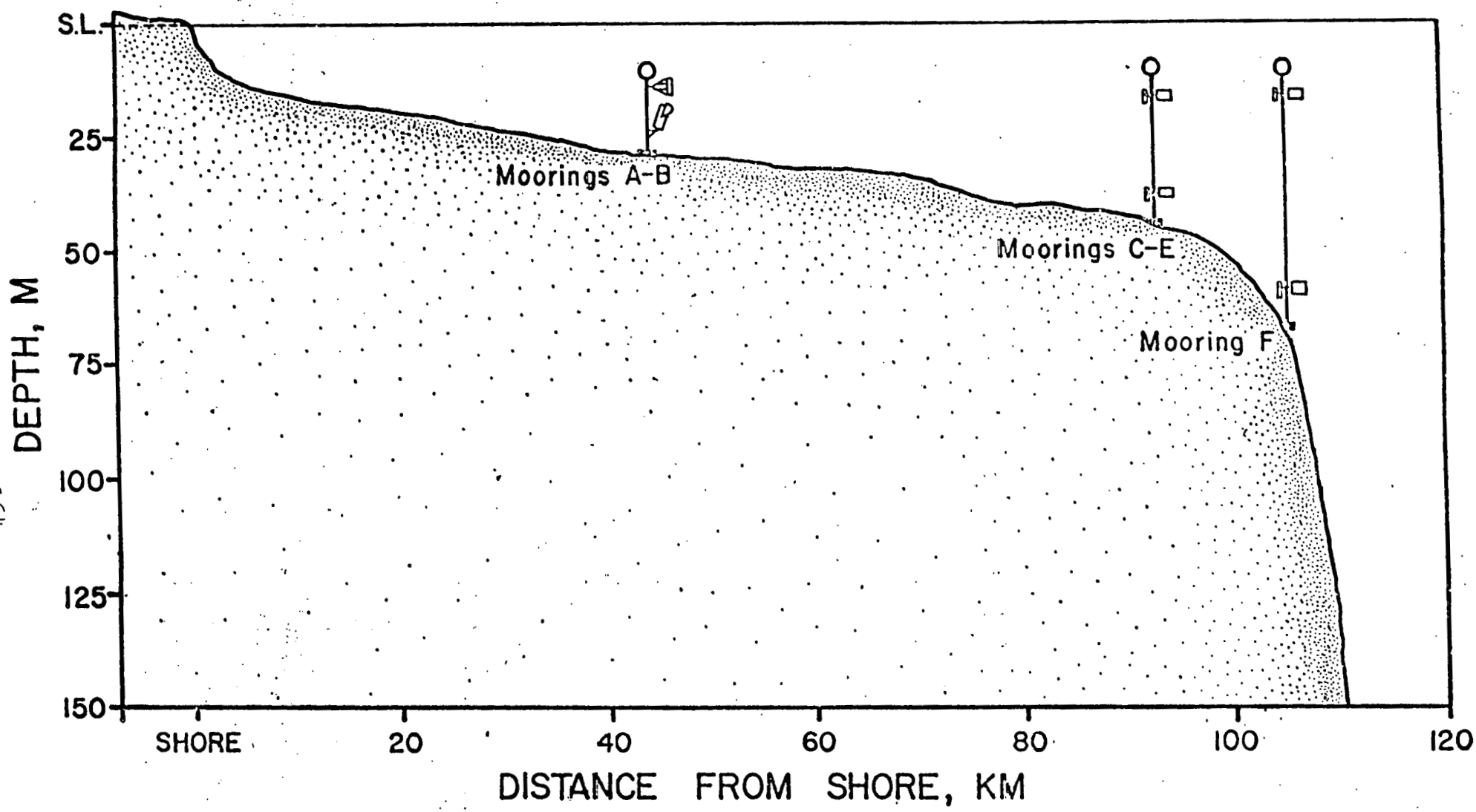

Figure 98 Vertical section of instrument depths

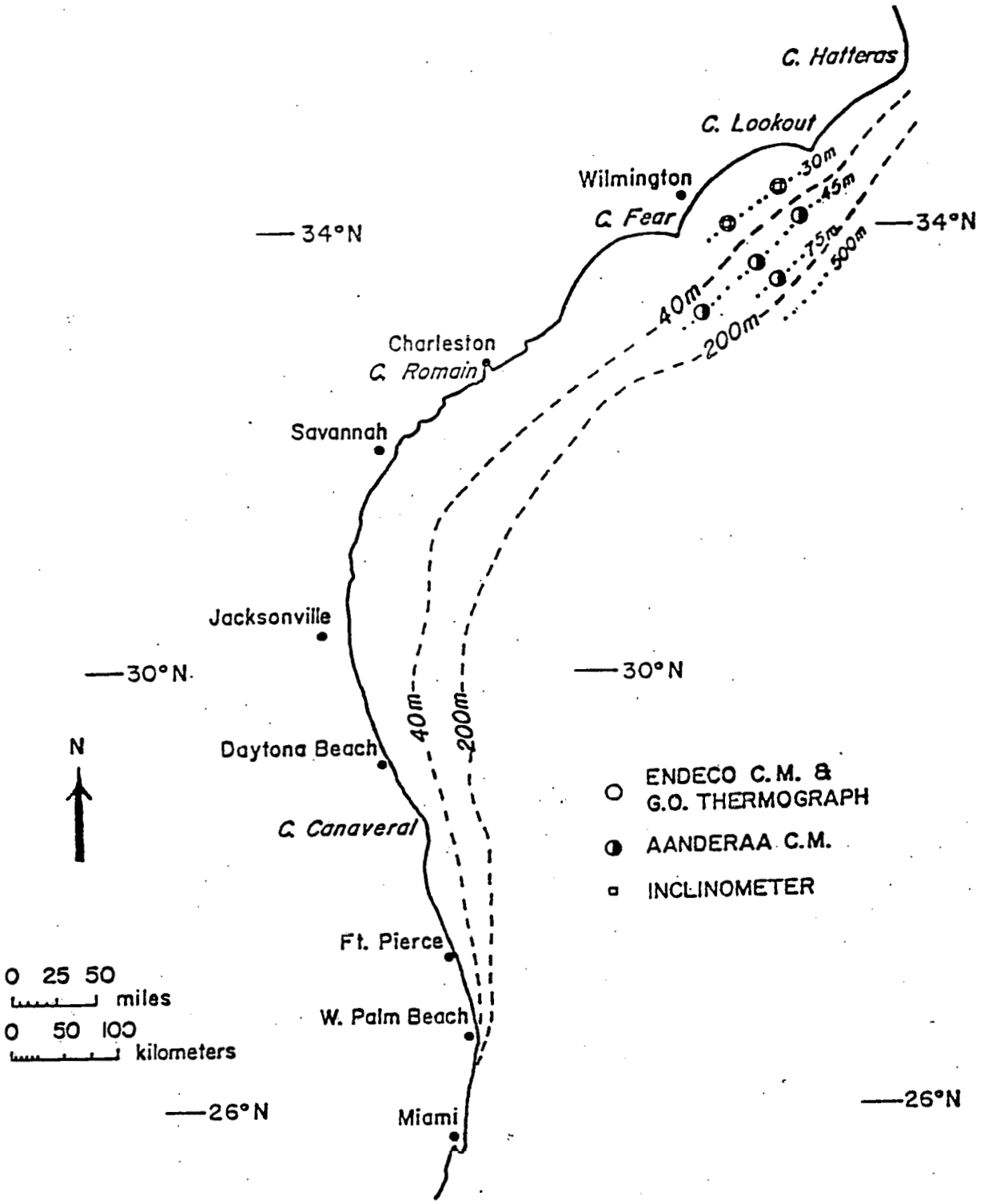

Figure 99. Mooring site locations for Fall-Winter, 1976 experiment

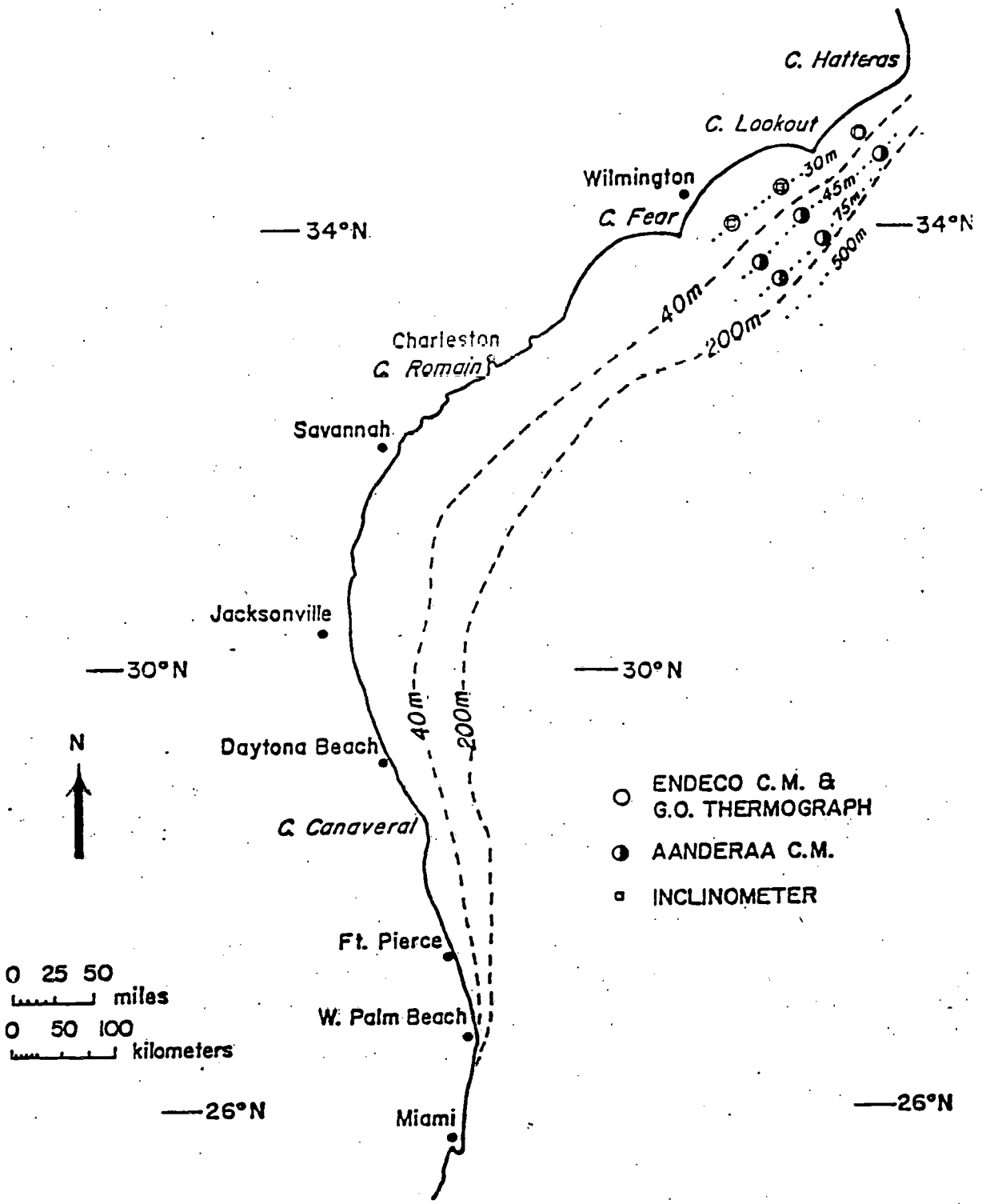

Figure 100 Mooring site locations for Summer, 1977 experiment

These moorings made use of AMF acoustic releases which served the dual function of helping locate and retrieve the mooring. The mooring configurations is depicted in Figure 101.

The operational logistics of installing moorings A-F were initiated in such a way as to maximize repeatability of location in subsequent experiments. The R/V Advance II was used during all deployment and retrieval phases of this 1976 experiment and mooring position locations (Table 6) were taken by the ship's Loran C system at the time of installation. The absolute error (accuracy) of the position is estimated to be less than ± 1 minute of latitude and longitude. The relative error (precision) is estimated to be less than ± 0.5 minute in either co-ordinate. Depths were taken by fathometer and are accurate to within ± 0.5 meters.

The recording instruments used on the shallow moorings (i.e. moorings A and B) were Endeco - 105 current meters, General Oceanics Model 2010 Inclinometer current meters and General Oceanics 3070, Thermographs; all film recording devices. The recording instruments used on the deep moorings (i.e. mooring C-F) were Aanderaa magnetic tape recording current meters and General Oceanics 3070 thermographs. Table 6 gives instrument types and depths used on all moorings. The specifications of the instruments are given in Pietrafesa, et. al. (1978 a and b).

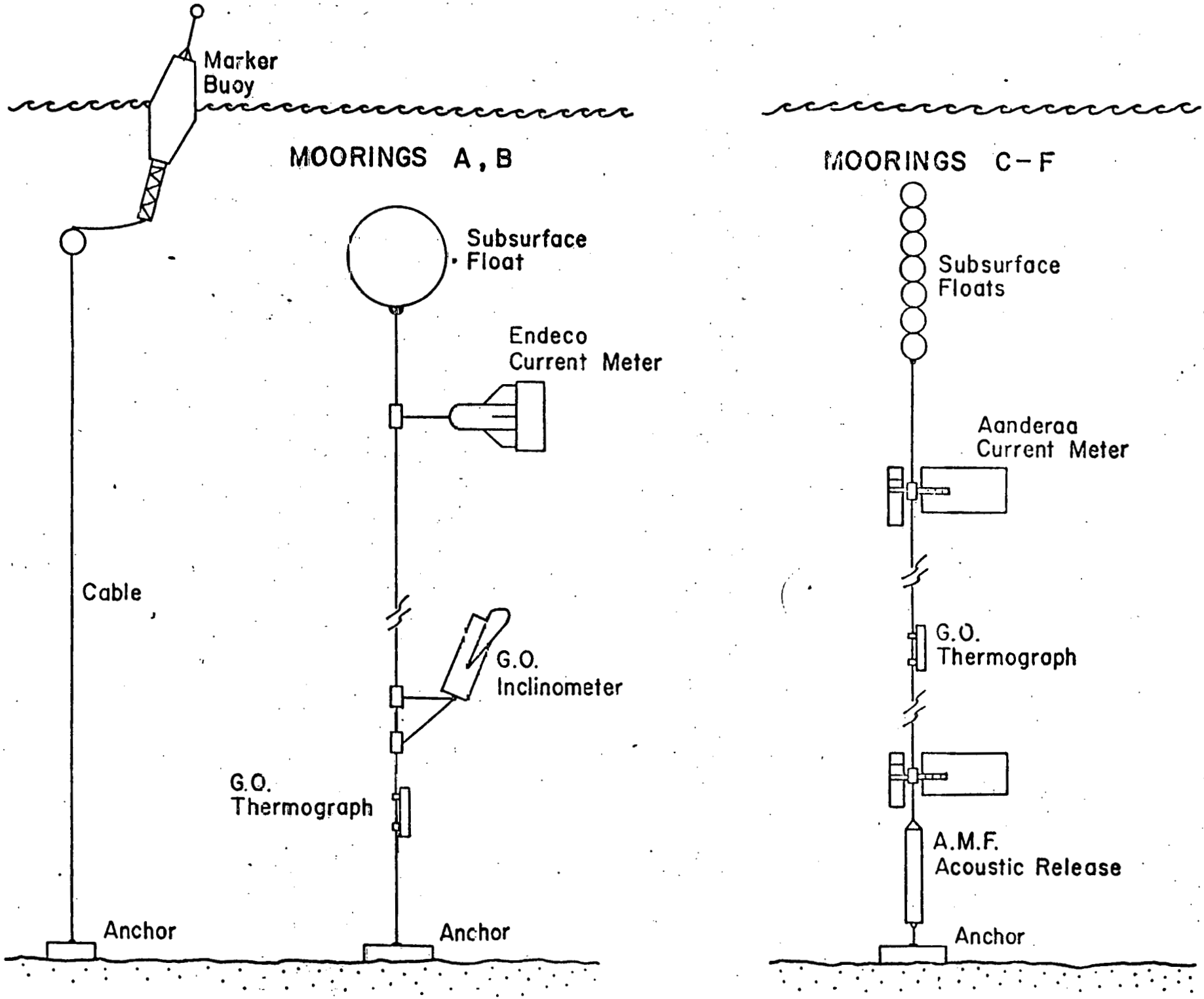

Figure 101 Fixed position current meter array

Table 6

Instrument Moorings and Element Locations

Mooring	Date	Lat./Long.	Loren A	Water Depth, m	Instr. Depth, m	Instr. Type	Inst. #
A	8 July,	34°18'N	4855	30	12	Endeco C.M.	316
(Albatross)	25 Aug. '76	76°50.6'W	2060		25	Inclimometer	M
						Thermograph	8
B	7 July,	33°58.2'N	4894	30	12	Endeco C.M.	247
(Brant)	25 Aug. '76	77°25.8'W	2493		25	Inclimometer	2
					26	Thermograph	5
C	22 June,	34°06.8'N	4780	40	22	Aanderaa	2254
(Cormorant)	21 Sept. '76	76°35.6'W	2030		28.5	Thermograph	4
					35	Aanderaa	1905
D	8 July,	33°46.7'N	4777	40	22	Aanderaa	2259
(Dunlin)	21 Sept. '76	76°55.1'W	2325		28.5	Thermograph	7
					35	Aanderaa	1908
E	22 June,	33°39'N	4774	40	22	Aanderaa	2256
(Eider)	21 Sept. '76	77°03'W	2445		28.5	Thermograph	3
					35	Aanderaa	1907
F	8 July,	33°34.6'N	4743	70	22	Aanderaa	2255
(Foster's Tern)	21 Sept. '76	76°56'W	2432		65	Aanderaa	1906

Mooring Deployment and Recovery

Deployment

Prior to the cruise, all wire, flotation and anchoring components are set up for each mooring. The wire is pre-cut and terminated appropriately. The flotation is assembled as several bouyancy units. The anchor and its hardware, including chain, swivel and eye hook on the anchor, are combined. The components of each mooring are labeled.

The moorings are transported, loaded and secured on the ship. As each mooring site comes up, the appropriate components are laid out and assembled on the fantail. The current meters are given a final check prior to putting them "in-line" on the wire. The release mechanism is attached and an in-air acoustic check is made. The entire mooring line is then scrutinized item by item to insure proper assembly.

As we approach the desired drop site, we begin to trail out the mooring over the stern, starting with the top. The ship is "bumped" ahead 1/3 on one engine by signals relayed from the fantail. This slow forward motion of the ship allows us to keep the mooring stretched as it is being played out. As the last of the mooring goes over, the acoustic release is gently lowered and allowed to hang from the mooring anchor. This anchor is then lowered to the water surface and held there by a deck-controlled quick release. We should at this time be over the drop site. If this is the case the release is pulled and the anchor and mooring drop away. Simultaneously a mark is given to the bridge to record the Loran A location. Also any other fixes at the deployment position such as Loran C and radar are recorded.

With the mooring in position the ship is immediately stopped and the hydrophone is lowered to interogate the acoustic release. After it has been found to be operating satisfactorily, the hydrophone is brought up and we proceed to the next mooring site.

Recovery

All bridge personel are informed prior to recovery as to what ship maneuvers will be required. The ship is brought to the same Loran A location at which a mooring was deployed. After the ship comes to a full stop the hydrophone is lowered and an attempt to interogate the mooring is made. If no contact is made or if the return signal is weak, the ship is maneuvered in a pattern so as to optimize the chances of getting a return signal. If the signal is strong an attempt will be made to release the mooring. Weather, amount of daylight and sea state are checked to ascertain that a released mooring can be brought on board. With these conditions met all available personel are called to a watch position on the upper decks. The release signal is sent. If the release mechanism responds that it has released, the word is sent out to begin a visual search for the free-floating mooring.

When the mooring is sighted, the ship maneuvers in on it from a down wind position. The bridge attempts to bring the stern in close proximity to the mooring. A grapnel line is thrown and usually after repeated attempts the mooring is hooked and pulled to the side of the ship. All ship locomotion ceases when the mooring is hooked. The mooring is then pulled in by hand, taking extreme care with the current meters and release mechanism. When all of the mooring is on board, the ship proceeds to the next site as a crew begins disassembl-

ing the mooring. The current meters are removed first. They are cleaned, taken inside, checked for damage, opened, turned off and inspected for amount of data collected. The tape from each meter is removed, labeled as to reference number, date, meter location, etc. and wrapped in aluminum foil. The tapes are then ready to be sent for processing. The meters are then closed up and stored for the return trip to Raleigh.

Calibration Techniques

Speed

Although the manner in which one obtains speed data differs widely among instruments, the same basic method of calibration may be used. The instrument may be a savonious rotor, inclinometer, impeller or hot film. All of these types may be calibrated in the same manner on a towed cart in a water channel when the speed of the cart is known.

This method, as used at N. C. State University, utilizes the facilities of EPA located in the Research Triangle Park. The facility consists of a 35 meter long, 2.4 meter wide and 1.2 meter deep channel with an overhead track capable of variable speeds from 0 to 50 cm/sec. Higher speeds are possible by setting up an opposing current.

Any number of points may be taken to establish the calibration curve depending on the resolution required. About every 10 cm/sec gives a satisfactory curve. Additional points at 5 cm/sec intervals can be used to "fill in" uncertain areas.

The actual method used consists of rigidly attaching the current meter to the cart. The meter is immersed in the tank to a depth of approximately 10 cm below the surface, 1 meter from the nearest sidewall. All supporting structures for the meter when immersed in the tank are designed to be down current of the meter so as not to interfere with

the flow around the meter. This may be checked from time to time by introducing dye in front of the meter while the cart is in motion.

With the meter in place on the frame, test runs are ready to begin. Starting at a slow speed, the cart travels the 25 meter length of the test section. The meter is tilted back out of the water when returning the cart to the start position to prevent inducing unnecessary turbulence in the channel. Each successive run is at a greater speed up to the 50 cm/sec limit.

This would complete the speed calibration for a given meter. The data is plotted and a speed calibration curve is obtained.

Direction

The Aanderaa meters have a mechanical compass. The compass produces a coded electrical signal, by means of potentiometer, which is recorded on magnetic tape. The 10 bit binary code yields a number from 0 to 1023. Thus a resolution of approximately 1/3 degree is possible. The Aanderaa specification sheet lists the accuracy of the compass as better than ± 2 degrees (meter out of the case). In the case, the accuracy is ± 7.5 degrees with a current of 2.5 to 5 cm/sec or 100 to 200 cm/sec and ± 5 degrees with a current of 5 to 100 cm/sec.

A non-magnetic stand was built by us and set on a concrete base in a remote area of the coast for the purpose of calibrating the meters. This stand is located near the State marine resource facility at Fort Fisher. The stand consists of a vertical base with a flat disk on top. A sheet of Teflon® (registered Dupont trademark) is placed on the disk. A cross piece with a matching disk is placed on top of the Teflon® sheet. Thirty six holes are drilled in the lower plate at 10 degree intervals. The upper plate has a single hole in it to allow a pin

to slide through to the lower plate. This locks the frame in a given position. There is no noticable give in the pin at any setting. The cross piece consists of two aluminum I-beams at 90 degrees. This makes a stand with four arms allowing four meters to be calibrated simultaneously.

Each arm is approximately two feet long. Each meter is placed on a pin at the end of an arm. This mounting is similar to that on the Aanderaa vane. The position of the stand was determined relative to true North by shooting Polaris and turning the angle to the zero or starting position of the stand.

To go through a calibration series, the crosspiece is rotated 10 degrees and allowed to record for three minutes. This is continued through all 36 positions.

This completes the compass calibration procedure. The data is plotted to correct future field data (see Fig. 9).

Pressure

A Heise pressure gauge is connected directly to the pressure sensor on the Aanderaa. With a hydraulic hand pump connected to this system, the pressure is increased in 10 psi increments up to the rated maximum pressure of the individual sensor. This is usually 100 or 200 psi. At each 10 psi step the coded Aanderaa value is noted and recorded. This value is determined by counting the ten binary pins and converting it into a number from 0 to 1023. This number may then be plotted against the Heise gauge reading to give a calibration curve for each sensor (Fig.9).

Temperature and Conductivity

We presently use the calibration formula provided with each sensor from Aanderaa for conductivity. For temperature a small constant temperature bath was used to generate a temperature calibration curve

for each sensor (see Figure 102). A constant temperature-salinity bath is being constructed at the present time to enable us to calibrate these parameters in the future.

Data Processing

Standard NCSU time series analysis programs based on both the FESTSA system (Brooks, 1976) and the programs of Dr. R.W. Weisberg of N.C.S.U. have been used to process the current and meteorological raw data.

Aanderaa Current Meters

The original Aanderaa data consisted of 10-bit binary words recorded on 1/4 inch magnetic tape. As this format was not computer-compatible, the original data tapes were sent to the University of Miami/RSMAS for decoding. As each reel was transcribed, the data frames were expanded to include frame count and flags for hardware-detectable errors, (Lee 1977). The expanded data files were returned to NCSU on standard 9-track tape, where they were transferred to disk files for convenient access. A primary editing pass was made to correct hardware-detected errors, after which the calibration vector for each meter were applied. The calibrated data was then converted to card-image format and plotted. These plots were visually scanned, and any errors detected were corrected by a second editing pass. The resulting files were then converted to FESTSA format for use in all further processing.

The calibrated data with an interval of 15 minutes was filtered using program CURFIL. A three-hour low pass filter (3HRLP) was first applied to reduce high frequency noise due to gravity wave aliasing and other contamination. The 3HRLP operation results in a data loss of 8 hours from each end of the record. The 3HRLP data were subsampled

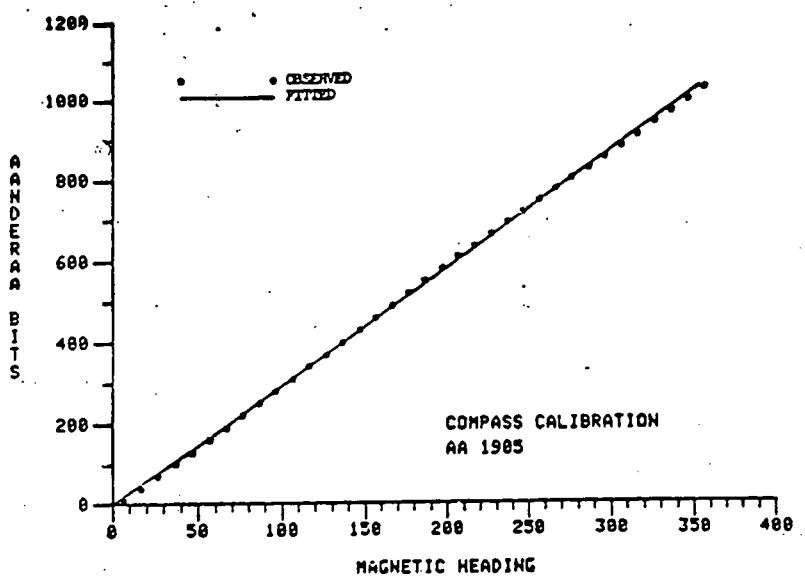

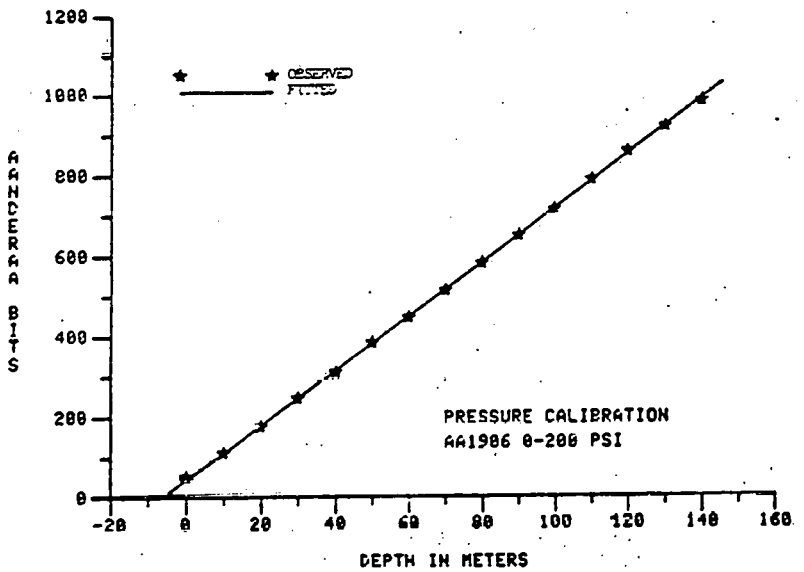

Figure 102
Sample Aanderaa calibration curves

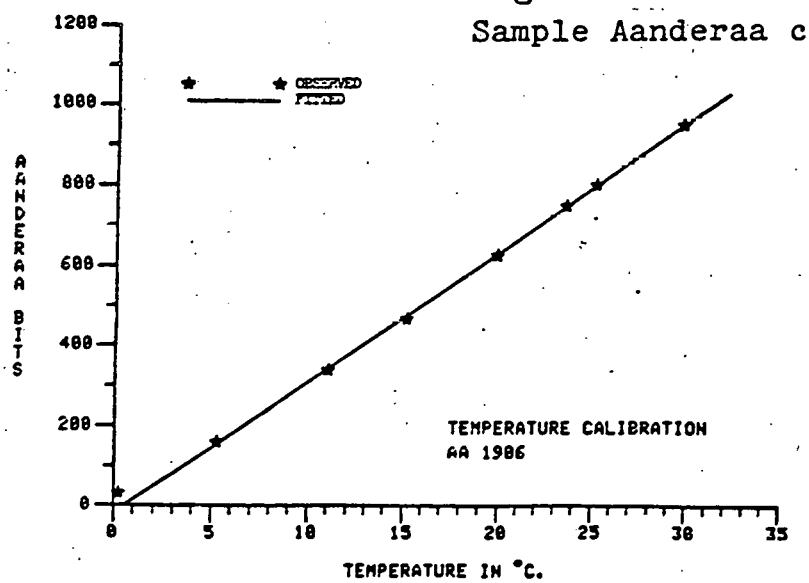

hourly. A 40 HRLP filter was then applied to the 3HRLP to separate the tidal and subtidal frequency bands, resulting in additional data loss of four days at each end. An hourly 3-40HRBP series was created by subtraction, and the 40HRLP series was then decimated to six-hourly samples for further analysis. The 40HRLP filter attenuation at the daily tidal frequency (1CPD) is greater than 10^6 (Fig. 53). The six hour interval was chosen to be commensurate with the filtered meteorological data. Table 7 gives the particulars on data sets.

The "Principal Axis" coordinate system (Fofonoff, 1969; Gonella, 1970; Mooers, 1973) was used for the current meter data. First order statistics are presented in Table 8 for the topographically aligned, 55.6° clockwise, rotation system (not used in this report) and Table 9 for the "Principal Axis" coordinate system.

Spectral representations of data are then given in two formats:

a) Graphs of variance (spectrum density times frequency) versus the logarithm of frequency. These are "quick look" calculations based on the fast Fourier transform (FFT). The FFT's of original data were smoothed by block averaging over five adjacent estimates, yielding about ten degrees of freedom for each averaged estimate. The FFT's of low passed data were not smoothed, yielding two degrees of freedom for each estimate.

b) Auto and cross spectra, phase and coherence squared computed for paired input time series. The spectral calculations were performed by Fourier transforming correlation functions. The maximum correlation lag, spectral bandwidth, degrees of freedom, and input time series names are shown on each figure. The first named time series corresponds to "spectrum x". Positive phase values indicate series y leading series x.

Table 7

Data Particulars

Mooring	Meter	Unfiltered Data Start time EST	Unfiltered Data End time EST	Unfiltered Data # of points	Unfiltered Data Δt (hr)	Filtered Data Start time EST	Filtered Data End time EST	Filtered Data # of points	Filtered Data Δt(hrs)
A	316	1830 hrs. 8 July	1330 hrs. 25 Aug.	2295	.50	0230 hrs. 13 July	0230 hrs. 21 Aug.	157	6
B	247	1730 hrs. 7 July	0600 hrs. 25 Aug.	2329	.50	0130 hrs. 12 July	1930 hrs. 20 Aug.	160	6
C	2254	1730 hrs. 22 Jun.'76	2130 hrs. 18 Sept.'76	8465	.25	0130 hrs. 27 Jan.'76	1330 hrs. 14 Sept.'76	319	6
	1905	1730 hrs. 22 Jun.'76	0415 hrs. 22 Aug.'76	5804	.25	0130 hrs. 27 Jun.'76	1930 hrs. 17 Aug.'76	208	6
D	2259	1445 hrs. 8 Jul.'76	1015 hrs. 21 Sept.'76	7183	.25	2245 hrs. 12 Jul.'76	2245 hrs. 16 Sep.'76	265	6
	1908	1445 hrs. 8 Jul.'76	0545 hrs. 21 Aug.'76	4189	.25	2245 hrs. 12 Jul.'76	1645 hrs. 16.Aug.'76	140	6
E	2256	0615 hrs. 22 Jun.'76	1130 hrs. 21 Sep.'76	8758	.25	1415 hrs. 26 Jun.'76	0215 hrs. 17 Sep.'76	331	6
	1907	0615 hrs. 22 Jun.'76	0530 hrs. 21 Sep.'76	8738	.25	1415 hrs. 26 Jun.'76	2015 hrs. 16 Sep.'76	330	6
F	2255	No data				No data			
	1906	1100 hrs. 8 Jul.'76	1230 hrs. 21 Sep.'76	7207	.25	1900 hrs. 12 Jul.'76	0100 hrs. 17 Sep.'76	266	6

Table 8

First Order Statistics (Rotation - 56°)

Meter	Meter Depth(m)	Min.	Max.	Mean	S.D.	Parameter Cm/sec
A_{top}(316)	12	-33.0	57.0	3.78	15.1	u
		-35.0	35.0	-1.1	10.9	v
B_{top}(247)	12	-29.0	32.0	0.13	9.9	u
		-42.0	37.0	-2.3	11.8	v
C_{top}(2254)	22	-42.11	51.35	0.18	12.42	u
		-26.09	52.68	9.55	13.64	v
C_{bottom}(1905_a)	35	-27.54	23.75	-1.60	10.32	u
		-26.31	35.80	7.14	10.14	v
D_{top}(2259)	22	-53.17	51.96	-2.45	18.07	u
		-16.87	72.61	4.70	20.37	v
D_{bottom}(1908)	35	-38.86	22.29	-2.72	9.80	u
		-18.20	28.42	3.16	6.46	v
E_{top}(2256)	22	-62.23	53.12	-1.86	15.58	u
		-55.90	91.03	8.41	20.70	v
E_{bottom}(1907)	35	-14.57	2.65	-0.18	1.10	u
		-1.50	24.69	0.37	1.27	v
F_{top}(2255)	22		- No Data -			u
						v
F_{bottom}(1906)	65	-27.00	76.79	1.48	8.80	u
		-56.21	42.93	-0.25	8.32	v

Table 9

First Order Statistics (Principal Axis angle = R)

Meter	Meter Depth(m)	Min.	Max.	Mean	S.D.	Parameter (Cm/sec)	R
A_{top}(316)	12	-39.0	58.0	2.30	16.0	u	18°
		-43.0	29.0	-3.18	9.4	v	
B_{top}(247)	12	-28.0	28.0	0.65	8.9	u	69°
		-44.0	38.0	-2.22	12.6	v	
C_{top}(2254)	22	-43.49	43.04	-2.14	11.67	u	69.65°
		-28.93	55.49	9.30	14.28	v	
C_{bottom}(1905_A)	35	-27.49	28.31	-0.3244	10.37	u	45.48°
		-27.31	37.89	7.32	10.09	v	
D_{top}(2259)	22	-53.57	51.68	-2.55	18.05	u	56.82°
		-57.24	72.59	4.66	20.38	v	
D_{bottom}(1908)	35	-20.00	22.14	-0.0082	6.99	u	14.99°
		-21.23	43.94	4.17	9.41	v	
E_{top}(2256)	22	-60.16	58.11	-1.00	15.52	u	49.79°
		-53.33	91.25	8.55	20.75	v	
E_{bottom}(1907)	35	- 9.16	8.72	-.086	1.03	u	41.18°
		- 1.50	24.10	.40	1.32	v	
F_{top}(2255)	22		- No Data -			u	
						v	
F_{bottom}(1906)	65	-27.23	79.60	1.42	8.70	u	46.10°
		-61.63	39.47	-0.49	8.42	v	

The speed and direction values were converted to u and v components in several ways. The Carolina Cape region is defined by an irregular, cuspate, scallop-like coastline which extends into shoals and consequently it is difficult to specify a spatial co-ordinate system. Coherency and phase relationships between components of a vector time series are functions of the co-ordinate system in which the components are specified. The natural tendencies are to choose either a north-south, east-west horizontal axis or to assume a straight coastline of uniform cross-section so that the horizontal co-ordinate system axes lie parallel to and perpendicular to the straight isobaths. Unfortunately, however, the isobaths in the Carolina Capes region are not uniform or straight and the choice of a co-ordinate system is less than obvious. Two tacks were taken herein. The first co-ordinate system chosen is one based on the direction of the local bathemetric contours at approximately mid-shelf to the shelf break, which tend to run southwest to northeast at an angle 56° clockwise from North (quantitatively "alongshore"). The second co-ordinate system used is one oriented on a basis determined by the characteristics of the data itself. A co-ordinate system which maximizes the variance in any given direction gives the so called "Principal Axis" of variance. This system, in which the estimated phase difference between u and v is identically $\pm 90^{\circ}$ is also called the "Normal" system (Fofonoff, 1969) and the "Hodograph" system (Mooers, 1970). As a function of the physical, dynamical processes causing the measured hydrodynamics, the principal axis of variance may vary with frequency and geographic location. The "Principal Axis" for a given vector time series is obtained by rotating the covariance matrix until the cross-covariance between orthogonal velocity components is zero. The rotation of the co-ordinate system into the principal axis does not fix the sign of the 90° phase shift

between u and v. This is determined by the data. Since the principal axis for a given vector time series will vary with frequency, we can construct hodographs which will allow for the vector time series to be decomposed into cyclonic and anticyclonic rotating motions of different amplitude and phase. The sum of these two polarized motions yields an ellipse whose semi-major axis is oriented along the principal axis of variance at that particular frequency. The principal axis herein is given as a function of frequency rather than as an average over a large frequency band.

In this report the "alongshore" co-ordinate system was used on the meteorological data. It was also used to generate first order statistics for the current meter velocity data. However, the "Principal Axis" system was used exclusively with the current meter velocity data for all data plotting.

IV. DATA PRODUCTS

To facilitate our understanding of the shelf "processes", we have presented the data in several forms. An example of these products is shown in the Summer, 1976 data report (Pietrafesa, et. al., 1978b), which is delineated below.

Figures following, within this section are representative of many of the products.

The current meter velocity information is presented in several forms. Displayed in unfiltered form are time series of current components u and v, FFT's, histograms and progressive vector diagrams (PVD's). The PVD's are presented for the full time series and also for interesting and/or confusing subsets. Displayed in 3HRLP are time series of current components u and v, spectra (only the crossing of the velocity components of the same meter) and hodographs. 40HRLP records were used to produce time series of velocity components, vector stick diagrams, FFT's and spectra. The spectra series crosses the velocity components for the top and bottom meters on the same mooring string, as well as of meters located on a line perpendicular to the shoreline for meters on an alongshore line. All this current velocity data is presented in the "Principal Axis" system, excepting for the hodographs and the histograms which are in a natural co-ordinate system.

The information from Aanderaa temperature and pressure sensors is displayed in time series plots of unfiltered, 3HRLP and 40HRLP form. FFT's are presented of unfiltered and 40HRLP records. Spectras of temperature vs. velocity components are also given.

Meteorological data from two stations, Wilmington, N. C. and Cape Hatteras, N. C. are presented in several forms. Displayed in unfiltered form are the time series of wind velocity components and their FFT's. Displayed in 40HRLP form is the temperature, pressure, wind velocity components and wind stress time series with their FFT's. Stick vector plots of wind stress are also displayed. A comparative look at the stick vector plots of current velocity and wind stress is presented and a series of spectras are presented crossing wind stress with current velocity components.

Kinetic energy density spectra for current meter u, v and T and of wind velocity and stress are presented. Momentum and heat correlation variance plots are displayed for all current meters. Co-spectra of temperature vs. velocity components for all current meters C-F are presented. Hodograph plots of wind velocity and stress are given. Mean current velocities, and tidal elipses are plotted, and Energy fraction vs. frequency plots for the mooring strings, for different current modes are presented.

Future products will include: 2 dimensional auto-regressive models to determine the percent of observed current due to direct atmospheric forcing; least tidal squares analyses; multiple regressions for a better assessment of atmospheric pressure and wind component input relationships to sea level response; in comparison of sea level and gradients thereof to moored meter data and gradients thereof; computations of the vertical modal structure of current and temperature data using an empirical orthogonal function analysis, like that of Kundu, et. al. (1975).

V. PRELIMINARY PHYSICAL DYNAMICAL ANALYSIS

This report contains a preliminary description of currents measured in Onslow Bay N. C., the generic term for the continental shelf region between Cape Lookout and Cape Fear; data from five moorings maintained during the summer of 1976 are presented in this report. Their locations are shown in Figure 97. The Onslow Bay measurement program continues to be active and a complete listing of available data is contained in the referenced data reports. We've chosen the summer 1976 data set included within for description. Data are also available from winter and summer of 1975 (Pietrafesa, et. al., 1978) on a more limited basis. These will also be discussed briefly.

Water motions on the continental shelf are caused by numerous physical processes. Synoptic and seasonal scale motions occur in response to direct forcing by the weather (principally wind and atmospheric pressure) at synoptic scales and variations in thermohaline inputs (heat and salt) at seasonal scales. Synoptic variability occurs predominantly over the range of time scales spanning 2-10 days, the scales of the cyclonic and anticyclonic perturbations of the wind field. Other low frequency fluctuations occur in response to external forcing from the deep ocean e.g. eddies and Gulf Stream intrusions. Due to its sloping bottom the continental shelf region can support free modes of oscillation generally spanning similar time scales as the atmospheric forcing. The free modes are commonly referred to as quasi-geostrophic, topographic Rossby, or continental shelf waves and a review of these oscillations is given by LeBlond and Mysak (1977). The combined low frequency oscillations observed at any position on the continental shelf is expected to reflect a complex mixture of these aforementioncd processes.

At higher frequencies, the astronomically forced semi-diurnal tides propagating shoreward from the deep ocean are a dominant feature observed in the South Atlantic Bight continental shelf. Between these semi-diurnal tides and the lower frequency weather continuum three processes occur in varying degrees across the shelf: diurnal tides, inertial oscillations, and sea breeze. These all have time scales of roughly one day. Processes occurring at frequencies higher than the semi-diurnal tides include internal inertia-gravity waves, edge waves, and finally the surface gravity waves.

We will view the summer 1976 data from Onslow Bay with these processes in mind, not for the purposes of scientific analysis, but rather as a conceptual overview delineating which candidate processes may be important.

The mooring locations in Onslow Bay during the ERDA/Sea Grant sponsored summer 1976 measurements are shown in Figure 97 and the corresponding instrument positions and sampling lengths are given in Tables 6, 7. Two different recording current meters: Aanderaa and Endeco, were used. These instruments as well as others have recently been intercompared by Beardsley et. al. (1977) and the results, for the present purposes, suggest that data from the two are qualitatively similar. The rectangular array had simulteneous records spanning 23 July to 22 Aug. These are presented in Figs. 103-111. Speeds are in cm/s with the u and v velocity components positively directed offshore and alongshore respectively, the alongshore direction being approximately at 55.6 degrees clockwise from true north. The time series were all low pass filtered with a half power point of 3 hours to remove high frequency noise. The most apparent features are semi-diurnal tidal currents superimposed upon a low frequency background. The only qualitative differences between the Aanderaa

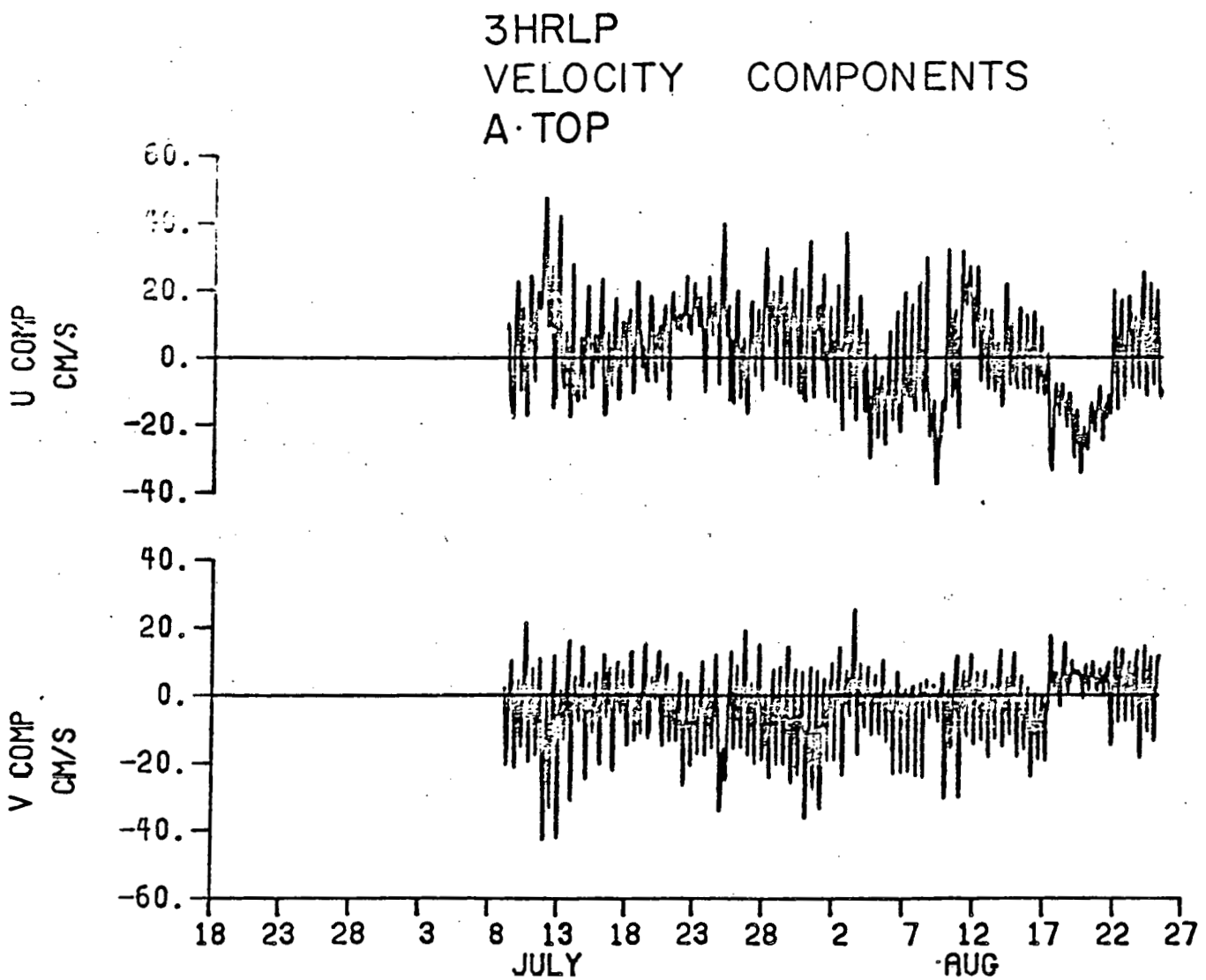

Figure 103. 3HRLP velocity components for A_{top}

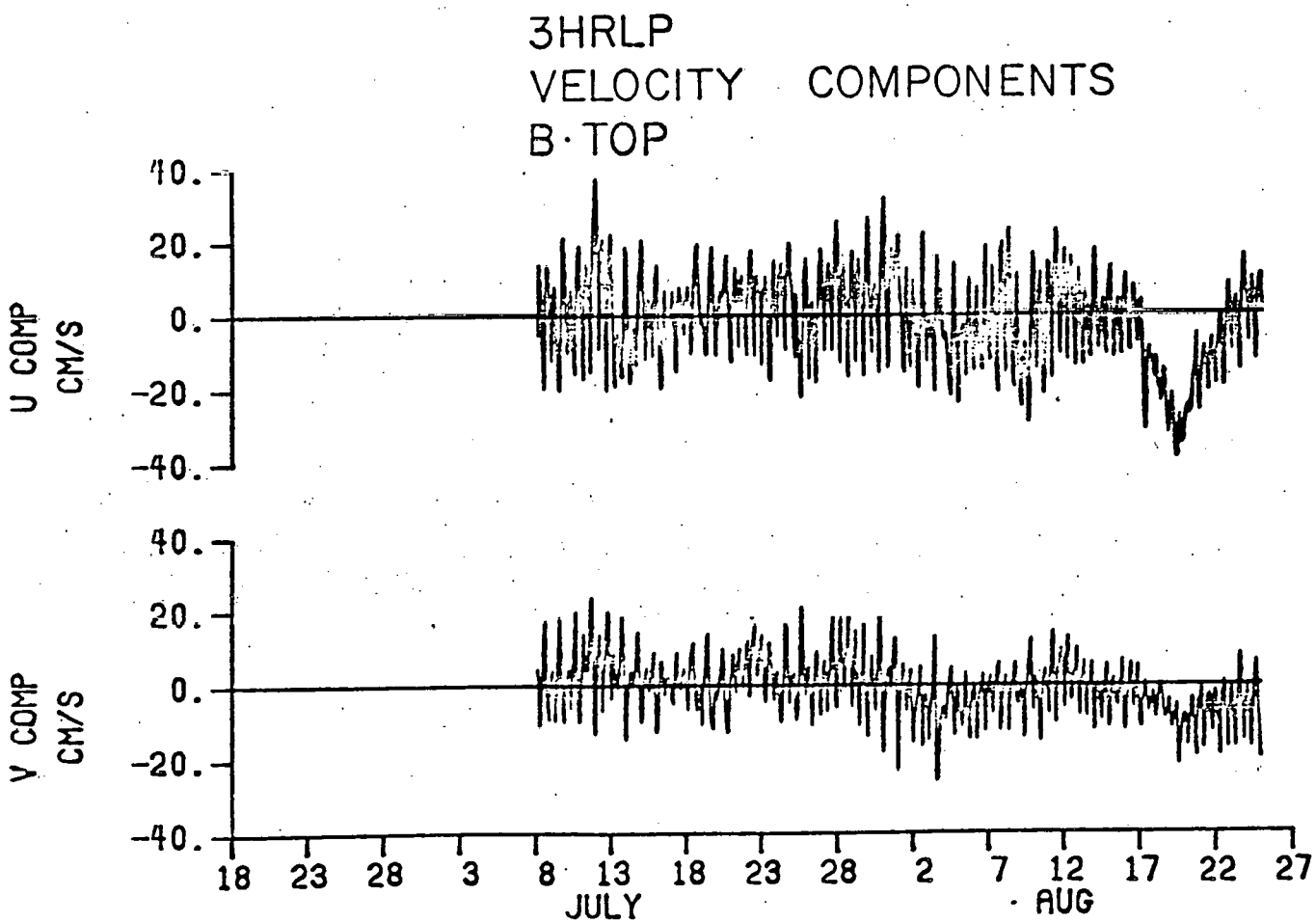

Figure 104. 3HRLP velocity components for B_{top}

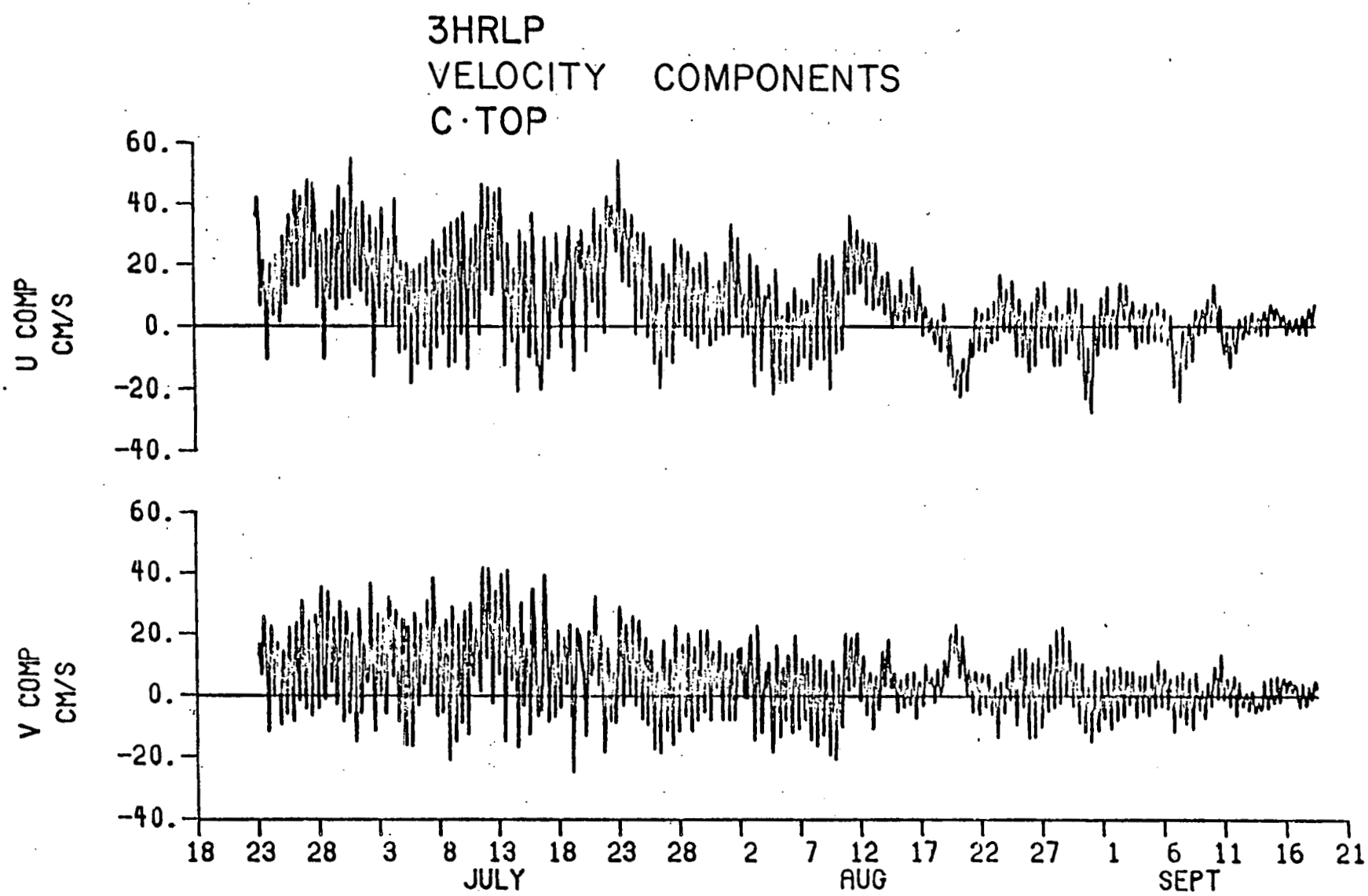

Figure 105. 3HRLP velocity components for C_{top}

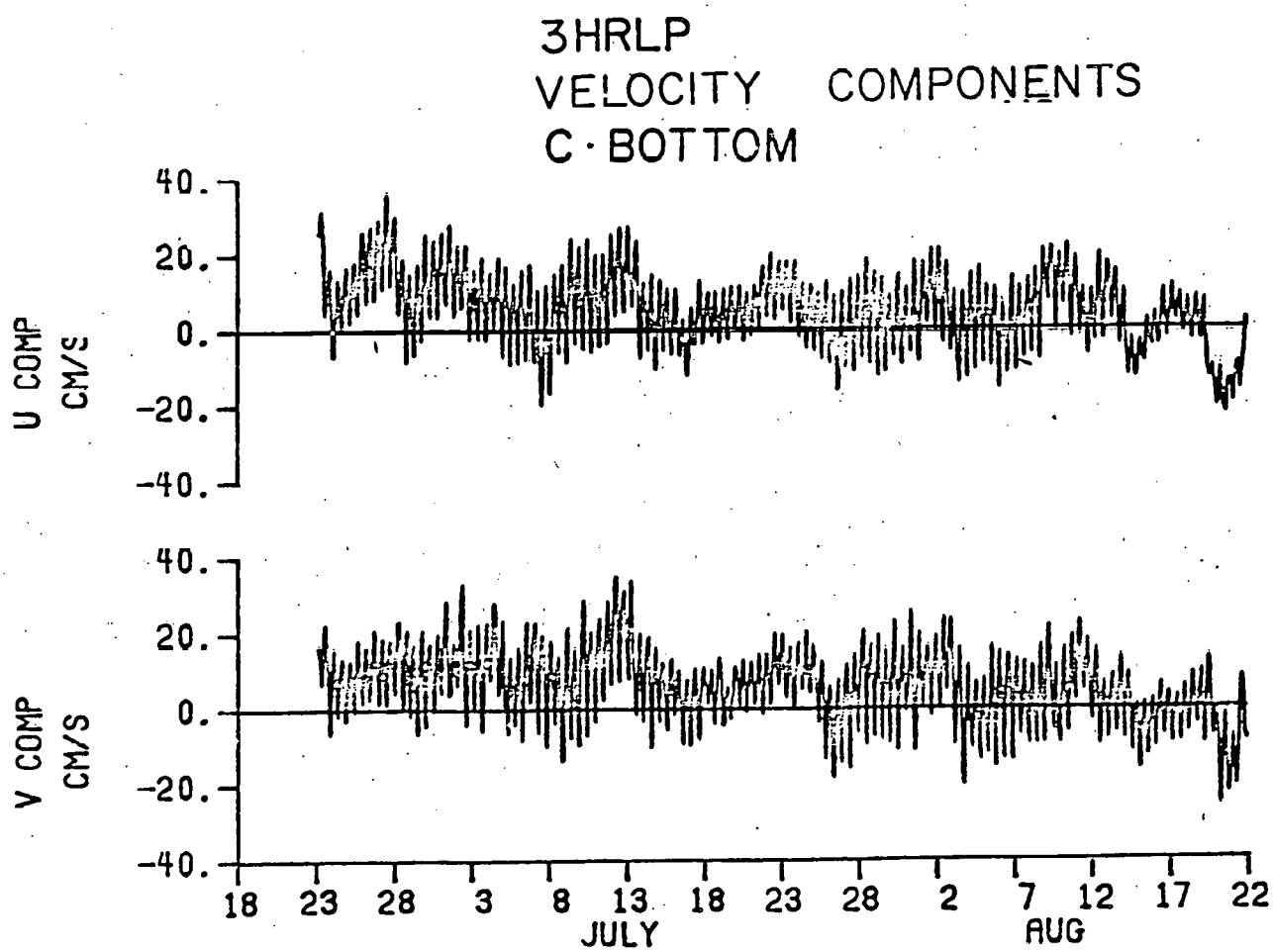

Figure 106. 3HRLP velocity components for C_{bot}

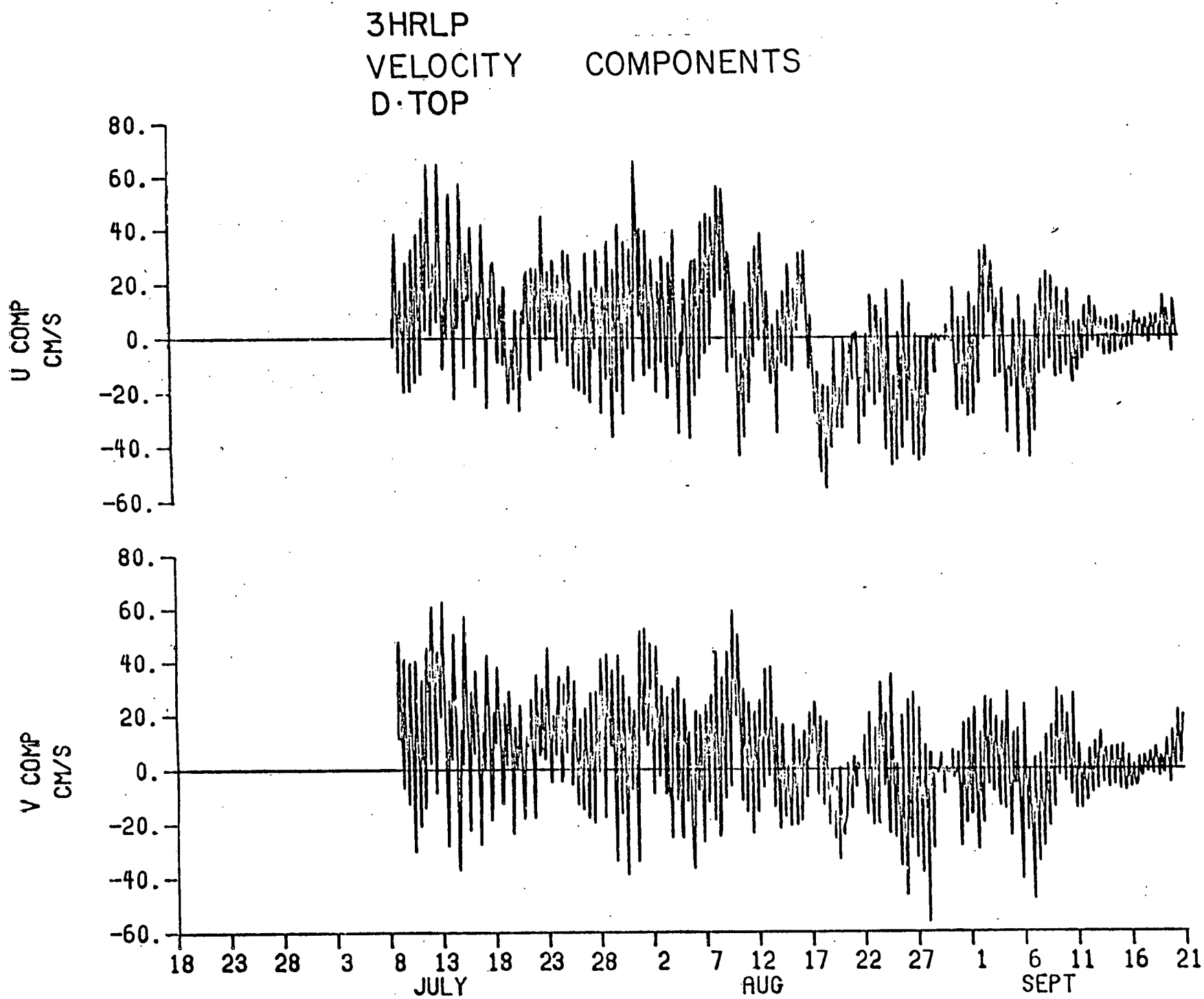

Figure 107. 3HRLP velocity components for D_{top}

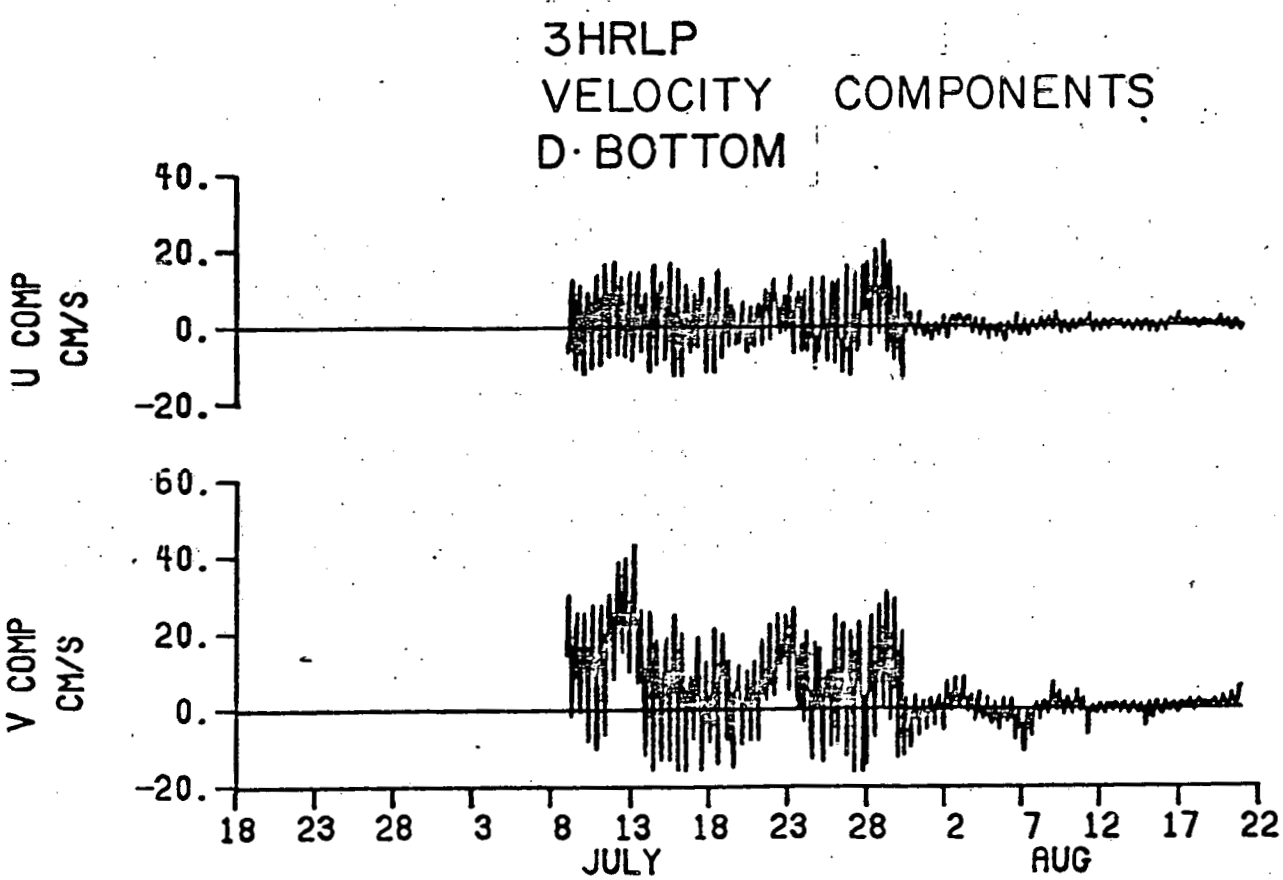

Figure 108. 3HRLP velocity components for D_{bot}

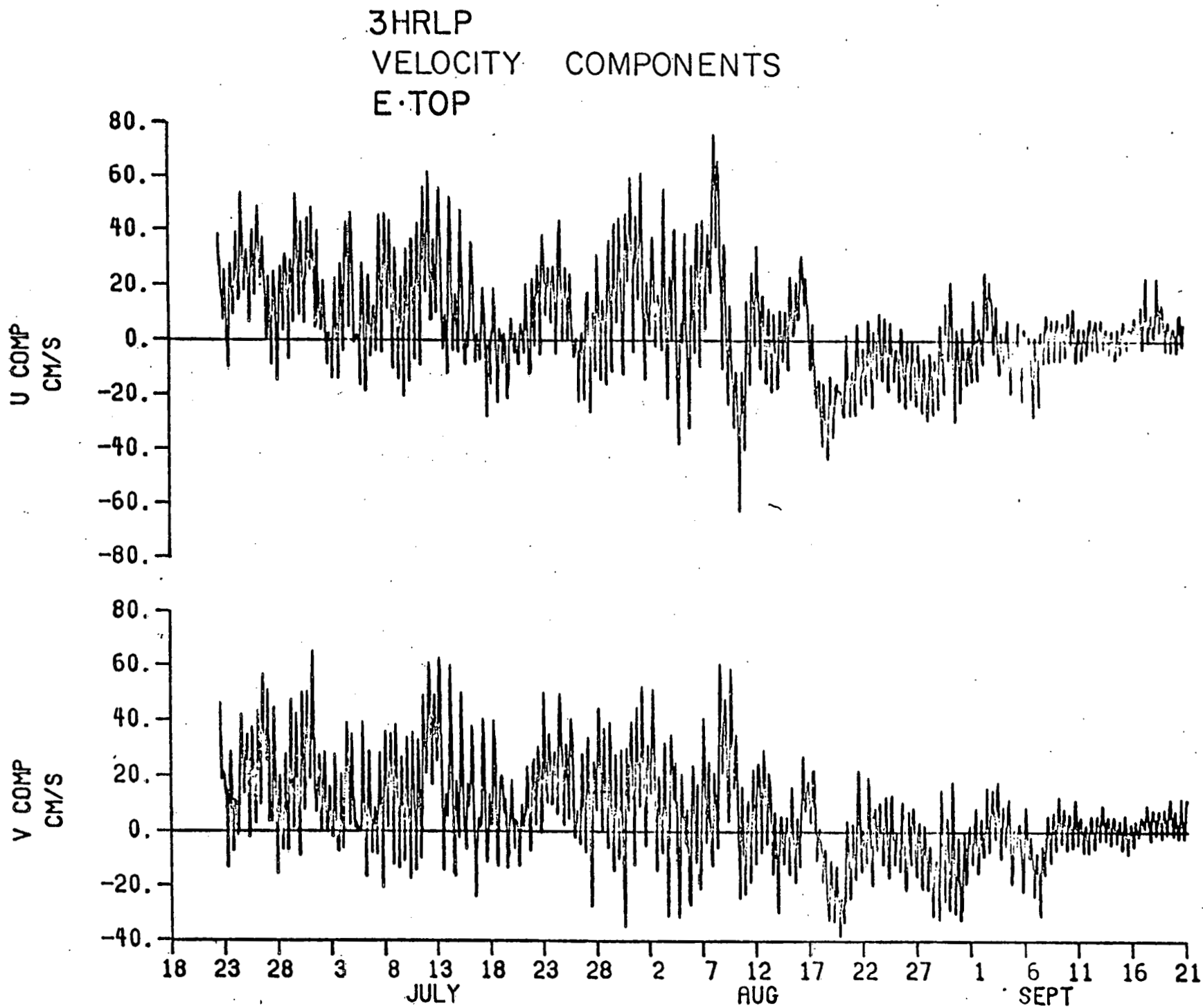

Figure 109. 3HRLP velocity components for E_{top}

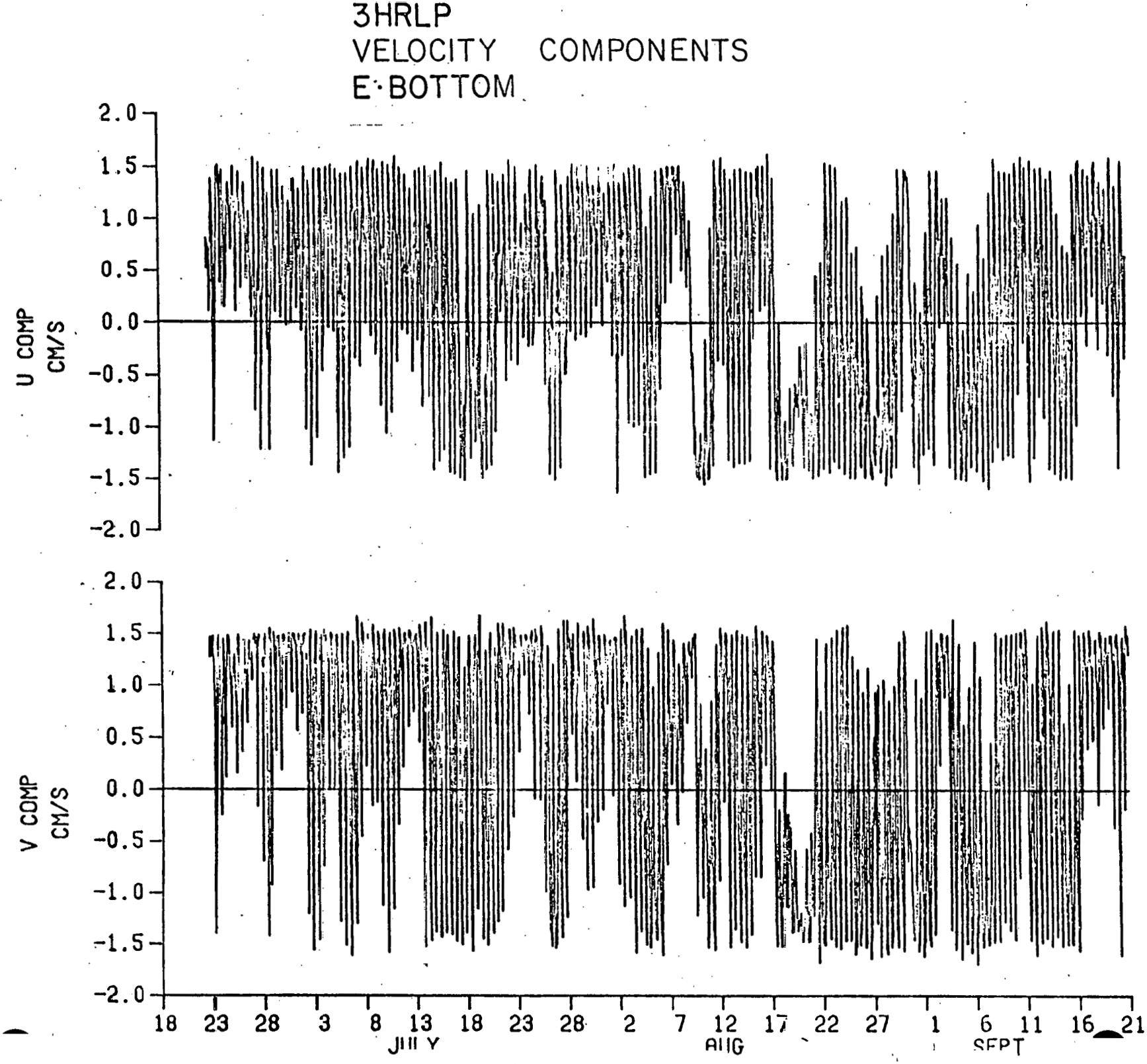
3HRLP
VELOCITY COMPONENTS
E·BOTTOM
U COMP
CM/S
V COMP
CM/S
2.0
1.5
1.0
0.5
0.0
-0.5
-1.0
-1.5
-2.0
18
23
28
3
8
13
18
23
28
2
7
12
17
22
27
1
6
11
16
21
JULY
AUG
SEPT

Figure 110.

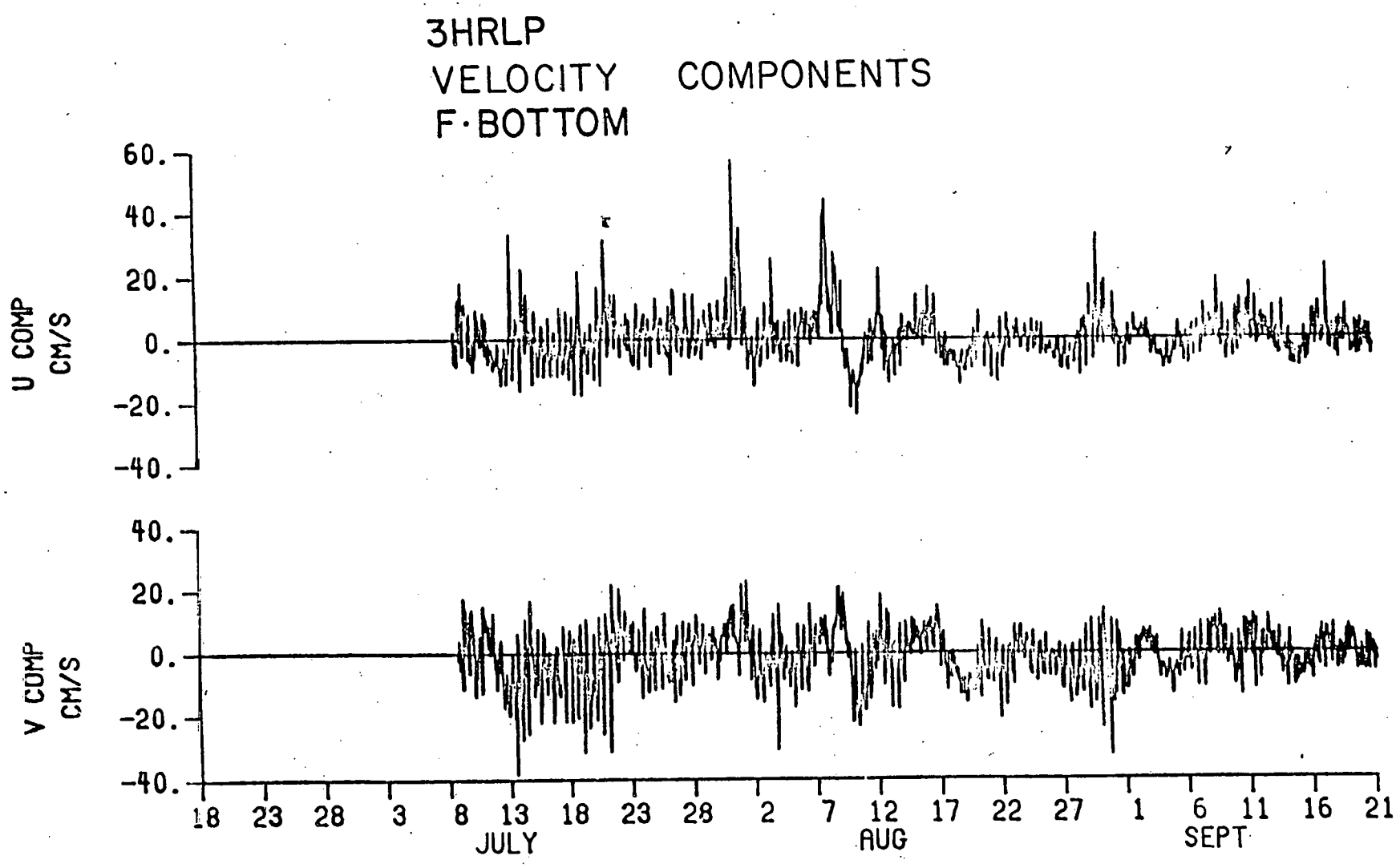

Figure 111. 3HRLP velocity components for F_{bot}

recordings (moorings C and E) and the Endeco recordings (mooring A and B) are the decrease in speed with time on the Aanderaa's due to fouling by barnacles. This affect will be discussed in a following section. Simultaneous recordings are also available at both the top and bottom locations of mooring C. These are shown in Figures 105 and 106 and records from moorings E (top) and F (bottom) are shown in Figures 109 and 110.

Mean velocity vectors are shown in Figures 112 and 113. Figure contains vectors at moorings C, E and F computed over the total available record length. Location C and E suggest an alongshore mean to the northeast compatible with the predominant wind direction during the summer. The slight offshore component in the upper level on mooring C and the corresponding onshore component at the lower level would seem capatible with the thermohaline convection brought about by river runoff. The situation is much more confusing however. Figure 113 shows upper level mean vectors computed over the common sampling duration of 7/23 - 8/22. Both B and E point toward the southeast, A points offshore, and C now has a slight onshore component. Clearly the record lengths are too short to compute statistically reliable mean values in the presence of energetic low frequency events. These results must be kept in mind when trying to interpret the progressive vector diagrams shown in (egs.) Figs. 114-119.

From velocity components (Figs. 120-121) typical speeds were observed to be around 10 cm/s at mooring C. Peak speeds of 58 cm/s and 35 cm/s occurred at the upper and lower levels respectively. An example of a polar histogram of current direction for mooring C top is given in Fig. 122

114 Progressive vector diagrams are used in some studies to estimate water particle trajectories (Lagrangian measurements) from Eulerian data. An example of the PVD's is mooring C in Fig. 116. PVD's may be of

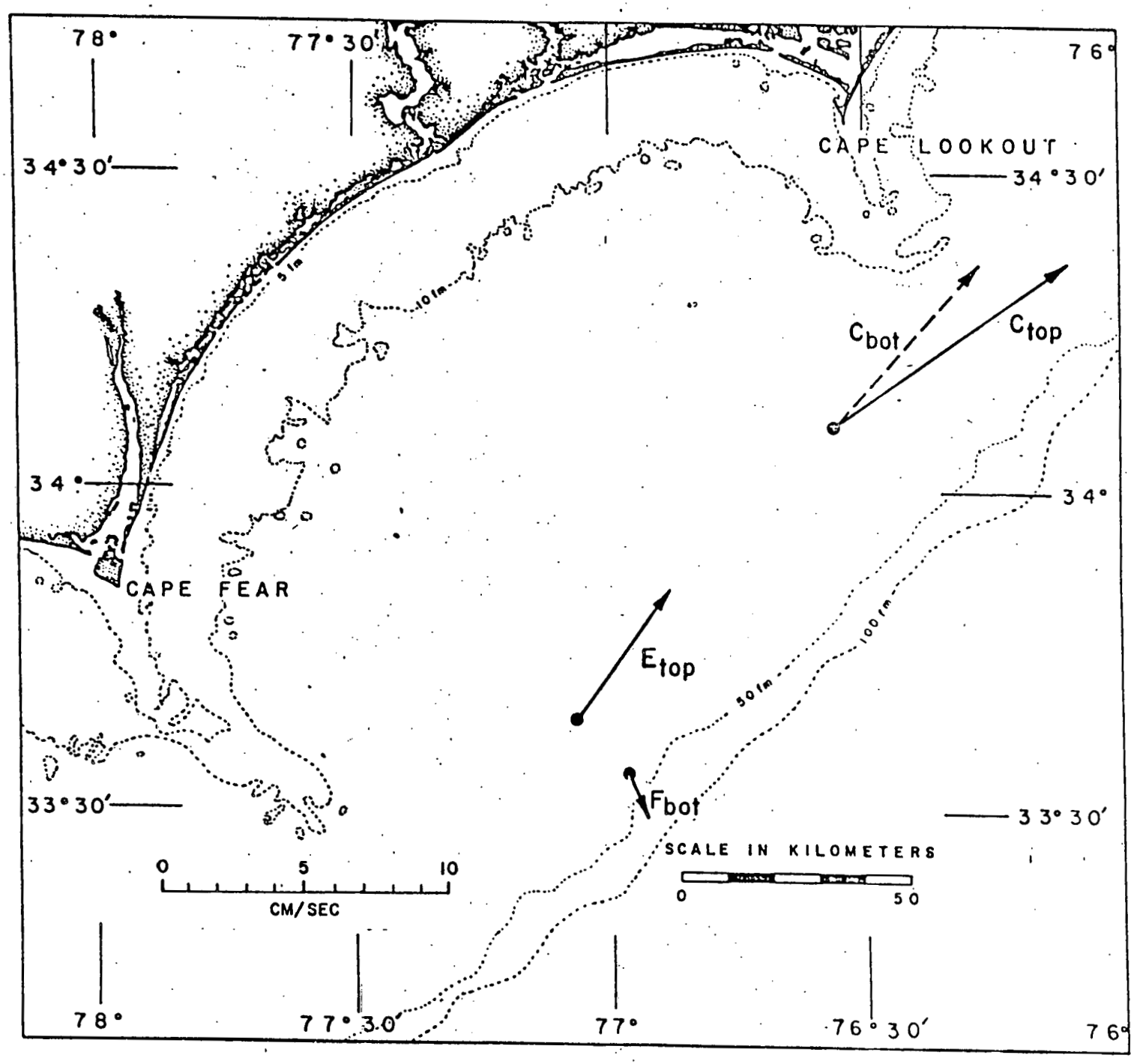

Figure 112. Mean velocity for Summer 1976

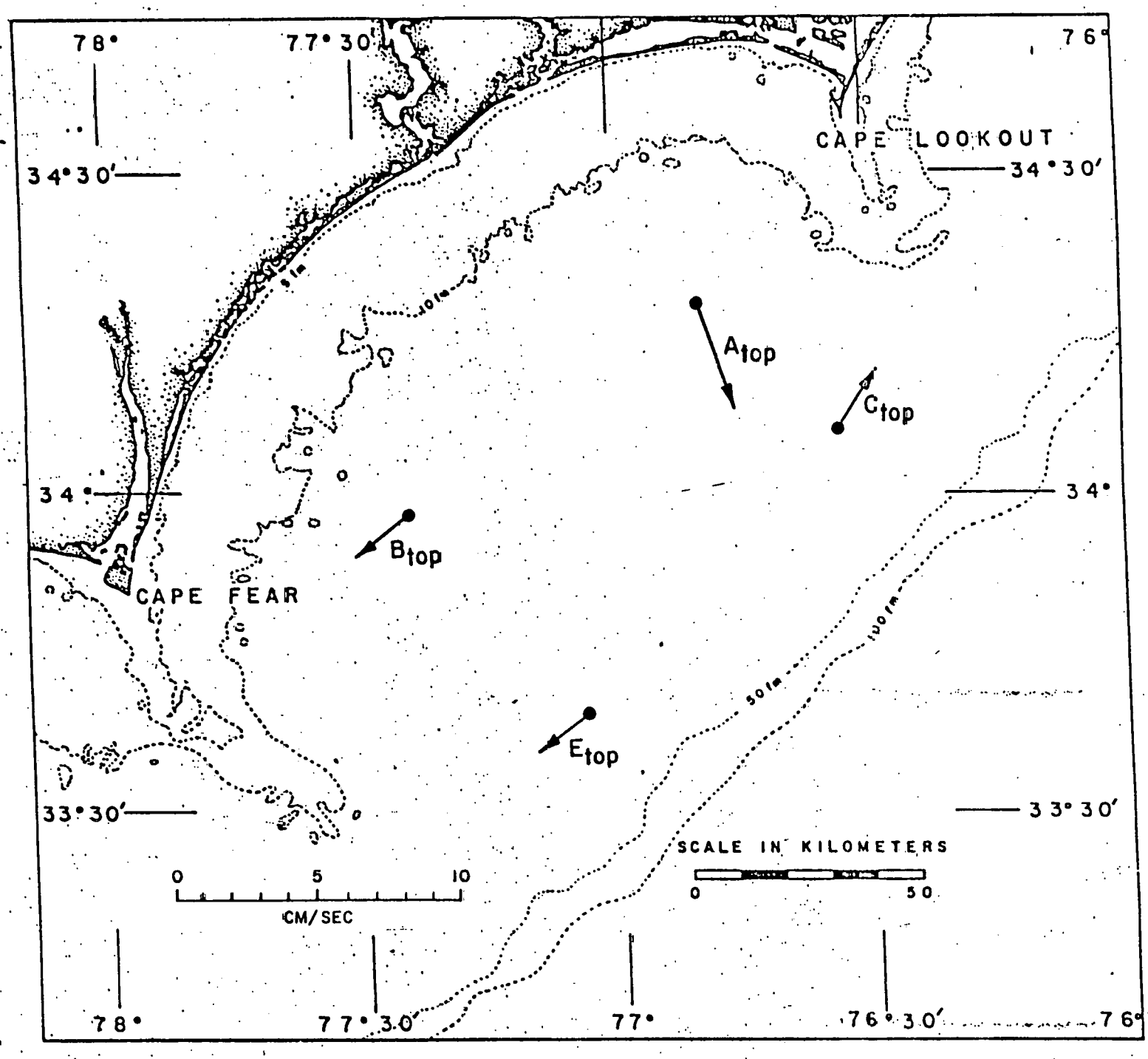

Figure 113. Mean velocity for July 23–Aug 22, 1976 (top meters)

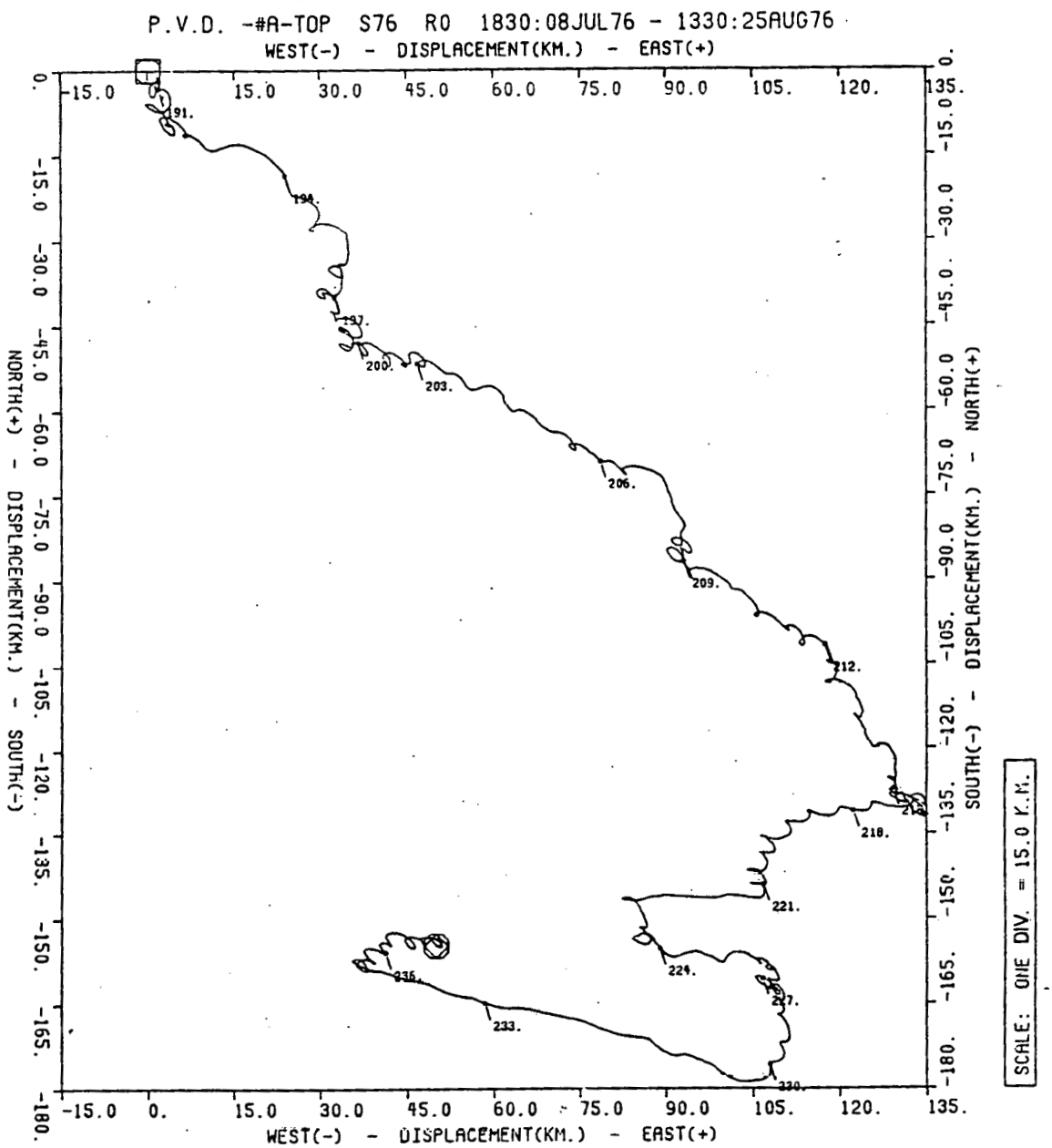

Figure 114. Progressive vector diagrams of unfiltered current velocity from meter A(Albatross)$_{top}$

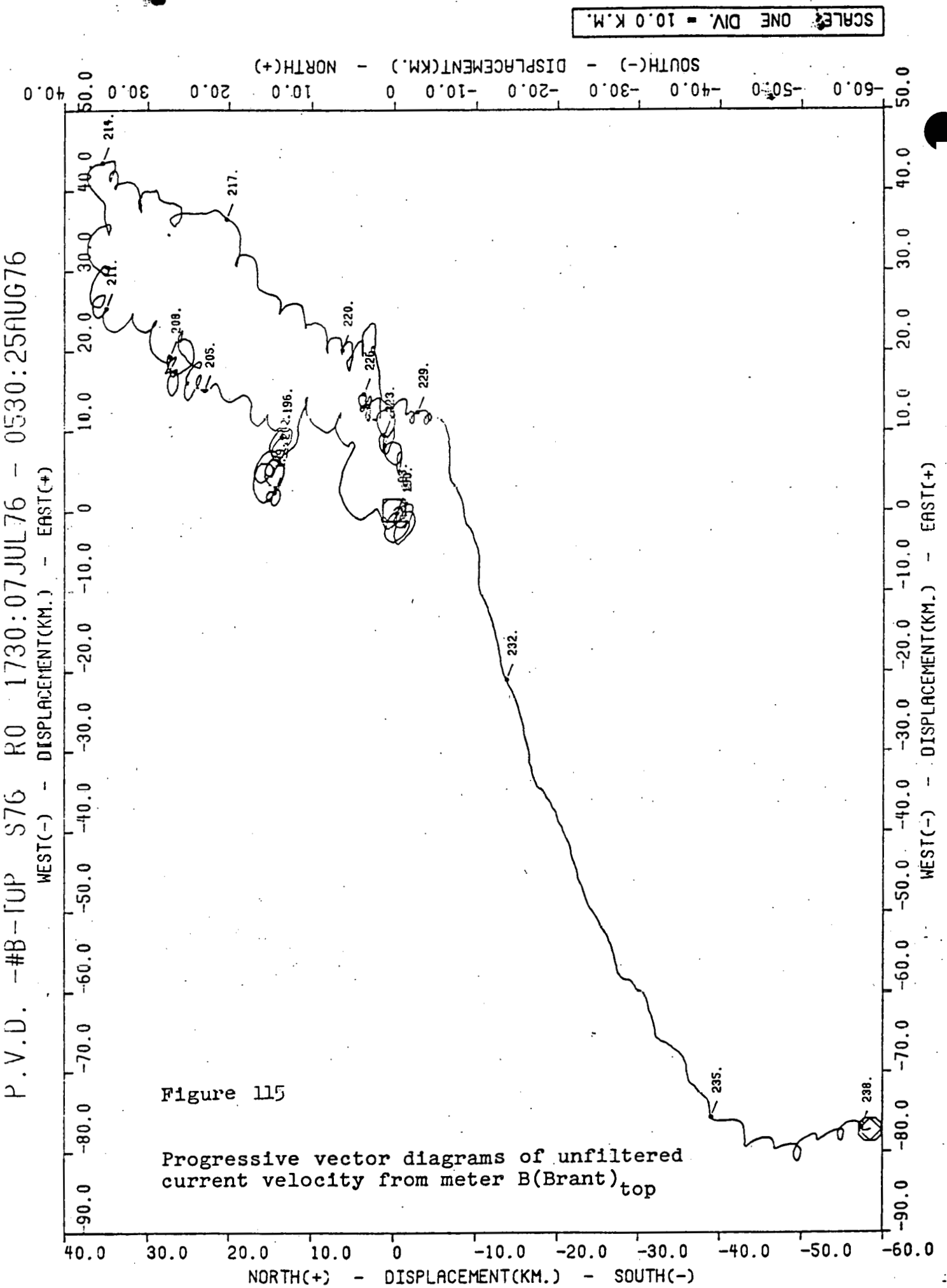

Figure 115

Progressive vector diagrams of unfiltered current velocity from meter B(Brant)$_{top}$

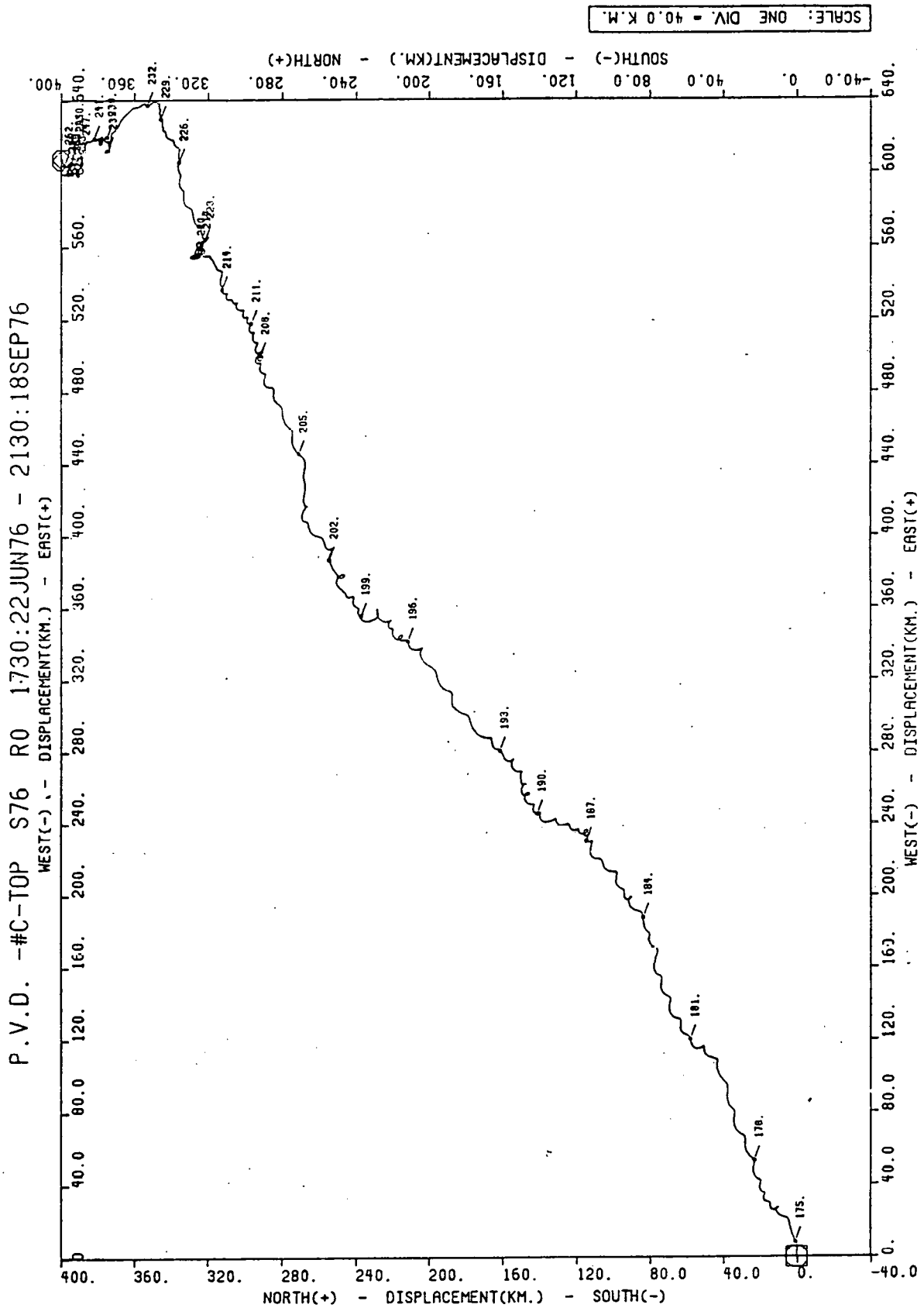

Figure 116. Progressive vector diagrams of unfiltered current velocity from meter C(Cormorant) top

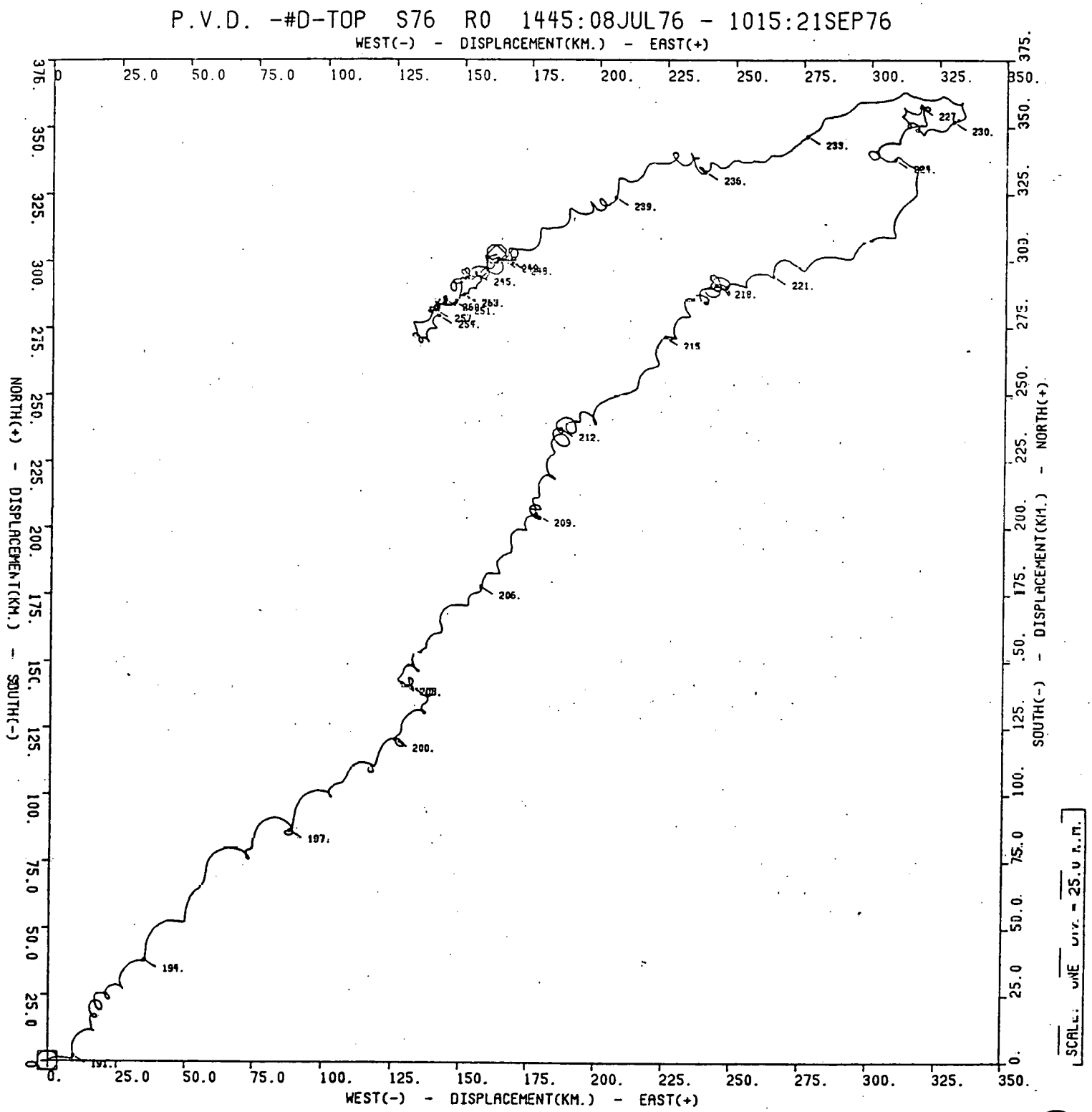

Figure 117. Progressive vector diagrams of unfiltered current velocity from meter D(Dunlin)$_{top}$

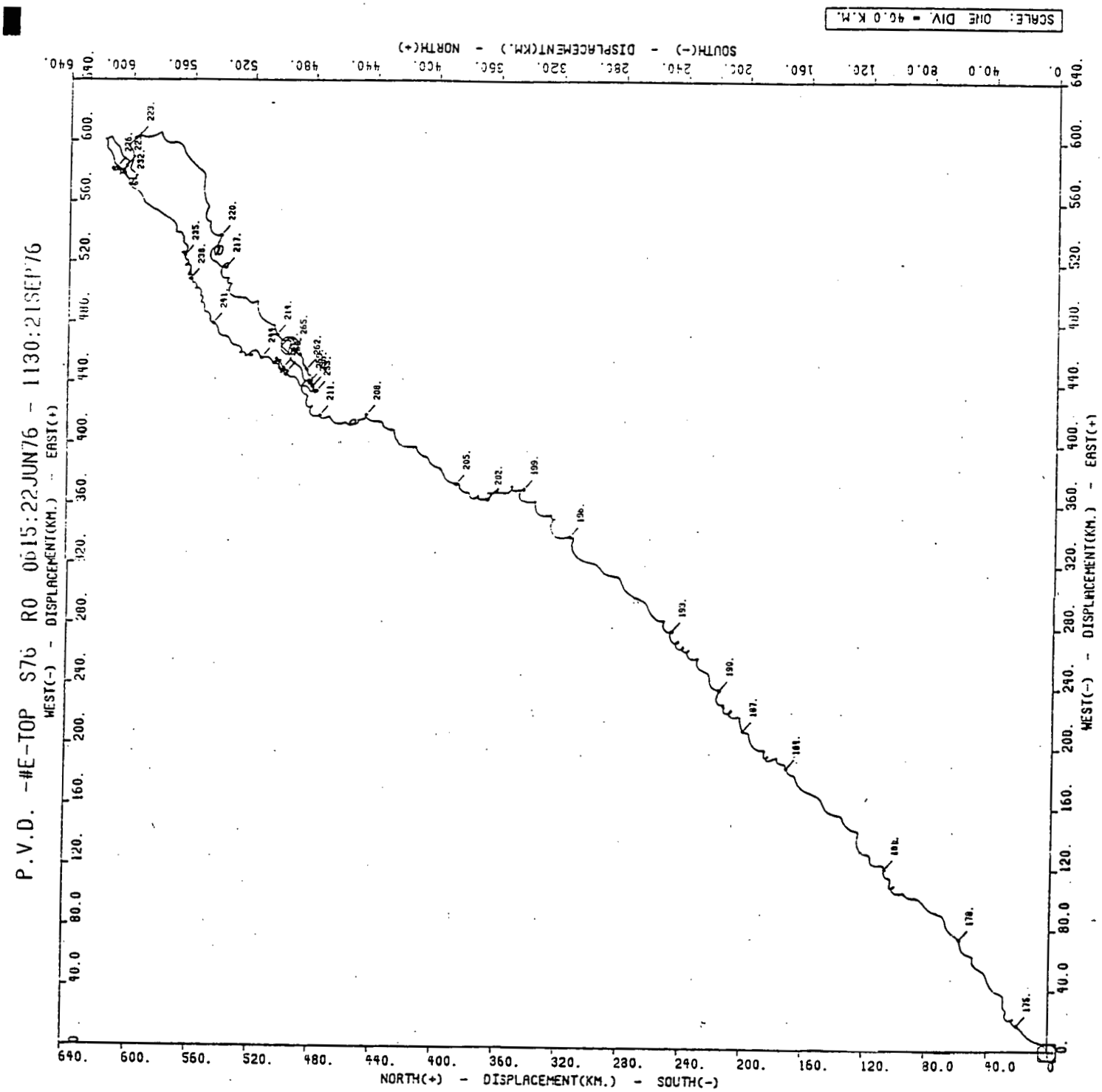

Figure 118 Progressive vector diagrams of unfiltered current velocity from meter E(Eider)$_{top}$

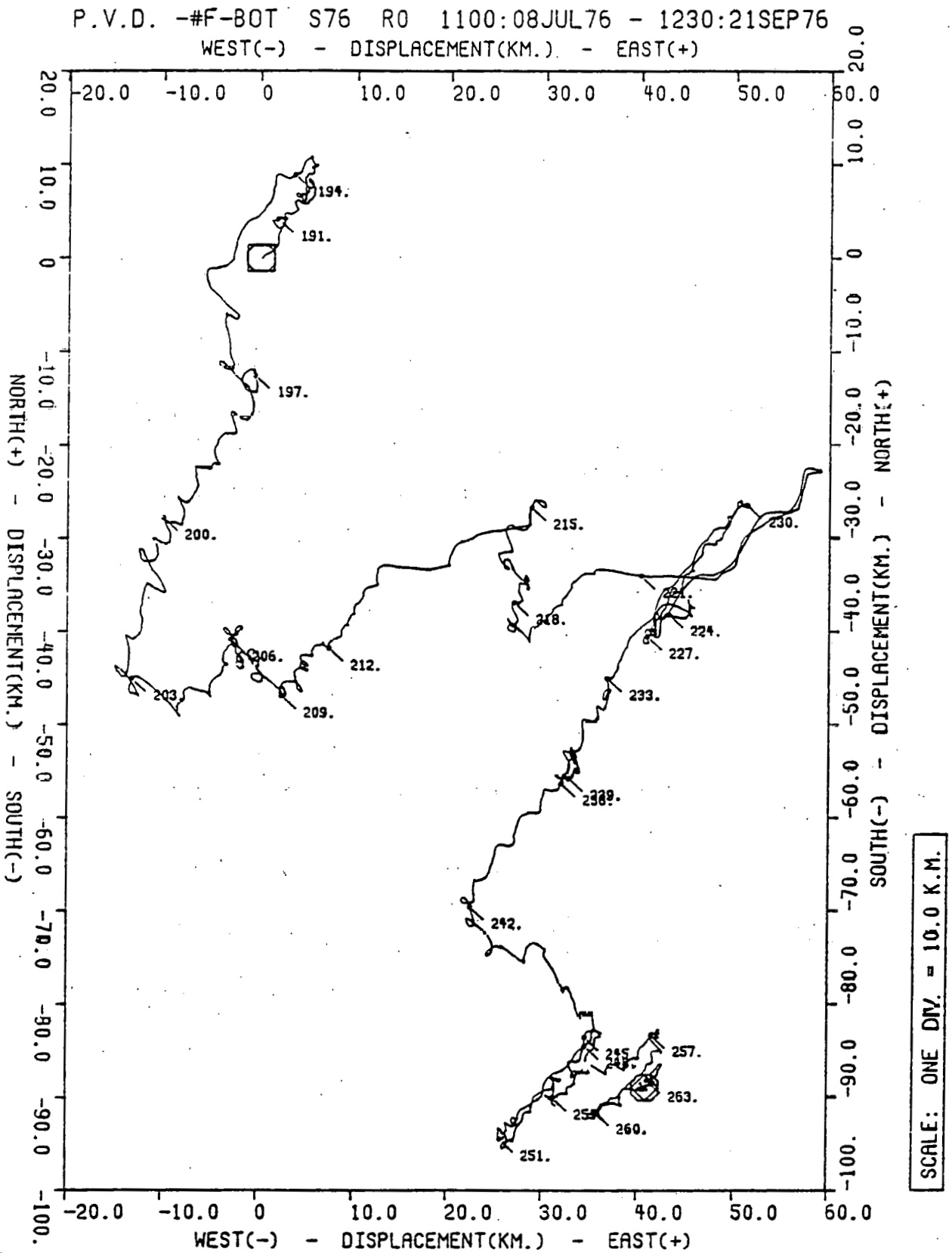

Figure 119 Progressive vector diagrams of unfiltered current velocity from meter F(Foster's Tern)$_{bot}$

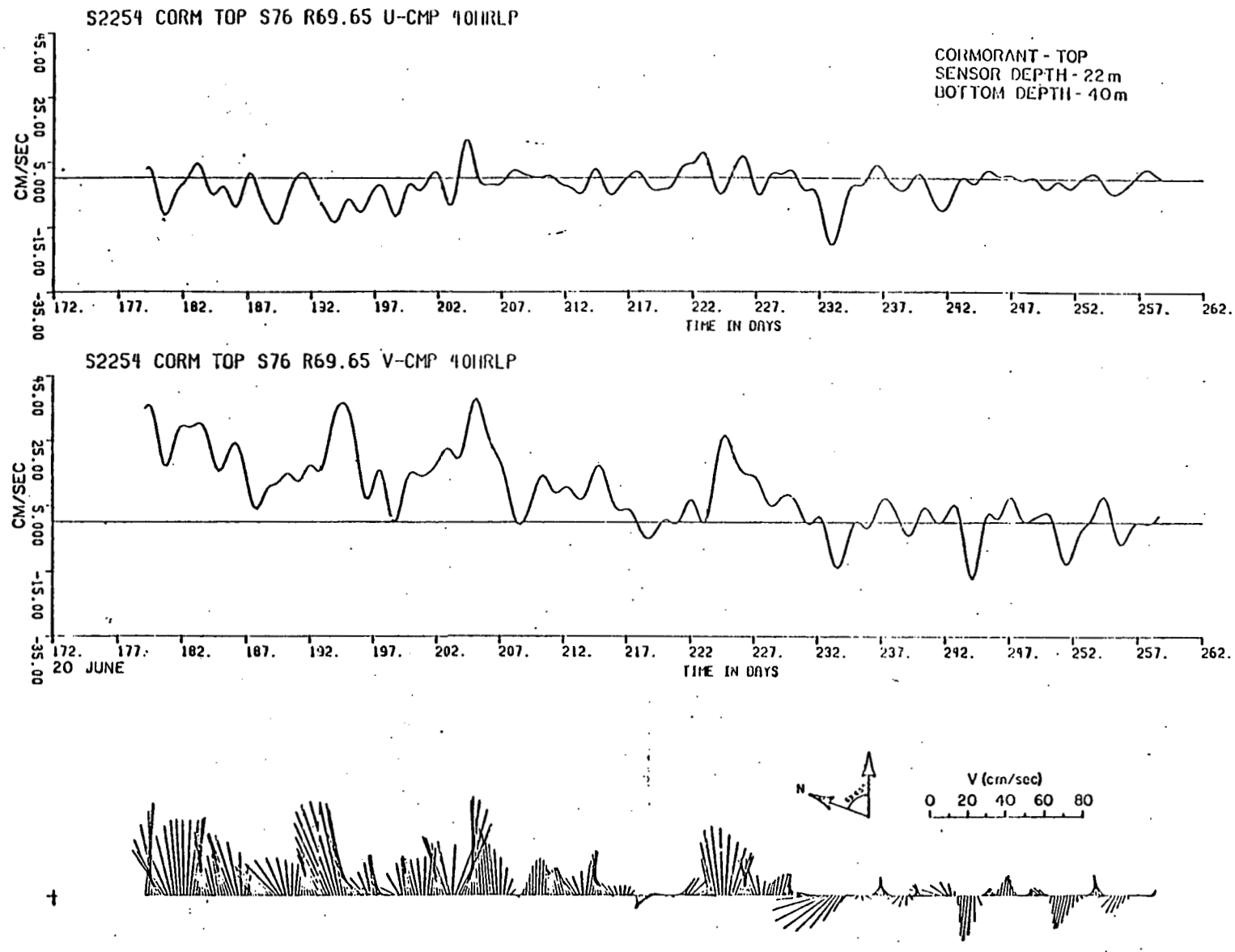

Figure 120 Low pass current velocity components and vectors from meter C(Cormorant)top

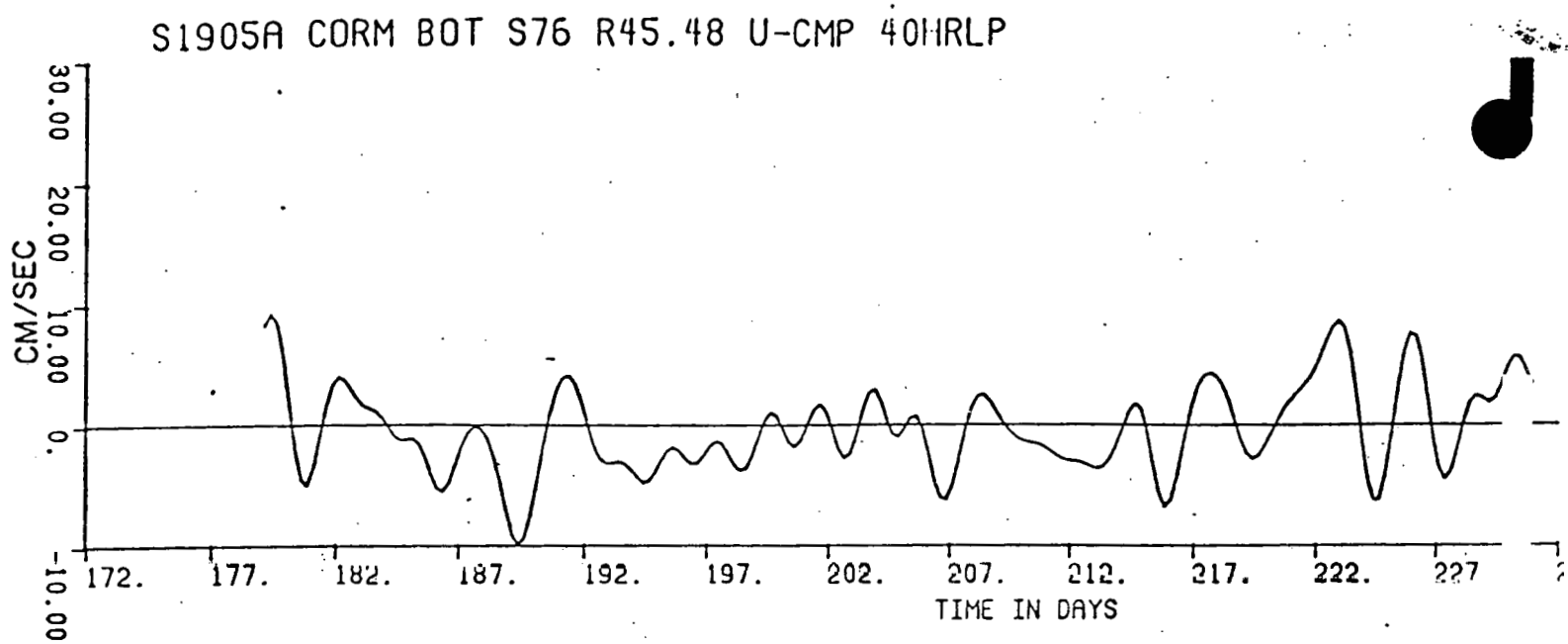

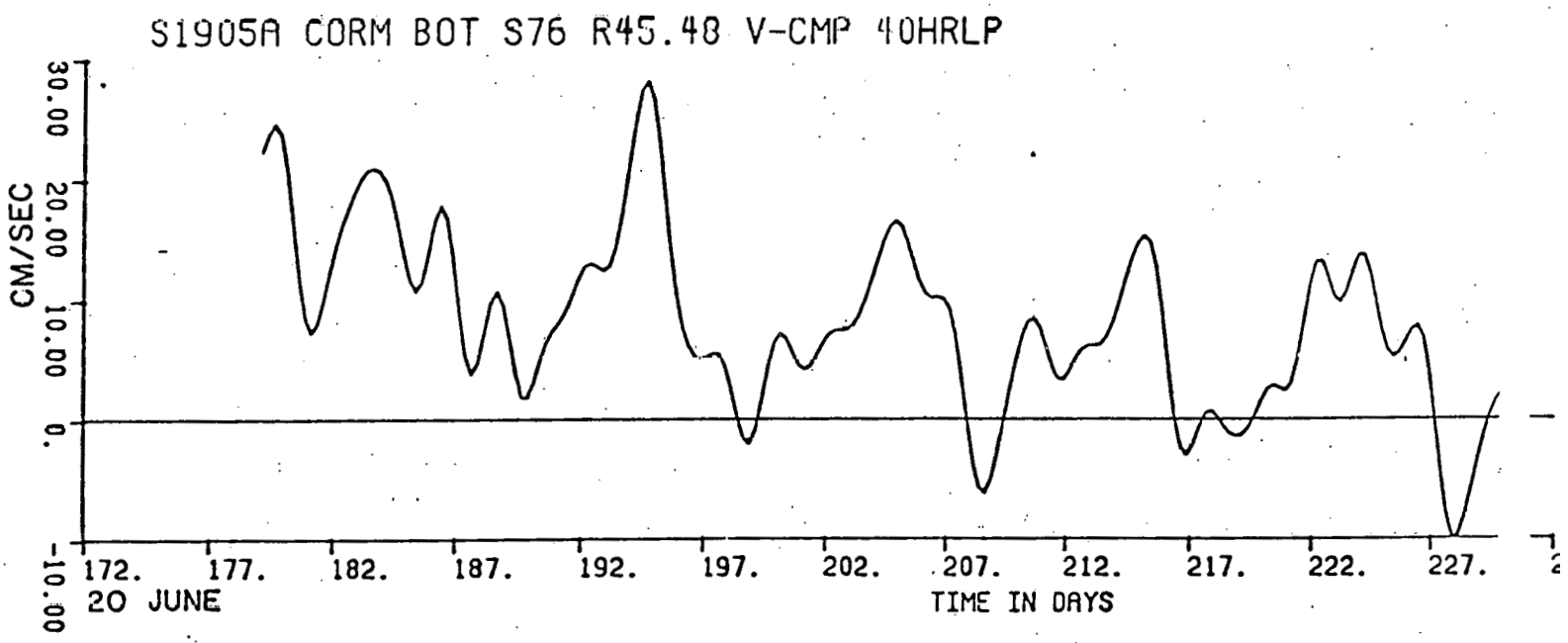

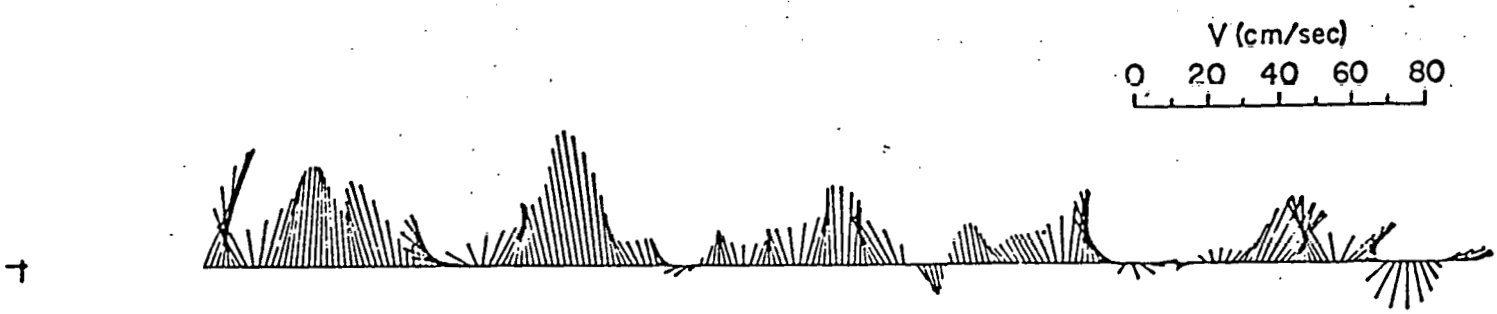

Figure 121 Low pass current velocity components and vectors from meter C(Cormorant)$_{bot}$

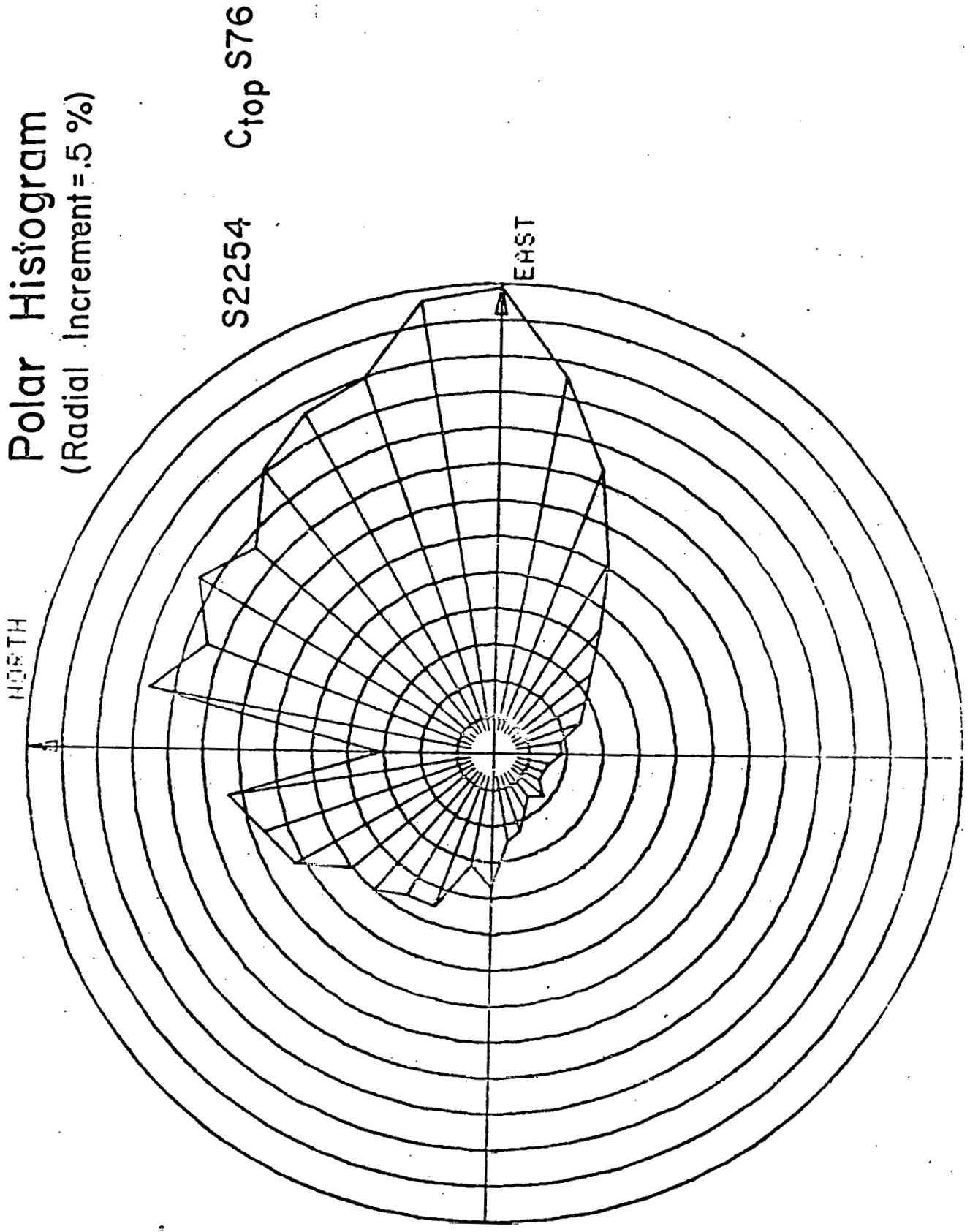

Figure 122 Histogram from meter C(Cormorant)$_{top}$

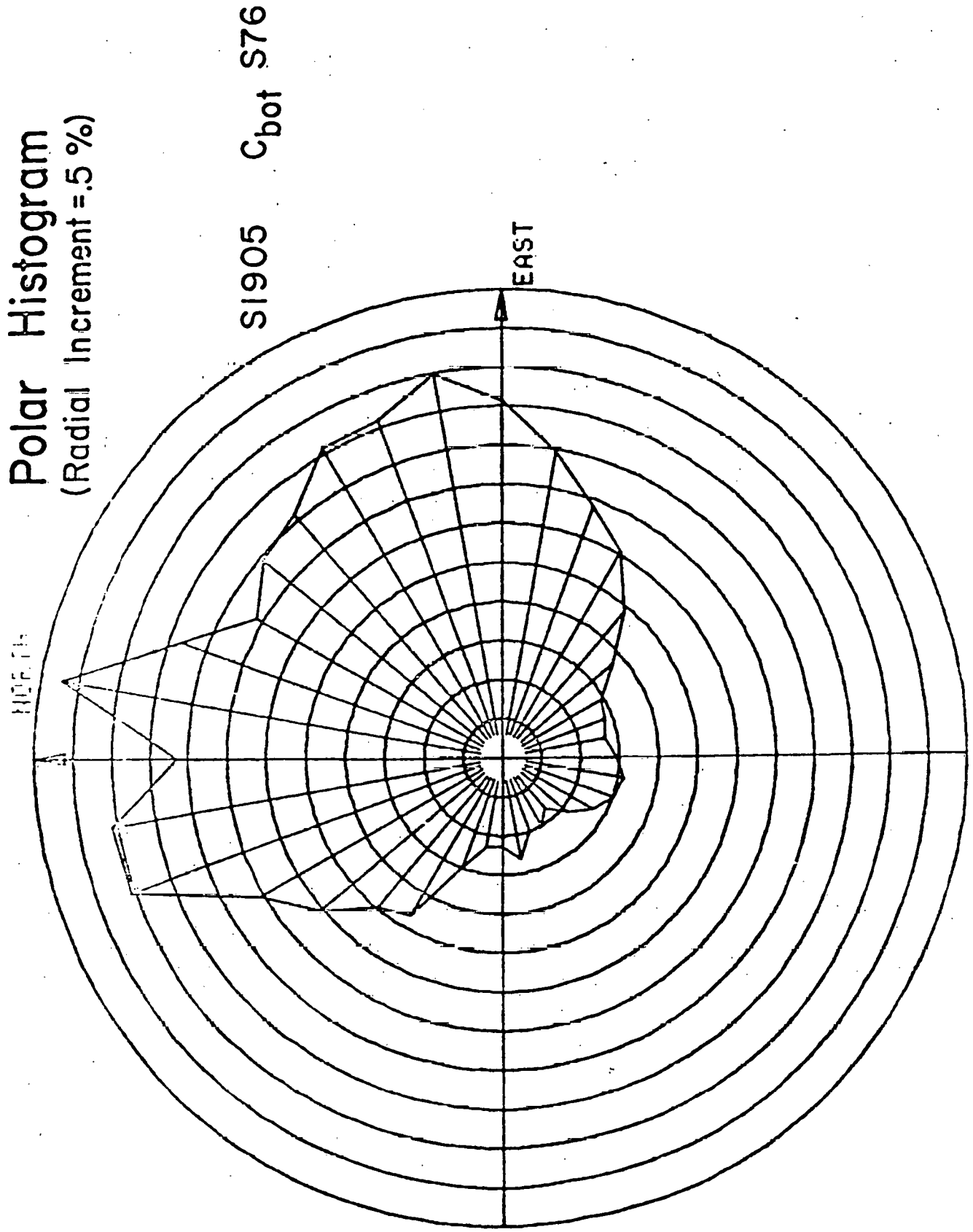

Figure 123 Histogram from meter C(Cormorant)$_{bot}$

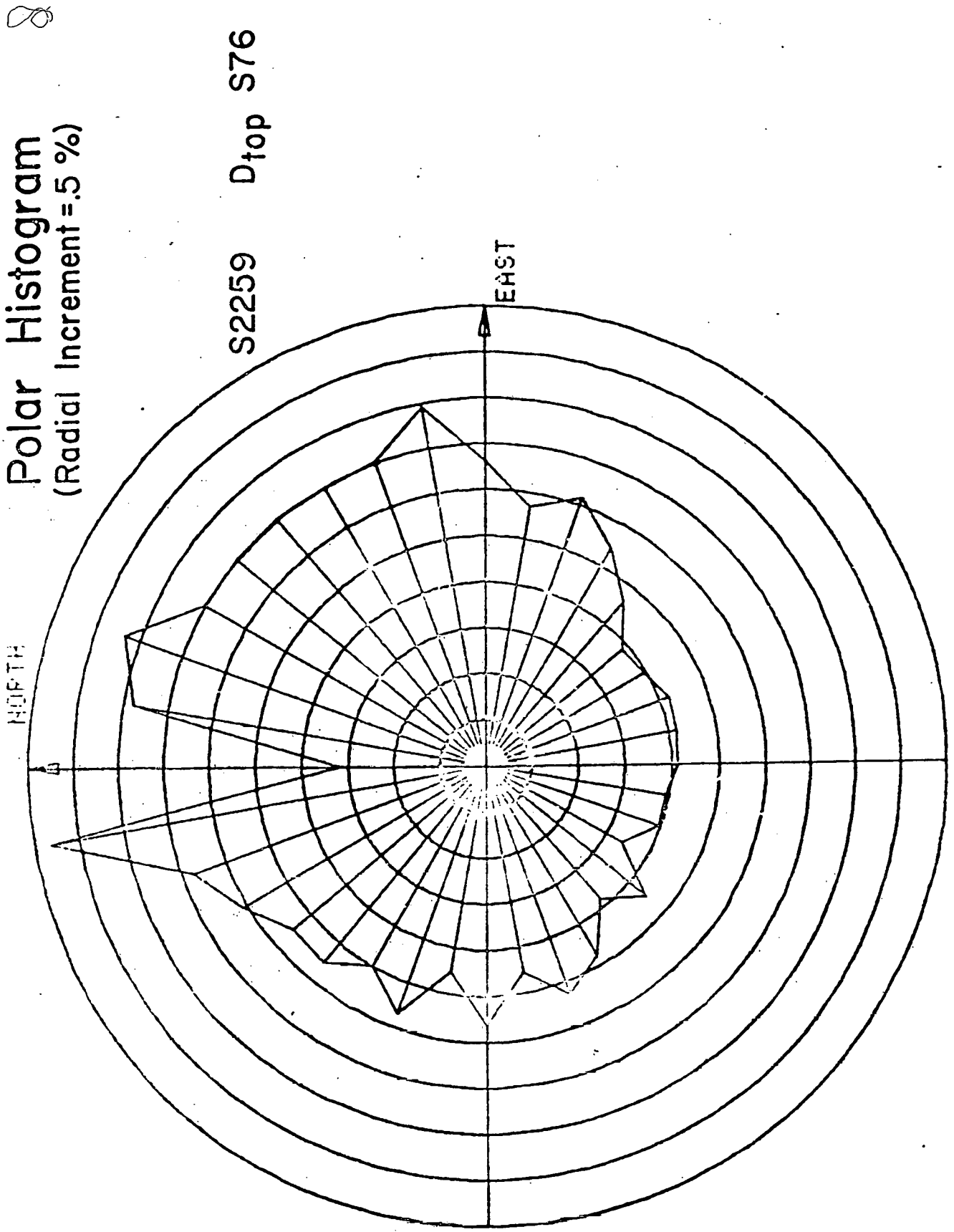

Figure 124 Histogram from meter $D(Dunlin)_{top}$

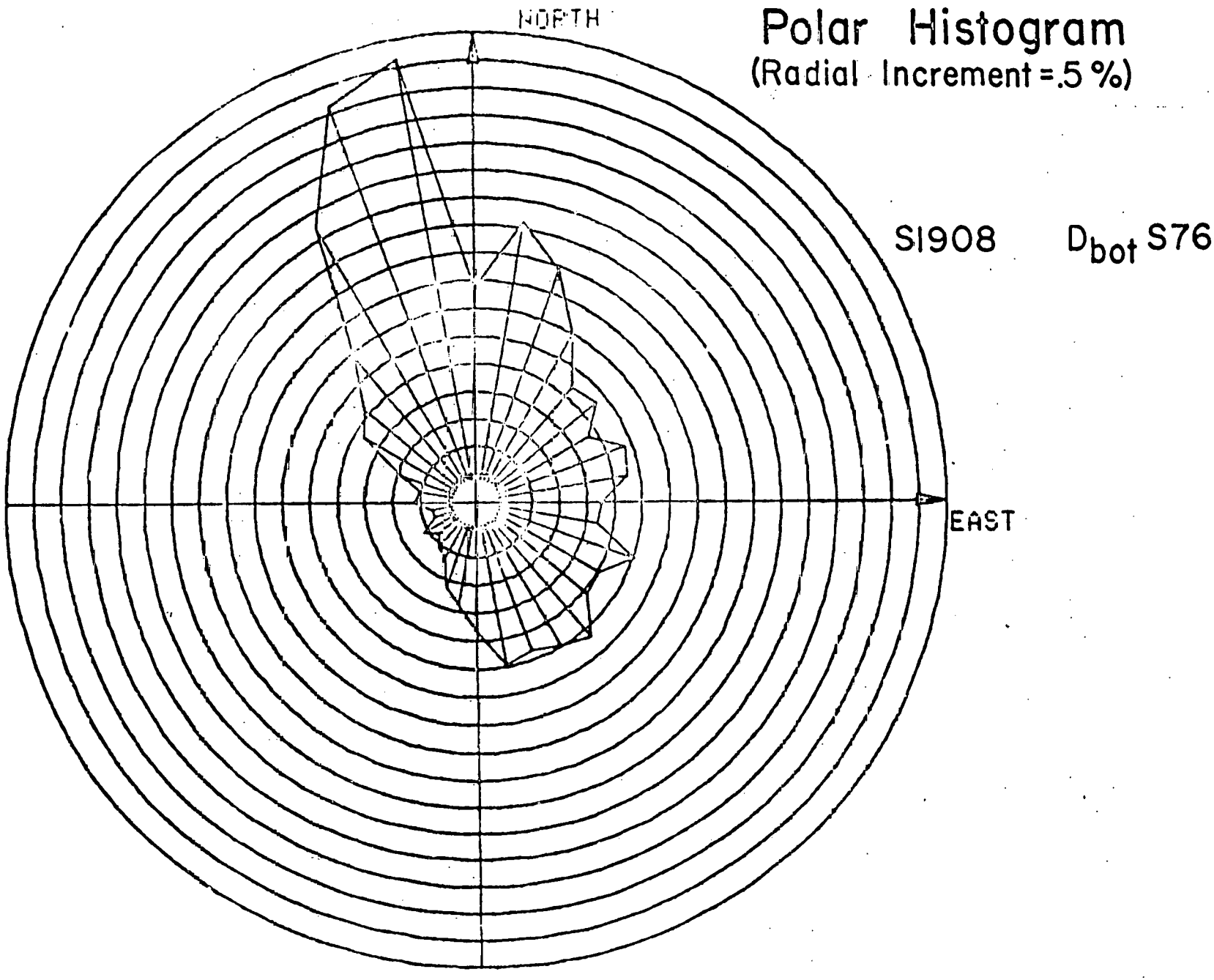

Figure 125. Histogram from meter $D(Dunlin)_{bot}$

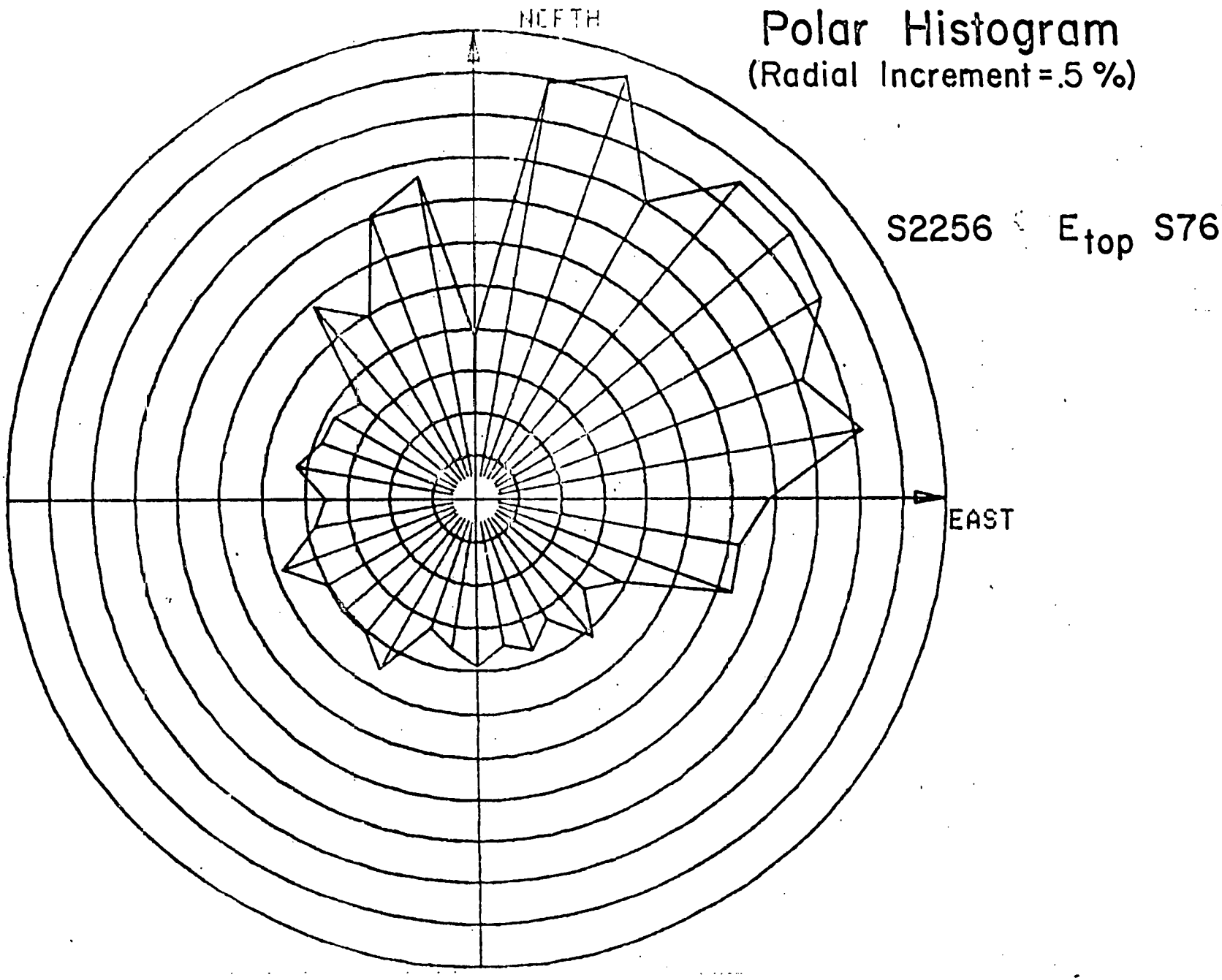

Figure 126 Histogram from meter $E(Eider)_{top}$

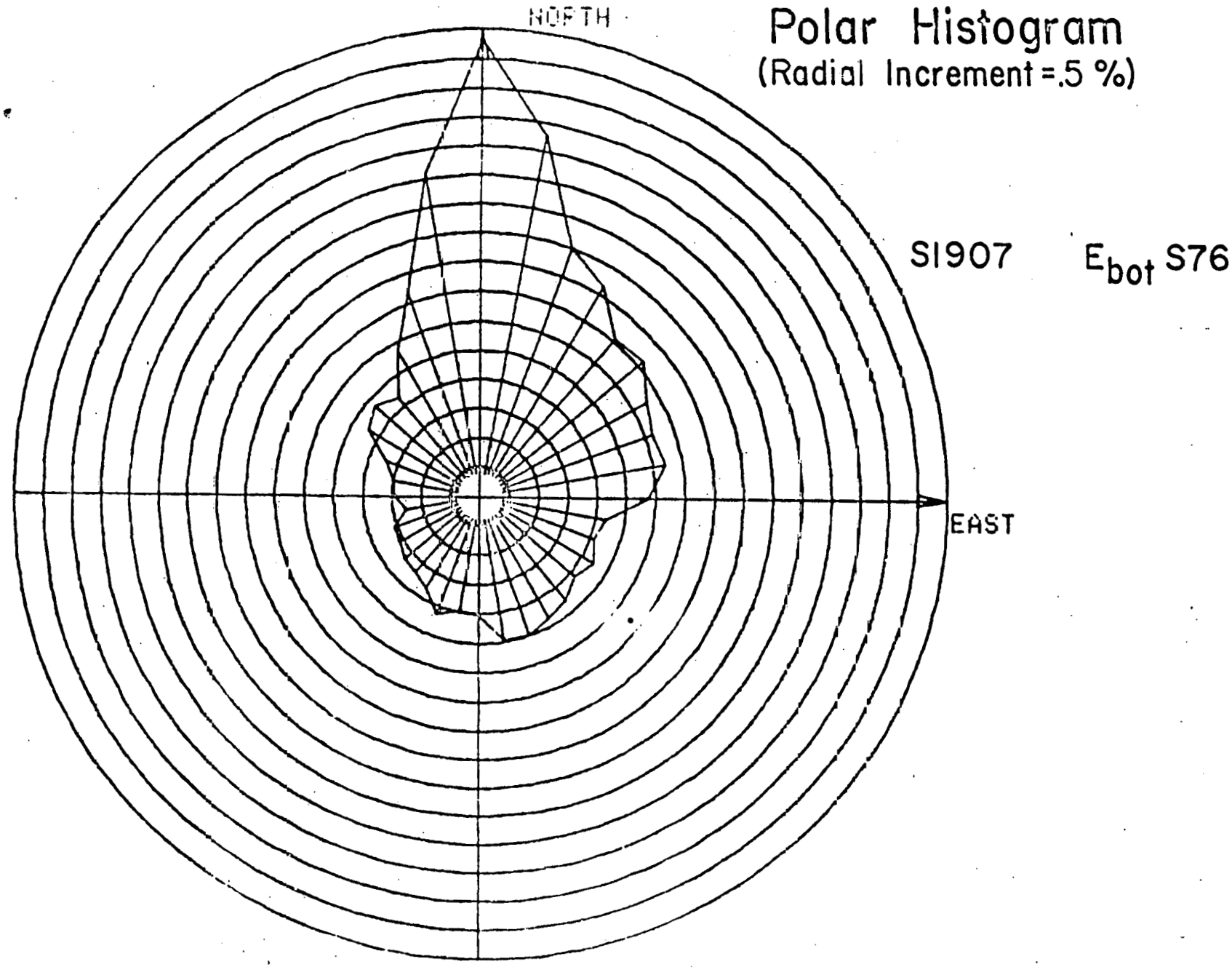

Figure 127 Histogram from meter $E(Eider)_{bot}$

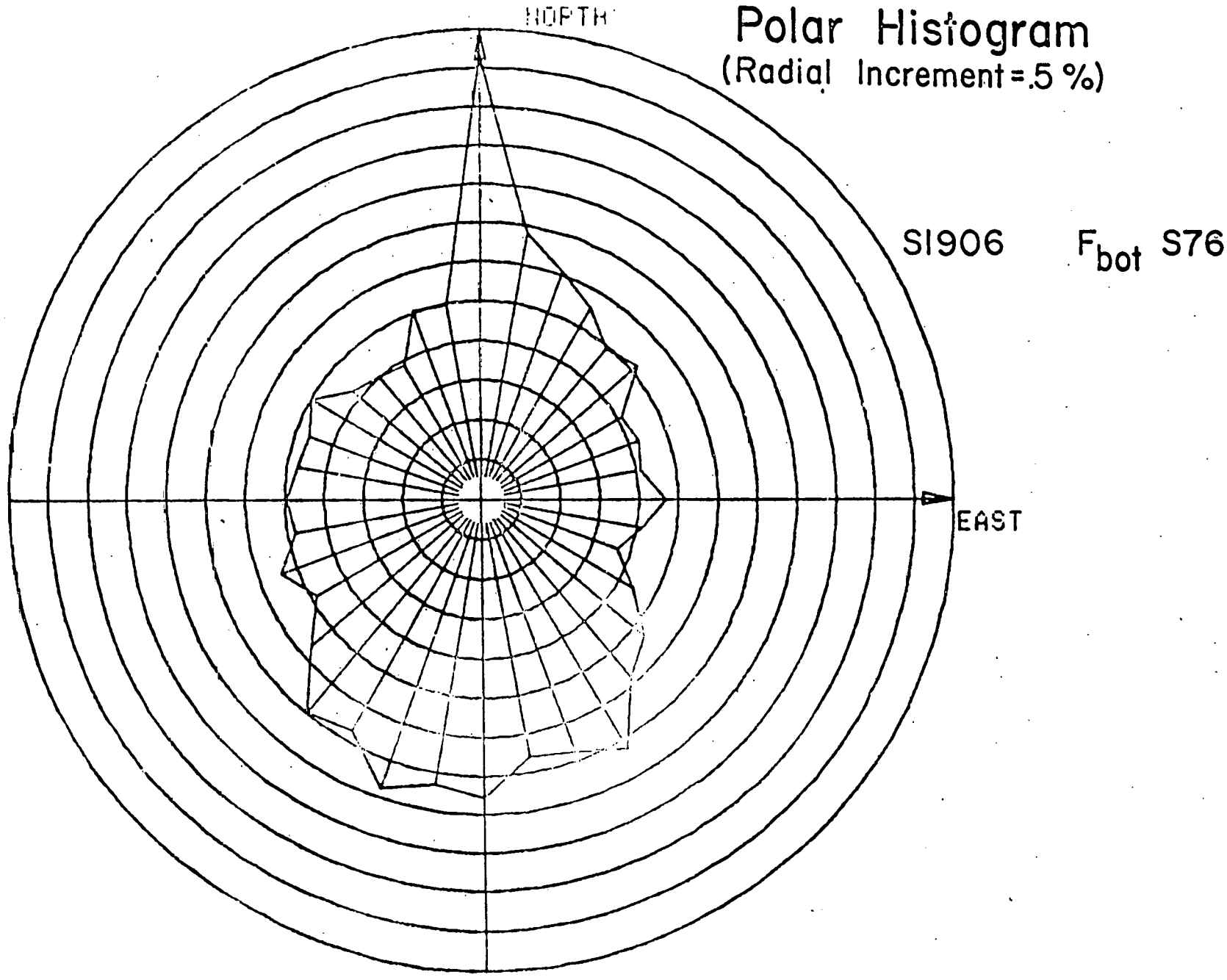

Figure 128. Histogram from meter F(Foster's Tern)$_{bot}$

use for estimating such quantities as tidal excursions which in this location are of a few kilometers in length.

Representative alongshore (aligned with the mean coastline at 55.6° true) and offshore kinetic energy density spectra from mooring C (top and bottom) are shown in Figures 129-132. Except for higher energy at the upper level both the upper and lower level spectra show similar features. Energy density decreases with increasing frequency to a combined diurnal tide and local inertial peak (local inertial period, 12 hr/sin 34° = 21.5 hrs.) followed by a pronounced semi-diurnal tidal peak and then a continuing decrease through the internal gravity wave range. Comparing alongshore with offshore energy levels we see a distinct, difference between the low frequency, presumably meteorologically driven, background and the tidal peak. The wind driven background has higher energy in the alongshore direction while the tidal currents have higher energy directed offshore. No marked directional preference appears in the higher frequency internal gravity wave portion of the spectrum.

Relative to any given current meter record, or velocity vector time series, the choice of a coordinate system oriented alongshore and offshore with respect to the coastline (or major bathymetric features) is quite arbitrary. A preferred coordinate system for many descriptive applications is one which maximizes the variance. Depending upon the physical processes causing the observed water motions, the principal axis of variance (normal coordinates) amy vary with location and frequency. The principal axis for a given vector time series may be obtained by rotating the covariance matrix until the cross-covariance between orthogonal velocity components is zero. These are shown in Figure 133 along with the

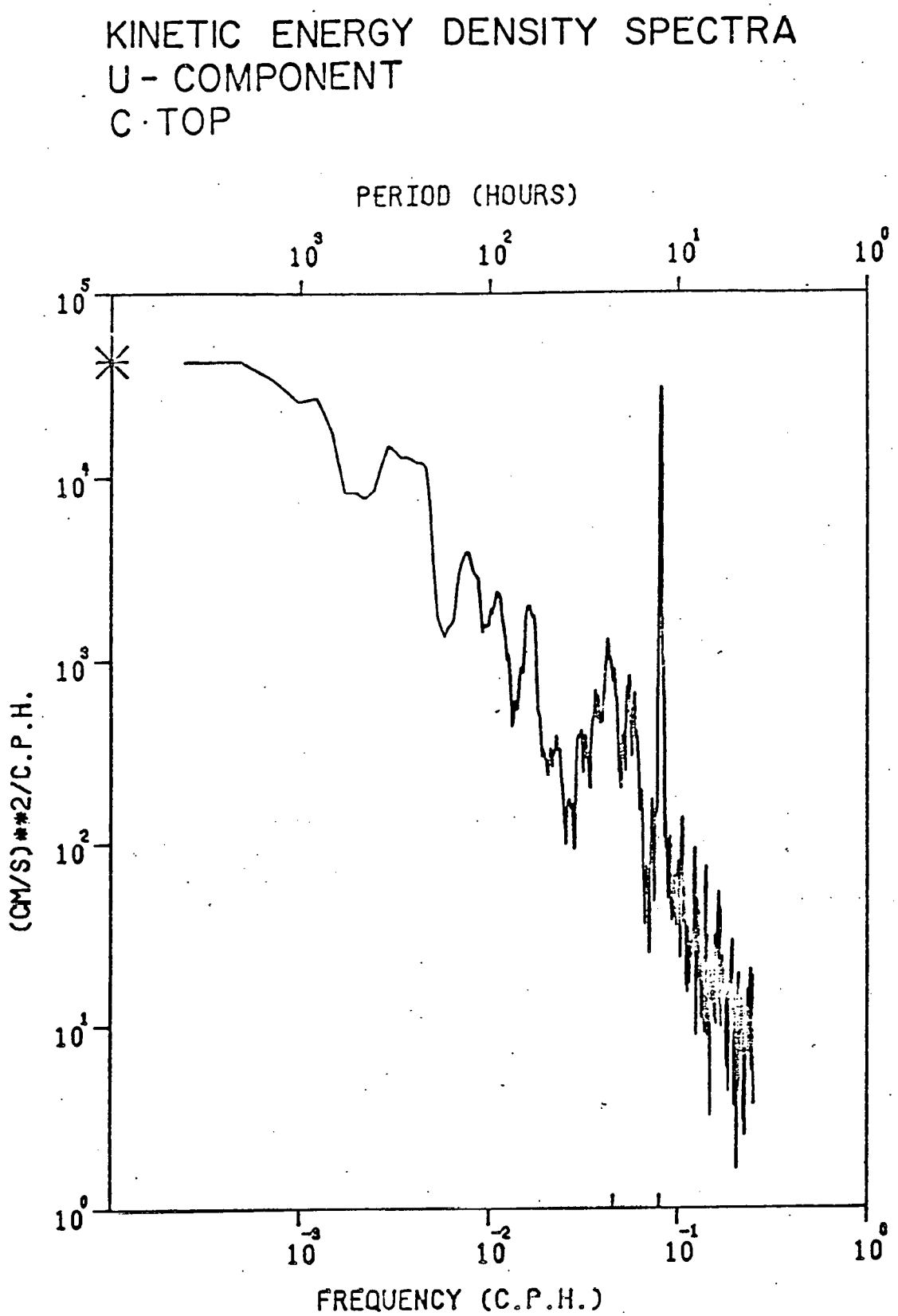

Figure 129 Kinetic energy density spectra for current velocity, ú-component, C_{top}

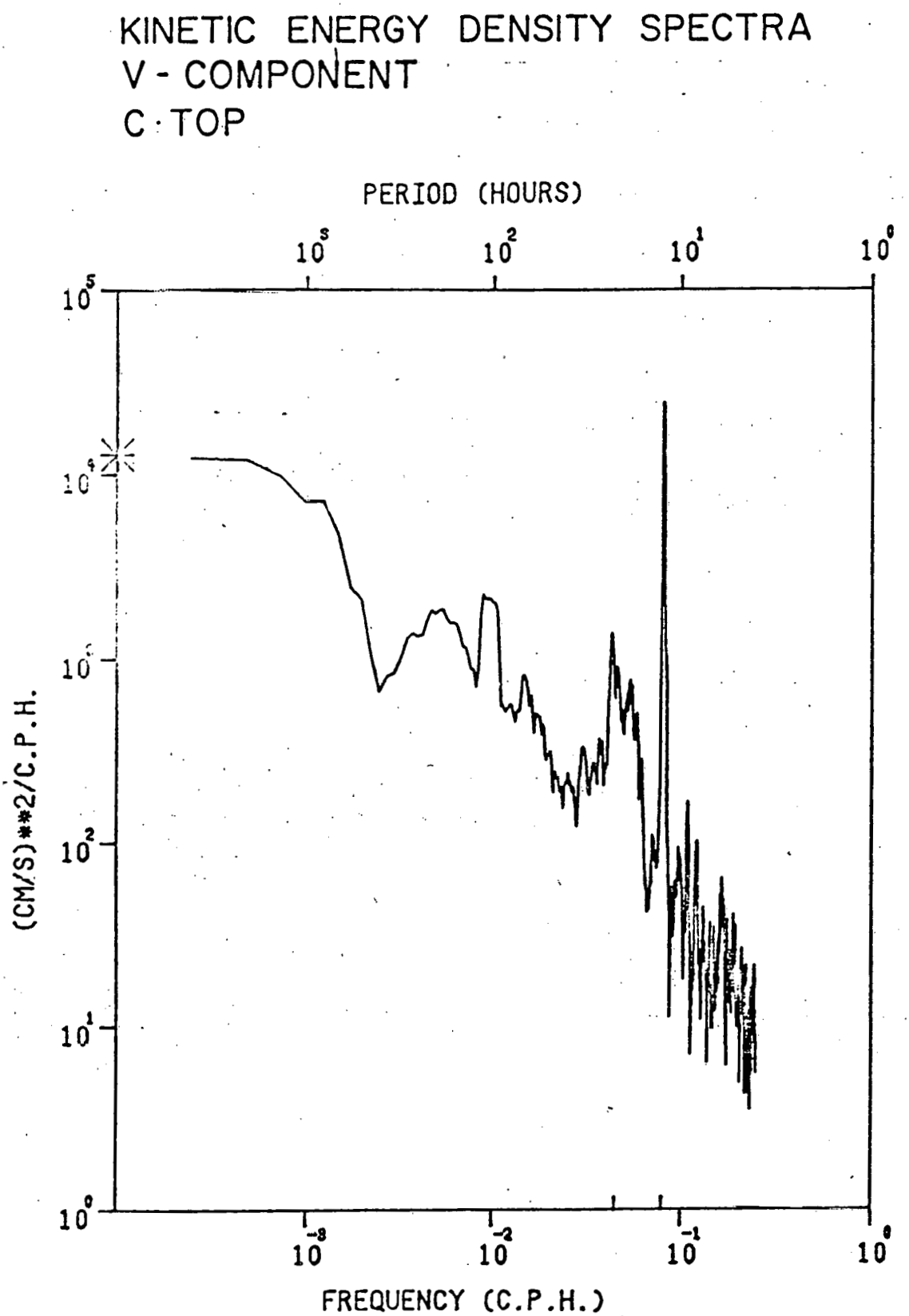

Figure 130 Kinetic energy density spectra for current velocity, v-component, C_{top}

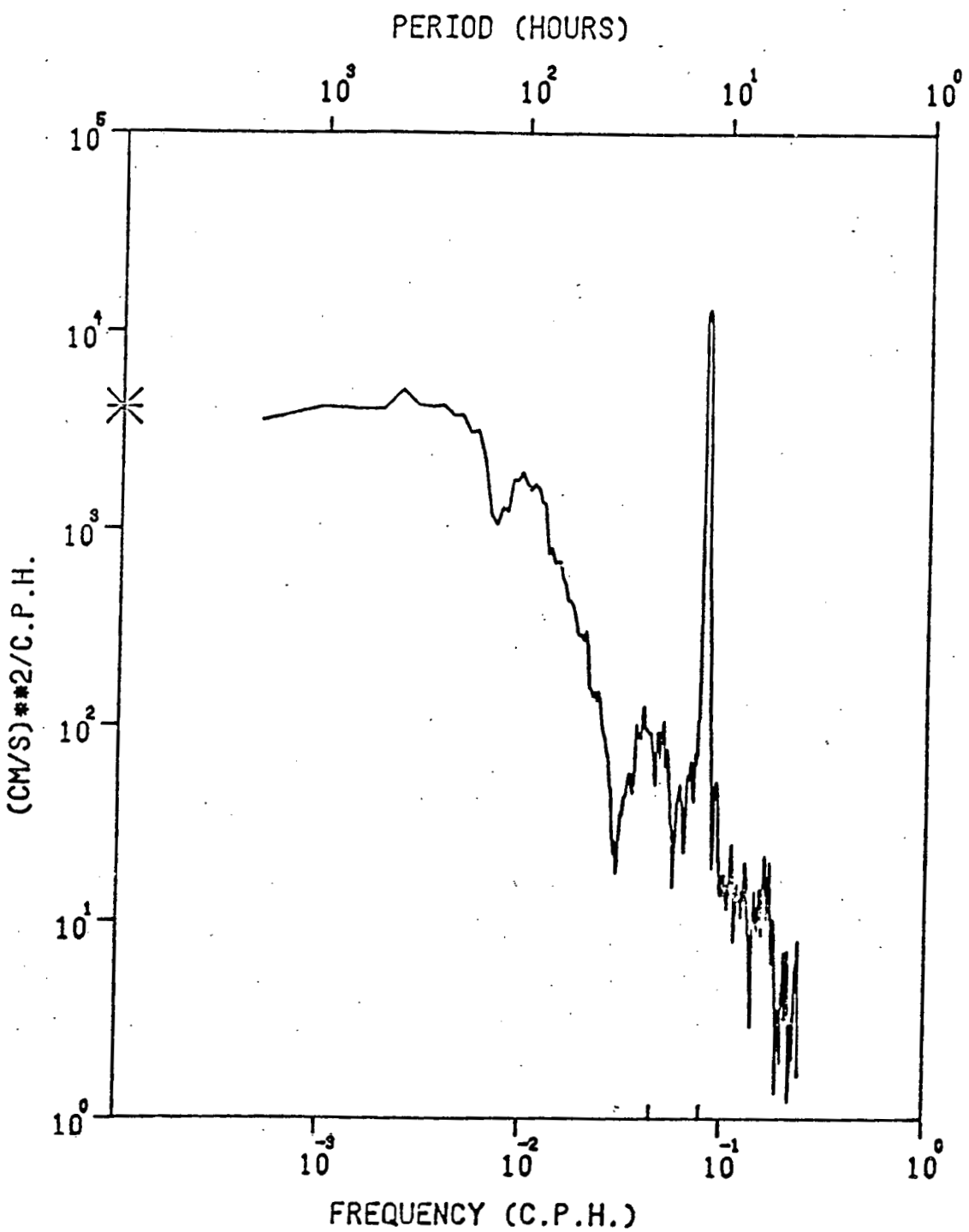

Figure 131 Kinetic energy density spectra for current velocity, u-component, C_{bot}

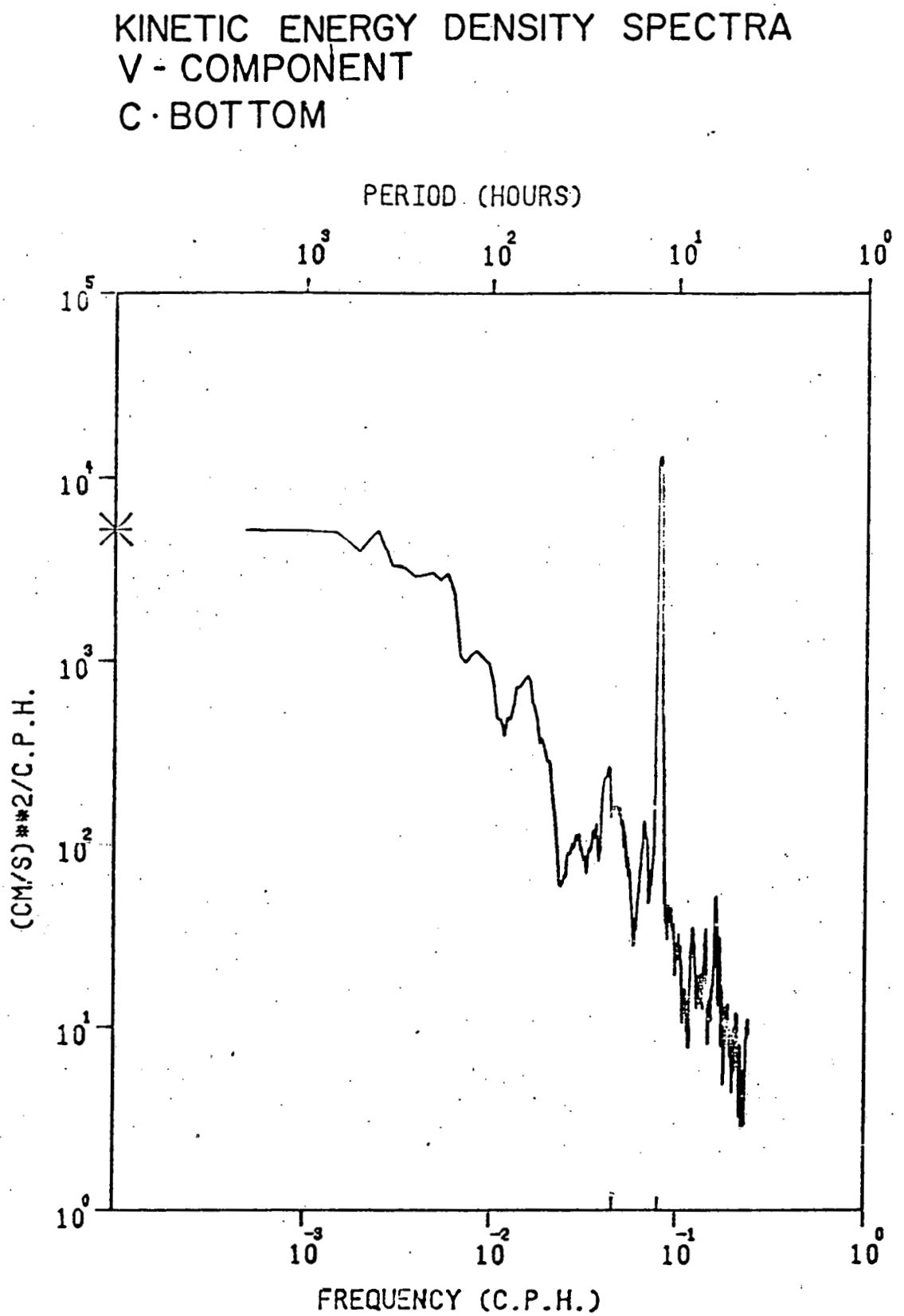

Figure 132 Kinetic energy density spectra for current velocity, v-component, C_{bot}

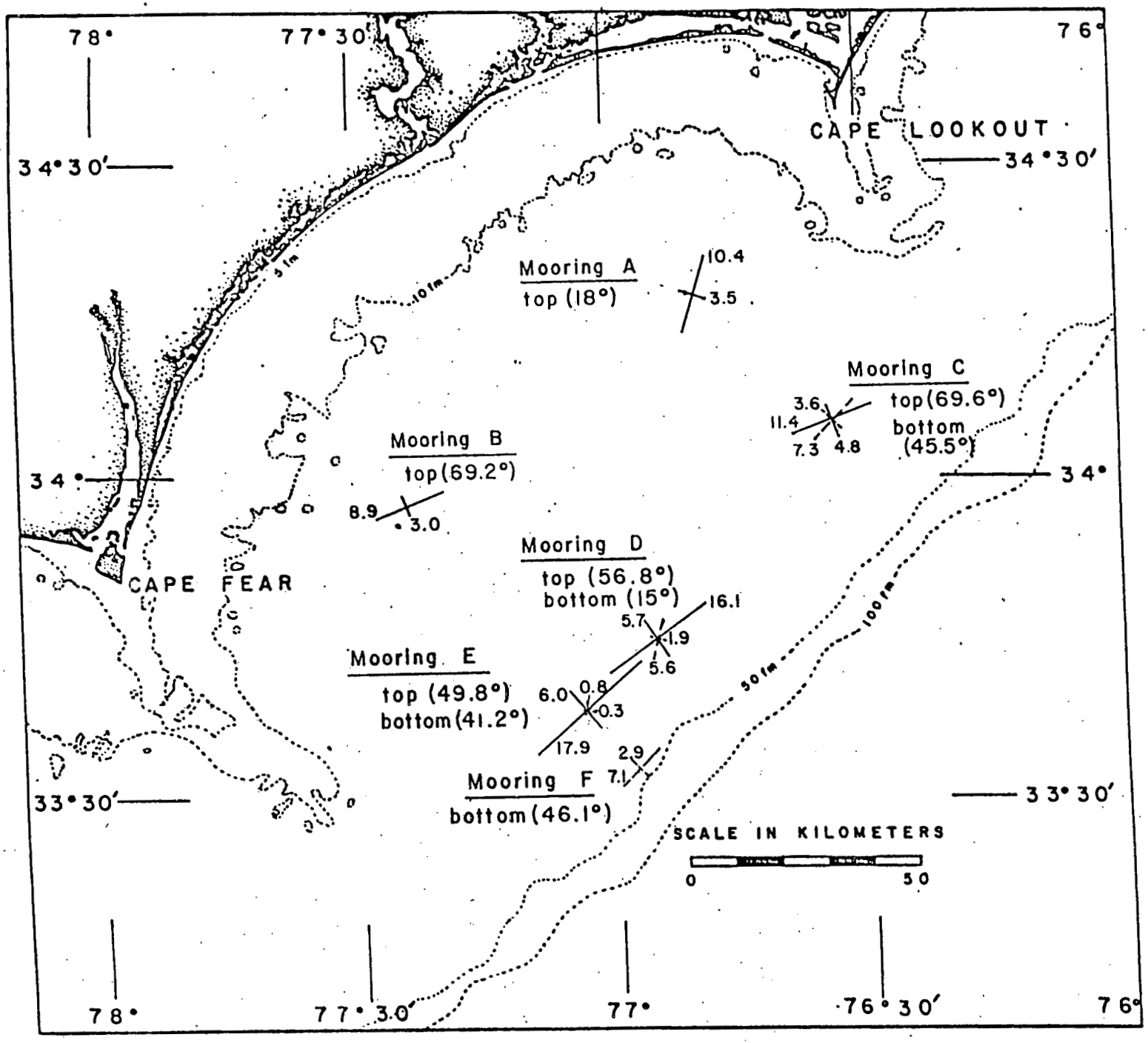

Figure 133 Principal axes and root mean square velocities for Moorings A-F

mean square (r.m.s. or standard deviation) of the velocity components relative to the normal coordinates. The computations were made using data low pass filtered to suppress the tides. Thus, the variance crosses represent only the low frequency portion of the spectrum where the motions are primarily induced by atmospheric forcing. Each mooring site contains one or two crosses: solid lines for the upper level and dashed lines for the lower level. The angle in parenthesis gives the rotation of the principal axis relative to true north and the numbers at the tips of the crosses are the standard deviations along the coordinate axis. Typical low frequency r.m.s. speeds are of order 10 cm/s. The principal axis exhibit topographic steering and the reduction in amplitude and rotation with depth is compatible with local Ekman dynamics.

The preceeding principal axis representation gives an overview of the low frequency motions. Since the principal axis may vary as a function of frequency (the physical processes giving rise to the motions differ) it is useful to construct a hodograph model. In so doing, the velocity vector time series are decomposed into clockwise and anticlockwise rotating motions of different amplitude and phase. The sum of these two polarized motions gives an ellipse whose semi-major axis is oriented along the principal axis of variance at that particular frequency. This form of analysis is generally referred to as rotary spectral analysis and a comprehensive description of the technique may be found in Mooers, 1973; Gonella, 1972; or Fofonoff, 1969. It is analogous to what was presented in Figure 133, except here the principal axis are computed as a function of frequency instead of just an average over a rather large frequency band. Examples of the anticlockwise and clockwise polarized kinetic energy density spectra are shown in Figures 134 and 135 for the upper level on mooring C. No consistent polarization preference is evident for time

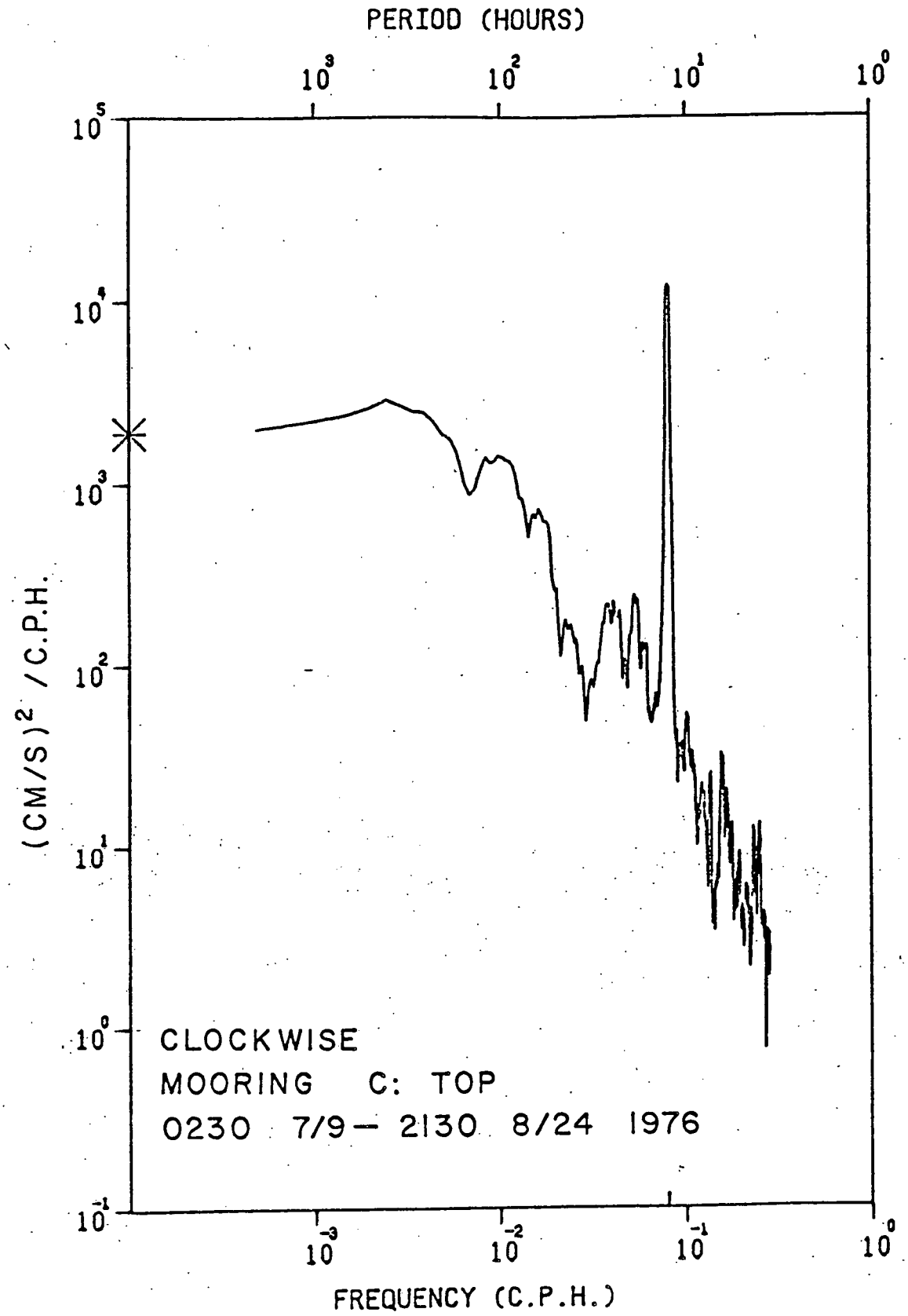
PERIOD (HOURS)
10^3
10^2
10^1
10^0
10^5
10^4
10^3
10^2
10^1
10^0
10^{-1}
$(CM/S)^2$ /C.P.H.
CLOCKWISE
MOORING C: TOP
0230 7/9 — 2130 8/24 1976
10^{-3}
10^{-2}
10^{-1}
10^0
FREQUENCY (C.P.H.)

Figure 134

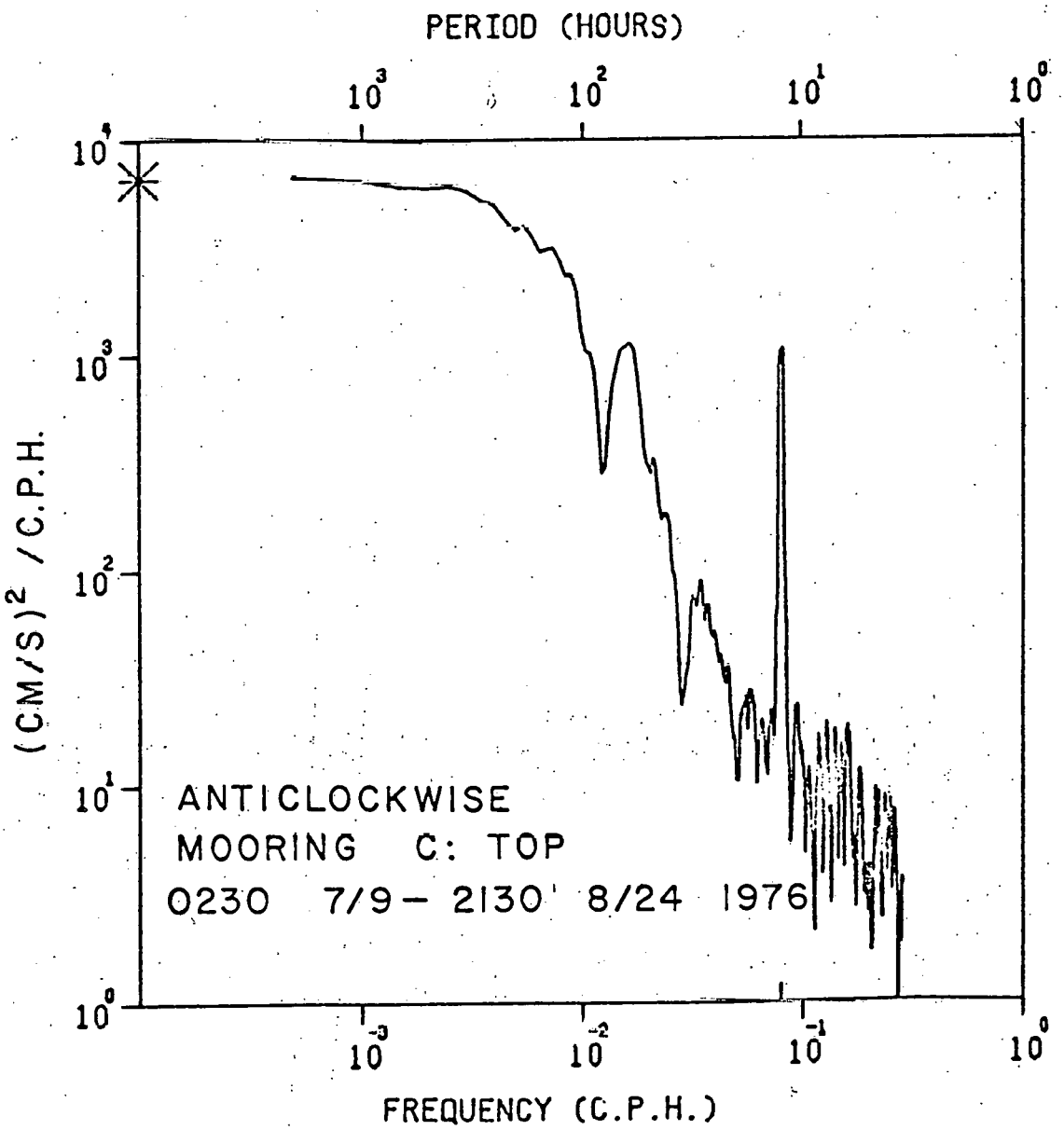
PERIOD (HOURS)
10^3
10^2
10^1
10^0
10^4
10^3
10^2
10^1
10^0
$(CM/S)^2$ /C.P.H.
ANTICLOCKWISE
MOORING C: TOP
0230 7/9 – 2130 8/24 1976
10^{-3}
10^{-2}
10^{-1}
10^0
FREQUENCY (C.P.H.)

Figure 135

scales longer than one pendulum day while at shorter time scales the preference is clearly for clockwise polarized motions compatible with the dynamics of inertia-gravity controlled oscillations. Various parameters are required to describe the hodograph ellipse; for example, the ellipse semi-major and semi-minor axis (analogous to the crosses shown in Figure 133), the ellipse orientation, and three different measures of coherency between the velocity component fluctuations; the minimum and maximum coherences and the ellipse stability. The minimum coherence is the coherence between velocity components measured relative to the normal coordinates; the maximum coherence is the coherence between velocity components measured relative to coordinates rotated 45° to the normal coordinates and the ellipse stability gives the coherence between anticlockwise and clockwise rotating components, i.e. it is a measure of the stability of the ellipse orientation. An example of these parameters is given in Figure 136 for the upper level on mooring C. The bottom plate contained the maximum (solid line) and minimum (dots) coherence squared as a function of frequency. The middle plate gives the stability (solid line) and the semi-minor to semi-major axis ratio (dots) with negative axis ratio designating clockwise hodograph rotation and vice-versa. The upper plate gives the ellipse orientation as a function of frequency which is useful when the stability is high. Regions of high maximum coherence but low minimum coherence generally designate coherent rectilinear motions where the stability mimicks the maximum coherency (the quadrative spectrum is small). Regions of both high maximum and minimum coherence designate coherent elliptical motions. For this case the stability can be either high or low. For example, the orientation of a nearly circular motion is arbitrary, therefore, the stability would

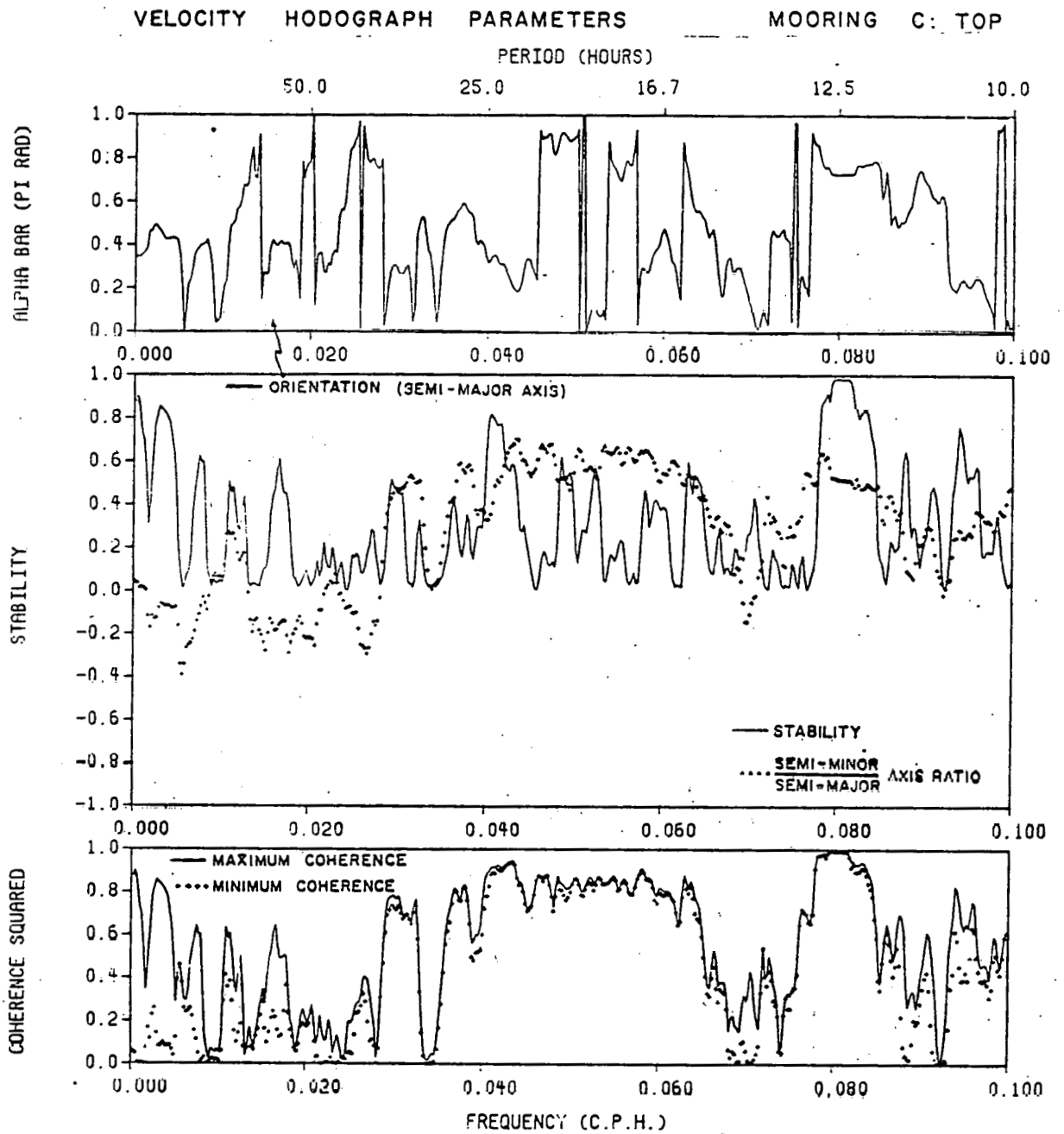

Figure 136 Hodograph parameters from meter C(Cormorant)$_{top}$

be low. Upon traversing from low to higher frequency motions in Figure 136, we see fairly coherent rectilinear motions at time scales longer than roughly 5 days oriented approximately along the principal axis shown in Figure 133. Note that orientation here is measured anticlockwise from the nominal offshore direction of 145.6° relative to true north. The units shown in the Figure have been normalized by π radians therefore one must multiply by π to get the radian measure. The motions are incoherent between time scales between 1 to 5 days except for a peak at about 32 hrs. A rather broad peak in both minimum and maximum coherence occurs spanning time scales of approximately 16-25 hours which incompasses the astronomical diurnal tidal species propagating onto the shelf from the deep ocean, local sea breeze effects, and local inertial period oscillations ($2\pi/f$ = 21.5 hrs.) as mentioned previously. The interaction between these three important processes is evident in the low ellipse stability and the varying orientation. The most coherent peak occurs centered at 12.41 hrs. which is the time scale of the principal luner semi-diurnal tide. This is the only time scale where the motions are truely coherent and stable because it is the only time scale dominated by a regular deterministic process.

Rodfield (1958) analyzed sea level records along the east coast of the U.S. to produce the co-tide and co-range lines and concluded that the principal luner semi-diurnal tide (M_2) on the eastern U.S. continental shelf is a co-oscillation caused by the reflection of an incident oceanic wave by the coast. The portion of the oceanic wave transmitted onto the shelf reflects off the coast resulting in an increase in the tidal amplitude with distance from the continental slope. Hence, the mean tidal range at

Savannah is 6.8 ft. whereas it decreases to 3.6 ft. at Cape Hatteras, since the shelf width at Savannah is larger than at Cape Hatteras. This type of reflected inertiagravity wave is called a Poincare wave. It has a maximum elevation slightly seaward of the coast and the associated water particle motions in the horizontal plane are elliptical, clockwise polarized, and oriented with the semi-major axis along the direction of propagation. The ratio of semi-minor to semi-major axis is theoretically predicted to be a pendulum day ($2\pi/f$) divided by the wave period (in this case 12.41 hr.). Thus the predicted axis ratio is 0.58 at the latitude of 34°N. The velocity data in Onslow Bay supports Redfields view. Example Figures 137 and 138 show the semi-diurnal tidal ellipses computed at all the mooring locations. Computations made from the entire record lengths are shown in Figure 137 and those made over the common length for the rectangular array are shown in Figure 138. The sense of rotation for all of the ellipses is clockwise, they are oriented onshore and their axis ratios are all close to the value predicted for a Poincare wave. At mooring C it is observed that the amplitude of the tidal current decreases with depth and the ellipse orientation is slightly rotated. Both of these effects may be attributed to bottom friction. A small phase shift (less than 1 hr.) also occurs between the upper and lower tidal current due to bottom friction.

Generally speaking, the Eastern U. S. continental margin supports tidal currents which are rotary, with the tidal current precessing to the right, as a function of time, due to the effect of the Earth's rotation and the nature of the tidal wave(s), forming (tidal) ellipses, over the temporal cycle of a particular tidal constituent. Tidal motion both north and south of Cape

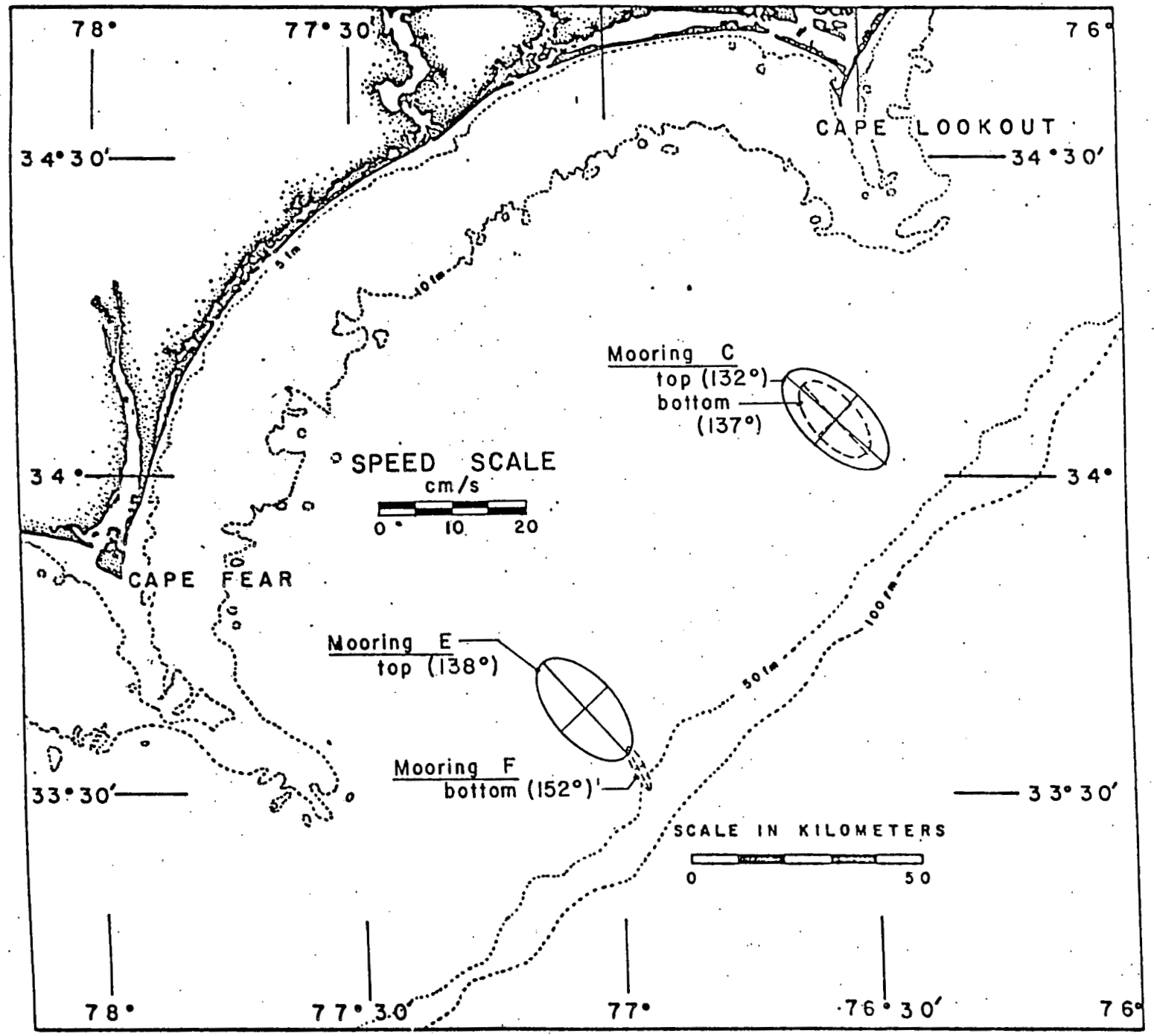

Figure 137 Tidal elipses for Summer 1976

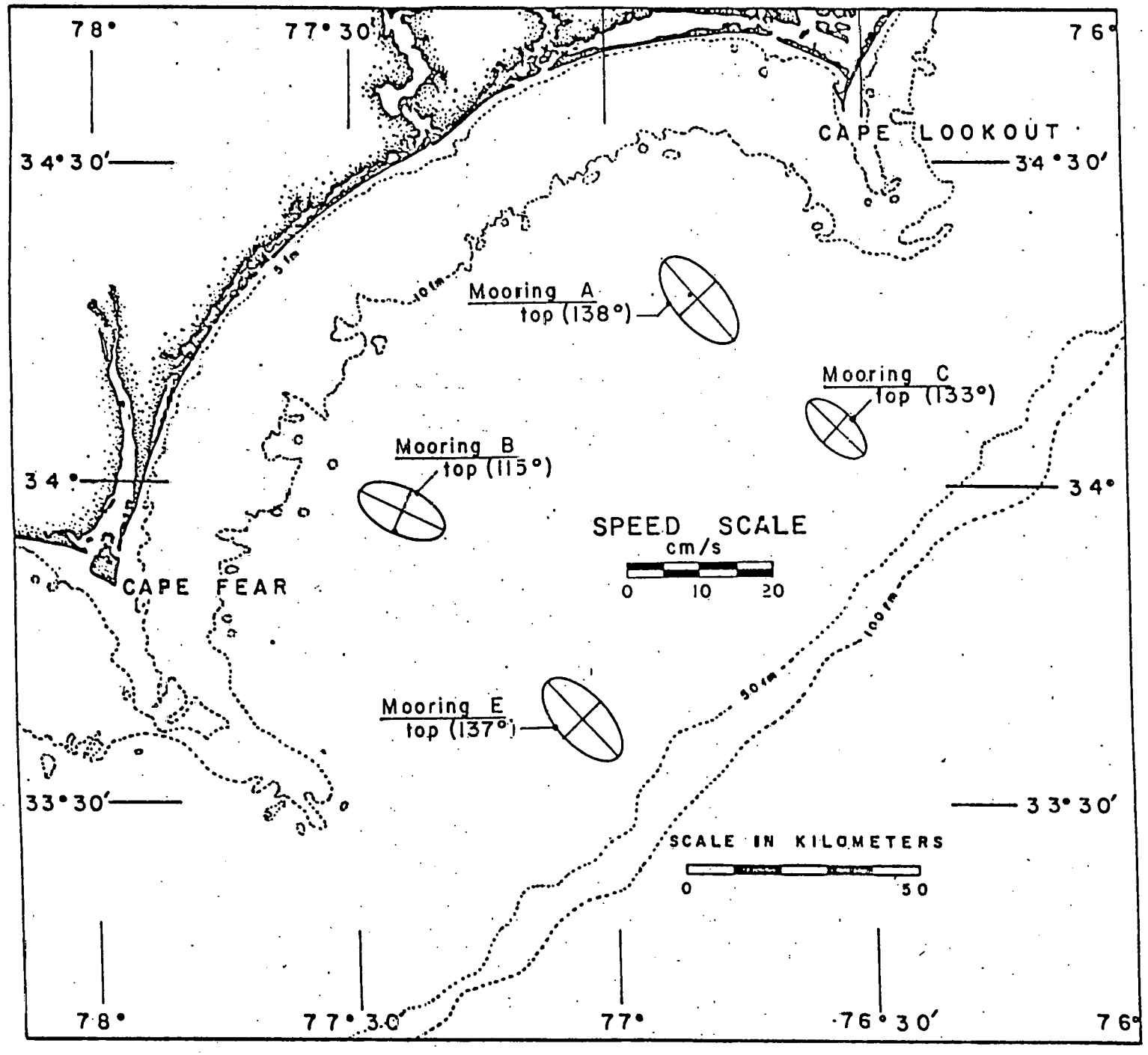

Figure 138 Tidal elipses for July 23-Aug. 22, 1976
(t[illegible] me[illegible]s)

Hatteras is principally semi-diurnal in frequency. This tidal constituent is called the M tide and completes two oscillations each lunar day, i.e., 24.84 hours. The diurnal tidal signature (S_2) is obvious, but of lesser magnitude than the M_2 signature, as indicated in Table 10 . Additional tidal constituents of higher order, are apparent in the data but tend to be of minor significance beyond the M_4 constituent.

Redfield (1958) presented a hypothesis, based on an analysis of sea level records, that the principal tide along the eastern U. S. continental margin was a co-oscillation of shelf waters with the Atlantic Ocean tide. A reflection of the incident oceanic tidal wave, off of the continental slope. The portion of the oceanic wave transmitted onto the continental shelf undergoes a reflection off of the coast thereby resulting in an increase in the tidal amplitude with distance from the continental slope. This further suggests that the (mean) tidal range seaward of Savannah, Ga. should be larger than that north or south of its latitude, with a northerly minimum occurring at Cape Hatteras, due to the fact that the continental shelf width is largest off ofSavannah and narrows both to the south and to the north. Hence, the mean tidal range of 2.1 meters at Savannah is contrasted with that of 1.1 meters at Hatteras.

This reflected inertiagravity wave is called a Poincare Wave. One can theoretically, analytically describe the basic motion of this tide by considering the following barotropic, inviscid, rotating model momentum balance:

TABLE 10

TIDAL CONSTITUENTS IN ONSLOW BAY OBSERVED DURING THE SUMMER OF 1976

		M_2			S_2			M_4		
Record	Length Hrs.	Orientation	Semi-Major CM/S	Axis Ratio	Orientation	Semi-Major CM/S	Axis Ratio	Orientation	Semi-Major CM/S	Axis Ratio
CT	1434	132	17.2	0.52	136	3.1	0.48	163	1.0	0.20
CB	"	137	13.2	0.43	136	2.3	0.39	163	0.8	0.12
ET	1784	138	16.3	0.55						
FB	"	152	6.8	0.26	163	2.1	0.29	136	1.3	0.25
AT	1123	138	14.5	0.45	143	2.3	0.52	073	2.4	0.35
BT	"	115	11.9	0.44	091	2.5	0.68	073	1.8	0.20
CT	"	133	9.4	0.55	136	2.5	0.52	163	0.6	0.10
ET	"	137	13.3	0.52	137	3.1	0.48	019	0.8	0.40

(1) $U_t - fv = -g\zeta_x$ in the on/off direction,
and
(2) $V_t + fu = -g\zeta_y$ in the alongshore direction,
and
(3) $P_z = -g\rho$ in the vertical,

where u and v are the "on/off" and "along" depth averaged current components, ζ is the surface elevation, g the gravitational acceleration, P the pressure, f the Coriolis parameter, ρ the density and subscrips denote partial differentiation. The time averaged depth is $h(x,y)$ and the vertically integrated equation of continuity is:

$$(4) \quad (hu)_x + (hv)_y = -\zeta_t \quad .$$

Nest, assuming $\zeta = G(x) \cos(\sigma t - ly)$, then (1) and (2) result in

$$(5) \quad u = \frac{g}{(f^2-\sigma^2)} (\sigma G_x - flG) \sin(\sigma t - ly)$$

and

$$(6) \quad v = \frac{g}{(f^2-\sigma^2)} (fG_x - \sigma lG) \cos(\sigma t - ly)$$

Equations (5), (6) and (4) can now be combined to yield the relation

$$(7) \quad (hG_x)_x + \left(\frac{(\sigma^2-f^2)}{g} - \frac{flh_x}{\sigma} - l^2h\right)G = 0 \quad .$$

This is the governing equation of the Sturm-Liouville type and with the conditions of G remaining bounded as $x \to \infty$, and with no singularities at $x = 0$ then the system is mathematically

proper. If the coefficient preceeding the G term is negative, then trignometric solutions are available and, furthermore if (for the sake of simplicity), h is a constant and if $\sigma > f$, then plane waves occur for $k^2 > 0$, where G(x) is proportional to e^{ikx} and $l \gtrless 0$. Inclusion of variable, regularly deepening h to seaward presents no major problems in the theory. These plane waves are called Poincare waves and the M_2 tidal component is an example of such a wave having a minimum elevation slightly seaward of the coast and an associated elliptical, clockwise polarized water particle motion in the horizontal plane. The semi-major axis of the tidal ellipse is oriented in the direction of wave propagation and the ratio of semi-minor to semi-major axes is theoretically predicted to be the wave period, eg. 12.41 hours for the M_2 component, divided by the local inertial period, 12/(sinθ) in hours. This ratio is 0.563, 0.578 and 0.593 for latitudes of 33, 34 and 35 degrees North, respectively. The velocity data in Onslow Bay is certainly consistent (Table 10) with both Redfield's view and with Poincare theory. It is of note that the ratios increase in the northerly direction, egs. ET vs. CT, 0.52 to 0.55 and BT vs. AT, 0.44 to 0.45, which is also consistent with the wave theory.

The minor to major axis ratios are somewhat lower than that predicted by wave theory, especially at the bottom sensors, and in shallower water. Additionally, it is noted that the amplitude of the tidal current decreases with depth and the ellipse orientation is slightly rotated both from top to bottom and from mooring to mooring. Finally, a small phase shift, less than 60

minutes, also occurs between the upper and lower current records with the lower leading the upper. These effects may all be ascribed to topographic influence, i.e., topographic steering and bottom friction. If one defines an effective pressure gradient as the resultant of the pressure gradient and tide generating forces, then the currents at any depth attain their maxima when the frictional forces are in balance with the effective pressure gradient. At this phase the effective pressure-gradients will be decreasing so the currents will attain their maxima before the effective pressure-gradients vanish.

The frictional forces arise from the bottom. If it is assumed that those near the bottom are greater than those higher up, then it follows that the bottom-currents will reach their maxima earlier than the higher currents and consequently it occurs that all phases of the bottom currents will occur earlier than corresponding phases of the higher currents.

Other tidal constituents were examined but only the principal lunar semi-diurnal M_2, the principal solar semi-durinal S_2, and a shallow water harmonic M_4 were found to have amplitudes over 1 cm/s. In some cases the other tidal constituents did not even stand out above the background noise level. The three major constituents for Onslow Bay tidal currents are summarized in Table 10, from which Figures 137 and 138 were constructed.

The S_2 tidal currents are very similar in orientation and axis ratio to the M_2 currents except for being much smaller in magnitude.

A preliminary look at the Onslow Bay velocity data from this experiment portrays the general character of water movements off the Carolina coasts. Except for the tidal oscillations, the picture is extremely complicated resulting from the superposition of numerous random processes operating over a broad range of frequencies.

Mean currents remain ill-defined. Velocity records of a months duration are too short to compute relatively small mean values in the presence of relatively large low frequency variability. Additional research is required (and has been conducted under DOE support, to date) to establish reliable mean fields and their seasonal variations.

The variance structure is summarized in Figures 139 - 144 , which is a plot of the fluctuation kinetic energy distribution as a function of frequency for the upper and lower levels at mooring C. The ordinate gives the energy fraction contained over any frequency band. For example, the semi-diurnal tidal current comprise percent of the variance at that location. Other pertainent fractions are labeled on the figure.

Earlier, it was mentioned that the low frequency portion of the spectrum could be attributable to either direct atmospheric forcing, intrusions or eddies from the deep ocean boundary, or propagation of free modes of oscillation supported by the bottom topography i.e. continental shelf waves. A firts impression from the data presented; particularly the velocity hodograph parameters, is that regular, coherent, wave like features on the continental shelf in Onslow Bay are of secondary importance to the transient wind induced motions and influence of the Gulf Stream.

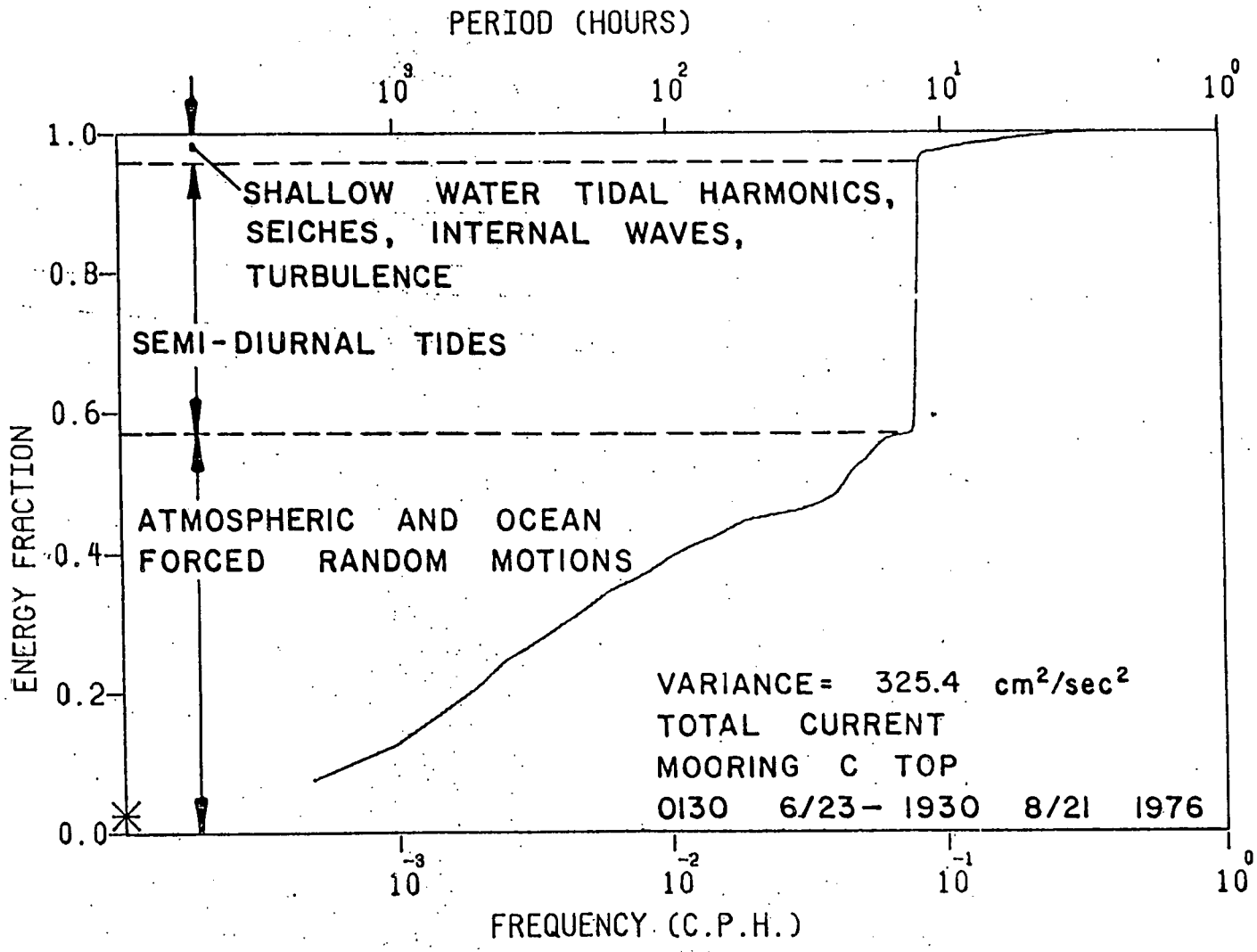

Figure 139 Energy fraction vs. frequency for C_{top} total current

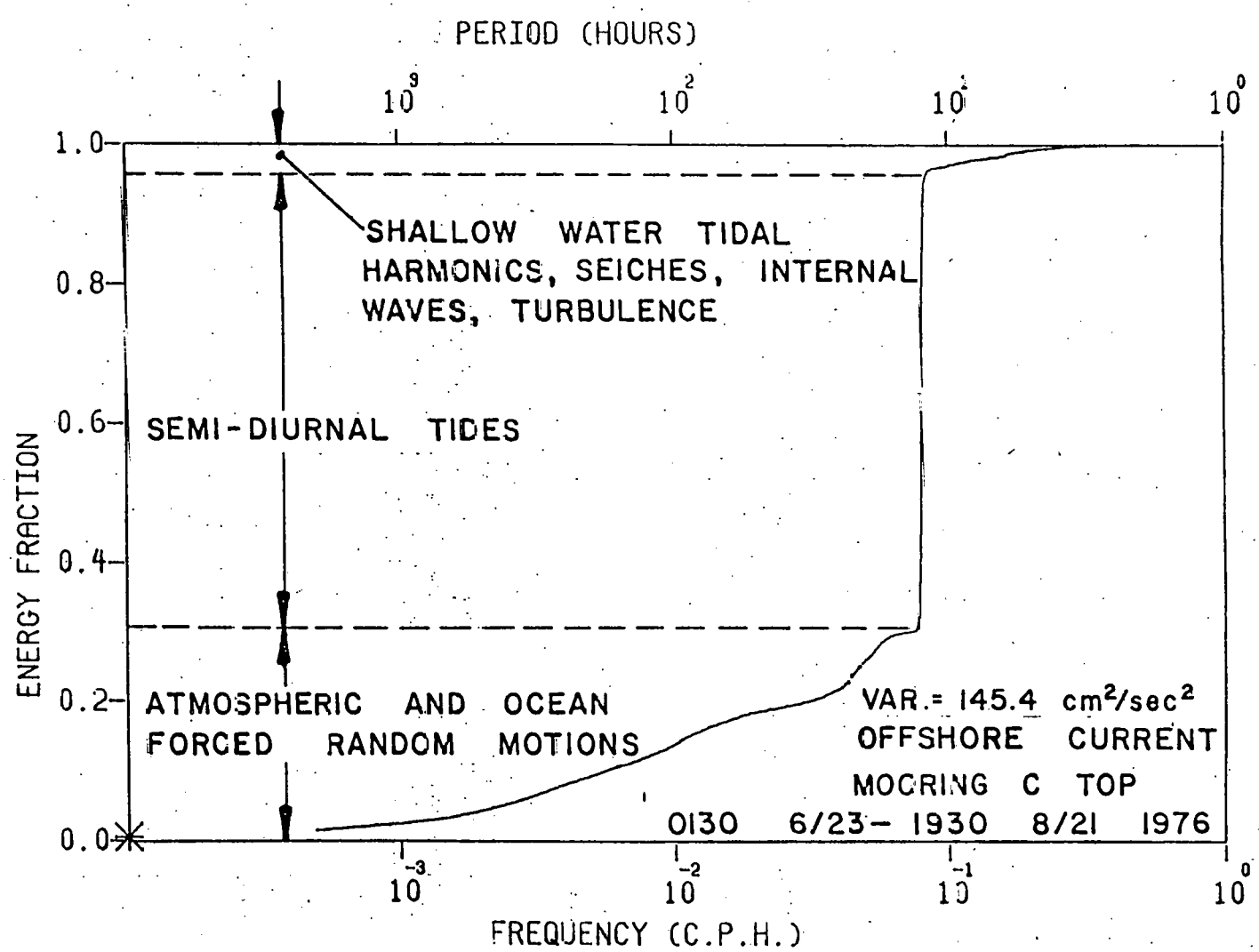

Figure 140 Energy fraction vs. frequency for C_{top} offshore current

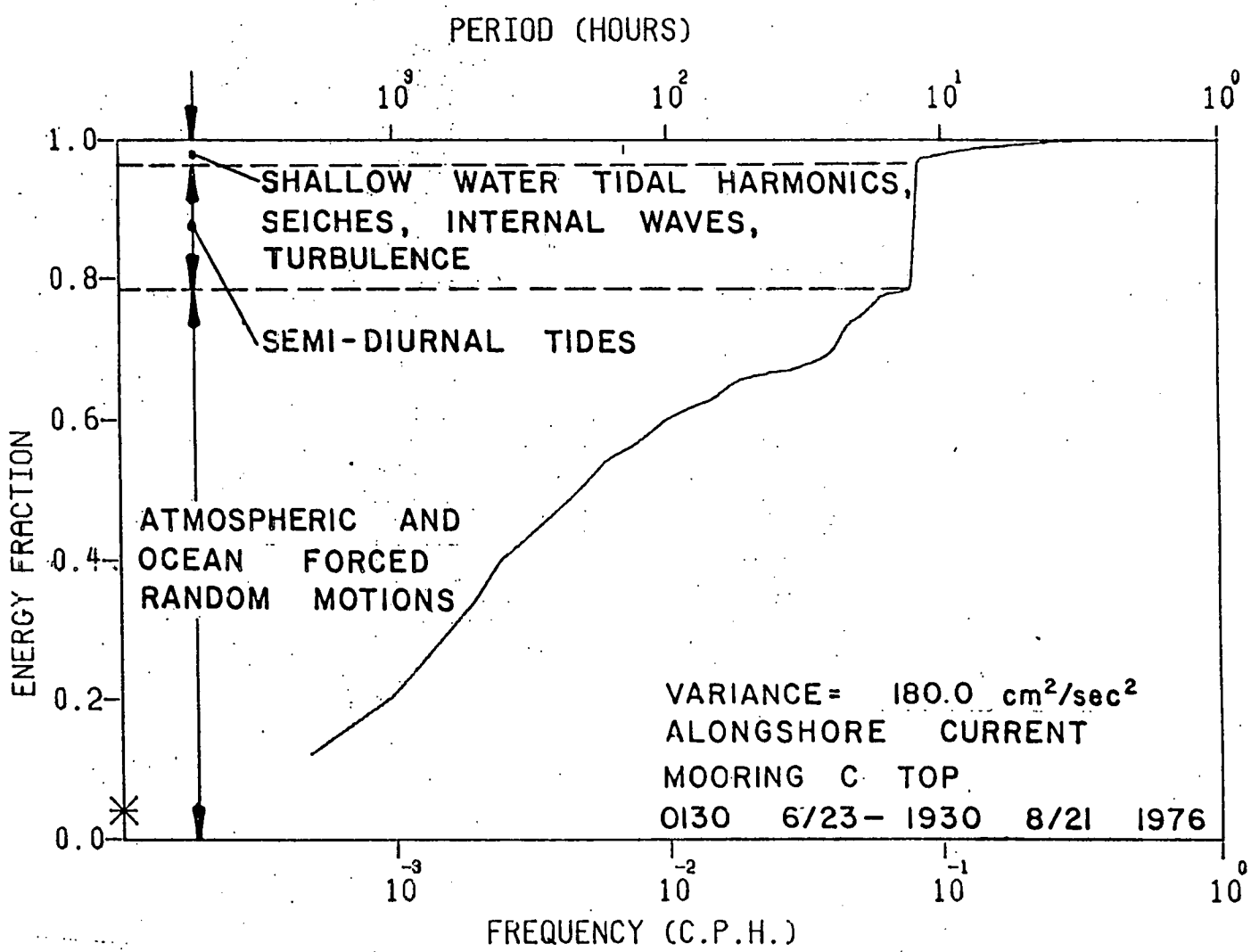

Figure 141 : Energy fraction vs. frequency for C_{top} alongshore current

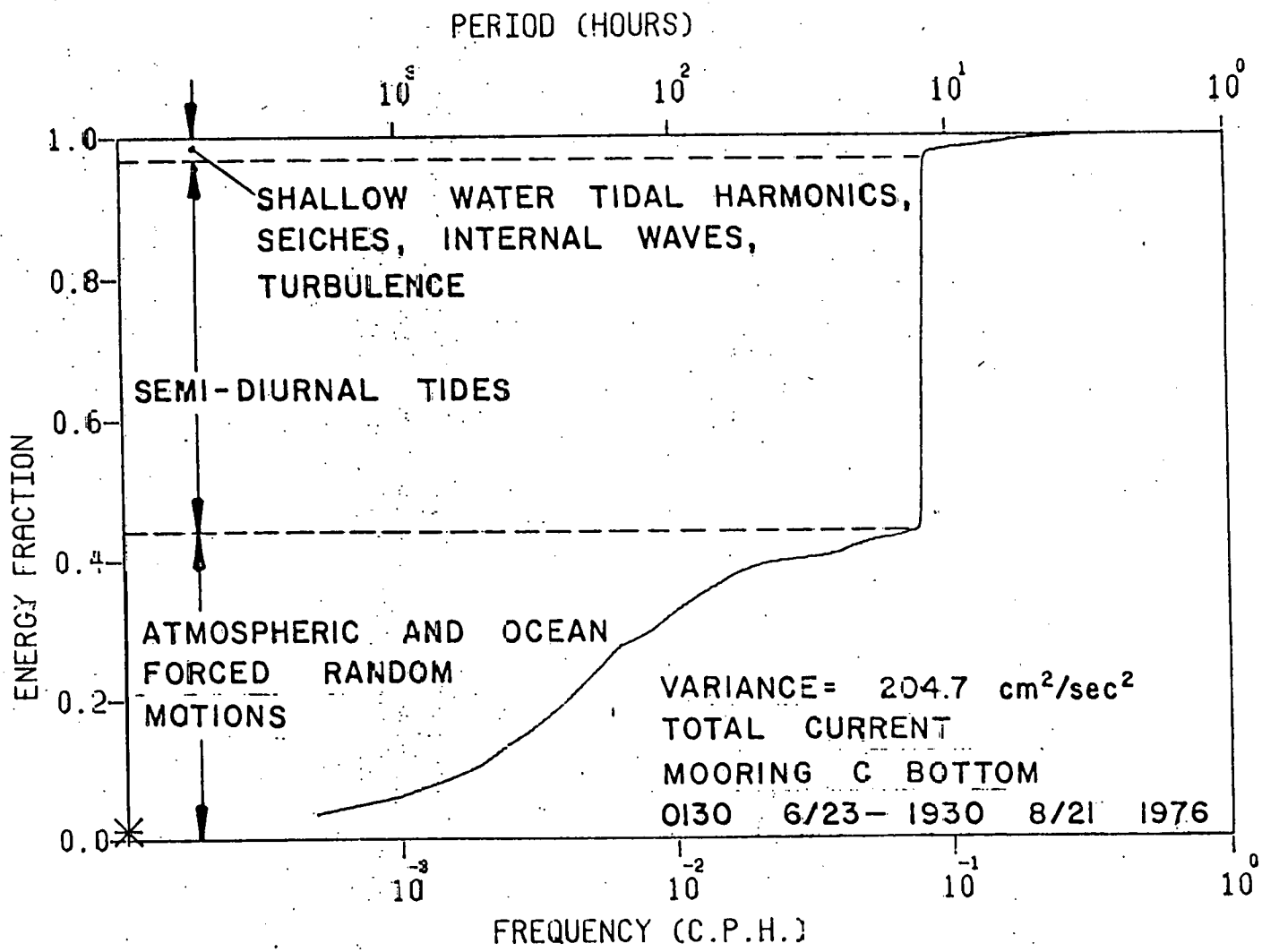

Figure 142: Energy fraction vs. frequency for C_{bot} total current

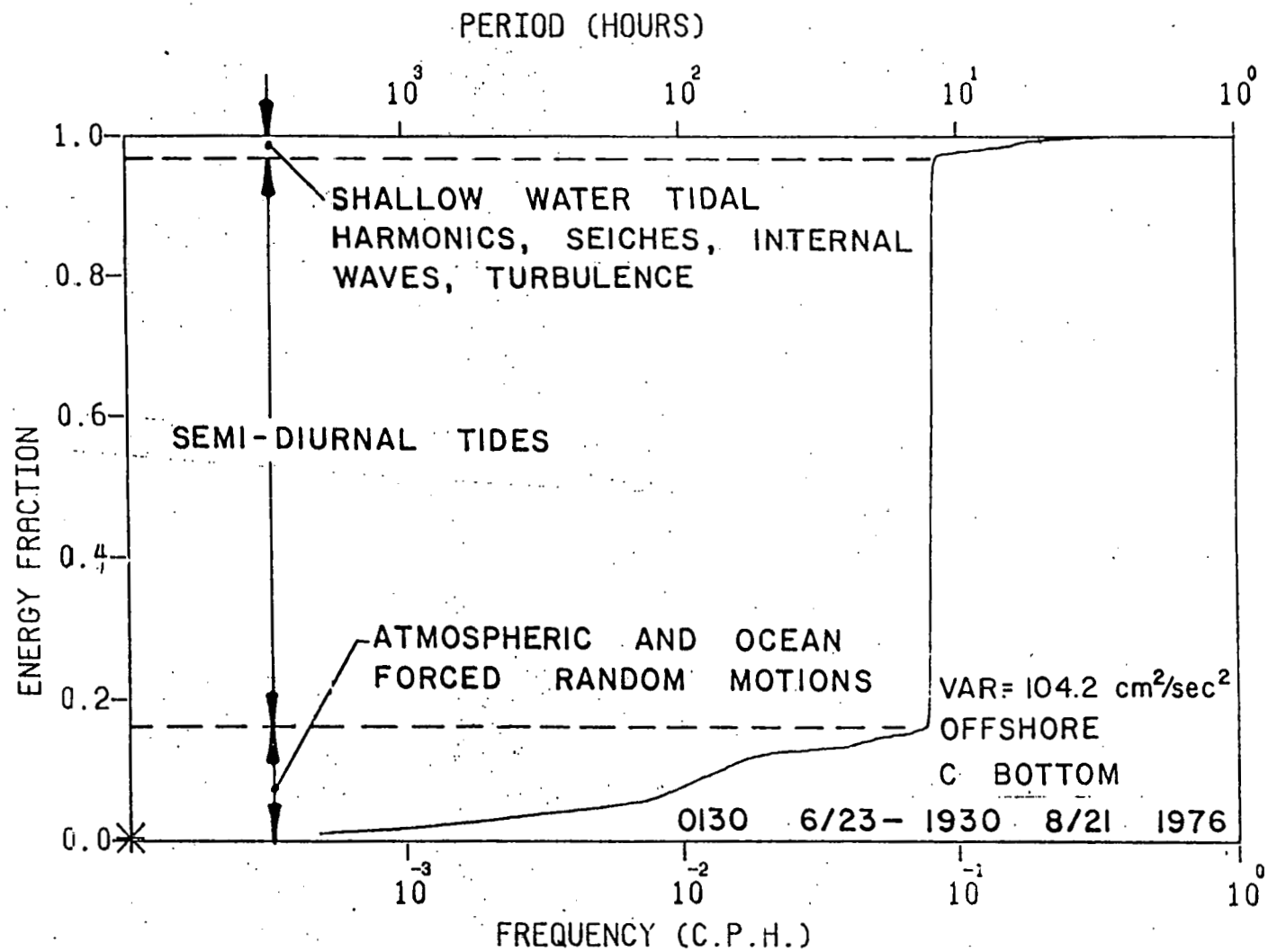

Figure 143 Energy fraction vs. frequency for C_{bot} offshore current

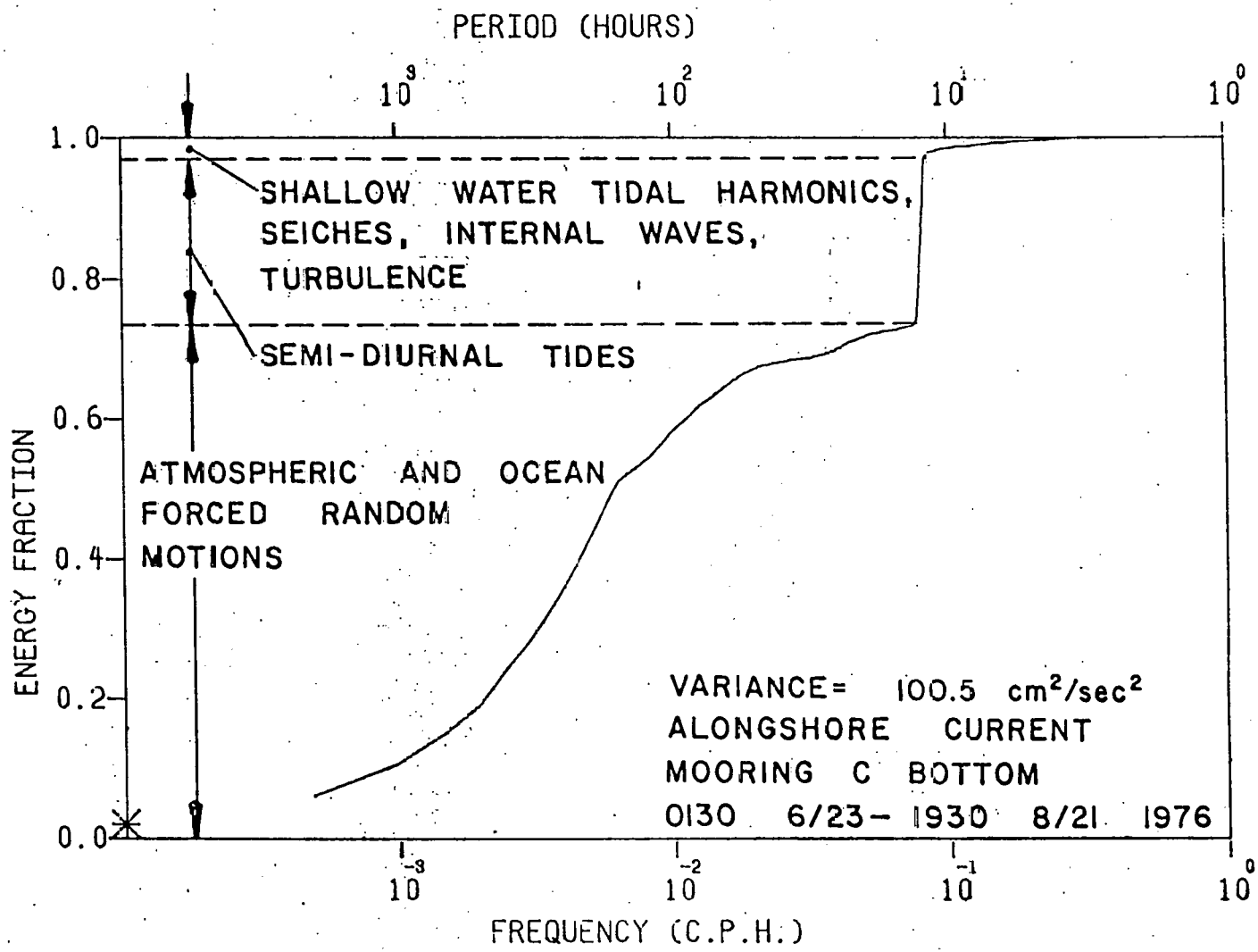

Figure 144. Energy fraction vs. frequency for C_{bot} alongshore current

Herein it should be noted that Brooks (1977) has used sea level data from BFT and WIL to predicate the existence of zero group speed continental shelf waves of the barotropic, clockwise rotating variety. It is the conclusion of this author (Pietrafesa) that the Brooks' conclusions were premature, at best, and that no new evidence yet exists for the southerly propagation of a barotropic continental shelf wave. In fact, and to the contrary of Brooks' contention, FPS vs. BFT and CHS vs. BFT (all sea level) both would argue that there is a northerly propagation of events, definitely atmospherically induced.

The passage of large scale meteorological disturbances, such as are seen to occur in the data shown within the met/sea level report (Pietrafesa, 1978c), along a coastline can generate waves of the continental shelf wave variety (Gill and Schumann, 1974). However, as suggested by Niiler and Mysak (1971), the vorticity associated with the mean current over a continental margin may be of the order of the Coriolis parameter and the shelf waves could be advected by the mean current or even by amplified and grow unstable. The former possibility has recently been investigated by McKee (1978) who showed that a sheared geostrophic current could change the direction of phase propagation of the waves. Grimshaw (1978) has extended McKee's work and found that the presence of a boundary sheared current in a continental shelf wave field could result in the continental shelf waves having negative phase speeds. Additionally, Grimshaw suggests that the background vorticity provided by the sheared boundary current may result in the amplitued of the shelf waves being modulated/increased and that the amplified waves may become unstable.

Pietrafesa (1978 a and b) shows evidence for the northerly propagation of events which show up as wavelike features in the current meter data, i.e.

u and v are in quadrature, with u leading v. This evidence is in contradiction with the Brooks' contention that southerly propagating barotropic CSW's exist since the Pietrafesa data was collected well within the offshore extend of the first node, within which the Brooks' wave must rotate clockwise contrary to the Pietrafesa evidence that the event rotates cyclonically at periods of 3-3½ days. What may be happening herein is that the shelf waves may be getting advected with the mean current, towards the north. If the waves have a phase speed within the range of that of the speed of the mean current, and moreover due to the fact that both v_x and h_x are large, in the region of the shelf break, slope, it may appear to the observed (the current meter) that the waves are propagating northward and rotating cyclonically. The fact that h_y is varying, in the Capes region, may also influence the characteristics of any possible shelf waves modes.

It should also be noted that there is little consistent co-herence within the period band of interest (eg. site D, Figures 145 - 146) from top to bottom at mooring sites, ruling out the possibility of a strictly barotropic phenomenon.

Superimposed on all of this is the fact that $\tau^{(y)}$, and $\tau^{(x)}$ are very coherent over these periods, with $\tau^{(y)}$ leading $\tau^{(x)}$, that currents are coherent with the wind at these periods and that, for example, in the inner shelf region, the southerly currents lead the northerly currents over the period bond 3-3½ days, consistent with the wind forcing.

Dr. T.N. Lee (UM) has reported (personal communication) findings in the Georgia Bight similar to those shown by this author (Pietrafesa) for Carolina Capes region so that the two regions are not a dynamical variance in qualitative comparison herein.

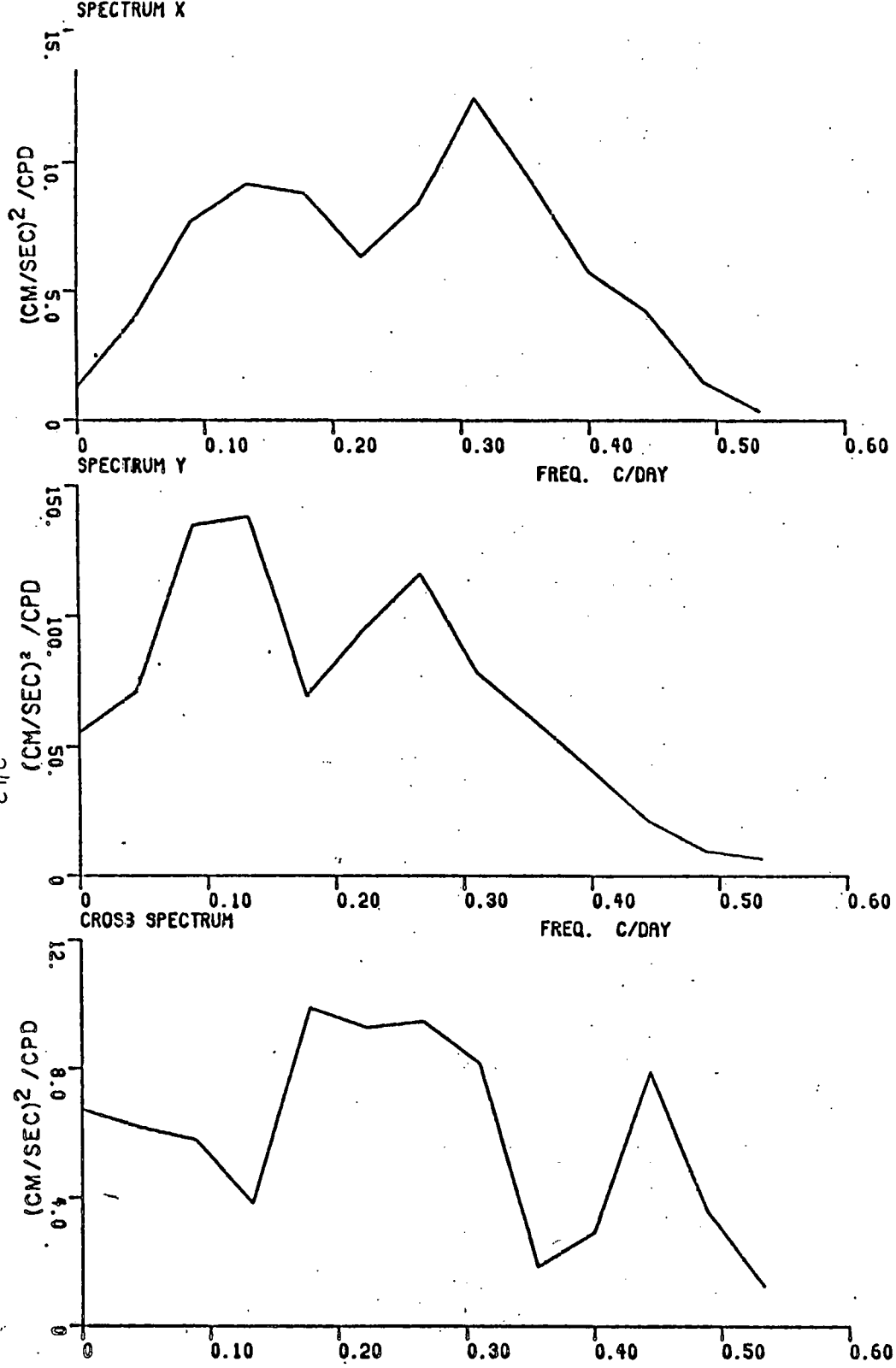

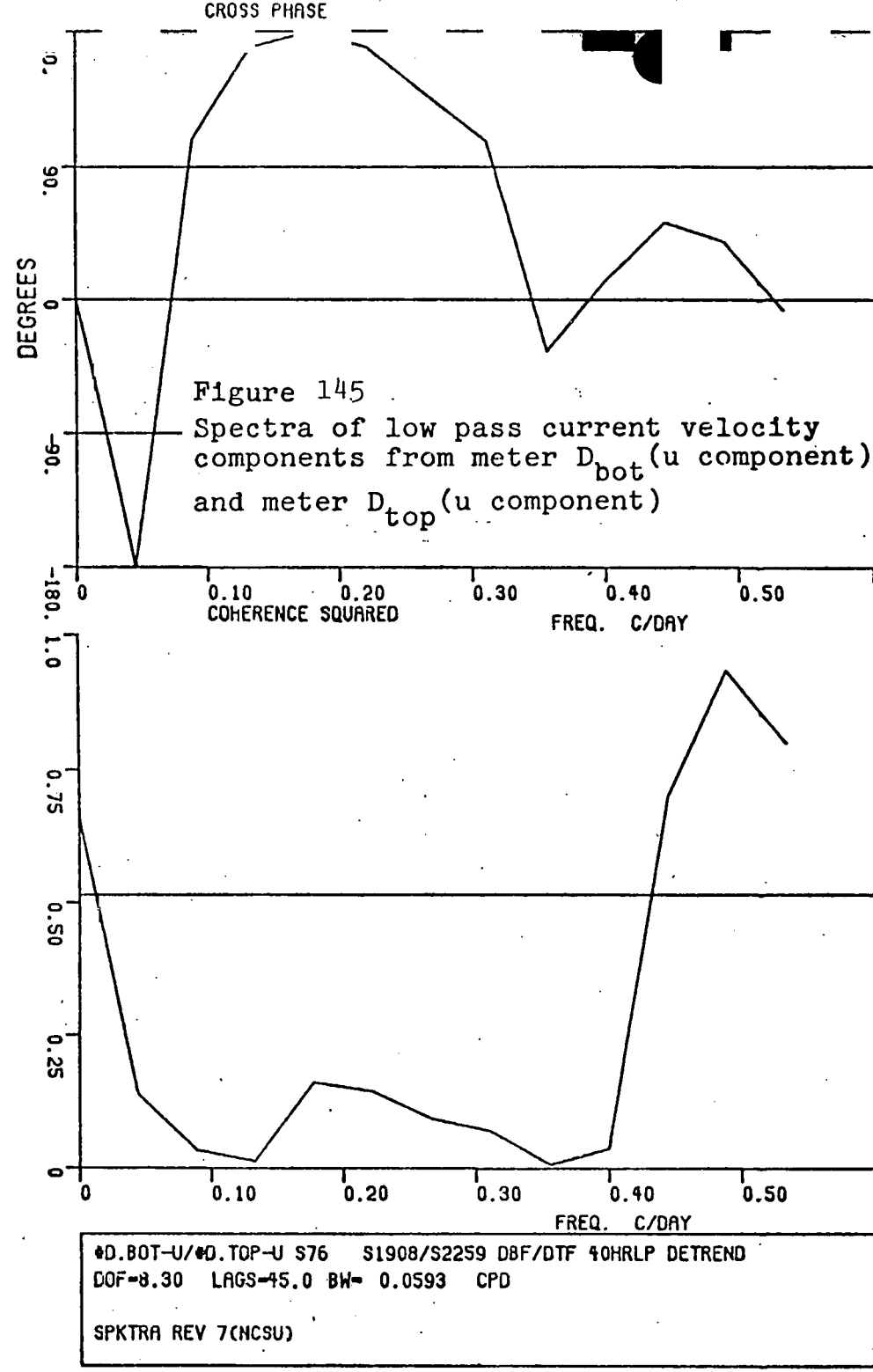

Figure 145
Spectra of low pass current velocity components from meter D_{bot} (u component) and meter D_{top} (u component)

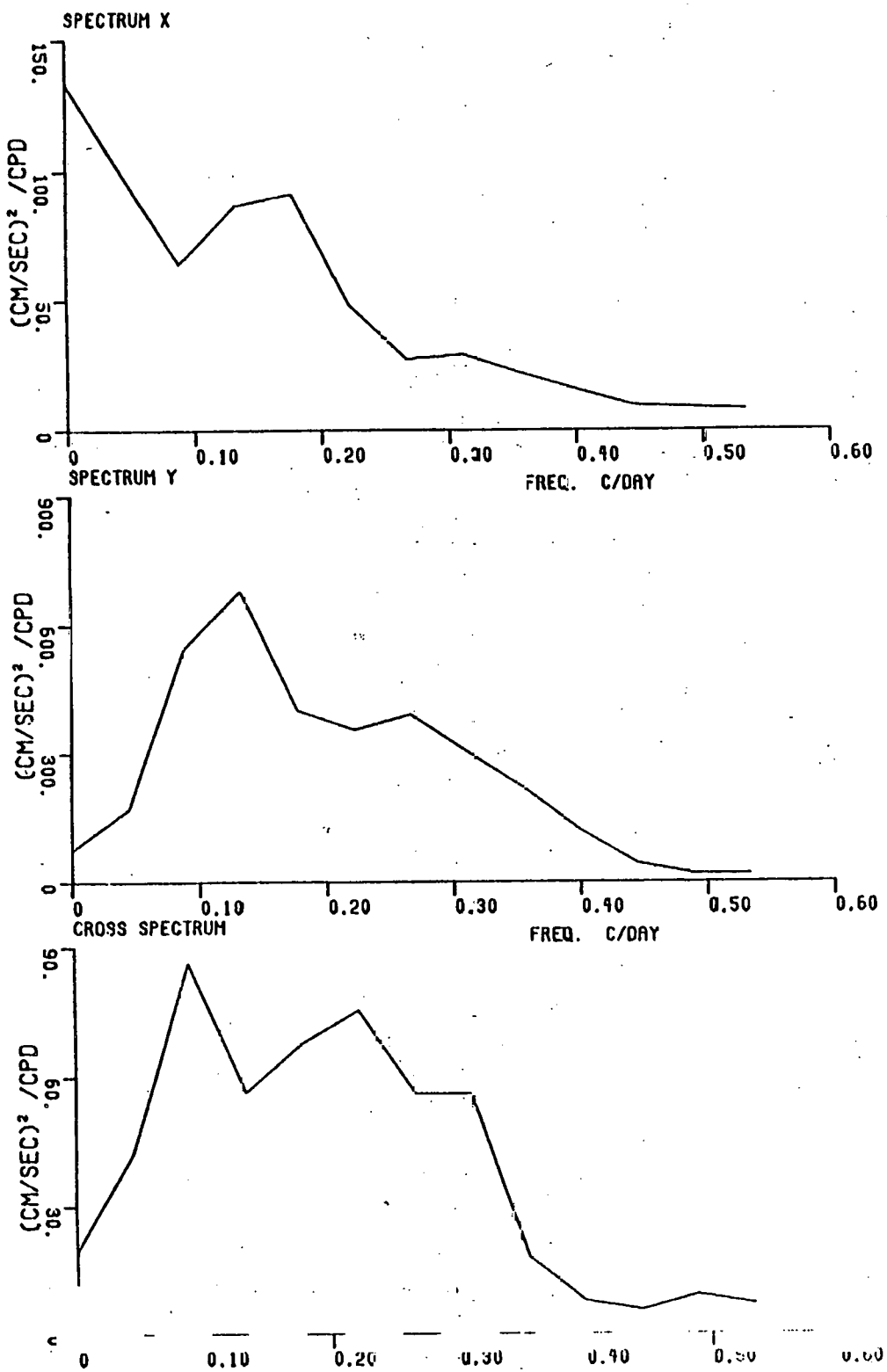

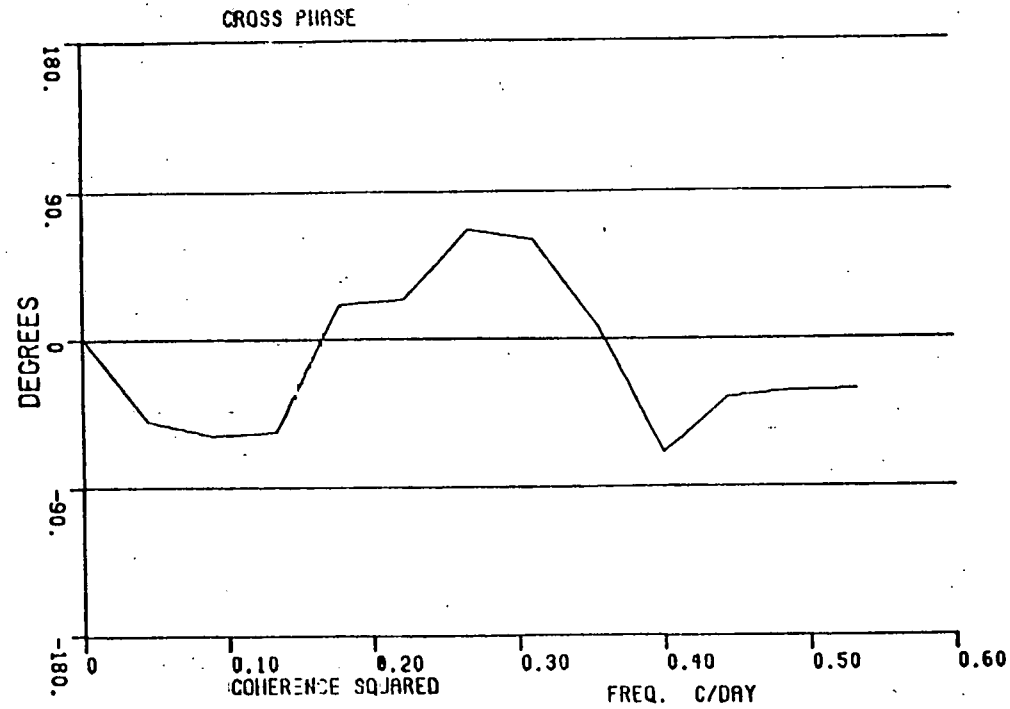

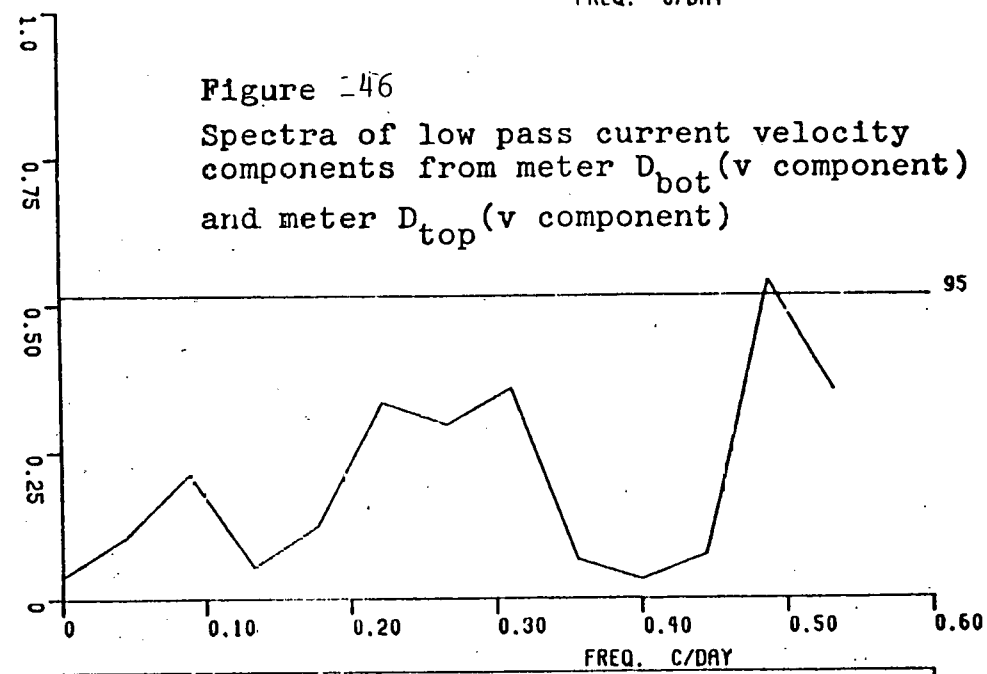

Figure 246
Spectra of low pass current velocity components from meter D_{bot} (v component) and meter D_{top} (v component)

#D.BOT-V/#D.TOP-V 376 S1908/S2259 DBF/DTF 40HRLP DETREND
DOF=8.30 LAGS=15.0 BW= 0.0593 CPD

SPKTRA REV 7(NCSU)

From the point of view of modelling, prediction of tidal currents appears to be tractable because of their regularity and orderliness. Prediction of the low frequency events will be much more difficult however since their driving functions tend to be random and non-stationary. Considerable diagnostic analysis will be required to define the important processes and their coupling with the shelf circulation before reliable predictive models can be realized. The DOE, N.C.S.U., S.K.I.O. and U.M. efforts represent a major step in acquiring such an understanding.

In summary, the velocity structure in Onslow Bay consists of low frequency atmospheric and deep ocean forced motions comprising about 45% of the variance (r.m.s. speed of order 10 cm/s) superimposed upon semi-diurnal tidal oscillations comprising about 53% of the variance (r.m.s. speed again of order 10 cm/s). The remainder of the variance is associated with internal gravity waves, along shore seiches and a associated with the bordering shoals, and turbulence. Mean currents remain poorly defined with magnitudes smaller than the r.m.s. fluctuations. The deterministic tidal currents seem amenable to predictive modelling; however, considerable more analysis of the data sets in hand will be required to understand the low frequency motions which can play a dominant role in mass transport. For example, typical tidal excursions are roughly 1-2 km while the low frequency excursions will typically be roughly ten times larger. Furthermore due to the transient at opposed to oscillatory nature of the low frequency motions their particle excursions are more likely to lead to net transports.

VI. MODELS

BIOLOGICAL MODELING

Consistent with the title of the Department of Energy's integrated Oceanography program in the South Atlantic Bight, we have tried to understand continental shelf processes affecting the oceanography and in that vein have tried to link physical oceanographic and biological observations through the development of mathematical models. It is our intention of developing these models so as to include the higher trophic levels but we have begun, in our effort, by attempting to model the distribution of nutrients, eg. nitrate, on the continental shelf under a variety of wind conditions and presumed offshore, Gulf Stream constraints.

The principal results of the model will deal with the subsequent unsteady distribution of nitrate on the continental shelf in a vertical plane, during an "intrusion" process. The basic intrusion mechanism is presumed to be the mechanical forcing of the wind, but the model is not limited to wind forcing as the driving mechanism. The model is flexible enough to accomodate any current distribution and the wind mechanism is simply presented for the sake of example.

Blanton (1971) proposed the following descriptive model for the intrusion process. During summer conditions, when the shelf water is stratified, intrusions of Gulf Stream water occasionally occur along the bottom. Under these conditions, the bottom velocity has a net onshore component. The colder, more saline, nutrient-rich water moving over the

shelf forms a strong pycnocline at the bottom. Once enough water has been forced onto the shelf and the intrusion has begun to weaken, the pycnocline is found approximately 10-15 meters off the bottom, thus separating the Gulf Stream water from shelf water. Mixing then weakens the pycnocline and Gulf Stream water is mixed upward into the surface layer.

The forcing phenomena for an intrusion is not clearly understood, but intrusions can be induced by the southerly and southwesterly winds associated with the summer northward migration of the Azores-Bermuda High, which would deflect surface waters offshore. The intrusions generated from this upwelling-type process are thus probably compensatory in nature. Meteorological data (Pietrafesa, et. al., 1978) show that during summer months, along the Carolina Coast, when intrusions are prevalent, the dominant winds are from the south-southwest.

Previous studies have not dealt specifically with the effects of intrusions on shelf waters since a common belief appears to be that intrusions are present only at the shelf break and do not extend shoreward of the outer one-third of the shelf. However, it has been observed by DOE investigators in this study, that intrusions quite often reach the near-shore zone (5-10 km. from the beach). Present date indicate that, during their existence, intrusions are a dominant factor controlling primary production in the South Atlantic Bight.

It is of reiterative note herein that we appreciate the fact that Gulf Stream meandering and "eddy" events may be of equal or even greater importance in supplying nutrients to the shelf and we are in fact attempting to include these events in our models presently being formulated.

The distribution of nitrate in intrusion waters is assumed to be governed by the following equation,

$$N_t + uN_x + wN_z - (D_1N_x)_x - (D_2N_z)_z = \text{Biological Terms (Source/Sink)} \quad (1)$$

where u is the horizontal velocity component, w is the vertical velocity component, D_1 is the horizontal diffusion coefficient, D_2 is the vertical diffusion coefficient and the biological terms include any source or sink of nitrate in the system.

The horizontal and vertical velocities have been redefined in terms of the streamfunction, ψ, such that

$$u = \psi_z \text{ and } w = -\psi_x,$$

which allows the continuity equation to be satisfied. Equation (1) now becomes

$$N_t + \psi_z N_x - \psi_x N_z - (D_1N_x)_x - (D_2N_z)_z = \text{Biological Terms (Source/Sink)} \quad (2)$$

Equation (2), a partial differential equation with variable coefficients, is very difficult to handle mathemati-

cally. Therefore, a method is needed to reduce it to a more workable form. In order to do this and for our purposes here, the mathematical technique of separation transformation (Hansen, 1964) has been employed.

Using this method, it is possible to redefine the concentration field of any physical, chemical or biological element in terms of the nondimensional position parameters η and ξ in the following way

$$\eta = \frac{z}{H_L} (\xi)^{\alpha} \text{ and } \xi = (x/L)$$

where x is the horizontal coordinate, L is a characteristic shelf width, z is the vertical coordinate and H_L is a characteristic depth. Alpha is the bottom offshore attenuation exponent. These nondimensional parameters allow one to "hide" the x and z dependence of the system.

In this model the following variable transformations were made.

$$N = N_{o,L} + \Delta N_L(\theta(\eta) \ (\tfrac{x}{L})^{\alpha 1} - \theta(o)) \ F_1(t)$$

$$\psi = \psi_L F_2(t) \ \phi(\eta) \ (\tfrac{x}{L})^{\alpha 2}$$

$$B = B_L F_3(t) G(\eta) \ (\tfrac{x}{L})^{\alpha 3}$$

$$D_1 = D_L F_4(t) \ (\tfrac{x}{L})^{\alpha 4}$$

$$D_2 = D_v F_5(t) \left(\frac{x}{L}\right)^{\alpha 5}$$

where N is the nitrate field transformation, ψ is the circulation pattern transformation, and B is the transformation for the biological terms. The significance of the terms in the nitrate transformation will be discussed and this description applies to all other transformations.

ΔN_L is a scaling parameter which represents some characteristic nitrate difference and $N_{O,L}$ is a characteristic nitrate concentration at the outer edge of the system. The time dependence for the nitrate field is included in the $F_1(t)$ terms. The transformed nitrate field is given by $\Theta(\eta)\xi^{\alpha 1} - \Theta(o)$ where $\Theta(o)$ is the transformed surface nitrate value and $\Theta(\eta)$ is the transformed nitrate field. The ξ term allows the curve that describes the nitrate field to stretch or shrink in the vertical as it moves about in the system. The similarity parameter, α_1, determines the horizontal gradient of the nitrate field and is referred to as an attenuation exponent. It is assumed that D_1 and D_2 change only in the horizontal direction, therefore the transforms for these variables do not include a function of η.

After substituting these transformations into equation 2, and assuming that $h(x) = h_L\left(\frac{x}{L}\right)^{-\alpha}$, as well as, that the system has a particular dependence on ξ which allows that parameter to be eliminated from the equation, one generates the similarity conditions

$$\alpha_1 = \alpha_2 + \alpha_1 + \alpha - 1 = \alpha_4 + \alpha_1 - 2 = \alpha_5 + \alpha_1 + 2\alpha = \alpha_3$$

and the transformed equation becomes

$$\alpha^2\eta^2 + \frac{D_v L^2 F_5(\tau)}{D_L H^2 F_4(\tau)} \frac{\partial^2\Theta}{\partial\eta^2}(\eta,\tau) - \frac{L^2}{TD_L F_4(\tau)} \frac{\partial\Theta}{\partial t}(\eta,\tau)$$

$$\alpha_1\alpha_4 + (2\alpha_1 + \alpha - 1)\alpha\eta - \alpha_2 \frac{\psi_L L F_2(\tau)}{D_L H_L F_4(\tau)} \phi(\eta) \frac{\partial\theta}{\partial\eta}(\eta,\tau) \tag{3}$$

$$\alpha_1\alpha_4 + \alpha_1(\alpha_1 - 1) + \alpha_1 \frac{\psi_L L F_2(\tau)}{D_L H_L F_4(\tau)} \frac{\partial\phi}{\partial\eta}(\eta) \quad \theta(\eta,\tau) =$$

$$- \frac{B_L L^2}{D_L \Delta N_L F_4(\tau)} \quad G(\eta,\tau)$$

which is now an equation in two variables η and τ.

Inspection of Equation 3 reveals three nondimensional numbers. The first gives a relationship between vertical and horizontal diffusion and the second is a relationship between advection and horizontal diffusion. Both are modified by the characteristic length and depth chosen for the system. The third nondimensional number indicates the relative importance of the biological terms to physical terms in the equation. It is by manipulating these nondimensional numbers and the similarity attenuation exponents that unique solutions are generated. Figure 147 shows the different bottom profiles that can be generated by simply varying the bottom offshore attenuation exponent.

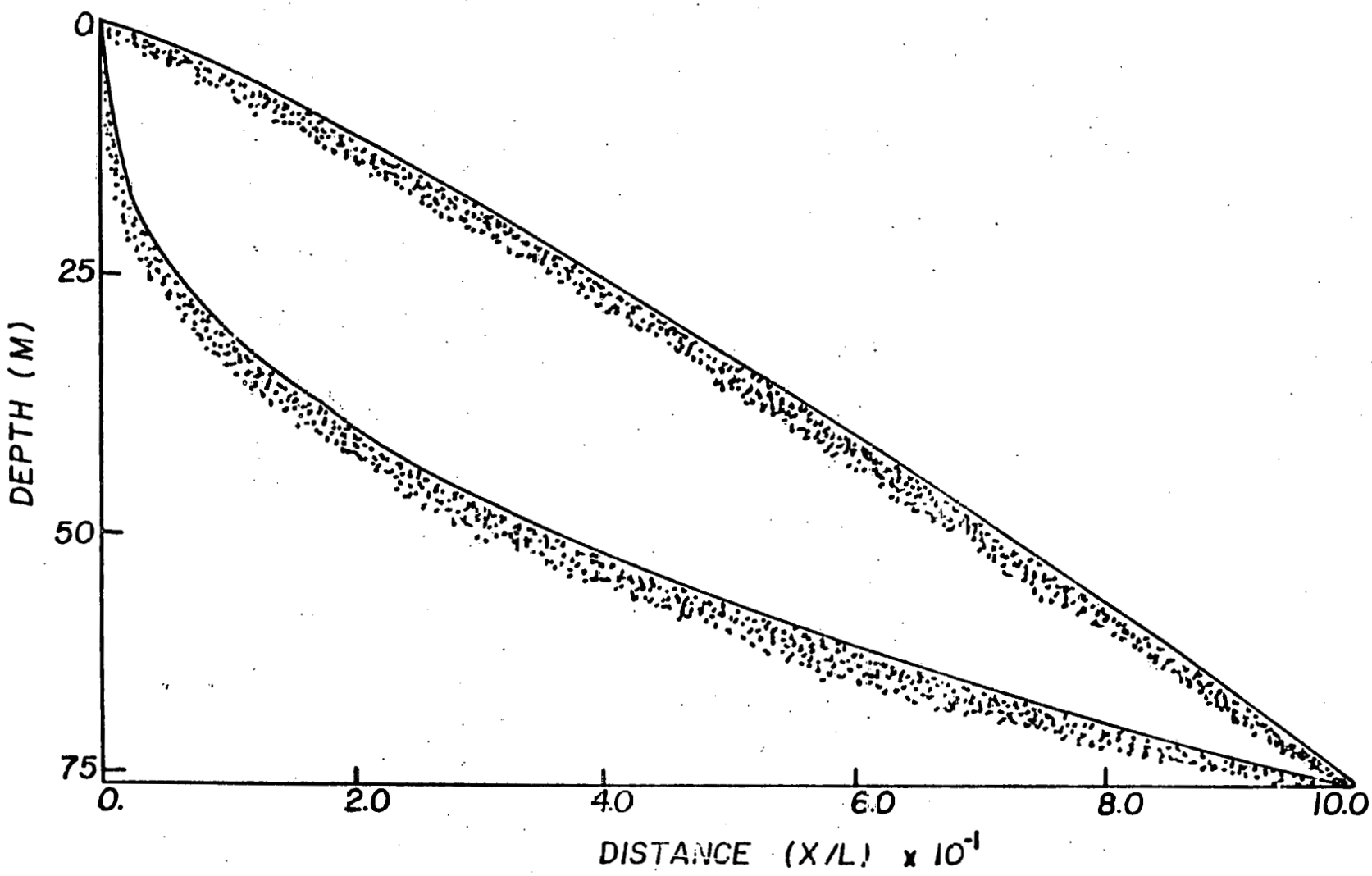

Figure 147 Bottom profiles generated with bottom offshore attenuation exponent equal to -.4 and -1.2. The x axis is nondimensional distance offshore.

In order to solve equation 3 it is necessary to impose certain constraints or boundary conditions on the system. These are as follows:

1. Flux of nutrients in or out of the surface is equal to N surface.

2. Flux of nutrients in or out of the bottom is equal to N bottom.

3. A difference condition imposed at the shelf break. The bottom nitrate concentration minus the surface nitrate concentration is equal to some number δN. This condition allows the system to "feel" the input or presence of the Gulf Stream.

The first two conditions are the conditions for the differential equation and the third condition determines the value given to the nitrate attenuation exponent, α_1.

Expressed mathematically these conditions become

1. $N_z = N_{surface}$ at $Z = 0$.
2. $D_2 N_z + D_1 N_x h_x = N_{Bottom}$ at $z = h$.
3. $N(L,H_L) - N(L,0) = \delta N$

and substituting the assumed transformations gives

1. $\theta_\eta(0) = N_s$ (where H surface = 0, for convenience here)
2. $\theta_\eta(1) + (H_L^2 D_L / L^2 D_v)\ (\theta_\eta(1)\ \alpha^2 + \theta(1)\ \alpha\alpha_1) = N_b$.
3. $\theta\ (1) - \theta(0) = \delta N / (N_L F_1(t))$

Thus, the complete mathematical system is second order

and is characterized by the eigen value, α_1.

The above model was coupled with the following barotropic circulation system based on Pietrafesa (1973) and Pietrafesa, et. al. (1978). The relationship defining the circulation is proposed, for the sake of this model, to be

$$\phi(\eta) = e^{T\eta}(A_1 \text{ Cos } T\eta + A_2 \text{ Sin } T\eta) + e^{-T\eta}(A_3 \text{ Cos } T\eta + A_4 \text{ Sin } T\eta) + A_5$$

where A_1, A_2, A_3, A_4, A_5 and T are constants.

This circulation model allows one to consider various wind directions. However, for this problem, the primary interest is in winds blowing from the south-southwest, since this will induce an Ekman transport offshore.

Two different time dependencies were used to describe the flow field regime. In the first the water column responds immediately to the wind and there is an onshore movement of Gulf Stream water at the bottom (Figure). By the fifth day, there is little change in the flow field except for further penetration of the Ekman layer (Figure).

The second time dependence includes the effect of a closkwise or anticlockwise rotating wind stress and it is evident that the response of the water column (Figure) is not as fast or dramatic as the previous case. It takes a wind system like this five days to reach the velocities

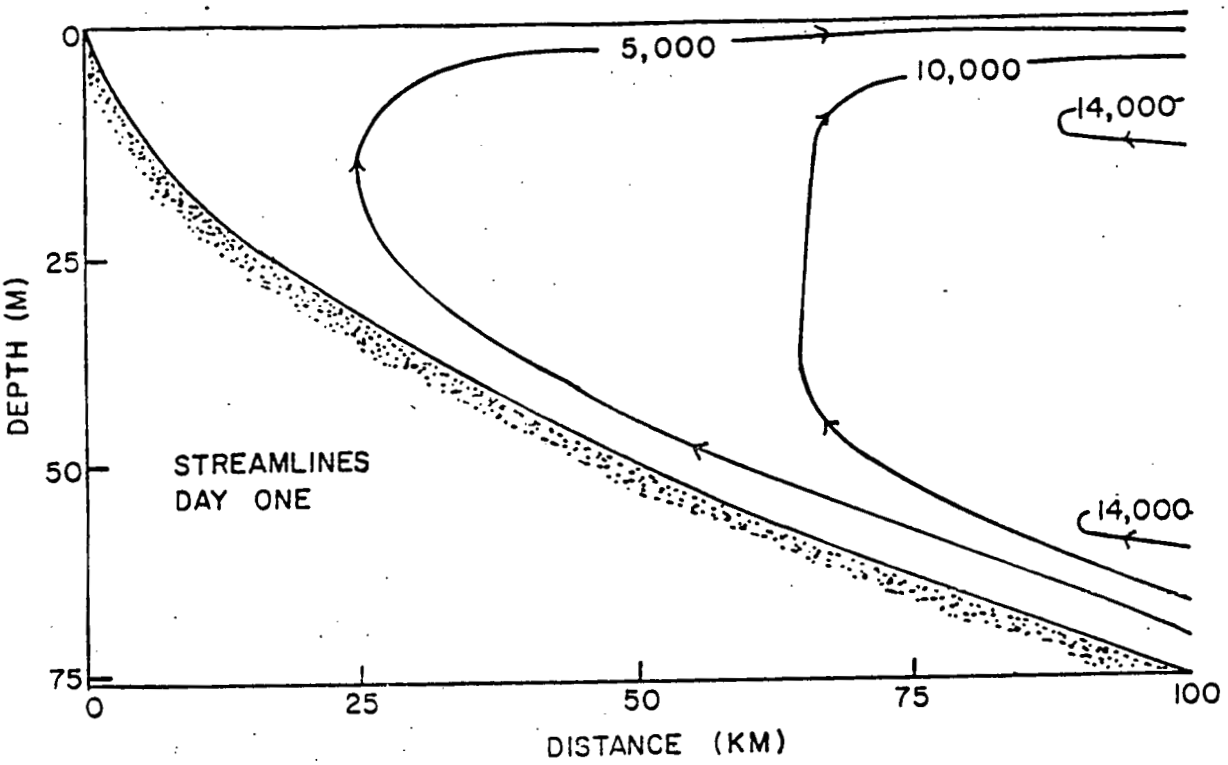

Figure 148 Streamline contours for case in which the water column responds immediately to the wind.

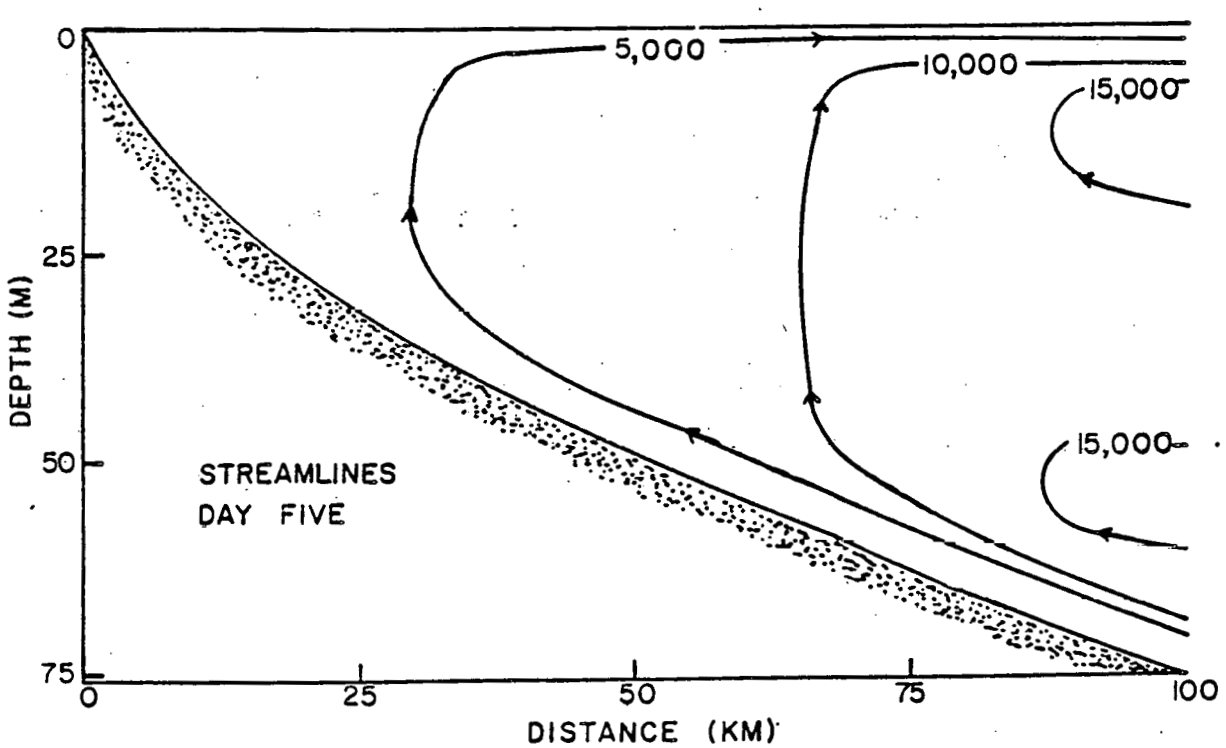

Figure 149 Streamlines show little change except for deepening of the Ekman layer.

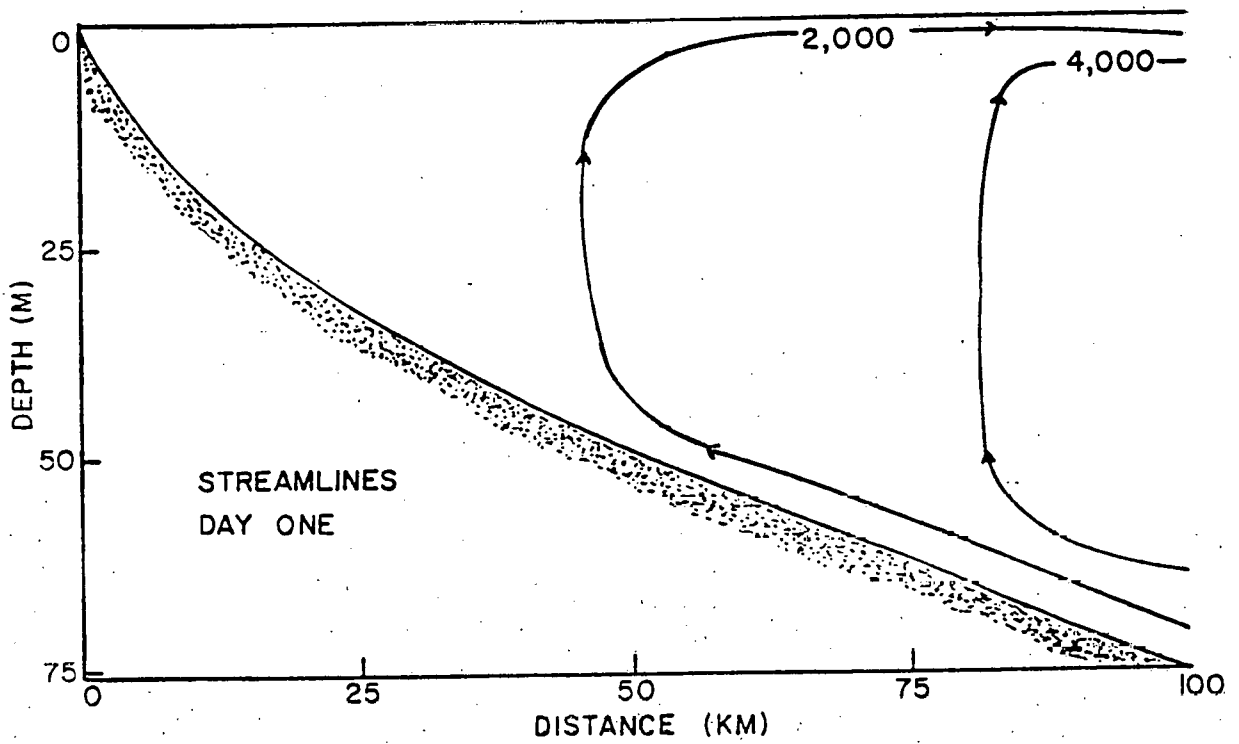

Figure 150 Streamline contours for case that includes the effect of a clockwise or anticlockwise rotating wind stress.

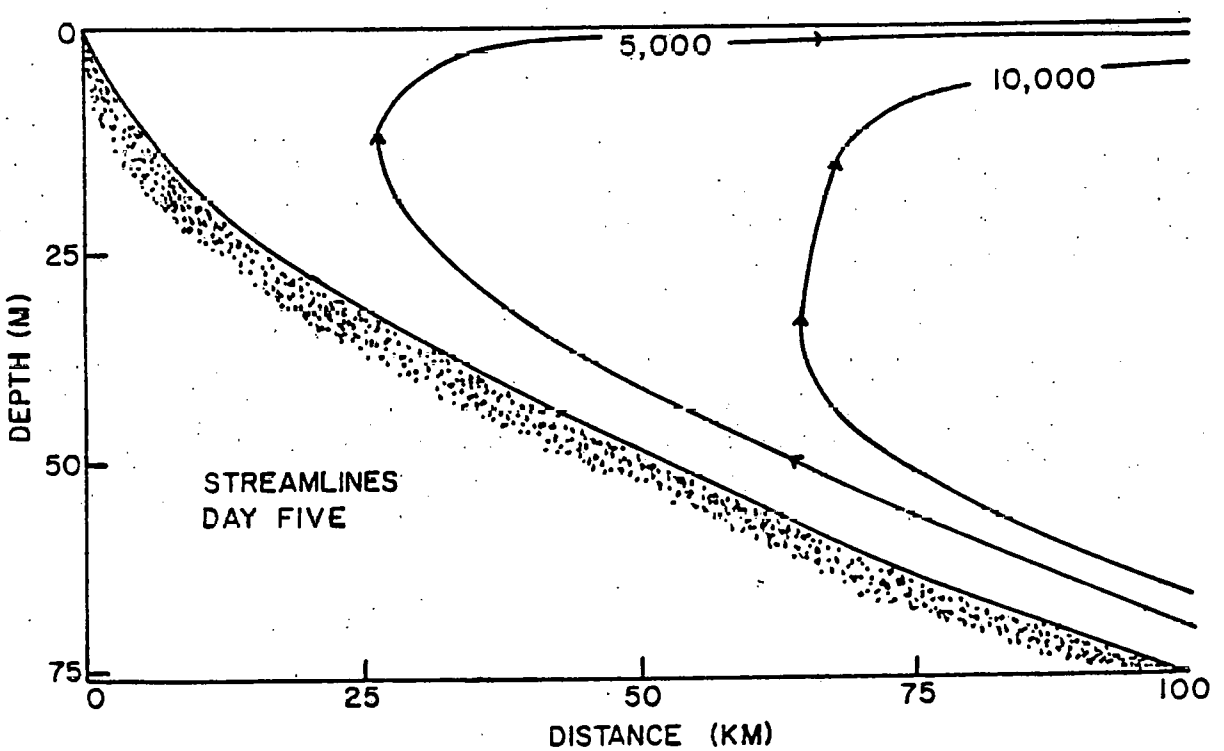

Figure 151 Streamlines after five days.

shown on the first day of the previous example (Figure 151) Current meter data (Pietrafesa, et. al., 1978) indicate that the first case is more like actual current response to wind forcing.

Biological Processes

The biolgocial terms included in this system are: phytoplankton uptake of nitrate, extracellular release by phytoplankton, excretion by zooplankton, excretion by fish, decomposition by detritus, nitrogen fixation by Blue-Greens, regeneration from bottom sediments. In the transformed system, equation 3, B_L is a scaling parameter and allows for scaling relative to the largest biological term.

Each biological term will be discussed and its importance will be determined. Values for the biological processes were obtained primarily from the literature, but when possible field measurements made during intrusions have been incorporated.

Nitrate Uptake

A basic assumption of this model is that nitrate uptake follows Michaelis-Menton kinetics (Dugdale, 1967) which is given by

$$V = \frac{V_m N}{K_s + N}$$

where V is the uptake rate of nitrate N, V_m, is the maximum uptake rate that can be obtained by elevating the nutrient

concentration and K_s is the Michaelis constant or half saturation constant.

The value used for uptake velocity in this model is 1.2×10^{-2} μg-at/l, which is the maximum uptake velocity determined for D. brightwelli. This value was chosen because D. brightwelli is similar in size to Rhizo. alata which field studies have shown to be the most abundant phytoplankton during an intrusion. This value was multiplied by 1.93×10^{5} cells (Rhizo.)/l to give an uptake velocity of 6.43×10^{-5} μg-at NO_3/l-sec.

Extracellular Release by Phytoplankton

Williams and Yentsch (1976) measured the chemical characteristics of the water column in which they carried out their phytoplankton excretion experiments. They determined a range for nitrate excretion of 0-.1 μg-at/l.

Using these values for nitrate excretion and a time scale for loss of the absorbed nutrient of 40 hours, a value on the order of 10^{-7} μg-at NO_3/l-sec for extracelluar release of phytoplankton can be calculated.

Zooplankton Excretion

The zooplankton excretion term was determined in the following manner. Data collected by Raffenhöfer (Skidaway Institute) on copepod species and density in Georgia coastal waters indicate seasonal variation in the copepod populations, the most abundant population being present in August. Using

these values and the ash free weights for the various copepod species, values ranging from 20-120 μg ash-free st/l are obtained. Corner and Newell (1967) have determined excretion rates for zooplankton populations in Plymouth Sound of 2-5 μg-at N/mg dry body wt-day. If it is assumed that 1% of the nitrogen excreted is in the form of nitrate, a number for zooplankton excretion on the order of 10^{-8} μg-at NO_3/ l-sec is obtained.

Fish Excretion

Fish densities on the order of 10^{-5} grams of fish /l can be calculated for Onslow Bay waters using catch figures determined by Struhasker (1969). Using data presented by Wood (1958) excretion rates of approximately 10^{-8} μg-at N/l-sec per fish can be calculated. If 1% of this is considered to be in the form of nitrate, an excretion rate for marine fish of approximately 10^{-10} μg-at NO_3/ l-sec per fish is calculated. When multiplied by the calculated fish density a number on the order of 10^{-15} is obtained. This number is extremely small and can be neglected since it will not significantly contribute to the nitrate concentration in Onslow Bay waters.

Decomposition of Particulate Matter

Particle data collected by Paffenhöfer for Onslow Bay waters show approximately 120 μg C/l. Chlorophyll a data collected at the same time show values of 0.7 μg chlorophyll a /l, a very low value. This concentration converts to

approximately 40 μg C/l for a well growing phytoplankton population and when subtracted from the particle value, a value of 80 μg C/l is obtained. This value is high and leads one to believe that particulate matter could be an important source of nutrients (Von Brand, et. al., 1937) in the system as well as an important food source for zooplankton. (Baylor, et. al., 1963; Paffenhofer, et. al., 1970; Poulet, 1976).

If one assumes that 2-15% of the particulate matter decomposition is nitrate, then values ranging from 1.6 to 12 μg-at NO_3/ are obtained. If one further assumes a regeneration rate of approximately two days, a range of values from 7.86×10^{-6} μg-at NO_3/l-sec to 6.94×10^{-5} μg-at NO_3/l-sec is obtained for detrital decomposition.

Nitrogen Fixation by Blue-Greens

Dunstan, et. al., (1976) found Oscillatoria sp. to be present in Georgia coastal waters in concentrations of approximately 1000 filaments/l. Using this concentration and nitrogen fixation rates determined by Carpenter and McCarthy (1975) for Oscillatoria thie. in the western Sargasso Sea he calculated a nitrogen fixation rate of 1.4 μg-at/l-year for Georgia Bight waters. When converted to a per second basis the value for nitrogen fixation becomes 3.65×10^{-6} μg-at/lsec. This value is substituted into the right-hand side of the surface boundary condition and allows a flux of nutrients across the surface.

Regeneration From Bottom Sediments

Rowe *et al*. (1976) performed *in situ* experiments in which a given amount of bottom sediment was incubated for various lengths of time and the amount of nutrient regeneration measured. Their results show bottom regeneration rates of nitrate ranging from 0.15-21.08 μg-at NO_3/m^2-h. When converted to a per second basis this gives values of order 10^{-5}-10^{-3} μg-at NO_3/m^2-sec. This value is substituted in the right-hand side of the bottom boundary condition and allows for a flux of nutrients into or out of the bottom.

Scale Analysis

Scale analysis provides a method for deciding the important components of a system and determining the importance of one component relative to another. Scaling of this model indicates that the biological processes are of the same order of magnitude as the advective-diffusive physical processes and cannot be neglected. Substitution of the values determined for the biological processes into the right hand side of equation 3 yields

$$\text{LHS} = \frac{B_L L^2}{D_L N_L} \left(\underset{\text{uptake}}{10^{-5}} - \underset{\substack{\text{Det.}\\\text{Decomp.}}}{10^{-6}} - \underset{\substack{\text{Zoo}\\\text{exc.}}}{10^{-8}} - \underset{\substack{\text{phyto.}\\\text{exc.}}}{10^{-7}} - \underset{\substack{\text{fish}\\\text{exc.}}}{10^{-15}}\right)$$

and scaling relative to uptake gives

$$\text{LHS} = \frac{10^{-5} L^2}{D_L \quad N_L} \left(1 - \underset{\text{uptake}}{} \underset{\substack{\text{Det.}\\\text{Decomp.}}}{10^{-1}} - \underset{\substack{\text{Zoo}\\\text{exc.}}}{10^{-3}} - \underset{\substack{\text{phyto.}\\\text{exc.}}}{10^{-2}} - \underset{\substack{\text{fish}\\\text{exc.}}}{10^{-10}}\right.$$

This indicates that detrital decomposition could play a role in the regeneration of nutrients and possibly in the absence of an intrusion could supply an important source of nutrients.

From the scaling analysis, it seems that the basic terms involved in the nitrate balance are; time dependence, advective-diffusive processes and biological terms. Since the solutions for this model were obtained numerically, all orders of effects are included.

Examples of Results

It is recognized that many combinations of parameters are possible; however, the cases presented here represent what is considered to be a meaningfully adequate minimum number of situations.

In this first example case the ranking of the physical processes (determined by the values given the nondimensional numbers) is as follows: vertical diffusion weaker than horizontal diffusion and horizontal advection of the same order as horizontal diffusion.

The results (Figures 152-3) show little change in the nitrate contours from day one to day four, except for a slight shoreward migration of the nitrate isopleths. This type of situation is not typically found in field data.

Next, for a second example let vertical diffusion be slightly larger than horizontal diffusion and horizontal advection stronger than horizontal diffusion.

After the first day (Figure 154 the 2 μg-at/L isopleth

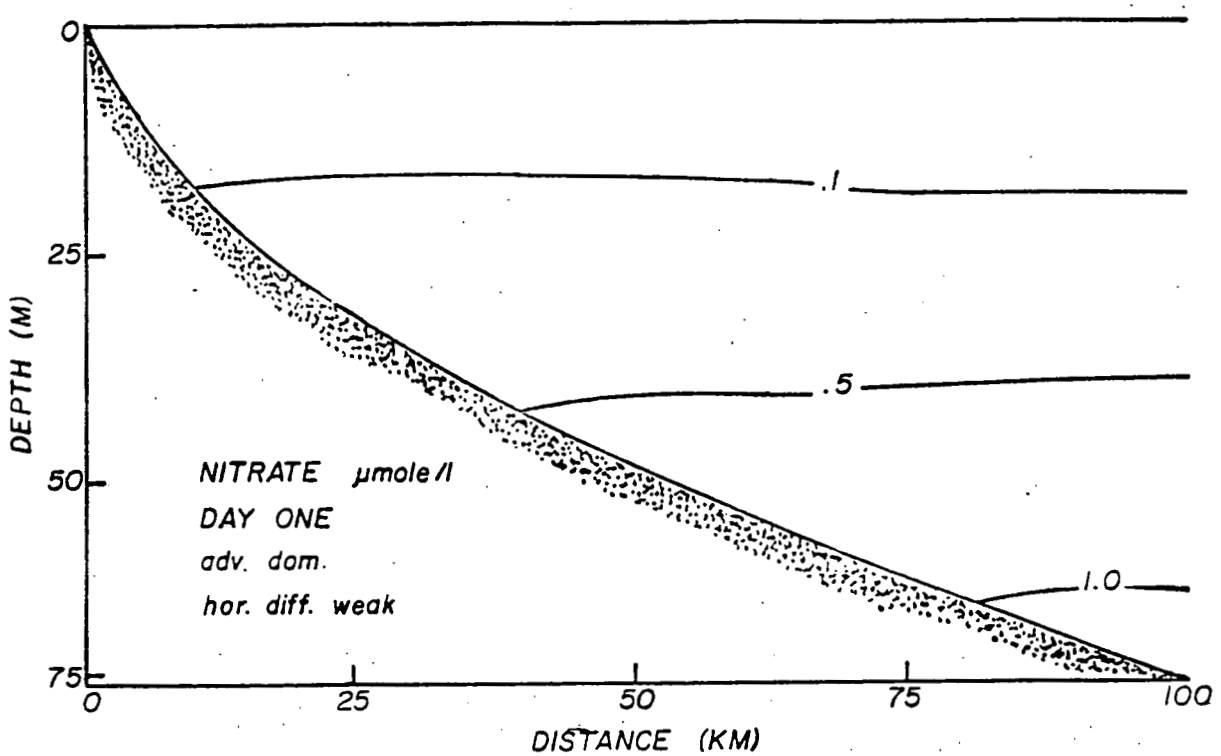

Figure 152 Nitrate profile after one day.

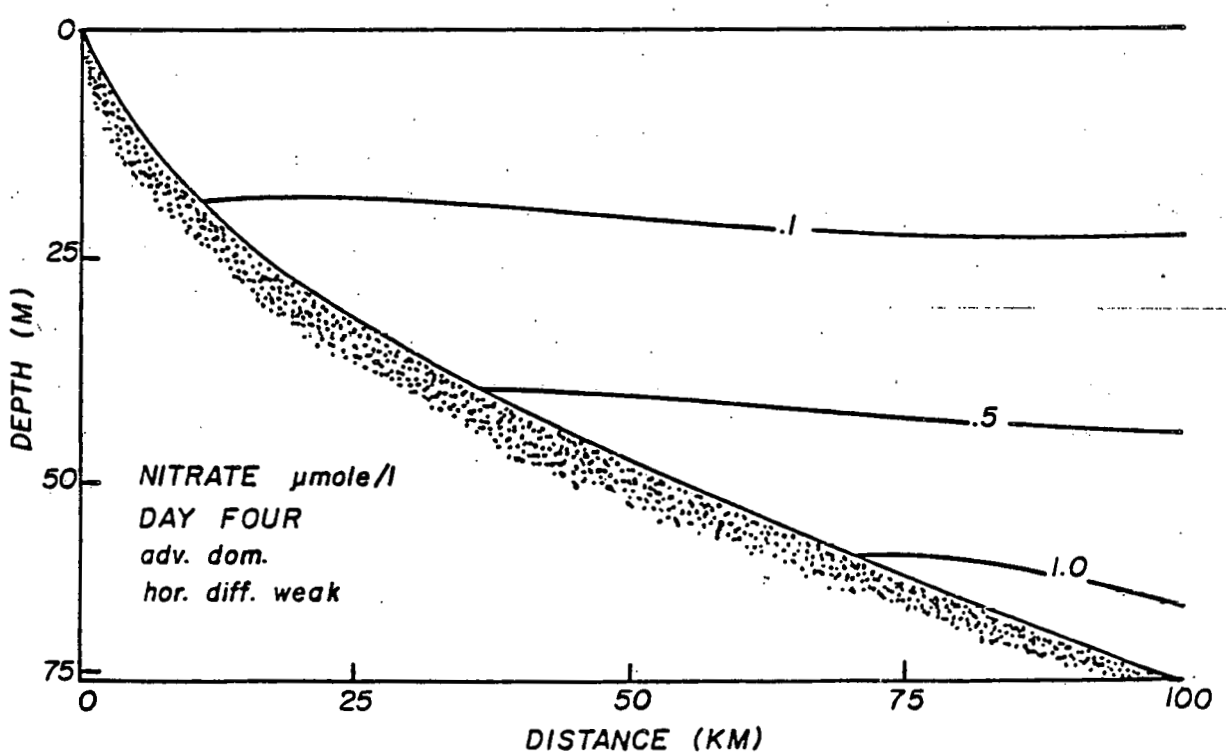

Figure 153 Nitrate profile after four days.

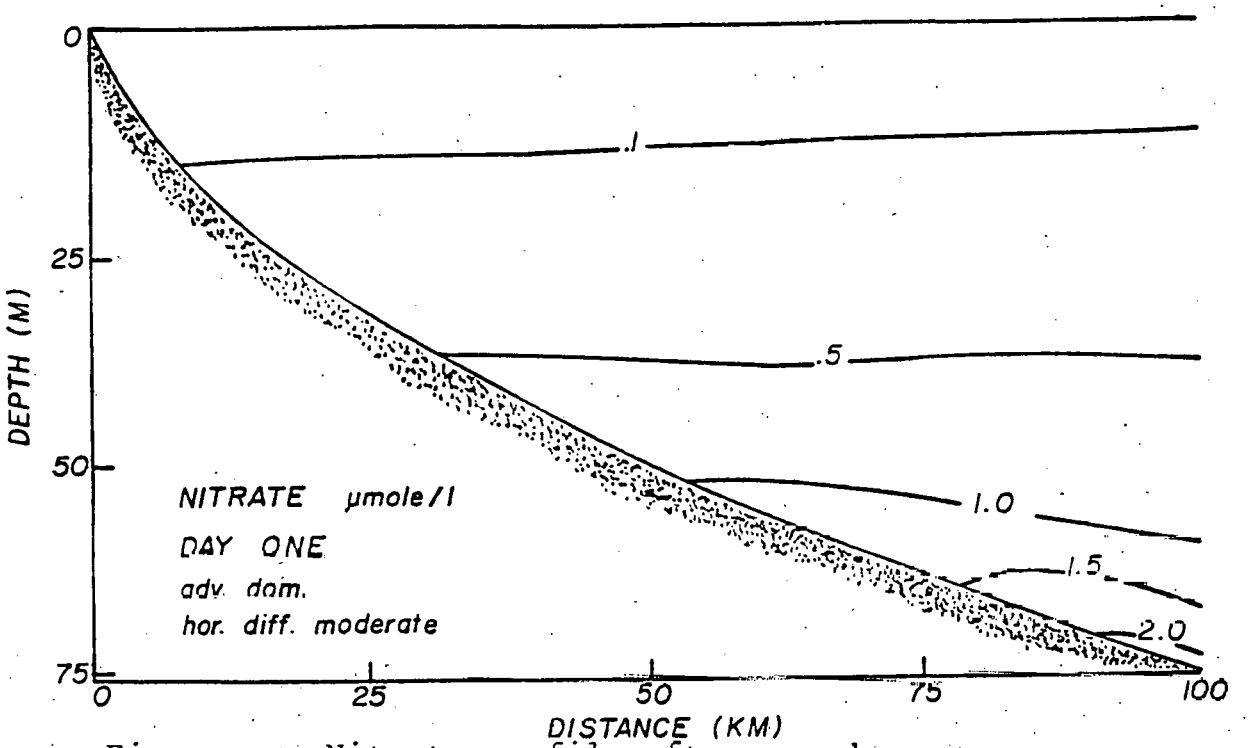

Figure 154 Nitrate profile after one day.

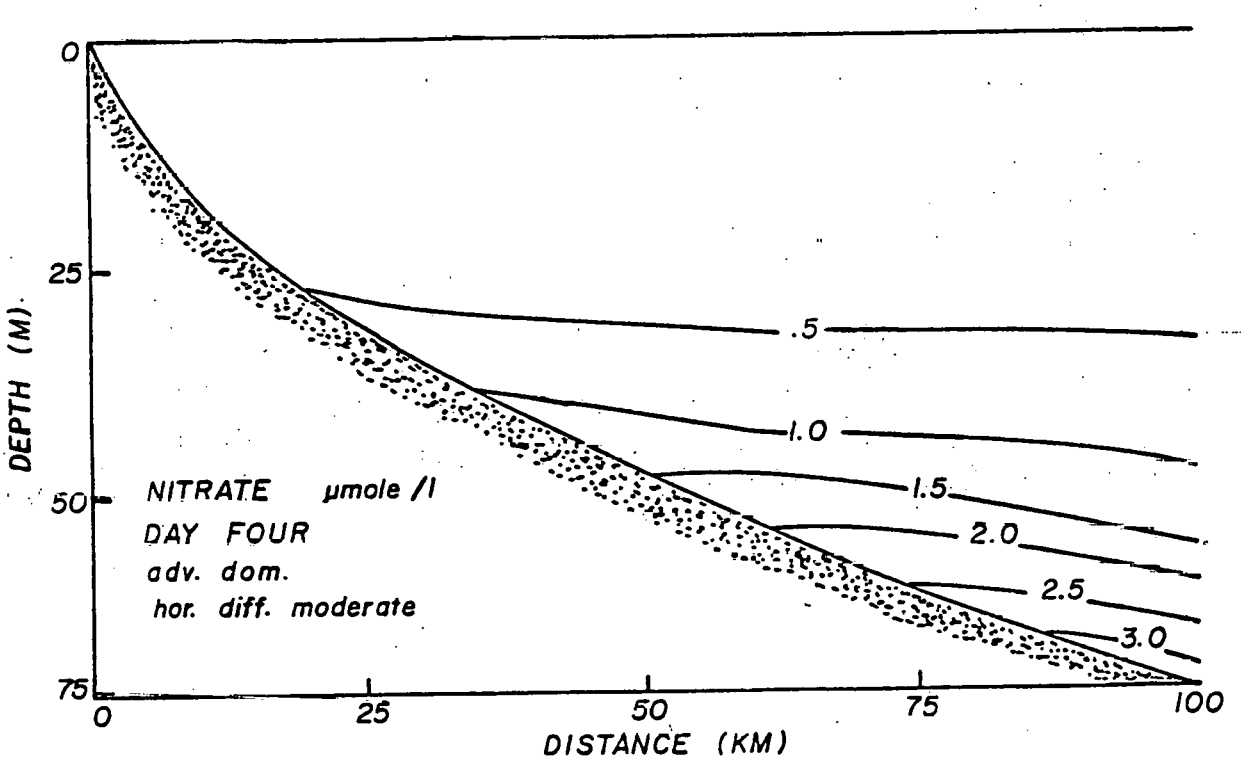

Figure 155 Nitrate profile after four days.

appears at approximately seventy meters. There is a gradual build up of nitrate, until by day four (Figure 155 the 3.0μg-at/L isopleth appears at the shelf break. By this time the wind has decreased in intensity which slows the upwelling of nitrate, while phytoplankton uptake is continuing to remove nitrate. Therefore, there are no rapid changes in nitrate concentration. It is important to note that by the fourth day the 1.0 μg-at/L isopleth has moved up onto the shelf and is about one-half to two-thirds of the way across the shelf.

Figure 156 is a nitrate profile characteristic of intrusions seen in Onslow Bay. It is apparent that the simulation results correspond to the measured nitrate distribution; however, the simulated nitrate field does not extend as far shoreward.

The order of the physical processes for the third example case is: vertical diffusion much stronger than horizontal diffusion.

After the first day, the 1.0 μg-at/L isopleth is already approximately two-thirds of the way across the shelf and the vertical profile seen after four days shows a strong vertical gradient of nitrate (Figures 158-159). This type of profile is not typical for Onslow Bay, but a similar profile was seen in field data after the passage of Hurricane Belle (August 9, 1976). Figure 157 shows the high nitrate concentrations found on the shelf four to five days after the passage of the

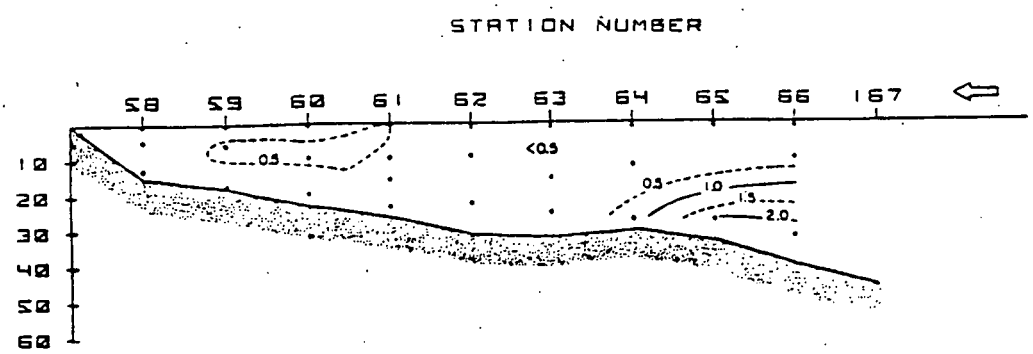

Figure 156 Nitrate profile seen in Onslow Bay July 14-15, 1976. Data from Singer, et.al., 1976.

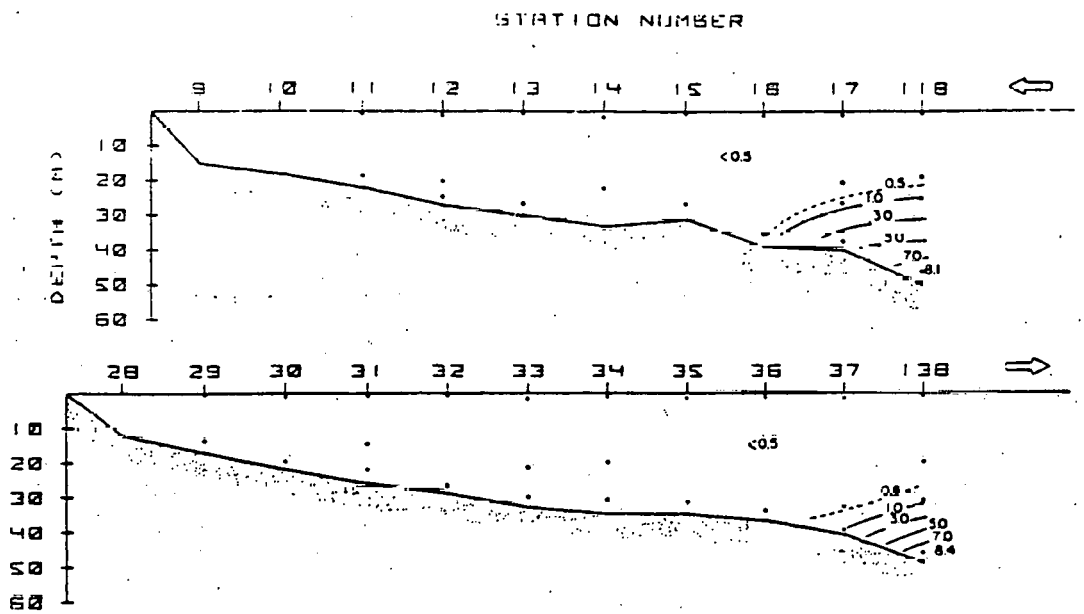

Figure 157 Nitrate profiles seen in Onslow Bay August 14-16, 1976. Data from Singer, et.al., 1976.

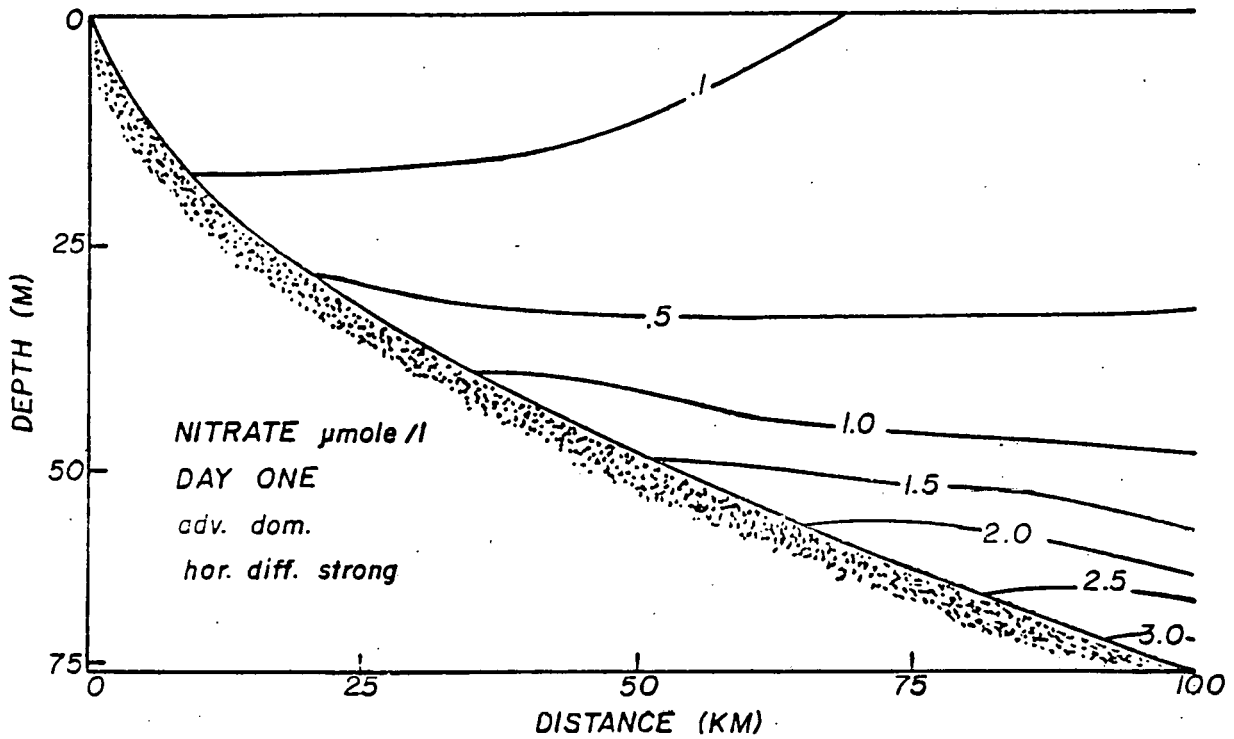

Figure 158 Nitrate profile after one day.

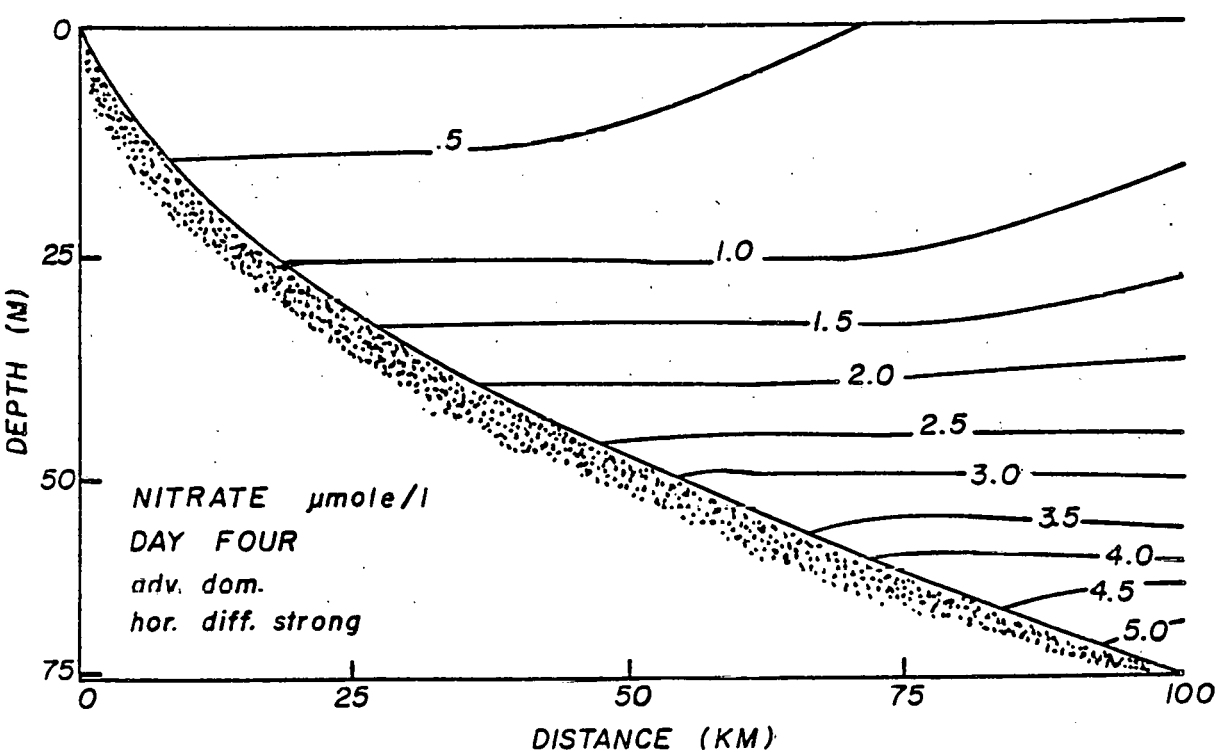

Figure 159 Nitrate profile after four days. Note high nitrate valves and strong stratification.

hurricane.

One intriguing aspect of this system is the effect of the vertical diffusion coefficient. A value of 30 cm^2/sec was used which can be considered as an average over the water column and is larger than values generally quoted for shelf waters. However, Marchuk et al. (1977) report values ranging from 80 to 390 cm^2/sec for surface eddy viscosity coefficients during a tropical storm. Since this coefficient changes dramatically with depth, an average value of 30 cm^2/sec may be reasonable for a vertical diffusion coefficient. This leads one to believe that the hurricane produced intense currents (supported by Pietrafesa's current meter data) which resulted in the movement of large amounts of nutrient rich water onto the shelf.

Introducing a light attenuation term in the left hand side of equation (3) gives depth dependence to the biological processes, i.e., they decrease exponentially with depth. Also, a time lag was incorporated into the nitrate uptake term, since it is not likely that phytoplankton begin removal of nitrate immediately (Eppley, et. al., 1969). Adding these two refinements to the previously discussed system, the nitrate profiles shown in Figures 160 thru 163 are produced.

The intrusion seen in Figures 160 and 164 is similar to the one seen in Figures 152 and 153 except that in the first case the horizontal diffusion coefficient has been reduced by an order of magnitude. Comparison of Figures 162 and 163 with

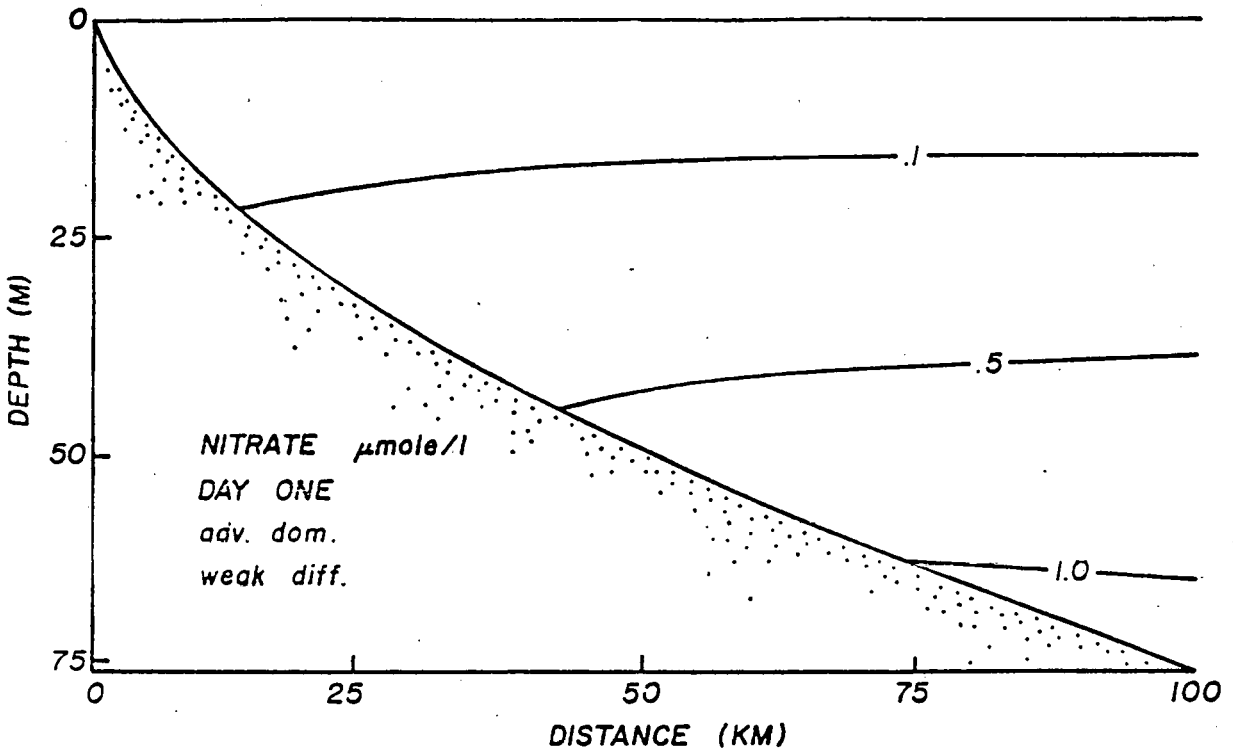

Figure 160 Nitrate profile after one day.

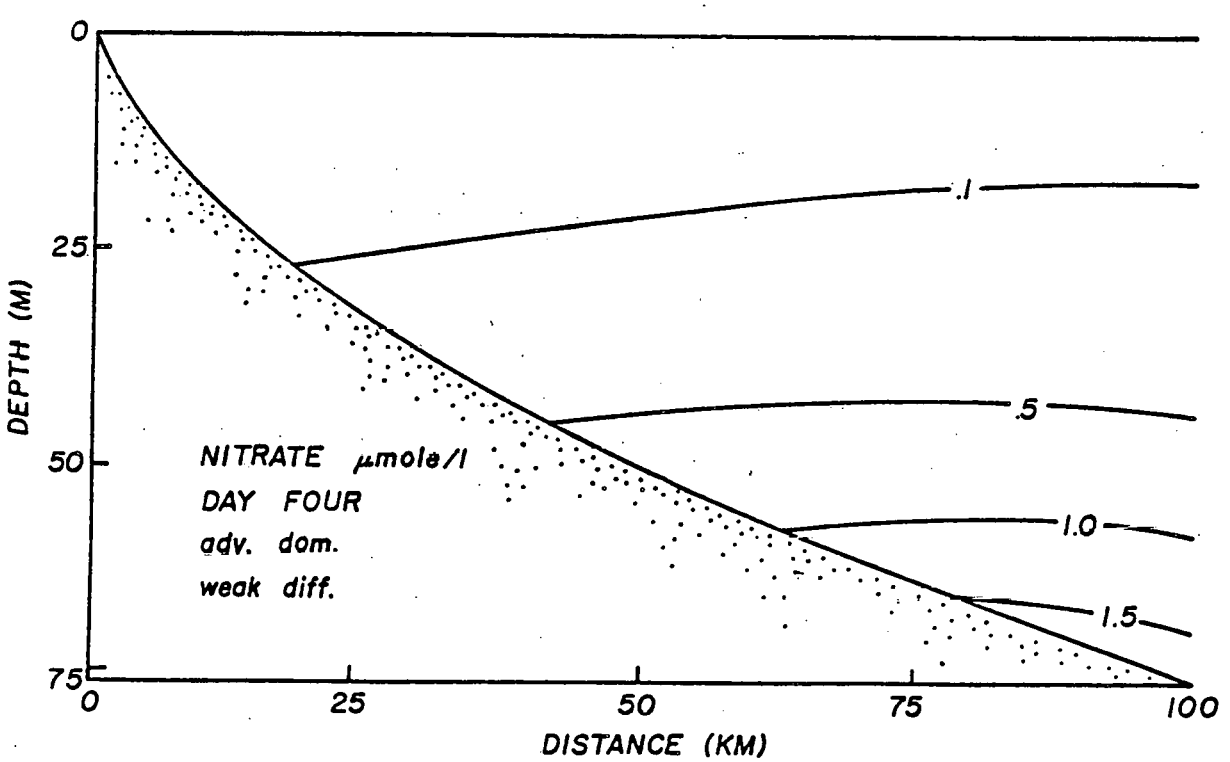

Figure 161 Nitrate profile after four days.

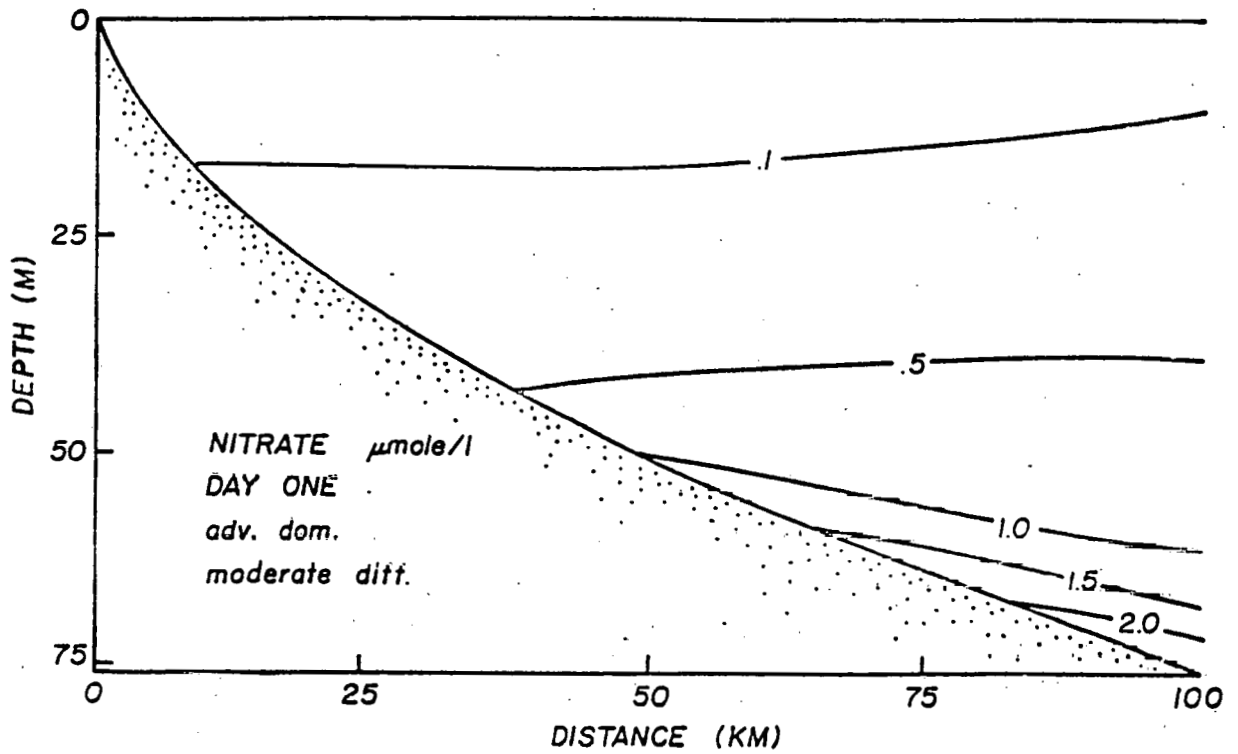

Figure 162 Nitrate profile after one day.

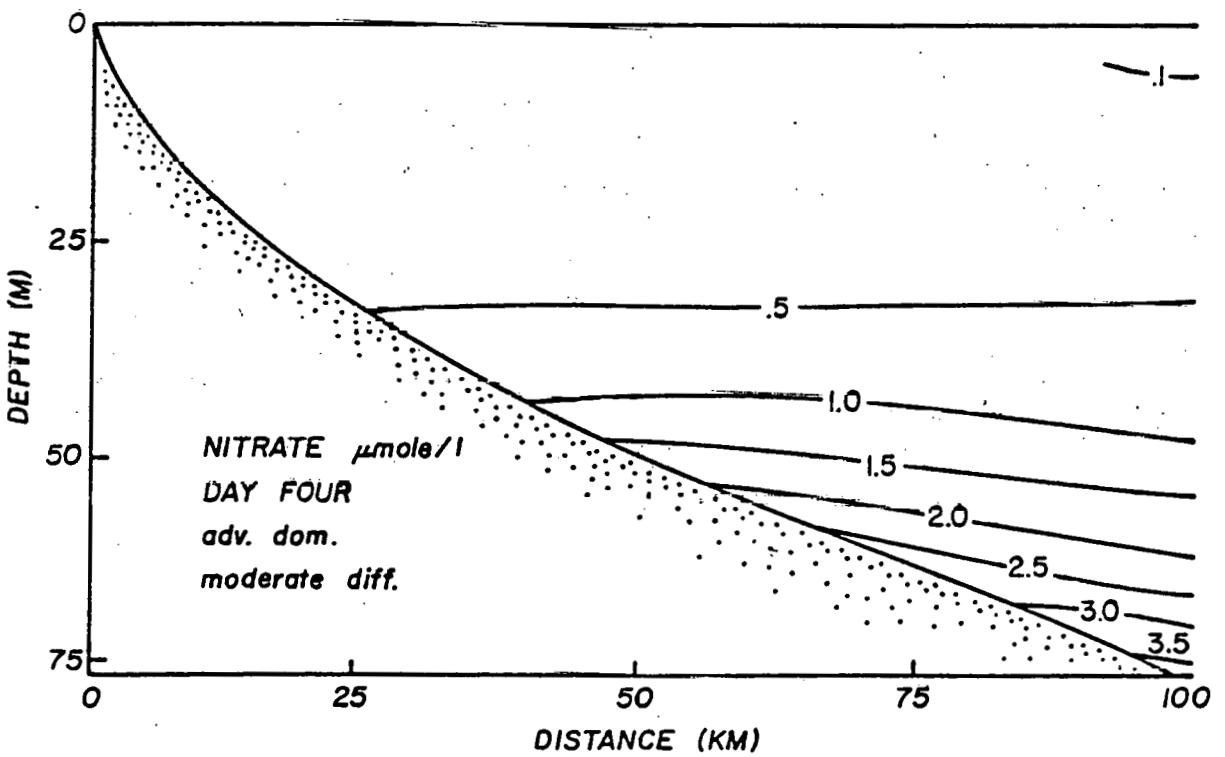

Figure 163 Nitrate profile after four days.

Figs. 154 and 155 also show similar profiles and again the horizontal diffusion coefficient has been reduced by an order of magnitude. The vertical structure of the nitrate field in Figure 162 is more like those seen in field data since the stratification is confined to the lower twenty-five meters of the water column.

Figures 164 thru 167 show that the vertical structure of the nitrate field can be modified by changing the bottom similarity attenuation exponent. The bottom topography primarily affects the flow velocities and this has an important secondary effect on the nitrate distribution.

The nitrate profiles generated with $\alpha = -.2$ and $\alpha = -1.0$ do not resemble any seen in field data. The nitrate isopleths extend too far shoreward and the depths of the nitrate isopleths are not consistent with measured values. Also, the bottom profile is not similar to that of Onslow Bay.

Comparison of these figures to Figures 162 and 163 show that the concentrations of nitrate are correct, but the "bubble" of nitrate formed near the bottom in an intrusion has not developed.

Conclusion

The results generated by this model clearly indicate that it is possible to stimulate primary productivity in Onslow Bay by periodic "intrusions" of nutrient-rich subsurface Gulf Stream water. This is in keeping with the hy-

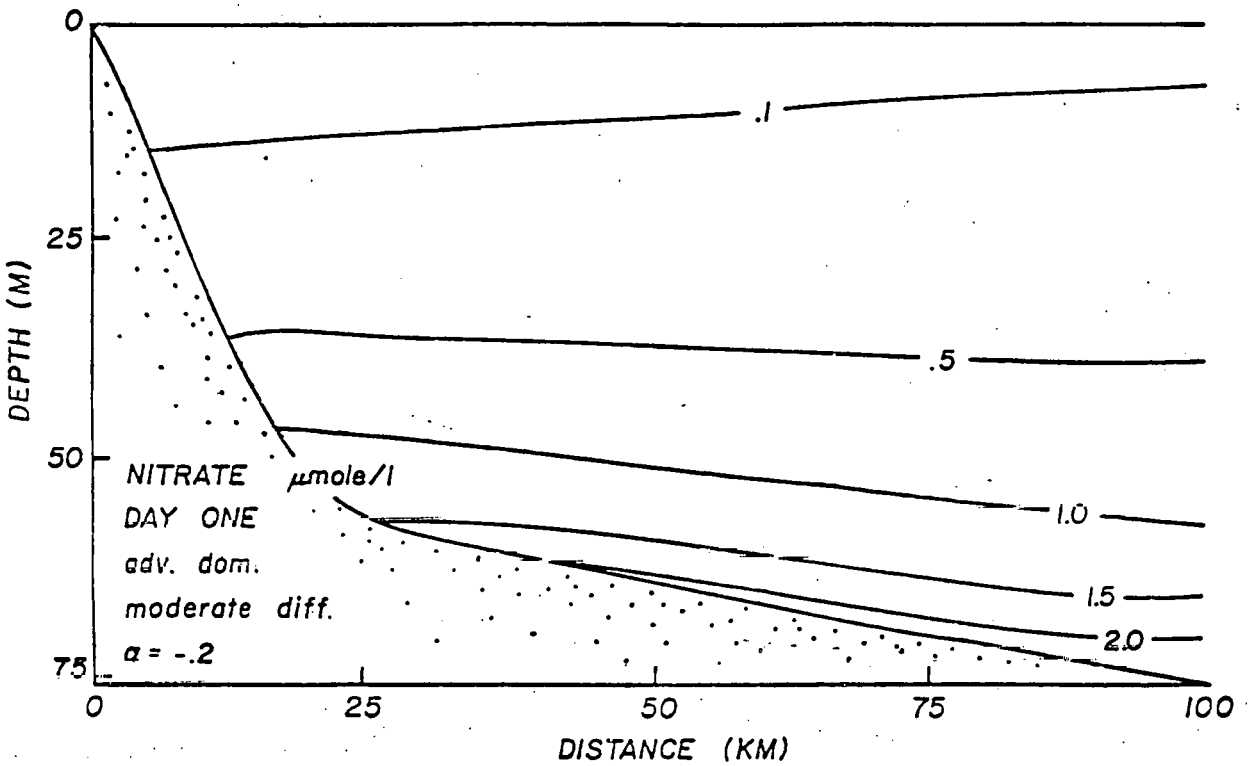

Figure 164 Nitrate profile after one day.

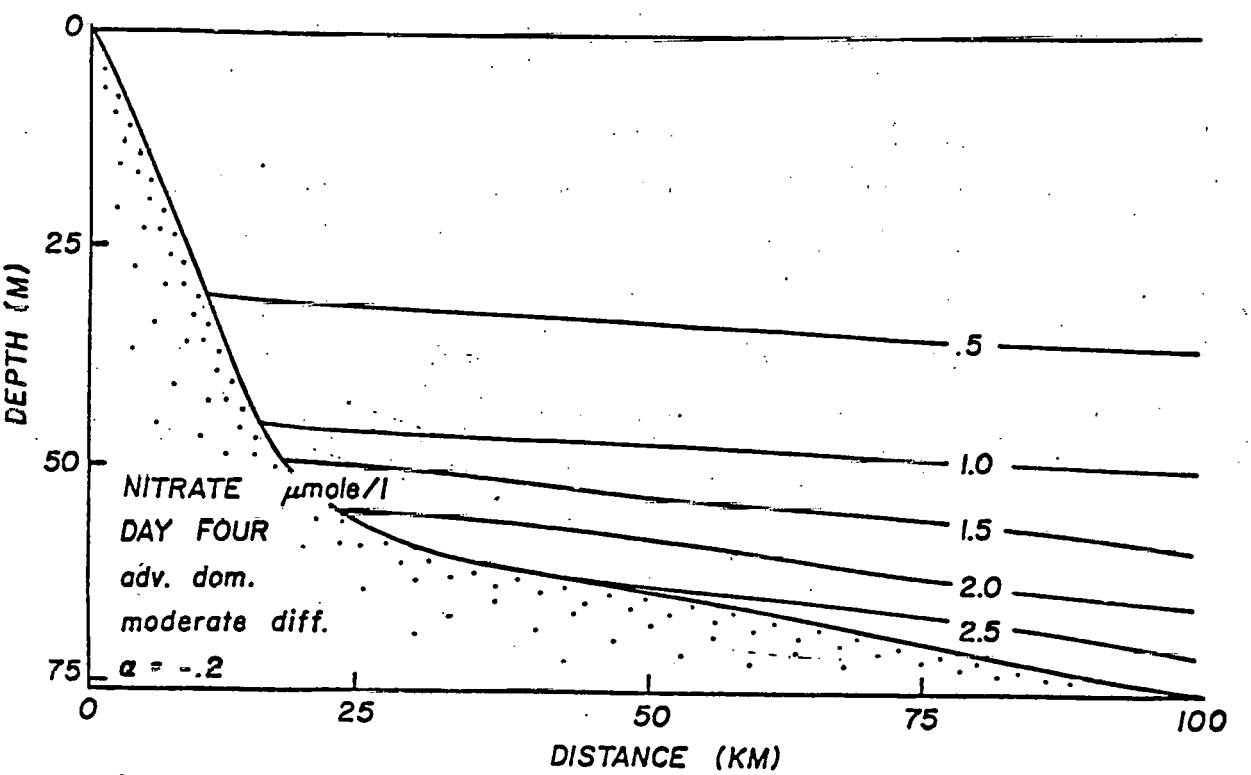

Figure 165 Nitrate profile after four days.

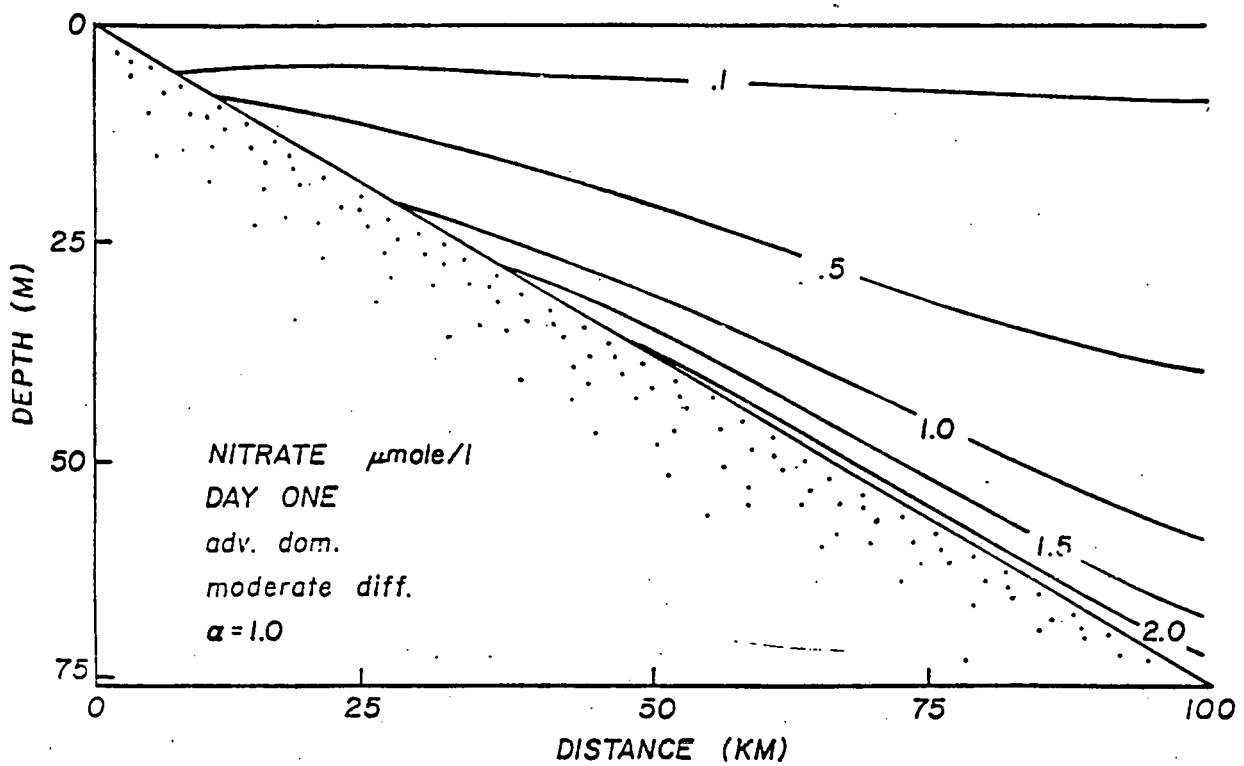

Figure 166 Nitrate profile after one day.

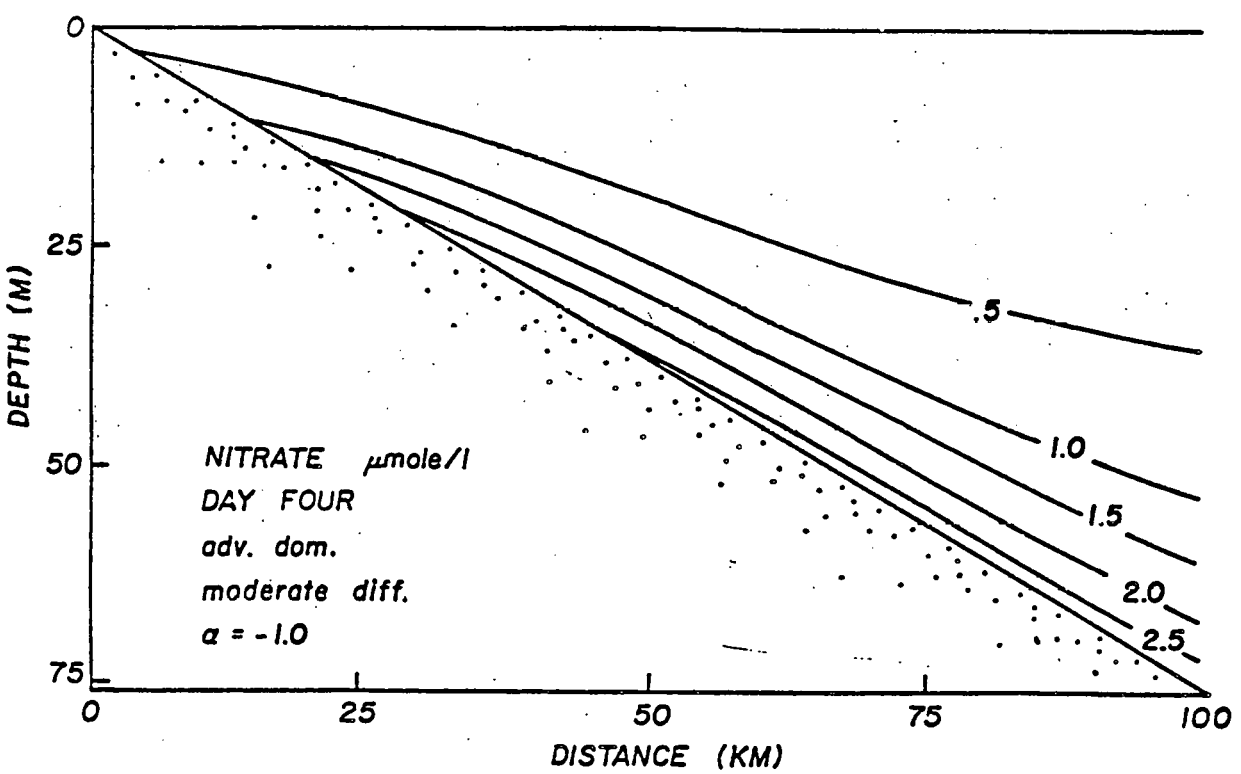

Figure 167 Nitrate profile after four days.

pothesis proposed by Dunstan and Atkinson (1976).

It is obvious that the intrusion process is advectively dominant and that the relative strength of vertical and horizontal diffusion determine the vertical gradient of nitrate produced. Also, the inclusion of a light term in the biological components gives a more realistic intrusion profile with reasonable values for diffusion coefficients. By comparing model results to field data, ranges of reasonable values for the non-dimensional ratios can be determined, which give an indication of the most important processes in coastal shelf water. These are order of magnitude estimates instead of specific constants.

Since this model is for a two-dimensional, time dependent system and does not allow lateral movement, comparison of model results to field data should be done carefully. However, the simulation results are very encouraging since the concentrations and general structure of the nitrate field are like those seen in field data.

BUOYANCY FLUX MODEL

The relative importance of the various ocean surface processes which influence the dynamics and mass field distribution on a continental shelf have not yet been fully established either by theory or field observations. It is generally acknowledged that the effects of mechanical surface wind forcing are dominant in the relatively shallow continental margin regions of the earth. Consequently, most field programs and theoretical attempts aimed at deducing the physics of the continental shelves tend to overlook or simply ignore the fundamental influence of non-zero buoyancy flux at the free surface of the coastal zone. Buoyancy flux constraints or impositions may most generally be derived by mass or heat exchange with the atmosphere or by assuming that lateral coastal freshwater input, such as river and or estuarine outwelling and pluming occurs as either a coastal surface feature or at least as a surface excess in the departure of a vertical integral density or volume constraint from a zero vertical plane, cross-sectional balance. There are several noteworthy exceptions to the apparent neglect of nonmechanical surface exchange forcing: Stommel and Leetma (1972) attempted to discriminate between wind-driven and river runoff modes of shelf circulation; Pietrafesa (1974) presented theory which differentiated between buoyancy and wind driven modes of circulation in the Red Sea; and Pietrafesa and Janowitz (1976) presented theoretical insights into modes of circulation associated with mass and heat exchange at the surface of a two-dimensional continental shelf.

Though there have been many attempts to actually measure the physics of continental margins, it was not until 1970 that a concerted,

co-ordinated effort to understand the fundamental oceanography of the upwelling phenomenon was begun. This project, known as the Coastal Upwelling Ecosystems Analysis program is ongoing and includes data from the continental margins of Oregon-Washington, West Africa and Peru. Additionally, programs sponsored by DOE (formerly: ERDA; AEC), NOAA, BLM, NOS and NSF have increased the physical/dynamical data base of continental margins.

In essence, the Pietrafesa-Janowitz solutions demonstrate the interacting, mutual control of both stratification and circulation by both momentum and buoyancy sources at the surface. These authors show that the effects of buoyancy flux at the surface of a two-dimensional, steady state, continuously stratified continental shelf have been considered. Similarity solutions have been generated using an interative technique. The solutions incorporate the influences of mechanical wind forcing, eddy diffusion, surface buoyancy flux and bottom topography. The traverse circulation can be decomposed into modes associated with the surface wind stress and the surface buoyancy flux and modified by stratification, mixing and bottom topography.

For the special cases of a wind stress with zero curl or for zero wind stress, upwelling circulations can be induced by both the sloping bottom and by gravitational convective effects. Alongshore interior currents counter to the direction of the wind are observed and are attributed to baroclinic pressure gradients.

The nature of the transverse and alongshore flows are characterized in terms of dimensionless ratios of: Coriolis to frictional forces, buoyancy to frictional forces; convective to diffusive forces; and horizontal to vertical mixing time scales and length scales.

Table 11 defines all of the models run for various relative sizes of the dimensionless coefficients used in the model.

The behavior of the system is characterized by dimensionless coefficients; E is the vertical Ekman No., Li is the Lineykin No., δ is an aspect ratio, γ is a relative measure of the strength of circulation to horizontal mixing; the quantity $Ra\gamma$ is the density i.e., ΔS, ΔT convective Raleigh No.; RaE^2 is a measure of the effect of stratification on the circulation; $\delta = h_L/L$ is an aspect ratio; and Γ is a ratio of vertical to horizontal mixing time scales,

with $Ra = h^4_L\, g\hat{\rho}/A_L\psi_L L)$, $E = A_L/fh_L^2$, $\Gamma = \dfrac{K_L L^2}{D_L h^2_L}$

and $\psi_L = (\tau_a^2 + \tau_o^2)^{\frac{1}{2}}$ or $\dfrac{g|q|A_L}{Lf^2K_L}$, which ever

is larger, $\Gamma = \dfrac{K_L L^2}{D_L h_L^2}$, $Li = \dfrac{g|q|h_L A_L}{L^2 f^2 K_L}$ (17)

and $\psi = \dfrac{\psi_L L}{K_L h_L}$.

Some results of the model are shown in Figures 168 - 170 for case 18.

SHOHAT RENORMALIZATION TECHNIQUE

As a part of this DOE work, Pietrafesa has attempted to obtain advanced analytical solutions to the equations governing the balances

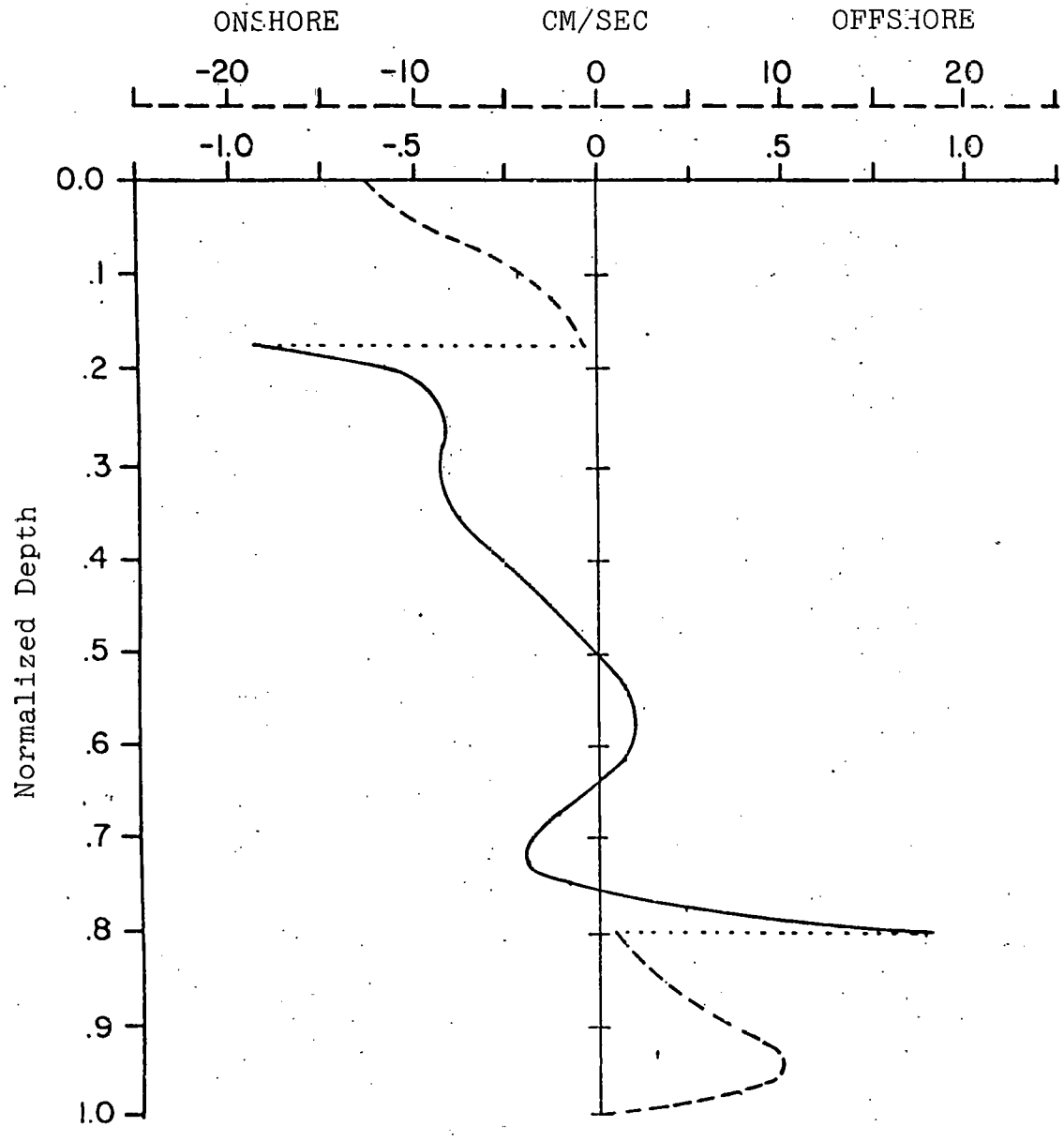

Figure 168. Case 18, u velocity profile

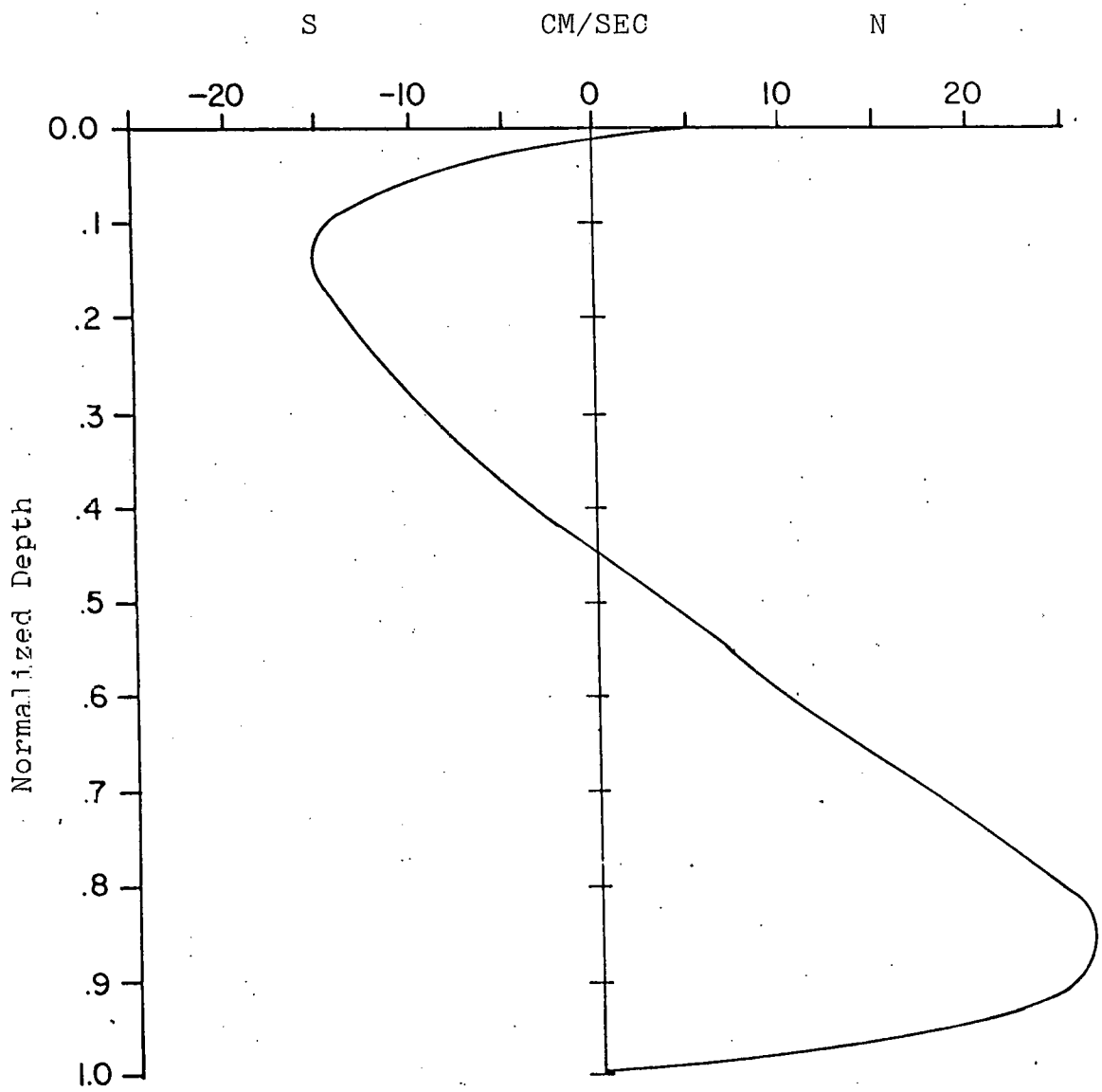

Figure 169. Case 18, v velocity profile

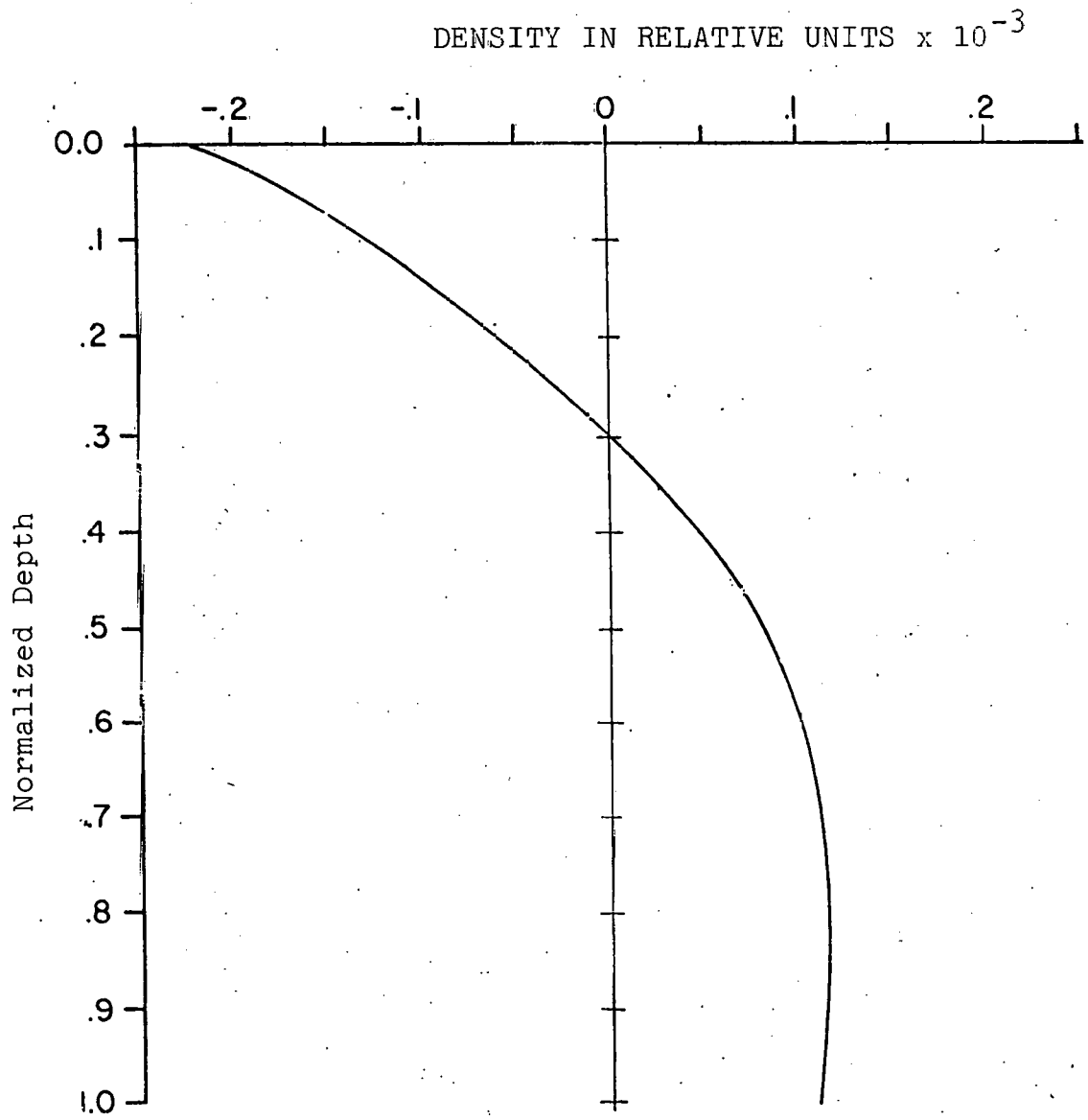

Figure 17C. Case 18, temperature profile

Table 11

Case No.	Ra/Ta	$(Ta)^{1/4}$	M	α	α_2	α_{10}	I	$\tau^{(x)}$	$\tau^{(y)}$	H	$\rho(L,h_L)$	$\rho(L,0)$
1	0	20	1	-0.4	0.2		1	0	1	+1		
2	0	20	1	-0.4	0.2		1	0	-1	-1		
3	0	20	1	-0.4	2.2		1	0	1	+1		
4	0	20	1	-1.5	-2		1	0	1	+1		
5	0	20	1	-1.5	-2		1	0	-1	+1		
6	0	20	1	-1.5	0		1	0	-1	+1		
7	0	29	1	-1.5	0		1	0	1	+1		
8	0	20	1	-1.5	1		1	0	1	+1		
9	0	20	1	-1.5	1		1	0	-1	+1.0		
10	1	20	0	-1.5	-0.5		1	0	0	+1		
11	0.5	20	1	-1.5	1		1	1	1	+1		
12	0	20	1	-0.4	0.2		1	0	0	-1		
13	0.5	20	1	-0.4	0.2		1	0	1	-1		
14	0	20	1	-0.4	0.2		1	0	-1	1		
15	0.5	20	1	-0.4	0.2		1	0	-1	1		
16	0.5	20	1	-0.4	2.2		1	0	-1	1		
17	0.5	20	1	-0.4	2.2		1	0	1	1		
18	0.5	20	1	-1.5	-2		1	0	1	1		
19	0	20	1	-1.5	-2		1	0	-1	-1		
20	0.2	20	1	-0.4	2.2		1	0	-1	1		
21	0	20	1	-0.4	2.2		1	0	1	-1		
22	0.1	20	1	-0.4	2.2		1	0	-1	+1		
23	0	20	1	-0.4	1		1	1	0	1		
24	0	20	1	-0.4	1		1	-1	0	1		
25	1	20	0.2	-0.4	0.6		1	0	0	+1		
26	0.5	20	1	-1.5	-2		1	0	-1	-1		
27	0	20	1	-1.5	0.2		1	0	-1	+1		
28	0	20	1	-1.5	0.2		1	0	1	+1		
29	0.5	20	1	-1.5	1		1	0	1	+1		
30	0.1	20	1	-0.4	2.2		1	0	1	-1		
31	0.2	20	1	-0.4	2.2		1	0	1	-1		
32	0.1	20	1	-0.4	2.2		1	0	-1	+1		
33	0.3	20	1	-0.4	2.2		1	0	-1	+1		
34	0.5	20	1	-0.4	1		1	1	0	+1		
35	0	20	1	-0.4	2.2		1	0.0	1	+1		
36	0.2	20	1	-0.4	2.2		1	0	1	+1		

Table 11(Cont'd)

Case No.	Ra/Ta	$(Ta)^{1/4}$	M	α	α_2	α_{10}	I	$\tau^{(x)}$	$\tau^{(y)}$	H	$\rho(L,h_L)$	$\rho(L,0)$
37	0.5	20	1	-0.4	2.2		1	0	1	+1		
38	0.2	20	1	-0.4	2.2		1	0	-1	+1		
39	0.5	20	1	-0.4	1		1	-1	0	+1		
40	0.5	20	1	-1.5	1		1	-1	0	+1		
41	1	20	0.2	-1.5	-0.5		1	0	0	+1		
42	0	20	0	-1.5	0.2		1	0	-1	+1		
43	0	20	0.5	-1.5	0.1		1	0	-1	+1		
44	0	20	1	-1.5	0.2		1	0	-1	+1		
45	0.25	20	0	-1.5	0.2		1	0	-1	+1		
46	0.25	20	0.5	-1.5	0.2		1	0	-1	+1		
47	0.25	20	1	-1.5	0.2		1	0	-1	+1		
48	0.5	20	0	-1.5	0.2		1	0	-1	+1		
49	0.5	20	0.5	-1.5	0.2		1	0	-1	+1		
50	0.5	20	1	-1.5	0.2		1	0	-1	+1		
51	0.5	20	1	-0.5	1		1	1	0	+1		
52	0.5	20	1	-0.4	1		1	-1	0	+1		
53	1	20	0	-0.4	0.6		1	0	0	+1		
54	1	20	0.2	-0.4	0.6		1	0	0	+1		
55	0	20	1	-0.4	0.6		1	0	-1	+1		
56	0.5	20	1	-0.4	0.6		1	0	-1	+1		
57	0.5	20	1	-0.4	2.2		1	0	1	-1		
58	0	20	1	-0.4	2.2		1	0	-1	+1		

of heat, momentum, mass, energy and nutrients in the SAB marine environment and has developed (in concern with a colleague, Dr. R.A. Struble of N.C.S.U.) a modified version of a classical perturbation expansion, approximation technique which yields insights into the field data. Not only have Pietrafesa and Struble used their technique successfully to solve the governing equations but they have proven a theorem which validates the use of the method and the integrity of the solutions. The method is presented in a separate report (Pietrafesa, Struble and Klinck, 1978).

DIAGNOSTIC AND PROGNOSTIC MODELS

The first model, the diagnostic model, uses a prescribed density field, wind stress field, and reasonable conditions on the streamfunction at the lateral boundaries to compute a velocity field. The dynamics include the Coriolis force, the pressure gradient, and vertical friction. The boundary conditions will be discussed in a later report. The programs for this model have been written and tested. The region under consideration includes the waters from the coast out to approximately the 75 - 3000 meter isobaths, in the region defined by Onslow Bay.

The second model, the prognostic model, is calculated on the same horizontal grid as the first but includes a time dependent diffusion equation. The density field fixed on the boundaries. The density field is allowed to adjust with time to a steady state value with the dynamics also adjusting. The dynamics now include unsteady and nonlinear accelerations as well as horizontal turbulent mixing terms. The output from the

diagnostic model, i.e., the velocity field calculated in that model, promises the initial conditions for this prognostic model. The program for this model is written and is now being tested.

Sinse the prescribed density field used in the diagnostic model is, in general, not the steady state field under existing wind conditions, we proceed to the prognostic model which allows for the adjustment of the density with time under a prescribed wind field and with the conditions on the enclosed boundary through advection-diffusion processes.

SHELF RESPONSE TO A MOVING STORM MODEL

The coastal meteorological and sea level data (Pietrafesa, et. al., 1978c) represent the Carolina Capes climatology as one which is consistently pulsed by several day to several week atmospheric storms, especially during the fall, winter and spring seasons. The data (Pietrafesa, et. al. 1978 a,b,c) indicate that sea level and currents and hydrography as well as possibly Gulf Stream local offshore location and local dynamics may be significantly affected by the passage of atmospheric anticyclones and cyclones (including tropical storms and hurricanes). Consequently, within our objective of understanding continental shelf processes, we (Ph.D. candidate Mr. J. M. Klinck and Dr. L. J. Pietrafesa) are attempting to model the response of a baroclinic, sloping, unsteady continental shelf to the passage of a storm. Consider the following system of equations and boundary conditions for the surface, interior and bottom layers of a continental shelf:

$$u_t - fv = \tau_z^{(x)}$$

$$v_t + fu = \tau_z^{(y)}$$

$$u_x + w_z = 0$$

Interior

$$u_t - fv = - P_x$$

$$v_t + fu = - P_y$$

$$\rho'_t + w\bar{\rho}_z = 0$$

$$P_z = - g\rho$$

$$u_x + w_z = 0$$

Bottom

$$u_t - fv = (Au_z)_z$$

$$v_t + fu = (Av_z)_z$$

$$u_x + w_z = 0$$

under atmospheric forcing which is defined by a, $\bar{\tau}_w$, wind stress:

$$\tau_w = x \pm u_w t \text{ (at } z = \text{surface)}$$

$$u_w = \text{wind velocity magnitude in x-direction}$$

or

$$\bar{\tau}_w = \bar{i}\tau_w^{(x)} + \bar{j}\tau_w^{(y)}$$

where

$$\tau_w^{(x)} = F(x \pm ut)$$

$$\tau_w^{(y)} = G(x \pm ut).$$

This is a brief model description of the complete model which will be presented in a report to follow.

VII. MOMENTUM AND HEAT FLUX CALCULATIONS

Using the Summer, 1976 data sets from Pietrafesa, et. al. (1978b), one can start to compute not only the co-spectra, i.e. the real part of the cross-spectrum between, u, v, t, S and P, in all combinations but one can also take the original time series of the various variables and form a time average of the product of products which represent departures from some temporal mean value, eg. $\overline{u'T'}$, $\overline{u'v'}$, etc. where the primed quantities represent increment departures (fluctuations) from a temporal mean over some specified window length.

The quantities have been averaged over a number of ways, egs.: 1 and 2 day discrete, 1 and 2 day running, cumulative, etc. Spatial gradients will also be taken of the various products. The intention is to compute statistically reliable estimates of horizontal momentum, heat, and vorticity fluxes onto and off of the continental shelf in the Carolina Cape region of the South Atlantic Bight. It is expected that these fluxes are provided by detached eddies and modulations of the Gulf Stream; by strong meteorological forcing, e.g., cold fronts; and by tides. As is discussed in the section "Plans and Objectives", for such calculations, it is essential to know at least the following: the magnitude and shape of the horizontal kinetic and potential energy spectra as a function of position; the magnitude and shape of the horizontal Reynolds stress and heat flux spectra as a function of position; and the along-shelf and trans-shelf coherence scales as a function of frequency and the distribution of the above quantities over vertical modes; It is then hoped that we will be able to qualitatively and quantitatively identify and calculate the source of the mesoscale turbulent, momentum flux fields along the shelf break strip and the alongshore boundaries of the Carolina Capes,

specifically Onslow Bay, and to assess the properties of the cross-spectral and covariance fields for their stationarity, homogeneity and anisotropy. We can then address questions concerning: the frequency of occurrence, intensity, persistence and characterizing signature of the most energetic fluctuation events; the characterization of the inner, mid and outer shelfs to strong atmospheric forcing; the determination of the minimum record lengths needed to compute momentum and heat flux estimates; and the spatial and temporal sampling rates and locations, resp., required to compute momentum, and heat flux estimates.

The 1976 Summer data set appears to be offering the kind of information necessary to compute these estimates, specifically as they relate to the minimum record lengths needed to compute such estimates; cf. Figures 171 - 173 are indicative of a leveling off of all of the fluctuation product quantities at about a period of 60 days at site E_{top}. The quantities suggest a cumulative flux of heat onto the shelf which is consistent with the E_{top} u vs. T cross-correlation, (Figure 174) where over the period band 3½ to 10 days, C^2 peaks at 0.75 and the co-spectral curve (Figure 175) which indicates a large magnitude of heat flux onto the shelf at site E_{top}.

The above are all presented for the sake of example and it is noted that the "leveling off" at site E_{top} may be due to the imposition of biological fouling and though the temperature sensor was not affected, the currents were somewhat at this site.

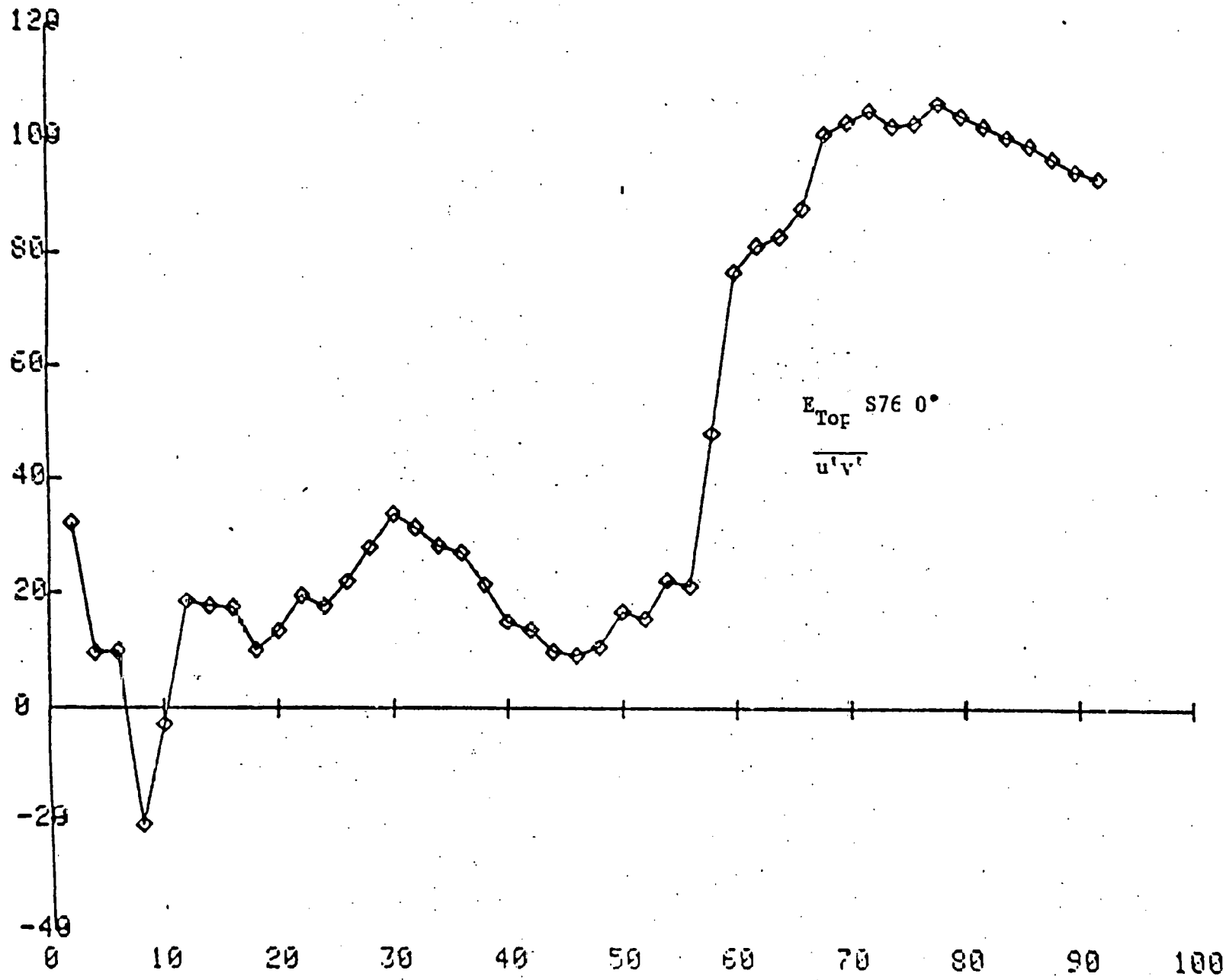

Figure 171: Momentum correlation variance in horizontal plane for E_{top} Summer, 1976 (cumulative)

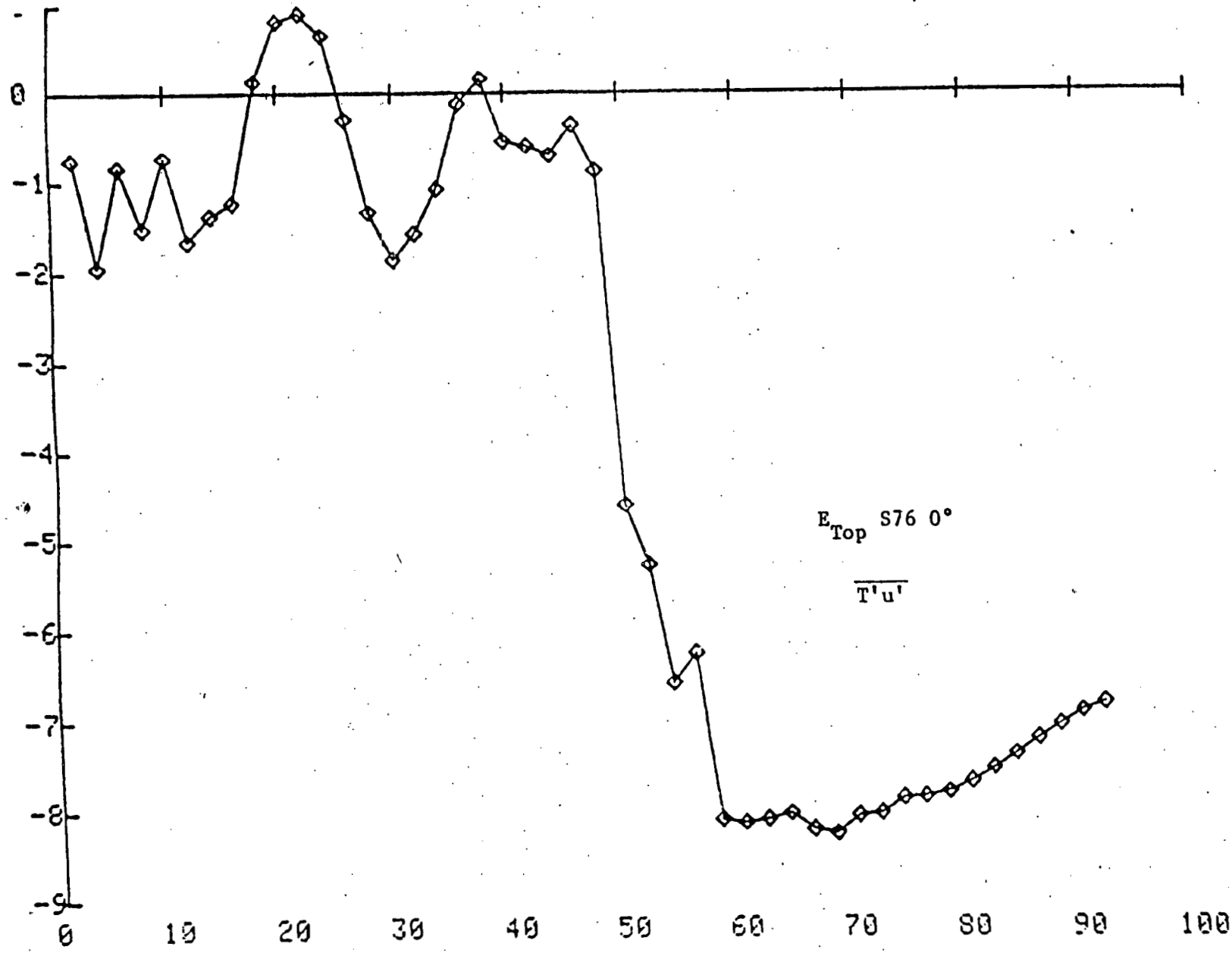

Figure 172 Heat correlation variance in x-direction for E_{top} Summer, 1976 (cumulative)

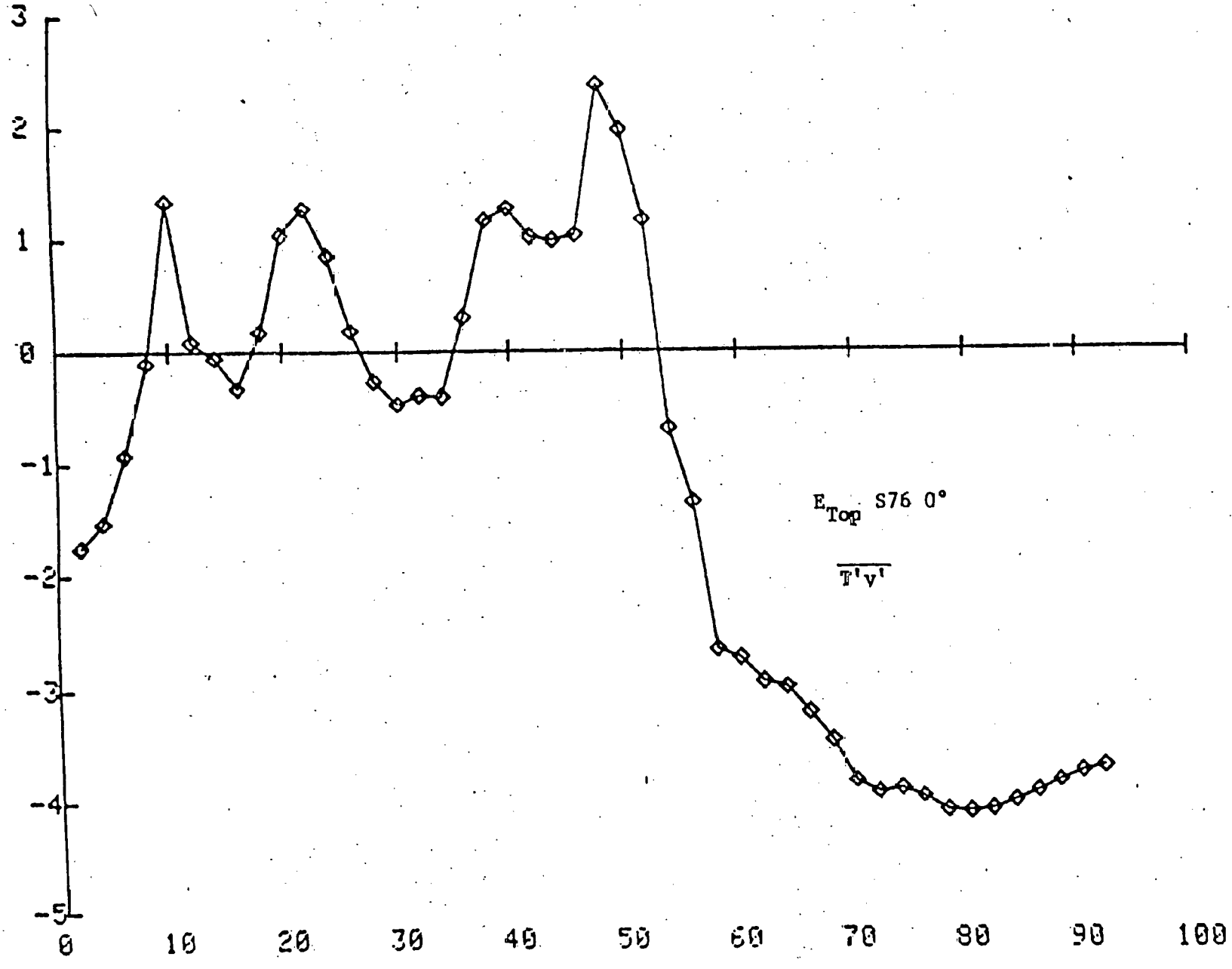

Figure 173 Heat correlation variance in y-direction for E_{top} Summer, 1976 (cumulative)

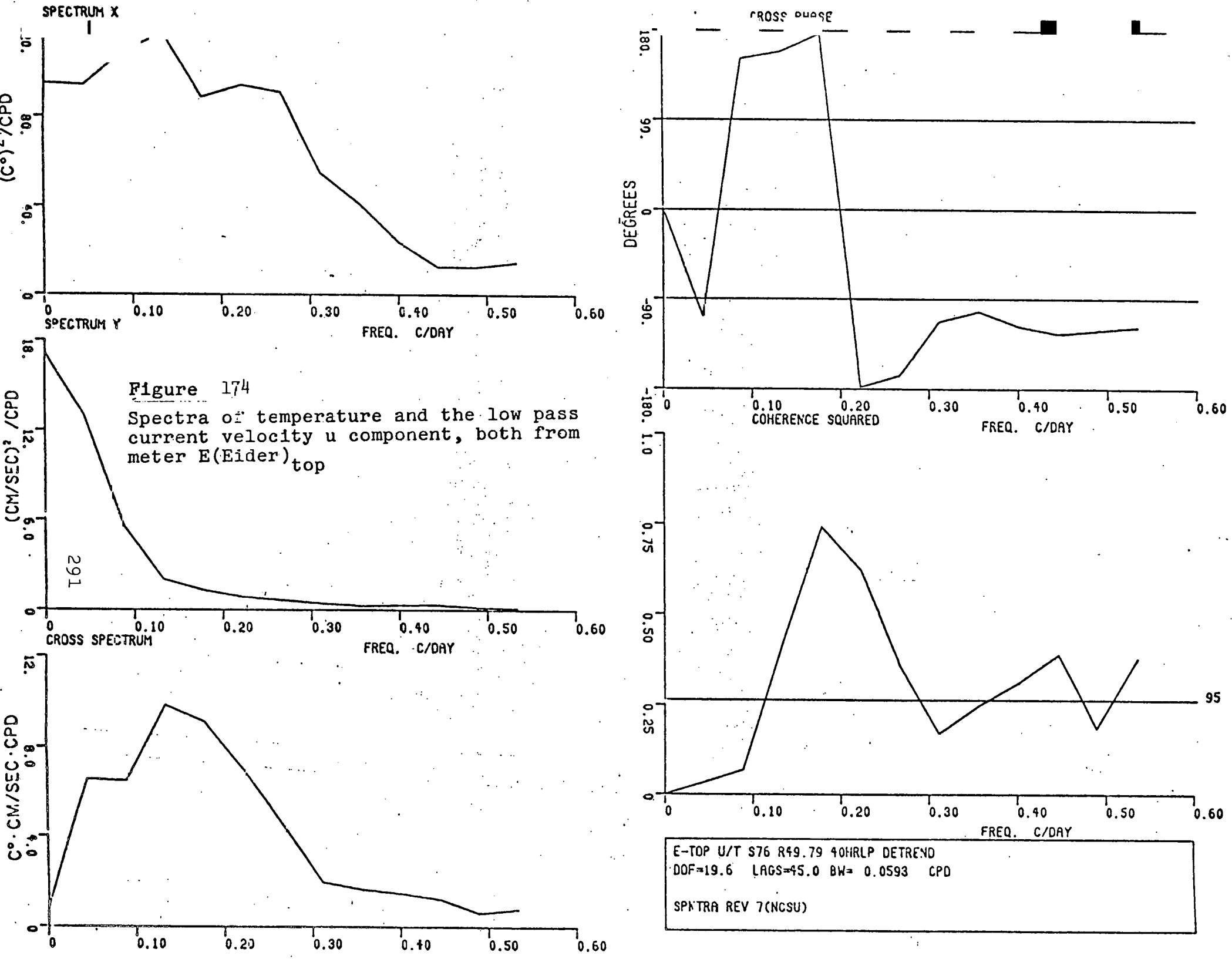

Figure 174

Spectra of temperature and the low pass current velocity u component, both from meter $E(\text{Eider})_{top}$

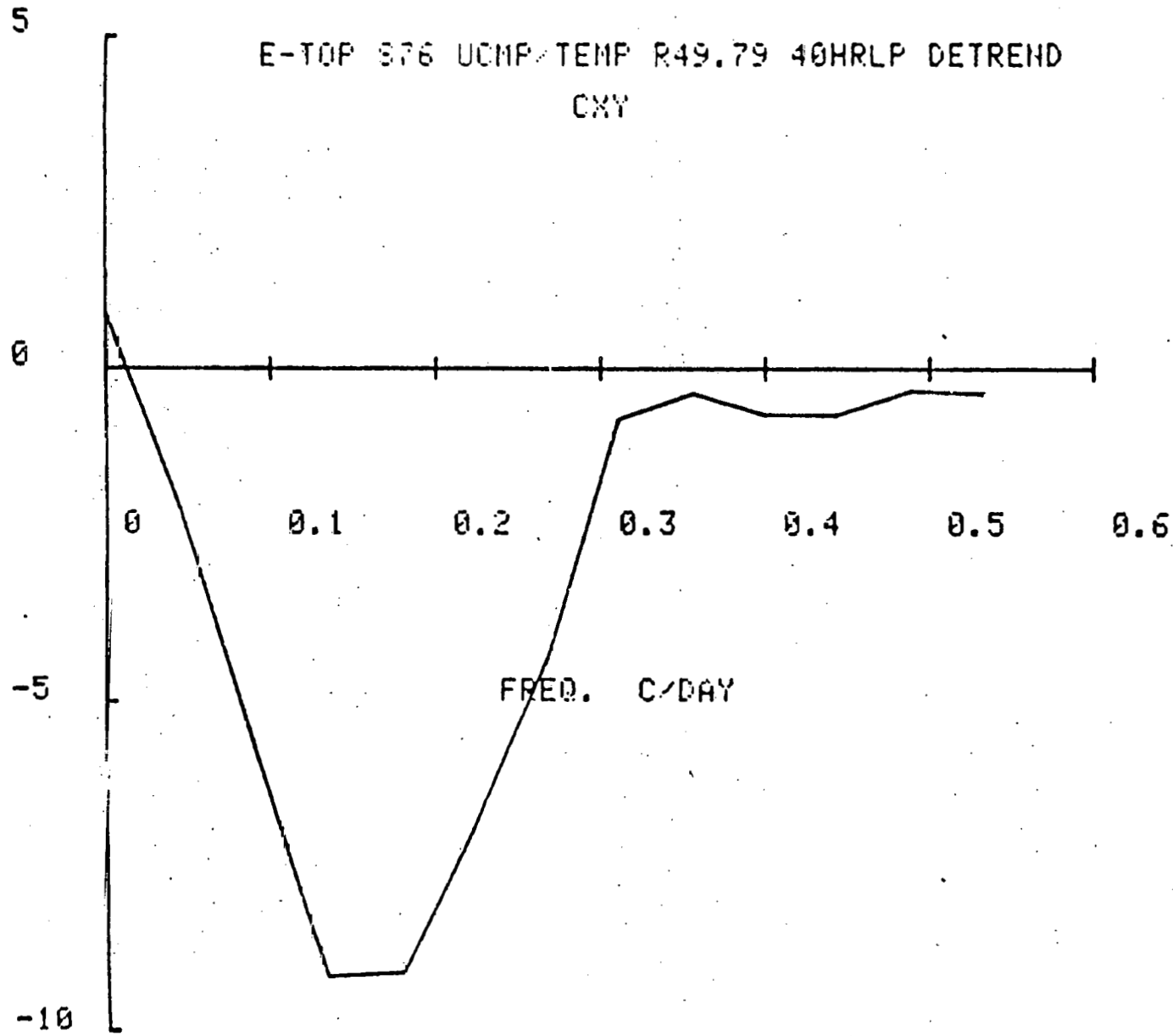

Figure 175 Cospectra of temperature vs. u-component for meter E_{top}

VIII. BIOLOGICAL FOULING

During the moored meter periods of observation of this study, biological fouling of the unattended, on-site instruments has not had any substantial effects upon the measurements, save for the Summer, 1976 period of observation (Pietrafesa, et.al., 1978b.).

As can be seen from Figures 103 - 111, we encountered an unusually excessive, and unexpected, amount of biological fouling which apparently increased the lower threshold speeds of several of the current meters and obviously reduced the current velocity magnitudes. The Aanderaa current meters were more dramatically affected than were the Endeco's which may suggest that either the latter instruments are less susceptible to the types of fouling encountered, than the former due to construction design (Pietrafesa, 1978a) or more likely that the instruments in near coastal waters are not as frequently in a nutrient enriched, biologically rich environment, as are the offshore instruments. The major collapse of the current magnitude envelopes seems to have occurred in the latter part of July, 1976 (cf. Figure 108) perhaps reflecting a large flux of nutrients, etc. onto the Carolina shelf by Gulf Stream intrusion, upwelling, etc.

It will be difficult to retrieve the mollified magnitudes of the currents but given the fact that the M_2 semi-diurnal lunar tidal constituent is so prominent, stable, regular, and deterministic, we will use the tide as a guide to, hopefully, reconstruct the current speed time series.

IX. HURRICANE BELLE

On 5 August 1976, the twentieth tropical system to be tracked east to west across the Atlantic Ocean during 1976, appeared approximately east of the northern Bahamas. By 6 August, VHRR satellite imagery (Dr. R. Legeckis, NOAA/NESS, personal communication) indicated a well-defined vortex of tropical storm intensity. During the next several days, NOAA aircraft reported high altitude winds of 130 knots and a meridional propagation speed of 25 knots. On the 8th of August, Belle had appeared east of Charleston, S. C. and by the 9th to 10th had extended itself to the Virginia border.

Though the storm track was centered essentially along the 75° meridian (cf. Figure 1 for geographic perspective) and though the storm was an intensely packed vortex, its effects had obviously been detected both in Gulf Stream VHRR imagery (NOAA/NESS) and in our moored instruments. (Pietrafesa, et. al. 1978b). Obvious current responses to this event are visible in the figure series 103-111 of this report during the period 6 - 20 August. Temperatures varied the order of 2°-9°C as the effects of this event passed by the arrays. Some of this dramatic temperature change can be attributed to mooring lay-over, but F_{bot} showed a decrease in temperature of 8 C (25°C down to 16.8°C) between day 225 and 228, and this sensor was located 3m from the bottom in 75m of water, so lay-over cannot explain away the dramatic ΔT.

Analyses of the shelf response to this event, including the Hydro/Bio observations made by SKIO immediately after the event (Singer, et. al., 1977), are ongoing.

X. PLANS AND OBJECTIVES

Given the description of the Southeast Continental Shelf Program, touched upon in the Introduction of this report, it is obvious that we (DOE - SAB investigators) are attempting to develope and understanding of the biological/chemical/physical functioning of the nearshore and continental shelf regimes and as nearly as possible to quantify general circulation patterns that control biological production and the dispersal of pollutants, whatever their source.

The natural environment is subject to changes which take place in time scales ranging from minutes to decades. Life processes on the S. E. continental shelf are largely controlled by water circulation which produce dramatic changes on scales of days to years. Without an understanding of the coupling of circulation and biological production, the magnitude of these influences and where they occur, little in the way of predictive capability or establishing cause and effect relationships can be achieved. For example, relatively small deviations in the average position of the Gulf Stream may greatly influence continental shelf production, the spawning and dispersal of larval fishes, etc. Marked changes in land runoff will influence the position of turbidity fronts and the exchange of pollutants across these.

The S. E. continental shelf program, developed in sequences listed below, is aimed at understanding natural processes which control biological activity and the dispersal of selected potential pollutants. Over the long run, with such knowledge, it should be possible to separate and explain natural changes from those which may be induced by man's activities in the coastal-continental shelf environment. The basic philosophy applied

is that effective management decisions are ultimately based on obtaining predictive capability and to achieve this an understanding of ecosystem function is required.

Our long-term objectives include: Differentiating and describing the biological/chemical responses of different shelf environments to fresh water input and coastal circulation patterns (i.e., Georgia Bight, Carolina Embayment, north Florida shelf, etc.); Determining the response of biological components on the shelf to quantified flux rates of nutrients and trace elements due to Gulf Stream motion, wind, runoff events and density fields; Quantifying the rates of input, distribution and exchange of trace elements and radioistopes into and between nearshore zones and the shelf; Determining the role of interfacial transfer mechanisms (e.g., density fronts) in the exchange of trace elements/nutrients/radioisotopes to continental shelf waters and their effect on the biology of the near shore zone.

Our specific objectives include: Characterizing physical and biological processes in Onslow Bay, utilizing data previously acquired under contract to ERDA (1975-1978) and newly acquired (1978-1979).

The specific objectives for studies in the Georgia Bight (5 year plan; 1978-1982) include: Determining the influence of Gulf Stream interactions on transport, flushing and dispersal rates and their effect on biological processes in the Georgia Bight area; Determining the influence of estuarine inputs on biological processes on the shelf; Determining the rates of input to and dispersion of trace elements and radioisotopes in estuaries and on the continental shelf.

Sub-objectives (Georgia Bight) - 2-3 years (1978 - 1980) are: Determining the contribution of atmospheric forcing, air-sea interaction, Gulf

Stream influence, and thermohaline effects (e.g., density gradients from runoff and air-sea interactions) on inner, mid- and outer shelf circulation and exchange processes (Lee, Pietrafesa, Atkinson, SRL); Determining the specific trajectories of water due to discrete events when encountered, such as (a) Gulf Stream meanders and "eddy events"; (b) fluctuations in density discontinuities; passage of cold fronts, etc. (all investigators); Determining the role of frontal zones in the nearshore region in controlling the dispersal to the shelf of inputs derived from rivers, estuaries and marshes (SRL - Blanton; Atkinson, Windom); Describing the spatial/temporal abundances and control of production of phyto-zooplankton as influenced by average circulation patterns (Paffenhöfer, Menzel); Determining the role of autotrophic and heterotrophic microorganisms in the cycling of essential elements and organic matter. Special attention will be placed on ascertaining the influence of horizontal and vertical discontinuities on element and organic matter distribution, microbiological activity and their relation to the physical and chemical regimes of the continental shelf (Pomeroy/Wiebe); Quantifying the input of trace elements to the Georgia Bight area by the atmosphere, Gulf Stream intrusions and their dispersion by average circulation patterns (Windom); Determining the rate of input and the longshore/offshore transport and dispersion of trace elements and radioisotopes (SRL - Blanton, Windom).

OBJECTIVES TO BE ADDRESSED: 1 March, 1978-31 May, 1979

Scientific objectives concerning the continental margin processes affecting the oceanography of the SAB, to be addressed within the next funding year (Present to 31 May, 1979) by N.C.S.U. personnel (at the direction of L.J. Pietrafesa) include: The calculation of statistically

reliable estimates of horizontal momentum, heat, and vorticity fluxes onto and off of the continental shelf in the Carolina cape region of the South Atlantic Bight. It is expected that these fluxes are provided by detached eddies and modulations of the Gulf Stream; by strong meteorological forcing, e.g., cold fronts; and by tides. For such calculations, it is essential to know the following: The magnitude and shape of the horizontal kinetic and potential energy spectra as a function of position; The magnitude and shape of the horizontal Reynolds stress and heat flux spectra as a function of position; The along-shelf and trans-shelf coherence scales as a function of frequency; The distribution of the above quantities over vertical modes; The synoptic-scale temporal and spatial structure of the meteorological forcing; The properties of the tidal forcing in terms of the amplitude and phase fields of the principal constituents.

We then hope to be able to definitively, qualitatively identify and calculate the source of the mesoscale turbulent, momentum flux fields along the shelf break strip and the alongshore boundaries of the Carolina Capes, specifically Onslow Bay, in order to estimate their role in the driving or damping of the persistent circulation along the shelf.

We will attempt to assess the properties of the cross-spectral and covariance fields for their stationarity, homogeneity and anisotropy. We will at least address, if not answer, questions concerning: the frequency of occurrence, intensity, persistence and characterizing signature of the most energetic fluctuation events; the characterization of the inner, mid and outer shelfs to strong atmospheric forcing, such as cold fronts and tropical storms; the determination of the minimum record lengths needed

to compute momentum and heat flux estimates; and the spatial and temporal sampling rates and locations, resp., required to compute momentum, and heat flux estimates.

Finally, we shall attempt to definitively determine: the signature of Gulf Stream derived events, including spin off eddies, filaments or meanders and to discriminate between the types of events; eg., an offshore meander causes a decrease in the surface temperature and an increase in the surface temperature at the shelf break while a spin off eddy causes an increase in temperature at the surface and a decrease near the bottom; the three dimensional temperature, salinity, nutrient and dissolved oxygen fields within the events; the relationships between surface, interior and bottom fluxes of mass, heat and momentum throughout a Gulf Stream derived event; to determine the percentages of current fluctuation due to tides, mechanical wind forcing and Gulf Stream influences; and to develope diagnostic and prognostic models of the physical dynamics.

REFERENCES

Abbe, C. Jr. 1895. Remarks on the Cuspate Capes of the Carolina Coast. Proc. Boston Soc. of Nat. Hist., 26, 489-497.

Atkinson, L.P., J.J. Singer, W.M. Dunstan, L.J. Pietrafesa 1976. Hydrography of Onslow Bay, North Carolina. September 1975 (OBIS II). Georgia Marine Science Center Technical Report, 76-2.

Atkinson, L.P., J.J. Singer, and L.J. Pietrafesa 1976. Onslow Bay intrusion study. Hydrographic observations during current meter servicing cruises in August, October and December 1975 (OBIS 1, 111, and IV). Georgia Marine Science Center Technical Report 76-4.

Atkinson, L.P., J.O. Blanton, and E. Haines 1977. Shelf flushing rates based on the distribution of salinity and freshwater in the Georgia Bight. Coastal and Estuarine Marine Science (in press).

Atkinson, L.P. and L.J. Pietrafesa 1978. Volume, Frequency and Effect of Subsurface Gulf Stream Intrusion into Onslow Bay, North Carolina (in press).

Baylor, E. R. and W. P. Sutcliffe, Jr. 1963. Dissolved organic matter in seawater as a source of particulate food. Limnol. Oceanog. 8:369-371.

Beardsley, R.C., W. Boicourt, L.C. Huff, J. Scott 1977. CMICE 76: A current meter intercomparison experiment conducted off Long Island in February-March, 1976. Woods Hole Oceanographic Institute Technical Report 77-62.

Blanton, J.O. 1971. Exchange of Gulf Stream Water with North Carolina Shelf Water in Onslow Bay during Stratified Conditions. Deep Sea Res., 18, 167-178.

Blanton, J.O. and L.J. Pietrafesa 1978. Flushing of the Continental Shelf South of Cape Hatteras by the Gulf Stream. (in press)

Bosart, L., C. Vando and J. Helsdon 1972. Coastal frontogenesis. J. of Appl. Meteor. 11 (8), 1236-1258.

Bosart, L. 1973. Detailed analysis of precipitation patterns associated with meso scale features accompanying United States east coast cyclogenesis. Mon. Wea. Rev. 101 (1), 1-12.

Bosart, L. and J. Cussen 1973. Gravity wave phenomena accompanying east coast cyclogenesis. Mon. Wea. Rev. Mon. Wea. Rev. 101 (5), 446-454.

Brooks, D.A. 1976. Festsa: fast and easy time series analysis at N.C.S.U. Center for Marine and Coastal Studies, North Carolina State University.

Brooks, D.A. and C.N.K. Mooers 1977. Tidal and longer period motions in the Florida Current. Summer 1970. Deep Sea Res. 24, 399-425.

Brooks, D.A. Sea level Fluctuations off the Carolina Coasts and their relation to atmospheric forcing. Center for Marine and Coastal Studies, North Carolina State University, Technical Report 77-6.

Bumpus, D.F. 1954. The circulation over the Continental Shelf south of Cape Hatteras. Trans. Amer. Geophys. Un. 36 (4), 601-611.

Bumpus, D.F. 1973. A description of the circulation on the continental shelf of the east coast of the United States. Progress in Oceanography, Vol. 6., New York, Pergamon, 111-156.

Carpenter, E. J. and J. J. McCarthy. 1975. Nitrogen fixation and uptake of combined nitrogenous nutrients by Oscillatoria (Trichodesmium) thiebautii in the Western Sargasso Sea. Limnol. Oceanog. 20: 389-401.

Corner, E. D. S. and B. S. Newell. 1967. On the nutrition and metabolism of zooplankton. IV. The forms of nitrogen excreted by Calanus. J. Mar. Biol. Ass. U. K. 47:113-120.

Cragg, J. and W. Sturges 1974. Wind induced currents and sea surface slopes in the eastern Gulf of Mexico. Florida State University Technical Report. June.

Curtin, T.B. 1978. Bureau of Land Management Outer Continental Shelf, southeast USA (in preparation)

Cutchin, P.L. and R.L. Smith 1973. Continental shelf waves: low frequency variations in sea level and currents over the Oregon continental shelf. J. Phys. Oceanogr. 3 (1), 73-82.

DeRycke, R.J. and P.K. Rao 1973. Eddies along a Gulf Stream boundary from a very high resolution radiometer. J. Phys. Oceanogr., 3, 490-492.

Deszoeke, R. 1975. Some effects of bottom topography in baroclinic stability. J. Mar. Res., 33 (1), 93-122.

Dugdale, R. C. 1967. Nutrient limitations in the sea: Dynamics, identification and significance. Limnol. Oceanog. 12:685-695.

Duing, W. 1975. Synoptic studies of transients in the Florida Current. J. Mar. Res. 33, 53-73.

Duing, W., C.N.K. Mooers and T.N. Lee 1977. Low Frequency variability in the Florida Current and relations to atmospheric forcing from 1972 to 1974. J. Geophys. Res. (in press).

Dunstan, W. M. and L. P. Atkinson. 1976. Sources of new nitrogen for the South Atlantic Bight. Estuarine Processes. 1:69-78.

Ekman, V.W. 1905. On the influence of the earth's rotation on ocean currents. Arkiv. fur Matematik, Astronomi ock Fysik 2, 1-52.

Eppley, R. W., J. L. Coatsworth and L. Solorzano. 1969. Studies of nitrate reductase in marine plankton. Limnol. Oceanog. 14:194-205.

Fofonoff, N.P. 1969. Spectral characteristics of internal waves in the Ocean. Deep Sea Res. 16 (supplement), 59-72.

Fuglister, F.C. 1951. Multiple currents in the Gulf Stream System. Tellus 3, 230-233.

Fuglister, F.C. and L.V. Worthington 1951. Some results of a multiple ship survey of the Gulf Stream. Tellus 3, 1-14.

Garvine, R.W. 1971. A simple model of coastal upwelling dynamics. J. Phys. Oceanogr. 1, 169-179.

Gill, A.E. and E.H. Schumann 1974. The generation of long shelf waves by the wind. J. Phys. Oceanogr. 4, 83-90.

Gonella, J. 1972. A rotary-component method for analyzing meteorological and oceanographic vector time series. Deep Sea Res., 19 (12), 833-846.

Green, C.K. 1944. Summer Upwelling-northeast coast of Florida. Science, 100 (2607), 546-547

Grimshaw, R. 1978. Stability of continental shelf waves in the presence of boundary current shear (unpub. M.S.).

Hamon, B.V. 1962. The spectrums of mean sea level at Sydney, Coff's Harbor and Lord Howe Island. J. Geophys. Res. 67, 5147-5155. 1963 (correction) J. Geophys. Res., 68 4635.

Hamon, B.V. 1966. Continental shelf waves and the effects of atmospheric pressure and wind stress on sea level. J. Geophys. Res. 71, 2883-2893

Hansen, A. G. 1964. Similarity Analyses of Boundary Value Problems in Engineering. Prentice Hall, Inc., Englewood Cliffs, New Jersey, p. 114.

Hansen, D.V. 1970. Gulf Stream meanders between Cape Hatteras and the Grand Banks. Deep Sea Res. 17, 495-511.

Hidaka, K. 1953. Wind-driven sea level change over a continental shelf. Tech. Rept. No. 9, Texas A and M Research Foundation, October.

Huyer, A., B.M. Hickey, J.D. Smith, R.L. Smith, and R.P. Pillsbury 1975. Alongshore coherence at low frequencies in currents observed over the Continental shelf off Oregon and Washington. J. Geophys. Res. 80 (24), 3495-3505.

Iselin, C.O'D. 1940. Preliminary report on long period variations in the transport of the Gulf Stream System. Pop. Phys. Oceanogr. and Meteor., Vol. 8, No. 1, 40 pp.

Kundu, P.K., J.S. Allen, R.L. Smith 1975. Modal decomposition of the velocity field near the Oregon Coast. J. Phys. Oceanogr. 5, 683-704.

LeBlond,P.H. and L.A Mysac. 1977. Trapped coastal waves and their role in shelf dynamics. The Sea, Vol. 6. pp.459-495.

Lee, T.N. 1975. Proposal to Energy Research and Development Administration.

Lee, T. N. 1977. Measurement of Gulf Stream and wind induced shelf circulation in the South Atlantic Bight. Progress Report to ERDA on contract E(40-1)-5163.

Lee, T.N. and R.L. Shutts 1977. Technical program for Aanderaa current meter moorings on continental shelves. University of Miami Technical Report. TR 77-5.

Lee, T.N., and D.A. Mayer 1977. Low frequency current variability and spin-off eddies along the shelf off southeast Florida. J. Mar. Res., 35(1), 193-220.

Legeckis, R. 1975. Applications of synchronous meteorological satellite data to the study of time dependent sea surface temperature changes along the boundary of the Gulf Stream. Geophys. Res. Lett., 2, 435-438.

Marchuk, I. G., V. P. Kochergin, V. I. Klimok and V. A. Sukhorukov. 1977. On the Dynamics of the Ocean Surface Mixed Layer. J. Phys. Oceanog. 7(6):865-875.

McKee, W.D. 1978. Continental shelf waves in the presence of a sheared geostrophic current (unpub. M.S.).

Miller, A.R. 1957. The effect of steady winds on sea level at Atlantic City. Meteoral. Monogr. 2, 29-31.

Miller, A.R. 1958. The effects of winds on outer levels on the New England Coast. Limnol. and Oceanogr. 3, 1-14.

Mooers, C.N.K. 1973. A technique for the cross spectrum analysis of pairs of comples-valued time series, with emphasis on properties of polorized components and rotational invariants. Deep Sea Res., 20 (12), 1129-1142.

Mooers, C.N.K. and R.L. Smith 1968. Continental Shelf Waves off Oregon. J. Geophys. Res. 73, 549-557.

Mysak, L.A., and B.V. Hamon 1969. Low frequency sea level behavior and continental shelf waves. J. Geophys. Res., 74, 1397-1405.

Niiler, P.P. 1975. Variability in Western Boundary currents. Numerical Models of Ocean Circulation, National Academy of Sciences, Washington, D.C. p216-236.

Niiler, P.P. 1975. The deepening of the wind mixed layer. J. Fluid. Mech. (in press).

Niiler, P.P. and L.A. Mysak 1971. Barotropic waves along the eastern continental shelf. Geophys. Fluid Dyn. 2, 273-288.

Niiler, P.P. and W.S. Richardson 1973. Seasonal variability of the Florida Current. J. Mar. Res. 31(3), 144-167.

NOAA 1970. Environmental conditions within specific geographical regions: offshore east and west coasts of the United States and in the Gulf of Mexico. Final Report, NODC, Environmental Data Service, NOAA, Washington, D.C.

Oort, A.H. 1964. Computations of the eddy heat and density transports across the Gulf Stream. Tellus, 16, 55-63.

Oort, A.H., and A. Taylor 1969. On the kinetic energy spectrum near the ground. Mon. Wea. Rev. 97, 623-636.

Orlanski, I. 1969. The influence of bottom topography on the stability of jets in a baroclinic fluid. J. Atm. Sci. 26, 1216-1232.

Orlanski, I. and M.D. Cox 1973. Baroclinic instability in ocean currents. Geophys. Fluid Dyn. 4, 297-332.

Paffenhöfer, G. - A. and J. D. H. Strickland. 1970. A note on the feeding of Calanus helgolandicus on detritus. Mar. Biol. 5:97-99.

Panshin, D.A. 1967. Sea level, winds and upwelling along the Oregon Coast. MS thesis, Oregon State University, Corvallis.

Parr, A.E. 1933. A geographic-ecological analysis of the seasonal change in temperature correlations in shallow water along the Atlantic coast of the U.S. Bull. Bingham Oceanogr. Coll. 4 (3), 1-90.

Pedlosky, J. 1964. The stability of currents in the atmosphere and the ocean. Part I. J. Atm. Sci. 21, 201-219.

Pedlosky, J. 1971. Geophysical Fluid Dynamics. Mathematical Problems in the Geophysical Sciences. American Mathematics Society, 1-60.

Petterson, S. 1969. Introduction to Meteorology 3rd edition. McGraw-Hill, New York, 333 pp.

Pietrafesa, L.J. 1970. Trapped and leaky shelf wave modes. unpublished M.S.

Pietrafesa, L. J. 1973. Steady baroclinic circulation on a continental shelf. Ph.D. dissertation, Department of Oceanography and Geophysics Group, University of Washington, Seattle. University Microfilms, Ann Arbor, Michigan.

Pietrafesa, L.J. 1974. Continental Shelf processes affecting the Oceanography of the South Atlantic Bight. Proposal to Atomic Energy Commission.

Pietrafesa, L.J. 1976. Proposal to Energy Research and Development Administration for renewal of Contract E(B8-1)-902.

Pietrafesa, L.J. and L.P. Atkinson 1975. Continental Shelf processes affecting the Oceanography of the South Atlantic Bight. Proposal to Energy Research and Development Administration.

Pietrafesa, L.J. and G.S. Janowitz 1976. AGU presentation. abstract. EOS 57 (12), 934.

Pietrafesa, L.J., D.A. Brooks, L.P. Atkinson, R.D'Amato, and J. Bane 1977. Preliminary data report, physical/dynamical observations made in Onslow Bay; summer, fall and winter 1975. Center for Marine and Coastal Studies, North Carolina State University, Technical Report, 77-05.

Pietrafesa, L.J., D.A. Brooks, R.D'Amato, L.P. Atkinson 1978(a). Onslow Bay physical/dynamical experiments; summer - fall, 1975. Center for Marine and Coastal Studies, North Carolina State University. Technical Report, 78-2.

Pietrafesa, L.J., R. Struble and J.M. Klinck 1978. Applications of a revised euler - Shohat pertubation expansion technique in the study of ocean circulation (in press).

Pietrafesa, L.J., R. D'Amato, C.D. Gabriel, R.J. Sawyer and D.A. Brooks 1978(b). Onslow Bay Physical/Dynamical Experiments, Summer, 1976. Vols. I and II. Center for Marine and Coastal Studies Technical Report, 78-3.

Pietrafesa, L.J., R. D'Amato, C.D.Gabriel and R.J. Sawyer 1978(c). Continental Margin Atmospheric Climatology and Sea Level. (Historical Setting 1974-1975). Center for Marine and Coastal Studies Technical Report, 78-4.

Pietrafesa, L.J., G.S. Janowitz, L.P. Atkinson and J.O. Blanton 1978. Effects of the Charleston "Bump" on Continental Margin Processes in the South Atlantic Bight. (Manuscript in preparation).

Pietrafesa, L.J., T.N. Lee and J.O. Blanton, 1978. Marine Climatology and Sea Level in the South Atlantic Bight: An Overview. (Manuscript in preparation).

Pillsbury, J.E. 1891. The Gulf Stream. Rept. Supt., U.S. Coast and Geod. Surv. for year ending June, 1890 p. 459-620.

Pond, S. 1975. The exchanges of momentum, heat and moisture at the ocean-atmospher interface. Numerical Models of Ocean Circulation, National Academy of Sciences, Washington, D.C. p 26-38.

Poulet, S. A. 1976. Feeding of *Pseudocalanus minutus* on living and nonliving particles. *Mar. Biol.* 34:117-125.

Redfield, A.C. 1958. The influence of the continental shelf on the tides of the Atlantic Coast of the U.S. J. Mar. Res., 17, 432-448.

Richardson, W.S., W.J. Schmitz, Jr. and P.P. Niiler 1969. The velocity structure of the Florida Current from the Straits of Florida to Cape Fear. Deep Sea Res., 16(supplement), 225-231.

Roden, G.I. 1960. On the nonseasonal variations in sea level along the west coast of North America. J. Geophys. Res. 65, 2809-2826.

Rowe, G. T., C. H. Clifford, K. L. Smith and A. L. Hamilton. 1975. Benthic nutrient regeneration and its coupling to primary productivity in coastal waters. Nature. 255:215-217.

Ruzecki, E.P. 1974. A socio-economic environmental baseline summary for the south atlantic region between Cape Hatteras, North Carolina and Cape Canaveral, Florida: Vol. II - Climatology. Virginia Institute of Marine Science Technical Report, September.

Saltzman, B. and C. Tang. 1975. Formation of meanders, fronts and cutoff thermal pools in a baroclinic ocean current. J. Phys. Oceanogr., 5, 86-92.

Saunders, P.M. 1977. Wind stress on the ocean over the eastern continental shelf of North America. J. Phys. Oceanogr. 7, 555-566.

Schmitz, W.J., Jr. 1969. On the dynamics of the Florida Current. J. Mar. Res., 27(1), 121-150.

Schmitz, W.J. and W.S. Richardson 1968. On the transport of the Florida Current. Deep Sea Res., 15, 679-693.

Schmitz, W.J., Jr. and P.P. Niiler, 1969. A note on the kinetic energy exchange between fluctuations and mean flow in the surface layer of the Florida Current. Tellus 21, 814-819.

Singer, J.J., L.P. Atkinson, W.S. Chandler, and P.G. O'Malley 1977. Hydrographic observations in Onslow Bay, North Carolina, July-August 1976 (OBIS V), Data Graphics. Georgia Marine Science Center Technical Report 77-6.

Smith, R.L. 1974. A description of current, wind and sea level variations during coastal upwelling off the Oregon coast, July-August 1972. J. Geophys. Res. 79 (3), 435-443.

Stommel, H.M. and A. Leetma 1972. Circulation on the continental shelf, Proc. Nat. Acad. Sci., USA., 69 (11), 3380-3384.

Strong, A.E. and R.J. DeRycke 1973. Ocean current monitoring employing a new satellite sensing technique Science, 182(4111), 432-484.

Stumpf, H.G. and P.K. Rao 1975. Evolution of Gulf Stream eddies as seen in satellite infrared imagery. J. Phys. Oceanogr., 5, 388-393.

Sturges, W. 1974. Sea level slope along Continental boundaries. J. Geophys. Res., 79(6), 825-830.

Struhsaker, P. 1969. Demersal fish resources: Composition, distribution and commercial potential of the continental shelf stocks of southeastern United States. Fish. Ind. Res. 4(7):261-300.

Taylor, C.B. and H.B. Stewart, Jr. 1959. Summer Upwelling along the east coast of Florida. J. Geophys. Res. 64 (1), 33-40.

U.S. Navy 1970. Summary of Synoptic meteorological observations (SSMO) for North American coastal Marine areas. Naval Weather Service Environmental Detachment, Fed. Bldg., Asheville, N. C.

Von Arx, W.S., D. Bumpus and W.S. Richardson 1955. On the fine structure of the Gulf Stream front. Deep Sea Res., 3, 46-65.

VonBrand, T., N. W. Bakestraw and R. E. Renn. 1937. The experimental decomposition and regeneration of nitrogenous organic matter in seawater. Biol. Bull. 72:165-175.

Ward, R. 1925. The Climates of the United States. Ginn, Boston, 338 pp.

Webster, F. 1961a. The effects of meanders on the kinetic energy balance of the Gulf Stream. Tellus, 13, 392-401.

Webster, F. 1961b. A description of Gulf Stream Meanders off Onslow Bay. Deep Sea Res., 8, 130-143.

Welander, P. 1957. Wind action on a shallow sea: Some generalization on Ekamn's theory. Tellus, 9, 45-52.

Williams, P. J. LeB. and C. S. Yentsch. 1976. An examination of photosynthetic products, and heteorotrophic utilization of dissolved organic compounds with reference to results from a coastal subtropical sea. Mar. Biol. 35:31-40.

Wood, J. D. 1958. Nitrogen excretion in some marine teleosts. Can. J. Biochem. and Phys. 36:1237-1242.

Wunsch, C., D.V. Hansen, and B.D. Zetler. 1969. Fluctuations of the Florida Current inferred for sea level records. Deep Sea Res. 16 (supplement), 447-470.